JOURNAL OF THE MECHANICS AND PHYSICS OF SOLIDS

EDITORIAL ADVISORY BOARD

J. F. BAKER—Cambridge W. M. BALDWIN—Cleveland
E. BRANDENBERGER—Zürich G. BUSCH—Zürich
A. H. COTTRELL—Cambridge C. CRUSSARD—Paris M. J. DRUYVESTEYN—Delft
A. KOCHENDÖRFER—Düsseldorf N. F. MOTT—Cambridge
A. NADAI—Pittsburgh, Pa. G. SACHS—Syracuse, N.Y. E. SIEBEL—Stuttgart
V. V. SOKOLOVSKY—Moscow

EDITOR-IN-CHIEF

R. HILL
University of Nottingham

Volume 8
1960

PERGAMON PRESS · OXFORD · LONDON · NEW YORK · PARIS

Contents of Volume 8

NUMBER 1

Page

T. B. KAMMASH, S. A. MURCH and P. M. NAGHDI : The elastic–plastic cylinder subjected to radially distributed heat source, lateral pressure and axial force with application to nuclear reactor fuel elements 1

A. F. B. WOOD : On the photoelastic examination of vibrating bodies and the photoelastic effect in optically active media 26

H. PAYNE and S. J. CZYZAK : On the torsion of a thin-wall cylinder following a plastic extension 39

W. A. ZAMA, D. D. LANG and F. R. BROTZEN : Steady-state creep of tin near the melting point 45

SHOI-YEAN HWANG and N. DAVIDS : Graphical analysis of the formation of shock fronts in materials 52

J. W. CRAGGS : On the propagation of a crack in an elastic-brittle material .. 66

Research Note

R. C. BREWER and J. M. ALEXANDER: A new technique for engraving and measuring grids in experimental plasticity 76

Book Reviews :

" Solid State Physics : Advances in Research and Applications," Vol. 6, edited by F. SEITZ and D. TURNBULL (reviewed by J. D. ESHELBY) 79

" Solid State Physics : Advances in Research and Applications," Vol. 7, edited by F. SEITZ and D. TURNBULL (reviewed by J. D. ESHELBY) 79

" Theoretical Elasticity and Plasticity for Engineers," by D. E. R. GODFREY (reviewed by F. A. GAYDON) 80

NUMBER 2

T. YOKOBORI : Stress criterion for fatigue fracture of steels 81

W. A. BASSALI : The classical torsion problem for sections with curvilinear boundaries 87

D. S. DUGDALE : Yielding of steel sheets containing slits 100

R. HILL and M. J. SEWELL : A general theory of inelastic column failure—I .. 105

R. HILL and M. J. SEWELL : A general theory of inelastic column failure—II .. 112

A. N. STROH : A simple model of a propagating crack 119

W. A. BASSALI : Bending of a singularly loaded thin circular annulus with free boundaries 123

E. O. IMEGWU : Plastic flexure and torsion 141

Book Reviews :

" Theoretical Elasticity," by C. E. PEARSON (reviewed by R. J. KNOPS) 147

" Proceedings of the 3rd U.S. National Congress of Applied Mechanics," (reviewed by R. HILL) 147

" Mechanical Properties of Non-metallic Brittle Materials," edited by W. H. WALTON (reviewed by R. HILL) 147

" Introduction to Plasticity," by W. PRAGER (reviewed by R. HILL) 148

" Progress in Metal Physics," Vol. 7, edited by B. CHALMERS and R. KING (reviewed by S. G. GLOVER) 148

" Linear Structural Analysis," by P. B. MORICE (reviewed by M. R. HORNE) 149

" Non-Homogeneity in Elasticity and Plasticity," edited by W. OLSZACK (reviewed by R. HILL) 149

" Proceedings of the Fourth Midwestern Conference on Solid Mechanics," (reviewed by J. E. ADKINS) 150

Books Received 151

NUMBER 3 *Page*

P. G. HODGE, Jr. and R. SANKARANARAYANAN : Plastic interaction curves for annular plates in tension and bending 153

H. DERESIEWICZ : Effect of boundaries on waves in a thermoelastic solid : Reflexion of plane waves from a plane boundary 164

S. C. REDSHAW and K. R. RUSHTON : An electrical analogue solution for the stresses near a crack or hole in a flat plate 173

F. A. MCCLINTOCK and S. P. SUKHATME : Travelling cracks in elastic materials under longitudinal shear 187

J. P. BERRY : Some kinetic considerations of the Griffith criterion for fracture—I. Equations of motion at constant force 194

J. P. BERRY : Some kinetic considerations of the Griffith criterion for fracture—II. Equations of motion at constant deformation 207

Book Reviews :

" An Introduction to the Mechanics of Solids," by S. H. CRANDALL and N. C. DAHL (reviewed by M. J. SEWELL).. 217

" Theory of Elasticity," by L. D. LANDAU and E. M. LIFSHITZ (reviewed by J. E. ADKINS) .. 217

" Fracture," edited by B. L. AVERBACH *et al.* (reviewed by D. V. WILSON) 218

NUMBER 4

S. C. HUNTER : The Hertz problem for a rigid spherical indenter and a viscoelastic half-space 219

C. D. DAVIS and S. C. HUNTER : Assessment of the strain-rate sensitivity of metals by indentation with conical indenters 235

M. REINER : Plastic yielding in anelasticity 255

A. J. M. SPENCER : The dynamic plane deformation of an ideal plastic–rigid solid 262

D. S. BERRY : An elastic treatment of ground movement due to mining—I. Isotropic ground 280

Notice 293

Author Index

(B) denotes Book Review

ADKINS, J. E. pp. 150, 217 (B).
ALEXANDER, J. M. p. 76.
BASSALI, W. A. pp. 87, 123.
BERRY, D. S. p. 280.
BERRY, J. P. pp. 194, 207.
BREWER, R. C. p. 76.
BROTZEN, F. R. p. 45.
CRAGGS, J. W. p. 66.
CZYZAK, S. J. p. 39.
DAVIDS, N. p. 52.
DAVIS, C. D. p. 235.
DERESIEWICZ, H. p. 164.
DUGDALE, D. S. p. 100.
ESHELBY, J. D. p. 79 (2) (B).
GAYDON, F. A. p. 80 (B).
GLOVER, S. G. p. 148 (B).
HILL, P. pp. 105, 112; pp. 147 (2), 148, 149 (B).
HODGE, P. G. p. 153.
HORNE, M. R. p. 149 (B).
HUNTER, S. C. pp. 219, 235.
HWANG, S. p. 52.
IMEGWU, E. O. p. 141.
KAMMASH, T. B. p. 1.
KNOPS, R. J. p. 147 (B).
LANG, D. D. p. 45.
MCCLINTOCK, F. A. p. 187.
MURCH, S. A. p. 1.
NAGHDI, P. M. p. 1.
PAYNE, H. p. 39.
REDSHAW, S. C. p. 173.
REINER, M. p. 255.
RUSHTON, K. R. p. 173.
SANKARANARAYANAN, R. p. 153.
SEWELL, M. J. pp. 105, 112; p. 217 (B).
SPENCER, A. J. M. p. 262.
STROH, A. N. p. 119.
SUKHATME, S. P. p. 187.
WILSON, D. V. p. 218 (B).
WOOD, A. F. B. p. 26.
YOKOBORI, T. p. 81.
ZAMA, W. A. p. 45.

J. Mech. Phys. Solids, 1960, Vol. 8, pp. 1 to 25. Pergamon Press Ltd., London. Printed in Great Britain

THE ELASTIC–PLASTIC CYLINDER SUBJECTED TO RADIALLY DISTRIBUTED HEAT SOURCE, LATERAL PRESSURE AND AXIAL FORCE WITH APPLICATION TO NUCLEAR REACTOR FUEL ELEMENTS*

By T. B. KAMMASH†, S. A. MURCH‡ and P. M. NAGHDI‡

(*Received* 20 *July* 1959)

SUMMARY

THE elastic–plastic deformation of a solid cylinder in the presence of a distributed heat source and subjected to a lateral pressure p and an axial fource F is considered in detail using Tresca's yield function, its associated flow law, and a linear workhardening law. Particular attention is given to the class of problems in which the radial stress, and not the axial stress, is the intermediate principal stress. The general results are applied to the cylindrical nuclear reactor fuel element in the state of plane strain with a radially distributed Gaussian heat source, acting in its fissionable interior. The solution is expressed in closed form in terms of the exponential integral and the incomplete gamma function and is found to exhibit three stages of plastic deformation. In stage I the plastic domain consists of two concentric and adjacent zones with different stress fields and different rates of propagation which expand outward from the centre of the cylinder ; in stage II the elastic domain vanishes, while the inner plastic zone continues to propagate ; and in stage III a third plastic zone is formed at the outer radius which propagates inward. Throughout the deformation the states of stress are found to exhibit regular progression. A numerical example is included.

1. INTRODUCTION

THE brief list of existing complete solutions to elastic–plastic problems in the incremental strain theory of plasticity has been enriched in recent years by a number of thermoelastic–plastic investigations, e.g., PARKUS (1954), BLAND (1956) WEINER (1956), WILHOIT (1958) and COWPER (1958). Of the problems solved in the above collection, all but the first and third employ Tresca's yield condition ; and of the plane strain solutions all contain, as do the isothermal solutions obtained to date, the axial stress σ_z as the intermediate principal stress. Furthermore, in all cases the state of stress is statically determinate.

An exception may be found in the recent work of WEINER and HUDDLESTON (1959) who have obtained, for an incompressible nonhardening cylinder in the presence of a temperature gradient, a radially symmetric solution for the stress rates which for certain regimes of the Tresca yield surface is necessarily statically indeterminate.

*The results presented in this paper were obtained in the course of research sponsored by the Office of Ordnance Research, U.S. Army. The investigation was initiated under Contract DA-20-018-ORD-14447 with the University of Michigan, and was completed under Contract DA-04-200-ORD-171 with the University of California at Berkeley.

† University of Michigan, Ann Arbor, Michigan.

‡ University of California, Berkeley, California.

Among the existing radially symmetric solutions associated with the problem of the elastic–plastic cylinder, that of the thick-walled tube has been the subject of numerous investigations. Of particular interest is the work of KOITER (1953) who obtained a simple and satisfactory solution in closed form for a nonhardening compressible elastic–plastic material, using Tresca's yield condition and its associated flow rule. This was extended by BLAND (1956) to include workhardening and a steady state temperature gradient. In both of these investigations (a) σ_z is the intermediate principal stress so that, on account of the symmetry of the problem, the stress field is statically determinate, (b) no singular regime of the Tresca loading function is encountered and (c) the initial yield begins at the inner surface, developing a plastic region with a surrounding elastic annulus.

The problem considered here is that of the quasi-static deformation of an elastic–plastic cylinder, which, with reference to cylindrical polar coordinates (r, θ, z) occupies the region $0 \leqslant r \leqslant a$ and is subjected to a lateral pressure p, an axial force F and a radially distributed heat source Q, all of which increase monotonically with time t. The solution is obtained for an inviscid workhardening material, with Tresca's loading function, its associated flow rule, and a workhardening law based on the plastic work per unit volume expended; the nonhardening elastic–plastic solution is also deduced as a special case for comparison purposes. Depending upon the relative values of the independently varying 'load parameters,' p, Q and F, the initial yield may occur at any radius $0 \leqslant r \leqslant a$, while the axial component of stress σ_z may or may not be the intermediate principal stress. Indeed, in the class of problems considered, the initial yield occurs along the axis of the cylinder $r = 0$, when the state of stress reaches the singular regime $\sigma_\theta - \sigma_z = \sigma_r - \sigma_z = 2k_0$, where σ_r and σ_θ are respectively the radial and tangential components of stress, and k_0 is the yield limit in simple shear. The ensuing state then consists of an elastic annulus $(\rho \leqslant r \leqslant a)$ surrounding a plastic region $(0 \leqslant r \leqslant \rho)$, with the elastic–plastic boundary $r = \rho$. The solution in the plastic domain $(0 \leqslant r \leqslant \rho)$ does not lend itself to description by a single stress field; instead, continuity requirements, imposed on the stresses and displacement, at the elastic–plastic boundary ρ, together with consideration of the elastic loading paths as well as the possible paths that the stress might follow in the plastic range demand that the plastic domain $(0 \leqslant r \leqslant \rho)$ be composed of two concentric zones, separated by an interface $r = \rho_1 < \rho$, each with different stress fields and different rates of propagation. In this manner the state of stress is found to exhibit regular progression (following the terminology of HODGE 1956); i.e., the state of stress upon yielding first lies on a regular face of the yield surface and then moves toward a singular regime where it stays throughout the remainder of the plastic deformation.

An interesting feature of the problem is the continued propagation of the interface boundary ρ_1, after the elastic–plastic boundary ρ has reached the outer surface $r = a$, so that the cylinder may sustain further loading. A second stage of the problem (referred to as Stage II) is thus entered in which the elastic region has vanished entirely. Stage II of the problem is short-lived, however, as the state of stress at $r = a$ reaches the regime B before the boundary ρ_1 has moved appreciably (Fig. 1), and a third and final stage of the problem (Stage III) is entered. In Stage III the state of stress again exhibits regular progression, giving rise to a new zone $\rho_2 \leqslant r \leqslant a$ (in which the state of stress corresponds to regime B), initiating at

$r = a$ with the interface boundary ρ_2 propagating inward ; hence the two interfaces ρ_2 and ρ_1 approach each other. It is found that these boundaries never meet but approach limit values as the temperature tends to infinity. This observation is similar to that made by WILHOIT (1958) for a ring subjected to a temperature gradient, and the work of COWPER (1959) for a hollow sphere subjected to a temperature gradient.

Specifically, the contents of the paper are arranged in two parts. In Part I (Sections 1–4) of the present paper, following some preliminaries, the character of the initial yield for a given class of temperature distributions is discussed in detail. The differential equations for the stress fields corresponding to various regimes of the Tresca yield surface are derived for an arbitrary, radially symmetric, temperature distribution and without the specifications of any particular hardening law. Also included, is the solution for the case of a nonhardening elastic–plastic material.

As an application of the foregoing results in Part II (Sections 5–7), cylindrical nuclear reactor fuel elements in the state of plane strain are considered in detail. The solid cylinder of fissionable material forms the heat generating portion of the fuel element and is surrounded by a hollow cylinder of nonfissionable material called 'cladding.' The uniform pressure between the two cylinders is then a consequence solely of the temperature field generated (precluding a shrink fit for simplicity). Using a Gaussian heat source and a linear hardening law, the general differential equations for stress and the displacement derived in Part I, corresponding to the regimes which arise in the various stages of the problem, are solved and applied in the plastic regime. A numerical example is worked out and complete results presented for a workhardening material as well as a nonhardening material for comparison. A further comparison is made of the solution of the coupled mechanical-thermal problem considered here with that obtained by a simple superposition of solutions to the separate mechanical and thermal problems.

PART I. GENERAL CONSIDERATIONS

2. PRELIMINARY BACKGROUND

With reference to cylindrical polar coordinates (r, θ, z), we recall for future reference that for axisymmetric problems in the state of plane strain the stress differential equations of equilibrium in the absence of body forces become simply

$$\frac{\partial \sigma_r}{\partial r} + \frac{\sigma_r - \sigma_\theta}{r} = 0, \tag{2.1}$$

and the nonvanishing plane components of strain are given by

$$\epsilon_r = \frac{\partial u}{\partial r}, \qquad \epsilon_\theta = \frac{u}{r}, \tag{2.2}$$

where u is the radial displacement. The elastic components of strain ϵ_r', ϵ_θ', ϵ_z' are related to the stresses through the generalized Hooke's law, while the plastic components of strain ($\epsilon_r'' = \epsilon_r - \epsilon_r'$, etc) are expressed for workhardening materials by

$$\{\dot{\epsilon}_r'', \dot{\epsilon}_\theta'', \dot{\epsilon}_z''\} = h \left\{\frac{\partial f}{\partial \sigma_r}, \frac{\partial f}{\partial \sigma_\theta}, \frac{\partial f}{\partial \sigma_z}\right\} \dot{f}, \tag{2.3}$$

where the plastic potential f is regular, dot denotes differentiation with respect to time, and h is a positive function (HILL 1950). When the hardening is zero the quantity $h\dot{f}$ on the right-hand side of (2.3) is to be replaced by $\dot{\lambda}$.

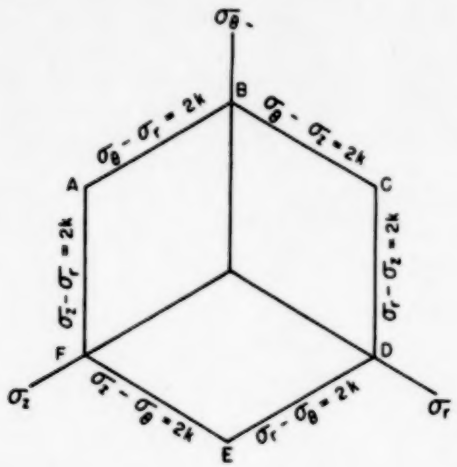

FIG. 1. Tresca's yield hexagon when σ_r, σ_θ, σ_z are the principal stresses.

Throughout this paper the plastic potential is taken as Tresca's yield function

$$f = \max\left[|\sigma_r - \sigma_\theta|, \quad |\sigma_\theta - \sigma_z|, \quad |\sigma_z - \sigma_r|\right] = 2k, \tag{2.4}$$

keeping in mind that the flow rule in the form (2.3) is valid only at regular regimes of (2.4); the function f is shown schematically in Fig. 1 with the various regimes labelled. The material is assumed to harden according to the law

$$2\dot{k} = \eta\, W_p, \tag{2.5}$$

where k is the yield stress in simple shear, η is a constant which depends on the material, and

$$W_p = \sigma_r \dot{\epsilon}_r'' + \sigma_\theta \dot{\epsilon}_\theta'' + \sigma_z \dot{\epsilon}_z'' \tag{2.6}$$

is the rate of plastic work per unit volume.

Although more general constitutive equations for non-isothermal plasticity have been recently proposed by PRAGER (1958), the thermal effect is here accounted for only in the generalized Hooke's law, so that the condition of compressibility is

$$\epsilon_r + \epsilon_\theta + \epsilon_z = \frac{1-2\nu}{E}(\sigma_r + \sigma_\theta + \sigma_z) + 3\alpha T, \tag{2.7}$$

where T is the change in temperature. The mechanical and thermal parameters E, ν and α (modulus of elasticity, Poisson's ratio and the coefficient of linear expansion, respectively), as well as the initial yield limit k_0, are assumed independent of temperature.

Since, for the problem being considered, the deformation is a direct consequence of the change in temperature arising from a distributed heat source within the body, any temperature difference that might occur due to the deformation itself

(as in thermoelastic damping) may be ignored, thus uncoupling the thermal and mechanical problems; furthermore, if the loading (thermal as well as mechanical) occurs quasi-statically, the heat conduction equation is characterized (e.g., THOMPSON and ROGERS 1956, p. 165) by

$$K \nabla^2 T = -Q, \tag{2.8}$$

where K is the thermal conductivity and Q is a radially distributed thermal source expressible in terms of units of heat per unit time per unit volume, and

$$\nabla^2 \equiv \frac{\partial^2}{\partial r^2} + \frac{1}{r}\frac{\partial}{\partial r}.$$

3. THERMOELASTIC SOLUTION AND INITIAL YIELD

While our main concern is with the elastic–plastic cylinder occupying the region $0 \leqq r \leqq a$, for future reference it is necessary to consider the corresponding thermoelastic problem. Specifically, we recall the (quasi-static) thermoelastic solution to the axisymmetric problem of a hollow cylinder ($\rho \leqq r \leqq a$) in the state of plane strain and subjected to a temperature distribution T, superposed on the elastic solution due only to a uniform axial stress $\sigma_z = C_3$ (e.g., TIMOSHENKO and GOODIER 1951, p. 409):

$$\left.\begin{aligned}
u &= \frac{1+\nu}{1-\nu}\frac{\alpha}{r}\int_\rho^r Tr\,dr + C_1 r + \frac{C_2}{r} - \frac{\nu}{E} C_3 r,\\
\sigma_r &= -\frac{\alpha E}{1-\nu}\frac{1}{r^2}\int_\rho^r Tr\,dr + \frac{E}{1+\nu}\left(\frac{C_1}{1-2\nu} - \frac{C_2}{r^2}\right),\\
\sigma_\theta &= \frac{\alpha E}{1-\nu}\frac{1}{r^2}\int_\rho^r Tr\,dr - \frac{\alpha E T}{1-\nu} + \frac{E}{1+\nu}\left(\frac{C_1}{1-2\nu} + \frac{C_2}{r^2}\right),\\
\sigma_z &= -\frac{\alpha E T}{1-\nu} + \frac{2\nu C_1 E}{(1-2\nu)(1+\nu)} + C_3,
\end{aligned}\right\} \tag{3.1}$$

where
$$C_3 = \frac{-2\nu}{1-2\nu}\frac{C_1 E}{1+\nu} + \frac{2}{a^2-\rho^2}\frac{\alpha E}{1-\nu}\int_\rho^a Tr\,dr + \frac{F}{\pi(a^2-\rho^2)}.$$

The thermoelastic solution for the solid cylinder ($0 \leqslant r \leqslant a$) may be deduced from (3.1) by allowing in the integrals the lower limit $\rho \to 0$, and by setting the coefficient $C_2 = 0$, which ensures the regularity of the solution at $r = 0$. When this solution is subjected to the boundary conditions appropriate to the solid cylinder subjected to a radial temperature distribution T, a lateral pressure p, and an axial force F (which includes the effects of both C_3 as well as that arising from the plane strain solution) the stresses are found to be

$$\left.\begin{aligned}
\sigma_r &= \frac{\alpha E}{1-\nu}\left[\theta(a) - \theta(r)\right] - p,\\
\sigma_\theta &= \frac{\alpha E}{1-\nu}\left[\theta(a) + \theta(r) - T\right] - p,\\
\sigma_z &= \frac{\alpha E}{1-\nu}\left[-T + 2\theta(a)\right] + \frac{F}{\pi a^2},
\end{aligned}\right\} \tag{3.2}$$

where
$$\theta(r) = \frac{1}{r^2}\int_0^r T(r)\,r dr.$$

According to Tresca's yield condition yielding occurs when one of the quantities

$$\left.\begin{aligned} |\sigma_r - \sigma_\theta| &= \left|\frac{\alpha E}{1-\nu}\left[T - \theta(r)\right]\right|, \\ |\sigma_r - \sigma_z| &= \left|\frac{\alpha E}{1-\nu}\left[T - \theta(r) - \theta(a)\right] - \frac{F}{\pi a^2} - p\right|, \\ |\sigma_\theta - \sigma_z| &= \left|\frac{\alpha E}{1-\nu}\left[\theta(r) - \theta(a)\right] - \frac{F}{\pi a^2} - p\right|, \end{aligned}\right\} \tag{3.3}$$

reaches the value $2k_0$. Since the determination of the maximum of (3.3) depends on the load parameters and especially on the distribution of T (which is so far arbitrary), we restrict ourselves to the class of monotone temperature distributions which assumes its maximum either at $r = 0$ or at $r = a$. With the notation

$$R = -\frac{F}{\pi a^2} - p, \qquad m = \frac{v_1}{v_2} - 1, \tag{3.4a}$$

$$\left.\begin{aligned} v_1 &= \frac{T(0) - T(a)}{Q_0} = \frac{2\theta(0) - T(a)}{Q_0}, \\ v_2 &= \frac{2\theta(a) - T(a)}{Q_0}, \end{aligned}\right\} \tag{3.4}$$

the expressions (3.3), when evaluated at $r = 0$ and $r = a$, read

$$\left.\begin{aligned} |\sigma_r - \sigma_\theta|_{r=0} &= 0, & |\sigma_r - \sigma_\theta|_{r=a} &= \left|-\frac{\alpha E}{1-\nu} v_2 Q_0\right|, \\ |\sigma_r - \sigma_z|_{r=0} &= \left|\frac{\alpha E}{1-\nu}\frac{Q_0 m v_2}{2} - R\right|, & |\sigma_r - \sigma_z|_{r=a} &= \left|-\frac{\alpha E}{1-\nu} v_2 Q_0 - R\right|, \\ |\sigma_\theta - \sigma_z|_{r=0} &= \left|\frac{\alpha E}{1-\nu}\frac{Q_0 m v_2}{2} - R\right|, & |\sigma_\theta - \sigma_z|_{r=a} &= |-R|, \end{aligned}\right\} \tag{3.5}$$

where the arbitrary constant Q_0 will be associated subsequently with a physical quantity related to the temperature field. A detailed comparison of the relative values of the five independent expressions appearing in (3.5) for the entire range of the load parameters, though straightforward, is lengthy and tedious. For our present purposes, however, we note that if the values of m, Q_0 and F are restricted to the range $1 \leqq m \leqq 2$, $Q_0 > 0$, then one is led to the result that the initiation of yield may occur in the three ways, summarized in Table 1. It may be noted here that the choice of the range of m in Table 1 was motivated by the temperature distribution employed in Section 5 for which $m \simeq 1{\cdot}12$.

TABLE 1. $(1 \leqq m \leqq 2)$

Range of the parameter R	*Yield condition*	*Location of initial yield*
$R \leqq \frac{\alpha E}{1-\nu} v_2 Q_0 \cdot \frac{m-2}{2}$	$\sigma_r - \sigma_z = 2k$ $\sigma_\theta - \sigma_z = 2k$	$r = 0$
$\frac{\alpha E}{1-\nu} v_2 \cdot \frac{Q_0}{2}(m-2) \leqq R \leqq 0$	$\sigma_r - \sigma_\theta = -2k$	$r = a$
$R \leqq 0$	$\sigma_r - \sigma_z = -2k$	$r = a$

4. Solutions in the Plastic Domain

The determination of the state of stress in the plastic domain generally, requires the solution of the system of nonlinear differential equations (2.1) to (2.7); however, it may be shown that for a *linear* workhardening material these equations can be directly integrated. To this end we observe that if f is a regular homogeneous function of degree n, then by (2.6), (2.3), and with an appeal to Euler's theorem on homogeneous functions, $W_p = h\dot{f}nf$. When f is the loading function associated with the regular regimes of (2.4), then $n = 1$, $f = 2k$, and

$$W_p = 2h\dot{f}k. \tag{4.1}$$

Substitution of (4.1) into (2.5) leads to $\dot{k}/k = \eta(h\dot{f})$, which upon integration becomes

$$\log(k/k_0) = \eta\lambda; \qquad \lambda = \int h\dot{f}\,dt, \tag{4.2}$$

indicating the nonlinear variation of k with λ. Expanding the left-hand side of (4.2) about $k/k_0 = 1$ and retaining only the linear term, results in

$$k = k_0(1 + \eta\lambda), \tag{4.3}$$

as the law for linear hardening which, since the flow rule (2.3) was employed, is valid only for regular regimes of the Tresca yield function. The corresponding result for the singular regimes of (2.4) requires different considerations, e.g., for the regime B in Fig. 1, $\sigma_r = \sigma_z$, $\sigma_\theta = \sigma_r + 2k$, (2.6) because of the vanishing of plastic volume change becomes

$$W_p = 2k\,\dot{\epsilon}_\theta''. \tag{4.4}$$

Repeating the steps between (4.2) and (4.3) we obtain

$$k = k_0(1 + \eta\,\epsilon_\theta''), \tag{4.5}$$

which is identical in form to (4.3), except that λ is replaced by ϵ_θ''. Expressions similar to (4.5) may be deduced in a similar manner for other singular regimes of (2.4).

The stress field is, in general, statically indeterminate, requiring the simultaneous solution of the seven equations (2.1) to (2.4), (2.7), (2.8) and one of the type (4.3) or (4.5). As this system is linear, it admits twelve solutions, corresponding to the six regular and six singular regimes of the piecewise linear loading function (2.4). These solutions for the radially symmetric stress and displacement fields are general and are valid either in full or in part for all radially symmetric temperature distributions, including the more specialized examples, where the initial yield occurs at $r = a$ or $r = 0$, discussed in Section 3.

We now proceed to consider the individual regular regimes of Tresca's loading functions as follows:

(a) *Regime AB* (σ_z, the intermediate principal stress). The solution here is included in the work of Bland (1956) and will not be repeated. It should be recalled that the workhardening parameter employed by Bland, namely the equivalent plastic strain (see Hill 1950, p. 30), differs from that used here (2.6); however, as shown subsequently by Bland (1957), the two parameters are equivalent

as long as the regime in question is regular and associated with either a linear or a quadratic loading function.

(b) *Regime BC* (σ_r, the intermediate principal stress). The presence of the axial component of stress σ_z in the loading function, corresponding to this regime, renders the stress distribution statically indeterminate, even in the nonhardening case. Substituting σ_z from the loading function, i.e., $\sigma_\theta - \sigma_z = 2k$, and σ_θ from (2.1) into the compressibility condition (2.7), gives

$$\frac{\partial u}{\partial r} + \frac{u}{r} + \epsilon_z(r, t) = \frac{1-2\nu}{E}\left(3\sigma_r + 2r\frac{\partial \sigma_r}{\partial r}\right) - \frac{2(1-2\nu)}{E}k + 3\alpha T, \quad (4.6a)$$

from which

$$u = \frac{1-2\nu}{E}\frac{1}{r}\left[2r^2\sigma_r - \int^r r\sigma_r\, dr\right] + \frac{3\alpha}{r}\int^r Tr\, dr - \frac{2(1-2\nu)}{E}\frac{1}{r}\int^r kr\, dr - \frac{1}{r}\int^r \epsilon_z r dr + \frac{B_1}{r}. \quad (4.6b)$$

Throughout this section σ_θ has been assumed greater than σ_z; when $\sigma_z > \sigma_\theta$ the sign of k need only be taken negative.

The flow law (2.3) gives upon integration with respect to time

$$\epsilon_r'' : \epsilon_\theta'' : \epsilon_z'' = 0 : 1 : -1,$$

so that

$$\epsilon_\theta = \epsilon_\theta' + \epsilon_\theta'' = \epsilon_\theta' - \epsilon_z'' = \epsilon_\theta' - \epsilon_z + \epsilon_z'.$$

By the generalized Hooke's law together with (2.1) and the loading function, the total tangential strain given above may be expressed as

$$\epsilon_\theta = \frac{u}{r} = -\epsilon_z + \frac{2(1-\nu)}{E}\cdot\left(\sigma_r + r\frac{\partial \sigma_r}{\partial r} - k\right) - \frac{2\nu}{E}\sigma_r + 2\alpha T. \quad (4.7)$$

Elimination of u between (4.6) and (4.7) after some manipulation results in the following differential equation for σ_r:

$$2(1-\nu)r^2\frac{\partial^2 \sigma_r}{\partial r^2} + 6(1-\nu)r\frac{\partial \sigma_r}{\partial r} + (1-2\nu)\sigma_r = -\alpha ET - 2\alpha Er\frac{\partial T}{\partial r} + 2k + 2(1-\nu)r\frac{\partial k}{\partial r} + E\epsilon_z + rE\frac{\partial \epsilon_z}{\partial r}. \quad (4.8)$$

It may be of interest to note that (4.8) may also be obtained from the appropriate differential equation of strain compatibility.

Since the yield stress k in general depends on parameters which may in turn be functions of the dependent variable σ_r, (4.8) cannot be solved until k is specified. The nature of the loading, however, is such that the axial strain is independent of σ_r, so that the solution of (4.8) is immediately attainable for a nonhardening material. The homogeneous solution of (4.8) for a nonhardening material is of the form

$$(\sigma_r)_h = \frac{A_1}{r^{s_1}} + \frac{A_2}{r^{s_2}}, \qquad \text{where} \quad \left.\begin{matrix} s_1 \\ s_2 \end{matrix}\right\} = 1 \mp \frac{1}{\sqrt{[2(1-\nu)]}}, \quad (4.9)$$

and the particular solution may be found by variation of parameters to be

$$\frac{(\sigma_r)_p}{k} = \frac{2}{1-2\nu} + \frac{\Phi}{2(1-\nu)(s_2-s_1)}\left\{\frac{1+2s_2}{r^{s_2}}\int\frac{T}{T_a}r^{s_2-1}\,dr - \frac{1+2s_1}{r^{s_1}}\int\frac{T}{T_a}r^{s_1-1}\,dr\right\} + \frac{E}{2(1-\nu)(s_2-s_1)}\left\{\frac{1}{r^{s_1}}\int\frac{\partial(r\epsilon_z)}{\partial r}r^{s_1-1}\,dr - \frac{1}{r^{s_2}}\int\frac{\partial(r\epsilon_z)}{\partial r}r^{s_2-1}\,dr\right\}, \tag{4.10}$$

where

$$\Phi = \frac{\alpha E T_a}{k_0}.$$

With σ_r known the tangential and the axial stress may be found through the equilibrium equation and the yield condition, respectively. The second expression in braces (4.10) leads to a term appearing in the expression for σ_z which may be identified with C_3, and results in

$$\epsilon_z = 2(1-\nu)\frac{k_0}{E}s_1 s_2 C_3 + \frac{C_4}{r}, \tag{4.11}$$

where C_4 is a function of time only. Thus, the stress distribution for a nonhardening material is given by

$$\left.\begin{aligned}
\frac{\sigma_r}{k_0} &= \frac{A_1}{r^{s_1}} + \frac{A_2}{r^{s_2}} + C_3 + \frac{2}{1-2\nu} - \frac{\Phi}{2(1-\nu)(s_1-s_2)}\left[\frac{1+2s_2}{r^{s_2}}\int\frac{T}{T_a}r^{s_2-1}\,dr - \frac{1+2s_1}{r^{s_1}}\int\frac{T}{T_a}r^{s_1-1}\,dr\right],\\
\frac{\sigma_\theta}{k_0} &= (1-s_1)\frac{A_1}{r^{s_1}} + (1-s_2)\frac{A_2}{r^{s_2}} + C_3 + \frac{2}{1-2\nu} - \frac{\Phi}{2(1-\nu)(s_1-s_2)}\left[\frac{(1-s_2)(1+2s_2)}{r^{s_2}}\int\frac{T}{T_a}r^{s_2-1}\,dr\right.\\
&\quad\left. - \frac{(1-s_1)(1+2s_1)}{r^{s_1}}\int\frac{T}{T_a}r^{s_1-1}\,dr + 2(s_2-s_1)\frac{T}{T_a}\right],\\
\frac{\sigma_z}{k_0} &= \frac{\sigma_\theta}{k_0} - 2.
\end{aligned}\right\} \tag{4.12}$$

Since the foregoing solution is not valid when $\nu = \frac{1}{2}$, the integrations leading to (4.12) requires separate consideration. Here the solution for an incompressible material may be obtained directly from (4.8); the result is similar to (4.12), the chief difference being that the leading terms are logarithmic in r, and that with reference to ϵ_z, corresponding for (4.11), a uniform axial stress gives rise to a uniform axial strain. These results, for an uncompressible material, when differentiated with respect to time, agree with the previously known solution (Weiner 1959) for the stress-rate and the displacement-rate of an incompressible material. In contrast to the solution for an incompressible material, it may be seen from (4.11) that for a compressible material a uniform axial stress may result in a non-uniform axial strain.

(c) *Regime CD* (σ_θ, the intermediate principal stress). As in (b) the stress distribution is again statically indeterminate, and the procedure leading to (4.6) and (4.8) gives

$$\left.\begin{aligned} u = \frac{1-2\nu}{E}\int^r\left(3r\sigma_r + r^2\frac{\partial\sigma_r}{\partial r}\right)dr - \frac{2(1-2\nu)}{Er}\int^r krdr \\ + \frac{3\alpha}{r}\int^r Trdr - \frac{E}{r}\int^r r\epsilon_z\,dr + \frac{B_2}{r}, \end{aligned}\right\} \tag{4.13}$$

$$\left.\begin{aligned} r^2\frac{\partial^2\sigma_r}{\partial r^2} + 3r\frac{\partial\sigma_r}{\partial r} - (1-2\nu)\sigma_r = -2k - 2\nu r\frac{\partial k}{\partial r} \\ - E\epsilon_z + \alpha ET - \alpha E\frac{\partial T}{\partial r}r, \end{aligned}\right\} \tag{4.14}$$

whose solution for a nonhardening material is

$$\left.\begin{aligned} \frac{\sigma_r}{k_0} &= \frac{A_3}{r^{s_3}} + \frac{A_4}{r^{s_4}} + C_3 - \frac{2}{1-2\nu} \\ &\quad + \frac{\Phi}{s_3 - s_4}\left[\frac{1+s_4}{r^{s_4}}\int\frac{T}{T_a}r^{s_4-1}\,dr - \frac{1+s_3}{r^{s_3}}\int\frac{T}{T_a}r^{s_3-1}\,dr\right], \\ \frac{\sigma_\theta}{k_0} &= (1-s_3)\frac{A_3}{r^{s_3}} + (1-s_4)\frac{A_4}{r^{s_4}} + C_3 - \frac{2}{1-2\nu} \\ &\quad + \frac{\Phi}{s_3 - s_4}\left[\frac{1-s_3^2}{r^{s_3}}\int\frac{T}{T_a}r^{s_3-1}\,dr - \frac{1-s_4^2}{r^{s_4}}\int\frac{T}{T_a}r^{s_4-1}\,dr + (s_4 - s_3)\frac{T}{T_a}\right], \\ \frac{\sigma_z}{k_0} &= \frac{\sigma_r}{k_0} - 2. \end{aligned}\right\} \tag{4.15}$$

The states of stress for the singular regimes *A*, *B*, *C*, *D*, *E* and *F* of Fig. 1 are also, in general, statically indeterminate for a workhardening material; for a nonhardening material, however, this is not the case, and the solutions may be obtained directly from the equilibrium equation and the yield condition:

$$\text{regime } A: \begin{cases} \sigma_r = 2k_0\log r + D_1 \\ \sigma_\theta = \sigma_z = \sigma_r - 2k_0 \end{cases} \tag{4.16}$$

$$\text{regime } B: \begin{cases} \sigma_r = \sigma_z = 2k_0\log r + D_2 \\ \sigma_\theta = \sigma_z - 2k_0 \end{cases} \tag{4.17}$$

$$\text{regime } C: \begin{cases} \sigma_r = \sigma_\theta = D_3 \\ \sigma_r = D_3 - 2k_0 \end{cases} \tag{4.18}$$

where D_1, D_2, D_3 are functions of time only. The states of stress at regimes *D*, *E* and *F* are obtained by replacing k_0 by $-k_0$ in (4.16), (4.17) and (4.18), respectively. The radial displacement associated with the above solutions, again obtained from (2.7), reads

$$u = \frac{\zeta_1 r}{2} + \zeta_2 k_0\frac{r}{2} + \frac{6\zeta_3 k_0}{r}(r\log r - r) + \frac{3\alpha}{r}\int^r Trdr + \frac{B_3}{r}, \tag{4.19}$$

where B_3 is an arbitrary function of time and the coefficients ζ_1, ζ_2 and ζ_3 for each of the singular regimes may be found from

$$\frac{1-2\nu}{E}(\sigma_r+\sigma_\theta+\sigma_z)=\zeta_1+\zeta_2 k_0+6\zeta_3 k_0 \log r \tag{4.20}$$

together with (4.16), (4.17) and (4.18).

PART II. APPLICATION TO CYLINDRICAL NUCLEAR REACTOR FUEL ELEMENTS

5. Temperature Distribution and the Character of Initial Yield

The fuel portion of a cylindrical reactor fuel element can be treated as a solid cylinder in the state of plane strain subjected to a thermal gradient and an external pressure; the former is due to heat generated by the nuclear fission of the element itself which thus behaves as a distributed heat source, while the latter is due to the expansion of the solid fissionable core against the nonfissionable hollow cylindrical cladding, which serves to conduct heat away. The pressure p at the interface ($r=a$) of the two cylinders is, therefore, not independent but rather a consequence of the temperature field. It is assumed for clarity that when Q is zero the stress field vanishes, i.e., there is no shrink-fit, although this may be easily included. A complete analysis of the reactor problem entails an elastic–plastic treatment of both cylinders, but here emphasis is placed on the elastic–plastic solid core and the parameters of the problem are selected with this goal in mind; the hollow cladding is mentioned only to the extent that it affects the solution of the solid core.

The heat source will be taken as Gaussian in character, i.e.,

$$Q=Q_0 \exp(-\mu r^2) \tag{5.1}$$

where μ^2 is a parameter. When $\mu^2=0$, Q reduces to Q_0, a distributed source of uniform strength. With (5.1) the solution of (2.8), subject to the boundary condition $T=Ta$ at $r=a$ and the regularity requirement at $r=0$, may be written as

$$T=T_a+\frac{Q_0}{4K_1\mu^2}\left[Ei(-\mu^2 r^2)-Ei(-\mu^2 a^2)-2\log\frac{r}{a}\right], \tag{5.2}$$

where

$$Ei(-x)=-\int_x^\infty \frac{e^{-y}}{y}\,dy. \tag{5.3}$$

is the exponential integral.

Since there is no heat source in the cladding ($a\leqq r\leqq b$), the temperature distribution is given by the homogeneous solution of (2.8), i.e.,

$$T=\frac{T_b-T_a}{(\log b/a)}\log\frac{r}{a}+T_a, \tag{5.4}$$

where the boundary conditions T_a and T_b have been utilized.

Before determining the location of the initial yield, as well as p^*, T^* and Q_0^* (i.e., the values, respectively, of p, T and Q_0 at the initiation of yield), it is necessary

to establish the functional relation between the parameters Q_0, T_a, F and p. One such relation is obtained by equating the radial displacements of the two cylinders at their interface $r = a$. Since prior to yielding both cylinders are entirely elastic, the displacements in each may be written from the first two of (3.1) as

$$u^{(i)} = -\frac{1+\nu_i}{Ei} r\sigma_r^{(i)} + 2C_1^{(i)} r \frac{1-\nu_i}{1-2\nu_i}, \tag{5.5}$$

where the index $i = 1, 2$, refers to the quantities appropriate to the solid core and the hollow cladding, respectively. If the pressure at the inner face is $-p$, then by (5.5)

$$p\left[\frac{1+\nu_1}{E_1} - \frac{1+\nu_2}{E_2}\right] = \frac{2(1-\nu_2)}{1-2\nu_2} C_1^{(2)} - \frac{2(1-\nu_1)}{1-2\nu_1} C_1^{(1)}, \tag{5.6}$$

and the coefficients $C_1^{(i)}$ are found from the second of (3.1) and the boundary conditions $\sigma_r(a) = -p$, $\sigma_r(b) = 0$:

$$C_1^{(1)} = \frac{(1-2\nu_1)(1+\nu_1)}{E_1}\left[-p + \frac{\alpha_1 E_1}{1-\nu_1}\theta(a)\right] \tag{5.7a}$$

$$C_1^{(2)} = \frac{(1-2\nu_2)(1+\nu_2)}{E_2}\left[-p\left(1 - \frac{1}{1-a^2/b^2}\right) + \frac{\alpha_2 E_2 T_a}{1-\nu_2}\left(\frac{\theta(b)}{T_a}\right)\frac{1}{1-a^2/b^2}\right] \tag{5.7b}$$

where by (5.2) and (5.4)

$$\theta(a) = \frac{1}{a^2}\int_0^a Trdr = \frac{T_a}{2} + \frac{Q_0}{8K_1\mu^2}\left(1 + \frac{\exp(-\mu^2 a^2) - 1}{\mu^2 a^2}\right), \tag{5.8a}$$

and similarly,

$$\theta(b) = \frac{1}{b^2}\int_a^b Trdr = \frac{T_a}{2}\left\{\frac{T_b}{T_a} + \left(\frac{T_b}{T_a} - 1\right)\left[\frac{a^2/b^2 - 1 + 2\log b/a}{2\log b/a}\right]\right\}. \tag{5.8b}$$

The relation between Q_0 and the interface temperature T_a, following the procedure employed by GLASSTONE (1955) for the case $\mu^2 = 0$, is obtained by equating the flux per unit length, produced in the core at $r = a$,

$$q(a) = -\frac{\pi Q_0}{\mu^2}\left[\exp(-\mu^2 a^2) - 1\right], \tag{5.9}$$

to that across any surface of the source-free cladding

$$q = \frac{(T_a - T_b)}{\log b/a} 2\pi K_2. \tag{5.10}$$

Hence

$$T_a = hQ_0, \tag{5.11a}$$

where

$$h = \frac{\log(b/a)}{(T_b/T_a - 1)\,2\mu^2 K_2} \cdot \left[\exp(-\mu^2 a^2) - 1\right], \tag{5.11b}$$

which reduces to GLASSTONE's results when $\mu^2 = 0$.

Substituting for $C_1^{(1)}$ and $C_1^{(2)}$ from (5.7), equation (5.6) becomes

$$p\left[\frac{1+\nu_1}{E_1}-\frac{1+\nu_2}{E_2}-\frac{2(1-\nu_2^2)}{E_2(b^2/a^2-1)}-\frac{2(1-\nu_1^2)}{E_1}\right]$$
$$=Q_0\left[2(1+\nu_2)\alpha_2 h\left(\frac{\theta(b)}{T_a}\right)\cdot\frac{1}{1-a^2/b^2}-\alpha_1(1+\nu_1)(h+\nu_2)\right], \quad (5.12)$$

where h and ν_2 are defined by (5.11b) and (3.4b), respectively.

We are now in a position to establish the character of initial yield. Since in the state of plane strain the superposed axial stress $C_3 = 0$, we observe by the last of (3.1) that when $\rho = 0$,

$$\frac{F}{\pi a^2} = -2\alpha_1 E_1 \theta(a) - 2\nu_1 p. \quad (5.13)$$

It then follows from Table 1 and the first of (3.4a) that initial yielding occurs at $r = 0$ if

$$-\alpha_1 E_1 T_a - \alpha_1 E_1 \nu_2 Q_0 + p(1-2\nu_1) < \frac{\alpha_1 E_1}{1-\nu_1}\nu_2 Q_0 \frac{m-2}{2}, \quad (5.14)$$

in which case (as may be seen from Table 1) the yield condition is characterized by

$$|\sigma_\theta - \sigma_z| = |\sigma_r - \sigma_z| = 2k_0. \quad (5.15)$$

Before proceeding further it is necessary to specify the ratios of the coefficients (both mechanical and thermal) in the core to those in the cladding, i.e.,

$$\frac{E_1}{E_2}=2, \qquad \frac{\alpha_1}{\alpha_2}=2, \qquad \frac{k_2}{k_1}=8, \qquad \frac{\nu_1}{\nu_2}=1, \qquad =0{\cdot}22, \quad (5.16a)$$

as well as

$$\frac{T_a}{T_b}=\frac{3}{2}, \qquad \frac{b}{a}=\frac{3}{2}. \quad (5.16b)$$

It may be noted here that the selection of the ratios (5.16a) is based on the assumption of a uranium core surrounded by an aluminium cladding.

If, with the aid of (5.12) and (5.11), p and T_a are eliminated from (5.14), then it may be easily shown that the ratios (5.16) render the inequality (5.14) valid. Hence if yielding occurs in the core before the cladding – which, subject to a later verification, is the case for the selected ratios (5.16) – then it must occur at $r = 0$ according to (5.15).

Substituting F from (5.13) into the second of (3.5) and equating the results to $2k_0$ in accord with (5.15) results in the following relation between Q_0^* and p^*,

$$\frac{\alpha_1 E_1}{2(1-\nu_1)}Q_0^*\left[2h(1-\nu_1)+\nu_1+\nu_2(1-2\nu_1)\right]-p^*(1-2\nu_1)=2k_0, \quad (5.17)$$

which may be solved together with (5.12) to obtain independent expressions for p^* and Q_0^*.

To confirm the statement that the solid core yields before the hollow cladding we need only compare p^* with the corresponding value of p obtained under the assumption that initial yield first occurs in the cladding instead. This value $\bar{p}^*$ is found by incorporating (5.12) into the results of Bland (1956), where it is sub-

sequently found that $p^* < \bar{p}^*$ for the parameters selected, so that yielding occurs first in the core. It is important to observe that having established the character of initial yield, the value of $\bar{p}^*$ ceases to be valid even for subsequent yielding of the cladding, since it was obtained through the use of the relation (5.12) which holds only when both elements are completely elastic. An exact value of $\bar{p}^*$ may be obtained using a relation similar to (5.12) but reflecting the true state of plastic deformation in the core.

6. Elastic–Plastic Solution for Linear Workhardening Material

Having determined the character of the initial yield, we now proceed to establish the mode of the plastic deformation in the solid core. Because of the symmetry the elastic–plastic boundary is a cylinder of radius ρ, defining the plastic ($0 \leqq r \leqq \rho$) and the elastic ($\rho \leqq r \leqq a$) domains. The solution in the elastic domain offers no difficulty and may be obtained from (3.1) by setting $C_3 = 0$. For the plastic domain all the possible fields of stress discussed in Section 4 are at our disposal. Attempts to characterize the state of stress in the plastic domain by a single regime (although satisfying all of the field equations) disclose that such solutions do not conform to all of the continuity requirements concerning the stresses and displacements at the elastic-plastic boundary and hence must be rejected. These continuity requirements, together with the consideration of (a) the loading paths during the purely elastic stage of deformation (Fig. 2) for any $r < 0$,

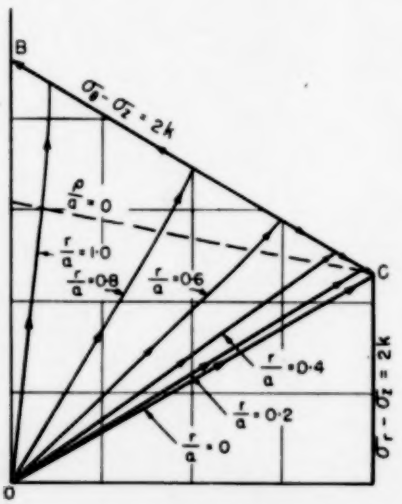

FIG. 2. A portion of Tresca's yield surface showing the stress profiles for a nonhardening material ($\gamma = 0$). The dashed curve corresponds to the state of stress at the initiation of yield.

(b) the fact that the initial yield occurs on an edge of the Tresca yield surface (the singular regime C), and (ç) the possible paths the state of stress may take following the initial yield, lead to the possibility of regarding the plastic domain ($0 \leqq r \leqq \rho$), as consisting of two concentric zones, separated by an interface

$r = \rho_1$, and with the state of stress in each zone characterized by a different regime of Tresca's loading function. For reasons that will become apparent later, the solution in the range of contained plastic deformation of the cylinder will be subsequently referred to as the solution for Stage I of deformation.

Stage I

The central zone *I* ($0 \leqq r \leqq \rho_1$) consists of stress states lying along an edge (regime *C* in Fig. 1) and are given by equations (4.18). The state of stress in the plastic annulus, zone II ($\rho_1 \leqq r \leqq \rho$), surrounding zone I, lies on the face

$$\sigma_\theta - \sigma_z = 2k \tag{6.1}$$

of the Tresca surface and thus satisfies equation (4.8) whose solution for a nonhardening elastic–plastic material is given by (4.12). However, before the stress field in zone II may be found for a workhardening material, the yield stress k appearing in (4.8) must be determined through the workhardening law (4.3), which by the flow rule (2.3) and for the state of plane strain ($\epsilon_z = 0$) becomes

$$k = k_0 (1 + \eta\, \epsilon_z'). \tag{6.2}$$

With the use of the generalized Hooke's law, (2.1) and (6.1), the elastic component of the axial strain may be written as

$$\epsilon_z' = \frac{1}{E_1}\left\{(1 - \nu_1)\, r \frac{\partial \sigma_r}{\partial r} + (1 - 2\nu_1)\, \sigma_r - 2k + \alpha_1 E_1 T\right\}, \tag{6.3}$$

so that by (6.2) k assumes the form

$$\frac{k}{k_0} = \frac{1}{1 + \gamma} + \frac{\kappa}{2}\left[(1 - \nu_1)\, r \frac{\partial}{\partial r}\left(\frac{\sigma_r}{k_0}\right) + (1 - 2\nu_1)\frac{\sigma_r}{k_0} + \Phi_1 \frac{T}{T_a}\right], \tag{6.4}$$

where

$$\gamma = \frac{2\eta k_0}{E_1}, \qquad \kappa = \frac{\gamma}{1 + \gamma}, \tag{6.5a}$$

and

$$\Phi_1 = \frac{\alpha_1 E_1 T_a}{k_0}. \tag{6.5b}$$

When (6.4) is substituted into (4.8), there results the following differential equation in σ_r:

$$b_1 r^2 \frac{\partial^2}{\partial r^2}\left(\frac{\sigma_r}{k_0}\right) + 3b_1 r \frac{\partial}{\partial r}\left(\frac{\sigma_r}{k_0}\right) + b_2 \frac{\sigma_r}{k_0} = \frac{2}{1 + \gamma} - \Phi_1 \frac{T}{T_a}\frac{1}{1 + \gamma}\Bigg] + \Phi_1 r \frac{\partial}{\partial r}\left(\frac{T}{T_a}\right)[(1 - \nu_1)\kappa - 2], \tag{6.6}$$

where

$$b_1 = 2(1 - \nu_1) - (1 - \nu_1)^2 \kappa,$$

$$b_2 = (1 - 2\nu_1)(1 - \kappa).$$

The homogeneous solution of (6.6) has the same form as (4.8) with s_1 and s_2 in (4.9) replaced by

$$\left.\begin{matrix} s_5 \\ s_6 \end{matrix}\right\} = 1 \mp \sqrt{\left(\frac{b_1 - b_2}{b_1}\right)}, \tag{6.7}$$

respectively; these reduce to s_1 and s_2 when $\eta = 0$.

The particular solution of (6.6) for any temperature distribution, as in Section 4, may be obtained by variation of parameters. However, since the character of the initial yield was established only for the class of temperature distributions for which $1 \leqslant m \leqslant 2$ (Table 1), in the

complete solution of (6.6) recorded below the specific temperature distribution (5.2) corresponding $m \simeq 1{\cdot}12$ has been used:

$$\frac{\sigma_r}{k_0} = \frac{A_5}{r^{s_5}} + \frac{A_6}{r^{s_6}} + \frac{2-\Phi_1}{1-2\nu_1}$$

$$- \frac{\Phi_1}{2K_1\mu^2 h}\left\{\frac{s_5+s_6}{s_5 s_6}(1+\gamma)\left[(1-\nu_1)\kappa - 2\right]\right.$$

$$+ Ei(-\mu^2 r^2) - Ei(-\mu^2 a^2) - 2\log\frac{r}{a}$$

$$- \frac{1}{2(1-2\nu)(s_5-s_6)}\left[\frac{s_5\left[1-2s_6+(1-\nu_1)s_6\kappa\right]}{\mu^{s_6} r^{s_6}}\Gamma_x(s_5/2)\right.$$

$$\left.\left. - \frac{s_6\left[1-2s_5+(1-\nu_1)s_5\kappa\right]}{\mu^{s_5} r^{s_5}}\Gamma_x(s_5/2)\right]\right\},$$

$$\frac{\sigma_\theta}{k_0} = (1-s_5)\frac{A_5}{r^{s_5}} + (1-s_6)\frac{A_6}{r^{s_6}} + \frac{2-\Phi_1}{1-2\nu_1} \tag{6.8}$$

$$- \frac{\Phi_1}{2K_1\mu^2 h}\left\{\frac{s_5+s_6}{s_5 s_6} - (1+(1+\gamma)\left[(1-\nu_1)\kappa - 2\right])\right.$$

$$+ Ei(-\mu^2 r^2) - Ei(-\mu^2 a^2) - 2\log\frac{r}{a}$$

$$- \frac{1}{2(1-2\nu_1)(s_5-s_6)}\left[\frac{s_5(1-s_6)\left[1-2s_6+(1-\nu_1)s_6\kappa\right]}{\mu^{s_6} r^{s_6}}\Gamma_x(s_6/2)\right.$$

$$\left.\left. - \frac{s_6(1-s_5)\left[1-2s_5+(1-\nu_1)s_5\kappa\right]}{\mu^{s_5} r^{s_5}}\Gamma_x(s_5/2)\right]\right\},$$

$$\frac{\sigma_z}{k_0} = \frac{\sigma_\theta}{k_0} - \frac{2k}{k_0},$$

where

$$\Gamma_x(n) = \int_0^{x=\mu^2 r^2} e^{-y}\, y^{n-1}\, dy$$

is the incomplete gamma function. It follows from (6.1) and (2.3) that for loading from an elastic state $\dot{\epsilon}_r'' = 0$, and hence the radial strain is purely elastic. Thus, the radial displacement corresponding to the solution (6.8) is most easily evaluated through (2.7) with $\epsilon_z = 0$, the generalized Hooke's law, and (6.1) by

$$\frac{E_1 u}{r} = -2\nu_1\sigma_r + 2(1-\nu_1)\sigma_\theta - 2(1-\nu_1)k + 2\alpha_1 E_1 T, \tag{6.9}$$

which with (6.8) completes the solution for zone II ($\rho_1 \leqq r \leqq \rho$).

Summarizing, the temperature field is given throughout the region $0 \leqq r \leqq a$ by (5.2), the stress and displacement fields are given:

(a) in plastic zone I ($0 \leqq r \leqq \rho_1$) by (4.18) and (4.19), respectively, and represented in stress space by the singular regime C in Fig. 1; (b) in plastic zone II ($\rho_1 \leqq r \leqq \rho$) by (6.8) and (6.9) respectively, and represented in stress space by the regime BC; and (c) in the elastic zone ($\rho \leqq r \leqq a$) by (3.1) with $C_3 = 0$.

With the form of the stress and displacement fields established in all three zones of the problem, it remains to determine the five coefficients D_3, A_2, A_1, C_1, C_2, as well as the relation between the boundaries ρ, ρ_1, and the load parameters p and Φ_1. Equilibrium together with continuity

of the yield condition and displacements requires that the stresses themselves be continuous not only at the elastic–plastic boundary ρ but at the interface ρ_1 between the two plastic zones. Furthermore, an examination of the compressibility equation reveals that continuity of u at $r = \rho_1$ is equivalent to the requirement that $\epsilon_r''(\rho_1) = 0$; this latter condition considerably simplifies the determination of the five coefficients mentioned above. In order to determine the foregoing unknowns, we require (a) continuity only of σ_r, σ_θ, and ϵ_r'' at $r = \rho_1$, since σ_z and u will automatically be continuous through the yield condition, and the compressibility equation, respectively; (b) continuity of σ_r, σ_θ, and σ_z at $r = \rho$, since u is continuous again through the compressibility equation and the vanishing of ϵ_r'' in zone II; (c) satisfaction of the boundary condition $\sigma_r(a) = -p$; and (d) the matching of the displacements of the solid cylinder with that of the hollow cladding, as was done previously in Section 5 for the purely elastic solution of the problem. For a given value of ρ this stage of the problem is thus statically indeterminate, requiring the solution of eight equations in eight unknowns.

In the central zone I the stresses through equilibrium and the loading function are found to have the same form as (4.18) except that k_0 is replaced by k; the radial displacement is found through the compressibility equation (2.7) to be

$$u = \frac{3}{2}\frac{1-2\nu_1}{E_1} r - \frac{2(1-2\nu_1)}{E_1}\frac{1}{r}\int_0^r krdr. \qquad + \frac{1}{r}\int_0^r 3\alpha\, Trdr, \tag{6.10}$$

from which with the use of Hooke's law and the plastic component of radial strain is found to be

$$\epsilon_r'' = \frac{1-2\nu_1}{2E_1} D_3 - \frac{2k}{E_1}(1-\nu_1) + \frac{(1-2\nu_1)}{E_1}\frac{2}{r^2}\int_0^r krdr + 2\alpha_1 T - \frac{3\alpha_1}{r^2}\int_0^r Trdr. \tag{6.11}$$

It may be seen from the compressibility relation (2.7) which holds throughout the cylinder, that since the stresses and displacement u are continuous at $r = \rho_1$, the elastic as well as the plastic components of the radial strain each must be continuous separately. Since $\epsilon_r'' = 0$ throughout zone II, then by (6.11)

$$\frac{1-2\nu_1}{E_1}\frac{D_3}{2} = \frac{2k(\rho_1)}{E_1}(1-\nu_1) - \frac{(1-2\nu_1)}{E_1}\frac{2}{\rho_1^2}\int_0^{\rho_1} krdr - 2\alpha_1 T(\rho_1) + \frac{3\alpha_1}{\rho_1^2}\int_0^{\rho_1} Trdr. \tag{6.12}$$

Substituting (4.18) into (6.2), though Hooke's law, the value of k throughout zone I is found to be

$$\frac{k}{k_0}(1+\gamma) = 1 + \frac{\gamma}{2}(1-2\nu_1)\frac{D_3}{k_0} + \frac{\Phi_1\gamma}{2}\frac{T(r)}{T_a}, \tag{6.13}$$

which, when solved with (6.12) after some simplification, yields

$$\frac{1-2\nu_1}{2}\frac{D_3}{k_0} = 1 - 2\Phi_1\frac{T(\rho_1)}{T_a} + 3\Phi_1\frac{\theta(\rho_1)}{T_a} + \gamma(1+\nu_1)\Phi_1\left[2\frac{\theta(\rho_1)}{T_a} - \frac{T(\rho_1)}{T_a}\right], \tag{6.14}$$

$$\frac{k}{k_0}(1+\gamma) = 1 + \gamma\left[1 - 2\Phi_1\frac{T(\rho_1)}{T_a} + \frac{\Phi_1}{2}\frac{T(r)}{T_a} + \frac{3\Phi_1(\rho_1)}{T_a}\right] + \\ + \gamma^2\left[2\frac{\theta(\rho_1)}{T_a} - \frac{T(\rho_1)}{T_a}\right](1+\nu_1)\Phi_1. \tag{6.15}$$

With D_3 and k known, the radial displacement may now be written as

$$\frac{E_1 u}{rk_0} = \frac{1-2\nu_1}{2}\frac{D_3}{k_0}\left[3-(1-2\nu_1)\kappa\right] - \frac{1-2\nu_1}{1+\gamma} + \Phi_1\frac{\theta(r)}{T_a}\left[3-(1-2\nu_1)\kappa\right], \tag{6.16}$$

which completes the solution for zone I.

Continuity of the plane components of stress [given by (3.1) in the elastic zone, and by (6.8) in the plastic zone II, and by (4.18) in the plastic zone I] at $r = \rho_1$ and $r = \rho$ gives, respectively,

$$\left.\begin{aligned} A_5 &= \frac{\rho^{s_5}}{s_5 - s_6}\left[\gamma_1(1 - s_5) - \beta_1\right], \\ A_6 &= \frac{\rho^{s_6}}{s_5 - s_6}\left[\gamma_1(1 - s_6) + \beta_1\right], \end{aligned}\right\} \tag{6.17a}$$

where

$$\left.\begin{aligned} \gamma_1 &= \frac{E_1 C_1}{(1+\nu_1)(1-2\nu_1)} - \frac{E_1 C_2}{1+\nu_1}\frac{1}{\rho_2} - \frac{\Phi_1}{1-\nu_1}k_0\frac{\theta(\rho)}{T_a} - \bar{\sigma}_r(\rho), \\ \beta_1 &= \frac{E_1 C_1}{(1+\nu_1)(1-2\nu_1)} - \frac{E_1 C_2}{1+\nu_1}\frac{1}{\rho^2} + \frac{\Phi_1}{1-\nu_1}k_0\frac{\theta(\rho)}{T_1} - \frac{\Phi_1 k_0}{1-\nu_1}\frac{T(\rho)}{T_1} - \bar{\sigma}_\theta(\rho), \end{aligned}\right\} \tag{6.17b}$$

and

$$A_5 = \frac{\rho_1^{s_5}}{s_5 - s_6}\left[\gamma_2(1 - s_6) - \beta_2\right], \qquad A_6 = \frac{\rho_1^{s_6}}{s_5 - s_6}\left[\gamma_2(1 - s_6) + \beta_2\right], \tag{6.18a}$$

where

$$\gamma_2 = D_3 - \bar{\sigma}_r(\rho_1), \qquad \beta_2 = D_3 - \bar{\sigma}_\theta(\rho_1). \tag{6.18b}$$

where the barred quantities correspond to the particular solution of (6.6).

The time parameters C_1, C_2 of the elastic domain appearing in (6.17b) are no longer given by (5.7) but must be redetermined from (3.1) with the additional boundary condition $(\sigma_\theta - \sigma_r)_{r=\rho} = 2k_0$ giving

$$\frac{E_1 C_1^{(1)}}{(1+\nu_1)(1-2\nu_1)k_0} = \frac{1}{D}\left[-\frac{1}{\rho_2}\frac{p}{k_0} + \frac{2}{a^2} + \frac{\alpha_1 E_1}{1-\nu_1}\frac{1}{k_0}\left(\frac{\theta(a)}{\rho^2} - \frac{\theta(\rho)}{a^2}\right)\right], \tag{6.19a}$$

$$\frac{E_1 C_2^{(1)}}{(1+\nu_1)a^2 k_0} = \frac{1}{Da^2}\left[(1-2\nu_1)\frac{p}{k_0} + 2 - \frac{\alpha_1 E_1}{1-\nu_1}\frac{1}{k_0}\left(\theta(\rho) - (1-2\nu_1)\theta(a)\right)\right], \tag{6.19b}$$

where $D = \dfrac{1}{\rho^2} + \dfrac{1-2\nu_1}{a^2}$.

With $C_1^{(1)}$ thus determined it is appropriate to record here the relation between p and Φ_1 for Stage I, which may be obtained from (5.6) through (5.7b) and (6.19a):

$$\frac{p}{k_0}\left[1 + \nu_1 - \frac{2(1-\nu_1^2)}{D\rho^2} - \frac{E_1}{E_2}\left(1 + \nu_2 + \frac{2(1-\nu_2^2)}{b^2/a^2 - 1}\right)\right]$$
$$= \Phi_1\left[\frac{2(1+\nu_2)}{1 - a^2/b^2}\frac{\alpha_2}{\alpha_1}\frac{\theta(b)}{T_a} - \frac{2(1+\nu_1)}{D\rho^2}\left(\frac{\theta(a)}{T_a} - \frac{\rho^2}{a^2}\frac{\theta(\rho)}{T_a}\right)\right] - \frac{4(1-\nu_1^2)}{Da^2}. \tag{6.20}$$

Equating (6.17a) and (6.18b), there results two equations in the unknowns Φ_1, ρ_1, and ρ which may be best solved numerically for various choices of ρ. With Φ_1 and ρ_1 determined, all of the coefficients C_1, C_2, A_1, A_2, D_3, given by (6.19a), (6.19b), (6.17a) and (6.14), respectively, may be evaluated, and the solution for this stage of the problem is complete.

Stages II and III

Due to the nature of the problem and the yield condition (6.1), when the elastic–plastic boundary ρ reaches the outer radius $r = a$, the interface boundary ρ_1 continues to propagate and the cylinder is still capable of accepting more load, even in the absence of workhardening.

Since zone II now extends to the interface $r = a$, the relation (6.20) ceases to be valid and a new relation between p and Φ_1 must be obtained. Since the cladding is still assumed to be elastic, (5.5) with $i = 2$ remains valid and is set equal to (6.9) at $r = a$.

A second relation between p and Φ_1 may be found by substitution of (6.18) (which remains valid in Stage II, since the form of the solution in zone I has not changed) into the boundary condition $\sigma_r(a) = -p$. The two new relations between p and Φ_1 may then be solved simultaneously for the two unknowns. Throughout Stage II, in the absence of an elastic–plastic boundary during Stage II, ρ_1 may be treated as the independent variable.

The description of the plastic deformation provided by Stage II continues to be valid, until the state of stress at the outer radius $r = a$ of the cylinder, represented during Stage II by a point moving in regime BC of Fig. 1, reaches the singular regime B, at which time the solution enters Stage III. As the states of stress at successive points in zone II of the cylinder enter regime B, a second interface ρ_2 is formed which moves inward from $r = a$ and forms a plastic domain III ($\rho_2 \leqq r \leqq a$), corresponding to states of stress lying in regime B.

The differential equation governing the radial stress σ_r (as well as σ_z, since $\sigma_r = \sigma_z$) in zone III, derived in a manner similar to (6.6) for zone II, is given by

$$\frac{\partial^2}{\partial r^2}\left(\frac{\sigma_r}{k_0}\right) + \frac{3}{r}\frac{\partial}{\partial r}\left(\frac{\sigma_r}{k_0}\right) - (1-2\nu)\frac{\kappa}{r^2}\frac{\sigma_r}{k_0} = \frac{4}{(1-\gamma)\,r^2} + \frac{\kappa\Phi_1}{r^2}\left[\frac{T}{T_a} - r\frac{\partial}{\partial r}\left(\frac{T}{T_a}\right)\right] \tag{6.21}$$

for a workhardening material. The tangential stress σ_θ is then obtained through the equilibrium equation (2.1) and the displacement u through the compressibility condition (4.6a). For a non-hardening material the stress field is given by (4.17). The method of determining the coefficients appearing in the solution is similar to that of Stage I with ρ replaced by ρ_2 and γ_1 and β_1, in (6.17a) replaced respectively by

$$\gamma_3 = \sigma_r(\rho_2) - \bar{\sigma}_r(\rho_2), \qquad \beta_3 = \sigma_\theta(\rho_2) - \bar{\sigma}_\theta(\rho_2), \tag{6.22}$$

where $\sigma_r(\rho_2)$ and $\sigma_\theta(\rho_2)$ in (6.22) refer to the components of stress in zone III found from (6.21) (or (4.17)).

Subsequent to the determination of a new relation between p and Q_0 for Stage III, and the redetermination of the time functions in the stress and displacement fields, it is found that the separation boundaries ρ_1 and ρ_2 approach each other monotonically but do not meet; each approaching a limit value as the temperature is indefinitely increased. This is reminiscent of the results given by Wilhoit (1958) for a ring in the state of plane stress, subjected to a temperature gradient, and by Cowper (1958) for a hollow sphere also in the presence of a temperature gradient.

This completes the solution of Stage III of the problem which remains valid until yield occurs in the cladding. It may be noted here that, once the cladding has yielded, a fourth stage of the deformation begins, since the interaction of the three boundaries ρ_1, ρ_2 and ρ_3 (the elastic–plastic boundary in the cladding) must be considered.

7. Discussion – Numerical Results

In the preceding Sections the character of the initial yield and the subsequent deformation was established for a class of radially symmetric temperature distributions ($1 \leqq m \leqq 2$), chosen to include (5.2) which was due to a Gaussian heat source, distributed throughout the region. The expressions in Section 6 are written in general terms to include any temperature distribution in this class. In order to gain an insight into the problem, it is desirable to consider a detailed example for one case. Since the expressions in Section 6 become involved and intricate, when (5.2) is inserted, for the sake of simplicity we allow the parameter μ^2 to approach zero. The temperature distribution (5.2) then assumes the simple form

$$T = T_a + \frac{Q_0 a^2}{4K_1}\left[1 - \left(\frac{r}{a}\right)^2\right], \tag{7.1}$$

and $\dfrac{\theta(r)}{T_a}$ becomes

$$\frac{\theta(r)}{T_a} = \tfrac{1}{2}\left\{1 + \delta\left[1 - \tfrac{1}{2}\left(\frac{r}{a}\right)^2\right]\right\}, \tag{7.2}$$

where

$$\delta = \frac{a^2}{4K_1 h}, \tag{7.3}$$

and by (5.11b)

$$h = -\frac{T_a}{Q_0} = \frac{a^2 \log b/a}{2(1 - T_b/T_a) K_2}. \tag{7.4}$$

Comparison plots of the functions specified by (5.2) and (7.1) as well as the integrals which appear in the solution reveal a qualitative similarity between the two temperature distributions, which together with the fact that both produce initial yield of the same character ($m = 1$, so that the results in Table 1 are applicable) justifies the use of (7.1) in place of the more realistic expression (5.2). The resulting equations are thus considerably simplified.

We now proceed to obtain explicit results for a workhardening material obeying (2.5) subjected to a uniformly distributed heat source ($\mu^2 = 0$) which gives rise to the temperature field (7.1). In each expression the nonhardening material may be obtained by setting $\gamma = \kappa = 0$.

For the values of the parameters (5.16a) selected in Section 5 we continue the example and obtain explicit expressions using the alternative temperature field (7.1) for the quantities discussed in Section 6. In zone I for all stages of the problem the state of stress and the displacement continue to be given by (4.18) and (6.16) with D_3 and k becoming through (6.14) and (6.15), respectively:

$$\left.\begin{aligned} \frac{1 - 2\nu_1}{2}\frac{D_3}{k_0} &= 1 - \frac{\Phi_1}{2}\left\{1 + \delta\left[1 - \left(\frac{\rho_1}{a}\right)^2 - \left[\tfrac{5}{2} + \gamma(1 + \nu_1)\right]\right]\right\}, \\ \frac{k}{k_0} &= 1 - \frac{\Phi_1 \delta\kappa}{2}\left\{\left(\frac{r}{a}\right)^2 - \left(\frac{\rho_1}{a}\right)^2\left[\tfrac{5}{2} + \gamma(1 + \nu_1)\right]\right\}. \end{aligned}\right\} \tag{7.5}$$

In zone II for all stages the stresses may be found by allowing μ^2 to approach zero in (6.8) or more easily from (6.6), the right-hand side of which upon substitution of (7.1) becomes

$$b_3 + b_4\left(\frac{r}{a}\right)^2, \tag{7.6}$$

where

$$\left.\begin{aligned} b_3 &= \frac{1}{1 + \gamma}\left[2 - \Phi_1(1 + \delta)\right], \\ b_4 &= \Phi_1 \delta\left[5 - (3 - 2\nu_1)\kappa\right], \end{aligned}\right\} \tag{7.7}$$

and consequently the stress field in zone II is

$$\left.\begin{aligned} \frac{\sigma_r}{k_0} &= \frac{A_5}{r^{s_5}} + \frac{A_6}{r^{s_6}} + A_7 + A_8\left(\frac{r}{a}\right)^2, \\ \frac{\sigma_\theta}{k_0} &= (1 - s_5)\frac{A_5}{r^{s_5}} + (1 - s_6)\frac{A_6}{r^{s_6}} + A_7 + 3A_8\left(\frac{r}{a}\right)^2, \\ \frac{\sigma_z}{k_0} &= \frac{\sigma_\theta}{k_0} - \frac{2k}{k_0}, \end{aligned}\right\} \tag{7.8}$$

where

$$A_7 = \frac{b_3}{b_2}, \qquad A_8 = \frac{b_4}{8b_1 + b_2}, \tag{7.9}$$

and k is given by (6.4).

By (7.5) and (7.9), A_5 and A_6 may be found through (6.18) to be

$$\left.\begin{aligned} A_5 &= \frac{-1}{s_5 - s_6}\frac{\rho_1^{s_5+2}}{a^2}\left\{\frac{s_6\,\Phi_1\,\delta}{1-2\nu_1}\left[5/2 + \gamma(1+\nu_1)\right] - (s_6+2)\,A_6\right\}, \\ A_6 &= \frac{1}{s_5 - s_6}\frac{\rho_1^{s_6+2}}{a^2}\left\{\frac{s_5\,\Phi_1\,\delta}{1-2\nu_1}\left[5/2 + \gamma(1+\nu_1)\right] - (s_5+2)\,A_6\right\}, \end{aligned}\right\} \tag{7.10}$$

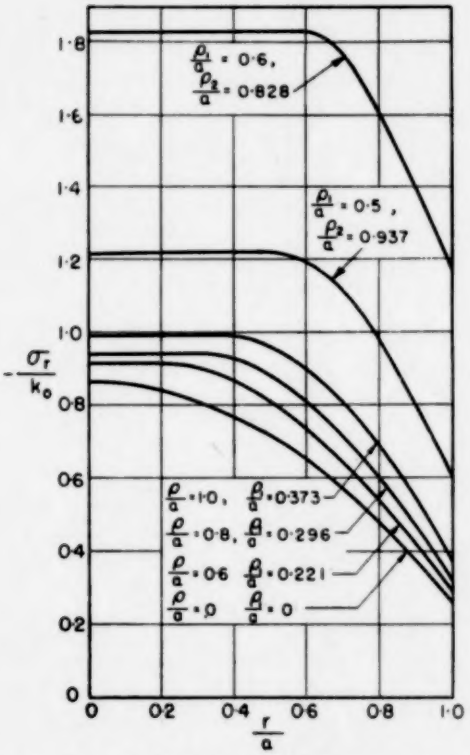

FIG. 3. Distribution of radial stress ($\gamma = 0$).

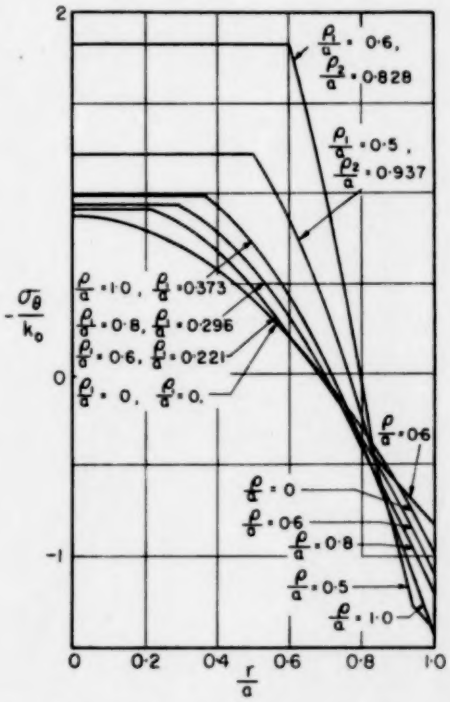

FIG. 4. Distribution of tangential stress ($\gamma = 0$).

Equating these values of A_5 and A_6 with those given by (6.17a) with subsequent elimination of ρ_1 between the two resulting equations leads to the following relation :

$$\left.\begin{aligned} \left(\frac{\rho}{a}\right)^{2(s_5-s_6)}&\left\{\frac{\gamma_1(1-s_6)-\beta_1}{\dfrac{-s_6}{1-2\nu_1}\,\Phi_1\,\delta\left[5/2+\gamma(1+\nu_1)\right]+(2+s_6)\,A_6}\right\}^{2+s_6} \\ &= \left\{\frac{\gamma_1(1-s_6)+\beta_1}{\dfrac{s_6}{1-2\nu_1}\,\Phi_1\,\delta\left[5/2+\gamma(1+\nu_1)\right]-(2+s_6)\,A_6}\right\}^{2+s_5}, \end{aligned}\right\} \tag{7.11}$$

which indicates the complex nature of the interaction between p, Φ_1 and ρ even for the simple distribution (7.1). Equation (7.11) may be solved simultaneously with (6.20) to determine p and Φ_1 in terms of ρ.

The values p^{**}, Q_0^{**} for which the cross-section becomes fully plastic, signifying the start of Stage II, may also be obtained from (7.11) and (6.20) by setting $\rho/a = 1$. During Stage II of the problem (7.5) continues to hold in zone I and (7.10) in zone II. Only the means of obtaining relations between p and Φ_1, discussed in Section 6, differs from Stage I. Stage II ends when $\sigma_r = \sigma_z$ at $r = a$ signifying that the state of stress has entered a singular regime (B), constituting the start of Stage III. The procedure used in the solution of Stage III parallels Stage I and for economy of space will not be included here.

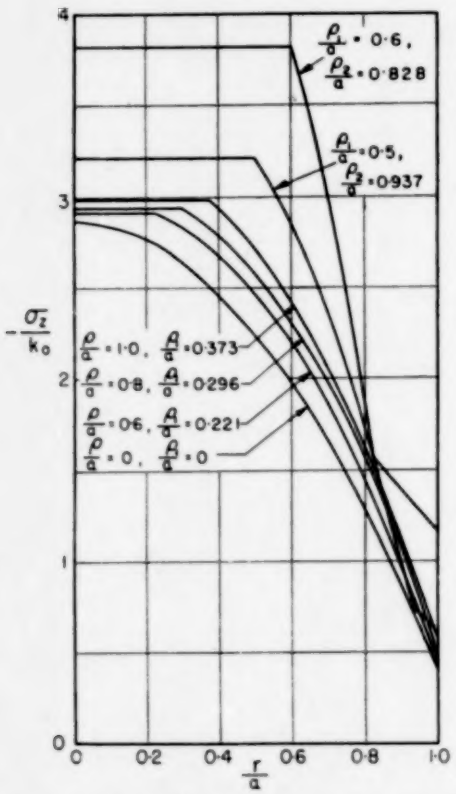
$\frac{\rho_1}{a}$ = 0·6, $\frac{\rho_2}{a}$ = 0·828
$\frac{\rho_1}{a}$ = 0·5, $\frac{\rho_2}{a}$ = 0·937
$\frac{\rho}{a}$ = 1·0, $\frac{\rho_1}{a}$ = 0·373
$\frac{\rho}{a}$ = 0·8, $\frac{\rho_1}{a}$ = 0·296
$\frac{\rho}{a}$ = 0·6, $\frac{\rho_1}{a}$ = 0·221
$\frac{\rho}{a}$ = 0, $\frac{\rho_1}{a}$ = 0
$-\frac{\sigma_z}{k_0}$
$\frac{r}{a}$
0 0·2 0·4 0·6 0·8 1·0
0 1 2 3 4

FIG. 5. Distribution of axial stress ($\gamma = 0$).

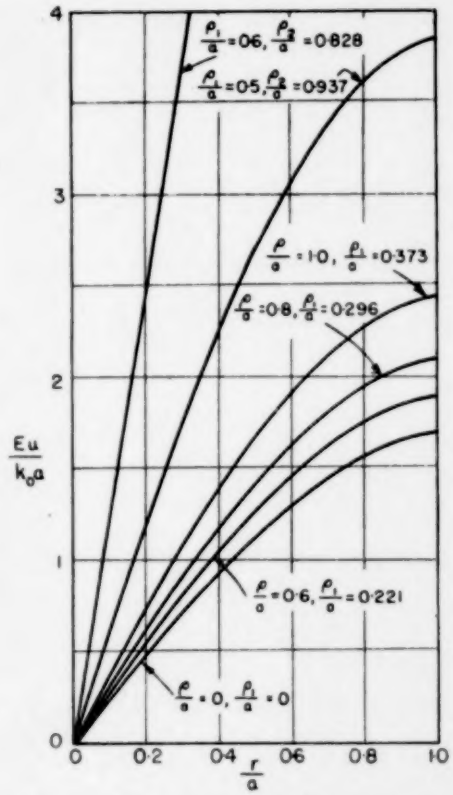
$\frac{\rho_1}{a}$ = 0·6, $\frac{\rho_2}{a}$ = 0·828
$\frac{\rho_1}{a}$ = 0·5, $\frac{\rho_2}{a}$ = 0·937
$\frac{\rho}{a}$ = 1·0, $\frac{\rho_1}{a}$ = 0·373
$\frac{\rho}{a}$ = 0·8, $\frac{\rho_1}{a}$ = 0·296
$\frac{\rho}{a}$ = 0·6, $\frac{\rho_1}{a}$ = 0·221
$\frac{\rho}{a}$ = 0, $\frac{\rho_1}{a}$ = 0
$\frac{Eu}{k_0 a}$
$\frac{r}{a}$
0 0·2 0·4 0·6 0·8 1·0
0 1 2 3 4

FIG. 6. Ratio of radial displacement to cylinder radius ($\gamma = 0{\cdot}3$).

For a nonhardening material ($\gamma = 0$) the stress distributions and displacements for various positions of ρ_1 are shown in Figs. 3–6, and the projection of the loading paths on a plane perpendicular to the axis of the yield surface is shown in Fig. 2.

To illustrate the effect of workhardening, a very drastic value 0·3 has been selected for γ; this corresponds roughly to the value of γ for uranium in compression (GURINSKY and DIENES 1956, p. 58).

Although not included in the Figures, it is found that at the completion of Stage I the greatest difference between the hardening and nonhardening cases occurs in the axial component of stress (7·2 per cent at $r = 0$); the plane components differ

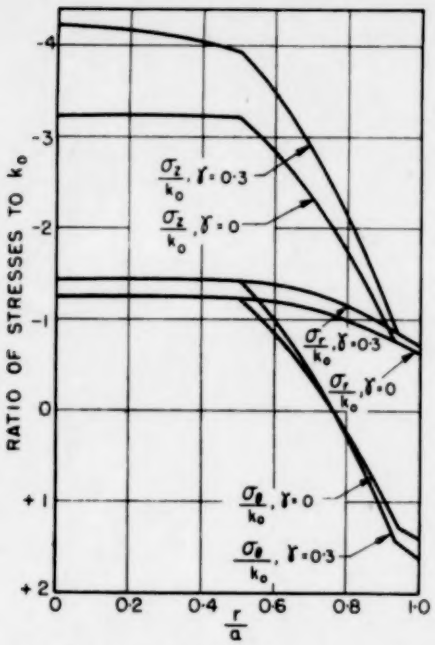

FIG. 7. Comparison of the three components of stress for hardening ($\gamma = 0{\cdot}3$) and non-hardening ($\gamma = 0$) materials when $\frac{\rho_1}{a} = 0{\cdot}5$ during Stage III.

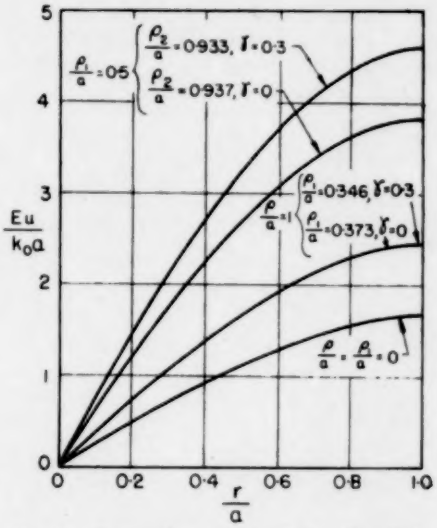
$\frac{Eu}{k_0 a}$
$\frac{\rho_1}{a} = 0.5$
$\frac{\rho_2}{a} = 0.933$, $\gamma = 0.3$
$\frac{\rho_2}{a} = 0.937$, $\gamma = 0$
$\frac{\rho}{a} = 1$
$\frac{\rho_1}{a} = 0.346$, $\gamma = 0.3$
$\frac{\rho_1}{a} = 0.373$, $\gamma = 0$
$\frac{\rho}{a} = \frac{\rho_1}{a} = 0$
$\frac{r}{a}$

FIG. 8. Comparison of the ratio of radial displacement to cylinder radius for hardening ($\gamma = 0{\cdot}3$) and nonhardening ($\gamma = 0$) materials.

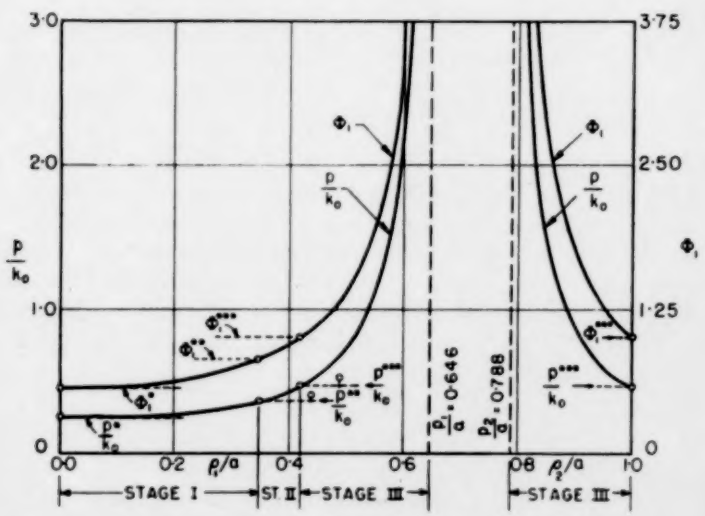

FIG. 9. Load parameters for various positions of the boundaries ρ_1, and ρ_2, showing values at initial yield (p^*, Q_0^*), at the start of Stage II (p^{**}, Q_0^{**}), and Stage III (p^{***}, Q_0^{**}), as well as the asymptotic values of ρ_1 and ρ_2.

by less than 2 per cent, while the radial displacements (Fig. 8) are indistinguishable. Larger differences occur during Stages II and III and in Figs. 7 and 8 the components of stress and displacement, respectively, for $\rho_1 = 0{\cdot}5$ of Stage III are compared. The character of the yield stress in simple shear for two values of ρ_1 is shown in Fig. 10. The load parameters for the workhardening case are shown in Fig. 9 as a function of ρ_1 and ρ_2. The boundaries ρ_1 and ρ_2 for a workhardening material are found to lag behind the nonhardening values for a given value of the load parameters p and Φ_1.

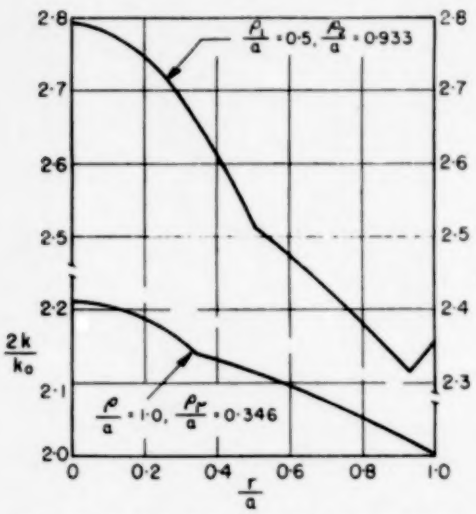

FIG. 10. Yield limit in shear at the completion of Stage I and when $\frac{\rho_1}{a} = 0{\cdot}5$ shortly after the start of Stage III.

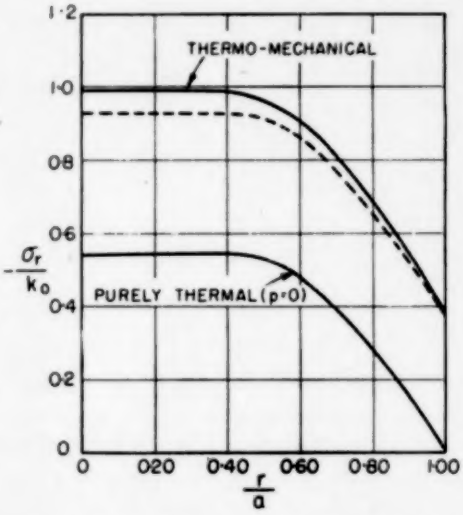

FIG. 11. Comparison of the thermo-mechanical solution at the completion of Stage I for the state of plane strain with that obtained by superposition of the purely thermal solution for the state of plane strain and hydrostatic pressure (shown by dashed lines) for $\gamma = 0$.

Finally it may be noted that the effect of adding $\sigma_r = -p$ to the purely thermal problem ($p = 0$) is not a matter of the simple super-position of a hydrostatic pressure. In fact the plane strain conditions prevent this so that the elastic–plastic deformation depends to a great extent on the relation between Φ_1 and p. To illustrate this, a comparison of σ_r at the completion of Stage I for the thermo-mechanical problem, considered in this paper, with the result obtained by superimposing a hydrostatic pressure upon the purely thermal solution* is shown in Fig. 11.

REFERENCES

BLAND, D. R. 1956 *J. Mech. Phys. Solids* **4**, 209.
1957 *Proc. 9th Int. Congr. Appl. Mech.* **8**, 45.
COWPER, G. R. 1958 Tech. Report No. 9, Nonr 562 (20), Division of Engineering, Brown University.

* It is easily verified by (5.14) that the character of initial yield is unchanged for the purely thermal problem.

Glasstone, S.	1955	*Principles of Nuclear Reactor Engineering* (Van Nostrand. New York).
Gurinsky, D. H. and Dienes, G. J.	1956	*Nuclear Fuels* (Van Nostrand, Princeton).
Hill, R.	1950	*Mathematical Theory of Plasticity* (Clarendon Press, Oxford).
Hodge, P. G.	1956	*J. Rat. Mech. Anal.* **5**, 917.
Koiter, W. T.	1953	*Biezeno Anniversary Volume on Applied Mechanics*, p. 232 (Haarem, Holland).
Parkus, H.	1954	*Proc. 2nd U.S. Nat. Congr. Appl. Mech.*, 307.
Prager, W.	1958	*Proc. Ken. Ned. Akad. v. Wetensch.* **B61**, 176.
Thompson, A. S. and Rodgers, O. E.	1956	*Thermal Power from Nuclear Reactors* (John Wiley. New York).
Timoshenko, S. and Goodier, J. N.	1951	*Theory of Elasticity* (McGraw-Hill, New York).
Weiner, J. H.	1956	*J. Appl. Mech.* **23**, 395.
Weiner, J. H. and Huddleston, J. V.	1959	*J. Appl. Mech.* **26**, 31.
Wilhoit, J. C.	1958	*Proc. 3rd U.S. Nat. Congr. Appl. Mech.*, 693.

J. Mech. Phys. Solids, 1960, Vol. 8, pp. 26 to 38. Pergamon Press Ltd., London. Printed in Great Britain

ON THE PHOTOELASTIC EXAMINATION OF VIBRATING BODIES AND THE PHOTOELASTIC EFFECT IN OPTICALLY ACTIVE MEDIA*

By A. F. B. Wood
Royal Holloway College, University of London†

(*Received 26th July*, 1959)

Summary

The interpretation of the photoelastic stress patterns of vibrating bodies is discussed, with particular reference to quartz crystals. An expression is derived for the change in velocity of a light wave propagated along the optic axis due to stresses acting in the plane normal to this axis. Such stresses should cause an increase in the effective rotary power and this is verified by experiment. This result offers an explanation of phenomena observed by earlier workers.

1. The Photoelastic Stress Patterns Produced by Oscillatory Stresses

In connexion with a photoelastic examination of vibrating quartz crystals it became necessary to consider the manner in which the isoclinics and isochromats observable in a statically stressed isotropic medium are modified by the vibratory nature of the stress and the optical activity of the *Z*-cut specimens used for the experiments.

The effects of vibration alone may easily be taken into consideration. The intensity of the light transmitted by a birefringent medium between crossed polarizer and analyser is

$$I = I_0 \sin^2 2\alpha \sin^2 (\delta/2) \qquad (1)$$

where I_0 is the incident intensity, α the acute angle between the polarizer axis and a principal axis of the medium and δ the relative phase retardation between the two plane polarized waves emerging from the specimen. The transmitted intensity is zero if $\alpha = 0$ or $\frac{1}{2}\pi$ or if $\delta = 2n\pi$, that is, if the principal axes of the medium are parallel to polarizer and analyser or the retardation is a whole number of periods. In a mechanically stressed isotropic medium the principal axes of the artificial birefringence are parallel to the principal axes of stress, and the difference between the propagation velocities in any direction is proportional to the difference between the secondary principal stresses acting normal to the direction of propagation. The case usually considered is that of a lamina in a state of plane stress, uniform throughout the thickness, the light being propagated along the thickness. If the stress varies across the specimen two sets of dark fringes are observed. One set, the isoclinic, joins points at which the principal stress directions are parallel

*This work forms part of a Ph.D. thesis (University of London, 1955).
†Now at Standard Telephones and Cables Limited, Crystal Division, West Road, Temple Fields, Harlow, Essex.

to the polarizer and analyser axes and its position is independent of the light wavelength. The other set, the isochromat, joins points at which the difference between the principal stresses causes a retardation of an integral number of periods and the position of the fringes for each non-zero value of n in equation (1) depends on the wavelength. The zero-order isochromat, for which there is no phase retardation and the principal stresses are equal, is common to all wavelengths.

Considering, now, an isotropic lamina subjected to an oscillatory plane stress system caused by vibration of the lamina in a normal mode, then a fundamental characteristic of such vibrations is that the displacements at all points are in phase and hence the directions and ratio of the principal stresses remain fixed throughout the vibration cycle. The retardation will vary sinusoidally with the stress at the frequency of vibration and, writing $\delta = \Delta \cos \omega t$ and finding the mean transmitted intensity over a whole period of the vibration, equation (1) becomes

$$I_m = I_0 \sin^2 2\alpha \, (1 - J_0 \, \Delta)/2. \tag{2}$$

This is zero when $\alpha = 0$ or $\frac{1}{2}\pi$ and also when $\Delta = 0$ since $J_0(0) = 1$. Thus the isoclinic and the zero-order isochromat are unaffected by the vibration. The expression $(1 - J_0 \, \Delta)$ oscillates about the value one with decreasing amplitude as Δ increases. The values of Δ for the minima are given by $\Delta = 2k\pi$ where k is no longer integral but takes the values 0, 1·117, 2·121, 3·122, 4·123. Although these minima do not have zero intensity, apart from the zero-order isochromat, the position is unaffected by the intensity distribution due to the $\sin^2 2\alpha$ term and they may be used in the same way as isochromats in the static case.

Thus, when an isotropic body is vibrating in a normal mode of a type giving rise to a plane stress system, the usual photoelastic observations may be made except that the number of isochromats visible is limited by the decrease in visibility with order and that the retardation associated with any order is not an integral number of periods as in the static case. In these experiments on vibrating quartz crystals, however, owing to the smallness of the photoelastic effect and the thinness of the specimens used, the retardation could not be increased sufficiently to produce the first intensity minimum without danger of exceeding the breaking stress. Hence only the isoclinics and zero-order isochromat were available for study.

2. The Photoelastic Effect in Quartz

Under the action of a general stress system the equation of the index ellipsoid of a crystalline medium, referred to the orthogonal crystal axes, changes from

$$a^0_{11} x^2 + a^0_{22} y^2 + a^0_{33} z^2 = 1 \tag{3}$$

to the general equation of an ellipsoid whose axes do not coincide with the coordinate axes:

$$a_{11} x^2 + a_{22} y^2 + a_{33} z^2 + 2a_{23} yz + 2a_{31} zx + 2a_{12} xy = 1 \tag{4}$$

where a^0_{ii} represent the squares of the principal velocities of light waves in the unstrained crystal relative to that *in vacuo*.

In general, each of the coefficients a_{ij} is a linear function of all of the six stress components. Pockels (1889) has shown that the strained index ellipsoid is obtained

from the unstrained by suitable changes in the lengths of the axes and, provided that $a_{ii} - a^0_{ii}$ and a_{ij} are all small compared with a^0_{ii} and $a^0_{ii} - a^0_{jj}$, by small rotations ϕ_i about each of the coordinate axes in turn. The magnitudes of these angles are given by:

$$\tan 2\phi_i = 2a_{jk}/(a_{jj} - a_{kk}) \simeq 2a_{jk}/(a^0_{jj} - a^0_{kk}). \tag{5}$$

In quartz the coefficients of the strained ellipsoid are given in terms of the stresses by the following equations:

$$\left.\begin{aligned}
a_{11} &= v^2_0 + \pi_{11}\sigma_1 + \pi_{12}\sigma_2 + \pi_{13}\sigma_3 + \pi_{14}\sigma_4 \\
a_{22} &= v^2_0 + \pi_{12}\sigma_1 + \pi_{11}\sigma_2 + \pi_{13}\sigma_3 - \pi_{14}\sigma_4 \\
a_{33} &= v^2_e + \pi_{31}\sigma_1 + \pi_{31}\sigma_2 + \pi_{33}\sigma_3 \\
a_{23} &= \pi_{41}\sigma_1 - \pi_{41}\sigma_2 + \pi_{44}\sigma_4 \\
a_{31} &= \pi_{44}\sigma_5 + 2\pi_{41}\sigma_6 \\
a_{12} &= \pi_{14}\sigma_5 + (\pi_{11} - \pi_{12})\sigma_6
\end{aligned}\right\} \tag{6}$$

where v_o and v_e are the ordinary and extraordinary velocities, π_{ij} the stress optic coefficients and σ_i the stress components.

Since $a^0_{11} = a^0_{22} = v^2_0$, ϕ_3 is large but the orientation of the index ellipsoid may still be found from the formula given, provided that the rotation ϕ_3 is carried out first and that it is calculated from the first part of (5). In the present discussion a state of plane stress in the XY-plane is considered. Since $\pi_{66} = \pi_{11} - \pi_{12}$ it is easily shown that in this case $\phi_3 = \theta$, the angle between the X and Y-axes and the principal stress directions. It may further be shown that for such a stress system the resultant effect of the rotations ϕ_1 and ϕ_2 is that the index ellipsoid is turned through an angle $(\phi^2_1 + \phi^2_2)^{\frac{1}{2}}$ about an axis in the XY-plane which makes an angle -2θ with the X-axis. Using POCKELS' values for the stress optic coefficients of quartz this angle is found to be about 1 or 2 per cent of the angle between the optic axes of the now biaxial quartz for a stress of 10^8 dyne cm^{-2} and will be ignored in what follows.

On substituting the values of the ellipsoid parameters from (6) and taking new X and Y-axes along the directions of the principal stresses, σ_p and σ_q, (4) transforms to the same form as (3):

$$\begin{aligned}
&(v^2_0 + \pi_{11}\sigma_p + \pi_{12}\sigma_q)\,x^2 + (v^2_0 + \pi_{12}\sigma_p + \pi_{11}\sigma_q)\,y^2 \\
&+ (v^2_e + \pi_{31}(\sigma_p + \sigma_q))\,z^2 = 1.
\end{aligned} \tag{7}$$

The difference between the principal velocities in the Z-direction is:

$$\sqrt{a_{22}} - \sqrt{a_{11}} \simeq (\pi_{11} - \pi_{12})(\sigma_p - \sigma_q)/2v_0. \tag{8}$$

Thus as regards the pure photoelastic effect a Z-cut lamina stressed in the XY-plane behaves as though isotropic to light propagated along the Z-axis because the section of the index ellipsoid by the wave front has axes parallel to the principal stress directions and the retardation is proportional to the difference between the principal stresses.

Since quartz is piezoelectric there is a secondary photoelastic effect due to the fact that the electric polarization produced by the stress causes further changes in

the parameters of the index ellipsoid by virtue of the electro-optic effect. The magnitude of the electric polarization will depend on the electric boundary conditions and will generally differ for static and oscillatory stresses. However, the effect is small in quartz, being a few per cent of the direct photoelastic effect and, more important, the symmetry of the direct effect is not altered by the secondary effect, for example the relation $\pi_{66} = \pi_{11} - \pi_{12}$ is still valid. For these reasons it will be ignored in this discussion.

3. Effect of Optical Activity

In a medium that is both birefringent and optically active two elliptically polarized waves of opposite hand may be propagated unchanged in any direction with slightly different velocities. The axes of the ellipses are parallel to those of the section of the index ellipsoid by the wave front and the ellipses themselves, although similar, lie oppositely, so that the minor axis of one is parallel to the major axis of the other.

In order to find the influence of such a medium upon the polarization state of an incident plane polarized wave, the wave is first resolved into plane polarized components along the axes of the section of the index ellipsoid by the wave front and then each of these is further resolved into two opposite elliptically polarized waves. After introducing the appropriate retardations due to the passage through the medium, these are recombined to give the emergent wave. Preston (1901) has considered the general case of the intensity transmitted by an optically active birefringent crystal between polarizer and analyser. If the axes of these make angles α and β respectively with one axis of the section of the index ellipsoid by the wave front, then the ratio of the transmitted to the incident intensity is

$$\frac{I}{I_0} = \left(\cos(\alpha - \beta)\cos\delta/2 - \frac{2h}{(1+h^2)}\sin(\alpha - \beta)\sin\delta/2\right)^2 + \left(\frac{1-h^2}{1+h^2}\right)^2 \cos^2(\alpha + \beta)\sin^2\delta/2 \tag{9}$$

where δ is the relative retardation of the emergent elliptically polarized waves and h is their axial ratio. Both terms of this expression are essentially positive and so the intensity can be zero only if they are simultaneously zero. The first term is zero when

$$(\beta - \alpha) = \pi/2 + \tan^{-1}\left(\frac{2h}{1+h^2}\tan\delta/2\right) \tag{10}$$

and the second when either

$$(\alpha + \beta) = \pi/2 \tag{11}$$

or

$$\delta = 2n\pi. \tag{12}$$

Since (10) must always hold good for zero intensity the polarizer and analyser axes must be misorientated by an angle

$$\tan^{-1}\left(\frac{2h}{1+h^2}\cdot\tan\delta/2\right)$$

from the crossed position so that the *effective* rotation is

$$\rho = \tan^{-1}\left(\frac{2h}{1+h^2} \cdot \tan \delta/2\right). \tag{13}$$

If $h = 1$, that is, if the waves are circularly polarized, which is the case when no birefringence is present, then there results the well-known equation

$$\rho = \delta/2. \tag{14}$$

Assuming that the polarizer and analyser have the correct relative setting, then from (11) and (12) extinction can occur when (a) the bisector of the angle between the polarizer and analyser axes is parallel to that of the angle between the axes of the section of the index ellipsoid or (b) the retardation is a whole number of periods.

Considering, now, a *Z*-cut quartz lamina statically stressed in the XY-plane it is assumed that the natural optical activity is affected by the stress only to the same extent as the refractive index so that such a change is negligible compared with the birefringence introduced in the direction of the optic axis. In general the difference between the principal stresses, and their directions, will vary over the field of view so that it would be fortuitous if (10) were satisfied simultaneously with (11) or (12). If, however, the light is reflected from the far side of the specimen so as to retrace its path exactly (10) may be fulfilled automatically. The reflexion results in a complicated expression for the intensity since a left-handed elliptic wave on incidence becomes a right-handed wave on reflexion ; but at points where the transmitted intensity would be zero if the analyser were correctly orientated, that is, at just those points in which we are interested, the light emergent from the specimen must necessarily be plane polarized and will, on reflexion, retrace its path exactly and leave the specimen in the same state as that in which it entered. It may therefore be stopped by an analyser with its axis crossed relative to the polarizer.

When observed under these conditions the specimen will exhibit two sets of dark fringes. One set joins points where the principal stress directions differ from those of the polarizer and analyser axes by half the effective rotation at the points concerned ; the other set joins points where the retardation is a whole number of periods. The sets correspond to isoclinics and isochromats with these differences :

(i) The rotation must be known at any point on the isoclinic to find the principal stress directions. Since the rotation depends upon phase difference and therefore upon stress the interpretation is difficult. It will be shown however that for sufficiently thin crystals the rotation hardly varies from the natural value and hence the directions of the polarizer and analyser axes differ by a constant angle from the principal stress directions.

(ii) Successive isochromats correspond to equal increments in the retardation but this does not now correspond to equal increments in stress owing to the influence of the optical activity, as will be seen later. In the work on vibrating crystals only the zero order isochromat is produced so this question does not arise.

4. Magnitude of Change in Effective Rotation with Stress

Drude (1905) has derived expressions for the propagation velocities v_1, v_2 and the axial ratio h of the two elliptically polarized waves in a birefringent optically active medium. In what follows the coordinate axes are taken parallel to the principal axes of the index ellipsoid as in (3) but the principal velocities relative to that *in vacuo* are now denoted by a_1, a_2 and a_3 for mathematical convenience. Drude gives

$$2v^2 = a^2_1 + a^2_3 + (a^2_1 - a^2_3)\cos g_1 \cos g_2 \pm \left[(a^2_1 - a^2_3)^2 \sin^2 g_1 \sin^2 g_2 + 4\eta^2\right]^{\frac{1}{2}} \tag{15}$$

$$h + 1/h = \left[(a^2_1 - a^2_3)^2 \sin^2 g_1 \sin^2 g_2 + 4\eta^2\right]^{\frac{1}{2}}/\eta \tag{16}$$

where g_1 and g_2 are the angles between the direction of propagation and each optic axis and η is a parameter proportional to the rotary power in the absence of birefringence and varying with the direction of propagation. In the present case the direction of propagation is the Z-axis and since the optic axis must split symmetrically into two new optic axes on the application of stress g_1 and g_2 are simply equal to $\pm\,\Omega$, the semi-angle between the optic axes. This has the value

$$\sin^{-1}\left[(a^2_1 - a^2_2)/(a^2_1 - a^2_3)\right]^{\frac{1}{2}}$$

and hence

$$\sin g_1 = +\left[(a^2_1 - a^2_2)/(a^2_1 - a^2_3)\right]^{\frac{1}{2}}, \tag{17}$$

$$\sin g_2 = -\left[(a^2_1 - a^2_2)/(a^2_1 - a^2_3)\right]^{\frac{1}{2}}, \tag{18}$$

$$\cos g_1 = \cos g_2 = +\left[(a^2_2 - a^2_3)/(a^2_1 - a^2_3)\right]^{\frac{1}{2}}. \tag{19}$$

Substitution of these values in (15) and (16) gives

$$v_1 - v_2 = (\eta/a_1)\left[1 + (a_1 - a_2)^2/(\eta/a_1)^2\right]^{\frac{1}{2}}, \tag{20}$$

$$h + 1/h = 2\left[1 + (a_1 - a_2)^2/(\eta/a_1)^2\right]^{\frac{1}{2}}. \tag{21}$$

If d is the thickness of the lamina, T the period of the light wave, and c the velocity of light *in vacuo* then the relative retardation of the emergent waves is

$$\delta = 2\pi d\,(v_1 - v_2)/Tc\,v_1 v_2 \simeq (2\pi\, d\eta/Tca^3_1)\left[1 + (a_1 - a_2)^2/(\eta/a_1)^2\right]^{\frac{1}{2}} \tag{22}$$

from (20). By (14) the rotation in the unstressed specimen is equal to half the retardation:

$$\rho_0 = \delta_0/2 = \pi d\eta/Tca^3_1. \tag{23}$$

Hence
$$\delta = 2\rho_0(1 + \epsilon^2)^{\frac{1}{2}} \tag{24}$$

where
$$\epsilon = (a_1 - a_2)/(\eta/a_1). \tag{25}$$

From (13) and (21) the effective rotation is

$$\rho = \tan^{-1}\left(\frac{2h}{1 + h^2}\tan\delta/2\right) = \tan^{-1}\left[\frac{\tan\left[\rho_0(1 + \epsilon^2)^{\frac{1}{2}}\right]}{(1 + \epsilon^2)^{\frac{1}{2}}}\right]. \tag{26}$$

In these expressions ϵ is directly proportional to the difference between the principal stresses; substituting from (8) into (25):

$$\epsilon = (\pi_{11} - \pi_{12})\ (\sigma_p - \sigma_q)/2\eta. \tag{27}$$

The resultant retardation is not proportional to the stress however. Fig. (1) shows the variation of the retardation δ and the effective rotation ρ with ϵ for two thicknesses of quartz, 0·5 mm and 3·06 mm. The first thickness is that of a Z-cut

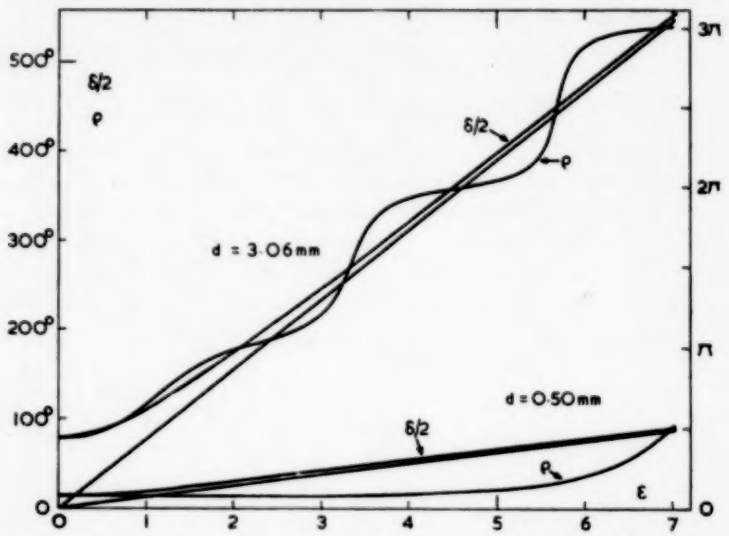

Fig. 1. Dependence of effective rotation on phase retardation in a birefringent optically active medium.

disk used for experiments on vibrations while the second is that of a Z-cut bar used for the experiments described in the next section to test this theory. It will be noticed that while ρ_0 and δ are proportional to the thickness ρ is definitely not. For the smaller thickness ρ hardly varies from the natural value ρ_0 since $(\tan K\rho_0)/K \to \rho_0$ as $\rho_0 \to 0$. Thus, for thin crystals, the rotation may be assumed constant and equal to the static value for all practical purposes. Owing to the flatness of the curves when ϵ is small the same will be true for thicker crystals provided the stresses are small enough. Two other features of these curves are notable. First, for sufficiently high stresses the retardation tends asymptotically to a straight line through the origin representing the retardation in the absence of optical activity. Second, whenever $\delta = n\pi$ then $\rho = \delta/2$ as for the case of optical activity in the absence of birefringence.

Finally, perhaps the most interesting feature of all in this theory is the fact that according to (24) the phase retardation between the two oppositely elliptically polarized waves can only *increase* when the quartz becomes artificially birefrigent along the optic axis. Thus the increase in effective rotation given by (26) is independent of the sign of the stress and depends only upon the difference between the principal stresses.

5. Experimental Test of the Theory

The results of Section 4 were tested by investigating the propagation of light through a Z-cut bar uniformly bent in the XY-plane. The bar had a rectangular section and its length was parallel to the X-axis. Fig. 2 shows how the stress was applied and Fig. 3 shows the optical arrangement. The polarizer axis was so orientated as to polarize the light in the plane of incidence on the half silvered mirror in order to avoid subsequent elliptic polarization. The thrust was provided by a calibrated spring rather than by weights as the stresses had to act in the horizontal plane owing to the geometry of the optical system. Before applying any stress the field of view was dark since the natural rotation of the quartz was cancelled by the double passage of the light through the crystal.

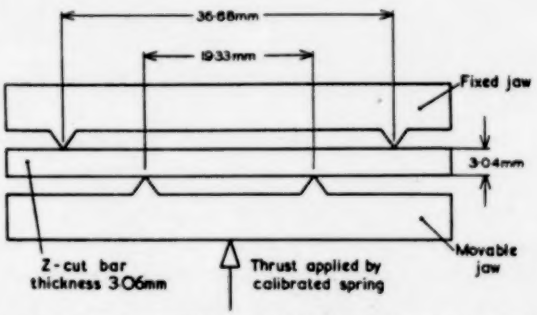

Fig. 2. Apparatus for applying static bending stress to a quartz bar.

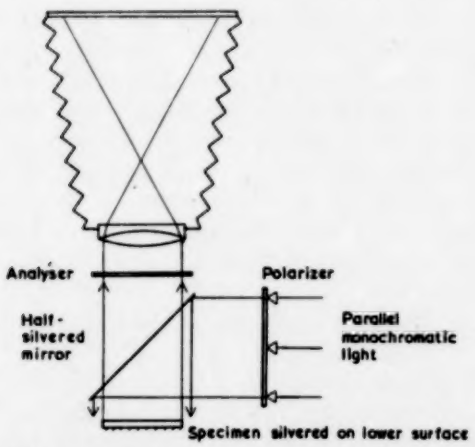

Fig. 3. Optical apparatus for observation of photoelastic stress patterns.

On applying a small stress the field brightened near the edges of the bar. At a slightly higher stress three distinct dark fringes could be seen parallel to the length of the bar, one along the axis and the other two symmetrically on either side. By rotating the bar and its bending jig about the Z-axis the latter fringes could be made to move outwards or, by a reverse rotation, coalesce with the centre fringe.

When the stress was increased still further the first-order isochromat appeared at the extreme edges of the bar. The thrust was increased slightly to a value of approximately 10^7 dyne so that these lay clear of the edges and then a series of photographs was taken in which the applied stress remained constant but the bar had various orientations relative to the polarizer axis. It was noticed that the zero and first-order isochromats at the centre and near the edges respectively retained their position throughout this series and also that the split ' isoclinic ' was approximately symmetrical throughout, although one side of the bar was in compression and the other in tension. Fig. 4 (Plate) shows a photograph of a typical photoelastic stress pattern under these conditions and Fig. 5 an explanatory diagram.

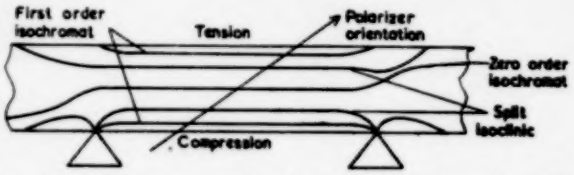

Fig. 5. Photoelastic stress pattern in a statically stressed quartz bar.

In the absence of optical activity there would have been a solitary isoclinic fringe blacking out the whole area over which the stress was substantially parallel to the axis, this being observed when the axis of the bar lay parallel to the polarizer or analyser axis. But from the theory of Sections 3 and 4 there is an effective rotation depending on the stress in the case of an optically active medium and darkness is only attained when there is a certain relation between polarizer orientation, principal stress directions and the magnitude of the stress, namely, that at any point on an isoclinic the stress results in an effective rotation equal to twice the angle between polarizer and analyser axes and the principal stress directions. The stress in a uniformly bent bar increases linearly from zero at the neutral axis to a maximum at the edges and so for a given applied stress and orientation of the bar relative to the polarizer axis the isoclinic fringe consists of two lines parallel to the neutral axis along the lines of appropriate tensile and compressive stress. If the orientation of the bar is altered the fringes move outwards or inwards to the regions of appropriate stress at which the necessary conditions are still fulfilled. Alternatively if the orientation is fixed but the stress is varied the isoclinic fringes move so that they are always in regions of the same stress and therefore the same effective rotation.

Although in this experiment the absolute stress was not known accurately, owing to poor mechanical construction of the bending jig, a graph of rotation against relative stress may be plotted from measurements made on the series of photographs taken under conditions of constant applied thrust. For each effective rotation the distance between the two parts of the isoclinic was measured and taken to be proportional to the stress. Fig. 6 shows these experimental points. The curve is part of Fig. 1 for a thickness of 3·06 mm and has been drawn to pass through the experimental point for which the rotation is 180° and the isoclinic coincides with the first-order isochromat. The values of ϵ relate to the theoretical curve. The agreement between the shapes of the two curves is very good. As the thrust

FIG. 4.

FIG. 4. Photoelastic stress pattern in a statically stressed quartz bar.

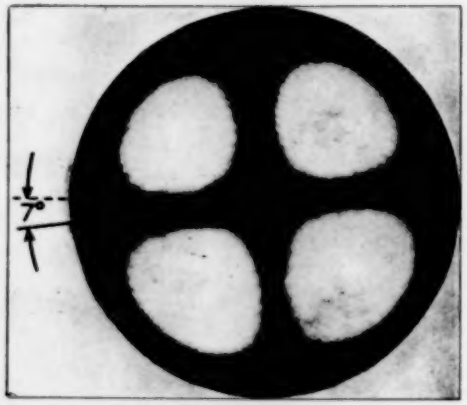

FIG. 7.

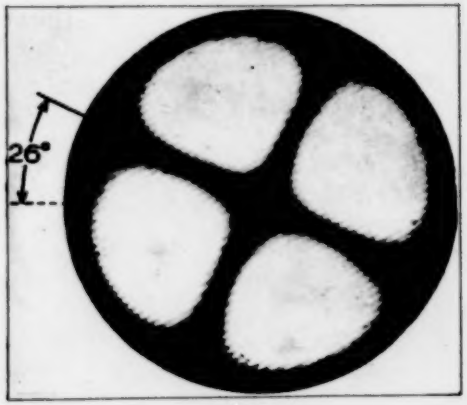

FIG. 8.

FIG. 9.

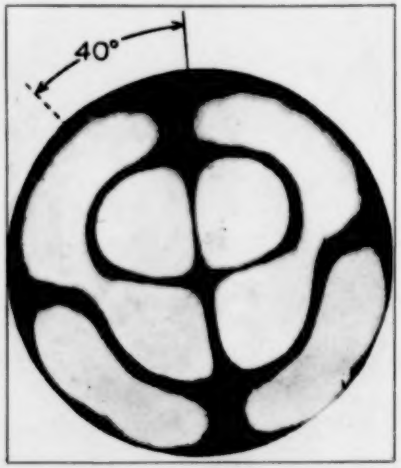

FIG. 10.

FIG. 11

FIGS. 7–11. Photoelastic stress patterns in vibrating quartz disks.

was known to be about 10^7 dyne for this experiment the stress in the region of the first order stress fringes was calculated from the geometry of the bar and the jig to be about $8{\cdot}41 \times 10^8$ dyne cm^{-2}, and it was possible to estimate the value of $\pi_{11} - \pi_{12}$.

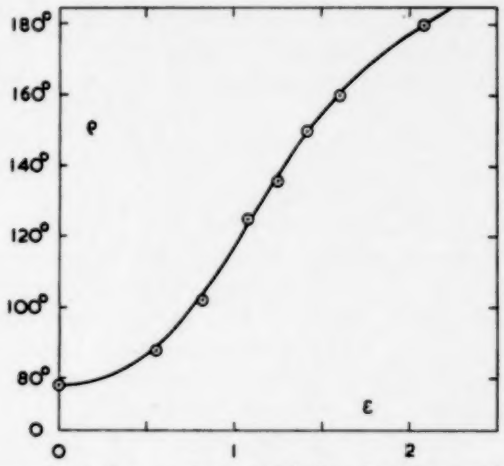

FIG. 6. Dependence of rotation on phase retardation showing experimentally determined points.

From (24)

$$\epsilon = (\delta^2/4\rho^2_0 - 1)^{\frac{1}{2}} \tag{28}$$

and, since $\rho_0 = 78°$ for the specimen used, ϵ is 2·08 for the first-order isochromat. From (23)

$$\eta = \rho_0 a^3_1 Tc/\pi d \tag{29}$$

and substituting in (27) gives

$$\pi_{11} - \pi_{12} = 2\rho_0 a^3_1 Tc\epsilon/(\sigma_p - \sigma_q)\pi d. \tag{30}$$

Taking a value of 1/1·55 for the ordinary velocity and using the experimental values quoted:

$$\pi_{11} - \pi_{12} = 10{\cdot}3 \times 10^{-14} \text{ dyne}^{-1} \text{ cm}^2 \text{ for } \lambda = 5461 \text{ Å}.$$

POCKELS' results give

$$\pi_{11} - \pi_{12} = 13{\cdot}95 \times 10^{-14} \text{ dyne}^{-1} \text{ cm}^2 \text{ for } \lambda = 5893 \text{ Å}$$

which is of the same order of magnitude.

6. PHOTOELASTIC EFFECT IN VIBRATING QUARTZ CRYSTALS

The work described in the previous sections is part of an extensive study of the longitudinal vibrations of thin, circular, *Z*-cut quartz disks, the results of which will be published elsewhere. Some examples are given here, however, to show how the theoretical predictions of Sections 1–3 are borne out in practice. *Z*-cut disks

behave substantially as though isotropic for normal modes of vibration involving a state of plane stress in the XY-plane. The theory of these vibrations in isotropic media has been given by Love (1927).

Of the multitude of modes of this type there are two series of symmetrical modes with simple displacements whose magnitude at any point depends only on the radial coordinate. In one series, type A, the displacements are everywhere along the radius vector while in the other, type B, the displacements are everywhere normal to the radius vector. The principal stresses at any point act along the radius and its normal for type A and at 45° to these directions for type B. In each case the nodes of the longitudinal displacements consist of the centre of the disk together with a number of concentric circles, the number increasing with mode order. Denoting successive modes by integers, including zero, the m^{th} type A mode has m nodes in addition to the centre while the m^{th} type B has $m + 1$. The zero-order isochromat joins points at which the principal stresses are precisely equal. In both types this occurs at the centre and on a series of concentric circles which lie between the nodes, except that there is never one between the centre and the first nodal circle. In the case of the type B modes the outermost circle of the isochromat is the periphery of the disk itself while for type A modes the outermost circle almost coincides with the periphery, except for the $m = 0$ mode.

The quartz disks, all about 2·5 cm diameter and of various thicknesses, were excited into vibration by a potential difference of appropriate frequency applied to six electrodes round the periphery, these being connected alternately in opposite phase so as to produce a field with trigonal symmetry in the XY-plane. The orientation of the crystal axes relative to the electrodes differed for types A and B modes since type A are dilatational modes and require a field along the X-axis while type B are shear modes and require a field along the Y-axis in order to excite suitable stresses. A suitable orientation was easily found by trial in every case. The crystals rested on a glass plate coated with a reflecting layer this being composed of dielectric multilayers to avoid short circuiting the electrodes. In the figures showing the photoclastic stress patterns the polarizer axis is always vertical. Apart from the photoelastic effects interference fringes can be seen in some of the photographs, these being formed by light reflected from the reflecting layer and the two crystal surfaces.

Fig. 7 (Plate) shows the type A, $m = 1$, mode for a crystal which is 0·5 mm thick. The isoclinic cross should have arms parallel to the polarizer and analyser axes but is misorientated by about 7°. The natural rotation of this specimen is 13°. Fig. 8 shows the same mode for a 2 mm thick crystal. The natural rotation of this crystal is 51°, and the misorientation is increased to 26°. The thinner crystal was right-handed, and rotated the light vector anticlockwise when looking in the direction of propagation while the thicker was left-handed so that the misorientations are both in the appropriate direction, that is, the isoclinics correspond to an orientation differing from the polarizer setting by half the natural rotation in the quartz. Fig. 9 shows the type B, $m = 1$, mode for a 0·5 mm thick crystal. The isoclinic cross, whose arms should make an angle of 45° with the polarizer axis, is misorientated by 7° as in the case of Fig. 7.

The radii of the zero-order isochromat circles have been measured on photographs of the 0·5 mm thick specimen for type A and B modes, $m = 0$ to 3. In

every case the radii agreed with the theoretical values to well within the accuracy of the measurements. In spite of this good agreement it is known from multiple-beam interference examination of the surface displacements normal to the plane of the disk that all of these modes are strongly coupled to flexural modes (Tolansky and Wood 1958). However, these flexural displacements do not influence the longitudinal displacements and they do not distort the photoelastic patterns since the stresses involved are antisymmetric about the median plane of the disk and the optical changes due to the stresses in laminae at equal distances on opposite sides of this plane cancel out, to the first order, in a sufficiently thin disk.

Fig. 10 shows the type B, $m = 1$, mode for a 3 mm thick crystal. For this thickness various second-order effects, both elastic and photoelastic, become significant and the stress pattern is correspondingly distorted. It is included, however, to demonstrate the increase of rotation for high stresses. In spite of the distortion it is seen that the isoclinic cross is misorientated by about 40° clockwise, the natural rotation being 78° and the crystal left-handed. Fig. 11 shows the crystal vibrating in the same mode at a much higher amplitude. Those parts of the isoclinic in between the zero-order isochromat have moved still further in the closewise direction indicating an increase in the effective rotation. It is, perhaps, surprising that the displaced isoclinic is so clearly defined, for it is actually moving to and fro at twice the frequency of vibration. The reason is that in the extreme position the isoclinic is momentarily at rest, the intensity of the rest of the field being then at a maximum, and the system acts stroboscopically. In the case of the 0·5 mm thick crystal there was no sign whatever of an increase in rotation with high stress; a 1·0 mm thick crystal showed some signs of increased rotation at stresses just short of the breaking point.

Thus, for thin quartz crystals of this type, the photoelastic stress patterns may be interpreted as though the quartz were isotropic and the stresses static except that the isoclinics correspond to a virtual polarizer setting differing by half the natural rotation in the quartz from the actual setting.

7. Comments on Phenomena Observed by Earlier Workers

(i) *Experiments of* Moens *and* Verschaffelt (1927). A vibrating quartz bar was studied by placing it between polarizer and analyser, so that white light passed along the optic axis, the transmitted light being examined with a spectrometer. The dimensions of the bar were 8, 34 and 12 mm along the X, Y and Z-axes respectively and the bar was excited into longitudinal vibrations along the X-axis at a frequency of about 450 kc/s by electrodes on the X-faces connected to a valve oscillator. Initially there was an extinction band in the spectrum of the transmitted light, due to the rotary dispersion of the quartz along the Z-axis, the position of which depended upon the precise relative setting of polarizer and analyser. Having moved this band to a suitable part of the spectrum the crystal was set into vibration and, as the amplitude was increased, the band was observed to move bodily towards the red end of the spectrum becoming less distinct as it did so. This occurred whatever the initial position of the band and indicated an increased rotation of some tens of degrees as shown by re-orientating the analyser to restore the band to its original position. The authors expressed surprise that the change in rotary power was in a fixed sense for an oscillatory stress. Moreover they stated that

the effect could be produced neither by a uniform compression perpendicular to the Z-axis of a Z-cut specimen nor by an intense electric field.

The change in rotation was clearly a manifestation of the effects discussed in Sections 3 and 4 of this paper which always result in an increase of the effective rotation irrespective of the sign of the stress. It is not possible to comment any more precisely than this since the experimental conditions are not very well described. The light admitted to the spectrometer for instance, was probably collected from a large area of the specimen over which the magnitude of the stress varied considerably. As to their failure to produce the effects by a static mechanical or electrical stress, this was probably due to their failure to appreciate the enormous stresses present in a resonating piezoelectric crystal. They do not mention the dimensions of the specimen used for the static experiments but considering that used for the dynamic experiments, a force of about 200 kg wt would be needed to produce rotations of the order of 20–30° by uniform compression along the X-axis, from the experimental results of Section 5. Using Pockels' data for the electro-optic effect (1890) the same result could be produced by a potential difference of several hundred kilovolts between the X-faces. Evidently they did not go to these extremes although, as seen in Section 5, the necessary stress is easily realized in a suitable specimen by simple bending.

(ii) *Experiment of* Pan Tcheng Kao (1935). It was noticed that the high order modes of a vibrating rectangular Z-cut quartz crystal often had the appearance of a regular array of red and green spots when the crystal was examined in reflexion by white plane polarized light, using a crossed analyser. Now this is the optical arrangement used in the work described in Sections 5 and 6 and so Pan Tcheng Kao was observing, although he did not realize it, the isoclinic patterns corresponding to principal stress directions differing by half the rotation in the quartz from the directions of polarizer and analyser axes. Since white light was used the isoclinic parameter varied for each wavelength, owing to the rotary dispersion of quartz. At any point of the crystal where there was the correct relation between the principal stress directions and the rotation for a particular colour, that colour would be stopped and the complementary colour would show up. Thus the general appearance was that of diffuse isoclinics coloured red on one side and green on the other. Owing to the gridlike nature of the isoclinics for many of the high order modes of a rectangular crystal the colours appear as a regular array of spots.

Acknowledgments

The author is grateful to Professor S. Tolansky for his keen interest and encouragement in this work and to the Department of Scientific and Industrial Research for a maintenance grant.

References

Drude, P.	1905	*The Theory of Optics* (London: Longmans Green).
Love, A. E. H.	1927	*The Mathematical Theory of Elasticity* (Cambridge: University Press).
Moens, R. and Verschaffelt, J. E.	1927	*C.R. Acad. Sci. Paris*, **184**, 1645.
Pan Tcheng Kao	1935	*C.R. Acad. Sci.* Paris, **200**, 563.
Pockels, F.	1889	*Ann. Phys. Lpz.* **28**, 737.
	1890	*N. Jahrb. f. Miner. Beil.* **7**, 224.
Preston, T.	1901	*The Theory of Light* (London: Macmillan).
Tolansky, S. and Wood, A. F. B.	1958	*Physica* **24**, 508.

J. Mech. Phys. Solids, 1960, Vol. 8, pp. 39 to 44. Pergamon Press Ltd., London. Printed in Great Britain

ON THE TORSION OF A THIN-WALL CYLINDER FOLLOWING A PLASTIC EXTENSION*

By H. PAYNE and S. J. CZYZAK
Physics Department, University of Detroit

(*Received 24th August*, 1959)

SUMMARY

THE problem of a thin-wall polycrystalline cylinder subjected to a torsional strain following a plastic tensile strain according to an extension of TAYLOR'S theoretical model has been investigated. Some agreement with experimental results has been obtained.

1. INTRODUCTION

TAYLOR'S model (1938) for calculating the stress–strain relation for a crystalline aggregate in the plastic region following a linear strain path has recently been extended (PAYNE 1959) to include the complete stress–strain relation for a non-linear strain path. To test this modified theory, the problem of a thin-wall cylinder of face-centred cubic polycrystalline material subjected to an incremental torsional strain on an existing tensile or compressive plastic strain has been investigated.

This problem has been studied from another point of view by BATDORF and BUDIANSKY (1949). TAYLOR, to simplify the mathematics, assumed the same strain in each crystal of the aggregate, whereas BATDORF and BUDIANSKY assumed the same stress. TAYLOR'S model leads to a violation of Newton's third law at the grain boundaries, in the plastic region, while BATDORF and BUDIANSKY'S violates the continuity of material. In the former circumstance six or eight slip systems may become active ; in the latter usually only one can become active. The true situation is presumably a compromise between these limiting cases. However, the success of the TAYLOR model in approximating the experimental tensile stress–strain curve for aluminium in the plastic region suggests that it is the more realistic.

2. APPLICATION OF THE THEORY TO THE TORSION PROBLEM

The deviator of the tensile strain tensor of the aggregate at the inception of the torsional strain is represented in the principal axes of the specimen by

$$\epsilon = \epsilon_3 \begin{pmatrix} -\frac{1}{2} & 0 & 0 \\ 0 & -\frac{1}{2} & 0 \\ 0 & 0 & 1 \end{pmatrix}.$$

*Research supported by the Solid State Physics Branch, Office of Air Research, Air Research and Development Command, U.S. Air Force under Contract No. 18 (600) 1466.

TAYLOR's simplifying assumption of uniform strain assigns ϵ to the individual crystal. By transformation it may be referred to the crystalline axes as a function of θ and ϕ, the spherical polar coordinates defining the direction of the cylindrical axis in the crystal. Then the elastic portion of ϵ may be designated by

$$\bar{\epsilon} = (\tau_c/\sqrt{2}\,\mu)\,\mathbf{A}_i, \tag{1}$$

where τ_c is the critical stress, μ is the shear modulus of elasticity, and $\mathbf{A}_i$ (PAYNE 1959) defines on the yield surface of the crystal a vertex which denotes the purely plastic state. Either six or eight slip systems in which slip may occur are associated with the vertex. We designate these by $\alpha = 1, 2 \ldots\ldots m$ ($m = 6$ or 8). The plastic portion may be expressed by

$$\bar{\epsilon} = \sum_{\alpha=1}^{m} g_\alpha\, \mathbf{B}^{(\alpha)},$$

where g_α is $1/\sqrt{2}$ times the slip in the αth system. The $\mathbf{B}^{(\alpha)}$ for face-centred cubic crystals have been listed (PAYNE 1959) and are selected as to sense such that $g_\alpha \geqslant 0$.

The differential torsional strain, which becomes simple shear in a thin-wall cylinder, may be represented by

$$d\epsilon = d\gamma_{13}\begin{pmatrix} 0 & 0 & 1 \\ 0 & 0 & 0 \\ 1 & 0 & 0 \end{pmatrix} \tag{2}$$

in the principal axes of the specimen. Referred to the crystalline axes, $d\epsilon$ becomes a function of the Eulerian angles θ, ϕ and ψ, which describe the orientation of the cylinder with respect to the crystal. By neglecting the small effect produced by workhardening during the torsional strain, i.e., by assuming $d\tau_c = 0$, the conditions imposed on the elastic and plastic components of $d\epsilon$ may be expressed in the notation of PAYNE (1959):

$$d\epsilon + d\bar{\epsilon} = d\epsilon, \tag{3a}$$

$$\mathbf{B}^{(\alpha)} \cdot d\epsilon \leqslant 0 \quad \text{for} \quad \alpha \leqslant m, \tag{3b}$$

$$d\bar{\epsilon} = \sum_{\alpha=1}^{m} dg_\alpha\, \mathbf{B}^{(\alpha)}, \tag{3c}$$

with

$$dg_\alpha \geqslant 0, \tag{4a}$$

$$dg_\alpha\, \mathbf{B}^{(\alpha)} \cdot d\epsilon = 0. \tag{4b}$$

The set of active systems, $\alpha = 1, 2, \ldots\ldots m$, as a function of θ and ϕ for the crystals of the aggregate under simple tension (or compression) has been determined by BISHOP (1953). Of the 44 sets of values of θ and ϕ employed by TAYLOR, we found that it was sufficient for our calculations to use 37, since these results were practically the same as those for 27. For each such direction the values of ψ were selected at 30° intervals. For each choice of θ, ϕ and ψ relations (3) and (4) were solved for the given $d\epsilon$ according to the following procedure:

1. Determine $d\epsilon \cdot \mathbf{B}^{(\alpha)}$ for $\alpha = 1, 2, \ldots\ldots m$. Let the system for which the maximum value is attained be designated $\alpha = 1$. Then, if $d\epsilon \cdot \mathbf{B}^{(1)} \leqslant 0$, relations (3) and (4) are satisfied by $d\epsilon = d\epsilon$ and $d\bar{\epsilon} = 0$.

2. However, if $d\epsilon \cdot \mathbf{B}^{(1)} > 0$, let $d\epsilon_1 = d\epsilon - d\mu_1 \mathbf{B}^{(1)}$ with $d\mu_1$ of such magnitude that $d\epsilon_1 \cdot \mathbf{B}^{(1)} = 0$. Then, determine $d\epsilon_1 \cdot \mathbf{B}^{(\alpha)}$ for $\alpha = 2, 3, \ldots, m$. Assume that the maximum value is attained for $\alpha = 2$. If $d\epsilon_1 \cdot \mathbf{B}^{(2)} \leqslant 0$, relations (3) and (4) are satisfied by $d\bar{\epsilon} = d\epsilon_1$, $d\bar{\bar{\epsilon}} = d\mu_1 \mathbf{B}^{(1)}$.

3. However, if $d\epsilon_1 \cdot \mathbf{B}^{(2)} > 0$, let $d\epsilon_2 = d\epsilon_1 - d\mu_2 \mathbf{B}^{(2)} - d\nu_1 \mathbf{B}^{(1)}$ with $d\mu_2$ and $d\nu_1$ of such magnitudes that $d\epsilon_2 \cdot \mathbf{B}^{(1)} = 0 = d\epsilon_2 \cdot \mathbf{B}^{(2)}$. Then, determine $d\epsilon_2 \cdot \mathbf{B}^{(\alpha)}$ for $\alpha = 3, 4, \ldots, m$. Assume that the maximum value is attained for $\alpha = 3$. If $d\epsilon_2 \cdot \mathbf{B}^{(3)} \leqslant 0$, relations (3) and (4) are satisfied by $d\bar{\epsilon} = d\epsilon_2$ and $d\bar{\bar{\epsilon}} = (d\mu_1 + d\nu_1)\, \mathbf{B}^{(1)} + d\mu_2 \mathbf{B}^{(2)}$ (if $d\mu_1 + d\nu_1 \geqslant 0$, $d\mu_2 \geqslant 0$).

4. However, if $d\epsilon_2 \cdot \mathbf{B}^{(3)} > 0$, continue this process until it is determined that $d\bar{\epsilon} = d\epsilon_n$ for $n < 5$ or $d\epsilon_4 \cdot \mathbf{B}^{(5)} > 0$. The latter would indicate that $d\bar{\epsilon} = 0$ and $d\bar{\bar{\epsilon}} = d\epsilon$.

The results for $\theta = 60°$, $\phi = 45°$, referred to the principal axes of the specimen, are presented in Tables 1 and 2. Tables for other orientations are given in the

TABLE 1. *Elastic strain tensor* $d\bar{\epsilon}$ *referred to cylinder axes at* 30° *intervals of* ψ *for* $\theta = 60°$ *and* $\phi = 45°$

ψ \ $d\bar{\epsilon}_{ij}/d\gamma_{13}$	$d\bar{\epsilon}_{11}/d\gamma_{13}$	$d\bar{\epsilon}_{22}/d\gamma_{13}$	$d\bar{\epsilon}_{33}/d\gamma_{13}$	$d\bar{\epsilon}_{12}/d\gamma_{13}$	$d\bar{\epsilon}_{23}/d\gamma_{13}$	$d\bar{\epsilon}_{31}/d\gamma_{13}$
0°	0·1082	0·4328	− 0·5412	0	0	0·5625
30°	0·2306	0·2474	− 0·4781	− 0·1949	0·1906	0·4341
60°	0·4599	0	− 0·4605	0·0190	− 0·0160	0·3059
90°	0·1571	0·2355	− 0·3929	0·2406	− 0·2722	0·4723
120°	− 0·0531	0·4741	− 0·4210	0·0458	− 0·0734	0·7004
150°	0·1575	0·2709	− 0·4285	− 0·2801	0·1065	0·6398
180°	0·4939	0	− 0·4939	0	0	0·5777
210°	0·1575	0·2709	− 0·4285	0·2801	0·1065	0·6398
240°	− 0·0531	0·4741	− 0·4210	− 0·0458	0·0734	0·7004
270°	0·1571	0·2355	− 0·3929	− 0·2406	0·2722	0·4723
300°	0·4599	0	− 0·4605	− 0·0190	0·0160	0·3059
330°	0·2306	0·2474	− 0·4781	0·1949	− 0·1936	0·4341

TABLE 2. *Plastic strain tensor* $d\bar{\bar{\epsilon}}$ *referred to cylinder axes at* 30° *intervals of* ψ *for* $\theta = 60°$ *and* $\phi = 45°$

ψ \ $d\bar{\bar{\epsilon}}_{ij}/d\gamma_{13}$	$d\bar{\bar{\epsilon}}_{11}/d\gamma_{13}$	$d\bar{\bar{\epsilon}}_{22}/d\gamma_{13}$	$d\bar{\bar{\epsilon}}_{33}/d\gamma_{13}$	$d\bar{\bar{\epsilon}}_{12}/d\gamma_{13}$	$d\bar{\bar{\epsilon}}_{23}/d\gamma_{13}$	$d\bar{\bar{\epsilon}}_{31}/d\gamma_{13}$
0°	− 0·1083	− 0·4331	0·5413	0	0	0·4376
30°	− 0·2310	− 0·2473	0·4782	0·1949	− 0·1903	0·5662
60°	− 0·4606	0	0·4610	− 0·0196	0·0163	0·6939
90°	− 0·1572	− 0·2355	0·3927	− 0·2405	0·2723	0·5277
120°	0·0532	− 0·4742	0·4209	− 0·0458	0·0735	0·2996
150°	− 0·1578	− 0·2709	0·4283	0·2801	0·1064	0·3603
180°	− 0·4938	0	0·4937	0	0	0·4223
210°	− 0·1578	− 0·2709	0·4283	− 0·2801	0·1064	0·3603
240°	0·0532	− 0·4742	0·4209	0·0458	− 0·0735	0·2996
270°	− 0·1572	− 0·2355	0·3927	0·2405	− 0·2723	0·5277
300°	− 0·4606	0	0·4610	0·0196	− 0·0163	0·6939
330°	− 0·2310	− 0·2473	0·4782	− 0·1949	0·1903	0·5662

ASTIA Reports (1957, 1958). The $d\varepsilon$ were averaged first with respect to ψ and then with respect to the set of values of θ and ϕ lying within a zone ; the zone is a locus of directions for which the same set of slip systems become active — or for which the same vertex on the yield surface is reached — during a plastic tensile strain. Then, with Ω_i representing the solid angle subtended by the ith zone and $d\varepsilon_i$ representing the average of $d\varepsilon$ over the selected values of θ and ϕ within this zone as well as of ψ, $d\varepsilon_{av}$, the average $d\varepsilon$ over the specimen, was obtained from the relation

$$\sum_i \Omega_i \, d\varepsilon_i = \Omega \, d\varepsilon_{av},$$

where

$$\Omega = \sum_i \Omega_i.$$

The result,

$$d\varepsilon_{av} = d\gamma_{13} \begin{pmatrix} 0{\cdot}1953 & -0{\cdot}0013 & 0{\cdot}5771 \\ -0{\cdot}0013 & 0{\cdot}1953 & 0{\cdot}0015 \\ 0{\cdot}5771 & 0{\cdot}0015 & -0{\cdot}3906 \end{pmatrix},$$

represents the deviator of the elastic strain tensor for the aggregate under torsion. To it must be added the hydrostatic component $d\eta\,\mathbf{I}$, where $\mathbf{I}$ represents the unit matrix.

From the theory of elasticity the corresponding stress on the specimen becomes

$$d\mathbf{S} = 2\mu \left(d\varepsilon_{av} + \frac{1+\rho}{1-2\rho} \, d\eta \, \mathbf{I} \right), \tag{5}$$

where ρ is Poisson's ratio. For

$$d\eta = -0{\cdot}1953 \left(\frac{1-2\rho}{1+\rho} \right) d\gamma_{13}$$

the condition that the tensile components of $d\mathbf{S}$ normal to the cylindrical axis vanish is satisfied. Setting $\rho = \frac{1}{3}$ for aluminium and substituting the resulting value for $d\eta$ in equation (5) gives $d\mathbf{S}$ in the desired form

$$d\mathbf{S} = \begin{pmatrix} 0 & 0 & d\tau_{13} \\ 0 & 0 & 0 \\ d\tau_{13} & 0 & d\sigma_3 \end{pmatrix}, \tag{6}$$

where

$$\frac{d\tau_{13}}{d\gamma_{13}} = 1{\cdot}154\,\mu \tag{7a}$$

$$\frac{d\sigma_3}{d\tau_{13}} = -1{\cdot}015. \tag{7b}$$

The addition of the hydrostatic component $d\eta\,\mathbf{I}$ to $d\varepsilon$ changes the elongation along the axis of the specimen. Since it was desired to determine the stress producing a torsional strain unaccompanied by such an elongation change, the above computations were repeated for three sets of values of θ and ϕ in different zones substituting for $d\varepsilon$ in (2) the expression

$$\begin{pmatrix} -\frac{1}{2}\,d\eta & 0 & d\gamma_{13} \\ 0 & -\frac{1}{2}\,d\eta & 0 \\ d\gamma_{13} & 0 & d\eta \end{pmatrix},$$

which overcorrects for the effect of the hydrostatic component. However, in none of these instances did a significant change in the value of $d\bar{\varepsilon}$ averaged over ψ occur. Consequently, we concluded that equations (6) and (7) suffice to represent the stress which, according to the model of this paper, produces the torsional strain $d\gamma_{13}$ – with a contraction of the specimen in the plane normal to the cylindrical axis – following a tensile stress σ_3 into the fully plastic region.

According to the model under consideration both $d\tau_{13}/d\gamma_{13}$ and $d\sigma_3/d\tau_{13}$ are constant for increasing torsional strain until a point on the yield surface of one of the crystals is reached at which one of the previously inactive systems ($\alpha > m$) becomes active. For the $\mathbf{B}^{(\alpha)}$ representing this system, it is readily shown (Payne 1959) that $\mathbf{B}^{(\alpha)} \cdot \mathbf{A}_i = 0$, where $\mathbf{A}_i$ designates the vertex occupied by the particular crystal just prior to the torsional strain. Then, for this system to become active, it is necessary that $\delta\bar{\varepsilon} \cdot \mathbf{B}^{(\alpha)} = \tau_c/\sqrt{2}\,\mu$. From equation (1) and the relations $\sqrt{5/2} \leqslant |\mathbf{A}_i| \leqslant \sqrt{6}$ and $|\mathbf{B}^{(\alpha)}| = 1$, it is apparent that under this circumstance $|\delta\bar{\varepsilon}| \sim |\bar{\varepsilon}|$ and, therefore, $\delta\tau_{13} \sim \sigma_3$. This model, then, predicts a linear relationship between (a) the tensile and torsional components of the stress that is required to produce a torsional strain and (b) the torsional stress component and resulting strain. The slopes of the curves are given by equation (7). This relationship is maintained until the torsional stress component exceeds a value of the order of magnitude of the tensile stress at the start of the torsional strain.

3. A Comparison of Theoretical and Experimental Results

The experimental results reported by Peters *et al.* (1949) appear to be the only ones to which these conclusions may be compared. A thin-wall cylinder of polycrystalline aluminium alloy was subjected first to compression beyond the elastic limit and then to torsion with no further change in the axial dimension.

Although the maximum torsional stress (12 k.s.i.) was substantially smaller than the tensile stress (32 k.s.i.) in effect at the beginning of the torsional strain, the $\delta\tau_{13}$ vs. $\delta\gamma_{13}$ curve is nonlinear. The quantity $d\tau_{13}/d\gamma_{13}$ approaches the elastic value $2\,\mu$ at $\delta\tau = 0$, but attains what appears to be a nearly uniform value of about $1{\cdot}35\,\mu$ for $\delta\tau_{13} > 8$ k.s.i. Furthermore, the $\delta\sigma_3$ vs. $\delta\tau_{13}$ curve is nonlinear, with $d\sigma_3/d\tau_{13}$ varying from about $\frac{1}{4}$ for $\delta\tau_{13} = 0$ to about $\frac{4}{5}$ for $\delta\tau_{13} > 8$ k.s.i. Thus, the experimental values of both $d\tau_{13}/d\gamma_{13}$ and $d\sigma_3/d\tau_{13}$ come into approximate agreement with our predictions, but only after a torsional stress approximately one fourth the tensile stress in effect at its inception is reached.

In attempting to account for this discrepancy for $\delta\tau_{13} < \frac{1}{4}\,\sigma_3$, it should first be noted that at the start of the torsional strain in the experiment the ratio of the axial compressive stress σ_3 to the axial compressive strain was $0{\cdot}80\,E$, where E represents Young's modulus. Thus, the plastic component constituted only one fifth of the total strain. Previous calculations of the tensile stress–strain relation for a face-centred cubic polycrystal (Payne *et al.*, 1958) indicate that the model under consideration requires a much larger ratio of the plastic to the total strain

to ensure that in nearly every crystal a vertex on its yield surface is reached. Accordingly, if the torsional strain were begun before a given crystal had achieved its vertex, fewer slip systems would be available for the plastic component of the torsional strain than assumed in the above analysis. This would require a greater initial stiffness in torsion. The additional slip systems would become active after a torsional stress amounting to a fraction of σ_3 since, although the vertex had not been attained, its approach must have rendered to these additional systems resolved shear stresses constituting substantial fractions of the critical stress.

Such a qualitative explanation of the discrepancy receives some support from the results of two other measurements performed by these investigators. The latter experiments differed from the first in that the axial load, rather than the elongation, was maintained constant during the torsion. Although the results cannot be compared quantitatively to those of this paper, they do show the initial stiffness in torsion disappearing for successively smaller values of $\delta\tau_{13}$ as the ratio of the axial compressive stress to the corresponding strain prior to the torsion was reduced first to $0{\cdot}74E$ and then to $0{\cdot}44E$.

However, it is believed that a more realistic model (i.e. than the one using the assumption of the same strain in each crystal) would not show the vertex of the yield surface attained in each crystal no matter how large the plastic component of the tensile strain. This would follow, as mentioned earlier, in order to satisfy the conditions imposed on the stress at the grain boundaries. (Presumably, the strain would not be uniform over the grain. This would require a device such as the consideration of an average strain for a crystal or a uniform strain over only a portion thereof). Hence, greater initial stiffness in torsion than predicted by the model presented in this paper would be expected.

REFERENCES

BATDORF, S. B. and BUDIANSKY, B.	1949	*NACA Tech.* Note No. 1871.
BISHOP, J. F. W.	1953	*Phil. Mag.* **43**, 51.
PAYNE, H.	1959	*J. Mech. Phys. Solids* **7**, 126.
PAYNE, H., CZYZAK, S. J., GREINER, J. and LIN, T. H.	1958	*J. Mech. Phys. Solids* **6**, 314.
PAYNE, H., CZYZAK, S. J. and LUCAS, W.	1957	AFOSR TR 57-61 ASTIA AD – 136 545. Armed Services Technical Information Agency, Arlington 12, Va. U.S.A.
PAYNE, H. and CZYZAK, S. J.	1958	AFOSR TR 57-61 ASTIA AD – 232 000. Armed Services Technical Information Agency, Arlington 12, Va. U.S.A.
PETERS, R. W., DOW, F. and BATDORF, S. B.	1949	*Proc. Soc. Exp. Stress Anal.* **7** (No. 2), 127.
TAYLOR, G. I.	1938	*J. Inst. Metals* **62**, 307.

J. Mech. Phys. Solids, 1960, Vol. 8, pp. 45 to 51. Pergamon Press Ltd., London. Printed in Great Britain

STEADY-STATE CREEP OF TIN NEAR THE MELTING POINT*

By W. A. Zama†, D. D. Lang‡ and F. R. Brotzen†

(*Received 26th August*, 1959)

Summary

The steady-state creep rates of commercial tin were investigated at temperatures between 180 and 230 °C. Torsional creep equipment was developed for this purpose. At temperatures below 215 °C results indicate that the steady-state creep process is one governed by a single activation energy of 22,500 cal/mole. At higher temperatures, however, the simple Arrhenius-type equation cannot properly express the creep behaviour.

1. Introduction

Virtually all investigations of metallic creep have been limited to temperatures well below the melting point of the materials. Only a few reports in the literature cover studies of mechanical properties at temperatures higher than 95 per cent of the absolute melting point. Yet even these few investigations were restricted to relatively low stresses. It was thought, therefore, that an investigation of steady-state creep under the combined influence of high stresses and of temperatures approaching the melting point would test the range of validity of presently accepted creep concepts.

Tin was chosen as the material for this investigation primarily because of experimental convenience. Its low melting temperature and ready availability are particularly desirable features. Furthermore, creep data for tin over wide temperature ranges have been published and permit comparison with experimental results obtained in this investigation.

In most metals the activation energies of steady-state creep correspond to the activation energies of self-diffusion. In tin, however, a relatively low creep activation energy seems to prevail at low temperatures and a relatively high one at temperatures above 130 °C (Breen and Weertman 1955, 1956). The latter is substantially greater than the activation energy for self-diffusion determined through radioactive tracer techniques by Fensham (1950). Weertman and Breen (1956) arrived at the conclusion that these activation energies could be reconciled with self-diffusion activation energies if Zener's ring mechanism were to play a part in the self-diffusion process.

*This research was carried out under the sponsorship of Army Ballistic Missile Agency, U.S. Army Ordnance contract No. DA-23-072-ORD-1167.

†The Rice Institute, Houston, Texas.

‡Formerly at the Rice Institute; present address—Chance-Vought Aircraft Co., Dallas, Texas.

At very high temperatures and under the influence of high stresses it becomes exceedingly difficult to discern the various mechanisms that may contribute to the creep rate. Among the processes that might contribute substantially to the deformation are (1) slipless deformation through movement of point defects; (2) grain-boundary slip; (3) dislocation climb. An effort will be made to discuss the results in the light of these basic possibilities.

2. Equipment and Procedure

Specimens were tested in torsion. This eliminated variation of cross-section during the test and simplified the maintenance of a uniform temperature along the length of the specimen. The specimens were heated in a small resistance furnace (Fig. 1) which was operated at constant current. The furnace was surrounded by a constant-temperature oil bath to isolate it from external temperature variations. With this equipment it was possible to reduce temperature fluctuations to a maximum of 0·3 °C with less than 0·3 °C variation along the entire length of the specimen. All temperature measurements were made in the centre of the specimen with a calibrated copper-constantan thermocouple and a Leeds and Northrup potentiometer.

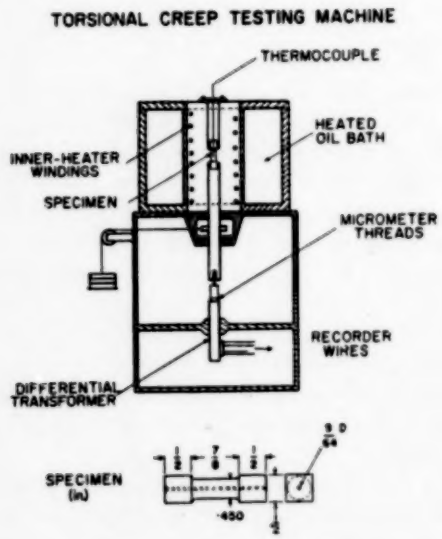

Fig. 1. Torsional creep-testing machine and specimen.

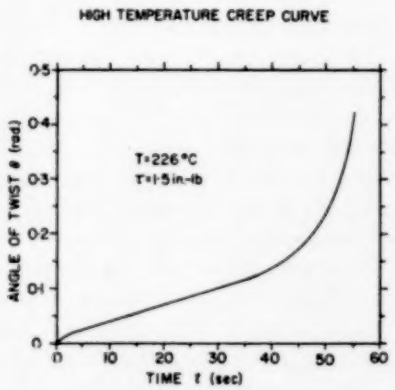

Fig. 2. Typical high-temperature creep curve at constant torque.

A constant torque was applied to the specimen through a weight and pulley. The angular deformation produced by the torque was converted into linear motion by a micrometer screw. The latter moved the core of a differential transformer which, in turn, activated a Sanborn recorder. This instrument recorded the angle of twist as a function of time with a maximum sensitivity of 0·05 rad. at full-scale deflexion, 5 cm, on the recorder chart. The equipment was calibrated prior to each test.

The specimens were prepared by casting commercial tin in steel moulds. They were then machined to the dimensions given in Fig. 1. Spectrographic analysis of a number of specimens revealed them to be of 99·80 per cent purity, with the following major impurities: (Found Pb, 0·51; Sb, 0·09; and As 0·06%). All specimens were annealed at 224 °C for 20 min and air cooled. The resulting grain size varied from 50 to 200 grains per cm^2.

In carrying out the experiments the specimens were placed into the furnace and allowed to reach the testing temperature. The load was applied gradually. Test runs lasted anywhere from 20 sec to 1 hr. A typical high-temperature creep curve obtained in this manner is illustrated in Fig. 2.

Since the results obtained by this method were expressed in terms of the angle of twist as a function of time at constant torque, it was necessary to convert the data into conventional terms of strain and stress. Under the assumption that the deformation was one of pure torsion, an equation was developed (see Appendix) by means of which the shear stress at the surface of the specimen could be calculated. It was found that a constant torque was equivalent to a constant stress.

3. Results

At temperatures below about 215 °C the steady-state creep rates at constant torques followed closely the established relation

$$\dot{\epsilon} = S(\sigma) \exp(-Q/RT) \tag{1}$$

where $\dot{\epsilon}$ = creep rate, $S(\sigma)$ = a stress-dependent constant, Q = heat of activation, R = universal gas constant and T = absolute temperature. For this temperature range Q was 22·5 ± 1·0 kcal/mole as computed from the data in Fig. 3.

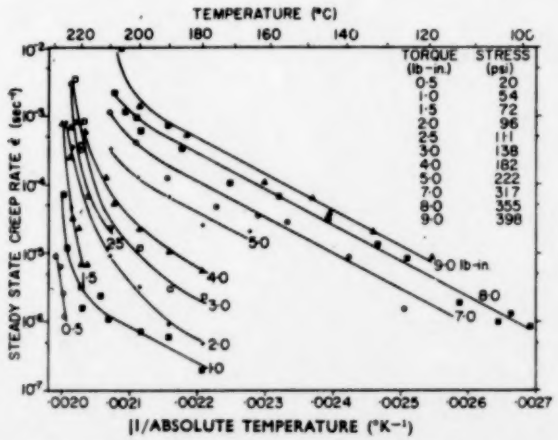

Fig. 3. Plot of the steady-state creep rate vs. reciprocal of absolute temperature at different torques.

This is in good agreement with the findings of several investigators: Frenkel *et al.* (1955) found Q = 21·0 ± 2·0 kcal/mole while Wiseman *et al.* (1957) found Q = 23·0 kcal/mole. Weertman and Breen (1956) and Weertman (1957),

whose observations were made with tin single crystals, observed $Q = 22{\cdot}0$ kcal/mole. At temperatures below 215 °C the heat of activation appeared to be independent of stress, strain and temperature, as is usual with creep of metals (Dorn 1955).

At temperatures above 215 °C the results indicated that the Arrhenius-type equation (1) is no longer applicable. Judging from the high-temperature portions of the curves in Fig. 3, the process can no longer be viewed as one having a single activation energy. The slope of the curves tends toward very high values as the melting point is approached. The only other creep results in that temperature region with polycrystalline tin were those by Breen and Weertman (1955). The few data collected by those authors in the range near the melting point are not sufficient to corroborate or contradict the results given in Fig. 3.

The creep curves observed at high temperatures still exhibited a definite linear portion (Fig. 2). Yet, as the temperature was increased, this steady-state creep portion tended to take up an increasingly smaller part of the entire creep curve. In the immediate vicinity of the melting point, i.e., at 228 °C, it became very difficult to distinguish between secondary and tertiary creep.

Creep rates at constant temperatures, as a function of stress, are shown in Fig. 4. The data for this diagram were obtained from the curves in Fig. 3, since it was not convenient to perform tests for different torques at exactly the chosen temperatures. By and large, the exponential expression by Dorn (1955),

$$\dot{\epsilon} = A\,(T)\,\sigma^n, \tag{2}$$

is consistent with the results given in Fig. 4. In this equation $A\,(T) =$ temperature-dependent constant, $\sigma =$ the applied shear stress. The values for the exponent

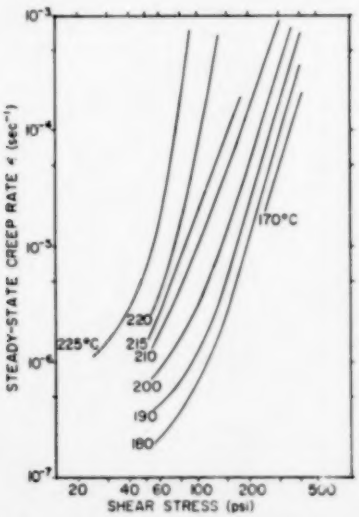

Fig. 4. Logarithmic plot of steady-state creep rate vs. shear stress at different temperatures.

n varied between 4·5 and 5·0 at temperatures up to 215 °C; and appeared to reach higher values at temperatures above 215 °C, Breen and Weertman (1955) found the exponent to be about 4·6. Attempts were made to extend the observations

of the stress-creep relationship in a more definite way to temperatures close to the melting point. This was not possible because steady-state creep data could be obtained for only very small torques. Higher torques were precluded by the extremely short duration of the high-temperature runs.

4. Discussion

The results obtained with tin at temperatures below about 215 °C, summarized in Figs. 3 and 4, confirm the observations made by other investigators. On the other hand, the departure from normal behaviour at higher temperatures is striking and stimulates speculation as to the possible underlying causes.

It has been postulated by Nabarro (1948) and Herring (1950) that the movement of point defects could account for creep. According to Herring, such a mechanism leads to a linear stress dependence of the creep rate. If such a mechanism were to become pronounced at high temperature, it would lead to an apparent lowering of the stress exponent n in (2). This was clearly not the case; indeed, the exponent appears to be greater than 5 at temperatures above 215 °C. Moreover, the Nabarro-Herring mechanism requires a temperature dependence which parallels that of the self-diffusion coefficient of tin. As mentioned earlier, the activation energy for self-diffusion in tin is substantially lower than that for steady-state creep. The observations made here, however, point toward a rapidly increasing energy of activation at elevated temperatures. The Nabarro-Herring mechanism therefore cannot account for the anomaly in the creep behaviour observed near the melting point of tin.

It is conceivable that, at very high temperatures, grain boundary slip could contribute to the overall deformation in such a manner as to increase the total strain-rate. In such a case the creep-rate at constant torque would be the sum of the creep-rate $\dot{\epsilon}_{LT}$ extrapolated from temperatures below 215 °C and of the creep rate $\dot{\epsilon}_{HT}$ due to an additional process, such as grain boundary slip. Thus,

$$\dot{\epsilon}_{HT} = \dot{\epsilon}_{Total} - \dot{\epsilon}_{LT}. \tag{3}$$

By using the observed data for $\dot{\epsilon}_{Total}$ and extrapolating the data $\dot{\epsilon}_{LT}$ to temperatures above 215 °C, this approach yields the relation

$$\dot{\epsilon}_{HT} = B \exp(-Q'/RT) \tag{4}$$

where B is a constant depending on the applied torque, and Q' is the activation energy of the high-temperature process. Q' has the unusually high value of 60–70 kcal/mole. In view of the difficulty of obtaining precise creep data at these very high temperatures it cannot be said with certainty that Q' is independent of applied torque. Nevertheless, the observed activation energy is much higher than that reported by Puttick and King (1952) for boundary slip in bicrystals of tin, namely 19·0 kcal/mole. Even the higher degree of impurity in the material used in this investigation compared to that of Puttick and King can hardly account for the differences in activation energies.

Weertman and Breen (1956) speculated that immobile Lomer dislocations might be formed in tin. This would make it possible to apply the analysis by Weertman (1955) of dislocation climb to creep in tin. Such sessile dislocations might break down under the combined effects of high temperature and stress

(STROH 1956). Should this take place, the effective length of piled-up groups of dislocations would increase. According to WEERTMAN's formulation the creep-rate should be proportional to the square of this length, so that the breakdown of sessile dislocations would enhance the creep-rate. In view of the uncertainty of this hypothesis it would be idle to attempt a quantitative analysis.

5. CONCLUSIONS

(1) The steady-state torsional creep of commercial tin is dominated by a process requiring a single activation energy up to about 215 °C. At higher temperatures an increasingly rapid rise of the creep rate is observed.

(2) The activation energy at temperatures below 215 °C was found to be 22·5 $\pm$ 1·0 kcal/mole, in good agreement with data obtained by methods other than torsion.

(3) The stress dependence of the creep rates follows an exponential law of the type $\dot{\epsilon} = A(T)\,\sigma^n$ at temperatures below 215 °C. It continues to do so at higher temperatures, though with larger values of the exponent n.

ACKNOWLEDGMENTS

The authors wish to acknowledge gratefully the assistance of Mr. J. R. BAKER and Mr. J. E. MERWIN in carrying out this research.

REFERENCES

BREEN, J. E. and WEERTMAN, J. 1955 *J. Metals* **7**, 1230.
DORN, J. E. 1955 *J. Mech. Phys. Solids*, **3**, 85.
FENSHAM, P. J. 1950 *Australian J. Sci. Res.* **3**, 91.
FRENKEL, R. E., SHERBY, O. D. and DORN, J. E. 1955 *Acta Met.* **3**, 470.
HERRING, C. 1950 *J. Appl. Phys.* **21**, 437.
HOFFMAN, O. and SACHS, G. 1953 *Introduction to the Theory of Plasticity for Engineers*, p. 137. (McGraw-Hill).
NABARRO, F. R. N. 1948 *Report on a Conference on the Strength of Solids*, 75-90. (Physical Society, London).
PUTTICK, K. E. and KING, R. 1952 *J. Inst. Metals* **80**, 537.
STROH, A. N. 1956 *Phil. Mag.* **1**, 489.
WEERTMAN, J. 1955 *J. Appl. Phys.* **26**, 1213.
1957 *Ibid.*, **28**, 196.
WEERTMAN, J. and BREEN, J. E. 1956 *J. Appl. Phys.*, **27**, 1189.
WISEMAN, C. D., SHERBY, O. D. and DORN, J. E. 1957 *J. Metals* **9**, 37.

APPENDIX

Consider a section of the cylindrical portion of the specimen. Let σ_r be the shear stress at a distance r from the axis due to a torque τ. During steady-state creep at a constant temperature T and creep rate $\dot{\theta}$ assume that (i) σ_r is a function of r and $\dot{\theta}$ only; (ii) planes perpendicular

to the axis remain plane. Due to the constraints on the ends of the specimen, the following formulae may be used to compute the strain ϵ and strain rate $\dot{\epsilon}$.

$$\epsilon = r\theta/L, \quad \dot{\epsilon} = r\dot{\theta}/L. \tag{5}$$

Following a derivation similar to that of Ludwik (Hoffman and Sachs 1953) it may be shown that

$$\sigma_b - \sigma_a (a/b)^3 = \left(\theta \frac{\partial \tau}{\partial \theta} + 3\tau\right) \Big/ 2\pi b^3 \tag{6}$$

where σ_a and σ_b are the stresses at the inner and outer radii of the specimen. Since the stress σ_a near the axis of the specimen cannot exceeed the stress σ_b on an outer fibre, and since $(a/b)^3 \ll 1$, $\sigma_a (a/b)^3$ may be neglected compared to σ_b. This gives the formula used to compute the stresses shown in Fig. 3:

$$\sigma = \sigma_b = \left(\theta \frac{\partial \tau}{\partial \theta} + 3\tau\right) \Big/ 2\pi b^3. \tag{7}$$

Tests were run at different values of τ and T so that a curve of τ vs. $\ln \dot{\theta}$ could be plotted. The slope gives the first term in the numerator of (7). At a given torque it was observed that $\dot{\theta}\, \partial\tau/\partial\dot{\theta}$ was essentially constant and had a value close to 1·0 lb-in. Any variation in the stress computed for a given torque in this manner was negligible so that, for all practical purposes, a constant torque gave a constant stress at all temperatures tested.

J. Mech. Phys. Solids, 1960, Vol. 8, pp. 52 to 65. Pergamon Press Ltd., London. Printed in Great Britain

GRAPHICAL ANALYSIS OF THE FORMATION OF SHOCK FRONTS IN MATERIALS

By Shoi-Yean Hwang and N. Davids
Dept. of Engineering Mechanics, Pennsylvania State University

(*Received* 31*st August*, 1959)

Summary

Contour-plotting methods are applied to non-linear materials with a two-straight-line stress–strain relation, such as certain types of rubber or foam plastic. The multiple scabbing phenomenon of materials due to tensile reflexion from a free boundary is analysed and presented graphically. General rules governing the structure of the characteristics field are obtained.

1. Introduction

This paper extends the one-dimensional graphical method, as described by Kumar and Davids (1958) for analysing stress-wave propagation effects, to the study of the formation of shock fronts under non-linear stress–strain behaviour of the material. When such behaviour is present, additional complicating factors arise; essentially these phenomena are classified according as the wave-velocity under high loading is smaller or larger than under low loading. In the former case a trailing plastic wave is known to result, while in the latter shock fronts tend to be formed analogous to those which have received intensive study in fluids. In this paper we shall discuss first these general conditions in more detail; then show by means of examples and plots how these fronts are formed and how they interact, after successive reflexions from boundaries, with each other and with different kinds of waves.

Graphical analyses have been applied to various wave problems by De Juhasz (1949), Lee (1953), Karman and Duwez (1950), Lee and Tupper (1954), Malvern (1951), White and Griffis (1948), and others.

2. Stress–Strain Wave Effects

It is known that stress–wave phenomena depend basically on whether the stress–strain diagram for the material is concave down or concave up. In the former case, the slope $d\sigma/d\epsilon$ decreases as the stress and strain increases. This implies that large strains are propagated with lower velocity. In the latter case the situation is just reversed, and shock fronts may appear, as will be seen. For example, raw rubber (Houwink and Burgers 1953), soft rubber (Marin and Sauer 1954) and foam plastic have either concave upward stress–strain curves or even combination concave up followed by convex up (Fig. 1). For foam plastic

or raw rubber the stress–strain relation is convex upward, and hence $d\sigma/d\epsilon$ increases with increasing ϵ; large strains will travel faster than small ones and any large pulse travelling through the medium acquires a steep front. In the case of soft rubber the wave in some middle range of stress travels with slower velocity than in the low or the high range.

We may say in general that wave effects in compression are similar to those in tension, provided the proper behaviour of the material is allowed for. In common brittle materials, such as cast iron and concrete, the considerably lower ultimate strength in tension is another important non-linear effect relevant to intense waves.

Another non-linear effect arises from repeated loading and unloading beyond the proportional limit, giving a diagram such as shown in Fig. 2. For the construc-

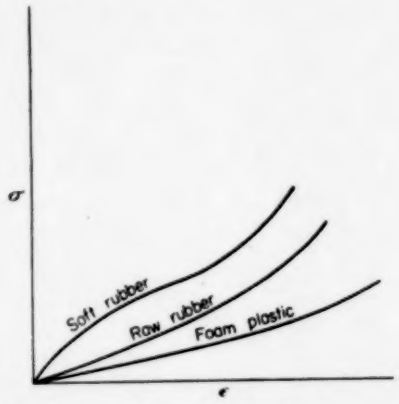

FIG. 1. Some idealized stress–strain curves.

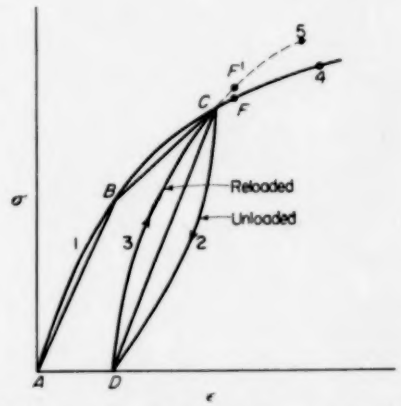

FIG. 2. Complete cycle of stress–strain for mild steel under tension.

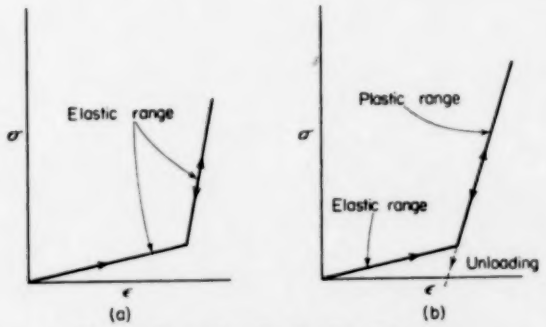

FIG. 3. Examples of unloading behaviour.

tion of X–T diagrams a simplification will be made by replacing the curved arcs of the characteristic by straight-line segments. Thus, repeating the loading results in the line DF, the arc $F4$ can be considered as a prolongation of the curve BC. If an interval of time, say several days, is allowed to elapse after unloading, then upon reloading a higher yield point than F may be obtained as indicated by the dotted line $F5$.

Two possible, significantly different, unloading curves may occur for the materials under study in this paper. Thus, in Fig. 3 (a) it is supposed that the material unloads along the same two-slope diagram as for loading. Foam plastic is approximately in this category. On the other hand, in Fig. 3 (b), unloading takes place along the prolongation of the line of higher slope ; here a residual strain is left in the material.

3. CONTOUR RELATIONSHIPS FOR STRESS PULSE PROPAGATION

As developed by DAVIDS and KUMAR (1958) the relationship between the slope m_ϵ of the strain contour and m_v, the velocity contour at a given point of the X–T diagram is

$$m_v\, m_\epsilon = \frac{\rho}{S} = \frac{1}{c^2} \tag{1}$$

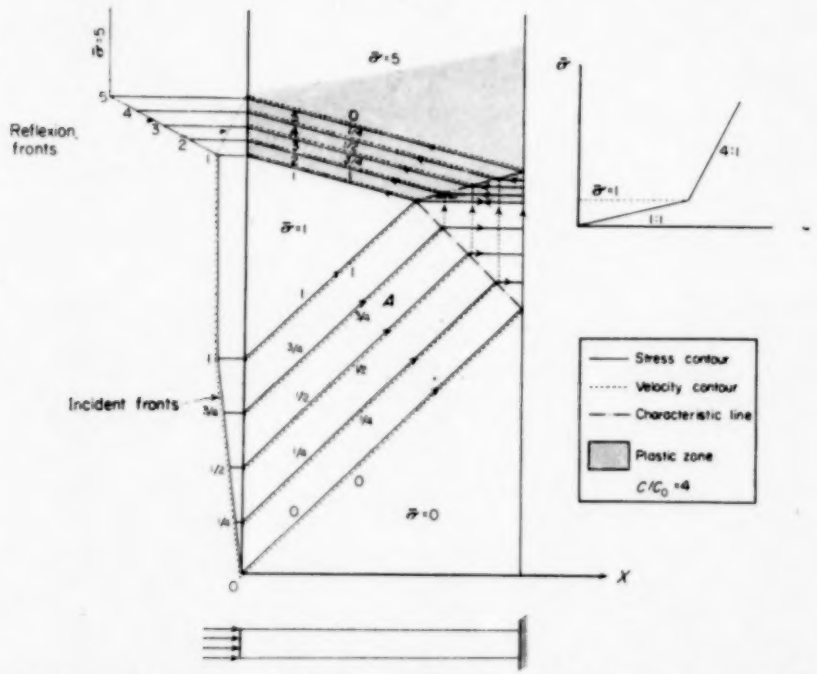

FIG. 4. Reflexion of an elastic wave into a plastic wave at a fixed end (second reflexion, at front boundary, not shown).

where S is the slope of the σ, ϵ – curve. It may be noted that, for a wave in which only loading occurs, the stress σ is a unique function of ϵ so that the stress contours coincide with the strain contours. Upon unloading, because of the lack of a single value of stress, this no longer holds.

When either $m_\epsilon = 1/c$ or $m_v = 1/c$ then the other slope also has the same value from (1).

This means the velocity and strain contours run parallel, and represent a wave travelling with velocity c without change of shape. This is shown in region A of Fig. 4, for example.

When velocity and strain contours are not parallel the relationship (1) must still hold. We call this an interaction region since such a pattern occurs whenever two different waves meet each other. Such regions are bounded by *characteristics*, i.e., lines where contours change direction suddenly, or partly by physical boundaries. The exact shape of such regions and the individual contours in them must be worked out by using the boundary and other conditions (formulated as 'rules' by DAVIDS and KUMAR (1958) as follows:

1. Contours of different values cannot cross or meet.
2. A contour must start or terminate at either end of the X–T region (i.e., $x = 0$ or $x = L$).
3. The product of the slopes of velocity and strain contours at a point is given by ρ/S. In particular, if one of the contours is horizontal, the other must be vertical.

4. EXAMPLES

Some X–T diagrams for basic case were plotted by DAVIDS and KUMAR (1958). The diagrams of this section form a supplemental study for the types of non-linear materials of Fig. 1, as exemplified by rubber and foam plastics.

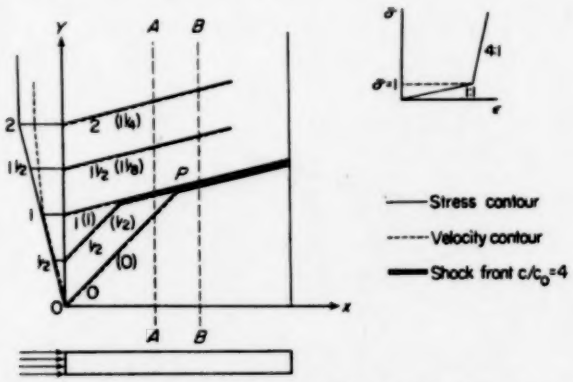

FIG. 5. Illustration of shock fronts (reflexion at boundary not shown).

A. *Plastic reflexion of elastic wave at fixed boundary*

When elastic waves of sufficient intensity in rods of rubber-like materials propagate towards a fixed end (Fig. 4), after reflexion a plastic wave results. The numbers in black written on the contours represent a non-dimensional stress defined as the ratio of actual stress to the critical stress $\bar{\sigma} = 1$. The construction procedure for the figure is described by DAVIDS and KUMAR (1958). It is worth noting how the reflected pulse, because of the higher propagation velocity, tends to acquire a steeper front than the incident pulse.

B. *Formation of shock fronts*

The basic situation where such a front arises is a loading beyond the critical stress $\bar{\sigma} = 1$, as shown in Fig. 5. As the Fig. 5 illustrates, the wave of higher velocity overtakes the initial elastic slower wave. Each stress contour below the

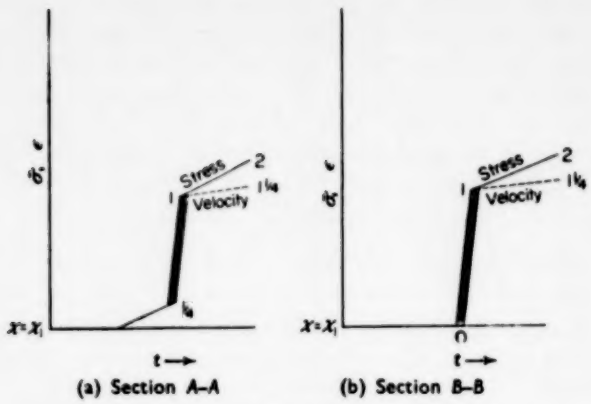

FIG. 6. Stress profiles showing shock fronts.

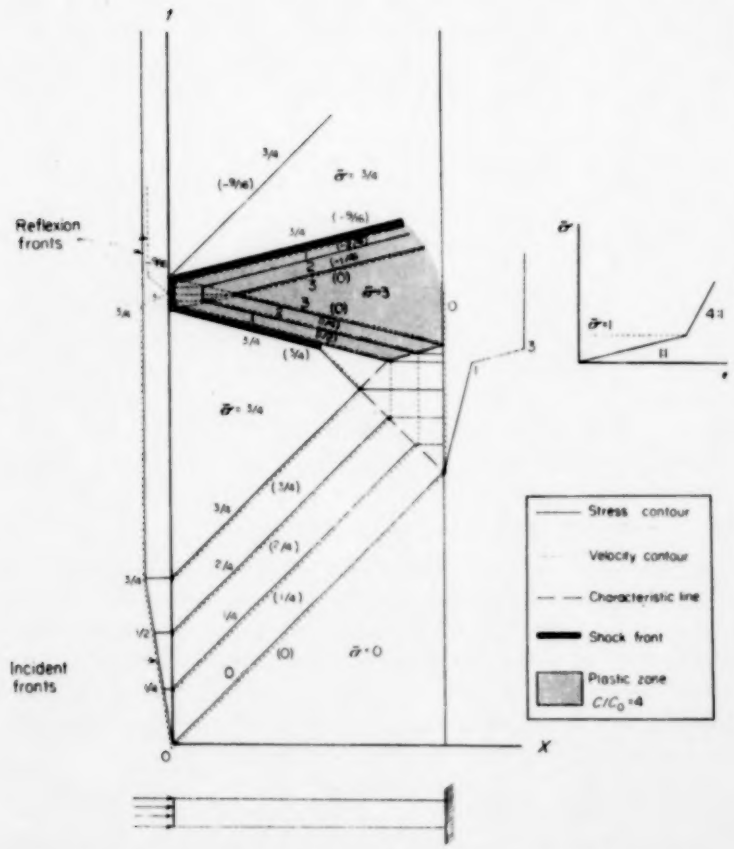

FIG. 7. Elastic-plastic reflexion and shock front formation from an elastic pulse at a fixed end.

critical one is suddenly deflected when met by the line $\bar{\sigma} = 1$, and thereafter coincides with this line. The discontinuity in stress thus created grows in magnitude until all the lines have been 'gathered in' at P; after this it continues as a unit jump through the medium. Cross-sections of the pulse as observed at two stations along the bar are shown in Figs. 6 (a) and 6 (b), illustrating this situation. The justification for the result is that all the rules for contours remain satisfied.

C. *Elastic–plastic reflexion of an elastic pulse from a fixed boundary*

When an incident elastic wave carries contour values from zero to a value less than one, there is both an elastic and a plastic wave on reflexion. The stress and velocity contours in this case can be drawn in a similar way as has been done previously. The new feature is that shock waves are initiated, as shown in Fig. 7, after reflexion of the initial wave. The discontinuity, however, is only 1/4 in magnitude, unlike that in Fig. 5.

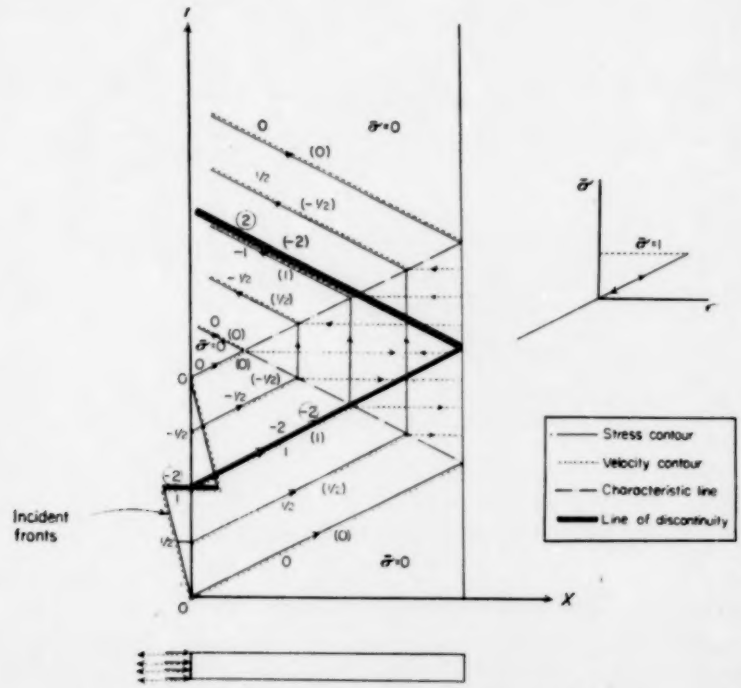

FIG. 8. Reflexion of a triangular pulse with discontinuity.

D. *Reflexion of a triangular pulse having an initial discontinuity at a free end*

A situation similar to shock waves is encountered by using the discontinuity method, which is based on following the course of initial discontinuities through the medium, as shown by an example in Fig. 8. The diagram is made for the case of a disturbance consisting of a gradually increasing compressive pulse, followed by a sudden unloading, with complete reversal of stress, as shown in the Figure. The discontinuity has a structure similar to a shock front, although it is desirable

to reserve the latter term for a front which develops of itself inside the medium, rather than one which is excited externally.

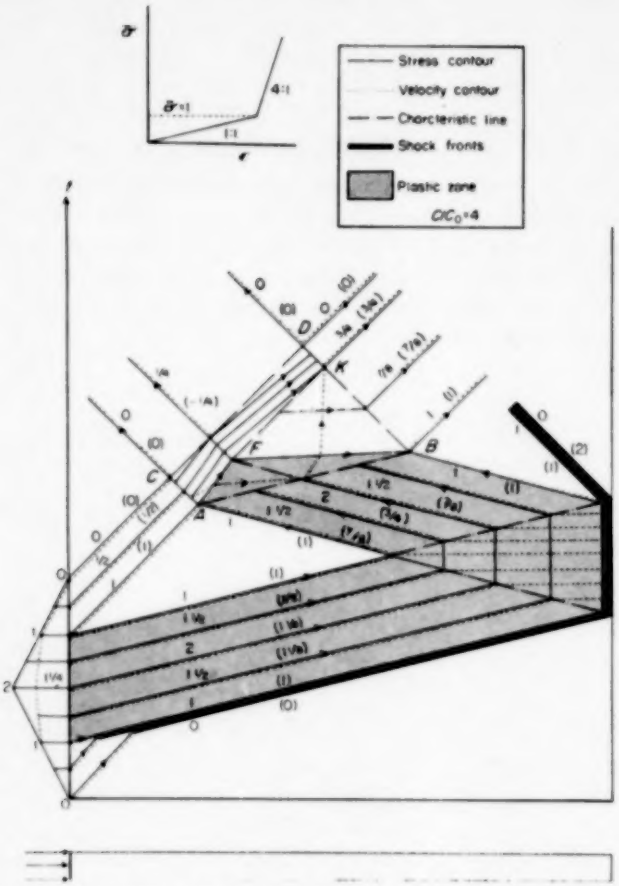

FIG. 9. Interaction of elastic–plastic contours for a triangular pulse.

E. *Interaction of elastic–plastic contours for a triangular pulse*

The formation of a shock front and the later reflexion and interaction of elastic plastic pulses are shown in Fig. 9. A more complicated interaction pattern arises when the reflected plastic wave meets the oncoming elastic unloading wave at the tail of the pulse. In order to clarify the construction of the diagram some additional properties of the contours are listed, as further general rules:

4. In an interaction region, contours of a given kind are parallel.

5. Whenever a triangle is formed consisting of two characteristic lines and a contour (such as ***FKB***, Fig. 10), the conjugate contour from the vertex ***K***, meets the opposite side at its mid-point. (This follows from Rules 3 and 4 which permit all the contours to be drawn after the interaction regions have been located).

6. If a slower moving set of contours are overtaken by a faster moving set, the former are deflected to the slope of the latter, thereby generating a shock front.

7. The zero-stress-contour follows a free boundary, while the zero-velocity-contour follows a fixed boundary.

8. Unless a dissipative mechanism is assumed, shock fronts persist, once generated.

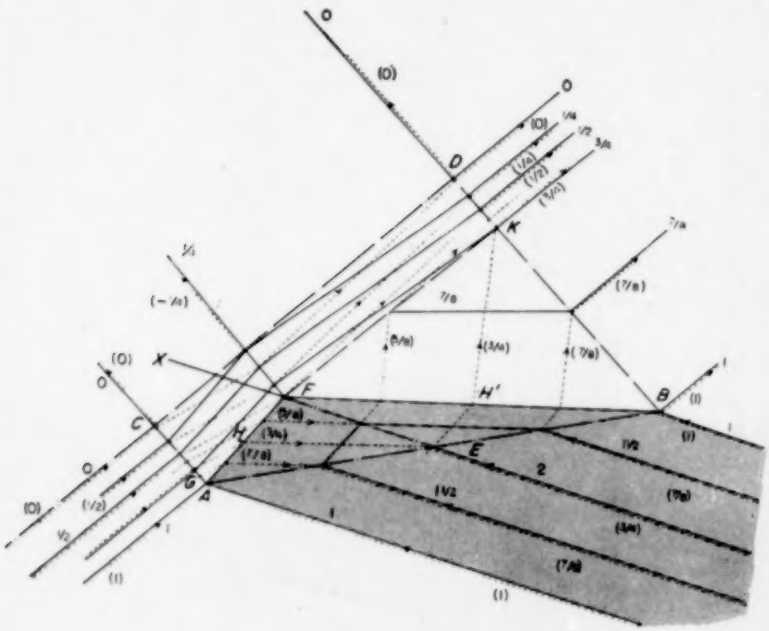

FIG. 10. Detail of interaction region $ABCD$ in Fig. 9.

The drawings of Fig. 9 and 10 are made stepwise as follows:

(i) Point A is located as the first interaction point between the two waves. Next B and C are located from the known slopes of the characteristic lines AB and AC.

(ii) Point D is then located as the intersection of two elastic characteristic lines, and the values $\sigma = v = 0$ are fixed since the emergent waves must retain their increments of stress and velocity.

(iii) The value $\sigma = 2$ is a maximum, and the corresponding contour appears to stop at E; actually it makes a 180° turn there and returns coincident with itself. Its prolongation EFX serves as a characteristic line to reverse all the contours within the triangle AFB.

(iv) The remaining step is to determine point F. For this we note next, since $\sigma = 1$ at A, that AF is a contour which separates the elastic and plastic

regions. Also CD is a characteristic line which links two equal values of stress and velocity. We may postulate the existence of a line GK in the same manner as CD, and which runs parallel to CD, meeting line DB at K and line EX at F, thus determining the required point F. However, this is not a unique way to determine F; another way arises from the fact that the velocity line EH and EH' where $v = \frac{3}{4}$ must meet AF and BF at the midpoints of these segments (see Rule 5).

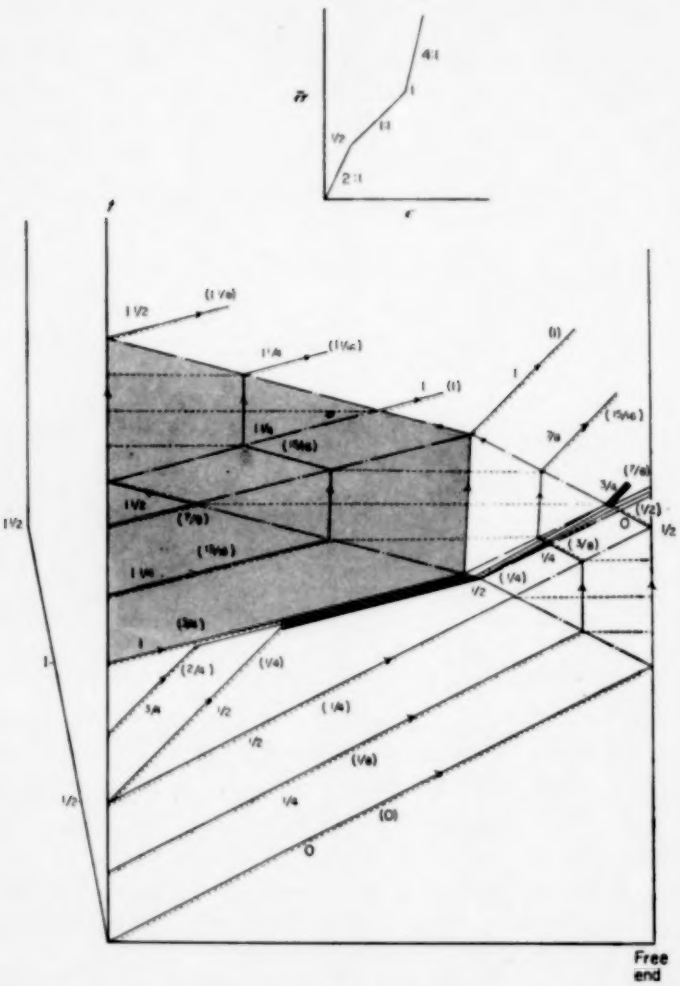

FIG. 11. Elastic–plastic reflexion from a free end with three propagation velocities.

(v) After F has been determined, the completion of the diagram is a straightforward procedure, outlined earlier. The construction should be checked to see that the conditions given by the rules for X–T diagrams are satisfied.

F. ***Elasto-plastic contours starting from a strong triangular pulse for a soft-rubber like material***

The stress–strain relation and the resulting diagram for a soft rubber-like material is shown in Fig. 11. This illustration intends to show the effect of a material behaviour with three values of propagation velocities. In this case a shock front will form due to the occurrence of the larger velocity at intermediate strains.

G. ***Interaction of elastic-plastic contours by fast elastic overtaking wave***

Suppose a uniformly increasing load from $\bar{\sigma} = 0$ to $\bar{\sigma} = 1\frac{1}{4}$ is followed by unloading to zero stress. Fig. 12 shows in outline how the elastic unloading wave overtakes the plastic wave at point A. The details of what happens then is shown in the diagram of Fig. 13. The plastic wave is so narrow here that point C falls beyond the advancing front of the plastic wave.

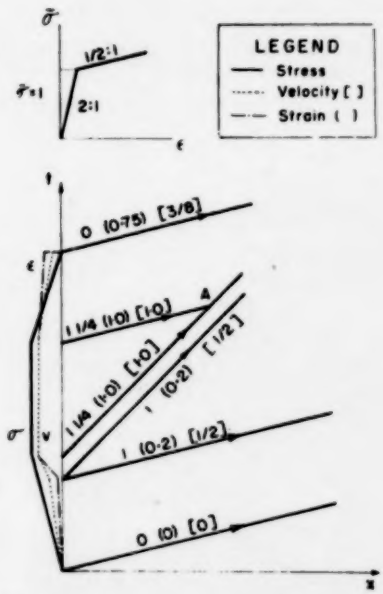

Fig. 12. Strong elastic wave overtaking a plastic wave.

Some features of the result are:

(a) A reflected elastic loading wave is generated, starting at point A.

(b) The plastic wave disappears completely.

(c) A continually widening region of permanent strain develops, starting at point A which always separates the elastic from the plastic waves and the incident from the transmitted waves.

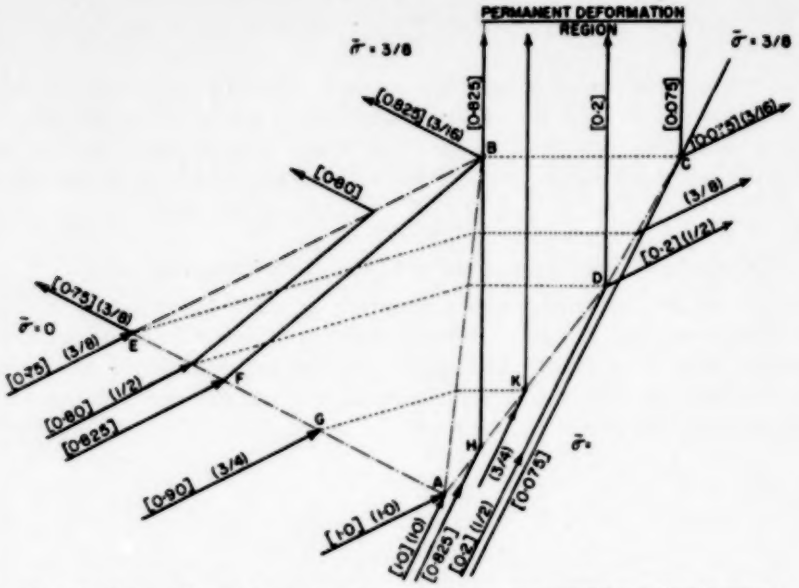

FIG. 13. Interaction contours of a strong elastic wave overtaking a plastic wave.

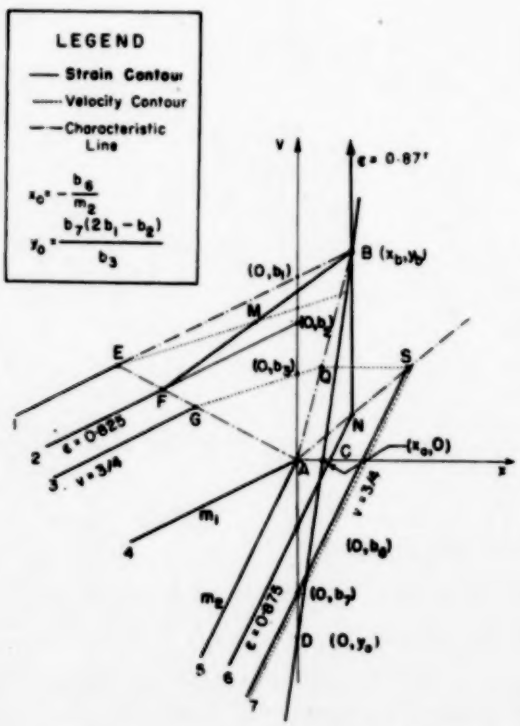

FIG. 14. Construction of wave interaction.

A brief description of the construction of this diagram follows. The stresses and strains in the two incident waves are given information and are shown on the diagram. The boundary conditions $v(B) = v(C)$, $\sigma(B) = \sigma(C)$, give around the path ADC, which crosses successively two elastic waves,

$$v(B) - v(A) = \frac{\sigma(E) - \sigma(A)}{\rho C_0} + \frac{\sigma(B) - \sigma(E)}{\rho(-C_0)}.$$

For the path ADC,

$$v(C) - v(A) = \frac{\sigma(D) - \sigma(A)}{C_1} + \frac{\sigma(C) - \sigma(D)}{\rho(-C_0)}.$$

Using $\sigma(D) = 1$, $\sigma(A) = 1\frac{1}{4}$, $\sigma(E) = 0$, $C_0 = 2$, $C_1 = \frac{1}{2}$, $\sigma(B) = \sigma(C)$, we obtain $\sigma(B) = \frac{3}{8}$ and $\epsilon(B) = 0{\cdot}825$. The remaining part of the procedure then consists of the following graphical steps (Fig. 14):

(i) Through point A draw a horizontal axis x and a vertical axis y.

(ii) Point B will lie somewhere along the prolongation of line (1). The interception of the y axis by line (1) is a known quantity, say b_1.

(iii) Similarly, b_2, b_3, b_6 and b_7 can be obtained by the same procedure as (ii).

(iv) The slopes of lines (1), (2), (3), (4) are designated by m_1, and lines (5, 6, 7) by m_2.

(v) The conditions of intersection for the strain and for the velocity contours are just sufficient to locate the point B on the Figure. One such condition is that B must lie on the continuation of line (1). Then, after writing the known x and y coordinates of points E, F and G, it is possible to express the coordinates of M in terms of those of B, using the fact that M is the midpoint of FB. The next steps consist in writing the equations for the line EM, the parallel line GQ, and the line ANS. Finally, a second condition arises from the fact that points Q and S lie on the same horizontal line. These two conditions are just sufficient to determine the coordinates of B:

$$x_b = \frac{b_6 b_7 (2b_1 - b_2) - b_1 b_3 b_6}{m_1 b_3 b_6 - m_2 b_7 (2b_1 - b_2)}, \qquad y_b = \frac{b_7 (m_1 b_6 - m_2 b_1)(2b_1 - b_2)}{m_1 b_3 b_6 - m_2 b_7 (2b_1 - b_2)}.$$

For convenience in graphical plotting it is simpler to locate the points C and D on the x and y axes respectively, with the following coordinates:

$$C: \quad x_c = -\frac{b_6}{m_2}; \quad y_c = 0$$

$$D: \quad x_D = 0; \qquad y_d = \frac{b_7 (2b_1 - b_2)}{b_3}.$$

It can easily be shown that a line joining C and D meets line (1) at B.

(vi) After point B has been determined, the remainder of the diagram may be completed in a straightforward way.

Another type of strong elastic overtaking-wave is illustrated by Fig. 15. The plotting procedure is similar to the previous case. A special feature of the diagram is that the same magnitudes on the incident plastic waves and on the unloading

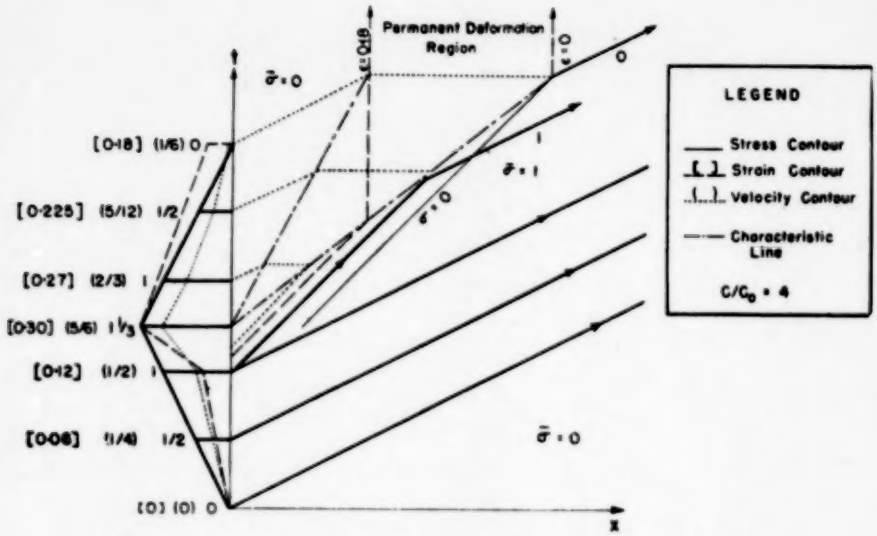

FIG. 15. Overtaking of a plastic wave by an elastic unloading wave.

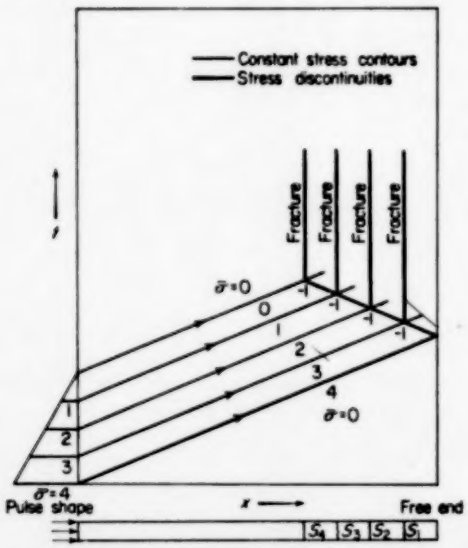

FIG. 16. Formation of scabs by a triangular pulse. Fracture stress = − 1.

elastic waves should be linked by either vertical lines (strain contours) or horizontal lines (velocity contours) in the interaction regions. This condition, in addition to the boundary conditions, enables the diagram to be constructed.

H. *Multiple scabbing of materials due to tensile reflexion of a compression pulse*

Since many materials have a smaller strength in tension, reversal of stress leads to the formation of scabs once a critical dynamic stress is reached. If the pulse is sufficiently long its trailing end will suffer reflexion at the newly fractured surface. By the same process this causes a second scab to form. The process continues until the reflected pulse becomes too weak to cause any further fracture.

Fig. 16 shows the application of the contour method to such a scabbing problem. The construction of the diagram is based on the assumptions that the magnitude of dynamic stress is entirely relieved after the fracture, and the fractured surface becomes a new free boundary. The construction of the diagram is then straightforward (the critical dynamic stress is assumed to be -1 in Fig. 16).

5. Discussion and Conclusions

The contour method is useful in solving theoretically many non-linear problems of the one-dimensional wave equation. In these problems the state of stress, strain, and particle velocity at any position and time can be presented on an X–T diagram. The formation of scabs may also be shown on this diagram. The resulting features of course need to be verified by experiments, but this method should greatly reduce the difficulty and complexity of solving wave-propagation problems in non-linear materials.

Some general conclusions can be drawn from the analysis of the problems presented here:

(i) The shock-front ideally tends to persist indefinitely, unless some further dissipative mechanism in the material is assumed.

(ii) When a fast elastic unloading wave overtakes a plastic wave in the same direction, a region of permanent deformation is generated by the interaction of the two waves.

(iii) Based on the assumption that the dynamic stress is relieved at a fracture surface, the methods discussed here enable the scabbing surfaces to be located.

Acknowledgments

This work has been sponsored by the Office of Ordnance Research, U.S. Army and the Department of Engineering Mechanics, The Pennsylvania State University.

References

Davids, N. and Kumar, S. 1958 *Proc. 3rd U.S. Congr. Appl. Mech.* 503.
De Juhasz, K. J. 1949 *J. Franklin Inst.* **248**, 113.
Houwink, R. and Burgers, W. G. 1953 *Elasticity, Plasticity and Structure of Matter* (Harren Press – Washington).
Karman, T. Van and Duwez, P. 1950 *J. Appl. Phys.* **21**, 977.
Kumar, S. and Davids, N. 1958 *J. Franklin Inst.* **265**, 371.
Lee, E. H. 1953 *Quart. Appl. Math.* **10**, 335.
Lee, E. H. and Tupper, S. J. 1954 *Trans. Amer. Soc. Mech. Engrs.* **76**, 63.
Malvern, L. E. 1951 *Trans. Amer. Soc. Mech. Engrs.* **73**, 203.
Marin, J. and Sauer, J. A. 1948 *J. Appl. Mech.* **70**, 256.

J. Mech. Phys. Solids, 1960, Vol. 8, pp. 66 to 75. Pergamon Press Ltd., London. Printed in Great Britain

ON THE PROPAGATION OF A CRACK IN AN ELASTIC-BRITTLE MATERIAL*

By J. W. Craggs
King's College, Newcastle-upon-Tyne

(*Received 2nd September*, 1959)

Summary

The Griffith theory of brittle cracking is extended to a dynamic problem, in which a semi-infinite crack in an infinite medium is extended by finite forces. The conclusion is drawn that the force required to maintain a steady rate of extension of the crack decreases as the rate increases. It is also observed that various criteria which may be assumed for crack division lead to limiting velocities of propagation of a single crack.

1. Introduction

The wide discrepancy between the measured breaking strength of a brittle material and the theoretical estimate, based on the cohesive forces between the molecules, was explained by Griffith (1921) in terms of stress concentration near incipient cracks. He postulated the existence of such a crack, in the form of an ellipse of small minor axis, and used the solution of the equations of elasticity in elliptic coordinates, as developed by Inglis (1913), to determine the stress field near the ends of the crack, assuming a given limiting form for the stress distribution far from the crack. Finally, by comparing the elastic energies corresponding to cracks of different sizes, and allowing for the different surface energies of the cracks, Griffith obtained an estimate of the stress required to enlarge a given crack, and showed good agreement with experimental results.

Yoffé (1951) considered the stresses in the neighbourhood of a moving crack. She assumed a crack of constant length, moving with constant speed through a fixed material, and obtained a solution by superposition of surface waves. Her analysis showed a singularity at the end of the crack, which reduced to that required by the Griffith solution as the speed of the crack approached zero. It also included the interesting property that for large enough speeds the direct stress over a radius near the end of the crack had a maximum value when the radius was at an angle to the axis of the crack. Thus some explanation was offered to account for the curved cracks often observed, for example, in glass. The analysis, however, suffers from the disadvantage that no estimate of the forces required to maintain the motion of the crack can be obtained from it.

*The results presented in this paper were obtained in the course of research sponsored by the Office of Naval Research, under contract Nonr.-562(10) with Brown University.

The present method differs from YOFFÉ's method mainly in that a semi-infinite crack is postulated. Two advantages follow: first, the solution may be obtained by much more elementary methods and, second, an estimate of the force required to extend the crack can be included. Near the end of the crack the solution agrees with YOFFÉ's solution, having the same limiting form as the singularity is approached.

2. MATHEMATICAL SPECIFICATION OF THE PROBLEM

Consider an infinite elastic body in a state of plane strain, in planes parallel to the x, y plane in rectangular Cartesian coordinates. Assume a cut over the half-plane $y = 0$, $x < Vt$, where V is a constant and t is the time. Assume further that the surface tractions σ_{yy}, σ_{xy} on the two sides of the cut are equal, and of the form

$$\sigma_{yy} = -f(x - Vt), \quad \sigma_{xy} = g(x - Vt), \quad -\infty < x - Vt < 0, \tag{1}$$

where f, g are differentiable any number of times, except perhaps at a finite number of isolated points, and that

$$R\sigma_{xx}, \quad R\sigma_{xy}, \quad R\sigma_{yy} \to 0 \tag{2}$$

as

$$R = \{(x - Vt)^2 + y^2\}^{\frac{1}{2}} \to \infty, \quad \text{uniformly in } y > 0.$$

The condition (2) may be modified to

$$R(\sigma_{xx} - A) \to 0, \quad R(\sigma_{xy} - B) \to 0, \quad R(\sigma_{yy} - C) \to 0, \quad R \to \infty, \tag{3}$$

where A, B, C are given constants, by superposition of a uniform stress field, and a suitable change in the conditions (1). The situation described by (3) may be loosely called ' uniform stress at infinity.'

Note that the length of the cut increases with constant speed V.

Let (u_x, u_y) be Cartesian components of the displacement of an element, and use scalar and vector potentials ϕ, ψ such that

$$u_x = \frac{\partial \phi}{\partial x} + \frac{\partial \psi}{\partial y}, \quad u_y = \frac{\partial \phi}{\partial y} - \frac{\partial \psi}{\partial x}. \tag{4}$$

Then the usual linear theory of dynamic elasticity (e.g. BULLEN 1953, p. 86) shows that

$$\frac{\partial^2 \phi}{\partial t^2} = c_1^2 \nabla^2 \phi = c_1^2 \left(\frac{\partial^2 \phi}{\partial x^2} + \frac{\partial^2 \phi}{\partial y^2} \right), \tag{5}$$

$$\frac{\partial^2 \psi}{\partial t^2} = c_2^2 \nabla^2 \psi, \tag{6}$$

where

$$\rho c_1^2 = (\lambda + 2\mu), \quad \rho c_2^2 = \mu, \tag{7}$$

and ρ is the density, and λ, μ are the Lamé elastic constants, of the material considered. Following SNEDDON (1952) assume solutions of (5) and (6) of the form

$$\phi = \phi(x - Vt, y); \quad \psi = \psi(x - Vt, y).$$

Write

$$X = x - Vt; \tag{8}$$

then (5) and (6) become

$$(1 - V^2/c_1^2)\frac{\partial^2 \phi}{\partial X^2} + \frac{\partial^2 \phi}{\partial y^2} = 0 \tag{9}$$

and

$$(1 - V^2/c_2^2)\frac{\partial^2 \psi}{\partial X^2} + \frac{\partial^2 \psi}{\partial y^2} = 0, \tag{10}$$

while the boundary conditions (1) become

$$\sigma_{yy} = -f(X), \quad \sigma_{xy} = g(X), \quad -\infty < X < 0. \tag{11}$$

Assume now that $V < c_2 (< c_1)$; then equations (9) and (10) are both elliptic. Write

$$z_1 = X + i(1 - V^2/c_1^2)^{\frac{1}{2}} y \tag{12}$$

and

$$z_2 = X + i(1 - V^2/c_2^2)^{\frac{1}{2}} y, \tag{13}$$

then

$$w_1 = \phi + i\chi = w_1(z_1), \quad w_2 = \psi + i\kappa = w_2(z_2) \tag{14}$$

where χ, κ are introduced to complete the complex potentials w_1 and w_2.

When ϕ, ψ are known, the stress components at the point $X (= x - Vt)$, y are given by

$$\begin{aligned}\mu^{-1}\sigma_{xx} &= \lambda\mu^{-1}\nabla^2\phi + 2\frac{\partial^2 \phi}{\partial x^2} + \frac{\partial^2 \psi}{\partial y\,\partial x} \\ &= c_1^2 c_2^{-2}\frac{\partial^2 \phi}{\partial X^2} + (c_1^2 c_2^{-2} - 2)\frac{\partial^2 \phi}{\partial y^2} + 2\frac{\partial^2 \psi}{\partial y\,\partial X} \\ &= (2 + V^2 c_2^{-2} - 2V^2 c_1^{-2})\frac{\partial^2 \phi}{\partial X^2} - 2(1 - V^2 c_2^{-2})^{\frac{1}{2}}\frac{\partial^2 \kappa}{\partial X^2},\end{aligned} \tag{15}$$

$$\mu^{-1}\sigma_{xy} = -2(1 - V^2 c_1^{-2})^{\frac{1}{2}}\frac{\partial^2 \chi}{\partial X^2} - (2 - V^2 c_2^{-2})\frac{\partial^2 \psi}{\partial X^2}, \tag{16}$$

and

$$\mu^{-1}\sigma_{yy} = -(2 - V^2 c_2^{-2})\frac{\partial^2 \phi}{\partial X^2} + 2(1 - V^2 c_2^{-2})^{\frac{1}{2}}\frac{\partial^2 \kappa}{\partial X^2}. \tag{17}$$

The problem, then, is to determine the complex potentials $w_1(z_1)$, $w_2(z_2)$ of (14) in the regions

$$-\pi < \arg z_1 < \pi, \quad -\pi < \arg z_1 < \pi, \tag{18}$$

subject to the conditions

$$(X^2 + y^2)^{\frac{1}{2}}\frac{d^2 w_1}{dz_1^2} \to 0, \quad |z_2| \to \infty \tag{19}$$

$$(X^2 + y^2)^{\frac{1}{2}}\frac{d^2 w_2}{dz_2^2} \to 0, \quad |z_2| \to \infty \tag{20}$$

(from (2)), and

$$-2(1 - V^2 c_1^{-2})^{\frac{1}{2}}\frac{\partial^2 \chi}{\partial X^2} - (2 - V^2 c_2^{-2})\frac{\partial^2 \psi}{\partial X^2} = \mu^{-1} g(X),$$

$$\arg z_1, \quad \arg z_2 = \pm\pi, \tag{21}$$

and

$$(2 - V^2 c_2^{-2}) \frac{\partial^2 \phi}{\partial X^2} - 2 (1 - V^2 c_2^{-2})^{\frac{1}{2}} \frac{\partial^2 \kappa}{\partial X^2} \to \mu^{-1} f(X),$$

$$\arg z_1, \quad \arg z_2 \to \pm \pi, \tag{22}$$

from (1), (16) and (17).

3. A Formal Solution

Write

$$\xi_1 + i\eta_1 = \zeta_1 = i z_1^{\frac{1}{2}}, \quad \xi_2 + i\eta_2 = \zeta_2 = i z_2^{\frac{1}{2}}, \tag{23}$$

and

$$W_1 = \frac{d^2 w_1}{dz_1^2}, \quad W_2 = \frac{d^2 w_2}{dz_2^2}. \tag{24}$$

Then W_1, W_2 may be regarded as functions of ζ_1, ζ_2 respectively, analytic in the upper half planes, $0 < \arg \zeta_1 < \pi$, $0 < \arg \zeta_2 < \pi$, and subject to boundary conditions as $\arg \zeta_1 \to 0, \pi$, $\arg \zeta_2 \to 0, \pi$.

Now when any function $W(\zeta)$ is analytic in $0 < \arg \zeta < \pi$, and $|W(\zeta)| \to 0$ as $|\zeta| \to \infty$, uniformly in $0 < \arg \zeta < \pi$, Cauchy's theorem, applied to a semicircle, $\zeta = Me^{i\theta}$, $0 \leqslant \theta \leqslant \pi$, together with the real axis, as $M \to \infty$, gives

$$W(\zeta) = \frac{1}{2\pi i} \int_{-\infty}^{\infty} \frac{W(t)}{t - \zeta} \, dt, \tag{25}$$

and

$$0 = \frac{1}{2\pi i} \int_{-\infty}^{\infty} \frac{W(t)}{t - \zeta^*} \, dt,$$

leading to

$$0 = -\frac{1}{2\pi i} \int_{-\infty}^{\infty} \frac{W^*(t)}{t - \zeta} \, dt, \tag{26}$$

where in each case convergence is assumed, the integration is along the real axis; $0 < \arg \zeta < \pi$; and the asterisk denotes the complex conjugate. But at $\zeta_1 = \zeta_2 = t$, real, equations (21) and (22) give

$$2i (1 - V^2 c_1^{-2})^{\frac{1}{2}} \{W_1(t) - W_1^*(t)\} - (2 - V^2 c_2^{-2}) \{W_2^*(t) + W_2(t)\} = 2\mu^{-1} g(t^2)$$

and

$$(2 - V^2 c_2^{-2}) \{W_1^*(t) + W_1(t)\} + 2i (1 - V^2 c_2^{-2})^{\frac{1}{2}} \{W_2(t) - W_2^*(t)\} = 2\mu^{-1} f(t^2)$$

so

$$\frac{1}{\mu\pi i} \int_{-\infty}^{\infty} \frac{g(t^2)}{t - \zeta} \, dt = 2i (1 - V^2 c_1^{-2})^{\frac{1}{2}} W_1(\zeta) - (2 - V^2 c_2^{-2}) W_2(\zeta) \tag{27}$$

and

$$\frac{1}{\mu\pi i} \int_{-\infty}^{\infty} \frac{f(t^2)}{t - \zeta} \, dt = (2 - V^2 c_2^{-2}) W_1(\zeta) + 2i (1 - V^2 c_2^{-2})^{\frac{1}{2}} W_2(\zeta). \tag{28}$$

$W_1(\zeta)$, $W_2(\zeta)$ may be eliminated successively from (27) and (28) to give

$$\{4 (1 - V^2 c_1^{-2})^{\frac{1}{2}} (1 - V^2 c_2^{-2})^{\frac{1}{2}} - (2 - V^2 c_2^{-2})^2\} W_1(\zeta_1)$$

$$= -\frac{1}{\pi\mu} \int_{-\infty}^{\infty} (t - \zeta_1)^{-1} \{2 (1 - V^2 c_2^{-2})^{\frac{1}{2}} g(t^2) - i (2 - V^2 c_2^{-2}) f(t^2)\} \, dt \tag{29}$$

and

$$\{4(1-V^2c_2^{-2})^{\frac{1}{2}}(1-V^2c_1^{-2})^{\frac{1}{2}}-(2-V^2c_2^{-2})^2\}\,W_2(z_2)$$

$$=-\frac{1}{\pi\mu}\int_{-\infty}^{\infty}(t-\zeta_2)^{-1}\{i(2-V^2c_2^{-2})g(t^2)+2(1-V^2c_1^{-2})^{\frac{1}{2}}f(t^2)\}\,dt. \quad (30)$$

Equations (29) and (30) constitute a formal solution of the problem, subject to the following conditions:

(i) The integrals converge, $0<\arg\zeta_1<\pi$, $0<\arg\zeta_2<\pi$.

(ii) The integrals have limits as $\arg\zeta_1\to 0,\ \pi$, $\arg\zeta_2\to 0,\ \pi$, except possibly near isolated singular points.

(iii) The factor

$$D\equiv 4(1-V^2c_2^{-2})^{\frac{1}{2}}(1-V^2c_1^{-2})^{\frac{1}{2}}-(2-V^2c_2^{-2})^2\neq 0. \quad (31)$$

(iv) The behaviour as $|\zeta_1|\to\infty$, $|\zeta_2|\to\infty$ is correct.

Now D has real zeros for $V^2=0$ and $V^2=C^2$ where C is the velocity of Rayleigh waves on a free surface. It is shown later that, for the solution to be physically meaningful, one must take $V<C$.

The conditions (ii) and (iv) require further comment. First, note that W_1, W_2 may have singularities on the real axes of ζ_1, ζ_2. Any discontinuity, for example, in $f(t^2)$ or $g(t^2)$ will give rise to logarithmic singularities in W_1, W_2, and singularities at $\zeta_1=0$, $\zeta_2=0$ cannot be excluded *a priori*, since singular transformations have been used. Secondly, the real parts of W_1, W_2 on the real axis would be unchanged by the addition of any functions

$$W'_1=iF_1(\zeta_1),\quad W'_2=iF_2(\zeta_2)$$

such that F_1, F_2 are real wherever ζ_1, ζ_2 are real. Moreover if F_1, F_2 tend uniformly to zero as $|\zeta_1|$, $|\zeta_2|\to\infty$ the application of Cauchy's theorem remains valid. It follows that the functions $W_1(\zeta_1)$, $W_2(\zeta_2)$ are not uniquely determined by (29) and (30). However, a function real on the real axis, bounded at infinity, and having no essential singularity is a rational function with real coefficients and poles on the real axis. Hence uniqueness can be achieved by specifying the singularities of W_1, W_2 on the respective real axes. In the particular application which follows, two singularities arise from discontinuities in the given functions $f(X)$ and $g(X)$ and a third singularity, at the origin, is introduced to ensure the specified behaviour of W_1, W_2 for large values of their arguments.

No attempt will be made to specify general conditions which ensure the convergence of the integrals in (29) and (30). It is sufficient to establish the convergence for any particular choice of $f(X)$ and $G(X)$ which is envisaged.

4. A Specific Problem

As a simple application of the foregoing analysis, take

$$\left.\begin{aligned} f(x-Vt)&=0, \quad x-Vt<-a,\\ &=P, \quad 0>x-Vt>-a, \end{aligned}\right\} \quad (32)$$

and

$$\left.\begin{aligned} g(x - Vt) &= 0, \quad x - Vt < -a \\ &= S, \quad 0 > x - Vt > -a, \end{aligned}\right\} \tag{33}$$

where a is a positive real constant.

Then (29) and (30) give

$$DW_1(z_1) = -\frac{1}{\pi\mu}\int_{-a^{\frac{1}{2}}}^{a^{\frac{1}{2}}} (t - \zeta_1)^{-1} \left\{2(1 - V^2 c_2^{-2})^{\frac{1}{2}} S - i(2 - V^2 c_2^{-2}) P\right\} dt$$

$$= -\frac{1}{\pi\mu}\left\{2(1 - V^2 c_2^{-2})^{\frac{1}{2}} S - i(2 - V^2 c_2^{-2}) P\right\} \log\left[\frac{a^{\frac{1}{2}} - iz_1^{\frac{1}{2}}}{a^{\frac{1}{2}} + iz_2^{\frac{1}{2}}}\right], \tag{34}$$

using (23), and

$$DW_2(z_2) = -\frac{1}{\pi\mu}\left\{i(2 - V^2 c_2^{-2}) S + 2(1 - V^2 c_2^{-2})^{\frac{1}{2}} P\right\} \log\left[\frac{a^{\frac{1}{2}} - iz_2^{\frac{1}{2}}}{a^{\frac{1}{2}} + iz_2^{\frac{1}{2}}}\right]. \tag{35}$$

Now in order to ensure that the applied forces are resisted by the material near the end of the crack, one must add terms singular at the origin, to reduce the stresses at large distances in accordance with the condition (2). It may be conjectured that only the lowest power of z_1^{-1}, z_2^{-1} consistent with (2) should be introduced. This conjecture can be supported on physical grounds by the observation that a singularity with exponent $-m$, $m > 1/2$, leads to expressions for the elastic energy per unit volume of order z_1^{-2m}, z_2^{-2m} and hence to an infinite concentration of energy in a small circle with centre $z_1 = z_2 = 0$. These considerations suggest the final answers

$$\pi\mu D(V) W_1(z_1) = -\left\{2(1 - V^2 c_2^{-2})^{\frac{1}{2}} S - i(2 - V^2 c_2^{-2}) P\right\}\left\{\log\frac{a^{\frac{1}{2}} - iz_1^{\frac{1}{2}}}{a^{\frac{1}{2}} + iz_1^{\frac{1}{2}}} + i\pi - \frac{2ia^{\frac{1}{2}}}{z_1^{\frac{1}{2}}}\right\} \tag{36}$$

$$\pi\mu D(V) W_2(z_2) = -\left\{i(2 - V^2 c_2^{-2}) S + 2(1 - V^2 c_1^{-2})^{\frac{1}{2}} P\right\}\left\{\log\frac{a^{\frac{1}{2}} - iz_2^{\frac{1}{2}}}{a^{\frac{1}{2}} + iz_2^{\frac{1}{2}}} + i\pi - \frac{2ia^{\frac{1}{2}}}{z_2^{\frac{1}{2}}}\right\}. \tag{37}$$

The stress components follow from (15) to (17), and it is easily verified directly that all the conditions of the problem are satisfied.

5. The Flow of Energy

Next consider the energy balance in the problem. Then it is easily verified that the stress components, and the velocity components, are $0(R^{-3/2})$ as $R \to \infty$. Thus the energy density is $O(R^{-3})$ and there is no transport of energy to infinity. The energy fed into the material by the forces P, S must therefore escape through the singularities. Now near the points $x - Vt = -a$, $y \to 0+$, $y \to 0-$, the stress and velocity components are $0(\log r)$ where $r^2 = (x - Vt + a)^2 + y^2$. The rate at which work is done on the circumference of a circle of radius r is therefore $0\{r(\log r)^2\}$ and tends to zero with r. The only loss of energy is therefore

associated with the singularity at the origin of the (X, y) coordinates, and all the work done by P, S is lost at $X = y = 0$. It is natural to equate the rate of loss of mechanical energy at this point to the rate of increase of surface energy of the material, which is $2\,TV$, where T is the energy per unit area of the surface.

Now from the form of the solution,

$$\frac{\partial u_x}{\partial t} = -V\frac{\partial u_x}{\partial x} = -V\left(\frac{\partial^2 \phi}{\partial x^2} + \frac{\partial^2 \psi}{\partial x\,\partial y}\right) = -V\left\{\frac{\partial^2 \phi}{\partial x^2} - (1 - V^2 c_2^{-2})^{\frac{1}{2}}\frac{\partial^2 \kappa}{\partial x^2}\right\} \tag{38}$$

and

$$\frac{\partial u_y}{\partial t} = V\left\{(1 - V^2 c_1^{-2})^{\frac{1}{2}}\frac{\partial^2 \chi}{\partial x^2} + \frac{\partial^2 \psi}{\partial x^2}\right\} \tag{39}$$

using (4), (12), (13) and (14).

The rate at which the external forces do work is

$$U = \int_{-a}^{0}\left\{P\left[\frac{\partial u_y}{\partial t}\right]_{y=0} - S\left[\frac{\partial u_x}{\partial t}\right]_{y=0}\right\} dX.$$

But from (36), (37), (38) and (39)

$$D\pi\mu\left[\frac{\partial u_x}{\partial t}\right]_{y=0+} = V^3 c_2^{-2}(1 - V^2 c_2^{-2})^{\frac{1}{2}} S\left\{\log\frac{a^{\frac{1}{2}} + \tau^{\frac{1}{2}}}{a^{\frac{1}{2}} - \tau^{\frac{1}{2}}} - \frac{2a^{\frac{1}{2}}}{\tau^{\frac{1}{2}}}\right\}$$
$$+ \pi P V\left\{2 - V^2 c_2^{-2} - 2(1 - V^2 c_1^{-2})^{\frac{1}{2}}(1 - V^2 c_2^{-2})^{\frac{1}{2}}\right\} \tag{40}$$

and

$$D\pi\mu\left[\frac{\partial u_y}{\partial t}\right]_{y=0+} = \pi S V\left\{2 - V^2 c_2^{-2} - 2(1 - V^2 c_1^{-2})^{\frac{1}{2}}(1 - V^2 c_2^{-2})^{\frac{1}{2}}\right\}$$
$$- V^3 c_2^{-2}(1 - V^2 c_2^{-2})^{\frac{1}{2}} P\left\{\log\frac{a^{\frac{1}{2}} + \tau^{\frac{1}{2}}}{a^{\frac{1}{2}} - \tau^{\frac{1}{2}}} - \frac{2a^{\frac{1}{2}}}{\tau^{\frac{1}{2}}}\right\} \tag{41}$$

where $\tau = -X$. Hence

$$D\pi\mu U = V^3 c_2^{-2}\left\{(1 - V^2 c_1^{-2})^{\frac{1}{2}} P^2 + (1 - V^2 c_2^{-2})^{\frac{1}{2}} S^2\right\}\int_0^a\left\{\frac{2a^{\frac{1}{2}}}{\tau^{\frac{1}{2}}}\right.$$
$$\left. - \log\frac{a^{\frac{1}{2}} + \tau^{\frac{1}{2}}}{a^{\frac{1}{2}} - \tau^{\frac{1}{2}}}\right\} d\tau$$
$$= \frac{2aV^3}{c_2^2}\left\{1 - V^2 c_1^{-2})^{\frac{1}{2}} P^2 + (1 - V^2 c_2^{-2})^{\frac{1}{2}} S^2\right\}. \tag{42}$$

The equations corresponding, on the other side of the crack, to (40) and (41) are obtained merely by changing the sign of S in (40) and P in (41). The rate at which the forces do work is then the same as in (42). If now the assumption is made that T is the same, whether the surface is formed by direct or tangential stress, the result of equating the rate of working to the rate of creation of new surface energy is

$$\frac{4aV^2}{c_2^2}\left\{(1 - V^2 c_2^{-2})^{\frac{1}{2}} P^2 + (1 - V^2 c_2^{-2})^{\frac{1}{2}} S^2\right\} = 2\pi\mu\, DT$$
$$= 2\pi\mu T\left\{4(1 - V^2 c_2^{-2})^{\frac{1}{2}}(1 - V^2 c_2^{-2})^{\frac{1}{2}} - (2 - V^2 c_2^{-2})^2\right\}. \tag{43}$$

6. Incipient Motion

Equation (43) gives the condition that the applied forces, P, S are sufficient to maintain the steady extension of the crack. If P, S were reduced, the crack would spread more slowly, and incidentally the kinetic energy of the whole medium would be reduced. On the other hand, if P, S were to be increased, work would be available to increase the kinetic energy of the material and the rate of propagation of the crack. Now if P, S are increased from zero in a medium initially at rest, extension of the crack will begin when P, S reach values such that (43) is satisfied for V just greater than zero. Note that both sides of (43) vanish for $V = 0$. The condition for incipient motion is that (43) should have a quadruple root at $V = 0$, and this is seen to be the case when

$$a\,(P^2 + S^2) = \pi\mu\, T\,(1 - c_2^2/c_1^2). \tag{44}$$

Now Griffith found the stress P_1 required to initiate spreading of a thin crack of length l, in a thin plate, to be given by

$$P_1^2 = 4ET/\pi l, \tag{45}$$

and since his crack extends at both ends one may tentatively set $l = 2a$. Also for a plate (plane stress)

$$c_1^2/c_2^2 = 4\,(\lambda + \mu)/(\lambda + 2\mu) \tag{46}$$

and Griffith worked with $\nu = 1/4$, $\lambda = \mu$. Setting $l = 2a$, $S = 0$, $\mu = E/2\,(1 + \nu)$ $P_1^2/P^2 = 8/\pi^2$, and $P/P_1 = 1{\cdot}11$, approximately. One would expect the dynamic method to give a higher force than the static one, since it takes into account the kinetic energy associated with movement of the crack, but the above numerical result is not to be taken too literally, as it depends on the equation $l = 2a$, which is only conjecture.

Note too that the present method implies the same limiting force for direct or tangential stress of the material. Again this is not in agreement with Griffith's results, and again his own result is the more appropriate to the experiments which he performed.

7. Higher Velocities of Crack Propagation

Table 1 shows the variation of P with V for $S = 0$, and of S with V for $P = 0$, calculated from equation (43). The second line represents the direct stress required

Table 1. ($\nu = 0{\cdot}25$)

V/c_2	0·0	0·1	0·2	0·3	0·4	0·5
$a^{\frac{1}{2}}P/(\pi\mu T)^{\frac{1}{2}}$	0·8165	0·8137	0·8002	0·7878	0·7629	0·7284
$a^{\frac{1}{2}}S/(\pi\mu T)^{\frac{1}{2}}$	0·8165	0·8150	0·8098	0·8004	0·7860	0·7675

V/c_2	0·6	0·7	0·8	0·9	c'/c_2
$a^{\frac{1}{2}}P/(\pi\mu T)^{\frac{1}{2}}$	0·6799	0·6092	0·4957	0·2305	0·0000
$a^{\frac{1}{2}}S/(\pi\mu T)^{\frac{1}{2}}$	0·7363	0·6893	0·6026	0·3228	0·0000

$c' = 0{\cdot}9194\,c_2$ is the velocity of a Rayleigh wave on a free surface.

to maintain the motion of a crack, in the absence of shear, and the third line represents the tangential stress needed, in the absence of normal stress.

Note that, as V increases, the force require to maintain the motion decreases. Thus, if a stress is applied which causes a crack to spread, the crack may well continue to spread even when the applied stress is decreased. Catastrophic cracking may therefore occur even under a load which, after reaching a maximum, decreases fairly rapidly. Note also that as $V \to c'$ the rate of working of a finite force tends to infinity, and the cracking process would appear to be self-maintaining. However, crack division will certainly occur before this velocity is reached.

8. Crack Division

Consider the stresses near the end of the crack ($X = y = 0$). Then the dominant terms in (36) and (37) give

$$\pi\mu D(V)\, W_1(z_1) = 2(2 - V^2 c_2^{-2})\, P a^{\frac{1}{2}} z_1^{-\frac{1}{2}} + 4i(1 - V^2 c_2^{-2})^{\frac{1}{2}}\, S a^{\frac{1}{2}} z_1^{-\frac{1}{2}} + O(1)$$

$$\pi\mu D(V)\, W_2(z_2) = 4i(1 - V^2 c_1^{-2})^{\frac{1}{2}}\, P a^{\frac{1}{2}} z_2^{\frac{1}{2}} - (2 - V^2 c_2^{-2})\, S a^{\frac{1}{2}} z_2^{-\frac{1}{2}} + O(1).$$

Write $X = r\cos\theta$, $Y = r\sin\theta$, $z_1 = r_1 e_1^{2i\theta}$, $z_2 = r_2 e_2^{2i\theta}$ where

$$r_1^2 = r^2(1 - V^2 c_2^{-2}\sin^2\theta), \quad r_2^2 = r^2(1 - V^2 c_2^{-2}\sin^2\theta) \tag{47}$$

and

$$\tan 2\theta_1 = V c_1^{-1}\tan\theta, \quad \tan 2\theta_2 = V c_2^{-2}\tan\theta, \tag{48}$$

and express the stress tensor near $r = 0$ in terms of the polar coordinates (r, θ). Then

$$\sigma_{\theta\theta} = \sigma_{xx}\sin^2\theta + \sigma_{yy}\cos^2\theta - 2\sigma_{xy}\sin\theta\cos\theta, \tag{49}$$

$$\sigma_{r\theta} = (\sigma_{yy} - \sigma_{xx})\sin\theta\cos\theta + \sigma_{xy}\cos 2\theta, \tag{50}$$

$$\sigma_{rr} = \sigma_{xx}\cos^2\theta + \sigma_{yy}\sin^2\theta + 2\sigma_{xy}\sin\theta\cos\theta. \tag{51}$$

Use of equations (15) to (17) then leads to

$$\begin{aligned} a^{-\frac{1}{2}}\pi D(V)\,\sigma_{\theta\theta}(\theta) = {} & -4(1 - V^2 c_1^{-2})^{\frac{1}{2}}\sin 2\theta\,\{(2 - V^2 c_2^{-2})\, P\sin\theta_1 \\ & - 2(1 - V^2 c_2^{-2})^{\frac{1}{2}}\, S\cos\theta_1\}\, r_1^{-\frac{1}{2}} + 2\{V^2(c_2^{-2} - c_1^{-2}) \\ & - (2 - V^2 c_2^{-2})\}\cos 2\theta\,\{(2 - V^2 c_2^{-2})\, P\cos\theta_1 + 2(1 - V^2 c_2^{-2})^{\frac{1}{2}}\, S\sin\theta_1\}\, r_1^{-\frac{1}{2}} \\ & + 2(2 - V^2 c_2^{-2})\sin 2\theta\,\{2(1 - V^2 c_1^{-2})^{\frac{1}{2}}\, P\sin\theta_2 - (2 - V^2 c_2^{-2})\, S\cos\theta_2\}\, r_2^{-\frac{1}{2}} \\ & + 4(1 - V^2 c_2^{-2})^{\frac{1}{2}}\cos 2\theta\,\{2(1 - V^2 c_1^{-2})^{\frac{1}{2}}\, P\cos\theta_2 + (2 - V^2 c_2^{-2})\, S\sin\theta_2\} \\ & r_2^{-\frac{1}{2}} + O(1). \end{aligned} \tag{52}$$

There is a similar equation for σ_{rr} obtainable by changing the sign of each trigonometrical function of 2θ in (52), and

$$\begin{aligned} a^{-\frac{1}{2}}\pi D(V)\,\sigma_{r\theta}(\theta) = {} & -2(2 - V^2 c_1^{-2})\sin 2\theta\,\{(2 - V^2 c_2^{-2})\, P\cos\theta_1 \\ & + 2(1 - V^2 c_2^{-2})^{\frac{1}{2}}\, S\sin\theta_1\}\, r_1^{-\frac{1}{2}} + 4(1 - V^2 c_2^{-2})^{\frac{1}{2}}\sin 2\theta\,\{2(1 - V^2 c_1^{-2})^{\frac{1}{2}}\cos\theta_2 \\ & + (2 - V^2 c_2^{-2})\sin\theta_2\}\, r_2^{-\frac{1}{2}} - 4(1 - V^2 c_1^{-2})^{\frac{1}{2}}\cos 2\theta\,\{(2 - V^2 c_2^{-2})\, P\sin\theta_1 \\ & - 2(1 - V^2 c_2^{-2})^{\frac{1}{2}}\, S\cos\theta_1\}\, r_1^{-\frac{1}{2}} - 2(2 - V^2 c_2^{-2})\cos 2\theta\,\{2(1 - V^2 c_1^{-2})^{\frac{1}{2}}\, P\sin\theta_2 \\ & - (2 - V^2 c_2^{-2})\, S\cos\theta_2\}\, r_2^{-\frac{1}{2}}. \end{aligned} \tag{53}$$

Now, following YOFFÉ, assume that the cracking of the material is caused by large direct stress. Take $S = 0$ in (52); then, as $V \to 0$, $\sigma_{\theta\theta}(\theta)$ has a maximum for $\theta = 0$, but as V increases through a critical value, V_1, at which $[d^2\sigma_{\theta\theta}/d\theta^2]_{\theta=0} = 0$, the value of $\sigma_{\theta\theta}$ at $\theta = 0$ becomes a minimum and maxima occur on each side of $\theta = 0$. This suggests that V_1 is the limiting velocity of propagation of a simple crack, and that division occurs if the applied stresses are further increased.

On the other hand, it might be conjectured that rupture is associated with strain, rather than stress. The limiting velocity V_2 will then be that for which $[d^2e_{\theta\theta}/d\theta^2]_{\theta=0} = 0$, where $e_{\theta\theta}$ is the strain component, proportional to $(1-\nu\sigma_{\theta\theta}-\nu\sigma_{rr}$. Again, if it were assumed that hydrostatic stress is unimportant, the limiting velocity, V_3 would be given by considering $\sigma_{\theta\theta} - \sigma_{rr}$.

Finally, if rupture is associated with shearing stress, one should take $P = 0$ in (53) and crack division will occur at a speed V_4 such that $[d^2\sigma_{r\theta}/d\theta^2]_{\theta=0} = 0$. The values of V_1/c_2, V_2/c_2, V_3/c_2, V_4/c_2 are given in Table 2 for $\nu = 1/4$, $\nu = 1/3$. The third, fourth and fifth lines, marked with asterisks, are the corresponding results for plane stress.

TABLE 2.

ν	V_1/c_2	V_2/c_2	V_3/c_2	V_4/c_2
1/4	0·629	0·611	0·565	0·772
1/3	0·667	0·621	0·571	0·810
1/4*	0·612	0·598	0·562	0·762
1/3*	0·629	0·597	0·565	0·772
1/2*	0·667	0·571	0·571	0·810

IRWIN (1958) quotes measured values of the limiting velocity of crack propagation in thin plates of varying materials. The values vary between $V/c_2 = 0{\cdot}44$ (cellulose acetate) and $V/c_2 = 0{\cdot}59$ (silica glass). The velocities derived from the present analysis are therefore consistently too high, but may perhaps be regarded as lying within the limits of experimental error, particularly since, from the nature of the experiment, the measured values are likely to be too low rather than too high.

REFERENCES

BULLEN, K. E. 1953 *Introduction to the Theory of Seismology* (Cambridge University Press).

GRIFFITH, A. A. 1921 *Phil. Trans. Roy. Soc.* A **221**, 163.

INGLIS, C. E. 1913 *Engineering* **95**, 415.

IRWIN, G. R. 1958 *Fracture Mechanics. First Symposium on Naval Structural Mechanics.*

SNEDDON, I. N. 1952 *Rendiconti Circ. Math di Palermo* Series II, 1.

YOFFÉ, E. H. 1951 *Phil. Mag.* **42**, 739.

J. Mech. Phys. Solids, 1960, Vol. 8, pp. 76 to 78. Pergamon Press Ltd., London. Printed in Great Britain

RESEARCH NOTE

A new technique for engraving and measuring grids in experimental plasticity

By R. C. Brewer and J. M. Alexander
Imperial College of Science and Technology

(*Received* 23 *July* 1959)

As part of Imperial College's extended programme of experimental research into the plastic flow of metals, particularly in metal working processes, it has been necessary to engrave and measure grids on metal specimens. By this technique grids are engraved on interior sections of specimens, which are then subjected to some metal working process, the operation being interrupted when the steady state is obtained so that measurements can be made of the deformed grid. In this way it is possible to determine a slip-line field (or the orthogonal network of lines which lie in the direction of principal shear strains), and obtain information about the detailed pattern of stress and strain which exists in the material. Typical examples of specimens partly deformed in rolling and machining are shown diagrammatically in Fig. 1, the specimen being formed in two or more laminae so that the grid can be brought to the interior of the specimen where edge effects will not give spurious results, and then secured together either by pressure welding or some form of adhesive. Photographs of typical deformed grids in these processes are shown in Fig. 2.

Apart from the difficulties associated with the securing together of the laminae to give effectively a single homogeneous specimen which can be deformed under truly plane strain conditions, one of the major limitations of these researches has been the difficulty of engraving a sufficiently accurate grid. In a University, metal working machines, due to limitations of power and space, are incapable of applying large forces to a specimen so that specimens are necessarily of rather small size. This means that in order to get a reasonable accuracy it is necessary to engrave the grid with as fine a mesh as possible and this in turn requires the width of the engraved lines to be small enough to enable the nodal points to be located to the same order of accuracy. In the past no better method could be found than that of using a razor blade as the scriber; this was firmly secured in the fixed arbor of a milling machine, the table being traversed underneath it to scribe a line, and indexed transversely to provide the spacing. This method produced a line which in addition to being rather thicker than was desirable, also suffered from the coronet effect; in general it did not justify the use of a more accurate measuring instrument than the tool-makers microscope. A further disadvantage was that the nodal pitch of the grid could only be achieved as a nominal dimension since the thimbles indicating the table movements of the milling machine were not reliable even to the order of accuracy of the tool-makers microscope. This meant that the grid has to be measured both before and after deformation.

The expansion programme of the College has included the establishment of a Metrology Laboratory with a wide range of equipment and with the necessary atmospheric control for making fine measurement. One of the two basic measuring instruments is the MU 214 B Universal Measuring Machine manufactured by the Société Genevoise d'Instruments de Physique. This is a coordinate measuring machine with a longitudinal movement of 16 in., a transverse movement of 4 in. and a vertical movement of 6 in. The high measuring accuracy is due to the fact that the principle of measurement is the microscopic observation of standard scales which are graduated at intervals of 0·05 in. The graticule of the microscope head can be moved (through a range a little greater than 0·05 in.) by means of a very accurate micrometer screw, the amount of movement

being observed on a rotating scale graduated in units of 0·00005 in. A further sub-division by eye enables the reading to be estimated to the nearest ten μ in.

The greatest accuracy which the Société Genevoise is prepared to guarantee is 0·00004 in. but if the instrument is used in accordance with good metrological principles, the accuracy should be higher than this figure. The limiting factor in the present application is undoubtedly the thickness of the engraved lines ; normally this could not be made less than 0·0002 in. and, even on a specular-ground steel surface, 0·00015 in. would be the absolute limit. It is perhaps sobering to reflect that the larger of these two figures is only of the order of one-twentieth of the diameter of the average human hair ! One further advantage was that the machine could be used not only for the measurement of the grids but also for engraving them. It was proposed to employ a tracelet mechanism similar to that used for engraving the lines on standard scales and line standards.

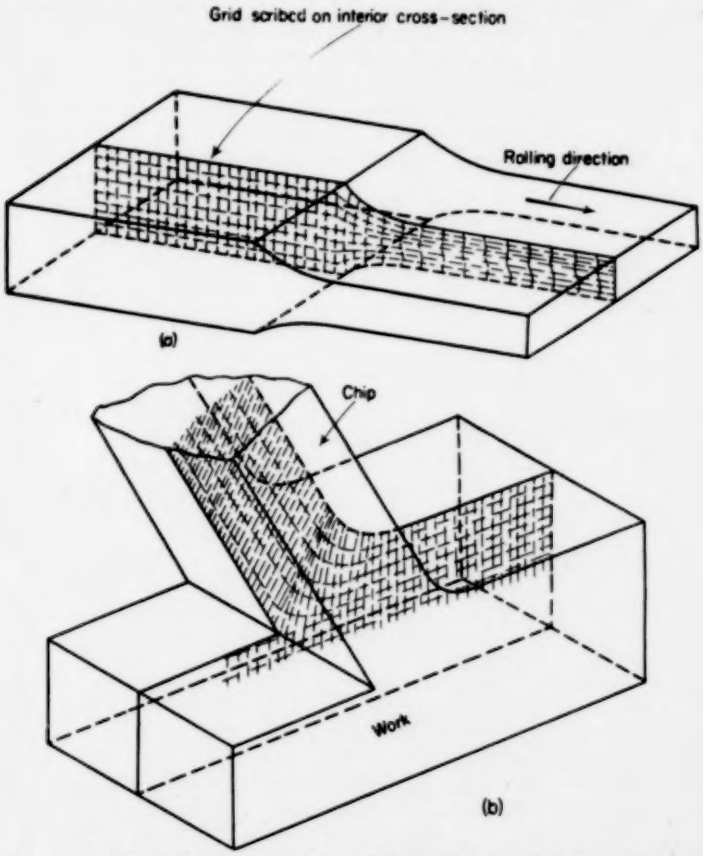

FIG. 1. (a) Partially rolled specimen. (b) Partially machined specimen.

It was clear, however, that this would have to differ in two ways from the tracelet mechanism used on a linear dividing engine. In the first place, the construction would need to be much lighter so that it could be attached to the location microscope and secondly, the normal tracelet mechanism is used to engrave lines on materials with a very narrow range of hardness. The proposed application entailed a much greater range and made necessary some means of adjusting the normal force between the engraving tool and the work.

Fig. 3 shows the tracelet mechanism which the Société Genevoise manufactured, in position on the measuring machine. The actual engraving tool is of high carbon tool steel, hardened,

ground and lapped to a wedge form of 30° included angle, and is held at one end of a lever pivoted in conical bearings carried in the main member. The force between the tool and the specimen may be adjusted by moving the jockey weight along the counter-balance arm of this lever. The height of the engraving tool can be easily adjusted so that the engraved line is in the focal plane of the microscope. Thus the position of the engraved line can be measured during the actual engraving operation.

It has been found, however, that such measurement of the undeformed grid is unnecessary. It is relatively easy to produce a grid of lines 0·0025 in. apart, even in material as soft as commercially pure aluminium, the resolution of the lines being quite satisfactory. In practice a certain amount of experiment is required to find the rake angle of the engraving tool which gives the most clearly defined line. If the ' cutting speed ' is too high the engraving tool tends to bounce, giving an intermittent line ; the highest speed of cutting which will give a continuous line is naturally governed by the extent to which the upper surface of the specimen is plane. This is an inevitable consequence of the low normal force between the tool and the specimen.

In the past there has been a lack of fundamental data concerning the detailed deformation pattern in many metal working processes and it is hoped to investigate several of these processes with the aid of this technique. If an accuracy of $\pm$ 50 μ in. can be achieved on a grid of 0·010 in. mesh, it should be possible to measure a strain in the material of the order of 1 per cent which is little more than the yield point elastic strain for many materials.

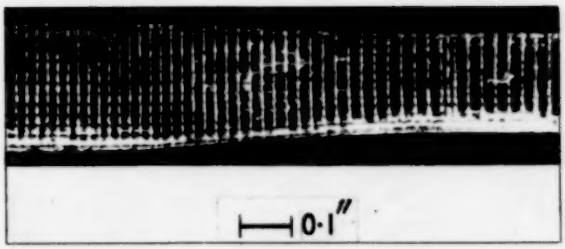

FIG. 2 (a).

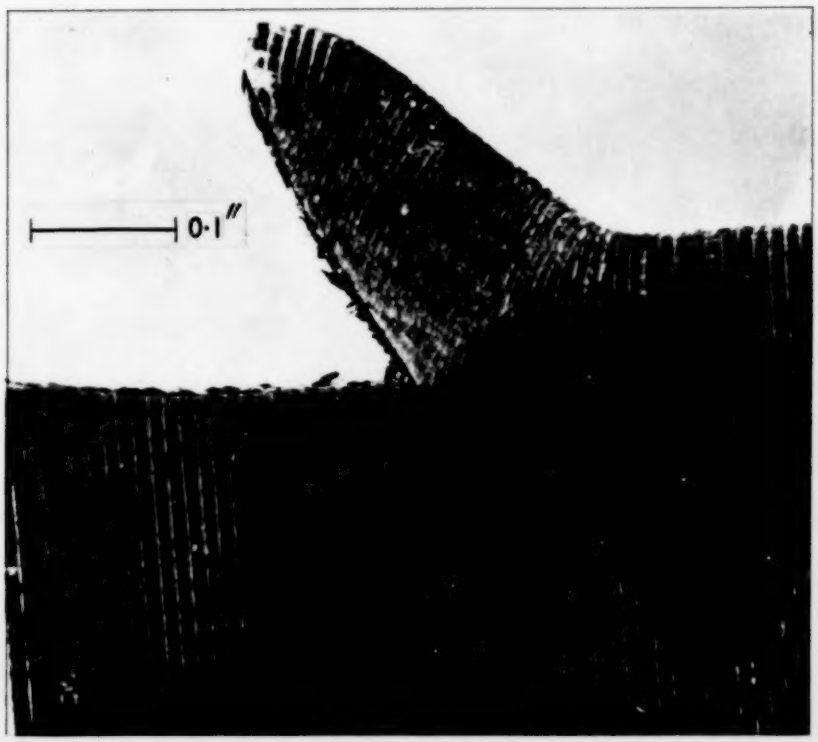

FIG. 2 (b).

FIG. 2 (a) Typical deformed grid in rolling (courtesy of MR. F. ELLIS).
(b) Typical deformed grid in machining (courtesy of MR. S. C. SHAH).

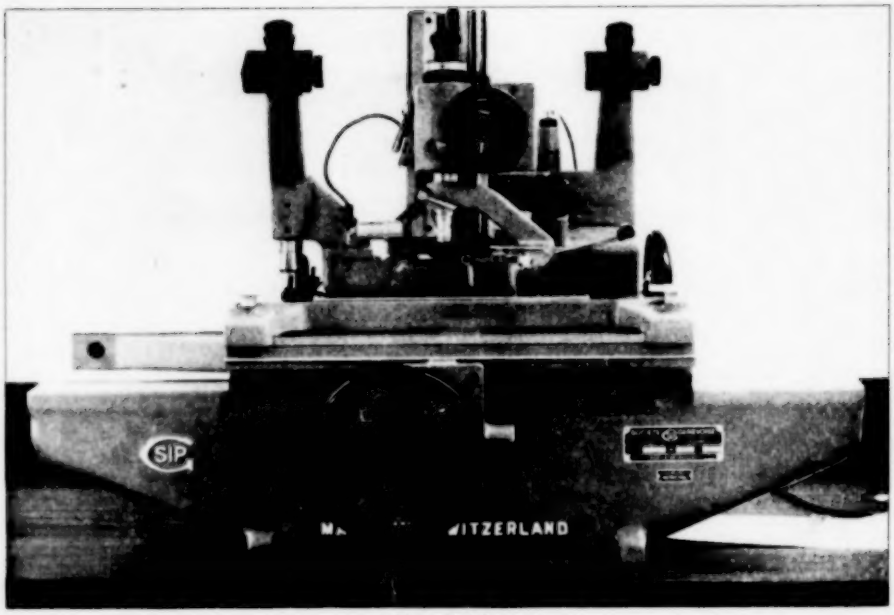

FIG. 3 (a)

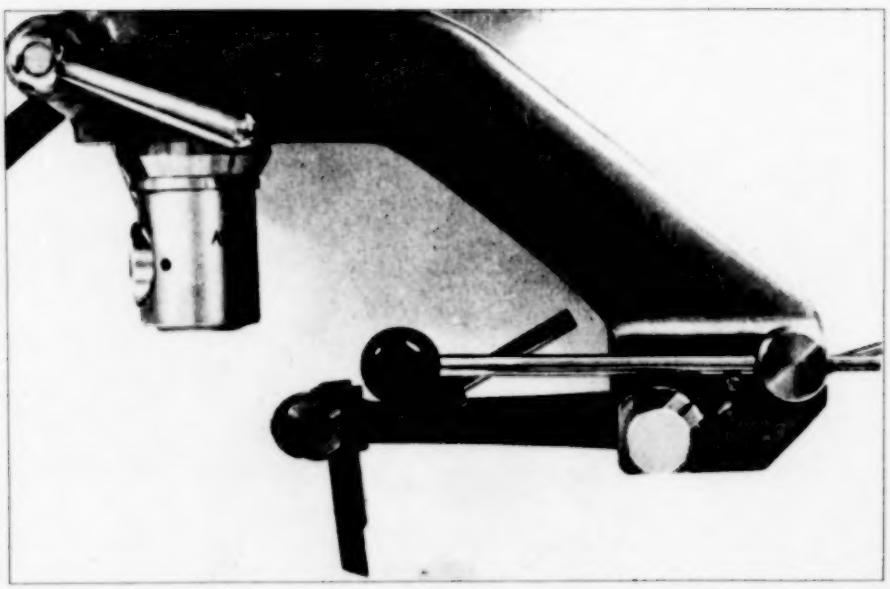

FIG. 3 (b).

FIG. 3. (a) The MU 214 B Universal Measuring Machine with the tracelet mechanism.
(b) The tracelet mechanism.

BOOK REVIEWS

Solid State Physics: Advances in Research and Applications, Vol. 6. Edited by F. Seitz and D. Turnbull. Academic Press Inc., New York, Academic Books Ltd., London. 429 pp. $12.

The sixth volume of this well-known series contains three articles directly relating to the mechanical properties of solids. The article "Compression of Solids by Strong Shock Waves," by Rice, McQueen and Walsh, reports work carried out at Los Alamos in which metals were subjected to pressures of up to several hundred thousand atmospheres with the help of explosives. From velocity measurements a Hugoniot curve can be constructed, that is, a curve showing the pressure and volume behind a shock wave with the shock wave velocity as parameter. The authors show how more orthodox thermodynamic curves (e.g. pressure-volume isotherms) can be deduced from the Hugoniot curve and a knowledge of the Grüneisen constant of the material. Data for twenty-seven metals are plotted and tabulated. The theme of Professor Borelius' article, "Changes of State of Simple Solid and Liquid Metals" is closely related; he shows that a division of thermo-dynamic quantities into a vibrational part (given by a Debye function) and a remaining 'structural' part leads to a satisfactory correlation of the experimental facts.

In "Macroscopic Symmetry and Properties of Crystals," Charles S. Smith derives, largely by direct physical arguments, the restrictions which the symmetry of a crystal imposes on the arrays of coefficients which describe its physical properties. Tensors of up to the fourth rank are considered. As his primary example of a fourth-rank tensor the author considers not the familiar elastic constants, but the piezo-resistivity coefficients. Results for the elastic constants then follow at once on imposing the additional requirement that (with the usual two-suffix notation) the array of coefficients be symmetric.

The rest of the volume is concerned with the electronic properties of solids. The articles by Piper and Williams ("Electroluminescence"), Dekker ("Secondary Electron Emission") and Givens ("Optical Properties of Metals") each contain experimental material and a theoretical discussion. In the final article ("Theory of the Optical Properties of Imperfections in Non-Metals") Dexter guides the reader along the chain of approximations which leads from a precise quantum-mechanical formulation to a manageable theory.

J. D. Eshelby

Solid State Physics: Advances in Research and Applications, Vol. 7. Edited by F. Seitz and D. Turnbull. Academic Press Inc., New York, Academic Books Ltd., London 525 pp. $12.

The longest article in the present volume is Huntington's comprehensive 160-page review of "The Elastic Constants of Crystals." It begins with an outline of macroscopic and atomic theory (including a sceptical look at the Laval theory) and a summary of methods of measurement. This is followed by tables of experimental results (with accompanying theoretical commentary) and an account of the effects of pressure and temperature. The final section discusses the influence of (among other things) lattice imperfection and superconductivity.

A. F. Wells gives a refreshing treatment of "The Structures of Crystals." His starting point is not the theory of space-groups but rather the topological problem of linking atoms together. In "Electron Energy Bands in Solids" Callaway outlines modern methods of calculating band structures and gives a critical review of the results which have been obtained so far. Becker's article ("Study of Surfaces by Using New Tools") is concerned with two new devices for investigating crystal surfaces. One is the simple and elegant field emission electron microscope of Müller, and its more powerful offshoot the field-ion microscope, in which electrons are replaced by ions

in order to increase the resolving power. The other is a rapid-acting ion gauge with which pressure-changes associated with adsorption and desorption can be studied.

The remaining two articles deal with transport processes. Klemens ("Thermal Conductivity and Lattice Vibrational Modes") is concerned with the thermal conductivity of non-metals and the lattice component of the thermal conductivity of metals and alloys. As often in solid state theory it proves easier to estimate the effect of imperfections that to solve the problem for the perfect crystal. Lewis's article "Wave Packets in Metals" discusses a troublesome technical point in conductivity theory. Roughly speaking, the difficulty is that for the usual perturbation theory to be valid the time occupied by an electron-phonon collision ought to be small compared with the time between collisions, and this condition, or rather its quantum-mechanical analogue, is commonly not satisfied. Specialists in this field will find the author's point of view instructive. Others, even if they are not prepared to follow the argument in detail, will, perhaps, be reassured by his conclusion that results obtained by the orthodox treatment are in fact correct.

J. D. ESHELBY

D. E. R. GODFREY: **Theoretical Elasticity and Plasticity for Engineers,** Thames and Hudson, London, 1959, 311 + x pp., 42s.

THE FIRST part of this book would appear to be based on a course of lectures on elasticity delivered a few years ago by A. C. Stevenson to post-graduate mathematicians at University College, London. The first two chapters analyse stress and infinitesimal strain using the vector method, these are then related for an isotropic, homogeneous elastic body by invoking Hooke's Law and the depen dence of the strain-energy on the strains only. Chapters III and V deal with pure bending and bending with shear respectively. The treatment of torsion in Chapter IV presents the well-known analytical solutions. A brief application of the conformal transformation method is given. The reviewer believes that the author has missed an opportunity in failing to introduce to engineers the idea of approximating to the value of the torsional rigidity by bounding methods. The torsion problem is particularly convenient as an introduction to such methods. Chapter VI is concerned with two-dimensional elasticity. This chapter serves a useful purpose by introducing the complex variable technique to the notice of the engineer, a thorough grasp of the methods here will help those going on to the advanced treatise by N. I. MUSKHELISHVILI *Some Basic Problems in the Mathematical Theory of Elasticity*. Chapter VII on curvilinear coordinates deals with the spherically and axially symmetric theory while Chapter VIII explains the ideas involved in the theory of concentrated and discontinuous loads in two and three dimensions. Chapter IX is concerned with the theory of thin flat plates and here, the reviewer, although he agrees that Stevenson's notation for stress-couples is logically superior to that usually used, cannot believe that it is useful to introduce it to engineers.

Chapters X, XI and XII are entitled theory of plasticity, plastic bending and torsion of a beam and plane problems of plasticity respectively. It is the reviewer's opinion that this part is so sketchy as to be practically worthless and as an introduction for engineers does not come up to PRAGER and HODGE *The Theory of Perfectly Plastic Solids*. The problems and solutions are a useful addition to the book. In the solution at the top of page 299, the error should read 27 per cent and not 6 per cent.

The book is unfortunately marred by poor proof-reading (or bad printing), 60 being a lower bound for the number of accents over the stresses which have been omitted!

F. A. GAYDON

J Mech. Phys. Solids, 1960, Vol. 8, pp. 81 to 86. Pergamon Press Ltd., London. Printed in Great Britain

STRESS CRITERION FOR FATIGUE FRACTURE OF STEELS

By T. Yokobori
Tohoku University, Sendai, Japan

(*Received 3rd November*, 1959)

Summary

An approach is presented to the problem of correlating the macroscopic fatigue strength of steels with microscopic explanations of present dislocation theory. The stress concentration or notch effect due to the obstacle itself against which the dislocations pile up is taken into account in addition to assuming that stress concentration at the piled-up dislocations plays an important role in fatigue fracture of steels. The agreement with the characteristic features in stress criterion for fatigue fracture of steels is good.

1. Introduction

In this article an approach is presented to the problem of correlating the macroscopic behaviour of engineering materials with microscopic explanations of present dislocation theory. It has been pointed out by Wood (1958) that in the case of OFHC copper and α-brass the fatigue failure at large stress amplitudes appears to be started by stress concentrations at a point where dislocations are piled up. On the other hand, since in the case of steels the stress criterion for fracture corresponding to the early part of a S/N curve appears to be similar to that for the later part of the curve, it is assumed in this article that stress concentration at the piled-up dislocations plays an important role in fatigue fracture under stress amplitudes corresponding to the later part of S/N curve including endurance limit. A salient feature, however, of this article is that the stress concentration or notch effect due to the obstacle itself against which the dislocations pile up is taken into account in addition. Attempts were made previously to derive the stress criterion for fatigue fracture along these lines (Yokobori 1957a, b). In this article the model is considered in more detail ; the argument is an order-of-magnitude or qualitative one and agreement with data is dependent upon appropriate choices of the constants related to notch stress concentration. However, the characteristic features in stress criterion for fatigue fracture of steel appear to be well explained.

2. Theoretical Considerations

In fatigue of steels under alternating stresses some of the dislocations may be in cyclic motion, and pushed and piled up cyclically against such obstacles as inclusions and pearlite or carbides during moving forward and backward. Let us assume the obstacle is an elliptic cylinder. The following notation is used :

AA' = the cross-section of the specimen

XX' = the active slip plane on which dislocations pile up

YY' = the plane containing the long axis of the ellipse of the obstacle and being perpendicular to the plane of the ellipse

ZZ' = the axis of the specimen

θ = the angle YQX' between planes XX' and YY'

ϕ = the angle between the planes YY' and AA'.

It may be reasonable to consider that the active slip-plane nearest to the tip P of the obstacle (Fig. 1) intersects the obstacle at a distance from the tip not greater than the mean distance l between Frank-Read sources (FRANK and READ 1950). For Frank-Read sources further than l from the tip toward the slip plane XX' intersecting the obstacle may already have been operated. Then we assume the average distance between X and P (Fig. 1) as $\frac{1}{2}l$, taking the mean value from zero

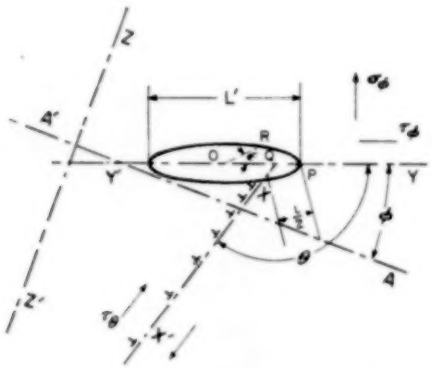

FIG. 1. Fatigue crack initiation based on this present model.

to l. Now there exists a concentrated tensile stress $q_3\,\tau_\theta$ due to the piled-up dislocations, where τ_θ = the applied shear stress component on the XX' plane and in the XX' direction, q_3 = the stress concentration factor due to piled-up dislocations. q_3 is written (STROH 1954)

$$q_3 = \sqrt{\left(L \Big/ \frac{l}{2}\right)}\, F(\theta) \tag{1}$$

where L = slip distance (in this case one half the grain diameter), $F(\theta)$ = a factor depending on the relative orientation of YY' to XX'.

Let σ_ϕ denote the applied tensile stress component normal to the plane YY', and τ_ϕ the applied shear stress component on the plane YY'. Since this type of obstacle is considered to produce a stress concentration on the boundary due to notch effect, at a point R on the periphery of the obstacle the circumferential

tensile stresses $q_{1,\epsilon}\,\sigma_\phi$ and $q_{2,\epsilon}\,\tau_\phi$ are induced by σ_ϕ and τ_ϕ respectively, where $q_{1,\epsilon}$ and $q_{2,\epsilon}$ are stress concentration factors and $\epsilon = ROY$. Therefore, the total sum σ of these tensile stresses is

$$\sigma = q_{1,\epsilon}\,\sigma_\phi + q_{2,\epsilon}\,\tau_\phi + q_3\,\tau_\theta. \tag{2}$$

The value of ϵ, ϕ and θ giving the maximum value σ_m of σ in (2) will be denoted by ϵ_m, ϕ_m and θ_m, respectively. Suppose fatigue fracture (crack) initiates when σ_m reaches some critical value, say, one tenth of Young's modulus E. Then the fatigue fracture criterion is

$$q_{1,\epsilon_m}\,\sigma_{\phi_m} + q_{2,\epsilon_m}\,\tau_{\phi_m} + q_{3,m}\,\tau_{\theta_m} = \alpha\,E \tag{3}$$

where q_{1,ϵ_m}, q_{2,ϵ_m} and $q_{3,m}$ are the values of $q_{1,\epsilon}$, $q_{2,\epsilon}$ and q_3, respectively, corresponding to ϵ_m, ϕ_m and θ_m, and α is a numerical value of order of one tenth. It is assumed that the specimen contains obstacles and crystal grains with all orientations. The position of the maximum value of the stress concentration factor $q_{1,\epsilon}$ due to applied tensile stress component σ_ϕ is P in Fig. 1. The position of the maximum value of stress concentration factor $q_{2,\epsilon}$ due to applied shear stress component τ_ϕ is fairly remote from that of the maximum value of stress concentration factor $q_{1,\epsilon}$ due to the applied tensile stress component σ_ϕ. That is, the plane on which the maximum concentrated tensile stress due to τ_ϕ acts is inclined with the plane YY' on which the maximum tensile stress due to σ_ϕ acts. The former makes an acute angle with the piled-up plane XX', if we assume in a first approximation for convenience the maximum tensile stress concentration by piled-up dislocations is on the plane perpendicular to this slip plane. On this reasoning the concentrated tensile stress $q_{2,\epsilon}\,\tau_\phi$ due to the applied shear stress τ_ϕ in (2) was previously neglected (Yokobori 1957a, b).

Now, since the analytical solution of (3) is very complex, tensile (or bending) and torsion tests are considered in what follows. In a tensile test, $q_{1,\epsilon}\,\sigma_\phi + q_{2,\epsilon}\,\tau_\phi$ in (2) takes the maximum value $q_{mi}\,\sigma_i$ when $\epsilon = 0$ and $\phi = 0$, where

σ_i = applied tension stress,

$q_{mi} = \beta\sqrt{(L'/b)}$ (Inglis 1913),

L' = the length of the longitudinal axis of the ellipse of the obstacle,

b = radius of the tip of the ellipse,

β = numerical value of order of unity.

q_3 takes the maximum value $q_{3,m}$ when $\theta = 109{\cdot}5^\circ$ (Stroh 1954). On the other hand, τ_θ takes maximum value $\frac{1}{2}\,\sigma_i$ when $\phi = 0$ and $\theta = \frac{3}{4}\pi$. Therefore, for convenience in a first approximation, $q_3\,\tau_\theta$ in (2) is assumed to reach the maximum value $q_{3,m}\,\tau_{\theta m}$ for $\theta = \frac{3}{4}\pi$ and $\phi = 0$. Then, using (1), the tensile stress $q_{3,m}\,\tau_{\theta m}$ at the tip P due to piled-up dislocations is written

$$q_{3,m}\,\tau_{\theta m} = \gamma\sqrt{\left(\frac{L}{l}\right)}\,\frac{\sigma_i}{2} \tag{4}$$

where γ is a numerical value of order unity. Thus, the criterion (3) reduces to

$$\beta\sqrt{(L'/b)}\,\sigma_i + \gamma\sqrt{(L/l)}\,\tfrac{1}{2}\,\sigma_i = \alpha\,E. \tag{5}$$

In a torsion test $q_{1,\epsilon}\,\sigma_\phi + q_{2,\epsilon}\,\tau_\phi$ in (2) takes the maximum value $q_{ms}\,\tau_s$ when $\epsilon = 0$ and $\phi = \frac{1}{4}\pi$, where

τ_s = applied shear stress,

$q_{ms} = \delta\sqrt{(L'/b)}$,

δ = numerical value of order of unity.

τ_θ takes maximum value τ_s when $\phi = \frac{1}{4}\pi$ and $\theta = \frac{3}{4}\pi$. Therefore, $q_3\,\tau_\theta$ in (2) is assumed to reach the maximum value $q_{3,m}\,\tau_{\theta_m}$ for $\phi = \frac{1}{4}\pi$ and $\theta = \frac{3}{4}\pi$, assuming for convenience in a first approximation that q_3 takes the maximum value $q_{3,m} = \gamma\sqrt{(L/l)}$ for $\theta = \frac{3}{4}\pi$ as mentioned above. That is,

$$q_{3,m}\,\tau_{\theta m} = \gamma\sqrt{(L/l)}\,\tau_s. \tag{6}$$

Thus, the criterion (3) reduces to

$$\delta\sqrt{\left(\frac{L'}{b}\right)}\,\tau_s + \gamma\sqrt{\left(\frac{L}{l}\right)}\,\tau_s = \alpha E. \tag{7}$$

Therefore, the ratio τ_s/σ_t is obtained from (5) and (7) as

$$\tau_s/\sigma_t = \tfrac{1}{2}\left[1 + \left\{1 + \left(\frac{b}{l}\cdot\frac{L}{L'}\right)^{\frac{1}{2}}\right\}^{-1}\right] \tag{8}$$

where β, γ and δ are assumed as unity. If we assume fatigue fracture occurs when the average tensile stress over the distance ξ (NEUBER 1937) on the YY' plane from the tip P reaches some critical value, the $\sqrt{(bL/lL')}$ may only be replaced by $\sqrt{\{\xi L/(\xi + l)\,L'\}}$ in (8), that is,

$$\tau_s/\sigma_t = \tfrac{1}{2}\left[1 + \left\{1 + \left(\frac{\xi}{\xi + l}\cdot\frac{L}{L'}\right)^{\frac{1}{2}}\right\}^{-1}\right]. \tag{9}$$

Equations (8) and (9) reduce to

$$\tau_s/\sigma_t = 0{\cdot}5 \quad \text{for} \quad L/L' \to \infty,$$

$$\tau_s/\sigma_t = 1{\cdot}0 \quad \text{for} \quad L/L' \to 0,$$

and

$$1{\cdot}0 > \tau_s/\sigma_t > 0{\cdot}5 \quad \text{for} \quad \infty > L/L' > 0.$$

In other words, when the value of L'/L increases from zero towards infinity, the stress criterion for fatigue fracture changes from a maximum shear stress law towards a maximum tensile stress law. This result may explain the experimental features described later. In (9), putting $\xi L/(\xi + l)\,L' \simeq 30$, we get $\tau_s/\sigma_t = 0{\cdot}577$. This value is in agreement with the result obtained from a Mises type criterion (SINES and WAISMAN 1959), which appears held in many soft steels. Assuming $\xi \geqslant l$, L/L' must be about 30 to 60 in this case. This value appears to be not unreasonable, because L' should be the length of the region of the interface where there is no cohesion between the obstacle and the surrounding matrix (that is, the length of the region of mere contact), and such value of the length L' might be considered not so large.

3. Conclusions

From the theoretical considerations above, the following three features in fatigue fracture may be interpreted.

(1) Equations (8) or (9) predicts that in fatigue fracture of steels neither the maximum shear stress law nor maximum tensile stress law is obeyed, which is in agreement with the trend of data reported in the literature.

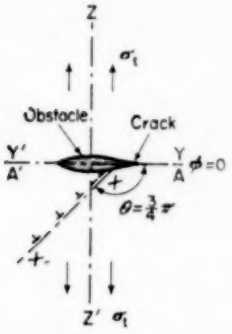

Fig. 2. Predicted crack direction in tensile fatigue test.

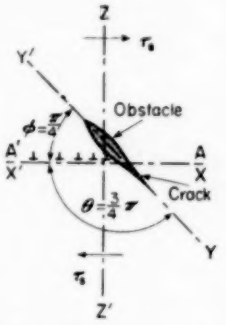

Fig. 3. Predicted crack direction in torsional fatigue test.

(2) Equation (8) predicts that the ratio τ_s/σ_t of torsional fatigue strength τ_s to tensile (or bending) fatigue strength σ_t increases when the ferrite path L decreases under the condition of equal size L' and shape of pearlite patches in carbon steels. Experimental results on carbon steel with various carbon content (Nishihara and Kawamoto 1940, 1941 ; Gough 1951 ; Sines and Waisman 1959) appear understandable from this viewpoint, although the size of pearlite patches also might be different.

(3) The fatigue strength is higher in spheroidized steel than in lamellar pearlitic steel with equal mean ferrite path L, and it has been inferred that the fatigue strength is independent of mean ferrite path (Dieter *et al.* 1955). However, the fact is interpreted in such a different way that from (5) the fatigue strength is understood to be higher in spheroidized steel with obstacles (carbides) of smaller length L' as stress raiser than in lamellar pearlitic steel with obstacles (lamellar carbides) of larger length L' since ferrite path L is equal for both in this case, although the fatigue strength is also dependent on ferrite path L.

(4) The length L' of inclusions as stress raiser may be considered as larger in steels with larger inclusions. Hence in such materials τ_s/σ_t may be larger as predicted by (8). Experimental results remarked by Sopwith (Peterson 1956) may well be interpreted on these lines.

(5) The theory predicts that, under both tension and torsion tests, fatigue cracks (fracture surface) will run normal to the principal stress (Figs. 2 and 3), which is in agreement with the data under stress amplitudes corresponding to the later part of S/N curve.

REFERENCES

DIETER, G. E., MEHL, R. F. and HORNE, G. T.	1955	*Trans. Amer. Soc. Met.* **47**, 423.
FRANK, F. C. and READ, W. T. Jr.	1950	*Phys. Rev.* **79**, 722.
GOUGH, H. J.	1951	*Aero. Res. Council R. and M.* 2522.
INGLIS, C. E.	1913	*Trans. Inst. Naval Arch.* **1**, 219.
NEUBER, H.	1937	*Kerbspannungslehre* (Julius Springer, Berlin).
NISHIHARA, T. and KAWAMOTO, M.	1940	*Trans. Jap. Soc. Mech. Engrs.* **6**, 8.
	1941	*Ibid.* **7**, 85.
PETERSON, R. E.	1956	*IUTAM Colloquium on Fatigue*, (Springer-Verlag, Berlin) 186.
SINES, G. and WAISMAN, J. L.	1959	*Metal Fatigue* (McGraw-Hill) 151.
STROH, A. N.	1954	*Proc. Roy. Soc.* A **223**, 404.
WOOD, W. A.	1958	*Phil. Mag.* **3**, 692.
YOKOBORI, T.	1957a	*J. Appl. Mech.* **24**, 77.
	1957b	*Tech. Reports of Tohoku Univ. Japan* **22**, 51.

J. Mech. Phys. Solids, 1960, Vol. 8, pp. 87 to 99. Pergamon Press Ltd., London. Printed in Great Britain

THE CLASSICAL TORSION PROBLEM FOR SECTIONS WITH CURVILINEAR BOUNDARIES

By W. A. Bassali
Faculty of Science, University of Alexandria

(*Received* 11*th November*, 1959)

Summary

This paper is concerned with the application of complex variable analysis to obtain solutions for the Saint-Venant torsion problem corresponding to certain sections with regular curvilinear boundaries. The area of the cross-section is conformally mapped on the unit circle by a transformation involving some parameters. By varying these parameters various shapes having several axes of symmetry are obtained. Sections bounded by $n\,(>2)$ equal and very approximately circular arcs are included as particular cases. Closed and exact expressions are derived for the complex torsion function, the torsional rigidity, and the shearing stresses at any point of the section. The distribution of shearing stress on the boundary is investigated in the general case and graphs showing its variation in four particular examples are plotted.

1. Introduction

Several methods have been used to solve the Saint-Venant torsion problem (linear small strain elasticity) for various sections; references are to be found in two recent papers by the author (1959, 1960). The method of images was applied by Hay (1939) to discuss sections bounded by a rectangle, an equilateral triangle, an isosceles right triangle and a 30° right triangle. Comprehensive reviews of the problem with extensive bibliographies have been given by Pöschl (1921) and Higgins (1942). An excellent survey of approximate mathematical methods has also been presented by the latter author (1943). An approximate method suitable for closed sections having several axes of symmetry has been discussed by Galimkhanov (1955). In a recent paper Poritsky (1958) has examined several graphical and exact analytical methods. A specialized text by Weber and Günther† (1958) contains a good collection of a number of torsion solutions useful in engineering problems.

Functions of a complex variable have been applied by many investigators. Cauchy integral methods have been introduced by Muskhelishvili (1949) and quoted by Sokolnikoff (1956), who gave a formal solution when the mapping function is written in the form

$$z = \sum_{n=0}^{\infty} a_n \zeta^n. \tag{1.1}$$

As illustrative examples Sokolnikoff (1956) treated sections with the shapes of the cardioid, the lemniscates of Bernoulli and Booth and the case of a section

†See the review of this book in *Math. Rev.* 1959, **20**, 81.

bounded by two circular arcs. TREFFTZ (1921) and SETH (1934) have used the Schwarz-Christoffel transformation to investigate the torsion problem concerning regular rectilinear polygons. Sections whose boundaries are the curves

$$r = a + b\,(1 + \cos\theta) \tag{1.2}$$

and

$$r^2 = a^2 + b^2 \cos 2\theta \tag{1.3}$$

have been considered by MUSHTARI (1933, 1935); his method consists essentially of assuming the complex torsion functions to have certain forms involving integral and fractional powers of the complex variable z. The solution for a circular shaft with two slits extending from the ends of a diameter to any depth along the diameter was obtained in closed form by WIGGLESWORTH (1940) who mapped the area of the cross-section of the shaft conformally on a half-plane and applied Schwarz's formula. The complex torsion function for beams whose boundaries consist partly of a straight line has been determined by GHOSH (1947) whose method was applied to a semi-circular area, a semi-loop of the lemniscate of Bernoulli and a semi-cardioid (MITRA 1949). Conformal transformations have been used by STEVENSON (1948) to study the Dirichlet problem for a ring space. His method was illustrated by determining the torsional rigidities of sections bounded by confocal ellipses or eccentric circles. Sections transformable to a ring space have been investigated by MORRIS and HAWLEY (1958).

STEVENSON (1943) and the author (1960) have treated sections bounded by regular curvilinear polygons of n sides and n rounded vertices (which may become cusps). The boundary curves, taken in the z-plane, can be mapped on the unit circle γ in the ζ-plane under the conformal transformations

$$z = c\,\zeta\,(1 + m\,\zeta^n), \quad c > 0, \quad 0 \leqslant |m|\,(n+1) \leqslant 1, \tag{1.4}$$

$$z = c\,\zeta/(1 + m\,\zeta^n), \quad c > 0, \quad 0 \leqslant |m|\,(n-1) \leqslant 1, \tag{1.5}$$

respectively. Sections bounded by the inverses of an ellipse with respect to any point on its major or minor axis have been recently considered by the author (1959). It was found that the mapping function in this case takes the form

$$z = c\,\zeta/(1 + n\,\zeta + m\,\zeta^2), \quad c > 0, \tag{1.6}$$

where m, n are real and $|m| < 1$, $|n| < 2$. In this paper we deal with sections which are mapped on the unit circle by the more general mapping function

$$z = c\,\zeta/(1 + m\,\zeta^n + p\,\zeta^{2n}), \quad c > 0, \tag{1.7}$$

where n is an integer and m, p are real coefficients restricted so that the roots of $z'(\zeta) = 0$ do not lie inside γ. It will be seen that the results include those of the two foregoing papers (BASSALI 1959, 1960) as particular cases. For $n > 2$, $m = -2/n\,(n-1)$ and $p = (n-2)/n^2\,(2n-1)$ we shall show in the next Section that the bounding curve consists of n equal and very approximately circular arcs. By varying the three parameters involved in the mapping function various sections having several axes of symmetry may be obtained.

2. Mapping Function

We now consider the classical torsion problem of an isotropic cylindrical beam whose section is bounded by the closed contour Γ_n in the z-plane* ($z = x + iy = r\,e^{i\theta}$), where Γ_n is conformally mapped on the unit circle in the ζ-plane by

$$z = c\zeta/(1 + m\zeta^n + p\zeta^{2n}), \quad c > 0, \quad \zeta = \xi + i\eta = \rho e^{i\phi}\,; \tag{2.1}$$

n being a positive integer and m, p are two real parameters. In order that this transformation shall be conformal at all points within Γ_n the parameters m and p must be restricted such that $z'(\zeta)$ does not vanish or become infinite within Γ_n. It is sufficient to consider either positive or negative values of m. This is due to the fact that the transformation (2.1) is equivalent to the transformation

$$z' = c\,\zeta'/(1 - m\,\zeta'^n + p\,\zeta'^{2n}),$$

where $z = z' \exp(i\pi/n)$ and $\zeta = \zeta' \exp(i\pi/n)$.

If Γ_n' is the inverse of Γ_n with respect to the circle $|z| = f$ and $z = x + iy$, $z' = x' + iy'$ are the points on Γ_n, Γ_n', respectively, which correspond to $\sigma = e^{i\phi}$ on γ then

$$z'\,\bar{z} = f^2. \tag{2.2}$$

Introducing (2.2) in (2.1) now leads to

$$z' = c'\,e^{i\phi}\,(1 + me^{-ni\phi} + pe^{-2ni\phi}), \tag{2.3}$$

where $c'\,c = f^2$. (2.4)

The parametric equations of Γ_n' are therefore

$$\left.\begin{aligned} x'/c' &= \cos\phi + m\cos n_1\phi + p\cos n_2\phi, \\ y'/c' &= \sin\phi - m\sin n_1\phi - p\sin n_2\phi. \end{aligned}\right\} \tag{2.5}$$

where

$$n_1 = n - 1, \quad n_2 = 2n - 1, \tag{2.6}$$

while those of Γ_n are

$$\left.\begin{aligned} cx/r^2 &= \cos\phi + m\cos n_1\phi + p\cos n_2\phi, \\ cy/r^2 &= \sin\phi - m\sin n_1\phi - p\sin n_2\phi. \end{aligned}\right\} \tag{2.7a}$$

where

$$c^2/r^2 = 1 + m^2 + p^2 + 2m\,(1 + p)\cos n\,\phi + 2p\cos 2n\,\phi. \tag{2.7b}$$

In general, it can be shown that each of Γ_n or Γ_n' is a certain regular curvilinear polygen with n sides and n rounded vertices (which may becomes cusps). For the contour Γ_n these rounded vertices or indentations occur when r is a minimum and become cusps when the critical points of the transformation, given by $z'(\zeta) = 0$, fall upon the boundary Γ_n. It is easily seen that if

$$mn_1 + p\,n_2 = 1, \qquad |p|\,n_2 \leqslant 1, \tag{2.8}$$

then the boundary Γ_n has n cusps which correspond to the points

$$\sigma_s = c\exp(2s\,i\,\pi/n) \quad (s = 0, 1, 2, \ldots, n - 1)$$

on γ. From (2.1) it follows that these cusps lie at the points

$$z_s = c\left[\exp(2si\,\pi/n)\right]/(1 + m + p) \quad (s = 0, 1, 2, \ldots, n - 1).$$

The case $n = 1$ leads to the transformation (1.6) which has been studied in detail in a previous paper (Bassali 1959), where some figures are drawn. We now consider the cases $n = 2$ and $n > 2$.

The case $n = 2$. Here we have the mapping function

$$z = c\,\zeta/(1 + m\,\zeta^2 + p\,\zeta^4), \tag{2.9}$$

*This is chosen to coincide with the plane $Z = 0$ perpendicular to the generators of the cylinder.

and the parametric equations for Γ'_2 simplify to

$$\left.\begin{aligned} x'/c' &= (1+m)\cos\phi + p\cos 3\phi, \\ y'/c' &= (1-m)\sin\phi - p\sin 3\phi, \end{aligned}\right\} \tag{2.10}$$

which represent a family of ovaloids symmetrical with respect to the coordinate axes. When $1+m=-9p$ it can be seen that Γ'_2 becomes a curvilinear rectangle whose sides are parallel to the coordinate axes and are of lengths $-16\,pc'$ and $4\,(1+5p)\,c'$. For $m=0$, $p=-1/9$ the contour Γ'_2 is a square hypotrochoid while if $m=2/7$, $p=-1/7$ then the ratio between the sides of the curvilinear rectangle Γ'_2 is $2:1$. The latter curve and its inverse Γ_2 with respect to a concentric circle are shown in Fig. 1

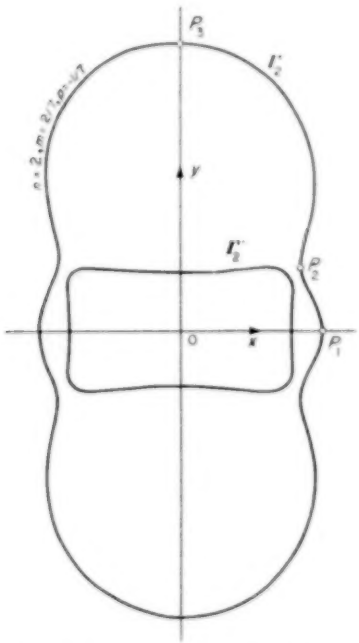

FIG. 1. Section bounded by the inverse of a curvilinear rectangle.

The case $n>2$. It is easily proved that the function

$$z' = c'\,\zeta'\left[1 - \sum_{\nu=1}^{\infty}\frac{2}{n}\left(\frac{2}{n}-1\right)\left(\frac{2}{n}-2\right)\cdots\left(\frac{2}{n}-\nu+1\right)\zeta^{-\nu n}/\nu!\;(\nu n-1)\right]\;(n>2) \tag{2.11}$$

maps the infinite region outside a regular rectilinear polygon with n sides in the z'-plane on the area outside the unit circle in the ζ'-plane. As an approximation to the right side of (2.11) we retain only the first two terms of the infinite summation appearing in it. Hence we obtain

$$z' = c'\,\zeta'\,(1 + m\,\zeta'^{-n} + p\,\zeta'^{-2n}), \tag{2.12}$$

where

$$m = -2/n\,(n-1), \quad p = (n-2)/n^2\,(2n-1). \tag{2.13}$$

Assuming that z is the inverse of z' with respect to the circle $|z'|=f$ in the z'-plane and ζ is the nverse of ζ' with respect to $|\zeta'|=1$ then

$$z z' = f^2, \quad \zeta\zeta' = 1, \tag{2.14}$$

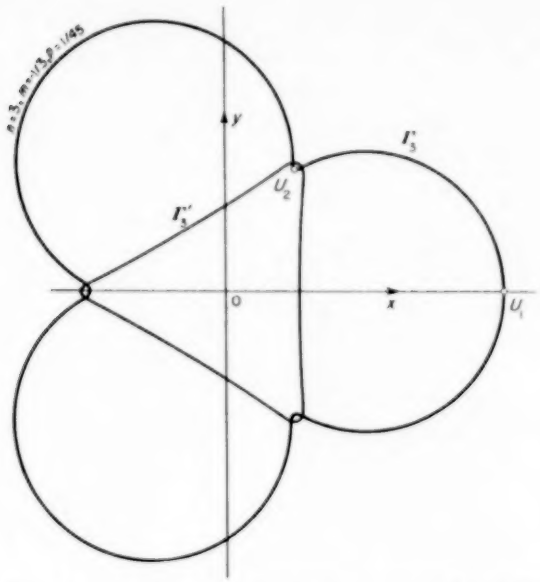

FIG. 2. Section bounded by three equal and approximately circular arcs.

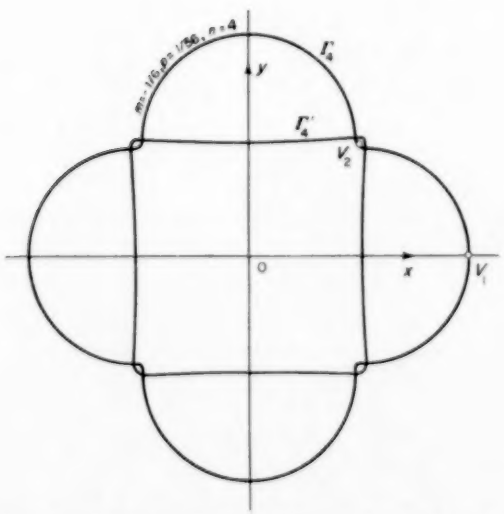

FIG. 3. Section bounded by four equal and approximately semi-circular arcs.

and combining (2.14) with (2.12) leads to the transformation (2.1). Thus it follows that, with the values (2.13), the closed curve Γ_n' is approximately a regular rectilinear polygon with n sides and the inverse curve Γ_n consists of the union of n equal and very approximately circular arcs each of which passes through the centre and two consecutive vertices of a regular rectilinear polygon with n sides. Figs. 2 and 3 illustrate the contours Γ_n and Γ_n' corresponding to $n = 3$, $m = -1/3$, $p = 1/45$ and $n = 4$, $m = -1/6$, $p = 1/56$, respectively. The curves Γ_3' and Γ_4' are also

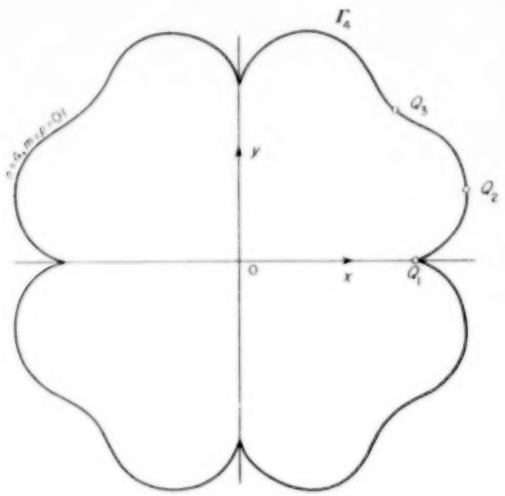

FIG. 4. Section with four axes of symmetry and four cusps.
$z = c\,\zeta/(1 + 0{\cdot}1\,\zeta^4 + 0{\cdot}1\,\zeta^8)$.

drawn in Figs. 41 and 43 of MUSKHELISHVILI's book (1949, pp. 371, 372). The section corresponding to the values $n = 4$, $m = p = 0{\cdot}1$ is shown in Fig. 4. These values satisfy the conditions (2.8) and the boundary Γ_4 has four cusps at the points $\pm 5c/6$ and $\pm 5ic/6$. For larger values of n the section bounded by Γ_n has grooves of a particular type.

3. COMPLEX TORSION FUNCTION

In the torsion problem it is known that the displacements u, v and w are furnished (STEVENSON 1943) by

$$u + iv = i\tau z\mathbf{Z}, \quad w = \tau\,\Phi(x, y) = \tfrac{1}{2}\,\tau\left[\Omega(z) + \bar{\Omega}(\bar{z})\right], \tag{3.1}$$

where τ is the constant twist per unit length of the cylinder and $\Omega(z) = \Phi(x, y) + i\,\Psi(x, y)$ is the complex torsion function which satisfies the boundary condition

$$\Psi(x, y) = \tfrac{1}{2}\,z\,\bar{z} \text{ along } \Gamma_n; \tag{3.2}$$

bars are used to denote conjugate complex quantities. Using (2.1), the function $\Omega(z)$ can be written in terms of ζ as

$$\Omega(z) = \omega(\zeta), \tag{3.3}$$

where $\omega(\zeta)$ is regular within γ. It is known (MUSKHELISHVILI 1949, p. 377) that

$$\omega(\zeta) = \frac{1}{2\pi}\int_{\gamma} \frac{z(\sigma)\,\bar{z}(\sigma^{-1})}{\sigma - \zeta}\,d\sigma + \text{constant}, \tag{3.4}$$

where ζ is any point inside γ. Introducing (2.1) in (3.4) yields

$$\omega(\zeta) = \frac{c^2}{2\pi} \int_\gamma \frac{\sigma^{2n}}{(1 + m\,\sigma^n + p\,\sigma^{2n})\,(\sigma^{2n} + m\,\sigma^n + p)\,(\sigma - \zeta)}\, d\sigma + \text{constant}. \tag{3.5}$$

Since the transformation (2.1) maps the area inside γ in the ζ-plane on the area inside Γ_n in the z-plane we see that the $2n$ roots of the equation

$$p\,\sigma^{2n} + m\,\sigma^n + 1 = 0 \tag{3.6}$$

must lie outside γ. If λ' and λ'' are the two roots of the quadratic equation

$$pt^2 + mt + 1 = 0,$$

so that

$$\lambda' + \lambda'' = -m/p, \quad \lambda'\,\lambda'' = 1/p, \tag{3.7}$$

then the $2n$ roots of (3.6) are λ_s', λ_s'' $(s = 1, 2, \ldots, n)$, where

$$\lambda_s'^n = \lambda', \quad \lambda_s''^n = \lambda''. \tag{3.8}$$

We therefore have

$$\zeta^n - \lambda' = (\zeta - \lambda_1')(\zeta - \lambda_2') \ldots (\zeta - \lambda_n'), \tag{3.9}$$

and by logarithmic differentiation this yields

$$\sum_{s=1}^{n} 1/(\zeta - \lambda_s') = n\,\zeta^{n-1}/(\zeta^n - \lambda'),$$

and hence

$$\sum_{s=1}^{n} \lambda_s'/(\zeta - \lambda_s') = n\,\lambda'/(\zeta^n - \lambda'). \tag{3.10}$$

If $m^2 \neq 4p$ then the integrand of (3.5), viewed as a function of σ, has $2n$ simple poles λ_s', λ_s'' $(s = 1, 2, \ldots, n)$, which lie outside the unit circle. For large values of $|\sigma|$ the integrand is of the order of $1/|\sigma|^{2n+1}$, and we have

$$\omega(\zeta) = -c^2\,i \sum_{s=1}^{n} (R_s' + R_s'') + \text{constant}, \tag{3.11}$$

where R_s' is the residue of the integrand at λ_s' and R_s'' is the corresponding value at λ_s''. Applying (3.8), it is easily shown that

$$R_s' = \lambda'\,\lambda_s'/\big[np\,(\lambda'' - \lambda')\,(\lambda'^2 + m\,\lambda' + p)\,(\zeta - \lambda_s')\big], \tag{3.12}$$

and then (3.10) gives

$$\sum_{s=1}^{n} R_s' = \lambda'^2/\big[p\,(\lambda'' - \lambda')\,(\lambda'^2 + m\,\lambda' + p)\,(\zeta^n - \lambda')\big]. \tag{3.13}$$

The corresponding expression for $\sum_{s=1}^{n} R_s''$ is obtained from (3.13) by interchanging λ' and λ''. Inserting these values in (3.11) and making use of (3.7), one finds

$$\omega(\zeta) = \frac{c^2\,i\,(1 + p + mp\,\zeta^n)}{(1 - p)\,\{(1 + p)^2 - m^2\}\,(1 + m\,\zeta^n + p\,\zeta^{2n})} + \text{constant}. \tag{3.14}$$

In the particular case $m^2 = 4p$ the integrand in (3.5) has n double poles outside γ and it can be shown that the same formula (3.14) remains valid. Taking for the constant in (3.14) the value

$$-c^2\,i\,(1 + p)/\big[2\,(1 - p)\,\{(1 + p)^2 - m^2\}\big],$$

we obtain for the complex torsion function

$$\omega(\zeta) = \frac{c^2\,i}{2k}\,\frac{q - m\,\zeta^n - p\,q\,\zeta^{2n}}{1 + m\,\zeta^n + p\,\zeta^{2n}}, \tag{3.15}$$

where

$$k = (1 + p)^2 - m^2, \quad q = (1 + p)/(1 - p). \tag{3.16}$$

The imaginary part of (3.15) is

$$\Psi = \frac{c^2}{2k}\frac{q(1-p^2\rho^{4n}) - m^2\rho^{2n} + m\rho^n(q-1)(1-\rho^{2n})\cos n\phi}{1+m^2\rho^{2n}+p^2\rho^{4n}+2m\rho^n(1+p\rho^{2n})\cos n\phi + 2p\rho^{2n}\cos 2n\phi}, \tag{3.17}$$

which reduces to $\frac{1}{2}r^2$ on putting $\rho = 1$ and using (2.7b).

4. Torsional Rigidity

The torsional rigidity D is known (Stevenson 1943) to be given by

$$D = \mu(I + J), \tag{4.1}$$

where μ is the rigidity of the material of the cylinder, I is the polar moment of inertia for the cross-section, or

$$I = -\tfrac{1}{4}i\int_\gamma z(\sigma)z'(\sigma)\bar{z}^2(\sigma^{-1})\,d\sigma, \tag{4.2}$$

and

$$J = \tfrac{1}{2}\int_\gamma z(\sigma)\bar{z}(\sigma^{-1})\,\omega'(\sigma)\,d\sigma. \tag{4.3}$$

Introducing (2.1) in (4.2) leads to

$$I = -\tfrac{1}{4}ic^4\int_\gamma \frac{\sigma^{4n-1}(1-mn_1\sigma^n - pn_2\sigma^{2n})}{(\sigma^{2n}+m\sigma^n+p)^2(1+m\sigma^n+p\sigma^{2n})^3}\,d\sigma, \tag{4.4}$$

where n_1 and n_2 are defined by (2.6). Let μ' and μ'' be the two roots of the equation

$$t^2 + mt + p = 0,$$

so that

$$\mu' + \mu'' = -m, \quad \mu'\mu'' = p. \tag{4.5}$$

The integrand in (4.4) has $2n$ double poles inside γ at the points μ_s', μ_s'' $(s = 1, 2, \ldots, n)$, where

$$\mu_s'^n = \mu', \quad \mu_s''^n = \mu''. \tag{4.6}$$

If P_s' and P_s'' denote the residues of this integrand at the points μ_s' and μ_s'', respectively, then

$$I = \tfrac{1}{2}\pi c^4\sum_{s=1}^{n}(P_s' + P_s''). \tag{4.7}$$

Setting $\sigma = \mu_s' + t$ in the integrand of (4.4) and expanding the resulting expression in powers of t, one finds after a fair amount of algebraic manipulation and using (4.6), that the coefficient of t^{-1} in the expansion may be written as

$$P_s' = \frac{p^2}{n(p-1)^3(m^2-4p)(p\mu'-\mu''^3}\left[\alpha + \alpha'\mu' + \alpha''\mu'' + \frac{\beta+\beta'\mu'}{\mu'-\mu''} + \frac{\gamma+\gamma'\mu'}{p\mu'-\mu''}\right], \tag{4.8}$$

where

$$\left.\begin{aligned} &\alpha = mn_1p(4-p)/(p-1), \quad \alpha' = p^2n_2(5-2p)/(p-1), \quad \alpha'' = 3/(1-p),\\ &\frac{\beta}{2} = \frac{\gamma}{3p} = -p(1+p^2n_2), \quad \frac{\beta'}{2} = \frac{\gamma'}{3p} = mp(n_1 - n_2p). \end{aligned}\right\} \tag{4.9}$$

Interchanging μ' and μ'' in (4.8) gives the value of P_s''. Both P_s' and P_s'' are independent of s, and hence (4.7) becomes

$$I = \tfrac{1}{2}\pi nc^4(P_s' + P_s''). \tag{4.10}$$

After some straightforward calculations and repeated application of (4.5) the following expressions are arrived at:

$$\frac{1}{(p\mu' - \mu'')^3} + \frac{1}{(p\mu'' - \mu')^3} = \frac{m(1-p)}{p^3 k^3}\left[(1 + p + p^2)m^2 - 3p(1+p)^2\right], \tag{4.11}$$

$$\frac{\mu'}{(p\mu' - \mu'')^3} + \frac{\mu''}{(p\mu'' - \mu')^3} = -\frac{1}{p^3 k^3}\left[m^4 - p(4 + 3p + p^3)m^2 + 2p^2(1+p)^3\right], \tag{4.12}$$

$$\frac{\mu''}{(p\mu' - \mu'')^3} + \frac{\mu'}{(p\mu'' - \mu')^3} = \frac{1}{p^2 k^3}\left[p^2 m^4 - (1 + 3p^2 + 4p^3)m^2 + 2p(1+p)^3\right], \tag{4.13}$$

$$\frac{1}{(p\mu' - \mu'')^3} - \frac{1}{(p\mu'' - \mu')^3} = \frac{1+p}{p^3 k^3}(\mu'' - \mu')\left[(1 - p + p^2)m^2 - p(1+p)^2\right], \tag{4.14}$$

$$\frac{\mu'}{(p\mu' - \mu'')^3} - \frac{\mu''}{(p\mu'' - \mu')^3} = \frac{m(\mu' - \mu'')}{p^3 k^3}(m^2 - 2p - 3p^2 + p^4), \tag{4.15}$$

$$\frac{\mu''}{(p\mu' - \mu'')^3} - \frac{\mu'}{(p\mu'' - \mu')^3} = \frac{m(\mu' - \mu'')}{p^2 k^3}(p^2 m^2 + 1 - 3p^2 - 2p^3), \tag{4.16}$$

$$\frac{1}{(p\mu' - \mu'')^4} + \frac{1}{(p\mu'' - \mu')^4} = \frac{1}{p^4 k^4}\left[(1 + p^4)m^4 - 4p(1+p)(1+p^3)m^2 + 2p^2(1+p)^4\right], \tag{4.17}$$

$$\frac{\mu'}{(p\mu' - \mu'')^4} + \frac{\mu''}{(p\mu'' - \mu')^4} = -\frac{m}{p^4 k^4}\left[m^4 - p(5 + 4p - p^4)m^2 + p^2(5 - 3p)(1+p)^3\right]. \tag{4.18}$$

Introducing these values in (4.10) we find, after considerable reduction and dividing by $m^2 - 4p$, that the polar moment of inertia of the section bounded by Γ_n is

$$I = \frac{\pi c^4}{2(p-1)^4 k^4}\left[(1+p)^4(1 + 4np^2 + p^4) + \{n_1(1 - 4p + 4p^3) + 6np^2\}m^4 + 2(1+p)^2\{n - 2(2n+1)p + 4np^2 - 2(4n-1)p^3 + np^4\}m^2\right]. \tag{4.19}$$

In the two particular cases $n = 1$ and $p = 0$, the foregoing expression simplifies to

$$I = \frac{\pi c^4}{2(1-p)^4 k^4}\left[(1+p)^4(1 + 4p^2 + p^4) + 2(1+p)^2(1 - 6p + 4p^2 - 6p^3 + p^4)m^2 + 6p^2 m^4\right], \tag{4.20}$$

$$I = \frac{\pi c^4(1 + 2n m^2 + n_1 m^4)}{2(1 - m^2)^2}, \tag{4.21}$$

respectively.

Inserting (2.1) and the torsion function defined by (3.15) and (3.16) in (4.3) yields

$$J = -\frac{c^4 in}{2(1-p)k}\int_\gamma \frac{\sigma^{3n-1}\{m(1 + p^2\sigma^{2n}) + 2p(1+p)\sigma^n\}}{(\sigma^{2n} + m\sigma^n + p)(1 + m\sigma^n + p\sigma^{2n})^3}\,d\sigma \tag{4.22a}$$

$$= \frac{\pi n c^4}{(1-p)k}\sum_{s=1}^{n}(Q_s' + Q_s''), \tag{4.22b}$$

where Q_s' and Q_s'' are the residues of the integrand in (4.22a) at the poles μ_s' and μ_s'', respectively. It is easily shown that

$$Q_s' = \frac{p^2}{n(p-1)^3}\frac{m(p^3\mu' + \mu'') + 2p^2(1+p)}{(\mu' - \mu'')(p\mu' - \mu'')^3}, \tag{4.23}$$

and Q_2'' is deduced from (4.23) by interchanging μ' and μ''. With these values inserted in (4.22b) and making use of (4.14)–(4.16) the expression for J reduces to

$$J = -\frac{\pi n\, c^4}{k^2}\left[\frac{2p^2}{(1-p)^4} + \frac{m^2(1+p)^2}{k^2}\right]. \tag{4.24}$$

When (4.19) and (4.24) are substituted in (4.1), it is found that the torsional rigidity is

$$D = \frac{\mu\pi c^4}{2(1-p)^4 k^4}\left[(1+p)^4(1+n_2 p^4) - 4p(1+p)^2(1-np+n_2 p^2)m^2 + (n_1 - 4n_1 p + 2n p^2 + 4n_1 p^3)m^4\right], \tag{4.25}$$

which reduces to

$$D = \frac{\mu\pi c^4}{2(1-p)^4 k^4}\left[(1+p)^4(1+p^4) - 4p(1+p)(1+p^3)m^2 + 2p^2 m^4\right], \tag{4.26}$$

$$D = \frac{\mu\pi c^4}{2(1-m^2)^4}(1+n_1 m^4), \tag{4.27}$$

in the special cases $n = 1$ and $p = 0$, respectively. These expressions are in agreement with those obtained before (BASSALI 1959, 1960).

5. SHEARING STRESSES

The shearing stresses $\widehat{\rho Z}$ and $\widehat{\phi Z}$ at any point of the cross-section are determined (MUSKHELISHVILI 1949, p. 579) by the convenient formula

$$\widehat{\rho Z} - i\,\widehat{\phi Z} = \left[\mu\tau\zeta/\rho\,|z'(\zeta)|\right]\left[\omega'(\zeta) - iz'(\zeta)\,\bar{z}(\zeta)\right]. \tag{5.1}$$

Substituting from (2.1) and (3.15), (3.16) in (5.1) we obtain

$$\widehat{\rho Z} - i\,\widehat{\phi Z} = -\mu\tau T^{-1} ci\left[\rho(1 + m\zeta^n + p\zeta^{2n})(1 - mn_1\zeta^n - pn_2\zeta^{2n}) + \frac{n}{(1-p)\rho k}\left\{m\zeta^{-n} + 2p(1+p) + mp^2\zeta^n\right\}(\zeta^n + m\lambda^2 + p\lambda^2\zeta^n)^2\right], \tag{5.2a}$$

where

$$T = \left|1 - mn_1\zeta^n - pn_2\zeta^{2n}\right|\left|1 + m\zeta^n + p\zeta^{2n}\right|^2 = \left\{1 + n_1^2 m^2\lambda^2 + n_2^2 p^2\lambda^4 + 2n_1 m\lambda(n_2 p\lambda^2 - 1)\cos\phi - 2n_2 p\lambda^2\cos 2\phi\right\}^{\frac{1}{2}} \times \left\{1 + m^2\lambda^2 + p^2\lambda^4 + 2m\lambda(1 + p\lambda^2)\cos\phi + 2p\lambda^2\cos 2\phi\right\}, \tag{5.2b}$$

$$\lambda = \rho^n, \quad \phi = n\phi. \tag{5.2c}$$

Setting $\zeta = \rho e^{i\phi}$ in (5.2a) and separating real and imaginary parts we find

$$\widehat{\rho Z} = \frac{\mu n c\tau}{(1-p)\rho k T}\left[m\lambda\left\{(1-p^2)kt_1 + (m^2 - 2p - 4p^2 + kp\sqrt{1-p}\,\rho^2)t_n + p^2(4 + 2p - m^2)t_{2n} + p^4 t_{3n}\right\}\sin\phi + 2p\lambda^2\left\{(1+p)(t_1 + p^2\rho^2 t_{n_2}) + (1-p)m^2\rho^2 t_{n_1}\right\}\sin 2\phi + mp^2\lambda^3 t_n \sin 3\phi\right], \tag{5.3}$$

$$\widehat{\phi Z} = \frac{\mu\tau c}{T}\left[\rho\left\{1 - n_1 m^2\lambda^2 - n_2 p^2\lambda^4 + m\lambda(2 - n + \sqrt{2-3n}\,p\lambda^2)\cos\phi - 2n_1 p\lambda^2\cos 2\phi\right\} + \frac{n}{(1-p)\rho k}\left\{2\lambda^2\left(m^2 + p(1+p)(m^2+2p)\lambda^2 + m^2 p^3\lambda^4\right) + m\lambda\left(1 + p^4\lambda^6 + (m^2+2p)(1+p^2\lambda^2)\lambda^2 + 4p(1+p)(1+p\lambda^2)\lambda^2\right)\cos\phi + 2p(1+p)(1 + m^2\lambda^2 + p^2\lambda^4)\lambda^2\cos 2\phi + mp^2(1+\lambda^2)\lambda^3\cos 3\phi\right\}\right], \tag{5.4}$$

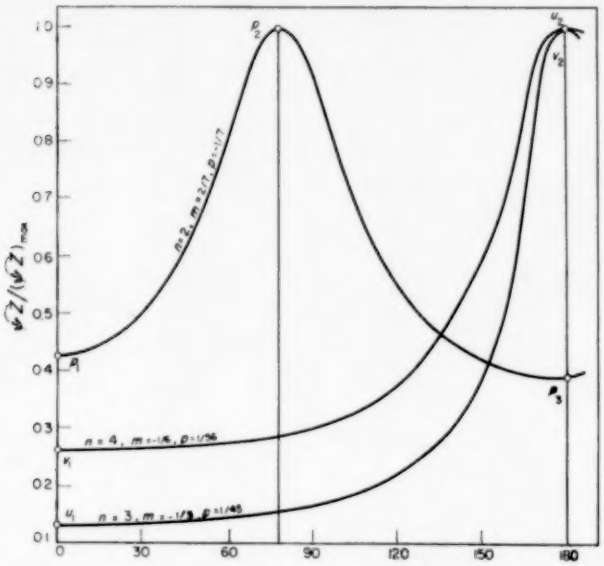

FIG. 5. Variation of shearing stress on the boundaries of the sections shown in Figs. 1–3.

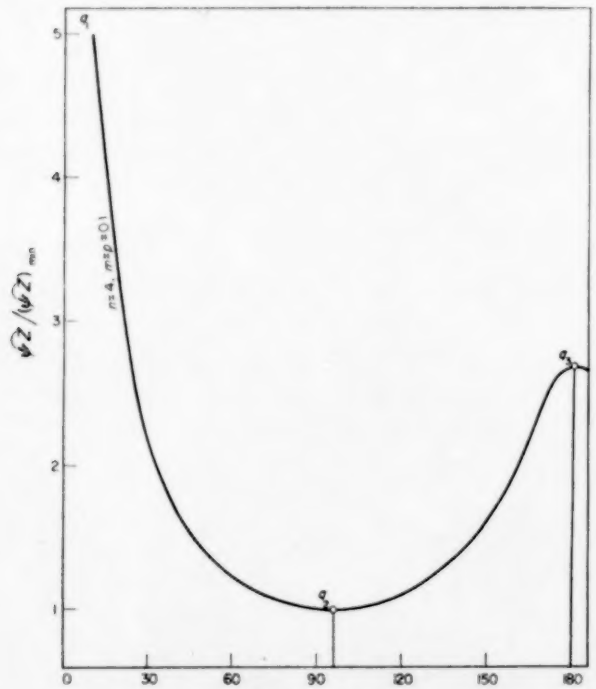

FIG. 6. Variation of shearing stress on the boundary of the section in Fig. 4.

where, for the sake of convenience, we have introduced the notation

$$l_n = 1 - \rho^{2n}. \tag{5.5}$$

Since the parameters m, p are chosen such that $z'(\zeta)$ does not vanish at any point within γ and the function $\omega(\zeta)$ is regular inside γ, it follows from (5.1) that the foregoing expressions for the stresses are necessarily finite and physically admissible across the section bounded by Γ_n. On the boundary Γ_n of the cross-section, $\rho = 1$ and (5.3) gives $\widehat{\rho Z} = 0$ as expected, while the peripheral shear stress (5.4) simplies considerably to

$$(\widehat{\phi Z})_{\rho=1} = \frac{\mu\tau c}{(1-p)k} \cdot \frac{A + B\cos\phi}{(C + 2D\cos\phi + E\cos^2\phi)^{\frac{1}{2}}}, \tag{5.6}$$

where $\phi = n\phi$ and

$$\left.\begin{aligned} A &= (1-p)\,n_1 m^2 + (1+p)(1+n_2 p^2), \\ B &= 2\,mnp, \\ C &= (1+n_2 p)^2 + m^2 n^2_1, \\ D &= n_1 m (n_2 p - 1), \\ E &= -4\,n_2 p. \end{aligned}\right\} \tag{5.7}$$

The maximum and minimum values of the tangential stress (5.6) on the boundary Γ_n occur alternately at the points $\phi = 0$, $\phi = \alpha$, and $\phi = \pi/n$, where

$$\cos n\,\alpha = \frac{AD - BC}{BD - EA}$$

$$= \frac{m}{2p} \cdot \frac{n_1(1+n_2 p^2)\{n_1 m^2 + (1+p)(1-n_2 p)\} + 2np(1+n_2 p)^2}{n_1 m^2\{2 - 3n + (2-n)n_2 p\} - 2n_2(1+p)(1+n_2 p^2)}, \tag{5.8}$$

on substitution from (5.7). The magnitudes of the shearing forces on the boundary at $\phi = 0$ and $\phi = \pi/n$ are determined from (5.6) and (5.7) as

$$(\widehat{\phi Z})_{\rho=1,\,\phi=0} = \frac{\mu\tau c}{(1-p)k} \cdot \frac{(1-p)\,n_1 m^2 + 2\,mnp + (1+p)(1+n_2 p^2)}{1 - n_1 m - n_2 p}, \tag{5.9}$$

$$(\widehat{\phi Z})_{\rho=1,\,\phi=\pi/n} = \frac{\mu\tau c}{(1-p)k} \cdot \frac{(1-p)\,n_1 m^2 - 2\,mnp + (1+p)(1+n_2 p^2)}{1 + n_1 m - n_2 p}. \tag{5.10}$$

Equations (2.8) and (5.9) show that the boundary value of the shearing stress at a cusp is infinite as expected. The considerable variation in peripheral shear due to the existence of grooves in the cylinder is illustrated in Figs. 5 and 6, where curves are plotted to show the distribution of shearing stress on the boundaries of the four sections sketched in Figs. 1–4. The points at which the stresses take their minimum and maximum values on the boundaries are indicated in all Figures†. As is usually the case the maximum values are attained at the bottoms of the grooves. This indicates the importance of considering stresses in slots and keyways of shafts.

REFERENCES

BASSALI, W. A.	1959	*J. Mech. Phys. Solids* **7**, 272.
	1960	*J. Math. Phys.* In press.
GALIMKHANOV, K. G.	1955	*Trud. Ufimsk. Aviats. in-ta* **1**, 66.
GHOSH, S.	1947	*Bull. Calcutta Math. Soc.* **39**, 107.
HAY, G. E.	1939	*Proc. London Math. Soc.* **45**, 382.
HIGGINS, T. J.	1942	*Amer. J. Phys.* **10**, 248.
	1943	*J. Appl. Phys.* **14**, 469.

†These points are shown in capital letters in Figs. 1–4 and in corresponding small letters in Figs. 5 and 6.

Mitra, D. N.	1949	*Bull. Calcutta Math. Soc.* **41**, 28.
Morris, R. M. and Hawley, F. J.	1958	*Qu. J. Mech. Appl. Math.* **11**, 462.
Mushtari, N. M.	1933	*Trans. Kazan Aviat. Inst.* **1**, 17.
	1935	*Trans. KIIKS* **1**, 53.
Muskhelishvili, N. I.	1949	*Some Basic Problems of the Mathematical Theory of Elasticity*, 3rd Ed. (Moscow).
Poritsky, H.	1958	*Proc. 3rd U.S. Nat. Congr. Appl. Mech.* (A.S.M.E., New York).
Pöschl, T.	1921	*Z. angew. Math. Mech.* **1**, 312.
Seth, B. R.	1934	*Proc. Camb. Phil. Soc.* **30**, 139.
Sokolnikoff, I. S.	1956	*Mathematical Theory of Elasticity*, 2nd Ed. (McGraw-Hill).
Stevenson, A. C.	1943	*Phil. Mag.* **34**, 114.
	1948	*Ibid.* **39**, 297.
Trefftz, E.	1921	*Math. Ann.* **82**, 306.
Weber, C. and Günther, W.	1958	*Torsiontheorie* (Vieweg, Braunschweig).
Wigglesworth, L. A.	1940	*Proc. London Math. Soc.* **47**, 20.

J. Mech. Phys. Solids, 1960, Vol. 8, pp. 100 to 104. Pergamon Press Ltd., London. Printed in Great Britain

YIELDING OF STEEL SHEETS CONTAINING SLITS

By D. S. Dugdale
Engineering Department, University College of Swansea*

(*Received 27th November*, 1959)

Summary

Yielding at the end of a slit in a sheet is investigated, and a relation is obtained between extent of plastic yielding and external load applied. To verify this relation, panels containing internal and edge slits were loaded in tension and lengths of plastic zones were measured.

1. Introduction

Notches, such as holes and slits, generally reduce the strength of sheet material. If no inelastic deformation is permissible, stresses must nowhere exceed the initial yield stress, though this may be subject to a size effect. If large-scale yielding is to be avoided, the applied load divided by minimum area of section should not reach the plastic flow stress. It is the purpose of the present work to trace the spread of plasticity from a centre of stress concentration as loads are increased.

Relaxation methods can often be applied to a particular problem for determining the field of plastic strain produced by given loads (Allen and Southwell 1950). However, in the present work, a prototype problem is sought which will allow a direct calculation of extent of yielding as a function of external load. When a very thin sheet containing a straight cut is loaded in a direction perpendicular to the cut, it may be expected that yielding will be confined to a very narrow band lying along the line of the cut.

2. Analysis of the Problem

An ideal elastic–plastic material is considered which flows after yielding at a constant uniaxial tensile stress Y. Uniform tensile stress T is applied to the edges of an infinite sheet in a direction perpendicular to an internal cut of total length $2l$. Yielding must occur over some length s measured from the end of the cut, as shown in Fig. 1 (a). It is suggested that the sheet may be considered to deform elastically under the action of the external stress together with a tensile stress Y distributed over part of the surface of a hypothetical cut of length $2a$ as shown in Fig. 1 (b). Since internally applied forces are in static equilibrium, the distribution of stress in the sheet must be independent of elastic constants (Coker and Filon 1957, p. 518).

The problem of a straight cut loaded over part of its edge has been examined by Muskhelishvili (1953, p. 340). His stress functions were found to assume a

*Present address: Metallurgical Engineering Dept., Illinois Institute of Technology, Chicago 16, Illinois, U.S.A.

simple form when account was taken of the symmetry of the present configuration. It is convenient to introduce variables α and β defined by $x = a \cosh \alpha$, $l = a \cos \beta$ (see Fig. 1). The stress σ_y acting at points on $y = 0$ was determined in the form of a series in ascending powers of α having a leading term $\sigma_y = -2Y\beta/\pi\alpha$. The

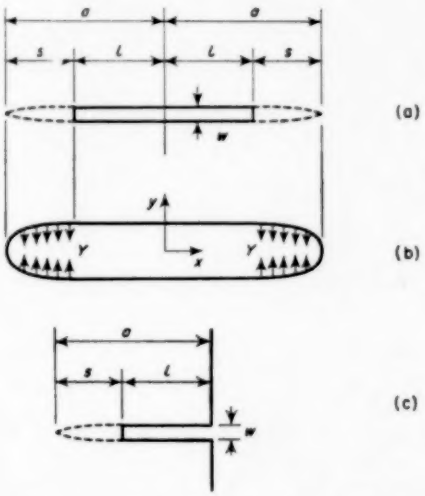

FIG. 1. Geometry of slit: (a) internal slit, (b) internal stresses acting on slit, (c) edge slit.

analogous expression for stress due to the external loading is $\sigma_y = T/\alpha$. When these stresses are superimposed, it is necessary that the stress at the point $\alpha = 0$ (i.e. $x = a$) should not be infinite, so the coefficient of $1/\alpha$ must vanish, viz. $T - 2Y\beta/\pi = 0$. This readily leads to the relation

$$\frac{s}{a} = 2 \sin^2 \left(\frac{\pi}{4} \frac{T}{Y} \right). \tag{1}$$

When T/Y approaches unity, this relation gives $s/a \simeq 1 - (\pi/2)(1 - T/Y)$. The last expression may be alternatively derived from stress functions given by WESTERGAARD (1939). By Saint-Venant's principle, stresses at $x = a$ should not depend on the exact distribution of stress over the segment $-l < x < l$ if l/a is small. Hence the partial loading required may be simulated by an inward tensile stress Y acting over the whole segment $-a < x < a$ together with central concentrated forces of magnitude $2lY$ acting outwards.

When T/Y is very small, equation (1) gives $s/l = 1{\cdot}23\,(T/Y)^2$. This relation gives the scale of plastic deformation if yielding actually occurs, but it need not imply that yielding must occur for any stress, however small.

3. TEST PANELS

The above analysis refers to an infinite sheet in a state of plane stress having a geometry defined by the length of slit. In practice, a sheet must have a definite thickness and a limited width. It was assumed that the sheet would be effectively

of infinite size if the total length of slit never exceeded one fifth of the sheet width. This point has been discussed by FROST and DUGDALE (1958). If the sheet is to yield when the tensile stress at any point reaches the uniaxial yield stress, it must be possible for shearing to occur without constraint on planes at 45° to the plane of the sheet. With two exceptions indicated later, slits were made of width w equal to the sheet thickness (0·050 in.).

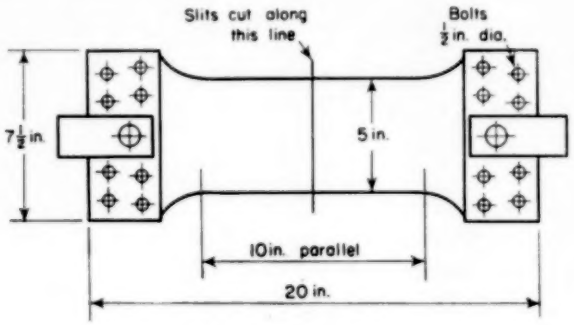

FIG. 2. Test panel.

Load was transmitted to the test panels through bolted joints as shown in Fig. 2. Measurements with extensometers on a panel without slits showed that stresses over the central section did not vary from the average value by more than 2 per cent. Steel produced by the Air Blown Bessemer process was selected, as this steel responds to strain-etching. The chemical analysis was: carbon 0·05 per cent, manganese 0·40 per cent, nitrogen 0·013 per cent. When cutting operations were completed, the panels were annealed at 900 °C, precautions being taken to avoid scaling.

TABLE 1. *Experimental values*

Internal slits			*Edge slits*		
Half-length of slit l (in.)	*Applied stress T* (tons/in²)	*Plastic zone length s* (in.)	*Length of slit l* (in.)	*Applied stress T* (tons/in²)	*Plastic zone length s* (in.)
0·50	3·3	0·042	0·50	3·7	0·057
0·40	5·0	0·088	0·50	4·6	0·093
0·25	6·2	0·087	0·40	5·7	0·116
0·25	6·9	0·122	0·40	7·0	0·197
0·25	8·0	0·185	0·25	8·3	0·204
0·25	10·0	0·470	0·25	9·5	0·350
0·10*	11·2	0·394	0·15*	10·8	0·448

*Width of slit $w = 0{\cdot}10$ in.

4. EXPERIMENTAL RESULTS

Tensile load was applied to each panel for 2 min. The stress T was calculated from the total width of the test section (5 in.) taking no account of the presence of slits (FROST and DUGDALE 1958). After being loaded, panels were aged at 250 °C

for a few hours and were dissected for examination. Portions including the slit and plastically deformed zone were polished on both sides and etched with Fry's reagent (Jevons 1925). The plastic zone tapered to a fine point, and its length was often uncertain to the extent of 0·003 in. It was measured with a steel rule and magnifying glass. Average values of the four measurements for each panel are shown in Table 1.

A strip was cut from each panel for a tensile test. When results for all panels were averaged, lower yield stresses of 12·0, 12·5 and 13·0 tons/in^2 were obtained for strain rates of 10^{-6}, 10^{-5} and 10^{-4} per second. For plotting Fig. 3, a value of 12·5 tons/in^2 was selected. Strain hardening was found to begin at a strain of 1·5 per cent.

5. Discussion of Results

In Fig. 3 experimental values are shown in relation to the curve calculated from equation (1). It should be noted that an edge slit was considered to have a length equivalent to half the total length of an internal slit, as shown in Fig. 1. It is thought that the experimental points fall sufficiently near the calculated curve to

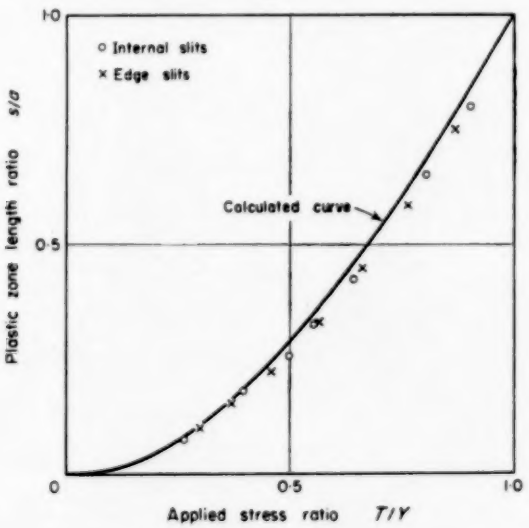

Fig. 3. Test results.

show that the analysis for internal slits is correct and that it applies also to edge slits. It can be seen that all experimental points fall slightly to the right of the curve. However, they may be brought into agreement with the curve by an adjustment of only about 3 per cent in the yield stress Y. As the yield stress corresponds to an arbitrarily chosen strain rate, it may be unwise to attach any significance to this discrepancy.

Acknowledgment

The writer is indebted to the Metallurgical Staff of Messrs. Richard Thomas and Baldwins, Ebbw Vale, for assistance in selecting steel of a suitable grade.

REFERENCES

ALLEN, D. N. DE G. and SOUTHWELL, R.	1950	*Phil. Trans.* A **242**, 379.
COKER, E. G. and FILON, L. N. G.	1957	*Photo-Elasticity* (Cambridge University Press)
FROST, N. E. and DUGDALE, D. S.	1958	*J. Mech. Phys. Solids* **6**, 92.
JEVONS, J. D.	1925	*J. Iron Steel Inst.* **111**, 191.
MUSKHELISHVILI, N. I.	1953	*Theory of Elasticity* (Noordhoff).
WESTERGAARD, H. M.	1939	*J. Appl. Mech.* **6**, A-49.

J. Mech. Phys. Solids, 1960, Vol. 8, pp. 105 to 111. Pergamon Press Ltd., London. Printed in Great Britain

A GENERAL THEORY OF INELASTIC COLUMN FAILURE—I

By R. Hill and M. J. Sewell
Department of Mathematics, University of Nottingham

(*Received* 16*th November*, 1959)

Summary

A continuum theory of uniqueness for general inelastic solids (Hill 1959) is applied to the basic column problem for any such material. The column is long, with arbitrary section, built in at one end, and axially loaded in compression at the other. A critical condition for bifurcation is obtained, generalizing and correcting the Shanley tangent-modulus formula.

1. Specification of the Material

A continuum theory of uniqueness and stability has recently been formulated for a broad class of inelastic solids (Hill 1959). In the present investigation the basic column problem is taken in illustration ; Part I is concerned with uniqueness and Part II with stability.

The solids covered by the theory have the defining property that in isothermal straining

$$\dot{\tau}^{\alpha\beta} = \frac{\partial W}{\partial \epsilon_{\alpha\beta}} \tag{1}$$

where $\tau^{\alpha\beta}$ are the contravariant components of the Kirchhoff stress tensor in curvilinear coordinates deforming with the material element (*op. cit.*, p. 219) ; the dot denotes the convected derivative ; and the ' potential ' W is a symmetrized homogeneous function of degree two in the strain-rate components $\epsilon_{\alpha\beta}$, with continuous first derivatives and at least piecewise continuous second derivatives. Any particular element of an extended body could be described as resilient or inelastic, or more especially elastic, plastic or elastic/plastic, according to a classification (*op. cit.*, Section 1) which depends on behaviour in vanishingly small closed cycles of further strain. This is governed by the form of W and the manner in which it changes with deformation. A solid cannot be classified purely from the rate equations (1) for a *single* state ; these may well be identical in essentially different materials. For the moment, however, it suffices to concern ourselves with just such a single generic instant, in an arbitrary process of distortion of an anonymous solid whose behaviour is unspecified beyond (1).

2. Criterion of Uniqueness

The question we have to answer is whether, at this instant, bifurcation is possible when a part S_v of the body surface is subject to prescribed velocities (perhaps zero) and the remainder S_F is subject to prescribed *nominal* traction-rates ;

that is, whether under these boundary conditions more than one mode of deformation is possible. The current shape and mechanical state of the body are regarded as given or previously determined.

A *sufficient* condition for uniqueness is expressible concisely through a related potential U, a function of the velocity gradients and not simply of the strain-rates, such that (*op. cit.*, equation (44))

$$U = W + \tfrac{1}{2}\,\tau^{\alpha\beta}\,v_{\gamma,\alpha}\,v^{\gamma}{}_{,\beta} \tag{2}$$

where v_α is the velocity, a comma signifies covariant differentiation in the current configuration, and the summation convention is adopted.

If the solid is ' linear ' at all points of the volume V, its potential W_L being a *quadratic form* $\frac{1}{2}\,\dot{\tau}^{\alpha\beta}\,\epsilon_{\alpha\beta}$, the solution is certainly unique if

$$\int U_L\,dV > 0 \tag{3}$$

for all continuous, once differentiable, velocity fields vanishing on S_v but not identically zero (*op. cit.*, p. 215). If, however,

$$\int U_L\,dV \geqslant 0, \tag{4}$$

any non-zero field producing the equality actually makes the functional *stationary* and is an *eigensolution* of the field equations: it represents a mode possible quasi-statically under *dead* loads on S_F and rigid constraints on S_v (*op. cit.*, pp. 216–8)*. Correspondingly, there is a bifurcation under *any* traction-rates on S_F and velocities on S_v since the solution is non-unique to the extent of an arbitrary additive multiple of the eigenfield. The stationary minimum property of the functional with respect to arbitrary variations from the eigenfield is vital to the effective use of approximation methods; it is a main reason for requiring the existence of a potential (1).

When the solid is non-linear, W not being a single quadratic form, (3) is no longer sufficient for uniqueness. The actual condition (*op. cit.*, equation (12)) is difficult to apply, however, and is replaced here by a more practicable ' comparison theorem ' involving the potential W_L of a certain linear solid (*op. cit.*, Section 4 (ii)). If, at each point of the body, (3) holds for U and in addition there can be chosen U_L and W_L such that $U - U_L = W - W_L$ is a *strictly convex* function of the strain-rates, a unique solution exists for the non-linear solid W, for any traction-rates on S_F and velocities on S_v, at least when (4) holds for the linear solid in the given state. If $W - W_L$ is merely *convex* there is a unique solution for the non-linear solid when the strict inequality (3) holds. But if $W - W_L$ is convex and only (4) is satisfied, so that we have an eigenstate of W_L, there may be *certain* boundary conditions under which a bifurcation occurs for the non-linear solid. In particular, when W coincides with the quadratic W_L in a part Q of strain-rate space (Q depends possibly on position in the body) it may happen that for certain boundary conditions some of the corresponding modes for W_L involve only strain-rates in Q; in that event these particular modes are also bifurcations for the non-linear solid W under the same boundary conditions. For convenience we shall refer to such a solid W_L as the ' linearization ' of solid W.

*Of course there are other eigensolutions in states where the functional is stationary but not one-signed; usually these are not practically important and we are not concerned with them here.

This situation is encountered in the column problem. We therefore begin with an analysis for a general linear solid.

3. Current State of the Column

The column is assumed to be currently straight with length l and uniform section of area A; the prior distortion is not necessarily infinitesimal. The column is built in at one end and otherwise unconstrained; at the other end a compressive load P acts in the line of centroids. The column is 'long' in the sense that $k/l \ll 1$, where Ak^2 is the second moment of area about the 'weaker' principal axis of section at a centroid. The present distribution of stress is assumed to be a uniform uniaxial compression of amount $\sigma = P/A$; here and later we consistently ignore possible local disturbances at the ends. We take the convected coordinates momentarily coincident with Cartesian axes of reference (x_1, x_2, x_3) with origin at the fixed end, x_3 along the line of centroids, and x_2 parallel to the weaker axis of section.

The potential of a general linear solid is

$$W_L = \tfrac{1}{2}\,\kappa^{\alpha\beta\gamma\delta}\,\epsilon_{\alpha\beta}\,\epsilon_{\gamma\delta}$$

where the tensor of coefficients is symmetric with respect to interchange of α, β; γ, δ; $\alpha\beta$ and $\gamma\delta$. In the column we suppose that the previous straining has resulted in a uniform orthotropic anisotropy such that the only non-zero coefficients in the Cartesian coordinates have either $\alpha = \beta$ and $\gamma = \delta$, or $\alpha = \gamma$ and $\beta = \delta$. We suppose, moreover, that the 1, 2 directions are alike in that

$$\kappa^{1111} = \kappa^{2222}, \qquad \kappa^{1313} = \kappa^{2323}, \qquad \kappa^{1133} = \kappa^{2233}.$$

When inverted, the rate equations in the current Cartesian coordinates now take the form

$$\left.\begin{aligned} \frac{\mu}{\nu}\,E\dot{\epsilon}_{11} &= \dot{\tau}_{11} - \lambda\dot{\tau}_{22} - \mu\dot{\tau}_{33}, & 2G\dot{\epsilon}_{23} &= \dot{\tau}_{23}, \\ \frac{\mu}{\nu}\,E\dot{\epsilon}_{22} &= \dot{\tau}_{22} - \lambda\dot{\tau}_{11} - \mu\dot{\tau}_{33}, & 2G\dot{\epsilon}_{31} &= \dot{\tau}_{31}, \\ E\dot{\epsilon}_{33} &= \dot{\tau}_{33} - \nu\,(\dot{\tau}_{11} + \dot{\tau}_{22}), & 2F\dot{\epsilon}_{12} &= \dot{\tau}_{12}, \end{aligned}\right\} \tag{5}$$

with a simplified notation. The only restrictions placed on the 'moduli' E, F, G are that they are positive and F/G is of order unity; E/G, however, is arbitrary. The 'contraction ratios' λ, μ, ν are required to be of order unity. Further, so that (5) has a unique inverse and a corresponding W_L, and so that this is a positive-definite quadratic form (and hence strictly convex – this ensures that bifurcation does not occur under a vanishingly small load),

$$-1 < \lambda < 1 - 2\,\mu\nu \quad \text{with} \quad 0 \leqslant \mu\nu < 1. \tag{6}$$

In an isotropic elastic solid after infinitesimal pre-strain E is of course Young's modulus, $F = G$ is the rigidity modulus, and $\lambda = \mu = \nu$ is Poisson's ratio.

It will appear that the bifurcation load of a long column depends essentially on E, G and ν. From a uniaxial compression test along x_3 ν could be obtained as the ratio $-\epsilon_{11}/\epsilon_{33}$ and E as the slope $\dot{\tau}_{33}/\epsilon_{33}$ at stress σ. Equivalently, $E - (1 + 2\nu)\,\sigma$ would be the ordinary 'tangent modulus,' i.e. the current slope of

the 'true stress' $\times$ strain curve, the component of true stress being with respect to the fixed axes. Similarly, $2G$ could be found as the slope $\dot{\tau}_{23}/\epsilon_{23}$ in a simple shear test parallel to the $x_1 x_2$ plane under constant normal pressure σ. Equivalently, the slope would be $2(G - \sigma)$ in terms of the fixed-axes component of true stress. Actually, however, the distinction between the rates of change of the convected component of Kirchhoff stress and the corresponding fixed-axes component of true stress is hardly significant in the present context, since σ/E is only of order $(k/l)^2$ at the bifurcation, while σ/G is even less in the range of E/G where it is necessary to know G accurately.

4. Bifurcation: Linear Solid

In the column $\tau_{33} = -\sigma$ and all other components are zero. Condition (3) reduces to

$$\int \left(\dot{\tau}_{ij}\, \epsilon_{ij} - \sigma \frac{\partial v_k}{\partial x_3} \frac{\partial v_k}{\partial x_3} \right) dV > 0$$

where the stress-rates must be eliminated via (5). Re-arranging this:

$$\sigma < \sigma_c = \text{Min} \left[\int \dot{\tau}_{ij}\, \epsilon_{ij}\, dV \Big/ \int \frac{\partial v_k}{\partial x_3} \frac{\partial v_k}{\partial x_3}\, dV \right] \tag{7}$$

where σ_c denotes the critical stress for which deflection is possible.

In view of the stationary property a close upper bound to σ_c is obtainable from a sufficiently wide subset of the admissible velocity fields. Here we consider the subset

$$\left.\begin{aligned} v_1 &= f(z) + \tfrac{1}{2}\nu \frac{x_1^2 - x_2^2}{l^2} f''(z), \\ v_2 &= \nu \frac{x_1 x_2}{l^2} f''(z), \\ v_3 &= -\frac{x_1}{l} f'(z), \end{aligned}\right\} \tag{8}$$

where $z = x_3/l$ and the dashes denote derivatives. This represents a deflexion $f(z)$ of the line of centroids in the $x_1 x_3$ plane, with bending about the weaker principal axis, and non-uniform shearing if $f''' \neq 0$. To the present approximation the built-in end condition is satisfied by $f(0) = 0 = f'(0)$. Note incidentally that $\dot{\tau}_{11}$, $\dot{\tau}_{12}$ and $\dot{\tau}_{22}$ corresponding to (8) all vanish identically (λ being unequal to either -1 or $1 - 2\mu\nu$ according to (6)); hence so do the x_1 and x_2 components of nominal traction-rate on the lateral surface of the column.

These fields were used by Pearson (1956) in an analysis of the stability of an isotropic elastic column. An extended investigation (Sewell 1960) for solids of type (5) has yielded nothing better in a more general class of fields for which $\epsilon_{11} = \epsilon_{22} = -\nu\epsilon_{33}$ and $\epsilon_{12} = 0$.

For fields (8)

$$\dot{\tau}_{ij}\, \epsilon_{ij} = E\epsilon^2_{33} + 4G(\epsilon^2_{13} + \epsilon^2_{23})$$

and so (7) gives

$$\frac{\sigma_c}{E} = \left(\frac{k}{l}\right)^2 \text{Min.} \frac{\int_0^1 (f'')^2\,dz + \gamma \int_0^1 (f''')^2\,dz}{\int_0^1 (f')^2\,dz} \tag{9}$$

where

$$\gamma = \left(\frac{j}{2k}\right)^4 \left(\frac{k}{l}\right)^2 \left(\frac{4\nu^2 G}{E}\right) \tag{10}$$

and

$$Ak^2 = \int\int_A x_1^2\,dx_1\,dx_2, \qquad Aj^4 = \int\int_A (x_1^2 + x_2^2)^2\,dx_1\,dx_2.$$

Ak^2 is the second moment of area about the weaker axis, already defined, while Aj^4 is the fourth moment of area about the centroidal axis; if, for example, the section is circular, $(j/2k)^4 = \frac{1}{4}$. Two terms have been omitted from the denominator in (9) since they are at most of order $(k/l)^2$ in comparison with the term retained, the three derivatives of f being comparable with one another.

The γ term in (9) represents the contribution of shear distortion. In a long column this is negligible when G/E is of order unity, owing to the factor $(k/l)^2$ in (10). In that event a minimum value $\frac{1}{4}\pi^2$ is obtained with $f = 1 - \cos(\frac{1}{2}\pi z)$, and

$$\frac{\sigma_c}{E} = \tfrac{1}{4}\pi^2 \left(\frac{k}{l}\right)^2,$$

where E is effectively the tangent modulus, as previously remarked. This confirms Euler's formula for the bifurcation load when the column is isotropic elastic and the pre-strain infinitesimal, as PEARSON showed. We have here obtained a result formally similar for a wide class of linear solids with no restriction on the magnitude of pre-strain.

At the other extreme the shear contribution is greatest when $G \to \infty$ but E remains finite, as in the transition between the linearizations of the conventional elastic/plastic and rigid/plastic solids*. Except when $f''' \equiv 0$ the quotient (9) can be made arbitrarily large by increasing G; consequently in the limit we must take $f \to z^2$ to obtain the minimum value, the shear distortion itself then being vanishingly small. The limiting minimum value is 3, which agrees with the *exact* result of HILL (1957) for the linearization† of an isotropic rigid/plastic solid treated on its merits and not as a limit. The rate equations for this solid have indeed the form (5), but with $\lambda = -1$, $\mu = 2$, $\nu = \frac{1}{2}$, values not allowed in (6): in fact the equations are then only of rank one and so there is neither a unique inverse nor a potential of type (1). Consequently $\dot{\tau}_{11}$, $\dot{\tau}_{12}$ and $\dot{\tau}_{22}$ need by no means vanish identically for the field (8).

As G/E increases, then, the Euler-type tangent modulus formula underestimates the bifurcation load by a factor which rises eventually to $12/\pi^2$; that is, an error of about 20 per cent. The discrepancy becomes appreciable when G/E is of order

*Conventional in the sense that the elastic/plastic potential is a quadratic form in the loading region of strain-rate space, which implies that the 'plastic part' of the strain-rate is always normal to the yield surface (compare equations (48) and (49), HILL 1959).

†This is tacitly introduced through equations (10) and (11) of the reference. The value 3 is exact since the *actual* field happens to be contained in the class (8).

$(l/k)^2$, as can happen in a structural metal with a rate of hardening small compared with the shear modulus.

The comparatively small range of the minimum in (9) suggests that a close estimate for intermediate values of G/E would be obtained from

$$f(z) = 1 - \cos(\tfrac{1}{2}\pi z) + \tfrac{3}{4}\pi\alpha z^2 \tag{11}$$

where α is disposable. With the best value,

$$\frac{\sigma_e}{E} = \tfrac{1}{4}\pi^2\left(\frac{k}{l}\right)^2\left(\frac{1+3\alpha}{1+\tfrac{1}{4}\pi^2\alpha}\right). \tag{12}$$

A simple approximate formula for the best α, with a negligible error in σ_e (never more than 0·05 per cent and vanishing at the extremes), is

$$\frac{\alpha}{\gamma} \simeq \left(\frac{12}{\pi^2} - 1\right)^{-1} = 4{\cdot}632\ldots \tag{13}$$

where γ is defined in (10).

5. Bifurcation: Non-linear Solid

According to the final remarks in Section 2 the result (12) is relevant to any non-linear solid having a potential W which is 'more convex' than the potential W_L of the linear solid (5). For a column of such non-linear material it can be asserted that the bifurcation load is certainly *not lower* than (12).

In what follows we discuss the important special case where an even more precise statement can be made, namely when W is a quadratic form in a part $\boldsymbol{Q}$ of strain-rate space and coincides there with W_L itself. This happens, for example, when the body is partly elastic and partly elastic/plastic: in an elastic element W coincides completely with W_L, while in an elastic/plastic element W_L is chosen as the quadratic which coincides with W in the 'loading' part $\boldsymbol{Q}$ of strain-rate space*.

Let $\mathbf{v}_e$ be the velocity vector in the eigenfield for the linear solid under dead loading on S_F. Let $\mathbf{v}$ be a solution in the same state under given nominal traction-rates not zero everywhere on S_F. Then $\mathbf{v} + \rho\mathbf{v}_e$ is also a solution for arbitrary constant ρ. It may happen that there are certain traction-rates for which the field $\mathbf{v}$ involves strain-rates which lie in the part $\boldsymbol{Q}$ of strain-rate space at every point of the body; if this is so then $\mathbf{v}$ is also a solution for the non-linear solid under these traction-rates. Moreover, by a continuity argument, there must in general be an interval of ρ containing $\rho = 0$ for which the fields $\mathbf{v} + \rho\mathbf{v}_e$ involve only $\boldsymbol{Q}$ and are consequently also solutions for the non-linear solid. It is then *certain* that bifurcations are possible for the non-linear solid, though this family of solutions is less extensive than for the linear solid and occurs only for certain traction-rates (these may or may not include dead loading). Of course, there may also be other types of bifurcation modes exclusive to the non-linear solid.

For the column under increasing axial load a uniform straining associated with a uniaxial stress-rate is one solution for any orthotropic material. Let the considered linear and non-linear solids have the same tangent modulus and contrac-

*For a proof of the overall convexity of $W - W_L$ see Hill (1958, Section 4, especially equation (13)). The proof is in terms of a related potential associated with the 'rigid-body derivative' of the Kirchhoff stress, not its convected derivative (cf. Hill 1959, p. 222, especially equation (40) and the footnote).

tion ratio in compression; they therefore have in common precisely the same uniform straining mode, which we suppose falls in $\boldsymbol{Q}$ so that it has all the properties ascribed to the field $\mathbf{v}$. Now the exact eigenfield $\mathbf{v}_e$ for the linear solid is not known, but we may perhaps regard (8) with (11) as an acceptable approximation (though naturally less good than the estimate of the bifurcation load itself).

As a specific example suppose that the column material is elastic/plastic. Region $\boldsymbol{Q}$ is defined (very nearly) by the loading condition

$$\epsilon_{33} < 0, \tag{14}$$

since the existing stress is a uniaxial compression. If the axial velocity at the centroid of the free end is arbitrarily set equal to unity (14) requires

$$1 + \rho \frac{x_1}{l} f''(z) \geqslant 0.$$

Since f'' is positive for $0 \leqslant z \leqslant 1$, its greatest value $f''(0)$ is most critical. With this inserted the inequality must be satisfied for $-a \leqslant x_1 \leqslant b$, say, where a, b are the greatest distances of the perimeter from the weaker axis of section on opposite sides. Hence

$$-\frac{l}{b} \leqslant \tfrac{1}{4}\pi^2 \left(1 + \frac{6\alpha}{\pi}\right) \rho \leqslant \frac{l}{a}. \tag{15}$$

Thus, there is a family of modes $\mathbf{v} + \rho\mathbf{v}_e$, where ρ lies in the interval (15) for α defined by (13). Note that the family still exists even in the limit as $\alpha \to \infty$ and $\rho \to 0$, since $\rho f \to \frac{1}{2}\beta z^2$ where

$$-\frac{l}{b} \leqslant \beta \leqslant \frac{l}{a}, \qquad \beta = \tfrac{3}{2}\pi\rho\alpha.$$

The column can therefore begin to deflect in a range of possible ways under *increasing* axial load at the stress (12), which in this sense is critical for the non-linear solid W.

We recall that this has been proved when $W - W_L \equiv 0$ for strain-rates satisfying (14), while $W - W_L$ is only restricted to be convex for other strain-rates and is otherwise unspecified.

Acknowledgment

The present work was done while one of us (M.J.S.) held a D.S.I.R. Studentship in the University of Nottingham.

References

Hill, R.	1957	*J. Mech. Phys. Solids* **5**, 153.
	1958	*Ibid.* **6**, 236.
	1959	*Ibid.* **7**, 209.
Pearson, C. E.	1956	*Quart. Appl. Math.* **14**, 133.
Sewell, M. J.	1960	Thesis, University of Nottingham. To be submitted.

J. Mech. Phys. Solids, 1960, Vol. 8, pp. 112 to 118. Pergamon Press Ltd., London. Printed in Great Britain

A GENERAL THEORY OF INELASTIC COLUMN FAILURE—II

By R. Hill and M. J. Sewell
Department of Mathematics, University of Nottingham

(*Received* 18*th December*, 1959)

Summary

General sufficient conditions are formulated respectively for either dynamic stability or instability of an inelastic continuum under dead loading. These indicate a criterion of stability, and the corresponding critical load is calculated for a built-in column under compression. This load is found to lie above the bifurcation (Shanley) value, as determined in Part I, and coincides (to within the approximation used) with the reduced modulus (Engesser-Karman) value modified to allow for the effect of shear deformation.

1. Scope of Investigation

At the present time it is not known what conditions are both necessary and sufficient for stability when the body concerned is inelastic. It is, however, possible to formulate sets of *sufficient* conditions either for stability or instability. Such a set has been given by Hill (1959, Section 3) for the stability of an inelastic solid of any kind, whose surface is subject to rigid constraints on a part S_v and to dead loading on the remainder S_F. We present these conditions here in a slightly relaxed form. A position of equilibrium is stable if, in configuration space, its representative point O is contained within a certain sequence of closed neighbourhoods, monotonically decreasing to zero at O, with the following property. On any geometrically-possible path from O to the boundary of a typical neighbourhood N the work absorbed in distortion algebraically exceeds the work of the dead loads by at least a positive quantity w_N, which decreases monotonically to zero with N. This ensures that a free inertial motion started with sufficiently small kinetic energy w from O by an arbitrary transitory disturbance can never escape from the neighbourhood such that $w_N = w$, no matter what the actual dynamic paths may be nor how long the motion may continue*. Moreover, when the disturbing energy is vanishingly small so is the neighbourhood containing the motion.

It is to be understood that a path to the boundary may be arbitrarily devious or repetitive (to allow for quasi-oscillatory or cyclical actual motions); in calculating the energy of distortion full account must naturally be taken of the accompanying changes in material properties (changes due to rate of strain and temperature variation are assumed negligible). On a *direct* path of *infinitesimal* total length, however, the net work defect is of second order and depends on the rate equations

*Disturbances such that the free motion starts from positions P near O are also permitted. w is not then the actual kinetic energy at P, but what would be the equivalent kinetic energy at O; that is, the total effective energy relative to O, with due allowance for the net work absorbed in the transition from O to P.

in the equilibrium state only. It has the sign of the volume integral $\int U\,dV$, where U is the potential function of velocity gradient evaluated for the velocity field defining the initial direction of the path (see Part I, Section 2). Consequently, the above set of conditions for stability includes the requirement that

$$\int U\,dV > 0 \tag{1}$$

for all continuous, once differentiable, velocity fields vanishing on S_v (but not identically zero). Additional restrictions have to be placed on the *variation* of the rate equations along arbitrary indirect paths in a sufficiently small neighbourhood of O, but we shall not discuss these here.

It is known that inequality (1) holds whenever a certain condition is satisfied guaranteeing uniqueness of the actual velocity field under prescribed nominal traction-rates on S_F (*op. cit.*, especially equations (5), (12) and foot of p. 213). On the other hand, when the solid is non-linear (U not a single quadratic form) there exists the possibility that (1) may hold and nevertheless bifurcation occurs under certain *varying* (not dead) loads on S_F. In Part I this was proved to happen for the built-in column under an increasing compressive stress σ, for a wide class of non-linear materials. For these the bifurcation stress σ_c was shown to coincide with that marking the fundamental eigenstate of a column of *linear* solid whose potential U_L is the linearization of U (a terminology introduced in Part I, Section 2). In this state

$$\int U_L\,dV \geqslant 0 \text{ for all admissible fields when } \sigma = \sigma_c. \tag{2}$$

$U - U_L$ was stipulated to vanish in a region Q of strain-rate space and to be convex in the remainder (and therefore positive); moreover, the eigenfield which produces the equality in (2) involves strain-rates outside Q in part of the column. It is evident that (1) is satisfied.

Our present concern is to calculate, for this class of non-linear solids, the critical stress $\bar{\sigma}_c$ such that

$$\left.\begin{aligned} &\int U\,dV > 0 \text{ for all admissible fields when } \sigma < \bar{\sigma}_c, \\ \text{and}\quad &\int U\,dV < 0 \text{ for some admissible fields when } \sigma > \bar{\sigma}_c. \end{aligned}\right\} \tag{3}$$

The question as to when a field exists such that $\int U\,dV = 0$ for $\sigma = \bar{\sigma}_c$ is not investigated here. If it does exist it is necessarily an eigenfield representing a mode possible under dead loading. For, in view of the first part of (3), the first variation of $\int U\,dV$ must vanish; this characterizes an eigenstate (by the converse of an argument given by Hill 1959, p. 214).

It is not apparent, however, whether the stress (3) need be critical for stability; that is, whether a state in which neither (1) nor (3) is satisfied must be unstable (according to some reasonable definition). For an *elastic* solid the classical argument of Kelvin shows that it is, in the dynamic sense, at least when gyroscopic forces are not induced by the motion and provided some viscous type of energy dissipation

is present, however small*. For inelastic solids it is unlikely that the question would admit a universal answer. Here we do not attempt a direct approach but instead formulate a set of conditions *sufficient* for instability, applying to any inelastic solid (linear or non-linear). Instability of a position of equilibrium is ensured if, in configuration space, its representation O is the point of accumulation of a sequence of points (typically P) contained in a bounded fixed neighbourhood N with the following property. Any equilibrium positions (including O) associated with arbitrary paths starting from any P and lying entirely within N are *energetically unattainable* in free inertial motion from momentary rest at P.† The proof is a refinement and generalization of Kelvin's argument. Among arbitrary transitory disturbances, however small, there are always those such that the ensuing free motion starts from rest at some P. This motion must eventually cease permanently at a position of equilibrium through the viscous dissipation. But, by hypothesis, any statically possible positions of equilibrium in N are energetically inaccessible from P, in that the work absorbed in distortion on any path to them from P algebraically exceeds the work of the dead loads — whereas no kinetic energy is available at P to supply this defect. Consequently the motion must eventually pass outside N (perhaps only temporarily). A *finite* displacement is therefore produced by certain *arbitrarily small* disturbances and so in that sense the position O is unstable. In order that O itself should be energetically inaccessible from rest at any P,

$$\int U \, dV < 0 \tag{4}$$

for the velocity field leading from O along the sequence.

For this set of sufficient conditions for instability, then, it is a pre-requisite that the functional should take negative values in at least some fields. On the other hand, for the sufficient conditions for stability it is a pre-requisite that the functional should always be positive. It is worthwhile, therefore, to give special attention to the stress characterized by (3).

2. Current State of the Column

With the notation of Part I the rate equations in the region Q of strain-rate space are

$$\left.\begin{aligned} \frac{\mu}{\nu} E \epsilon_{11} &= \dot\tau_{11} - \lambda \dot\tau_{22} - \mu \dot\tau_{33}, & 2G \epsilon_{23} &= \dot\tau_{23}, \\ \frac{\mu}{\nu} E \epsilon_{22} &= \dot\tau_{22} - \lambda \dot\tau_{11} - \mu \dot\tau_{33}, & 2G \epsilon_{31} &= \dot\tau_{31}, \\ E \epsilon_{33} &= \dot\tau_{33} - \nu (\dot\tau_{11} + \dot\tau_{22}), & 2F \epsilon_{12} &= \dot\tau_{12}, \end{aligned}\right\} \text{ in } Q. \tag{5}$$

In the remainder of strain-rate space, Q' say, we assume similar linear forms but with different coefficients. The potential U for this non-linear solid is then analytically composite, being obtained by adjoining a pair of quadratic forms.

*Viscous in the broad sense of being dependent on velocity and vanishing with it.

†The equilibrium positions are naturally in respect of the body *changed* in its material properties by the distortion on the paths from P.

In order to make the subsequent variation problem tractable it is virtually unavoidable to assume the same contraction ratio ν in Q and Q' for a uniaxial stress-rate along x_3, the axis of the column*. We therefore take in Q'

$$\left.\begin{aligned} \frac{\mu'}{\nu} E' \dot{\epsilon}_{11} &= \dot{\tau}_{11} - \lambda' \dot{\tau}_{22} - \mu' \dot{\tau}_{33}, & 2G' \dot{\epsilon}_{23} &= \dot{\tau}_{23}, \\ \frac{\mu'}{\nu} E' \dot{\epsilon}_{22} &= \dot{\tau}_{22} - \lambda' \dot{\tau}_{11} - \mu' \dot{\tau}_{33}, & 2G' \dot{\epsilon}_{31} &= \dot{\tau}_{31}, \\ E' \dot{\epsilon}_{33} &= \dot{\tau}_{33} - \nu (\dot{\tau}_{11} + \dot{\tau}_{22}), & 2F' \dot{\epsilon}_{12} &= \dot{\tau}_{12}, \end{aligned}\right\} \text{ in } Q'. \tag{6}$$

For any strain-rate in the hyper-plane surface separating Q and Q' the relations (5) and (6) must predict identical stress-rates. This requires the surface to be $\dot{\epsilon}_{33} = 0$ ($E' \neq E$), and we therefore suppose (as in Part I) that

$$\dot{\epsilon}_{33} \leqslant 0 \text{ in } Q, \quad \dot{\epsilon}_{33} \geqslant 0 \text{ in } Q'. \tag{7}$$

Moreover, it is necessary that

$$\left.\begin{aligned} F' &= F, \quad G' = G, \\ \frac{1+\lambda'}{1+\lambda} &= \frac{1-\mu'\nu}{1-\mu\nu} = \frac{\mu' E'}{\mu E}. \end{aligned}\right\} \tag{8}$$

Only one of the material constants in (6), say E', can thus be chosen independently of the constants in (5). It is, however, subject to the restriction

$$E' > E \tag{9}$$

in order that $U - U_L$ should be convex (as required in Part I), where U_L corresponds to (5) in both Q and Q'. In terms of E'/E equations (8) give explicity for λ', μ':

$$\frac{\mu E}{\mu' E'} = \frac{\lambda + \left[(1 - (E/E')\right] \mu\nu}{\lambda'} = 1 - \left(1 - \frac{E}{E'}\right) \mu\nu. \tag{10}$$

It will be recalled that λ, μ, ν are restricted by inequalities (6) in Part I; it is easily checked that similar ones are automatically satisfied by λ', μ', ν:

$$-1 < \lambda' < 1 - 2\mu'\nu, \quad 0 \leqslant \mu'\nu < 1. \tag{11}$$

3. Critical Load for Possible Instability

The compressive stress on the column at the load characterized by (3) is

$$\bar{\sigma}_c = g.l.b. \left[\int \dot{\tau}_{ij} \dot{\epsilon}_{ij} \, dV \Big/ \int \frac{\partial v_k}{\partial x_3} \frac{\partial v_k}{\partial x_3} \, dV \right]$$

in the class of admissible fields. This is formally analogous to (7) of Part I, but now we are dealing with the non-linear solid U and not its linearization U_L. Relations (5) apply only in the part of the column where $\dot{\epsilon}_{33} \leqslant 0$, while in the remainder relations (6) must be taken. We seek a close upper bound to the minimum through the subset

*The theory can then only be an approximation for the *conventional* elastic/plastic solid, where the ratios differ in the loading and unloading regions of strain-rate space. However, since the final formula for the critical load does not depend sensitively on the contraction ratio, a mean value should be adequate for practical purposes.

$$\left.\begin{aligned} v_1 &= g(z) + \tfrac{1}{2}\nu\,\frac{(x_1^2 - x_2^2 + 2dx_1)}{l^2}\,g''(z), \\ v_2 &= \nu\,\frac{(x_1 + d)\,x_2}{l^2}\,g''(z), \\ v_3 &= -\,\frac{(x_1 + d)}{l}\,g'(z), \end{aligned}\right\} \tag{12}$$

where $g(0) = 0 = g'(0)$, l is the length of the column, z denotes x_3/l, and dashes denote derivatives with respect to z. d is the distance between the centroidal axis and the surface of momentarily unstretched fibres, which in (12) is plane.

Two considerations governed the choice of these fields. First, the corresponding strain-rates satisfy $\epsilon_{11} = \epsilon_{22} = -\nu\epsilon_{33}$, $\epsilon_{12} = 0$, and so $\dot\tau_{11}$, $\dot\tau_{22}$ and $\dot\tau_{12}$ are identically zero through the column, making the x_1 and x_2 components of nominal traction-rate vanish on the lateral surface. Second, in every section the portion corresponding to $\boldsymbol{Q}$ (or $\boldsymbol{Q}'$) is the same:

$$\boldsymbol{Q}:\ x_1 \geqslant -d. \qquad \boldsymbol{Q}':\ x_1 \leqslant -d. \tag{13}$$

This greatly eases the extremum problem. No doubt the actual surface separating the portions is neither plane nor parallel to the axis, but nevertheless the optimum value determined for d probably represents a fair approximation to the mean $|x_1|$ on the actual surface.

With the field (12) the approximate critical stress is

$$\sigma_c = \left(\frac{k}{l}\right)^2 \mathrm{Min}\left[\frac{\displaystyle\int_0^1 (g'')^2\,dz + \bar\gamma\int_0^1 (g''')^2\,dz}{\displaystyle\int_0^1 (g')^2\,dz}\cdot\bar E\right] \tag{14}$$

where

$$Ak^2\,\bar E = E\iint_{\xi_1>0}\xi_1^{\,2}\,d\xi_1\,d\xi_2 + E'\iint_{\xi_1<0}\xi_1^{\,2}\,d\xi_1\,d\xi_2. \tag{15}$$

(ξ_1, ξ_2) are new Cartesian coordinates such that $\xi_1 = x_1 + d$, $\xi_2 = x_2$, and the double integrals extend over the parts of the section on either side of the chord $\xi_1 = 0$. The parameter $\bar\gamma$ represents the effect of shear deformation and is given by a formula similar to that for γ in Part I:

$$\left.\begin{aligned} &\bar\gamma = \left(\frac{j_d}{2k}\right)^4\left(\frac{k}{l}\right)^2\left(\frac{4\nu^2 G}{\bar E}\right) \\ &\text{where}\qquad Aj_d^{\,4} = \iint_A [(\xi_1 - d)^2 + \xi_2^{\,2}]\,[(\xi_1 + d)^2 + \xi_2^{\,2}]\,d\xi_1\,d\xi_2. \end{aligned}\right\} \tag{16}$$

The ' weighted modulus ' $\bar E$ is a function of d, given by (15); so also is the shear parameter $\bar\gamma$, given implicitly through $\bar E$ and j_d by (16). For fixed d the extremum problem (14) for $g(z)$ is precisely the same as that for $f(z)$ in (9) of Part I. If, therefore, the bifurcation stress is written in the form

$$\sigma_c = \tfrac{1}{4}\,\pi^2\left(\frac{k}{l}\right)^2\phi(\gamma)\,E,$$

the critical stress corresponding to (3) is expressible as

$$\bar{\sigma}_c = \tfrac{1}{4}\,\pi^2 \left(\frac{k}{l}\right)^2 \operatorname*{Min}_d \{\phi\,(\bar{\gamma})\,\bar{E}\}.$$

Now it was shown in Part I that ϕ only varies between 1 and $12/\pi^2$ as its argument ranges from 0 to ∞ [an approximation to ϕ was obtained in (12) there]. It should be sufficiently accurate, therefore, to take

$$\bar{\sigma}_c = \tfrac{1}{4}\,\pi^2 \left(\frac{k}{l}\right)^2 \phi\,(\bar{\gamma}) \operatorname*{Min}_d \bar{E} \tag{17}$$

where $\bar{\gamma}$ here is to be evaluated at that value of d which makes $\bar{E}$ least* (instead of at the value which makes $\phi\bar{E}$ least). This formula is in fact exact [i.e. with an error only of order $(k/l)^2$] at the extremes, namely when $\bar{\gamma}$ is either very small ($G/\bar{E}$ of order unity) or when it is very large ($G/\bar{E} \gg l^2/k^2$).

Special interest attaches to a material which is rigid for strain-rates in Q'. When $E' \to \infty$, while E remains finite, $\bar{E}$ is least when the part $\xi_1 < 0$ of the section vanishes. $\bar{E}/E$ is then equal to the ratio (second moment of area about the corresponding tangent parallel to the x_2 axis)/(second moment of area about the x_2 axis); that is, to $1 + (d^2/k^2)$ where d is the distance between the tangent and the axis of section. This ratio is, for example, four when the section is a rectangle and five when it is a circle. Further, since $G \to \infty$ also, so does $\bar{\gamma}$ ($\nu \neq 0$) and consequently the optimum $g(z) \to z^2$ [as did $f(z)$ in Part I]. This makes $\phi = 12/\pi^2$, and so finally

$$\bar{\sigma}_c = 3\,\frac{(d^2 + k^2)}{l^2}\,E. \tag{18}$$

The result previously obtained by Hill (1957) for a cylindrical column of the conventional rigid/plastic solid is in agreement with this general formula.

4. Critical Stress for Eigenstate

We now consider the stress at which the column can first deflect under dead load. Even if, for certain inelastic solids, the eigenstate stress should not coincide with the critical stress (3), it nevertheless has importance as a 'latent instability' (Ziegler's terminology, 1956). For example, additional arbitrary body-force rates (representing, in the slender column context, small transverse disturbing forces *steadily* applied) produce an unbounded strain-rate as the eigenstate stress is approached. The wellknown Engesser-Karman theory was prompted by such a static concept of instability.

The Engesser-Karman formula for the eigenstate stress was derived originally for a conventional elastic/plastic solid. For the class of non-linear solids considered here its formal generalization is

$$\tfrac{1}{4}\,\pi^2 \left(\frac{k}{l}\right)^2 \bar{E}\,(d_0) \tag{19}$$

where d_0 is the unique value of d for which

*This d always falls inside the section, and approaches the boundary as $E'\,E \to \infty$. It is zero when $E' = E$, and then (17) coincides with the approximation to the bifurcation stress obtained in Part I.

$$E \iint_{\xi_1 > 0} \xi_1 \, d\xi_1 \, d\xi_2 + E' \iint_{\xi_1 < 0} \xi_1 \, d\xi_1 \, d\xi_2 = 0. \tag{20}$$

$\bar{E}(d_0)$ is the so-called ' reduced modulus.'

It is worth noting that (20) is equivalent to the condition that the rate of increase of the x_3 component of total load on any section shall vanish for fields in the subset (12):

$$\iint (\dot{\tau}_{33} - \sigma \, \epsilon_{33}) \, d\xi_1 \, d\xi_2 = 0$$

with $$\dot{\tau}_{33} = \begin{cases} E\epsilon_{33}, & \xi_1 \geqslant 0 \\ E' \epsilon_{33}, & \xi_1 \leqslant 0 \end{cases} \quad \text{and} \quad \epsilon_{33} = -\xi_1 g''(z)/l^2.$$

On neglecting σ/E and σ/E' compared with unity, and dropping the factor $g''(z)$, (20) is obtained.

Now it is easily shown that the reduced modulus is actually the absolute minimum value of the weighted modulus for any value of d in the section* ; that is,

$$\text{Min } \bar{E}(d) = \bar{E}(d_0). \tag{21}$$

Consequently, when the shear effect is insignificant ($\phi \sim 1$), the Engesser-Karman approximation (19) to the eigenstate stress coincides with the upper bound approximation (17) to the critical stress (3) for non-linear solids of type (5) with (6).

However, the formula (19) is not a good approximation when the influence of shear deformation is significant. To see this, consider the limit when E'/E and $G/E \to \infty$, so that the region $\xi_1 < 0$ vanishes. The critical value (18) then *exceeds* the value (19), which therefore lies in the range where the functional (1) is positive, not only for the subset (12) but for *all* admissible fields (HILL 1957). In other words, there could not be an eigenstate at the stress (19) in these circumstances.

A modification of (19) which would not have this particular defect is of course (17) itself with (21):

$$\tfrac{1}{4} \pi^2 \left(\frac{k}{l}\right)^2 \phi \, \bar{E}(d_0) \tag{22}$$

where the function ϕ here is to be evaluated at $d = d_0$. The question whether this actually supplies a valid approximation to the eigenstate stress is left for further examination.

ACKNOWLEDGMENT

The present work was done while one of us (M.J.S.) held a D.S.I.R. Studentship in the University of Nottingham.

REFERENCES

HILL, R.	1957	*J. Mech. Phys. Solids* **6**, 1.
	1959	*Ibid.* **7**, 209.
HILL, R. and SEWELL, M. J.	1960	*J. Mech. Phys. Solids* **8**, 105.
ZIEGLER, H.	1956	*Advances in Applied Mechanics*, Vol. **4**, p. 352 (Academic Press, New York).

*For the second derivative of $\bar{E}(d)$ is positive everywhere in the section, while (20) holds at the stationary value.

J. Mech. Phys. Solids, 1960, Vol. 8, pp. 119 to 122. Pergamon Press Ltd., London. Printed in Great Britain

A SIMPLE MODEL OF A PROPAGATING CRACK

By A. N. Stroh
Department of Mechanical Engineering, Massachusetts Institute of Technology

(*Received* 1st *January*, 1960)

Summary

A model of a crack is developed in which the surface energy in the Griffith treatment is taken to depend on the temperature and strain rate. It is shown that such a crack shows a transition from brittle to ductile behaviour as the temperature is raised.

In a metal a crack may spread either in a brittle or in a ductile manner, depending on how readily plastic flow can occur. Little progress, however, has been made in relating quantitatively the type of crack propagation to the capacity of the material to deform plastically, and it has still to be shown how a relatively small change in the plastic behaviour of the material (such as may be obtained by a change in the operating temperature) can cause an abrupt change in the mode of crack propagation. A detailed calculation of the plastic flow near a moving crack presents a problem of some difficulty, especially since strain-rate effects are likely to be important. It may therefore be of interest to describe a simplified model of a propagating crack which nevertheless shows a brittle to ductile transition; the model is a development of one previously proposed by Gilman (1956).

Mott (1948) has shown how the velocity of a moving Griffith crack may be determined by taking into account the kinetic energy. The condition that the sum of the kinetic, elastic and surface energies be conserved as the crack spreads gives the velocity V of the crack to be

$$V = V_0(1 - U_S/2\,U_E), \tag{1}$$

where V_0 is the limiting velocity of a long completely brittle crack, U_E is elastic strain energy of the crack, and U_S its surface energy. In a metal a certain amount of plastic deformation will take place even when the fracture is of the type commonly regarded as brittle, and Orowan (1949) has pointed out that this can be allowed for by including a term in the surface energy representing the plastic work done. The magnitude of this plastic work is in general large compared with the true surface energy, which may therefore be neglected. It will be possible to represent the plastic work as a surface energy in this way if the deformation is confined to a thin layer near the crack, that is when the material is brittle; but in a fully ductile material, where plastic flow extends through a large volume, such a representation will not be even approximately correct.

In order to obtain a ductile–brittle transition we must suppose that the plastic work done, U_S, depends on the crack velocity and on the temperature. To deduce

a simple expression for this dependence consider a material which, when loaded under a constant stress, develops after time t a strain ϵ given by

$$\epsilon = (t/\tau)^n \tag{2}$$

where n is a constant and τ depends on the stress and the temperature. When $n = 1$, we have a quasi-viscous material which deforms at a constant strain rate. When n is large the strain is small for times $t < \tau$ and large for $t > \tau$; thus we have a material which shows delayed yield, τ being the delay time. Hence equation (2) is sufficiently general to include a variety of important types of strain behaviour. At each point near a moving crack the time of loading t will be inversely proportional to the crack velocity V, and so the strain will everywhere be proportional to V^{-n}. Hence we write the surface energy U_S as

$$U_S = A V^{-n} \tag{3}$$

where the factor A will depend on the temperature. Since plastic flow will occur most readily at high temperatures, we assume that A will increase with rising temperature.

On substituting (3) into equation (1) and writing $V/V_0 = v$, we obtain

$$v = 1 - \theta v^{-n} \tag{4}$$

where

$$\theta = A/2\, U_E\, V_0^n. \tag{5}$$

The relation (4) between v and θ is shown in Fig. 1. Since, from (5) and the assumed behaviour of A, θ will increase with rising temperature, Fig. 1 is essentially a plot

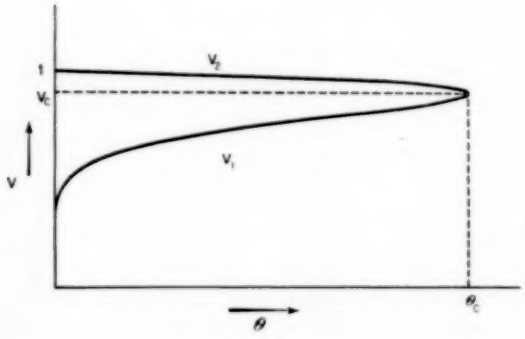

FIG. 1.

of crack velocity against temperature (though the temperature scale will in general not be linear). Above some temperature T_c corresponding to $\theta = \theta_c = n^n/(n+1)^{n+1}$ no velocity of crack propagation can be found which satisfies the assumptions on which our equations are based, showing that quasi-brittle propagation of the crack is impossible here. This therefore represents the ductile region and so we identify T_c with the transition temperature. Below the transition temperature we find two velocities v_1 and v_2 ($v_1 < v_2$) of brittle crack propagation. On the upper branch of the curve, v_2 varies between 1 and $v_c = n/(n+1)$, and so we have a high speed

crack, moving with a velocity which is only a little less than V_0 and which decreases slightly as the transition temperature is approached. We may reasonably identify this with the experimentally observed brittle crack. The other lower speed v_1 of crack propagation which is shown in Fig. 1 is, however, not observed. To understand this we must consider the stability of the crack velocity.

Let v denote the steady crack velocity satisfying equation (4), and suppose that at some instant the plastic work which is being done corresponds not to v, but to $v + \delta v$. (Such fluctuations may for example occur when the crack crosses a region which happens to be harder locally than the bulk of the material). Then on the right-hand side of equation (4) we must replace v by $v + \delta v$. This change in plastic work will produce a change Δv in the crack velocity given by

$$\Delta v = n\,\theta\, v^{-n-1}\,\delta v. \tag{6}$$

If $\Delta v < \delta v$, any fluctuation will be damped out and so the crack will propagate in a stable manner; while if $\Delta v > \delta v$ the propagation will be unstable. Hence from equations (4) and (6) we find that the crack will be stable if, and only if, $v > v_c$. Thus only the higher crack velocity, v_2, will be stable and so will be the only one to be observed.

Nevertheless the lower crack velocity v_1 does have a physical significance, as it represents the velocity at which the crack can propagate under its own momentum; once the crack has reached the velocity v_1 it will accelerate and become a fast-moving brittle crack. For velocities less than v_1 the crack will resemble a ductile crack in that (i) it will tend to come to rest unless its motion is maintained by the external load, and (ii), by equation (3), its propagation will be accompanied by a large amount of plastic work. This is in accord with the observations of Felbeck and Orowan (1955) who found that a crack always started to spread in a ductile manner before becoming brittle, and similarly reverted to ductile behaviour on coming to rest.

For a crack of length c the elastic energy U_E (equation 1) will be proportional to c^2, while the surface energy U_S will vary only as c. Hence the ratio U_S/U_E, and so the value of θ, will decrease as the crack grows. If this carries θ through the transition value θ_c there will be a change from ductile to brittle propagation when the crack reaches a certain critical size depending on the temperature. We suggest that this accounts for the observation of Wessel (1956) that near the transition temperature fracture may occur in a tensile specimen by a ductile crack starting at the centre, spreading outwards to a fraction of the cross-section, and then continuing as a brittle crack, the size of the ductile region increasing with temperature. In general, however, this effect will be complicated by the fact that the triaxial nature of the stress changes as the crack spreads from the centre to the edges of the specimen; this is not taken into account here.

The neglect of effects due to the triaxial nature of the stress is, indeed, the greatest limitation of the present model (apart from the fact that it says nothing about the initiation of the crack). Though such effects are certainly of importance it unfortunately does not seem possible to include them without greatly complicating the treatment.

In conclusion we note that although we have assumed the particular law of plastic flow contained in equations (2) and (3), this is by no means necessary; it is quite easy to see that if equation (3) is replaced by any relation which makes

U_S increase with rising temperature and decreasing crack velocity, very similar results are obtained. This suggests that the general features of brittle crack propagation are not very sensitive to the precise mechanism of plastic flow, though the value of the transition temperature will depend on the details of the mechanism.

Acknowledgments

I am glad to thank Professors E. Orowan and F. A. McClintock for their helpful comments.

References

Felbeck, D. K. and Orowan, E.	1955	*Weld. J.* **34**, 570s.
Gilman, J. J.	1956	*J. Appl. Phys.* **27**, 1262.
Mott, N. F.	1948	*Engineering* **165**, 16.
Orowan, E.	1949	*Rep. Progr. Phys.* **12**, 185.
Wessel, E. T.	1956	*Proc. ASTM.* **56**, 540.

J. Mech. Phys. Solids, 1960, Vol. 8, pp. 123 to 140. Pergamon Press Ltd., London. Printed in Great Britain

BENDING OF A SINGULARLY LOADED THIN CIRCULAR ANNULUS WITH FREE BOUNDARIES

By W. A. Bassali
Faculty of Science, University of Alexandria

(*Received 25th January*, 1960)

Summary

Series solutions are presented for the complex potentials and deflexion of a thin circular annular plate of constant thickness under any system of concentrated forces or concentrated couples in equilibrium, the edges of the annulus being free. The limiting cases when the radius of the inner edge tends to zero or the radius of the outer edge tends to infinity are investigated and exact solutions in closed forms are deduced. Worked out in detail are three particular problems; namely, those of circular ring plates subjected, respectively, to two bending couples, to two twisting couples, both applied at the ends of a diameter of a concentric circle, and to four forces applied at the ends of two perpendicular diameters of a concentric circle. The method of images is used to obtain the deflexion of a sectorial plate bounded by two free arcs of concentric circles and two radii when the plate is acted upon by a concentrated load at an arbitrary point and is simply supported along the straight edges.

1. Introduction

The technological importance of the study of the behaviour of normally loaded thin elastic slabs is sufficiently well established to require no elaboration. Thin perforated plates of material are structures which have considerable applications in engineering design and problems concerning their transverse flexure have been investigated both theoretically and experimentally by many authors. The influence of circular and elliptical holes on thin elastic plates under transverse flexure and transmitting constant bending moments, twisting moments, or shearing forces were first considered by Goodier (1936) through the use of curvilinear coordinates. Muskhelishvili's complex variable method of solving the biharmonic equation was applied by Friedmann (1941) to the case of a circular hole in a large plate transmitting constant bending or twisting moments. Problems relating to a circular ring plate have also been treated in the same paper. Solutions for an infinite plate with a cut-out in the form of an ovaloid have been given by Holgate (1946) who considered flexural couples distributed around all edges, cylindrical bending about one axis and uniform twist about one axis. The effects of a free hole or a rigid inclusion with the shape of an ovaloid on a large plate transmitting constant bending moments, twisting moments, or shearing forces have been discussed by Yu (1954a) with the aid of Muskhelishvili's complex variable method. Although Yu's results are exact only when the plate is infinite in size, they may also be applied to finite plates the sizes of which are large compared with the hole or the rigid inclusion. Goodier (1936) observed that in the case of a

circular hole the results may be applied to finite plates without significant error if the boundary does not come within a distance equal to five times the radius of the circle. Solutions for an infinite isotropic thin plate with free outer edge and an elastically restrained inner circular edge have been established (BASSALI 1957a, b), when the plate is subject to various distributions of normal thrust over the area of a circle. When both edges are free and the infinite plate is under the same normal pressures and is supported at several points the appropriate solutions have also been obtained (BASSALI 1957c, 1958a). The latter paper contains the solution for an infinite plate with a free circular hole and acted upon by any external system of isolated forces and couples in equilibrium. The corresponding problems for an elastically restrained circular plate or a circular plate with a free edge have also been solved in a series of papers (BASSALI and DAWOUD 1956; BASSALI 1956, 1957d, 1958b); extensive bibliographies are to be found at the ends of these papers.

Using the solution for an infinitely large plate clamped at an inner circular edge, with outer edge free and loaded by a concentrated force at an arbitrary point, SYMONDS (1946) has established solutions for ring-shaped plates of free finite outer radius, with the force applied either at the outer edge or at any point between the inner clamped edge and the outer edge. The first case, in which the force is applied at the outer edge was solved by REISSNER (1929). In his discussion of SYMOND's paper POLIVKA (1947) mentioned that he had applied the methods of FÖPPL and MICHELL to a ring-shaped plate clamped along its outer edge and that he was able to corroborate the results of his analysis by tests on models. Influence deflexions were measured and fair agreement with the analytical solution was found. The bending of circular annular plates under an isolated load has also been discussed by SEKIYA *et al.* (1952) who gave an explicit solution to the problem only when both edges are clamped. Circular plates with central holes and loaded over the arbitrary eccentric circular domain have also been treated by SEKIYA and WADA (1956) who gave Fourier expansions of the boundary conditions and applied their method to two numerical examples in which the boundaries are clamped. In a recent paper (BASSALI and GORGUI 1960) solutions for circular ring plates under a concentrated load or a concentrated couple at an arbitrary point have been found when both edges are elastically restrained with different restraining parameters or one edge is elastically restrained and the other is free. The finite circular plate with an eccentric circular hole and bent by a concentrated load at any point has been studied by KUDRIAVTZEV (1946) and SAITO (1957). The same problem has also been discussed by OLSZAK and MROZ (1956, 1957) through the use of the transformation of inversion.

The bending of circular ring plates of variable thickness has been considered by CONWAY (1948, 1958), the plates being either subject to symmetrical loadings or to systems of couples and normal forces on the edges. The corresponding problems for plates with constant thickness have been worked out by WAHL and LOBO (1930), LABROW (1941), TRUMPLER (1943) and GEORGIAN (1957).

In this paper expressions are determined, on the basis of the classical theory of bending of thin elastic plates, for the complex potentials and deflexions of circular ring plates with free edges and subject to any system of concentrated external couples or forces acting at a finite number of interior points. For convenience, concentrated couples and concentrated forces will be discussed separately. It

may be seen that this does not restrict us from loading the annulus with both couples and forces at the same time. No special treatment (Yu 1954b) is required when the forces or couples are applied at points of the edges, and the solutions can be derived from those for interior points by a limiting process of letting the points of application of forces or couples tend to the boundary. Solutions corresponding to certain distributions of couples or forces are carried out in detail. In limiting and special cases the results obtained are found to agree with those of previous authors.

2. Preliminary Results

It is well known that the small transverse displacement w, measured positively downwards, at any point $z = x + iy = re^{i\theta}$ of the middle plane of an isotropic homogeneous thin plate singularly loaded by isolated couples or forces satisfies the biharmonic equation

$$\nabla^4 w = \left[(\partial^2/\partial x^2) + (\partial^2/\partial y^2)\right]^2 w = 16\, \partial^4 w/\partial z^2\, \partial \bar{z}^2 = 0 \tag{2.1}$$

at all points of the plate except at the load point or points, bars being used to denote conjugate complex quantities. According to Muskhelishvili, the general solution of (2.1) may be represented by

$$w = z\,\overline{\phi}(\bar{z}) + \bar{z}\,\phi(z) + \chi(z) + \overline{\chi}(\bar{z}), \tag{2.2}$$

where $\phi(z)$ and $\chi(z)$ are analytic functions of the complex variable z, usually called the complex potentials.

With the usual assumptions (Conway 1948, p. 1) and nomenclature of small deflexion plate theory, the complex combinations of the bending moments M_r, M_θ, twisting moment $M_{r\theta}$ and shearing forces Q_r, Q_θ, all per unit of arc length at any point in the plate may conveniently be given (Lechnitzky 1938) by

$$M_r + M_\theta = -4D(1+\nu)\left[\phi'(z) + \overline{\phi}'(\bar{z})\right], \tag{2.3a}$$

$$M_r - M_\theta + 2iM_{r\theta} = -4D(1-\nu)\left[z\,\phi''(z) + (z^2\,\psi'(z)/r^2)\right], \tag{2.3b}$$

$$Q_r - iQ_\theta = -8Dz\,\phi''(z)/r, \tag{2.3c}$$

where

$$\psi(z) = \chi'(z), \tag{2.4}$$

$D = 2Eh^3/3(1-\nu^2)$ is the flexural rigidity of the plate; E, ν and h being, respectively, Young's modulus, Poisson's ratio, and the half-thickness of the plate.

Lechnitzky (1938) also derived the boundary condition for the plate problem in which the boundary moments and shear resultants are prescribed. For a free boundary Γ of a plate his result is reduced to

$$\kappa\,\phi(z) + z\,\overline{\phi}'(\bar{z}) + \overline{\psi}(\bar{z}) = \alpha + i\beta z \text{ on } \Gamma, \tag{2.5}$$

where

$$\kappa = (3+\nu)/(\nu-1). \tag{2.6}$$

α is a complex constant and β is a real constant, both arbitrary.

3. Circular Ring Plate Subjected to Concentrated Couples

We now consider the bending of a circular annular plate of constant thickness bounded by an outer circle Γ_1 of radius c_1 and an inner circle Γ_2 of radius c_2. Both

boundaries of the plate are assumed to be free and the plate is acted upon by the system of m concentrated couples G_s ($s = 1, 2, \ldots, m$) operating at the m interior points $z_s = r_s e^{i\theta_s}$, the planes of the couples being normal to the plate and making angles γ_s with the positive direction of the x-axis.

It was shown (BASSALI 1959, p. 132) that the singular parts of the complex potentials $\phi(z)$ and $x(z)$ at the point of application of the concentrated couple G_s are

$$\phi_{\sin}(z) = -k\,\lambda_s \log Z_s, \tag{3.1a}$$

$$x_{\sin}(z) = k\,(\lambda_s\,\bar{z}_s - \bar{\lambda}_s\,Z_s)\log Z_s, \tag{3.1b}$$

where

$$k = 1/(16\pi D), \tag{3.2}$$

$$\lambda_s = e^{i\gamma_s}, \quad Z_s = z - z_s. \tag{3.3}$$

From (2.4) and (3.1b) it follows that the singular part of the function $\psi(z)$ at the point z_s is

$$\psi_{\sin}(z) = k\left[(\lambda_s\,\bar{z}_s/Z_s) - \bar{\lambda}_s \log Z_s\right]. \tag{3.4}$$

The conditions of equilibrium of the plate readily give

$$\sum_{s=1}^{m} \lambda_s\,G_s = 0. \tag{3.5}$$

Guided by (3.1a) and (3.4) we now assume that the functions $\phi(z)$ and $\psi(z)$ which solve the circular ring plate problem under consideration have the forms

$$\phi(z) = k\left[-\sum_{s=1}^{m} \lambda_s\,G_s \log Z_s + \phi_0(z)\right], \tag{3.6a}$$

$$\psi(z) = k\left[\sum_{s=1}^{m} G_s\left\{(\lambda_s\,\bar{z}_s/Z_s) - \lambda_s \log Z_s\right\} + \psi_0(z)\right], \tag{3.6b}$$

where $\phi_0(z)$ and $\psi_0(z)$ are functions of z, regular over the annulus $c_2 \leqslant |z| \leqslant c_1$. We have now to determine these functions from the conditions that the boundaries Γ_j ($j = 1, 2$) are free. Substituting from (3.6) in (2.5) leads to

$$\kappa\,\phi_0(z) + z\,\bar{\phi}_0'(\bar{z}) + \bar{\psi}_0(\bar{z}) = \sum_{s=1}^{m} G_s\left[\lambda_s\,(\kappa \log Z_s + \log \bar{Z}_s) + (\lambda_s\,Z_s/\bar{Z}_s)\right] + \alpha_j + i\beta_j\,z \text{ on } \Gamma_j\ (j = 1, 2). \tag{3.7}$$

On Γ_1 we have $z\bar{z} = {c_1}^2$ and the expression on the right side of (3.7) may be expanded in the form

$$\alpha_1 + i\beta_1\,z + \sum_{s=1}^{m} G_s\left[\sum_{n=2}^{\infty}\left(\frac{z\bar{z}_s}{{c_1}^2}\right)^n\left\{\frac{\lambda_s\,({c_1}^2 - {r_s}^2)}{\bar{z}_s^{\,2}} - \frac{\lambda_s}{n}\right\} - \frac{z}{{c_1}^2}\,(\lambda_s\,\bar{z}_s + \bar{\lambda}_s\,z_s) - \kappa\,\lambda_s \sum_{n=1}^{\infty}\frac{1}{n}\left(\frac{z_s}{z}\right)^n\right], \tag{3.8a}$$

while on Γ_2 we have $z\bar{z} = {c_2}^2$ and the same expression has the expansion

$$\alpha_2 + i\beta_2\,z + \sum_{s=1}^{m} G_s\left[\frac{\lambda_s}{\bar{z}_s^{\,2}}\,({r_s}^2 - {c_2}^2) + \lambda_s\,(\kappa \log z_s + \log \bar{z}_s) - \frac{\bar{\lambda}_s\,z}{\bar{z}_s} + \sum_{n=1}^{\infty}\left\{\frac{\lambda_s}{\bar{z}_s^{\,2}}\,({r_s}^2 - {c_2}^2) - \frac{\lambda_s}{n}\right\}\left(\frac{{c_2}^2}{z\bar{z}_s}\right)^n - \kappa\,\lambda_s \sum_{n=1}^{\infty}\frac{1}{n}\left(\frac{z}{z_s}\right)^n\right]. \tag{3.8b}$$

To satisfy (3.7) we now assume tentatively that

$$\phi_0(z) = z \sum_{-\infty}^{\infty} P_n z^n, \tag{3.9a}$$

$$\psi_0(z) = z^{-1} \sum_{-\infty}^{\infty} Q_n z^n, \tag{3.9b}$$

where P_n and Q_n ($n = 0, \pm 1, \pm 2, \ldots$) are, in general, complex constants to be determined. Since a term iCz (C real) in $\phi_0(z)$ makes no contribution to the deflexion w we see that the constant P_0 may be taken as real. Furthermore, it follows from (2.5) that a term* iCz^{-1} (C real) in $\psi_0(z)$ does not affect the conditions of a free circular boundary. This term leads to a term $iC \log z$ in $\chi_0(z)$ and hence contributes a multiple-valued term to w. The constant Q_0 must therefore be taken as real.

With the values (3.9) inserted in (3.7) the left side may be written as

$$z \sum_{-\infty}^{\infty} [\kappa P_n z^n + (c_j^2/z)^n \{(n+1)\bar{P}_n + \bar{Q}_n c_j^{-2}\}] \text{ on } \Gamma_j \ (j = 1, 2). \tag{3.10}$$

When the expressions (3.8a), (3.8b) are equated to (3.10) with $j = 1, 2$, respectively, and the corresponding coefficients of powers of z in the resulting identities are compared the following equations are immediately arrived at:

$$\left.\begin{aligned} (1+\kappa) c_1^2 P_0 + Q_0 &= -2 \operatorname{Re} \sum_{s=1}^{m} \bar{\lambda}_s G_s z_s, \\ (1+\kappa) c_2^2 P_0 + Q_0 &= -(1+\kappa) c_2^2 \operatorname{Re} \sum_{s=1}^{m} \lambda_s G_s / z_s ; \end{aligned}\right\} \tag{3.11}$$

$$\left.\begin{aligned} \kappa P_n c_1^{2+2n} + (1-n) c_1^2 \bar{P}_{-n} + \bar{Q}_{-n} &= U_n' \ (n = 1, 2, \ldots), \\ \kappa P_n c_2^{2+2n} + (1-n) c_2^2 \bar{P}_{-n} + \bar{Q}_{-n} &= U_n'' \ (n = 1, 2, \ldots), \\ (1+n) c_1^2 P_n + \kappa \bar{P}_{-n} c_1^{2-2n} + Q_n &= V_n' \ (n = 2, 3, \ldots), \\ (1+n) c_2^2 P_n + \kappa \bar{P}_{-n} c_2^{2-2n} + Q_n &= V_n'' \ (n = 2, 3, \ldots), \end{aligned}\right\} \tag{3.12}$$

where

$$\left.\begin{aligned} U_n' &= \sum_{s=1}^{m} G_s \left[\frac{\bar{\lambda}_s}{\bar{z}_s^2}(c_1^2 - r_s^2) - \frac{\lambda_s}{1+n}\right] \bar{z}_s^{1+n}, \\ U_n'' &= -\kappa \sum_{s=1}^{m} \lambda_s G_s \frac{(c_2^2/z_s)^{1+n}}{1+n}, \\ V_n' &= \kappa \sum_{s=1}^{m} \bar{\lambda}_s G_s \frac{(c_1^2/\bar{z}_s)^{1-n}}{1-n}, \\ V_n'' &= \sum_{s=1}^{m} G_s \left[\frac{\lambda_s}{z_s^2}(r_s^2 - c_2^2) + \frac{\bar{\lambda}_s}{1-n}\right] z_s^{1-n}. \end{aligned}\right\} \tag{3.13}$$

Solving the foregoing equations and making use of the equilibrium conditions (3.5) lead to

$$\left.\begin{aligned} P_0 &= \frac{c_2^2}{(1+\kappa)(c_1^2 - c_2^2)} \operatorname{Re} \sum_{s=1}^{m} \frac{\lambda_s G_s}{z_s} \left(1 + \kappa - \frac{2r_s^2}{c_2^2}\right), \\ Q_0 &= -\frac{c_1^2 c_2^2}{c_1^2 - c_2^2} \operatorname{Re} \sum_{s=1}^{m} \frac{\lambda_s G_s}{z_s} \left(1 + \kappa - \frac{2r_s^2}{c_1^2}\right), \end{aligned}\right\} \tag{3.14}$$

*Equation (2.3b) shows that this term contributes a constant value to $M_{r\theta}$ over any circle $r =$ constant and hence the conditions $M_r = 0$, $Q_r - (\partial M_{r\theta}/r\partial\theta) = 0$ for a free circular boundary are not affected by such a term.

$$\left.\begin{aligned} P_1 &= \frac{1}{\kappa(c_1^4 - c_2^4)} \sum_{s=1}^{m} G_s \left[\frac{\lambda_s}{2z_s^2}(\kappa c_2^4 - r_s^4) - \bar{\lambda}_s r_s^2\right], \\ Q_{-1} &= -\frac{c_2^4}{c_1^4 - c_2^4} \sum_{s=1}^{m} G_s \left[\frac{\bar{\lambda}_s}{2\bar{z}_s^2}(\kappa c_1^4 - r_s^4) - \lambda_s r_s^2\right], \end{aligned}\right\} \tag{3.15}$$

$$\left.\begin{aligned} P_n &= J_n\left[\kappa t_{1-n}(U_n' - U_n'') - (1-n)\, t_1 (V_n' - V_n'')\right], \\ P_{-n} &= J_n\left[\kappa t_{1+n}(V_n' - V_n'') - (1+n)\, t_1 (U_n' - U_n'')\right], \\ Q_n &= c_1^2 c_2^2 J_n\left[\kappa^2 c_1^2 c_2^2 (V_n' c_1^{2n-2} - V_n'' c_2^{2n-2})\, t_{-n-1} - \right. \\ &\qquad \left. - (n^2-1)\, t_1 (V_n' c_1^{-2} - V_n'' c_2^{-2}) - \kappa(1+n)(U_n' - U_n'')\, t_{-n}\right], \\ Q_{-n} &= c_1^2 c_2^2 J_n\left[\kappa^2 c_1^2 c_2^2 (U_n' c_1^{-2n-2} - U_n'' c_2^{-2n-2})\, t_{n-1} - \right. \\ &\qquad \left. - (n^2-1)\, t_1 (U_n' c_1^{-2} - U_n'' c_2^{-2}) - \kappa(1-n)(V_n' - V_n'')\, t_n\right], \end{aligned}\right\} \tag{3.16}$$

where $n = 2, 3, \ldots,$

$$\left.\begin{aligned} J_n^{-1} &= \kappa^2 t_{1+n} t_{1-n} + (n^2-1)\, t_1^2, \\ t_n &= c_1^{2n} - c_2^{2n}. \end{aligned}\right\} \tag{3.17}$$

The constants P_{-1} in (3.9a) and Q_1 in (3.9b) are left arbitrary and since they have similar contributions to w it follows that one of them may be taken as zero. These terms together with a constant term in $x_0(z)$ contribute the linear expression $Ax + By + C$ to the deflexion w at any point of the plate; A, B and C being real constants that can be determined by knowing the deflexions at three given points of the plate.

To compute the moments and shears at any point of the annulus we substitute (3.9) into (3.6) and then apply (2.3). The results are

$$\left.\begin{aligned} \left.\begin{matrix} M_r \\ M_\theta \end{matrix}\right\} &= \frac{1-\nu}{8\pi} \operatorname{Re}\left[\sum_{s=1}^{m} \frac{G_s}{Z_s}\left\{\pm\frac{z}{r^2}\left(\frac{z\bar{z}_s - r^2}{Z_s}\lambda_s + \bar{\lambda}_s z_s\right) - (1+\kappa)\lambda_s\right\} + \right. \\ &\qquad \left. + \sum_{-\infty}^{\infty}\{(n+1)(\kappa \mp n + 1)\, P_n \mp (n-1)\, r^{-2} Q_n\} z^n\right], \\ M_{r\theta} &= \frac{1-\nu}{8\pi r^2} \operatorname{Im}\left[\sum_{s=1}^{m} \frac{zG_s}{Z_s}\left\{\frac{z\bar{z}_s - r^2}{Z_s}\lambda_s + \bar{\lambda}_s z_s\right\} - \right. \\ &\qquad \left. - \sum_{-\infty}^{\infty}\{n(n+1)\, r^2 P_n + (n-1)\, Q_n\} z^n\right], \\ \left.\begin{matrix} -Q_r \\ Q_\theta \end{matrix}\right\} &= \frac{1}{2\pi r} \begin{matrix} \operatorname{Re} \\ \operatorname{Im} \end{matrix}\left[z \sum_{s=1}^{m} \frac{\lambda_s G_s}{Z_s^2} + \sum_{-\infty}^{\infty} n(n+1)\, P_n z^n\right]. \end{aligned}\right\} \tag{3.18}$$

From (2.2), (2.4), (3.6) and (3.9) we find that the deflexion at any point is furnished by

$$w = 2k\left[-\sum_{s=1}^{m}(\lambda_s Z_s + \bar{\lambda}_s \bar{Z}_s) G_s \log R_s + P_0 r^2 + Q_0 \log r + \operatorname{Re}(r^2 P_1 z - Q_{-1} z^{-1}) + \right.$$
$$\left. + \operatorname{Re}\sum_{n=2}^{\infty}\left\{\left(r^2 P_n + \frac{1}{n} Q_n\right) z^n + \left(r^2 P_{-n} - \frac{1}{n} Q_{-n}\right) z^{-n}\right\} + Ax + By + C\right], \tag{3.19}$$

where $R_s = |Z_s|$, A, B and C are real constants.

We are now in a position to examine two limiting cases.

(a). Finite circular plate (without a concentric hole) having a free edge and subject to any system of concentrated couples in equilibrium. Let us now determine the limiting form of the foregoing solution as the radius c_2 of the inner circular boundary Γ_2 tends to zero. The following expressions for the coefficients in (3.9) are easily obtained:

$$\left.\begin{aligned} P_0 &= -\frac{1}{(1+\kappa)\,c_1^{\,2}}\sum_{s=1}^{m} G_s\,(\bar{\lambda}_s z_s + \lambda_s \bar{z}_s),\\ P_n &= \frac{1}{\kappa}\sum_{s=1}^{m} G_s \left(\frac{\bar{z}_s}{c_1^{\,2}}\right)^{n+1}\left[\frac{\bar{\lambda}_s}{\bar{z}_s^{\,2}}(c_1^{\,2}-r_s^{\,2}) - \frac{\lambda_s}{1+n}\right] (n=1,2,\ldots),\\ P_{-n} &= 0\,(n=2,3,\ldots), \end{aligned}\right\} \tag{3.20a}$$

$$\left.\begin{aligned} Q_n &= \frac{1}{\kappa}\sum_{s=1}^{m} G_s \left(\frac{\bar{z}_s}{c_1^{\,2}}\right)^{n-1}\left[\bar{\lambda}_s\left\{(n+1)\left(\frac{r_s^{\,2}}{c_1^{\,2}}-1\right) - \frac{\kappa^2}{n-1}\right\} + \frac{\lambda_s z_s^{\,2}}{c_1^{\,4}}\right] (n=2,3,\ldots),\\ Q_{-n} &= 0\,(n=0,1,2,\ldots). \end{aligned}\right\} \tag{3.20b}$$

When these values are inserted in (3.9) it is found that the regular function $\phi_0(z)$ and $\psi_0(z)$ can be put in the closed forms

$$\left.\begin{aligned} \phi_0(z) &= \frac{1}{\kappa}\sum_{s=1}^{m} G_s\left[\lambda_s \log\left(1-\frac{z\bar{z}_s}{c_1^{\,2}}\right) + \frac{\bar{\lambda}_s z Z_s}{c_1^{\,2}-z\bar{z}_s} + \frac{z\,(\lambda_s \bar{z}_s + \lambda_s z_s)}{(1+\kappa)\,c_1^{\,2}}\right] + C_1,\\ \psi_0(z) &= \frac{1}{\kappa}\sum_{s=1}^{m} G_s\left[\kappa^2\,\bar{\lambda}_s \log\left(1-\frac{z\bar{z}_s}{c_1^{\,2}}\right) + \frac{\lambda_s \bar{z}_s^{\,2}}{c_1^{\,2}-z\bar{z}_s} + \bar{\lambda}_s \frac{(r_s^{\,2}-c_1^{\,2})\,(2c_1^{\,2}-z\bar{z}_s)}{(c_1^{\,2}-z\bar{z}_s)^2}\right]. \end{aligned}\right\} \tag{3.21}$$

Substituting from (3.21) in (3.6) and integrating the resulting expression for $\psi(z)$ we find that the values obtained for $\phi(z)$ and $\chi(z)$ agree with those derived through the application of MUSKHELISHVILI's complex variable method (BASSALI 1958b, p. 274).

(b). Infinite plate with a free circular hole. Letting c_1 tend to ∞ in equations (3.14)–(3.17) yields

$$\left.\begin{aligned} P_n &= 0\,(n=0,1,2,\ldots),\\ P_{-n} &= \frac{1}{\kappa}\sum_{s=1}^{m} G_s\left[\frac{\bar{\lambda}_s^{\,2}}{\bar{z}_s^{\,2}}(r_s^{\,2}-c_2^{\,2}) - \frac{\lambda_s}{n-1}\right]\left(\frac{z_s}{c_2^{\,2}}\right)^{1-n} (n=2,3,\ldots), \end{aligned}\right\} \tag{3.22a}$$

$$\left.\begin{aligned} Q_0 &= -(1+\kappa)\,c_2^{\,2}\,\mathrm{Re}\sum_{s=1}^{m}\lambda_s G_s/z_s,\\ Q_n &= 0\,(n=2,3,\ldots),\\ Q_{-n} &= \frac{1}{\kappa}\sum_{s=1}^{m} G_s\left(\frac{c_2^{\,2}}{\bar{z}_s}\right)^{n+1}\left[\bar{\lambda}_s\left\{(n-1)\left(\frac{r_s^{\,2}}{c_2^{\,2}}-1\right) - \frac{\kappa^2}{n+1}\right\} - \frac{\lambda_s z_s^{\,2}}{c_2^{\,2}}\right] (n=1,2,\ldots). \end{aligned}\right\} \tag{3.22b}$$

Introducing these expressions in (3.9) and summing the infinite series obtained we get the closed formulae

$$\left.\begin{aligned} \phi_0(z) &= \frac{1}{\kappa}\sum_{s=1}^{m} G_s\left[\lambda_s \log\left(1-\frac{c_2^{\,2}}{z\bar{z}_s}\right) + \frac{\bar{\lambda}_s c_2^{\,2}(r_s^{\,2}-c_2^{\,2})}{\bar{z}_s^{\,2}(z\bar{z}_s - c_2^{\,2})}\right] + C_1,\\ \psi_0(z) &= \frac{1}{\kappa}\sum_{s=1}^{m} G_s\left[\bar{\lambda}_s\left\{\kappa^2 \log\left(1-\frac{c_2^{\,2}}{z\bar{z}_s}\right) + \frac{\kappa^2 c_2^{\,2}}{z\bar{z}_s} + \frac{(r_s^{\,2}-c_2^{\,2})\,c_2^{\,4}}{z\bar{z}_s\,(c_2^{\,2}-z\bar{z}_s)^2}\right\} + \right.\\ &\qquad \left. + \frac{\lambda_s \bar{z}_s c_2^{\,2}}{z\,(c_2^{\,2}-z\bar{z}_s)} - \kappa(1+\kappa)\frac{c_2^{\,2}}{z}\,\mathrm{Re}\left(\frac{\lambda_s}{z_s}\right)\right]. \end{aligned}\right\} \tag{3.23}$$

When equations (3.23) are combined with (3.6) and the second equation is integrated it is found that the results are in agreement with equations (49), p. 116 of BASSALI (1958a).

Special problems dealing with the transverse flexure of a finite circular plate, an infinite plate containing a free circular hole or a half-plane subjected to two bending or twisting couples have been worked out in detail (BASSALI 1958a, b). Two particular problems concerning the bending of a circular annulus by concentrated couples at interior or boundary points will now be discussed.

4. Circular Annulus Under Two Bending Couples

In the first problem the annulus of outer radius c_1 and inner radius c_2 is subjected to two equal and opposite concentrated bending couples each of magnitude G and acting at the ends $(\pm c, 0)$ of a diameter of a concentric circle. Here we have

$$\lambda_1 = \bar{\lambda}_1 = 1, \quad z_1 = c\,; \quad \lambda_2 = \bar{\lambda}_2 = -1, \quad z_2 = -c. \tag{4.1}$$

Substituting these values in (3.13) and introducing for convenience the dimensionless quantities

$$\delta_j = c/c_j, \quad \delta = \delta_1/\delta_2 = c_2/c_1, \tag{4.2}$$

we find that

$$\left.\begin{aligned} U_n' &= 2G\left(\delta_1^{-2} - 1 - \frac{1}{1+n}\right)c^{1+n}, & U_n'' &= -\frac{2\kappa G}{1+n}\,\delta_2^{-2n-2}\,c^{1+n}, \\ V_n' &= \frac{2\kappa G}{1-n}\,\delta_1^{2n-2}\,c^{1-n}, & V_n'' &= 2G\left(1 - \delta_2^{-2} + \frac{1}{1-n}\right)c^{1-n} \end{aligned}\right\} \tag{4.3}$$

for $n = 2, 4, 6, \ldots$ and they all vanish for odd values of n. Applying (4.1) to (3.14) and (3.15), introducing (4.3) in (3.16) and using the notations (4.2) we find that the expression (3.19) for the deflexion at any point $z = r\,e^{i\theta}$ of the annulus may be written in the form

$$\begin{aligned} \frac{4\pi D}{cG}\,w = {} & \left(1 + \frac{x}{c}\right)\log\frac{|z+c|}{2c} + \left(1 - \frac{x}{c}\right)\log\frac{|z-c|}{2c} + A_0(\rho^2 - 1) + B_0\log\rho + \\ & + \sum_{2,\,4,\,6,\,\ldots} T_n\left[A_n(\rho^{2+n}\cos n\,\theta - 1) + B_n(\rho^{2-n}\cos n\,\theta - 1) + \right. \\ & \left. + C_n(\rho^n\cos n\,\theta - 1) + D_n(\rho^{-n}\cos n\,\theta - 1)\right], \end{aligned} \tag{4.4}$$

where $\rho = r/c$, the deflexion is taken as zero at the points $(\pm c, 0)$ and

$$T_n^{-1} = (n^2 + \kappa^2 - 1)(\delta^{-1} - \delta)^2 - \kappa^2(\delta^{-n} - \delta^n)^2 \quad (n = 2, 4, 6, \ldots)\,; \tag{4.5a}$$

$$\left.\begin{aligned} A_0 &= \frac{\delta^2}{1-\delta^2}\left(1 - \frac{2\delta_2^{\,2}}{1+\kappa}\right), \\ B_0 &= \frac{\delta_2^{-2}}{1-\delta^2}(2\delta_1^{\,2} - 1 - \kappa)\,; \end{aligned}\right\} \tag{4.5b}$$

$$\left.\begin{aligned} A_n &= \kappa(\delta^{-2} - \delta^{-2n})\left\{\delta_1^{-2} - 1 + \frac{\kappa\,\delta_2^{-2n-2} - 1}{n+1}\right\}\delta_1^{2+2n} + \\ &\quad + (\delta^{-2} - 1)\left\{(n-1)(\delta^2 - \delta_1^{\,2}) + \delta_1^{\,2} - \kappa\,\delta_1^{\,2n}\right\}, \\ B_n &= \kappa(\delta^{-2} - \delta^{2n})\left\{\delta_2^{-2} - 1 + \frac{1 - \kappa\,\delta_1^{\,2n-2}}{n-1}\right\}\delta_1^{\,2-2n} + \\ &\quad + (1 - \delta^2)\left\{(n+1)(\delta_2^{\,2} - \delta^{-2}) + \delta_2^{\,2} - \kappa\,\delta_2^{-2n}\right\}, \\ C_n &= \frac{1}{n}\left[\kappa^2(\delta^{2n} - \delta^{-2})\left\{\delta_2^{-2} - 1 + \frac{1 - \kappa\,\delta_2^{\,2n-2}}{n-1}\right\} - (n^2-1)(\delta^{-2} - 1)\left\{\delta_2^{-2} - 1 + \right.\right. \\ &\quad \left.\left. + \frac{1 - \kappa\,\delta_2^{-2}\,\delta_1^{\,2n}}{n-1}\right\} - \kappa(\delta_1^{\,2n} - \delta_2^{\,2n})\left\{(n+1)(\delta_1^{-2} - 1) + \kappa\delta_2^{-2n-2} - 1\right\}\right], \\ D_n &= \frac{1}{n}\left[\kappa^2(\delta^{2n} - \delta^2)\left\{\delta_1^{-2} - 1 + \frac{\kappa\delta_1^{-2n-2} - 1}{n+1}\right\} - (n^2-1)(1 - \delta^2)\left\{1 - \delta_1^{-2} + \right.\right. \\ &\quad \left.\left. + \frac{1 - \kappa\delta_1^{-2}\,\delta_2^{-2n}}{n+1}\right\} - \kappa(\delta_1^{-2n} - \delta_2^{-2n})\left\{(n-1)(\delta_2^{-2} - 1) + 1 - \kappa\delta_1^{\,2n-2}\right\}\right]. \end{aligned}\right\} \tag{4.5c}$$

Letting $\delta_1 (= c/c_1)$ or $\delta_2 (= c/c_2)$ tend to unity in the foregoing expressions yields the solution corresponding to a circular ring plate subjected to two bending couples at the ends of a diameter of the outer or inner edge. It can now be shown that the logarithmic terms in (4.4) may be expanded in the forms

$$\left(1+\frac{x}{c}\right)\log\frac{|z+c|}{2c}+\left(1-\frac{x}{c}\right)\log\frac{|z-c|}{2c}=\rho^2-2\log 2+$$
$$+\sum_{2,4,\ldots}\left(\frac{1}{n-1}-\frac{2}{n}+\frac{\rho^2}{n+1}\right)\rho^n\cos n\theta\,(\rho\leqslant 1), \tag{4.6a}$$

$$\left(1+\frac{x}{c}\right)\log\frac{|z+c|}{2c}+\left(1-\frac{x}{c}\right)\log\frac{|z-c|}{2c}=1+2\log\frac{\rho}{2}+$$
$$+\sum_{2,4,\ldots}\left[\frac{1}{n+1}-\frac{2}{n}+\frac{\rho^2}{n-1}\right)\rho^{-n}\cos n\theta\,(\rho\geqslant 1). \tag{4.6b}$$

Substituting from (4.6a) in (4.4) and making use of (4.5) we find after some algebraic manipulation that, in the case of an annulus under two bending couples at the points $(\pm c_1, 0)$ of the outer edge, the deflexion at any point is furnished by

$$\frac{\pi\sigma D}{c_1 G}w=\frac{1}{1-\delta^2}\left\{\frac{1-\rho^2}{1+\kappa}+\delta^2\log\rho\right\}$$
$$+\sum_{2,4,\ldots}T_n\left[\left\{(n+1)(\delta^2-1)+\kappa(1-\delta^{-2n})+\frac{\kappa^2}{n-1}(\delta^2-\delta^{-2n})\right\}\frac{\rho^n\cos n\theta-1}{n}+\right.$$
$$+\left\{(n-1)(\delta^2-1)+\kappa(\delta^{2n}-1)+\frac{\kappa^2}{n+1}(\delta^2-\delta^{2n})\right\}\frac{\rho^{-n}\cos n\theta-1}{n}+$$
$$+\left\{\delta^{-2}-1+\frac{\kappa}{n+1}(\delta^{-2n}-\delta^{-2})\right\}(\rho^{2+n}\cos n\theta-1)+$$
$$\left.+\left\{\delta^{-2}-1+\frac{\kappa}{n-1}(\delta^{-2}-\delta^{2n})\right\}(\rho^{2-n}\cos n\theta-1)\right], \tag{4.7}$$

where $\rho = r/c_1$ and

$$\sigma = 1-\nu, \tag{4.8}$$

the deflexion being taken as zero at $(\pm c_1, 0)$. Allowing $\delta\,(= c_2/c_1)$ to tend to zero in (4.7) yields the solution

$$\frac{\pi\sigma D}{c_1 G}w=\frac{1-\rho^2}{1+\kappa}+\frac{1}{\kappa}\sum_{2,4,\ldots}\left[\frac{1}{n}\left(1+\frac{\kappa}{n-1}\right)(\rho^n\cos n\theta-1)+\frac{1-\rho^{n+2}\cos n\theta}{n+1}\right] \tag{4.9}$$

for a circular plate subjected to two bending couples at the ends of a diameter, a problem which has been considered in detail by Yu (1954b).

Applying (4.6b) to (4.4) and setting $\delta_2 = 1$, $\delta_1 = \delta$ it is found that the deflected form of a circular plate with a concentric hole of radius c_2 bent by the two couples $(G_1 = G, \lambda_1 = 1)$ and $(G_2 = G, \lambda_2 = -1)$ at the points $(c_2, 0)$ and $(-c_2, 0)$ is

$$\frac{\pi\sigma D}{c_2 G}w=\frac{1}{\delta^{-2}-1}\left\{\frac{1-\rho^2}{1+\kappa}+\delta^{-2}\log\rho\right\}+$$
$$+\sum_{2,4,\ldots}T_n\left[\left\{(n+1)(1-\delta^{-2})+\kappa(\delta^{2n}-1)+\frac{\kappa^2}{n-1}(\delta^{2n}-\delta^{-2})\right\}\frac{\rho^n\cos n\theta-1}{n}+\right.$$
$$+\left\{(n-1)(1-\delta^{-2})+\kappa(1-\delta^{-2n})+\frac{\kappa^2}{n+1}(\delta^{-2n}-\delta^{-2})\right\}\frac{\rho^{-n}\cos n\theta-1}{n}+$$
$$+\left\{1-\delta^2+\frac{\kappa}{n+1}(\delta^2-\delta^{2n})\right\}(\rho^{2+n}\cos n\theta-1)+$$
$$\left.+\left\{1-\delta^2+\frac{\kappa}{n-1}(\delta^{-2n}-\delta^2)\right\}(\rho^{2-n}\cos n\theta-1)\right], \tag{4.10}$$

where $\rho = r/c_2$, $\delta = c_2/c_1$ and the deflexion is zero at $(\pm c_2, 0)$.

5. CIRCULAR ANNULUS UNDER TWO TWISTING COUPLES

In the second problem the annulus is subjected to two equal and opposite concentrated twisting couples each of magnitude G and operating at the points $(\pm c, 0)$. In this case we have

$$\gamma_1 = \tfrac{1}{2}\pi,\ \lambda_1 = i,\ \bar{\lambda}_1 = -i,\ z_1 = c\,;\ \gamma_2 = -\tfrac{1}{2}\pi,\ \lambda_2 = -i,\ \bar{\lambda}_2 = i,\ z_2 = -c. \tag{5.1}$$

Introducing these values into (3.13) gives

$$\left.\begin{aligned} U_n' &= -2iG\left(\delta_1^{-2} - 1 + \frac{1}{1+n}\right)c^{1+n}, \qquad U_n'' = -\frac{2i\kappa G}{n+1}\,\delta_2^{-2n-2}\,c^{1+n}, \\ V_n' &= \frac{2i\kappa G}{n-1}\,\delta_1^{2n-2}\,c^{1-n}, \qquad V_n'' = 2iG\left(1 - \delta_2^{-2} + \frac{1}{n-1}\right)c^{1-n} \end{aligned}\right\} \tag{5.2}$$

for $n = 2, 4, \ldots$ and zero otherwise. When the values (5.1) are applied to (3.14) and (3.15) it is seen that

$$P_0 = Q_0 = P_1 = Q_{-1} = 0. \tag{5.3}$$

Substituting from (5.2) in (3.16) and inserting the resulting expressions together with (5.3) in (3.19) we find that the equation of the deflexion surface is

$$\frac{4\pi D}{cG}\,w = \frac{y}{c}\log\left|\frac{z+c}{z-c}\right| + \sum_{2,\,4,\ldots} T_n\left\{(A_n\rho^2 + C_n)\,\rho^n + (B_n\rho^2 + D_n)\,\rho^{-n}\right\}\sin n\theta, \tag{5.4}$$

where $\rho = r/c$ and

$$\left.\begin{aligned} A_n &= \kappa(\delta^{-2} - \delta^{-2n})\left(\delta_1^{-2} - 1 + \frac{1-\kappa\delta_2^{-2n-2}}{n+1}\right)\delta_1^{2+2n} + \\ &\quad + (\delta^{-2} - 1)\left\{(n-1)(\delta_1^{2} - \delta^{2}) + \delta_1^{2} - \kappa\delta_1^{2n}\right\}, \\ B_n &= \kappa(\delta^{-2} - \delta^{2n})\left(1 - \delta_2^{-2} + \frac{1-\kappa\delta_1^{2n-2}}{n-1}\right)\delta_1^{2-2n} + \\ &\quad + (1 - \delta^{2})\left\{(n+1)(\delta_2^{2} - \delta^{-2}) - \delta_2^{2} + \kappa\delta_2^{-2n}\right\}, \\ C_n &= \frac{1}{n}\left[\kappa^2(\delta^{2n} - \delta^{-2})\left(1 - \delta_2^{-2} + \frac{1-\kappa\delta_2^{2n-2}}{n-1}\right) - (n^2-1)(\delta^{-2} - 1)\left(1 - \delta_2^{-2} + \right.\right. \\ &\quad \left.\left. + \frac{1-\kappa\delta_2^{-2}\,\delta_1^{2n}}{n-1}\right) - \kappa(\delta_1^{2n} - \delta_2^{2n})\left\{(n+1)(\delta_1^{-2} - 1) + 1 - \kappa\delta_2^{-2n-2}\right\}\right], \\ D_n &= \frac{1}{n}\left[\kappa^2(\delta^{2n} - \delta^{2})\left(\delta_1^{-2} - 1 + \frac{1-\kappa\delta_1^{-2n-2}}{n+1}\right) - (n^2-1)(1 - \delta^{2})\left(1 - \delta_1^{-2} + \right.\right. \\ &\quad \left.\left. + \frac{\kappa\delta_1^{-2}\,\delta_2^{-2n} - 1}{n+1}\right) - \kappa(\delta_1^{-2n} - \delta_2^{-2n})\left\{(n-1)(1 - \delta_2^{-2}) + 1 - \kappa\delta_1^{2n-2}\right\}\right] \\ &\qquad\qquad (n = 2, 4, \ldots). \end{aligned}\right\} \tag{5.5}$$

The logarithmic term appearing in (5.4) has the Fourier expansions

$$\frac{y}{c}\log\left|\frac{z+c}{z-c}\right| = \sum_{2,\,4,\ldots}\rho^n\left(\frac{1}{n-1} - \frac{\rho^2}{n+1}\right)\sin n\theta\ (\rho < 1). \tag{5.6a}$$

$$\frac{y}{c}\log\left|\frac{z+c}{z-c}\right| = \sum_{2,\,4,\ldots}\rho^{-n}\left(\frac{\rho^2}{n-1} - \frac{1}{n+1}\right)\sin n\theta\ (\rho > 1). \tag{5.6b}$$

Inserting (5.6a) in (5.4) and collecting terms lead to the following solution for a circular ring plate bent by two twisting couples applied at the ends of a diameter of the outer edge ($\delta_1 = 1$, $\delta_2 = \delta^{-1}$):

$$\frac{\pi\sigma D}{c_1 G} w = \sum_{2,4,\ldots} T_n \sin n\theta \left[\left\{ (n+1)(\delta^2 - 1) + \kappa(\delta^{-2n} - 1) + \frac{\kappa^2}{n-1}(\delta^2 - \delta^{-2n}) \right\} \frac{\rho^n}{n} + \right.$$

$$+ \left\{ (n-1)(1 - \delta^2) + \kappa(\delta^{2n} - 1) + \frac{\kappa^2}{n+1}(\delta^{2n} - \delta^2) \right\} \frac{\rho^{-n}}{n} +$$

$$\left. + \left\{ \delta^{-2} - 1 + \frac{\kappa}{n+1}(\delta^{-2} - \delta^{-2n}) \right\} \rho^{2+n} + \left\{ 1 - \delta^{-2} + \frac{\kappa}{n-1}(\delta^{-2} - \delta^{2n}) \right\} \rho^{2-n} \right]. \tag{5.7}$$

Ad $\delta \to 0$ the solution (5.7) tends to

$$\frac{\pi\sigma D}{c_1 G} w = \frac{1}{\kappa} \sum_{2,4,\ldots} \rho^n \left[\frac{1}{n} \left(\frac{\kappa}{n-1} - 1 \right) + \frac{\rho^2}{n+1} \right] \sin n\theta \; (\rho = r/c_1). \tag{5.8}$$

The infinite series entering in (4.9) and (5.8) can be easily summed and the results obtained for these particular problems agree with those of Yu (1954b).

A solution similar to (5.7) can be established for the case of a circular plate with a central hole when the plate is bent by two twisting couples acting at the ends of a diameter of the hole. This follows immediately by introducing (5.6b) in (5.4) and then putting $\delta_2 = 1$, $\delta_1 = \delta$.

Equation (5.7) represents the deflected form of a plate with the shape of a quadrant of a circular ring bounded by the circular arcs $A_1 B_1$ of radius c_1, $A_2 B_2$ or radius c_2 ($c_1 > c_2$) and the radial edges $A_2 A_1$, $B_2 B_1$; the plate is simply supported along the straight edges, free along the circular edges and is under the action of an external isolated couple G at A_1 whose axis is along $A_2 A_1$.

6. Circular Ring Plate Subjected to Concentrated Forces

We now consider the transverse flexure of a circular annulus having free edges when it is acted upon by any general system of concentrated forces in equilibrium. Let F_s ($s = 1, 2, \ldots, m$) be the magnitudes of m concentrated forces acting at the m interior points $z_s = r_s e^{i\theta_s}$ in a direction normal to the plane of the plate. The conditions of equilibrium of the plate give

$$\sum_{s=1}^{m} F_s = 0, \quad \sum_{s=1}^{m} F_s z_s = 0. \tag{6.1}$$

The singular parts of the complex potentials $\phi(z)$ and $x(z)$ near the concentrated force F_s are given (Bassali 1957c) by

$$\phi_{\sin}(z) = k F_s Z_s \log Z_s, \tag{6.2a}$$

$$x_{\sin}(z) = -k F_s \bar{z}_s Z_s \log Z_s, \tag{6.2a}$$

and hence

$$\psi_{\sin}(z) = -k F_s \bar{z}_s \log Z_s, \tag{6.2c}$$

where k and Z_s are defined by (3.2) and (3.3), respectively. These forms of the singular parts corresponding to a concentrated force at an interior point are believed to have been used first by Lurie (1940). We now assume that

$$\phi(z) = k \left[\sum_{s=1}^{m} F_s Z_s \log Z_s + \phi_0(z) \right], \tag{6.3a}$$

$$\psi(z) = k \left[-\sum_{s=1}^{m} F_s \bar{z}_s \log Z_s + \psi_0(z) \right], \tag{6.3b}$$

where $\phi_0(z)$ and $\psi_0(z)$ are functions of z regular all over the annulus $c_2 \leqslant |z| \leqslant c_1$. When the functions (6.3) are applied to (2.5) it is found that the boundary conditions along Γ_1 and Γ_2 may be written as

$$\kappa\,\phi_0(z) + z\,\bar{\phi}_0'(\bar{z}) + \bar{\psi}_0(\bar{z}) = \alpha_j + i\beta_j\,z - \sum_{s=1}^{m} F_s Z_s\,(\kappa \log Z_s + \log \bar{Z}_s) \text{ on } \Gamma_j\,(j = 1, 2). \quad (6.4)$$

Taking the functions $\phi_0(z)$ and $\psi_0(z)$ in the forms (3.9) and expanding the expression on the right side of (6.4) in terms of positive and negative powers of z we find that the boundary conditions (6.4) together with the equilibrium conditions (6.1) yield the identities

$$\sum_{-\infty}^{\infty}\left[\kappa P_n z^n + \left(\frac{c_1^2}{z}\right)^n\{(n+1)\bar{P}_n + \bar{Q}_n c_1^{-2}\}\right] = \alpha_1 z^{-1} + i\beta_1 + \sum_{s=1}^{m} F_s\left[-\frac{r_s^2}{c_1^2} + \sum_{n=2}^{\infty}\left\{-\frac{\kappa\,(z_s/z)^n}{n(n-1)} + \left(\frac{z\bar{z}_s}{c_1^2}\right)^{n-1}\left(\frac{1}{n-1} - \frac{r_s^2}{nc_1^2}\right)\right\}\right] \text{ on } \Gamma_1, \quad (6.5a)$$

$$\sum_{-\infty}^{\infty}\left[\kappa P_n z^n + \left(\frac{c_2^2}{z}\right)^n\{(n+1)\bar{P}_n + \bar{Q}_n c_2^{-2}\}\right] = \alpha_2 z^{-1} + i\beta_2 + \sum_{s=1}^{m} F_s\left[\frac{c_2^2}{\bar{z}_s} - \frac{Z_s}{z}(\kappa \log z_s + \log \bar{z}_s) + \sum_{n=2}^{\infty}\left\{\frac{\kappa\,(z/z_s)^{n-1}}{n(n-1)} + \left(\frac{c_2^2}{z\bar{z}_s}\right)^n\left(\frac{1}{n} - \frac{r_s^2}{(n-1)c_2^2}\right)\right\}\right] \text{ on } \Gamma_2. \quad (6.5b)$$

Equating the coefficients of the same powers of z on both sides of each of the foregoing identities we get the equations

$$\left.\begin{aligned}(1+\kappa)c_1^2 P_0 + Q_0 &= -\sum_{s=1}^{m} F_s r_s^2,\\ (1+\kappa)c_2^2 P_0 + Q_0 &= -(1+\kappa)c_2^2\sum_{s=1}^{m} F_s \log r_s\end{aligned}\right\} \quad (6.6)$$

together with the same equations (3.12) where in this case

$$\left.\begin{aligned}U_n' &= \sum_{s=1}^{m} F_s \bar{z}_s^n\left(\frac{c_1^2}{n} - \frac{r_s^2}{1+n}\right), \qquad U_n'' = \kappa c_2^2\sum_{s=1}^{m}\frac{F_s\,(c_2^2/z_s)^n}{n(1+n)}\ (n = 1, 2, \ldots),\\ V_n' &= \kappa c_1^2\sum_{s=1}^{m}\frac{F_s\,(\bar{z}_s/c_1^2)^n}{n(1-n)}, \qquad V_n'' = \sum_{s=1}^{m} F_s z_s^{-n}\left(\frac{c_2^2}{n} + \frac{r_s^2}{1-n}\right)(n = 2, 3, \ldots).\end{aligned}\right\} \quad (6.7)$$

When these equations are solved and the equilibrium conditions (6.1) are used it is found that

$$\left.\begin{aligned}P_0 &= \frac{1}{c_1^2 - c_2^2}\sum_{s=1}^{m} F_s\left[c_2^2 \log r_s - \frac{r_s^2}{1+\kappa}\right],\\ Q_0 &= \frac{c_2^2}{c_1^2 - c_2^2}\sum_{s=1}^{m} F_s\left[r_s^2 - (1+\kappa)c_1^2 \log r_s\right];\end{aligned}\right\} \quad (6.8)$$

$$\left.\begin{aligned}P_1 &= \frac{1}{2(c_1^4 - c_2^4)}\sum_{s=1}^{m}\frac{F_s}{z_s}\left[\frac{r_s^2}{\kappa}(2c_1^2 - r_s^2) - c_2^4\right],\\ Q_{-1} &= \frac{c_2^4}{2(c_1^4 - c_2^4)}\sum_{s=1}^{m}\frac{F_s}{\bar{z}_s}\left[\kappa c_1^4 + r_s^2(r_s^2 - 2c_1^2)\right],\end{aligned}\right\} \quad (6.9)$$

and the constants P_n, P_{-n}, Q_n, Q_{-n} $(n = 2, 3, \ldots)$ are determined by (3.16), (3.17) in which U_n', U_n'', V_n', V_n'' are defined by (6.7). Here also the constants P_{-1} and Q_1 are left arbitrary and together with a constant term in $x_0(z)$ they contribute the linear expression $Ax + By + C$ to w.

From (6.3), (3.9), (2.3) and (2.2) we obtain after some straightforward computations the following formulae for the moments, shears and deflexion at any point of the annulus:

$$\left.\begin{aligned}
\left.\begin{matrix} M_r \\ M_\theta \end{matrix}\right\} &= \frac{1-\nu}{8\pi}\left[\sum_{s=1}^{m} F_s\left\{(1+\kappa)\log R_s \mp \frac{(r^2-r_s^2)^2 - r_s^2 R_s^2}{2\,r^2 R_s^2}\right\} + \right. \\
&\qquad \left. + \operatorname{Re}\sum_{-\infty}^{\infty}\{(n+1)(\kappa \mp n + 1)P_n \mp (n-1)Q_n r^{-2}\} z^n\right], \\
M_{r\theta} &= \frac{\nu-1}{8\pi r^2}\operatorname{Im}\left[\bar{z}\sum_{s=1}^{m} F_s z_s \frac{r^2 - r_s^2}{R_s^2} + \sum_{-\infty}^{\infty}\{n(n+1)P_n r^2 + (n-1)Q_n\} z^n\right], \\
Q_r &= -\frac{1}{2\pi r}\left[\sum_{s=1}^{m} P_s \frac{r^2 - r_s^2}{2R_s^2} + \operatorname{Re}\sum_{-\infty}^{\infty} n(n+1)P_n z^n\right], \\
Q_\theta &= \frac{1}{2\pi r}\operatorname{Im}\left[\bar{z}\sum_{s=1}^{m}\frac{F_s z_s}{R_s^2} + \sum_{-\infty}^{\infty} n(n+1)P_n z^n\right];
\end{aligned}\right\} \tag{6.10}$$

$$\begin{aligned}
w = 2k\Bigg[&\sum_{s=1}^{m} F_s R_s^2 \log R_s + P_0 r^2 + Q_0 \log r + \operatorname{Re}(r^2 P_1 z - Q_{-1} z^{-1}) + \\
&+ \operatorname{Re}\sum_{n=2}^{\infty}\left\{\left(r^2 P_n + \frac{1}{n}Q_n\right) z^n + \left(r^2 P_{-n} - \frac{1}{n}Q_{-n}\right) z^{-n}\right\} + Ax + By + C\Bigg].
\end{aligned} \tag{6.11}$$

Closed expressions for the functions $\phi(z)$ and $\psi(z)$ corresponding to the two limiting cases $c_2 \to 0$ or $c_1 \to \infty$ can now be derived.

(a) Letting c_2 tend to zero in equations (6.8), (6.9), (3.16), (3.17) and (6.7) we get

$$\left.\begin{aligned}
P_0 &= -\frac{1}{(1+\kappa)c_1^2}\sum_{s=1}^{m} F_s r_s^2, \\
P_n &= \frac{1}{\kappa c_1^2}\sum_{s=1}^{m} F_s\left(\frac{\bar{z}_s}{c_1^2}\right)^n\left(\frac{c_1^2}{n} - \frac{r_s^2}{1+n}\right)\ (n = 1, 2, \ldots), \\
P_{-n} &= 0\ (n = 2, 3, \ldots);
\end{aligned}\right\} \tag{6.12a}$$

$$\left.\begin{aligned}
Q_n &= \frac{c_1^2}{\kappa}\sum_{s=1}^{m} F_s\left(\frac{\bar{z}_s}{c_1^2}\right)^n\left[\frac{r_s^2}{c_1^2} - 1 - \frac{1}{n} + \frac{\kappa^2}{n(1-n)}\right]\ (n = 2, 3, \ldots), \\
Q_{-n} &= 0\ (n = 0, 1, 2, \ldots).
\end{aligned}\right\} \tag{6.12b}$$

With these values inserted in (3.9) the functions $\phi_0(z)$ and $\psi_0(z)$ are found as

$$\left.\begin{aligned}
\phi_0(z) &= \frac{1}{\kappa}\sum_{s=1}^{m} F_s\left\{\frac{r_s^2 z}{(1+\kappa)c_1^2} - Z_s \log\left(1 - \frac{z\bar{z}_s}{c_1^2}\right)\right\} + C_1, \\
\psi_0(z) &= \frac{1}{\kappa}\sum_{s=1}^{m} F_s\left\{\frac{(1-\kappa^2)c_1^2 + \kappa^2 z\bar{z}_s}{z}\log\left(1 - \frac{z\bar{z}_s}{c_1^2}\right) - \frac{c_1^2 - r_s^2}{c_1^2 - z\bar{z}_s}\bar{z}_s\right\},
\end{aligned}\right\} \tag{6.13}$$

which agree with the results obtained by setting $P_0 = 0$ in equations (2.34) and (2.35), p. 735 of Bassali (1957d). The same problem has also been considered by Friedmann (1951).

(b) Results pertaining to an infinite plate with a free circular hole and bent by any system of isolated normal forces at interior or boundary points can also be deduced by allowing c_1 to tend to ∞. This leads to

$$\left.\begin{aligned}
P_n &= 0\ (n = 0, 1, 2, \ldots), \\
P_{-n} &= \frac{1}{\kappa c_2^2}\sum_{s=1}^{m} F_s\left(\frac{c_2^2}{\bar{z}_s}\right)^n\left(\frac{c_2^2}{n} + \frac{r_s^2}{1-n}\right)\ (n = 2, 3, \ldots),
\end{aligned}\right\} \tag{6.14a}$$

$$\left.\begin{aligned} Q_0 &= -(1+\kappa)\,c_2^2 \sum_{s=1}^{m} F_s \log r_s, \\ Q_n &= 0 \;(n = 2, 3, \ldots), \\ Q_{-n} &= \frac{c_2^2}{\kappa} \sum_{s=1}^{m} F_s \left(\frac{c_2^2}{z_s}\right)^n \left[1 - \frac{1}{n} - \frac{r_s^2}{c_2^2} + \frac{\kappa^2}{n\,(1+n)}\right] \;(n = 1, 2, \ldots), \end{aligned}\right\} \tag{6.14b}$$

and hence

$$\left.\begin{aligned} \phi_0(z) &= -\frac{1}{\kappa} \sum_{s=1}^{m} F_s Z_s \log\left(1 - \frac{c_2^2}{z\bar{z}_s}\right) + C_1, \\ \psi_0(z) &= \frac{1}{\kappa z} \sum_{s=1}^{m} F_s \left\{\left((1-\kappa^2)c_2^2 + \kappa^2 z\bar{z}_s\right) \log\left(1 - \frac{c_2^2}{z\bar{z}_s}\right) + \frac{c_2^2 - r_s^2}{z\bar{z}_s - c_2^2} c_2^2 - \right. \\ &\qquad \left. - \kappa\,(1+\kappa)\,c_2^2 \log r_s \right\}. \end{aligned}\right\} \tag{6.15}$$

The expressions (6.15) are in agreement with those found after putting $P_0 = 0$ in equations (2.28) and (2.29), p. 748 of BASSALI (1957c) when it is remarked that only the real parts of the coefficients of ζ^{-1} and $\log \zeta$ in the expansions of $\Psi_0(\zeta)$ and $X_0(\zeta)$ $(\zeta = z/c_2)$ should be taken.

The foregoing results will now be applied to the transverse flexure of a circular annulus under two special distributions of normal forces in equilibrium.

7. Circular Annulus Under Four Forces at the Ends of Two Perpendicular Diameters of a Concentric Circle

Let us consider the case of a circular annular plate of outer radius c_1 and inner radius c_2 when the plate is acted upon by the four forces

$$\left.\begin{aligned} F_1 &= F \text{ at } z_1 = c, \quad F_2 = -F \text{ at } z_2 = ic, \\ F_3 &= F \text{ at } z_3 = -c, \quad F_4 = -F \text{ at } z_4 = -ic. \end{aligned}\right\} \tag{7.1}$$

Substituting these values into (6.7) yields

$$\left.\begin{aligned} U_n' &= 4F\left(\frac{c_1^2}{n} - \frac{c^2}{1+n}\right)c^n, \quad U_n'' = 4\kappa c_2^2 F \frac{(c_2^2/c)^n}{n\,(1+n)}, \\ V_n' &= 4\kappa c_1^2 F \frac{(c/c_1^2)^n}{n\,(1-n)}, \quad V_n'' = 4F\left(\frac{c_2^2}{n} + \frac{c^2}{1-n}\right)c^{-n} \end{aligned}\right\} \tag{7.2}$$

for $n = 2, 6, 10, \ldots$ and zero otherwise. From (7.1), (6.8) and (6.9) it follows that

$$P_0 = Q_0 = P_1 = Q_{-1} = 0. \tag{7.3}$$

Introducing (7.2) in (3.16) and inserting the resulting expressions together with (7.1) and (7.3) in (6.11) lead to

$$\frac{2\pi D}{Fc^2} w = \sum_{2,\,6,\,10,\,\ldots} T_n \left[A_n \rho^{2+n} + B_n \rho^{2-n} + C_n \rho^n + D_n \rho^{-n}\right] \cos n\theta + \frac{1}{4c^2}\left[|z-c|^2 \log|z-c| + \right.$$
$$\left. + |z+c|^2 \log|z+c| - |z-ic|^2 \log|z-ic| - |z+ic|^2 \log|z+ic|\right], \tag{7.4}$$

where $\rho = r/c$, T_n is given by (4.5a), the deflexion is taken as zero along $\theta = \pm \pi/4$ and

$$
\left.
\begin{aligned}
A_n &= \kappa(\delta^{-2}-\delta^{-2n})\left\{\left(\frac{1}{n}-\frac{{\delta_1}^2}{n+1}\right){\delta_1}^{2n}-\frac{\kappa\,\delta^{2n+2}}{n(n+1)}\right\}+\\
&\qquad+(1-\delta^2)\left\{{\delta_2}^2-1+\frac{1-\kappa\,\delta^{-2}\,{\delta_1}^{2n}}{n}\right\},\\
B_n &= \kappa(\delta^{-2}-\delta^{2n})\left\{\left(\frac{{\delta_1}^2}{n-1}-\frac{\delta^2}{n}\right){\delta_1}^{-2n}-\frac{\kappa}{n(n-1)}\right\}+\\
&\qquad+(1-\delta^{-2})\left\{1-{\delta_1}^2+\frac{1-\kappa\delta^2\,{\delta_2}^{-2n}}{n}\right\},\\
C_n &= \frac{1}{n}\left[\frac{\kappa^2}{n}(\delta^{2n}-\delta^{-2})\left\{\frac{n-\kappa{\delta_2}^{2n-2}}{n-1}-{\delta_2}^{-2}\right\}-(n+1)(1-\delta^2)\left\{\delta^{-2}-{\delta_1}^{-2}+\right.\right.\\
&\qquad\left.+\frac{{\delta_1}^{-2}}{n}(1-\kappa{\delta_1}^{2n})\right\}-\kappa({\delta_1}^{2n}-{\delta_2}^{2n})\left\{{\delta_1}^{-2}-1+\frac{{\delta_1}^{-2}-\kappa{\delta_2}^{-2n-2}}{n}\right\}\Bigg],\\
D_n &= \frac{1}{n}\left[\frac{\kappa^2}{n}(\delta^2-\delta^{2n})\left\{\frac{n+\kappa{\delta_1}^{-2n-2}}{n+1}-{\delta_1}^{-2}\right\}-(n-1)(1-\delta^2)\left\{1-{\delta_1}^{-2}+\right.\right.\\
&\qquad\left.\left.+\frac{{\delta_1}^{-2}}{n}(\kappa{\delta_2}^{-2n}-1)\right\}-\kappa({\delta_1}^{-2n}-{\delta_2}^{-2n})\left\{1-{\delta_2}^{-2}+\frac{{\delta_2}^{-2}-\kappa{\delta_1}^{2n-2}}{n}\right\}\right].
\end{aligned}
\right\}
\tag{7.5}
$$

It can be seen that (7.4) represents the deflexion of a plate having the form of the quadrant of a circular ring bounded by the two radial edges $\theta = \pm\,\pi/4$ when the plate is free along the circular edges, simply supported along the straight edges and is singularly loaded by an isolated force F on the axis of symmetry $\theta = 0$. The expression involving the logarithmic terms in (7.4) has the expansions

$$
\sum_{2,\,6,\,10,\,\ldots}\frac{\rho^n}{n}\left(\frac{1}{n-1}-\frac{\rho^2}{n+1}\right)\cos n\,\theta \quad \text{for } \rho < 1, \tag{7.6a}
$$

and

$$
\sum_{2,\,6,\,10,\,\ldots}\frac{\rho^{-n}}{n}\left(\frac{\rho^2}{n-1}-\frac{1}{n+1}\right)\cos n\,\theta \quad \text{for } \rho > 1. \tag{7.6b}
$$

Replacing the logarithmic terms in (7.4) by (7.6a) and then putting $\delta_1 = 1$, $\delta_2 = \delta^{-1}$ we obtain after simplification the following solution for a circular ring plate under four concentrated forces at the ends of two perpendicular diameter of the outer edge:

$$
\begin{aligned}
w = \frac{2F{c_1}^2}{\pi\sigma D}\sum_{2,\,6,\,10,\,\ldots}\frac{T_n}{n}\cos n\,\theta\,\Bigg[&\left\{(n+1)(\delta^2-1)+\kappa(\delta^{-2n}-1)+\frac{\kappa^2}{n-1}(\delta^2-\delta^{-2n})\right\}\frac{\rho^n}{n}+\\
&+\left\{(n-1)(1-\delta^2)+\kappa(\delta^{2n}-1)+\frac{\kappa^2}{n+1}(\delta^{2n}-\delta^2)\right\}\frac{\rho^{-n}}{n}+\\
&+\left\{\delta^{-2}-1+\frac{\kappa}{n+1}(\delta^{-2}-\delta^{-2n})\right\}\rho^{2+n}+\\
&+\left\{1-\delta^{-2}+\frac{\kappa}{n-1}(\delta^{-2}-\delta^{2n})\right\}\rho^{2-n}\Bigg] \quad (\sigma = 1-\nu).
\end{aligned}
\tag{7.7}
$$

Letting δ tend to zero in (7.7) and substituting for σ and κ from (4.8) and (2.6), respectively, we obtain the solution

$$
w = \frac{2F{c_1}^2}{(3+\nu)\,\pi D}\sum_{2,\,6,\,10,\,\ldots}\frac{\rho^n}{n}\left[\frac{1}{n}\left(1-\frac{\kappa}{n-1}\right)-\frac{\rho^2}{n+1}\right]\cos n\,\theta \quad \left(\rho=\frac{r}{c_1}\right), \tag{7.8}
$$

which agrees with Yu's results for the same problem (Yu 1954b).

A solution similar to (7.7) can be found when the four forces are applied at the ends of two perpendicular diameters of the inner edge. This follows by substituting (7.6b) for the logarithmic terms in (7.4) and then setting $\delta_2 = 1$, $\delta_1 = \delta$.

8. Sector of a Circular Ring Simply Supported Along the Radial Edges, Free Along the Circular Edges and Loaded by an Isolated Force

We now apply the general solution established in Section 6 to the special distribution of forces defined by

$$F_s = (-1)^s F \text{ at } z_s = c\, e^{i\theta_s} \; (s = 0, 1, 2, \ldots, 2m-1), \tag{8.1}$$

where m is an integer greater than 1 and

$$\left.\begin{aligned} \theta_s &= s\,\pi/m + \theta_0 \; (s = 0, 2, \ldots, 2m-2), \\ \theta_s &= (s+1)\,\pi/m - \theta_0 \; (s = 1, 3, \ldots, 2m-1). \end{aligned}\right\} \tag{8.2}$$

Inserting (8.1) in (6.7) yields

$$\left.\begin{aligned} U_n' &= \left(\frac{c_1^2}{n} - \frac{c^2}{1+n}\right) H_n, \quad U_n'' = \frac{\kappa c_2^2 \delta_2^{-2n}}{n(1+n)} H_n, \\ V_n' &= \frac{\kappa c_1^{2-2n}}{n(1-n)} H_n, \quad V_n'' = \left(\frac{c_2^2}{n} + \frac{c^2}{1-n}\right) c^{-2n} H_n, \end{aligned}\right\} \tag{8.3}$$

where

$$H_n = \sum_{s=0}^{2m-1} F_s z_s^n. \tag{8.4a}$$

It can be shown that

$$\left.\begin{aligned} &H_n = mF(z_0^n - z_0^n) = -2imF c^n \sin n\theta_0 \text{ if } n \text{ is a multiple of } m, \\ &H_n = 0 \text{ otherwise.} \end{aligned}\right\} \tag{8.4b}$$

When the values (8.1) are substituted in (6.8) and (6.9) it is seen that

$$P_0 = Q_0 = P_1 = Q_{-1} = 0. \tag{8.5}$$

Introducing (8.3), (8.4) in (3.12) and substituting the resulting expressions together with (8.1) and (8.5) in (6.11) it follows that the equation of the deflexion surface is

$$\frac{8\pi D w}{F} = 2mc^2 \sum_{m,\,2m,\,3m,\,\ldots} T_n (A_n \rho^{2+n} + B_n \rho^{2-n} + C_n \rho^n + D_n \rho^{-n}) \sin n\theta_0 \sin n\theta + \sum_{j=0}^{2m-1} (-1)^j R_j^2 \log R_j \quad \left(\rho = \frac{r}{c}\right), \tag{8.6}$$

where T_n is defined by (4.5a) and

$$R_j = |z - z_j| = \{r^2 + r_j^2 - 2r r_j \cos(\theta - \theta_j)\}^{\frac{1}{2}}, \tag{8.7}$$

$$\left.\begin{aligned} A_n &= (1-\delta^2)\left(\delta_2^2 - 1 + \frac{1}{n}\right) + \kappa\left(\frac{\delta_1^{2n} - \delta_2^{2n}}{n} + \frac{\delta_1^2\delta_2^{2n} - \delta_2^2\delta_1^{2n}}{n+1}\right) + \\ &\quad + \frac{\kappa^2(\delta^2 - \delta^{2n})}{n(n+1)}, \\ B_n &= (1-\delta^{-2})\left(1 - \delta_1^2 + \frac{1}{n}\right) + \kappa\left(\frac{\delta_2^{-2n} - \delta_1^{-2n}}{n} + \frac{\delta_2^2\delta_1^{-2n} - \delta_1^2\delta_2^{-2n}}{n-1}\right) + \\ &\quad + \frac{\kappa^2(\delta^{2n} - \delta^{-2})}{n(n-1)}, \end{aligned}\right\} \tag{8.8}$$

$$C_n = \left(1 + \frac{\kappa^2 - 1}{n^2}\right)\left\{(\delta^{-2} - 1)\left(\delta_2^{-2} - \frac{n}{n-1}\right) + \frac{\kappa\,(\delta_1^{-2}\,\delta_2^{2n} - \delta_2^{-2}\,\delta_1^{2n})}{n-1}\right\} -$$

$$- \frac{\kappa}{n}(1 - \delta^{2n})\left(\delta_2^{2n} + \frac{\kappa}{n-1}\right),$$

$$D_n = \left(1 + \frac{\kappa^2 - 1}{n^2}\right)\left\{(1 - \delta^2)\left(\delta_1^{-2} - \frac{n}{n+1}\right) + \frac{\kappa\,(\delta_2^{-2}\,\delta_1^{-2n} - \delta_1^{-2}\,\delta_2^{-2n})}{n+1}\right\} -$$

$$- \frac{\kappa}{n}(1 - \delta^{2n})\left(\delta_1^{-2n} - \frac{\kappa}{n+1}\right).$$

Using (8.7) it can be proved that the logarithmic terms in (8.6) have the expansions

$$\sum_{j=0}^{2m-1}(-1)^j R_j^2 \log R_j = 2mc^2 \sum_{m,\,2m,\,3m,\,\ldots} \frac{\rho^n}{n}\left(\frac{1}{n-1} - \frac{\rho^2}{n+1}\right)\sin n\,\theta_0 \sin n\,\theta \quad (\rho < 1), \tag{8.9a}$$

$$\sum_{j=0}^{2m-1}(-1)^j R_j^2 \log R_j = 2mc^2 \sum_{m,\,2m,\,3m,\,\ldots} \frac{\rho^{-n}}{n}\left(\frac{\rho^2}{n-1} - \frac{1}{n+1}\right)\sin n\,\theta_0 \sin n\,\theta \quad (\rho > 1). \tag{8.9b}$$

The solution furnished by (8.6)–(8.8) is appropriate to the case of a plate with the shape of the sector of the circular ring bounded by the radial edges $\theta = 0$ and $\theta = \pi/m$ (m an integer > 1) when the plate is simply supported along these edges, free along the circular edges and is subjected to the concentrated force F at the point $z_0 = c\,e^{i\theta_0}$. With the expansions (8.9) inserted in (8.6) it is easily checked that the obtained expression gives the appropriate solution corresponding to integral or non-integral values of $m > 1$. This follows from the fact that, whatever is the value of $m > 1$, this expression satisfies the biharmonic equation except at the load point and also satisfies the required boundary conditions along the radial and circular edges.

Problems relating to singularly loaded sectorial plates subjected to various boundary conditions along the straight and circular edges have been worked out by many investigators (Nowacki and Mossakowski 1953, Woinowsky-Kreiger 1953, Sekiya and Saito 1954, Holmyanski 1955, Bassali and Gorgui 1960).

References

Bassali, W. A.	1956	*Proc. Camb. Phil. Soc.* **52**, 734.
	1957a	*Ibid.* **53**, 248.
	1957b	*Bull. Calcutta Math. Soc.* **49**, 119.
	1957c	*Proc. Camb. Phil. Soc.* **53**, 744.
	1957d	*Ibid.* **53**, 728.
	1958a	*Bull. Calcutta Math. Soc.* **50**, 107.
	1958b	*Proc. Camb. Phil. Soc.* **54**, 265.
	1959	*Ibid.* **55**, 121.
Bassali, W. A. and Dawoud, R. H.	1956	*Proc. Camb. Phil. Soc.* **52**, 584.
Bassali, W. A. and Gorgui, M. A.	1960	*Proc. Camb. Phil. Soc.* **56**, 75.
Conway, H. D.	1948	*J. Appl. Mech.* **15**, 1.
	1958	*Ibid.* **25**, 386.
Friedmann, M. M.	1941	*Prikl. Mat. Mekh.* **5**, 93.
	1951	*Ibid.* **15**, 258.
Georgian, J. C.	1957	*J. Appl. Mech.* **24**, 306.
Goodier, J. N.	1936	*Phil. Mag.* **22**, 69.
Holgate, S.	1946	*Proc. Roy. Soc.* A **185**, 35.
Holmyanskii, M. M.	1955	*Inzh. Sborn.* **22**, 199.
Kudriavtzev, N. V.	1946	*Dokl. Akad. Nauk SSSR* **53**, 103.
Labrow, S.	1941	*Proc. Instn Mech. Engrs, Lond.* **145**, 155.

LECHNITZKY, S. G.	1938	*Prikl. Mat. Mekh.* **2**, 181.
LURIE, A. I.	1940	*Prikl. Mat. Mekh.* **4**, 93.
NOWACKI, W. and MOSSAKOWSKI, J.	1953	*Arch. Mech. Stos.* **5**, 237.
	1953	*Bull. Polsk. Akad. Nauk*, Otd. IV **1**, (3), 99.
OLSZAK, W. and MROZ, Z.	1956	*Mém. Ass. Int. Ponts Charp.* **16**, 399.
	1957	*Arch. Mech. Stos.* **9**, 125.
POLIVKA, J. J.	1947	*J. Appl. Mech.* **14**, 164.
REISSNER, H.	1929	*Ingen.-Arch.* **1**, 72.
SAITO, A.	1957	*Proc. Jap. Nat. Congr. Appl. Mech.* **7**, 99.
SEKITA, T. and SAITO, A.	1954	*Proc. Jap. Nat. Congr. Appl. Mech.* **4**, 195.
SEKITA, T., SAITO, A. and YAMADA, S.	1952	*Proc. Jap. Nat. Congr. Appl. Mech.* **2**, 113.
SEKIYA, T. and WADA, Y.	1956	*Proc. Jap. Nat. Congr. Appl. Mech.* **6**, 145.
SYMONDS, P. S.	1946	*J. Appl. Mech.* **13**, 181.
TRUMPLER, W. E.	1943	*Trans. Amer. Soc. Mech. Engrs.* **65**, 173.
WAHL, A. M. and LOBO, G.	1930	*Trans. Amer. Soc. Mech. Engrs.* **52**, 29.
WOINOWSKY-KREIGER, S.	1953	*J. Appl. Mech.* **20**, 77.
YU, Y. Y.	1954a	*Proc. U.S. Nat. Congr. Appl. Mech.* **2**, 381.
	1954b	*J. Appl. Mech.* **21**, 129.

J. Mech. Phys. Solids, 1960, Vol. 8, pp. 141 to 146. Pergamon Press Ltd., London. Printed in Great Britain

PLASTIC FLEXURE AND TORSION

By E. O. Imegwu
Department of Civil and Mechanical Engineering, University of St. Andrews

(*Received 2nd February*, 1960)

Summary

The paper deals with the plastic flexure and torsion of prismatic beams loaded by terminal bending and twisting moments which, acting together, cause full plastic flow. The material is assumed to behave according to the Tresca-Lévy-Mises hypotheses, and in nonhardening and rigid plastic.

The results were obtained by numerical solution of the second order non-linear differential equation derived by Handelman for a Lévy-Mises material, and the beam sections investigated were circular, square and triangular. The relationships obtained were found to give points lying virtually on a single interaction curve plotted with non-dimensional coordinates. The results are consistent with the two cases considered by Steele, who first reported a numerical solution for a square section.

The interaction curve obtained is compared with the lower bound curve given by Hill and Siebel.

1. Introduction

A straight prismatic solid beam of length L, with at least one axis of symmetry, is loaded from a stress-free state by terminal bending moment M about the axis of symmetry Oy and a terminal twisting moment T. The axis Ox is chosen arbitrarily in this instance to pass through the centroid of area of cross-section. Oz is parallel to the generators of the cylinder, and $z = 0$, $z = L$ are the end cross-sections. The material of the beam is assumed to be rigid–plastic and nonhardening. In consequence, no deformation takes place for any combination of M and T which cannot cause the yield of the whole cross-section. At this critical combination, plastic deformation starts and continues indefinitely without any further change in M or T (if changes in geometry were disregarded).

The differential equation was originally derived by Handelman (1944). A similar equation was obtained by Hill (1948) using his method of maximum plastic work. A solution of the differential equation has been attempted by Steele (1954) who considered a square cross-section and obtained two critical combinations of M and T.

Approximate solutions in the form of lower and upper bound curves have been proposed by Hill and Siebel (1953), Steele (1954) and Gaydon and Nuttall (1957).

In the present paper Handelman's equation is solved numerically, on lines similar to those adopted by Steele but for a larger number of values of the parameter $\dot{\beta}/\dot{\alpha}$, ratio of rate of twist to rate of curvature, and for several cross sections circular, square and triangular. The curve obtained is compared with the lower bound of Hill and Siebel which appears to be the best simple approximation to

the true curve. It is noted that the curve is the same for a Tresca or a Mises material (with identical yield function and plastic potential).

As far as the author is aware, the true curve, even for one cross-sectional shape, has not yet been published.

2. HANDELMAN'S EQUATION

On the lines adopted by HILL (1948) we may write the expressions for the velocities as follows:

$$\left.\begin{aligned} u_1 &= \tfrac{1}{2}\,\dot{\alpha}\,xy + \dot{\beta}zy, \\ u_2 &= \tfrac{1}{4}\,\dot{\alpha}\,(2z^2 - x^2 + y^2) - \dot{\beta}\,zx, \\ u_3 &= -\,\dot{\alpha}\,zy + \dot{\psi}\,(x, y, \beta). \end{aligned}\right\} \tag{1}$$

The stress function $\phi\,(x, y)$ is chosen such that the only stresses different from zero are

$$\left.\begin{aligned} \sigma_{zx} &= k\,\frac{\partial\phi}{\partial y} = k\,\phi_y, \quad \sigma_{zy} = -\,k\,\frac{\partial\phi}{\partial x} = -\,k\,\phi_x, \\ \sigma_{zz} &= -\,\lambda k\,\sqrt{(1 - \phi_x{}^2 - \phi_y{}^2)}, \end{aligned}\right\} \tag{2}$$

where $\lambda = \sqrt{3}$ in von Mises' yield criterion and $\lambda = 2$ in Tresca's; k is the yield stress in pure shear. The radical in (2) is chosen to have the same sign as y. Since the longitudinal surface of the beam is free from loading the boundary condition on the stress function is $\phi =$ constant on the section contour $= 0$ say. The rate of work of external forces per unit length of beam is

$$\dot{W} = \iint (\sigma_{zx}\,u_1 + \sigma_{zy}\,u_2 + \sigma_{zz}\,u_3)\,dx\,dy, \tag{3}$$

where the integration is carried out over the end faces. Substituting from (1) and (2) into (3) and simplifying, we have

$$\frac{\dot{W}}{kL} = \iint \{(2\dot{\beta}\phi + \dot{\alpha}\lambda y\,\sqrt{(1 - \phi_x{}^2 - \phi_y{}^2)}\}\,dx\,dy. \tag{4}$$

HILL's principle of maximum plastic work requires that the actual distribution of ϕ is the one that makes $\dot{W}$ a maximum. Applying the Euler-Lagrange formula of the calculus of variations to (4) gives

$$\frac{\partial}{\partial x}\left[\frac{y\phi_x}{\sqrt{(1 - \phi_x{}^2 - \phi_y{}^2)}}\right] + \frac{\partial}{\partial y}\left[\frac{y\phi_y}{\sqrt{(1 - \phi_x{}^2 - \phi_y{}^2)}}\right] + \mu = 0, \text{ where } \mu = \frac{2\dot{\beta}}{\lambda\dot{\alpha}}. \tag{5}$$

Equation (5) together with the boundary condition $\phi_s = 0$ is solved below for several cross-sections. If σ_{zx} and σ_{zy} vanish identically the problem is one of pure plastic bending:

$$\left.\begin{aligned} &T = 0, \quad \sigma_{zz} = \pm\,\lambda k, \quad \phi = 0, \\ &M = M_0 = -\iint y\,\sigma_{zz}\,dx\,dy = \lambda k A_0, \text{ say.} \end{aligned}\right\} \tag{6}$$

If, on the other hand, σ_{zz} vanishes identically the problem is one of pure plastic torsion:

$$\left.\begin{aligned} &M = 0, \quad \phi_x^2 + \phi_y^2 = 1, \\ &T = T_0 = \iint (x\,\sigma_{zy} - y\,\sigma_{zx})\,dx\,dy = 2k \iint \phi\,dx\,dy = 2kB_0. \end{aligned}\right\} \quad (7)$$

In (6) and (7) A_0 and B_0 are functions of the cross-sectional dimensions of the beam.

When both M and T are non-zero a point on the interaction curve may be represented by (m, t), where

$$\left.\begin{aligned} m &= M/M_0 = -\iint y\sqrt{(1 - \phi_x^2 - \phi_y^2)}\,dx\,dy/A_0, \\ t &= T/T_0 = \iint \phi\,dx\,dy/B_0. \end{aligned}\right\} \quad (8)$$

3. Numerical Solution

Before solving (5) numerically it is essential to write it in a non-dimensional form. The non-dimensional form is identical to (5). Consequently, (5) is hereafter considered to be non-dimensional.

It is observed that the parameter μ is the same using either the yield function and flow rule of von Mises or those of Tresca and the corresponding flow rule provided $\dot{\beta}/\dot{\alpha}$ used in the two cases is in the ratio $1 : \sqrt{(2/3)}$. It is evident that (m, t) of (8) or the interaction curve is the same in each case. The solution which follows is performed for $\lambda = \sqrt{3}$.

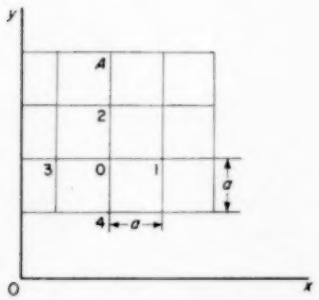

Fig. 1. Square mesh.

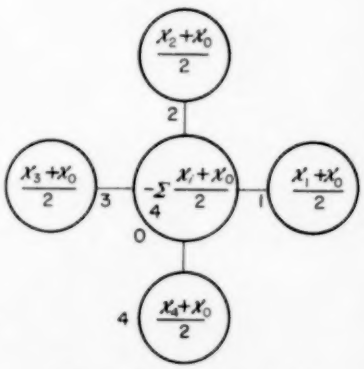

Fig. 2. Relaxation pattern.

(a) *Nature of the stress-function*

The function $\phi(x, y)$ must be symmetrical about an axis of symmetry of the cross section. In the neutral plane, $y = 0$, the direct stress σ_{zz} vanishes. Equation (5) cannot then apply. The normal gradient then has the same value, unity, as in pure torsion. In the numerical solution which follows the ϕ-surface is assumed, in the manner of Steele (1954), to be smooth on the neutral axis. Equation (5)

(3)

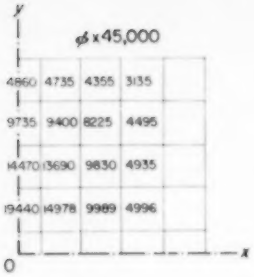

(4)

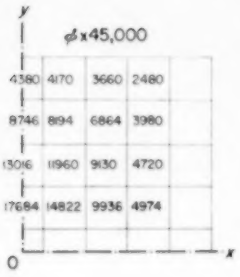

(5)

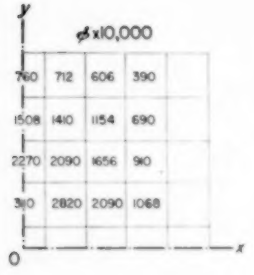

(6)

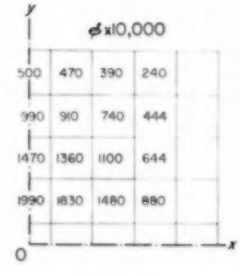

(7)

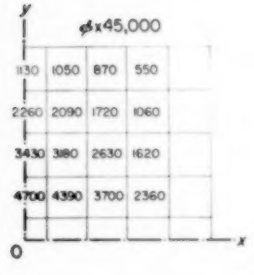

(8)

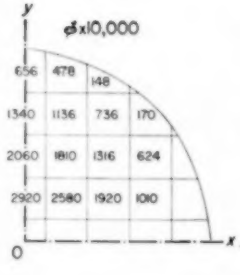

(9)

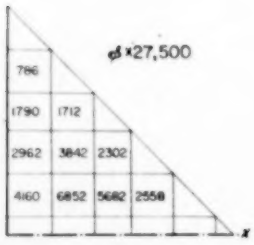

(10)

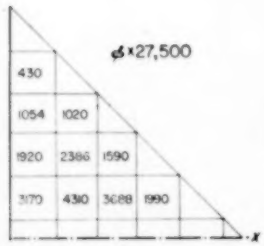

FIG. 3. Square, $\dot{\beta}/\dot{\alpha} = 4$. $(m, t) \equiv (0{\cdot}4510, 0{\cdot}9473)$.
FIG. 4. Square, $\dot{\beta}/\dot{\alpha} = 2$. $(m, t) \equiv (0{\cdot}6176, 0{\cdot}8605)$.
FIG. 5. Square, $\dot{\beta}/\dot{\alpha} = 1$. $(m, t) \equiv (0{\cdot}7887, 0{\cdot}6971)$.
FIG. 6. Square, $\dot{\beta}/\dot{\alpha} = \frac{1}{2}$. $(m, t) \equiv (0{\cdot}9184, 0{\cdot}4503)$.
FIG. 7. Square, $\dot{\beta}/\dot{\alpha} = \frac{1}{4}$. $(m, t) \equiv (0{\cdot}9835, 0{\cdot}2449)$.
FIG. 8. Circle, $\dot{\beta}/\dot{\alpha} = 1$. $(m, t) \equiv (0{\cdot}7914, 0{\cdot}6937)$.
FIG. 9. Triangle, $\dot{\beta}/\dot{\alpha} = \frac{1}{2}$. $(m, t) \equiv (0{\cdot}9602, 0{\cdot}3380)$.
FIG. 10. Triangle, $\dot{\beta}/\dot{\alpha} = 1$. $(m, t) \equiv (0{\cdot}8917, 0{\cdot}5130)$.

is assumed to apply but no mesh points are chosen to lie on the neutral axis. By repeating a solution using a finer mesh for a square section STEELE showed in the same paper that any error in (m, t) due to these assumptions is less than one half of one per cent, although errors in ϕ, σ_{zz}, σ_{zx} and σ_{zy} may be larger.

(b) *Finite difference method*

In solving (5) numerically the relaxation method (GREEN and SOUTHWELL 1944, SOUTHWELL 1946) was adopted. With a three-point formula of differentiation the equation may be written, with the notation of Fig. 1,

$$\left.\begin{aligned} &\tfrac{1}{2}\sum_4 \phi_i\,(x_i + x_0) - \tfrac{1}{2}\,\phi_0 \sum_4 (x_i + x_0) + \frac{2}{\sqrt{3}}\frac{\dot\beta}{\dot\alpha}\,a^2 = R_0, \\ &(\partial\phi/\partial y)_0 = (\phi_2 - \phi_4)/2a, \quad (\partial\phi/\partial y)_A = (\phi_0 - 4\,\phi_2 + 3\,\phi_A)/2a, \\ &x = y/\sqrt{(1 - \phi_x{}^2 - \phi_y{}^2)}, \end{aligned}\right\} \tag{9}$$

where $\phi_s = 0$ on the boundary; thus $\phi_A = 0$. The second and third of (9) are typical gradients for evaluating x; the third applies at a boundary point such as A. The correct solution of the finite difference equation is the distribution of ϕ which makes R, the residual, vanish at all internal points. The corresponding relaxation pattern is shown in Fig. 2. In most of the solutions the first of (9) was multiplied by $10{,}000/2a$ so that the second and third reduce to subtraction and decimal multiplication.

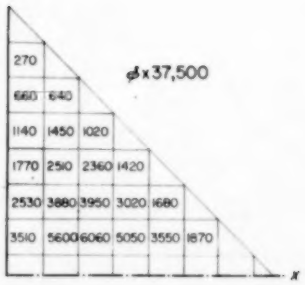

FIG. 11. Triangle, $\dot\beta/\dot\alpha = \frac{1}{4}$. $(m, t) = (0{\cdot}9627, 0{\cdot}3571)$.

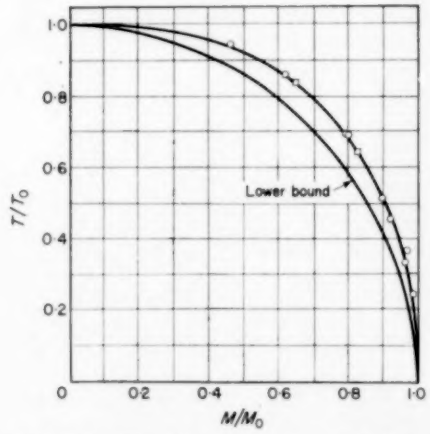

FIG. 12. The interaction curve and the lower bound curve. Points □ obtained by STEELE.

In solving the problem for the square section each side of the square was divided into nine, or $a = \frac{1}{9}$. Solutions were obtained for $\dot\beta/\dot\alpha = 4, 2, 1, \frac{1}{2}, \frac{1}{4}$. For the circle, whose boundary cut the mesh irregularly, each diameter was divided into nine, or $a = \frac{1}{9}$. A solution was obtained for $\dot\beta/\dot\alpha = 1$. For the right-angled isosceles triangle of unit height the neutral axis was chosen to bisect the right angle. Solutions were obtained for $\dot\beta/\dot\alpha = 1, \frac{1}{2}$, for the case in which the diagonal was divided

into eleven, or $a = \frac{2}{11}$. A solution with a finer mesh, $a = \frac{2}{15}$, was carried out for $\dot{\beta}/\dot{\alpha} = \frac{1}{4}$.

In each case $R \times 10{,}000$ was reduced below ± 10. At some isolated points, however, the residuals were higher owing to the fact that a change in $\phi \times 10{,}000$ of ± 1 at such points produced a residual of opposite sign, not necessarily small in magnitude. The solutions are shown in Figs. 3–11.

The integrals for m and t in equation (8) were obtained by the application of Simpson's $\frac{1}{3}$-rule in two dimensions. The resulting interaction curve is shown in Fig. 12.

CONCLUSION

The interaction curve obtained in this paper for the cross-sections considered shows a unique characteristic in that the curve seems to be virtually independent of the shape of the cross-section of the beam. This resembles the insensitivity of the interaction curve for combined bending and axial force as noted by ONAT and PRAGER (1952).

The interaction curve cuts the lower bound curve of HILL and SIEBEL at $M/M_0 = 0$ and at $T/T_0 = 0$ as shown in Fig. 12, and the difference between the two curves, measured along a radius vector, has a maximum less than 6 per cent.

ACKNOWLEDGMENT

The author is indebted to Professor JOHN DICK and Dr. N. JACKSON, both of the Department of Civil and Mechanical Engineering, University of St. Andrews, Queen's College, Dundee, for their generous advice in the writing of this paper.

REFERENCES

GAYDON, F. A. and NUTTALL, H. 1957 *J. Mech. Phys. Solids* **6**, 17.

GREEN, J. R. and SOUTHWELL, R. V. 1944 *Phil. Trans. Roy. Soc.* A **239**, 367.

HANDELMAN, G. H. 1944 *Quart. Appl. Math.* **1**, 351.

HILL, R. 1948 *Quart. J. Mech. Appl. Math.* **1**, 18.

HILL, R. and SIEBEL, M. P. L. 1953 *J. Mech. Phys. Solids* **1**, 207.

ONAT, E. T. and PRAGER, W. 1952 *J. Mech. Phys. Solids* **1**, 77.

SOUTHWELL, R. V. 1946 *Relaxation Methods in Theoretical Physics*, p. 144 (Clarendon Press).

STEELE, M. C. 1954 *J. Mech. Phys. Solids* **3**, 156.

BOOK REVIEWS

C. E. Pearson: Theoretical Elasticity. (Harvard Monographs in Applied Science, No. 6.) Harvard University Press, 1959. 218 pp., $6.

This book is excellent for those already acquainted with elasticity theory but is a rather difficult introduction to the subject. It provides a concise account of the present state of the general theory and touches upon most of its aspects, with the obvious exception of Saint-Venant's Principle. The author has made a valuable contribution to the literature of the field and the many suggestions scattered throughout the book will repay close reading by the active worker.

A welcome feature is the inclusion of a clear exposition of the mathematical elements required in treating the subject. The first chapters discuss vector and tensor analysis and the rotation of axes, and the later chapter on General Solutions starts with an introduction to potential theory. The remainder of the book is devoted to elasticity theory with the emphasis on results in the linear case. However, the chapter on Deformation fully treats non-linear strain, while the final chapter is concerned with non-linear stress-strain relations.

General solutions of the basic equations for a homogeneous body composed of isotropic or anisotropic material are discussed. All the classical methods are mentioned, such as those of Betti and Maxwell-Morera. Variational principles and approximation methods are treated: besides those of virtual displacement, virtual stress, and Rayleigh-Ritz, that based on the hypercircle technique is also described. The account of the latter is clear and comprehensive, unifying many of the conclusions spread through the literature and so is particularly useful. A chapter devoted almost entirely to elementary thermodynamics establishes the 'linked' thermoelastic equations. Another considers simple forms of elastic wave motion.

There are few misprints and the lay-out and printing of the book are good. One minor regret is that insufficient references are provided to original sources.

R. J. Knops

Proceedings of the 3rd U.S. National Congress of Applied Mechanics (1958) American Society of Mechanical Engineers, New York. 864 pp., $20.

This volume contains the complete text of papers presented at the Congress. There are four general lectures, three of which are concerned with solids: 'Linear Thermodynamics' by M. A. Biot, 'Theories of Creep Buckling' by N. J. Hoff, and 'Rotationally Symmetric Problems in Elastic Shells' by E. Reissner. This preponderance of solid over fluid mechanics at the Congress is to be seen also in the papers themselves. Almost all aspects of the subject are massively represented, an especial feature being the close blend of theory and experiment in many contributions. Interesting new trends and significant advances are reported over the whole range. This was beyond doubt a quite outstanding Congress.

R. Hill

Mechanical Properties of Non-metallic Brittle Materials. Edited by W. H. Walton. Butterworths, London; Inter-Science, New York, 1958. 492 pp., 90s.

This is the proceedings of a conference organized by the Mining Research Establishment of the National Coal Board in consultation with the Building Research Station, held in London in April,

1958. There are twenty-seven papers, with discussions, arranged in four sections: Strength in Compression, Tension, Bending and Shear; Elasticity and Creep; Dynamic Loading, Impact and Fragmentation; Action of Tools. Among the materials referred to are coal, carbon and graphite, rocks, ceramics, gypsum, concrete, brick and glass. The standard of the contributions is high and the book is very well illustrated and nicely produced.

R. HILL

W. PRAGER: **Introduction to Plasticity.** Addison-Wesley, Reading, Mass., 1959. 148 pp., $9.50.

THIS is a revised version of the author's *Probleme der Plastizitätstheorie* (Birkhäuser, Basel, 1955), reviewed in this Journal (1956 **4**, 206). The principal changes are the addition of numerous practice problems and more recent references. The textual changes are comparatively slight. Chapters I and II are changed only in details. In Chapter III the section on the influence of distortion in connexion with limit design has been amplified, and a new section added on the optimum weight design of plates and redundant frames. In Chapter IV some additional examples of large plastic flow are included.

This edition in English is a welcome addition to the existing introductory texts. It has been well produced, but the price of so short a book is likely to be considered high in this country.

R. HILL

Progress in Metal Physics. Vol. 7. Edited by B. CHALMERS and R. KING. Pergamon Press, London, 1958. 408 pp. 110s.

FOR THOSE familiar with previous volumes in this series it will be sufficient assurance to say that in Volume 7 the happy choice of authors and high standard of production characteristic of the series is well maintained. Each of the five review articles which comprise this volume is written by an expert directly engaged in the particular field; the presentation is such, however, that they all make their appeal both to fellow specialists and to those whose acquaintance with metal physics has not specifically included the subject of review.

H. M. ROSENBERG of the Clarendon Laboratory presents the results of many recent studies of the physical and mechanical properties of metals at low temperature and illustrates well the particular advantages of low temperature work in formulating the electronic structure of metals and the mechanism of plastic flow. A rather similar approach is taken by J. N. HOBSTETTER of Bell Telephone Laboratories who, in an article entitled 'Equilibrium, Diffusion and Imperfections in Semi-conductors,' seeks not merely to catalogue information in this field, but to bring out the wider significance of observations made on semi-conductors which contribute to the solution of problems in metal physics. Again, in a comprehensive review of the stored energy of cold work, A. L. TITCHENER and M. B. BEVER after summarizing the many measurements made of this quantity discuss how these have contributed to our understanding of such complex processes as deformation and annealing.

If a distinction between 'metal physics' and 'physical metallurgy' could be made then the remaining two articles would probably fall into the latter class. In an excellent contribution on martensitic transformations L. KAUFMAN and M. COHEN of M.I.T. present the modern view of the kinetics and thermodynamics of this intriguing mode of phase change. This is a subject in which there has been intense activity in recent years and a comprehensive account from a school which has played a leading role in the work is to be welcomed. Finally, the 'Physical Metallurgy of Titanium Alloys' is reviewed by R. I. JAFFEE of Battelle Memorial Institute. Without disputing the obvious merit of this article, the value to metal physics of what is commercially vital, but largely empirical information on certain alloys, must be very limited.

An exacting test of the value of a review series of this kind is the useful life of each volume. Judged on this basis the verdict is wholly satisfying for in the reviewer's experience even the first issue published a decade ago still does useful service, a quite remarkable achievement considering the rapidity of advancement of this branch of science. There is no reason to believe that this latest volume will have any less lasting merit and the only regret is that its price may exclude it from the personal library of many who would profit by its possession.

S. G. GLOVER

P. B. MORICE: **Linear Structural Analysis**. Thames and Hudson, London, 1959, xii + 170 pp., 35*s*.

THE SUB-TITLE to this book is 'An Introduction to the Influence Coefficient Method applied to Statically Indeterminate Structures.' This well expresses the limitations as well as the scope of the book.

The procedure followed is first to introduce sufficient cuts (or 'releases') into the structure to render it statically determinate. The influence coefficients then calculated are the flexibility coefficients relating the discontinuities at the cuts to the redundant forces which must be introduced to restore continuity after the external loads have been applied to the released structure. These flexibility coefficients are derived from the energy relations by the principle of least work, and the author enters in some detail into the numerical procedures involved. The equations establishing the continuity of the structure are then assembled, and this concludes that part of the treatise really concerned with the theory of structures. The remainder of the book describes how matrix methods may be used to solve these linear equations. There is a chapter summarizing some of the elementary properties of matrices, and another illustrating the numerical procedure for inverting a symmetrical matrix by triangular resolution. Matrix solutions are then discussed in relation to the derivation of the final stresses in the structure, the choice of release systems, the effect of choice of release system on the form of the flexibility matrix, and numerical solution by electronic digital computer.

The main defect of the book is that the treatment is too limited to give a balanced view of the general principles of linear structural analysis and the application of matrix methods. The use of the least work relations to set up the initial equations is by no means always the best procedure. The influence coefficient method is not ideally suited to machine computation, since the operator is required to carry out many processes which, using stiffness methods, are effectively carried out by the machine itself. On the other hand, the limited scope of the book does mean that a complete method of structural analysis and computation is expounded within a small compass, providing a useful introduction to matrix methods. Provided its limitations are recognized, the book can be thoroughly recommended both to advanced students and research workers in structures, and to practising structural engineers.

M. R. HORNE

Non-Homogeneity in Elasticity and Plasticity. Edited by W. OLSZAK. (Proceedings of I.U.T.A.M. Symposium, Warsaw, 1958). Pergamon Press, London, 1959, 528 pp., £5.

FIFTY-FIVE papers submitted to the Symposium are reproduced here in full, the languages being English and French. The papers are mostly grouped under five headings: Elasticity, Plasticity, Rheology, Wave Propagation, Statistical and Micro Non-homogeneity. The main theme is the formulation of field equations and methods of solution in the mechanics of homogeneous anisotropic continua or non-homogeneous isotropic continua, principally elastic, rigid/plastic, elastic/plastic, and visco-elastic solids.

The standard and interest of the contributions varies enormously. Among the most valuable are articles by OLSZAK and URBANOWSKI, reviewing mainly Polish work on plastic solids; HASHIN, on the effective moduli of a two-phase, elastic medium; BIOT, on stability in visco-elastic layered media; and SHERMAN, on an integral equation technique for solving plane strain problems in inhomogeneous elastic media.

Much recent work in Poland in solid mechanics has been concerned with the title subject of this Symposium. Unfortunately, certain Polish writers have tended to claim new results consisting merely of automatic 'generalizations' of existing theorems due to Western writers, under the erroneous impression that these had previously been proved only for isotropic homogeneous materials (often despite explicit contrary statements in the original proofs). This regrettable tendency appears also in the contribution by OLSZAK and PERZYNA on variational methods. They give, in essentially the original form, the systematic method of HILL (this Journal, 1956, **5**, pp. 66–74) and associated so-called 'convexity inequalities,' stating these to have been originally formulated only for isotropic materials; in fact, no such restriction was made. Moreover, OLSZAK and PERZYNA claim to have generalized the original formalism to apply to materials such that the stress-*rate* is derivable from a potential function of strain-rate; in fact, this also appears in HILL's paper (p. 69, especially equations (11) and (12)), together with examples for a conventional elastic/plastic solid and visco-elastic solids of Maxwell and Voigt types. The initial choice of stress and strain-rate as the related variables in the formal analysis was, of course, purely arbitrary, as the original paper made abundantly clear (or so one would think).

R. HILL

Proceedings of the Fourth Midwestern Conference on Solid Mechanics. Texas, 1959 (University of Texas), 530 pp., $12.50.

A CONSIDERABLE part of this volume is devoted to work on shells and plates but other topics which receive attention are dislocation theory, wave propagation and thermoelastic problems. The paper by DONNELL gives a summary of shell theory (including plates and beams as special cases) using the Kirchhoff–Love theory in which transverse shear strains and transverse normal strains are neglected. In dealing with compressor blade vibrations LANE and SLUTSKY formulate the shell theory in curvilinear coordinates appropriate to the blade middle surface and by using an energy method obtain an eigenvalue problem; the resulting equations are programmed for computing. Deflections of thin conical shells under asymmetrical loading are considered by THURSTON and SCHILE. In the former paper the equations of motion are derived by an energy method using Langhaar's theory and are solved numerically for particular loadings; in the latter paper Novozilov's equations for a thin shell of revolution are used and a series solution assumed. Work on thermal effects includes an analysis of curved plates by CHEN and FOSS who consider large deflections and derive approximate solutions of particular problems by using Reissner's variational method; these solutions are compared with results obtained in other ways. ANG and WILLIAMS examine the wave patterns due to the propagation of a plane dislocation in an infinite medium. From a solution of the elastic wave equations by transform methods, it emerges that for subsonic velocities two cylindrical waves are propagated from the origin, while in the transonic and supersonic cases there are, in addition, one and two shock waves respectively.

J. E. ADKINS

BOOKS RECEIVED

K. Lark-Horovitz and V. A. Johnson: Solid State Physics, Pt. A, Vol. 6. Academic Press, 1959, xvi + 446 pp., $11.80.

K. Lark-Horovitz and V. A. Johnson: Solid State Physics, Pt. B, Vol. 6. Academic Press, 1959, xiv + 416 pp., $11.00.

K. Swainger: Analysis of Deformation, Vol. 4. Waves and Vibrations. Chapman & Hall, 1959, 370 pp., 75s.

J. Mech. Phys. Solids, 1960, Vol. 8, pp. 153 to 163. Pergamon Press Ltd., London. Printed in Great Britain

PLASTIC INTERACTION CURVES FOR ANNULAR PLATES IN TENSION AND BENDING*

By P. G. Hodge, Jr. and R. Sankaranarayanan†
Illinois Institute of Technology, Chicago

(*Received 5th March*, 1960)

Summary

An annular plate made of a perfectly plastic material is subjected to a uniform normal load over its surface and a constant tensile load around its outer edge. Close bounds on the interaction curve are found for all values of the inner radius under various support conditions at the inner edge.

1. Introduction

There are many practical applications where it is necessary to have an aperture or cut-out in a thin-skinned structure. In general such a cut-out will weaken the structure; obviously it is desirable to know the amount of this weakening.

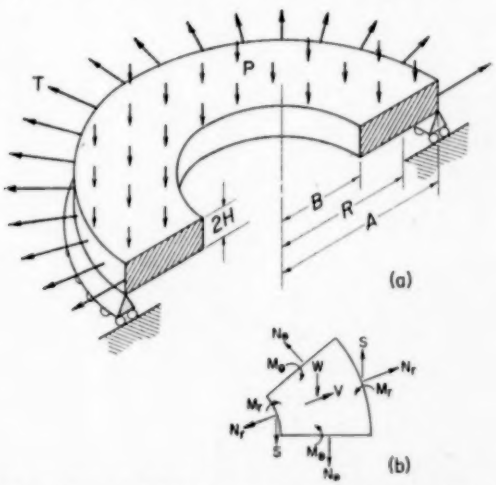

Fig. 1. Definition of problem. (a) Loaded plate, showing dimensions. (b) Plate element, showing stress resultants and velocities.

As a relatively simple problem of this type, we consider a circular plate with a concentric cut-out as shown in Fig. 1a. The plate is subjected to a uniform

*This investigation was sponsored by the Office of Naval Research.
†Now at the Polytechnic Institute of Brooklyn.

normal pressure P and to a uniform tension T around its circumference. The outer edge of the plate is simply supported.

The support conditions at the inner edge of the plate may be designed in several different ways. Basically, the cut-out may be directly connected to the frame structure with the plate attached to a gasket as shown in Fig. 2a, or the

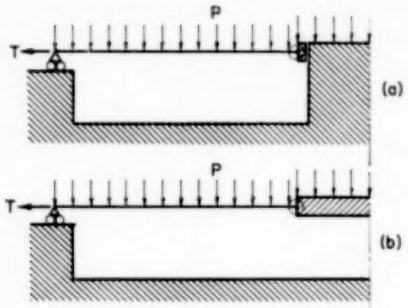

FIG. 2. Basic cut-out designs. (a) Pressure over cut-out supported by frame. (b) Pressure over cut-out supported by plate.

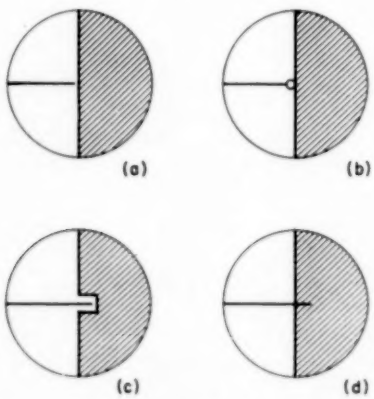

FIG. 3. Details of cut-out support. (a) Free to bend or expand. (b) Free to bend but not expand. (c) Free to expand but not bend. (d) Constrained against bending or expanding.

plate may be required to support the cut-out plug as shown in Fig. 2b*. Further, the method of attachment of the plate to the gasket or cut-out plug may independently restrain or permit slope changes or radial displacements as shown in Fig. 3. All eight of these possibilities will be considered in the following.

We are interested in the maximum load-carrying capacity of the plate acted upon by both normal and edge loads. As a measure of this capacity, we will take the yield-point load. This load is precisely defined for any given ratio of P/T as that magnitude for which an ideal rigid/plastic structure can undergo a small quasi-static deformation while remaining in equilibrium. It should be noted that

*A further possibility, that the cut-out is supported by the frame with the plate attached directly to the cut-out, will not be considered. We note, however, that such a design strengthens rather than weakens the plate, at least against bending.

the real plate may undergo elastic and elastic/plastic deformations for loads less than the yield point load. These deformations, as well as deformations at the yield point load, will change the plate geometry which will again affect the carrying capacity. However, despite these deviations from reality, the yield-point load should provide a meaningful estimate to the true carrying capacity.

The mathematical problem to be considered, then involves a plate of uniform thickness whose material is rigid/plastic and satisfies the Tresca yield condition of maximum shearing stress with its associated plastic potential flow law. In the next Section we state the basic equations of this problem in terms of appropriate generalized stresses. We also briefly review the theorems of limit analysis which will be used extensively in the treatment of the problem.

Sections 3 and 4 are concerned with the detailed analysis of one of the eight possible boundary value problems described above. In particular, Section 3 gives the elementary solutions for pure bending and for pure tension. Section 4 is then concerned with the establishment of close bounds for the interaction curve of combined bending and tension.

The other possible support conditions are all considered in Section 5 and general formulas are obtained for the interaction curve bounds. The results are summarized in tabular form and typical cases are shown graphically.

2. Basic Equations

The plastic problem is conveniently expressed in terms of a four-dimensional reduced stress vector

$$\mathbf{Q} = (n_\theta,\ n_r,\ m_\theta,\ m_r) \tag{1}$$

and reduced strain-rate vector

$$\mathbf{q} = (\lambda_\theta,\ \lambda_r,\ \kappa_\theta,\ \kappa_r). \tag{2}$$

Here the subscripts θ and r refer to the tangential and radial directions, respectively, and dimensionless quantities are defined by

$$\begin{aligned} r &= R/A, & b &= B/A, & h &= H/A, & v &= V/A, \\ w &= W/H, & n &= N/N_0, & m &= M/M_0, & s &= S/N_0, \\ N_0 &= 2\sigma_0 H, & M_0 &= \sigma_0 H^2, & t &= T/N_0, & p &= PA^2/6M_0, \\ & & \lambda &= \Lambda, & \kappa &= HK/2. \end{aligned} \tag{3}$$

In (3) σ_0 denotes the yield stress of the material ; plate dimensions, stress resultants, and velocities are all defined in Fig. 1 ; Λ and K are the extensions and curvatures, respectively, of the middle surface of the plate.

In terms of these variables the equilibrium equations are

$$(rn_r)' - n_\theta = 0, \tag{4a}$$

$$(rs)' - 3phr = 0, \tag{4b}$$

$$(rm_r)' - m_\theta = -(2/h)\, rs, \tag{4c}$$

where primes denote differentiation with respect to r. In terms of velocities the strain-rate vector is

$$\mathbf{q} = (v/r,\ v',\ -h^2 w'/2r,\ -h^2 w''/2). \tag{5}$$

Since both moments and forces are present, the problem must be treated as a special case of a rotationally symmetric shell. The expression for the yield surface in terms of **Q** was first derived by Onat and Prager (1954): it consists of several different curved surfaces in four-dimensional stress space. Since we will not need the entire surface, we list only the portions relevant to the present problem. These are the cylindrical surfaces

$$n_\theta^2 + m_\theta = 1, \tag{6a}$$

$$n_r^2 + m_r = 1, \tag{6b}$$

$$n_r^2 - m_r = 1; \tag{6c}$$

the intersection of the yield surface with the plane $m_\theta = m_r = 0$,

$$\max\left[|n_\theta|,\ |n_r|,\ |n_\theta - n_r|\right] = 1; \tag{7a}$$

and the intersection with $n_\theta = n_r = 0$,

$$\max\left[|m_\theta|,\ |m_r|,\ |m_\theta - m_r|\right] = 1. \tag{7b}$$

For part of the analysis we will also use an approximate yield surface first proposed by Hodge (1960):

$$\max\left[|n_\theta|,\ |n_r|,\ |n_\theta - n_r|,\ |m_\theta|,\ |m_r|,\ |m_\theta - m_r|\right] = 1. \tag{8}$$

The plastic potential flow rule states that the vector **q** is directed along the outward normal to the yield surface. Thus, corresponding to (6) we have

$$\mathbf{q} = \mu_1 (2n_\theta,\ 0,\ 1,\ 0), \tag{9a}$$

$$\mathbf{q} = \mu_2 (0,\ 2n_r,\ 0,\ 1), \tag{9b}$$

$$\mathbf{q} = \mu_3 (0,\ 2n_r,\ 0,\ -1), \tag{9c}$$

where the μ_i are arbitrary non-negative scalers. The flow rules for any of the linear surfaces in (7) or (8) are obvious; they will be written as required.

The outer edge of the plate is simply supported and hence

$$m_r = w = 0, \quad n_r = t, \quad \text{at} \quad r = 1. \tag{10a}$$

Boundary conditions at the inner edge depend upon the method of support. For the totally unsupported cut-out,

$$m_r = n_r = s = 0 \quad \text{at} \quad r = b. \tag{10b}$$

Boundary conditions for all possible support conditions are listed in Table 1.

A complete solution for the nonlinear problem defined above appears to be impractical. However, we may obtain reasonable bounds on the interaction curve by considering the upper and lower bound theorems of limit analysis [see, for example, Hodge (1959)]. In terms of the present problem, the upper bound theorem may be developed as follows:

Let v^* and w^* be any velocity field which satisfies the velocity boundary conditions. Compute the strain-rate vector $\mathbf{q}^*$ from (5) and compute a stress field $\mathbf{Q}^*$ from the flow law. Define the dimensionlesss internal rate of dissipation of energy by

$$d_i = \int_b^1 \mathbf{Q}^* \cdot \mathbf{q}^* \, r \, dr. \tag{11a}$$

Next, let t^+ and p^+ be the applied loads and compute the dimensionless external energy rate

$$d_e = 3p^+ h^2 \int_b^1 w^* \, r dr + bhs \, (b) \, w^* \, (b) + t^+ v^* \, (1). \tag{11b}$$

The upper bound theorem of limit analysis then states that the locus of points t^+, p^+ obtained from the relation $d_i = d_e$ is everywhere on or outside of the true interaction curve, i.e., it is an outer bound.

The lower bound theorem states that any load point t^-, p^-, for which there exists a stress state in internal and external equilibrium which nowhere violates the yield condition, is on or within the true interaction curve.

There are two useful corollaries to the lower bound theorem. The first of these states that, if a yield surface A is wholly within a yield surface B, then the interaction curve corresponding to A is an inner bound or the interaction curve for B. It has been shown by Hodge (1960) that the approximate yield surface (8) circumscribes the actual yield surface, but if the surface (8) is multiplied by $\frac{1}{2}(\sqrt{5} - 1) = 0{\cdot}618$ the resulting surface inscribes the actual one. Therefore, the interaction curve for the approximate surface can be used to obtain both inner and outer bounds for the true interaction curve.

The second corollary makes use of the fact that the yield surface is always convex to prove that the interaction curve must also be convex. Indeed, if $\mathbf{Q}_1$ and $\mathbf{Q}_2$ are the stress solutions corresponding to loads t_1, p_1 and t_2, p_2 on or within the interaction curve, then the stress solution $\lambda \, \mathbf{Q}_1 + (1 - \lambda) \, \mathbf{Q}_2$ is in equilibrium with the loads $\lambda t_1 - (1 - \lambda) \, t_2$, $\lambda \, p_1 - (1 - \lambda) \, p_2$ and nowhere violates the yield condition for all $0 > \lambda > 1$. Therefore, the straight line joining any two points of the interaction curve is on or within the interaction curve.

3. Elementary Solutions

We consider in detail the cut-out supported as in Figs. 2a and 3a under the action of tension or bending separately. Although similar problems have been treated earlier by Hodge and Prager (1951) and Hopkins and Prager (1953), we reconsider them here for the light they will throw on the more general problem.

If $p = 0$ there will obviously be no bending moments so that the problem is reduced to one in two stress dimensions n_θ and n_r. The yield curve of (7a), the equilibrium equation (4a) and the boundary conditions on n_r from (10) suffice to determine the stress solution

$$n_\theta = 1, \quad n_r = 1 - (1 - t)/r, \quad t = t_0 = 1 - b. \tag{12a}$$

The flow rule for $n_\theta = 1$ is

$$\mathbf{q}_1 = (v/r, \; v') = \mu \, (1, 0) \, ;$$

hence

$$v = C > 0 \tag{12b}$$

is the corresponding velocity solution.

If $t = 0$, then the problem is one of bending only. The yield curve of (7b), the equilibrium equations (4b and c) and the boundary conditions on m_r and s

from (10) now determine

$$m_\theta = 1, \quad m_r = 1 + 3pb^2 - pr^2 - (1 + 3pb^2 - p)/r, \tag{13a}$$

$$p = p_0 = (1 + b - 2b^2)^{-1}.$$

Since $m_\theta = 1$, the flow rule is

$$\mathbf{q}_2 = (-h^2 w'/2r, \; -h^2 w''/2) = \mu (1, 0);$$

hence

$$w = B(1 - r), \quad B > 0. \tag{13b}$$

4. Bounds for the Interaction Curve

We begin by constructing the complete interaction curve for the approximate yield condition (8). This consists of the rectangle ABC in Fig. 4. To show this for a point D on AB, let $\lambda = \overline{AD}/\overline{AB}$. Consider a stress field where n_θ, n_r, and t are given by (12a), m_θ, m_r and p are given by λ times the appropriate equation

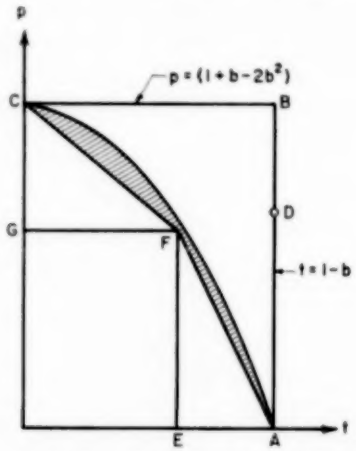

Fig 4. Discussion of bounds for interaction curve.

(13a), v is given by (12b), and $w = 0$. Evidently the above defined solution is in equilibrium with the load point D and satisfies the yield condition (8) with its associated flow rule. Therefore it is both an outer and inner bound on the interaction curve; hence it is part of the interaction curve. A similar argument holds for side BC of the rectangle.

Since ABC is the actual interaction curve for the approximate yield condition, it is an outer bound on the true interaction curve. Further, the rectangle EFG, obtained by multiplying ABC by 0·618 is a lower bound on the actual interaction curve.

The points A and C represent complete solutions for the actual yield surface; therefore, they must be on the actual interaction curve. Since the interaction curve must be convex, it follows that an improved lower bound is given by the broken line AFC in Fig. 4. Therefore the actual interaction curve must pass through A and C and lie in the region $ABCFA$.

To obtain an improved outer bound, we consider the velocity field defined by (12b) and (13b) and apply the upper bound theorem. Evidently (9a) is the appropriate part of the yield surface to use, and it follows from (5) that

$$\mathbf{q} = (Bh^2/r)\ (\beta,\ 0,\ \tfrac{1}{2},\ 0) = \mu_1\ (2n_\theta,\ 0,\ 1,\ 0) \tag{14}$$

where

$$\beta = C/Bh^2. \tag{15}$$

Equation (14) can be used to eliminate μ_1 and determine n_θ; m_θ is then given by (6a). Substituting these results into (11), we find

$$d_i = d_i^0 = (Bh^2/2)\ (\beta^2 + 1)\ (1 - b), \tag{16a}$$

$$d_e = d_e^0 = (Bh^2/2)\ \left[(1 - b)^2\ (1 + 2b)\ p + 2\ \beta t\right]. \tag{16b}$$

Equating the two equations (16) we obtain an outer bound curve in terms of the parameter β:

$$p = (1 - b)^{-2}\,(1 + 2b)^{-1}\left[(1 - b)\ \beta^2 - 2t\ \beta + (1 - b)\right]. \tag{17}$$

Obviously the ' best ' outer bound curve will be obtained if β is chosen so as to minimize p subject to a given t. Thus, setting $dp/d\beta = 0$, we find $\beta = t/(1 - b)$ and (17) becomes

$$(1 - b)^2\ (1 + 2b)\ p + t^2/(1 - b) = 1 - b. \tag{18}$$

This curve is a parabola through A with vertex at C which passes very slightly above F in Fig. 4. Therefore, the actual interaction curve must lie within the shaded region in Fig. 4.

Final outer and inner bounds for two specific values of b are shown in Figs. 5a, b.

5. Further Examples

The remaining support conditions may be systematically handled by the same methods used in Sections 3 and 4. The boundary conditions at the inner edge for each case are listed in the third, fourth, and fifth columns of Table 1.

Considering first the case of pure tension, we see that equations (12) are directly applicable to cases 2, 5 and 6 in Table 1. For the remaining cases the velocity solution (12b) will not satisfy the boundary condition $v\,(b) = 0$ from Table 1. However, due to the idealization of a perfectly plastic material, it is permissible to have a positive radial velocity discontinuity at $r = b$, provided only that $n_r\,(b) = 1$. With this boundary condition, the complete solution for cases 3, 4, 7 and 8 is

$$n_\theta = n_r = 1, \quad t = 1, \quad v = C. \tag{19}$$

For pure bending, equations (13) apply for case 3. Cases 2 and 4 are handled in the same manner, the results being

$$m_\theta = 1, \quad m_r = 1 - pr^2 - (1 - p)/r, \quad p = (1 + b + b^2)^{-1}. \tag{20}$$

The remaining cases can be satisfied only by a discontinuity of slope at $r = b$. Such a discontinuity requires $m_r\,(b) = 1$. The stress distribution for cases 5 and 7 is still given by the first two equations (13) but the load is now defined by

$$p = (1 - 3b^2 + 2b^3)^{-1}. \tag{21}$$

Similarly, the stresses for cases 6 and 8 are given by the first two equations (20) but the load is given by

$$p = (1 - b^3)^{-1}. \tag{22}$$

TABLE 1. *Summary of bounds* on interaction curves*

Case	Fig.		Requirements at $r = b^-$			t_0	p_0	Upper bound curve
	2	3	m_r, w'	n_r, v	s			
1	*a*	*a*	$m_r = 0$	$n_r = 0$	0	$1 - b$	$(1 + b - 2b^2)^{-1}$	$(1 + b - 2b^2)\,p + t^2/(1 - b)^2 = 1$
2	*b*	*a*	$m_r = 0$	$n_r = 0$	$\frac{3}{2}pbh$	$1 - b$	$(1 + b + b^2)^{-1}$	$(1 + b + b^2)\,p + t^2/(1 - b)^2 = 1$
3	*a*	*b*	$m_r = 0$	$v = 0$	0	1	$(1 + b - 2b^2)^{-1}$	$(1 + b - 2b^2)\,p + \alpha\,(t - b)^2/(1 - b)^2 = 1$
4	*b*	*b*	$m_r = 0$	$v = 0$	$\frac{3}{2}pbh$	1	$(1 + b + b^2)^{-1}$	$(1 + b + b^2)\,p + \alpha\,(t - b)^2/(1 - b)^2 = 1$
5	*a*	*c*	$w' = 0$	$n_r = 0$	0	$1 - b$	$(1 - 3b^2 + 2b^3)^{-1}$	$(1 - b)^2\,(1 + 2b)\,p + t^2/(1 - b) = 1$
6	*b*	*c*	$w' = 0$	$n_r = 0$	$\frac{3}{2}pbh$	$1 - b$	$(1 - b^3)^{-1}$	$(1 - b^3)\,p + t^2/(1 - b) = 1$
7	*a*	*d*	$w' = 0$	$v = 0$	0	1	$(1 - 3b^2 + 2b^3)^{-1}$	$(1 - b)^2\,(1 + 2b)\,p + t^2 = 1$
8	*b*	*d*	$w' = 0$	$v = 0$	$\frac{3}{2}pbh$	1	$(1 - b^3)^{-1}$	$(1 - b^3)\,p + t^2 = 1$

*Lower bound is formed by straight lines joining the points $(t_0, 0)$, 0·618 (t_0, p_0), and $(0, p_0)$. Upper bounds are the straight lines $t = t_0$ and $p = p_0$ and the curve defined in the last column above (for cases 3 and 4, $\alpha = 1$ if $t > b$, $\alpha = 0$ if $t < b$).

The appropriate ones of equations (12, 13, 19–22) can now be used to bound the interaction curve to a domain similar to $ABCFA$ in Fig. 4. Values of t_0 and p_0 which fully define this domain are summarized in Table 1.

Better upper bounds are obtained by modifying the energy expressions to fit the various boundary conditions. The internal energy is still given by (16a) for case 2, but in all other cases the energy dissipated in the discontinuity at $r = b$ must be accounted for. In cases 3 and 4, λ is discontinuous and w' is continuous, at $r = b$. If we regard the region from $r = b^-$ to $r = b^+$ as having small but finite thickness, the component v' of $\mathbf{q}$ will be very much larger than the other components, hence we may write

$$\mathbf{q} = (0, v', 0, 0).$$

It follows from (9) that this velocity field must be associated with the intersection of the cylindrical surfaces (6b) and (6c), hence the radial stresses at $r = b$ are $n_r = 1$, $m_r = 0$. Therefore, the internal energy rate is

$$d_i' = \int_{b^-}^{b^+} n_r \lambda_r r \, dr = b \int_{b^-}^{b^+} v' \, dr = b \, [v]_b = Bh^2 b\beta, \tag{23a}$$

where the symbol $[\ ]_b$ denotes the discontinuity of the bracketed quantity at $r = b$.

In the remaining cases w' is discontinuous and v may or may not be discontinuous, hence

$$\mathbf{q} = (0, v', 0, -h^2 w''/2).$$

Evidently (6b) is the applicable yield surface, and the flow rule (9b) yields

$$\mathbf{q} = \mu (0, 2n_r, 0, 1).$$

Eliminating μ from the two above equations, we obtain

$$n_r = v'/(-h^2 w'') = -(1/h^2)\,[v]_b/[w']_b.$$

Finally, we may use the above expression for n_r and (6b) to write the internal energy rate as

$$d_i = \int_{b^-}^{b^+} (n_r \lambda_r + m_r \kappa_r) r dr = b \{n_r [v]_b - (h^2/2) m_r [w']_b\}$$
$$= \frac{b}{2} \cdot \frac{[v]_b^2 + h^4 [w']_b^2}{-h^2 [w']_b}.$$

In particular, then, the energy dissipated at the discontinuity is given by

$$di'' = \tfrac{1}{2} Bh^2 b \tag{23b}$$

for cases 5 and 6, whereas for cases 7 and 8

$$di''' = \tfrac{1}{2} Bh^2 b (\beta^2 + 1). \tag{23c}$$

Since the internal energy over the interior of the plate is still d_i^0 as given by (16a) the total energy for the various cases is obtained by adding (16a) to the appropriate equation (23).

The external energy for cases 3, 5 and 7 is still given by (16b). For the remaining cases the shear energy at $r = b$

$$d_e^* = \tfrac{1}{2} Bh^2 [3pb^2 (1 - b)] \tag{24}$$

must be added to (16b).

The procedure now is similar to that used in Section 4. The internal and external energies appropriate for the given boundary conditions are equated and solved for p in terms of t and β. Then β is determined to minimize p for a given t. In most cases the minimum is a relative one determined from $dp/d\beta = 0$. However, if $t < b$ in cases 3 or 4, the minimum is restricted by the requirement that β be non-negative and hence occurs for $\beta = 0$.

The resulting formulas are listed in the last column of Table 1 and typical results are shown graphically in Fig. 5. In most cases, the curve gives the best outer bound, but in cases 5 and 6 the line $t = t_0$ is a better outer bound over part of the range.

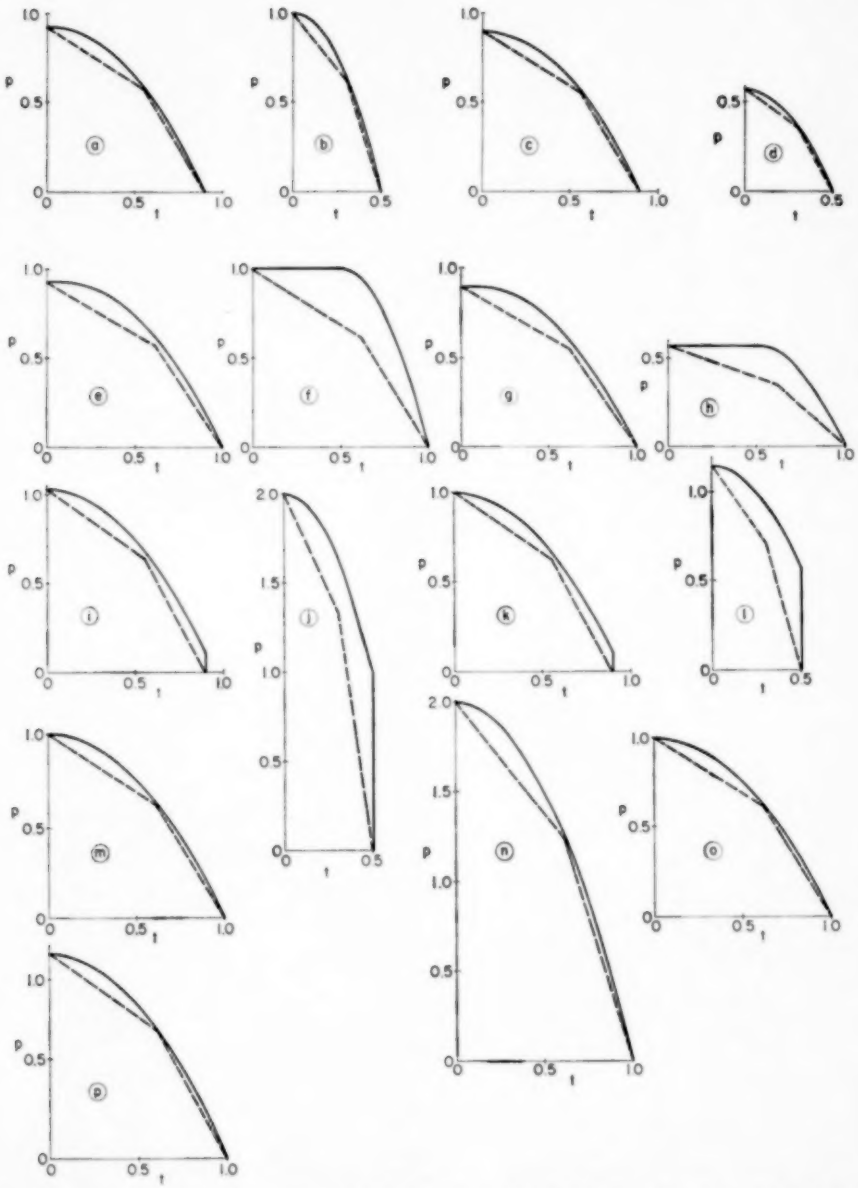

Fig. 5. Typical interaction curves. (a) Case 1, $b = 0{\cdot}1$. (b) Case 1, $b = 0{\cdot}5$. (c) Case 2, $b = 0{\cdot}1$. (d) Case 2, $b = 0{\cdot}5$. (e) Case 3, $b = 0{\cdot}1$. (f) Case 3, $b = 0{\cdot}5$. (g) Case 4, $b = 0{\cdot}1$. (h) Case 4, $b = 0{\cdot}5$. (i) Case 5, $b = 0{\cdot}1$. (j) Case 5, $b = 0{\cdot}5$. (k) Case 6, $b = 0{\cdot}1$. (l) Case 6, $b = 0{\cdot}5$. (m) Case 7, $b = 0{\cdot}1$. (n) Case 7, $b = 0{\cdot}5$. (o) Case 8, $b = 0{\cdot}1$. (p) Case 8, $b = 0{\cdot}5$.

It is evident from Fig. 5 that the bounds are reasonably close together except for large b in cases 5 and 6. Reference to Table 1 and Fig. 3 shows that the support conditions in this case appear to be rather artificial and not too likely to occur in practice. Therefore, for all cases of practical interest we may conclude that Table 1 and Fig. 5 give satisfactory bounds on the plastic interaction curve.

References

Hodge, P. G., Jr.	1959	*Plastic Analysis of Structures* (McGraw-Hill, New York).
	1960	*J. Appl. Mech.* **27**, 323.
Hodge, P. G., Jr. and Prager, W.	1951	*Limit Design of Reinforcements of Cut-outs in Slabs.* GDAM Rep. B.11-2, Brown University.
Hopkins, H. G. and Prager, W.	1953	*J. Mech. Phys. Solids* **2**, 1.
Onat, E. T. and Prager, W.	1954	*Proc. Roy. Netherlands Acad. Sci.* B **57**, 534.

J. Mech. Phys. Solids, 1960, Vol. 8, pp. 164 to 172. Pergamon Press Ltd., London. Printed in Great Britain

EFFECT OF BOUNDARIES ON WAVES IN A THERMOELASTIC SOLID: REFLEXION OF PLANE WAVES FROM A PLANE BOUNDARY†

By H. Deresiewicz
Columbia University, New York

(*Received 14th March*, 1960)

Summary

Investigated are some of the phenomena resulting from the incidence of plane thermoelastic waves on a plane, traction-free, thermally radiating boundary.

1. Introduction

In view of the interest manifested in recent years in the effects of finite thermal conductivity on wave propagation in an elastic medium, it appears desirable to examine the influence of boundaries on such motion. It has been shown previously (Deresiewicz 1957) that, in a medium of indefinite extent, the field equations of linear thermo-elasticity predict the existence of two plane dilatational waves, one predominantly elastic, the other predominantly thermal (referred to in the sequel as E and T waves, respectively). These disturbances are dissipative as well as dispersive, the amplitude of each undergoing a spatial attenuation for a given fixed frequency. In addition, the equations predict a purely elastic plane shear wave, of constant velocity and amplitude.

The present paper contains an investigation of the reflexion of such waves from a plane, traction-free, thermally radiating surface. It is found that an obliquely incident dilatational wave of either kind generates reflected waves of all three kinds, each of which (shear wave included) being dissipative and dispersive, the amplitudes diminishing with displacement normal as well as parallel to the boundary. An obliquely incident shear wave also gives rise to reflected waves of all three kinds, of which the shear wave, however, remains elastic, and the amplitude attenuation of the reflected E and T waves takes place only for displacement normal to the boundary.

An incident E wave gives rise to a reflected SV wave having a smaller phase velocity but a larger angle of reflexion than it would have in a non-conducting elastic medium; an incident SV wave generates a reflected E wave whose phase velocity and angle of reflexion are each smaller than in the corresponding elastic case. The T wave generated by either the incident E or the SV wave is reflected at an angle to the normal and with a phase velocity which are extremely small (for physically realizable frequencies and material properties).

†The support of the present work by (United States) National Science Foundation grant NSF-G 10242 to Columbia University is gratefully acknowledged.

The effect of thermal conductivity on the amplitude of the reflected E and SV waves is found to be greater for an incident SV wave than for an incident E wave; the effect on the amplitude of the reflected T wave is of the same order of magnitude in each case. It is found, also, that a normally incident E wave generates only the two reflected dilatational waves, whose amplitude ratios (to the incident amplitude) curiously enough are independent, for frequencies well into the megacycle range, of the thermal radiation at the boundary.

It must of course be kept in mind that, quantitatively, the effects discussed herein are quite small. Nevertheless, they assume importance in certain applications in ultrasonics: for example, in the design of high-frequency oscillators. The aim there is to evolve oscillators with ever larger mechanical admittance. However, it does not appear to be generally known that there is a limitation *imposed by the laws of thermoelasticity* on the maximum realizable value of the admittance, and that this limitation becomes practically important in the megacycle frequency range. In addition, since the phenomena under discussion are directly consequent upon the laws of thermodynamics, they have inherent theoretical interest.

Finally, it is evident that the problem of refraction of waves from one medium into a contiguous one across a plane boundary, with attendant reflexion at this boundary, may be handled analogously to the problem dealt with herein.

2. Solution of the Field Equations

A general solution of the field equations of linear isotropic elasticity for the displacement, $\mathbf{u}$, and the (small) deviation, T, of the temperature from equilibrium has been exhibited recently (Deresiewicz 1958) in the form

$$\left.\begin{aligned} \mathbf{u} &= (\sum_{j=1}^{2} \operatorname{grad} \bar{\phi}_j + \operatorname{curl} \mathbf{H})\, e^{pt}, \\ T &= -(\rho c_T^2/\bar{\beta}) \sum_{j=1}^{2} (\delta_j^2 + p^2/c_T^2)\, \bar{\phi}_j\, e^{pt}, \end{aligned}\right\} \tag{1}$$

where

$$\left.\begin{aligned} &(\nabla^2 + \delta_j^2)\, \bar{\phi}_j = 0, \quad j = 1, 2, \\ &(\nabla^2 + \delta_3^2)\, \mathbf{H} = 0. \end{aligned}\right\} \tag{2}$$

For a harmonic time variation (i.e., $p = i\omega$), the parameters $\delta_k\,(k = 1, 2, 3)$ which are associated, respectively, with E, T, and shear motion, are given by

$$\left.\begin{aligned} 2\,(\delta_1^2, \delta_2^2) &= \frac{\omega^2}{c_T^2}\left\{\left(1 - i\,\frac{1+\epsilon}{\Omega}\right) \pm \left[\left(1 + \frac{i}{\Omega}\right)^2 - \frac{\epsilon}{\Omega}\left(\frac{2+\epsilon}{\Omega} + 2i\right)\right]^{\frac{1}{2}}\right\}, \\ \delta_3^2 &= \frac{\omega^2}{c_2^2}. \end{aligned}\right\} \tag{3}$$

The material constants entering into the solution are ρ, the density; $c_T^2 = (\lambda + 2\mu)/\rho$, the phase velocity of isothermal dilatational waves (i.e., corresponding to a medium with infinite thermal conductivity); λ and μ, Lamé's constants; $\bar{\beta} = \tilde{\alpha}\,(3\lambda + 2\mu)$, where $\tilde{\alpha}$ is the coefficient of thermal expansion. Further, $\epsilon = \bar{\beta}^2\, T_0/\rho\, c_v\, c_T^2 = c_s^2/c_T^2 - 1$, where T_0 is the equilibrium temperature, c_v, the specific heat at constant

volume per unit volume, and c_s, the phase velocity of adiabatic dilatational waves (corresponding to a medium having zero thermal conductivity). Finally, $\Omega = a^2\,\omega/c_T{}^2$, where a^2 is the thermal diffusivity, is the (dimensionless) product of the frequency of the motion and the relaxation time due to thermal currents.

It should be noted that the solution represented by (1), (2) and (3) is complete (STERNBERG 1960).

3. INCIDENT E WAVE

We introduce a set of rectangular coordinates with origin at a point on the (horizontal) plane boundary, such that the xy plane coincides with this boundary and the z axis is normal to it and directed into the solid. Then, for waves of plane strain in the (vertical) xz plane, a solution of (2) appropriate to an *incident E wave* is

$$\phi'_1 \equiv \bar{\phi}_1\, e^{i\omega t} = A_1' \exp i\,(\omega t - \delta_1\, \mathbf{w}_1' \cdot \mathbf{r}), \tag{4}$$

where

$$\mathbf{w}_1' = \mathbf{i} \sin \alpha - \mathbf{k} \cos \alpha \tag{5}$$

is the unit normal to the wave front and $\mathbf{r} = x\mathbf{i} + z\mathbf{k}$ is the position vector with respect to the origin.

In view of the situation which exists in the purely elastic case, we may expect that the presence of a traction-free boundary will cause the appearance of reflected body waves of all three kinds. Accordingly we introduce the following solutions of (2):

reflected E wave

$$\phi_1'' = A_1'' \exp i\,(\omega_1 t - \delta_1\, \mathbf{w}_1'' \cdot \mathbf{r}), \tag{6a}$$

reflected T wave

$$\phi_2'' = A_2'' \exp i\,(\omega_2 t - \delta_2\, \mathbf{w}_2'' \cdot \mathbf{r}), \tag{6b}$$

reflected SV wave

$$\mathbf{H} = (0, H'', 0),$$

where

$$H'' = A_3'' \exp i\,(\omega_3 t - \delta_3\, \mathbf{w}_3'' \,.\, \mathbf{r}). \tag{6c}$$

The resultant displacement has components

$$\begin{aligned} u_x &= -\,i\,(\delta_1 \sin\alpha\, \phi_1' + \delta_1 l_1 \phi_1'' + \delta_2 l_2 \phi_2'' - \delta_3 n_3 H'') \\ u_y &= 0 \\ u_z &= i\,(\delta_1 \cos\alpha\, \phi_1' - \delta_1 n_1 \phi_1'' - \delta_2 n_2 \phi_2'' - \delta_3 l_3 H'') \end{aligned} \tag{7}$$

where $(l_k, 0, n_k)$ are the components of the unit vectors $\mathbf{w}_k''$.

Of the traction conditions on $z = 0$, $\tau_{zy} = 0$ is satisfied identically. The other boundary conditions require that

$$\omega_1 = \omega_2 = \omega_3 = \omega, \tag{8}$$

i.e., that each of the reflected waves have the same frequency as the incident wave, and

$$\delta_1 l_1 = \delta_2 l_2 = \delta_3 l_3 = \delta_1 \sin\alpha. \tag{9}$$

It is apparent from (9) that

$$l_1 = \sin\alpha, \quad n_1 = \cos\alpha\,; \tag{10}$$

thus, the angle of reflexion of the E wave is equal to its angle of incidence.

We note that, for materials within the scope of our theory, $\Omega \ll 1$ for frequencies as high as the megacycle range*. Accordingly, the expressions (3) for δ_1 and δ_2 may be approximated by expanding in powers of Ω and retaining only the first few terms:

$$\left.\begin{aligned} \delta_1 &\cong \frac{\omega}{c_s}(1 + k_1\,\zeta^4 - i\,\zeta^2/2), \\ \delta_2 &\cong \frac{\omega}{c_s}\cdot\frac{\eta}{2\zeta}\left[(1 + \zeta^2/2) - i\,(1 - \zeta^2/2)\right], \end{aligned}\right\} \tag{11}$$

where

$$\left.\begin{aligned} &\eta = (2\epsilon)^{\frac{1}{2}}, \quad k_1 = (4 - 3\epsilon)/8\epsilon, \\ &\zeta^2 = \epsilon\,\Omega/(1 + \epsilon)^2. \end{aligned}\right\} \tag{12}$$

On proceding to the remaining relations in (9), we find, with the aid of (11) and the last of (3),

$$\left.\begin{aligned} l_2 &= \frac{\delta_1}{\delta_2}\sin\alpha \cong \frac{\zeta\sin\alpha}{\eta}\left[(1 + \zeta^2 - k_2\,\zeta^4) + i\,(1 - \zeta^2 - k_2\,\zeta^4)\right], \\ n_2 &= (1 - l_2^2)^{\frac{1}{2}} \cong 1 + \frac{\zeta^4\sin^2\alpha}{8\epsilon^2}(\sin^2\alpha - 8\epsilon) - i\,\frac{\zeta^2\sin^2\alpha}{2\epsilon}, \end{aligned}\right\} \tag{13}$$

where $k_2 = (4 - 7\epsilon - 4\epsilon^2 - 2\epsilon^3)/8\epsilon$, and

$$\left.\begin{aligned} l_3 &= \frac{\delta_1}{\delta_3}\sin\alpha \cong q\sin\alpha\,(1 + k_1\,\zeta^4 - i\,\zeta^2/2) \\ n_3 &= (1 - l^2{}_3)^{\frac{1}{2}} \\ &\cong (1 - \Delta^2)^{\frac{1}{2}}\left[1 + \frac{\Delta^2\,\zeta^4}{(1 - \Delta^2)^{\frac{1}{2}}}\left(k_1\,\Delta^2 - \frac{1 - \epsilon}{2\epsilon}\right) - i\,\frac{\Delta^2\,\zeta^2}{2\,(1 - \Delta^2)}\right], \end{aligned}\right\} \tag{14}$$

where

$$q = c_2/c_s, \quad \Delta = q\sin\alpha. \tag{15}$$

Inserting (10), (13) and (14) in (6a, b, c), and again taking account of (11) and the last (3), we find

$$\left.\begin{aligned} \phi_1'' &\cong A_1''\,e^{-(\theta x + \psi_1 z)}\exp\left[\frac{i\omega}{v_1^{(1)}}\,(v_1^{(1)}\,t - x\sin\alpha - z\cos\alpha)\right], \\ \phi_2'' &\cong A_2''\,e^{-(\theta x + \psi_2 z)}\exp\left[\frac{i\omega}{v_2^{(1)}}\,(v_2^{(1)}\,t - x\sin\beta - z\cos\beta)\right], \\ H'' &\cong A_3''\,e^{-(\theta x + \psi_3 z)}\exp\left[\frac{i\omega}{v_3^{(1)}}\,(v_3^{(1)}\,t - x\sin\gamma - z\cos\gamma)\right]. \end{aligned}\right\} \tag{16}$$

In (16),

$$\theta = \frac{\omega}{2c_s}\,\zeta^2\sin\alpha \tag{17}$$

is the spatial attenuation factor parallel to the boundary (which, by virtue of the boundary conditions, is the same for each of the waves), and

*In addition, $\epsilon \ll 1$, although $\epsilon \gg \Omega$. Representative values are given by Deresiewicz (1957) and Chadwick and Sneddon (1958).

$$\left.\begin{aligned} \psi_1 &= \frac{\omega}{2c_s}\,\zeta^2 \cos\alpha, \\ \psi_2 &= \frac{\omega}{2c_s}\cdot\frac{\eta}{2\zeta}\left[1-(\sin^2\alpha-\epsilon)\,\zeta^2/2\epsilon\right], \\ \psi_3 &= \frac{\omega}{2c_s}\frac{\Delta^2\zeta^2}{q\,(1-\Delta^2)^{\frac{1}{2}}}, \end{aligned}\right\} \tag{18}$$

are the respective spatial attenuation factors normal to the boundary. Furthermore,

$$\left.\begin{aligned} v_1^{(1)} &= c_s(1-k_1\zeta^4), \\ v_2^{(1)} &= \frac{c_s\zeta}{\eta}\left(1-\frac{\epsilon+\sin^2\alpha}{2\epsilon}\zeta^2\right), \\ v_3^{(1)} &= c_2\left[1-\frac{\Delta^2\zeta^4}{8\,(1-\Delta^2)}\right], \end{aligned}\right\} \tag{19}$$

are the respective phase velocities, and α, β, γ, related by means of

$$\left.\begin{aligned} \sin\beta &= \frac{\zeta}{\eta}\left(1-\frac{\epsilon+\sin^2\alpha}{2\epsilon}\zeta^2\right)\sin\alpha, \\ \sin\gamma &= \left[1+\left(\frac{4}{\epsilon}-\frac{3-2\Delta^2}{1-\Delta^2}\right)\frac{\zeta^4}{8}\right]q\sin\alpha, \end{aligned}\right\} \tag{20}$$

are the angles of reflection of the E, T and SV waves, respectively.

It is seen that the dissipation is quite small in the E and SV waves, varying as $\exp(-\Omega)$, and very large in the T wave, varying as $\exp(-\Omega^{\frac{1}{2}})$. The phase velocity of the reflected shear wave is smaller than its corresponding value in the purely elastic case (i.e., for $\epsilon = 0$). Its angle of reflexion is greater than the corresponding angle in a perfectly non-conducting medium but (since $q = c_2/c_s = c_2/c_T(1+\epsilon)^{\frac{1}{2}}$) smaller than in a perfectly conducting medium. The phase velocity and the angle of reflexion of the T wave, each proportional to $\Omega^{\frac{1}{2}}$, are very small.

The amplitude ratios are obtained from the boundary conditions in the usual manner. Thus, on $z = 0$, the conditions

$$\left.\begin{aligned} \tau_{zx} &= \mu\left(\frac{\partial u_x}{\partial z}+\frac{\partial u_z}{\partial x}\right)=0, \\ \sigma_z &= 2\mu\left[\frac{\partial u_z}{\partial z}+\sum_{j=1}^{2}\left(\delta_j^2-\frac{\omega^2}{2c_2^2}\right)\phi_j\right]=0, \\ \frac{\partial T}{\partial z}+hT &= -\frac{\rho c_T^2}{\beta}\left(\frac{\partial}{\partial z}+h\right)\sum_{j=1}^{2}\left(\delta_j^2-\frac{\omega^2}{c_T^2}\right)\phi_j=0, \end{aligned}\right\} \tag{21}$$

reduce to the system of algebraic equations

$$\left.\begin{aligned} &(\delta_1^2\sin 2\alpha)\,z_1^{(1)}+(2\delta_2^2 l_2 n_2)\,z_2^{(1)}-\delta_3^2(n_3^2-l_3^2)\,z_3^{(1)}=\delta_1^2\sin 2\alpha, \\ &\left(2\delta_1^2\sin^2\alpha-\frac{\omega^2}{c_2^2}\right)z_1^{(1)}+\left(2\delta_2^2 l_2^2-\frac{\omega^2}{c_2^2}\right)z_2^{(1)}-2\delta_3^2 l_3 n_3 z_3^{(1)} \\ &\qquad\qquad =-2\delta_1^2\sin^2\alpha+\frac{\omega^2}{c_2^2}, \\ &\left(\delta_1^2-\frac{\omega^2}{c_T^2}\right)(i\delta_1\cos\alpha-h)\,z_1^{(1)}+\left(\delta_2^2-\frac{\omega^2}{c_T^2}\right)(i\delta_2\cos\alpha-h)\,z_2^{(1)} \\ &\qquad\qquad =\left(\delta_1^2-\frac{\omega^2}{c_T^2}\right)(i\delta_1\cos\alpha+h), \end{aligned}\right\} \tag{22}$$

where

$$z_k^{(1)} = A_k''/A_1', \quad (k = 1, 2, 3)$$

and l_2, n_2 are given by (13), and l_3, n_3, by (14).

Solution of (21) yields, to terms of $O(\zeta^2)$, the amplitude ratios of the reflected potentials* ϕ_1'', ϕ_2'', H'',

$$\left.\begin{aligned} z_1^{(1)} &= \frac{A-B}{A+B}(1 + e_1\zeta^2 + if_1\zeta^2), \\ z_2^{(1)} &= \frac{-2\zeta^2/\eta}{A+B}\left[(\xi A \sec\alpha - B) + i(\xi A \sec\alpha + B)\right], \\ z_3^{(1)} &= -\frac{2(1-\Delta^2)\sin 2\alpha}{A+B}(1 + e_2\zeta^2 + if_2\zeta^2), \end{aligned}\right\} \tag{23}$$

where

$$\left.\begin{aligned} A &= 2\Delta(1-\Delta^2)^{\frac{1}{2}}\sin 2\alpha, \quad B = (1-2\Delta^2)^2/q^2, \quad \xi = hc_s/\omega, \\ e_1 &= \frac{2}{\eta q\cos\alpha}\left[\frac{\xi A(\eta q A\sec\alpha + B^{\frac{1}{2}}) - B^{3/2}\cos\alpha}{A^2-B^2}\right], \\ f_1 &= \frac{2B^{\frac{1}{2}}}{\eta q\cos\alpha}\left(\frac{\xi A + B\cos\alpha + \eta AB^{\frac{1}{2}}}{A^2-B^2}\right) - \frac{3q^{-1}}{1-\Delta^2}\cdot\frac{AB^{\frac{1}{2}}}{A^2-B^2}, \\ e_2 &= \frac{1}{\eta\cos\alpha}\left[\frac{\eta\xi A\sec\alpha + (\xi+\cos\alpha)q^{-1}B^{\frac{1}{2}}}{A+B} - \tfrac{1}{2}\xi\tan\alpha\right], \\ f_2 &= \frac{1}{\eta\cos\alpha}\left[\eta - \xi\left(\frac{1}{\epsilon} + \tfrac{1}{2}\tan\alpha\right) - \frac{\eta A - (\xi-\cos\alpha)q^{-1}B^{\frac{1}{2}}}{A+B}\right] \\ &\quad + \frac{2\Delta^2}{1-2\Delta^2} + \frac{1}{A+B}\left[\frac{3-2\Delta^2}{2(1-\Delta^2)}A - \frac{4\Delta^2}{q}B^{\frac{1}{2}}\right]. \end{aligned}\right\} \tag{24}$$

At normal incidence (i.e., for $\alpha = 0$) $A = 0$, $B = q^{-2}$, $e_1 = -f_1 = 2/\eta$, $e_2 = (\xi+1)/\eta$, $f_2 = (\xi - \xi/\epsilon - 1 + \eta)/\eta$, so that (23) reduce to

$$\left.\begin{aligned} z_1^{(1)} &= -1 - (2\zeta^2/\eta)(1-i), \\ z_2^{(1)} &= (2\zeta^2/\eta)(1-i), \quad z_3^{(1)} = 0. \end{aligned}\right\} \tag{25}$$

It is worthy of note that for normal incidence the amplitude ratios, to terms of $\sigma(\zeta^2)$, are independent of the thermal radiation constant on the boundary, h.

The procedure leading to (23) is valid for angles of incidence, α, such that $\zeta\sec\alpha \ll 1$, or $\alpha < \arcsin(1-\zeta^2)^{\frac{1}{2}}$. In the range $\arcsin(1-\zeta^2)^{\frac{1}{2}} \leqslant \alpha \leqslant \frac{1}{2}\pi$, i.e., near grazing incidence, (23) must be replaced by one of two sets of expressions depending on whether or not the boundary is thermally insulated. Thus, for $h \neq 0$, as $\alpha \to \frac{1}{2}\pi$,

$$z_1^{(1)} \to -1, \quad z_2^{(1)} \to 0, \quad z_3^{(1)} \to -2iq^2\zeta/(1-2q^2), \tag{26}$$

while, for $h = 0$, as $\alpha \to \frac{1}{2}\pi$,

$$\left.\begin{aligned} z_1^{(1)} &\to -1 - \frac{2\zeta^2}{\eta(1-2q^2)}\left\{1 - i\left[1 + \frac{4\eta q^3(1-q^2)^{\frac{1}{2}}}{1-2q^2}\right]\right\}, \\ z_2^{(1)} &\to 2(1-i)\zeta^2/\eta, \quad z_3^{(1)} \to -4iq^2\zeta^2/(1-2q^2), \end{aligned}\right\} \tag{27}$$

q being given by the first of (15). Of course, as in the case of the classical elastic solution, the case of grazing incidence ($\alpha = \frac{1}{2}\pi$) must be handled separately. This will not be done here.

* The amplitude ratios of the corresponding displacements are obtained by multiplying the values given in (23) by δ_k/δ_1, $k = 1, 2, 3$.

4. Incident SV Wave

In accordance with the procedure employed in the preceding section, we choose a solution of (2) appropriate to an *incident SV wave* (whose wave front is inclined at an angle γ to the boundary),

$$H' = C'_3 \exp i\,(\omega t - \delta_3 x \sin\gamma + \delta_3 z \cos\gamma), \tag{28}$$

and attempt to satisfy the conditions on $z = 0$ by introducing *reflected E, T* and *SV* waves given, respectively, by

$$\left.\begin{aligned} \phi_1'' &= C_1'' \exp i\,(\omega t - \delta_1 \mathbf{d}_1'' \cdot \mathbf{r}), \\ \phi_2'' &= C_2'' \exp i\,(\omega t - \delta_2 \mathbf{d}_2'' \cdot \mathbf{r}), \\ H'' &= C_3'' \exp i\,(\omega t - \delta_3 \mathbf{d}_3'' \cdot \mathbf{r}), \end{aligned}\right\} \tag{29}$$

where the $\mathbf{d}_k''$ denote unit vectors having components $(\lambda_k, 0, \nu_k)$. Once again we find, as in (9),

$$\delta_1 \lambda_1 = \delta_2 \lambda_2 = \delta_3 \lambda_3 = \delta_3 \sin\gamma \tag{30}$$

from which it follows that

$$\lambda_3 = \sin\gamma, \quad \nu_3 = \cos\gamma. \tag{31}$$

Thus, the angle of reflexion of the SV wave equals its angle of incidence.

We find, further, that

$$\left.\begin{aligned} \lambda_1 &\cong \Lambda\,(1 - k_1 \zeta^4 + i\,\zeta^2/2), \\ \nu_1 &\cong [1 - \Lambda^2\,(1 - \zeta^4/\epsilon) - i\Lambda^2\,\zeta^2]^{\frac{1}{2}}, \end{aligned}\right\} \tag{32}$$

where

$$\Lambda = q^{-1} \sin\gamma. \tag{33}$$

For $0 \leqslant \Lambda \leqslant (1 - \zeta)^{\frac{1}{2}}$,

$$\nu_1 \cong (1 - \Lambda^2)^{\frac{1}{2}} \left(1 + \left[\frac{1}{2\epsilon} + \frac{\Lambda^2}{8\,(1 - \Lambda^2)}\right] \frac{\Lambda^2\,\zeta^4}{1 - \Lambda^2} - i\,\frac{\Lambda^2\,\zeta^2}{2\,(1 - \Lambda^2)}\right) \tag{34}$$

and, in this range of values of the angle of incidence,

$$\phi_1'' \cong C_1''\, e^{-\sigma_1 z} \exp\left[\frac{i\omega}{v_1^{(3)}}\,(v_1^{(3)}\, t - x \sin\alpha - z\cos\alpha)\right]; \tag{35}$$

the attenuation factor (normal to the boundary) is

$$\sigma_1 = \frac{\omega}{c_s} \cdot \frac{\zeta^2}{2\,(1 - \Lambda^2)^{\frac{1}{2}}}, \tag{36}$$

the phase velocity,

$$v_1^{(3)} = c_s\,[1 - k_3\,(1 - \Lambda^2)\,\zeta^4], \tag{37}$$

where $k_3 = [1 - 3\epsilon/4 - (1 - \epsilon)\,\Lambda^2]/2\epsilon\,(1 - \Lambda^2)^2$, and the angle of reflexion, α, such that

$$\sin\alpha = \Lambda\,[1 - k_3\,(1 - \Lambda^2)\,\zeta^4]. \tag{38}$$

Thus, the velocity and the angle of reflexion are smaller than in the isothermal case.

It can also be shown that the SV wave undergoes total reflexion whenever it is incident at an angle greater than a critical one, $\gamma_{cr.}$, whose value is bracketed by

$$\text{arc sin}\,\frac{c_2}{c_s}\left(1 - \frac{\zeta^4}{\epsilon}\right)^{-\frac{1}{2}} < \gamma_{cr.} < \text{arc sin}\,\frac{c_2}{c_T} \tag{39}$$

Finally, (30) yields

$$\left.\begin{aligned} \lambda_2 &\cong (2\zeta\Lambda/\eta)\left[(1+\zeta^2/2)+i\,(1-\zeta^2/2)\right], \\ v_2 &\cong 1+2\Lambda^2\,(\Lambda^2-\epsilon)\,\zeta^4/\epsilon^2-2i\Lambda^2\,\zeta^2/\epsilon, \end{aligned}\right\} \tag{40}$$

from which we find, in turn,

$$\phi_2'' \cong C_2''\,e^{-\sigma_2 z}\exp\left[\frac{i\omega}{v_2^{(3)}}\,(v_2^{(3)}\,t-x\sin\beta-z\cos\beta)\right], \tag{41}$$

$$\sigma_2 = \frac{\omega}{c_s}\cdot\frac{\eta}{2\zeta}\left(1+\frac{4\Lambda^2-\epsilon}{2\epsilon}\,\zeta^2\right), \tag{42}$$

$$v_2^{(3)} = (2c_s\,\zeta/\eta)\left[1+(2\Lambda^2-\epsilon)\,\zeta^2/2\epsilon\right], \tag{43}$$

$$\sin\beta = (2\zeta\Lambda/\eta)\left[1+(2\Lambda^2-\epsilon)\,\zeta^2/2\epsilon\right]. \tag{44}$$

It appears from (35) and (41) that attenuation of reflected E and T waves, generated by an incident SV wave, depends only on displacement normal, but not parallel, to the boundary. In addition, the reflected SV wave is undamped. This differs markedly from the behaviour of the reflected waves generated by an incident E wave, as is evident from (16).

The conditions on the boundary reduce to the set of equations governing the amplitude ratios $z_k^{(3)} = C_k''/C_3'$,

$$\left.\begin{aligned} (2\delta_1 v_1\sin\gamma)\,z_1^{(3)}+(2\delta_2 v_2\sin\gamma)\,z_2^{(3)}-(\delta_3\cos 2\gamma)\,z_3^{(3)} &= \delta_3\cos 2\gamma, \\ (\cos 2\gamma)\,z_1^{(3)}+(\cos 2\gamma)\,z_2^{(3)}+(\sin 2\gamma)\,z_3^{(3)} &= \sin 2\gamma, \\ (-i\delta_1 v_1+h)\,(\delta_1^2-\omega^2/c_T^2)\,z_1^{(3)}+(-i\delta_2 v_2+h)\,(\delta_2^2-\omega^2/c_T^2)\,z_2^{(3)} &= 0. \end{aligned}\right\} \tag{45}$$

At normal incidence, only the SV wave is reflected.

For an arbitrary angle of incidence $0 \leqslant \gamma \leqslant \arcsin\left[q\,(1-\zeta)^{\frac{1}{2}}\right]$, the amplitude ratios* in (45) may be written

$$\left.\begin{aligned} z_1^{(3)} &\cong D^{-1}\left[(\epsilon-\zeta)-i\,(\epsilon+a_2\,\zeta)\right]q^{-1}\sin 2\gamma\cos 2\gamma, \\ z_2^{(3)} &\cong -D^{-1}\left[\xi-i\,(1-\Lambda^2)^{\frac{1}{2}}\right]\eta\zeta^2\,q^{-1}\sin 2\gamma\cos 2\gamma, \\ z_3^{(3)} &\cong -D^{-1}\left\{\left[\epsilon\,(E-F)-\zeta\,(E-a_1\,F)\right]-i\left[\epsilon\,(E-F)+\zeta\,(a_2\,E-a_3\,F)\right]\right\}, \end{aligned}\right\} \tag{46}$$

where

$$\left.\begin{aligned} D &= \left[\epsilon\,(E+F)-\zeta\,(E+a_1\,F)\right]-i\left[\epsilon\,(E+F)+\zeta\,(a_2\,E+a_3\,F)\right], \\ E &= (2q)^{-1}\cos^2 2\gamma, \quad F=(1-\Lambda^2)^{\frac{1}{2}}\sin\gamma\sin 2\gamma, \\ a_1 &= 1+\epsilon-\epsilon\xi\,(1-\Lambda^2)^{-\frac{1}{2}}, \quad a_2 = 1-\eta\xi, \\ a_3 &= 1+\epsilon+\xi\left[\eta-\epsilon\,(1-\Lambda^2)^{-\frac{1}{2}}\right] \end{aligned}\right\} \tag{47}$$

and ξ is given in (24).

For a thermally impervious boundary (i.e., $h=0$) (46) reduce to

$$\left.\begin{aligned} z_1^{(3)} &\cong \frac{\sin 2\gamma\cos 2\gamma}{q\,(E+F)}\left(1+\frac{iE\zeta}{E+F}\right), \\ z_2^{(3)} &\cong -\frac{(1-\Lambda^2)^{\frac{1}{2}}\sin 2\gamma\cos 2\gamma}{q\,(E+F)}\cdot\frac{\zeta^2}{\eta}\,(1-i), \\ z_3^{(3)} &\cong -\frac{E-F}{E+F}\left(1+\frac{2i\,F\epsilon\zeta}{E-F}\right). \end{aligned}\right\} \tag{48}$$

*The amplitude ratios of the corresponding displacements are obtained from the values in (46) by multiplying by δ_k/δ_3, $k=1,2,3$.

REFERENCES

CHADWICK, P. and SNEDDON, I. N.	1958	*J. Mech. Phys. Solids* **6**, 223.
DERESIEWICZ, H.	1957	*J. Acoust. Soc. Amer.* **29**, 204.
	1958	*Proc. 3rd U.S. Nat. Congr. Appl. Mech.*, p. 287.
STERNBERG, E.	1960	*Arch. Rat. Mech. Anal.* In press.

J. Mech. Phys. Solids, 1960, Vol. 8, pp. 173 to 186. Pergamon Press Ltd., London. Printed in Great Britain

AN ELECTRICAL ANALOGUE SOLUTION FOR THE STRESSES NEAR A CRACK OR HOLE IN A FLAT PLATE

By S. C. Redshaw and K. R. Rushton
Department of Civil Engineering, University of Birmingham

(*Received* 25*th March*, 1960)

Summary

An electrical analogue for solving the biharmonic equation was used to determine the elastic stresses near a hole or crack in a flat rectangular plate subjected to uniaxial tension.

Problems concerning both simply and multiply connected regions were solved by the method and, where a comparison between the experimental results and existing analytical solutions was possible, the agreement was good.

The advantages and limitations of the method are discussed and the desirability of extending the method for the determination of the stresses after plastic yielding has occurred, is emphasized.

1. Introduction

The determination of the stresses in the region of a hole or crack in a stressed plate is of great engineering importance, particularly in components liable to fatigue, but unfortunately theoretical solutions are difficult to obtain and, indeed, very few solutions exist. Experimental methods such as photo-elasticity, strain gauge investigations and brittle lacquer techniques, have been used in an attempt to obtain reliable results but, although a hole can be made easily, a fine crack is difficult to manufacture. However, the principal difficulty lies in the inability to measure strains over a short length and at sufficient stations in the proximity of the crack or hole.

For this reason it was decided to attempt a solution to the problem by using an electrical analogue method, a technique which had already yielded satisfactory solutions to other elastic problems.

2. Outline of Problem

(i) *General*

The cases investigated all concerned the plane stress problem of a flat rectangular plate subjected to uniaxial tension, and having either a central hole or a central crack disposed perpendicularly to the direction of applied stress, or external cracks centrally disposed in the same direction. The problems are summarized in Fig. 1. It will be seen that the problems considered concern either simply or multiply connected regions.

Palmer and Redshaw (1955) have established an electrical analogue for the solution of the biharmonic equation and, for their analogy to be used in the present

instance, the problem has to be expressed in terms of the Airy stress function and the boundary conditions formulated accordingly. When the boundary conditions have been represented on the electrical analogue network the measurement of the electrical potentials at various nodes supplies the Airy stress function at those

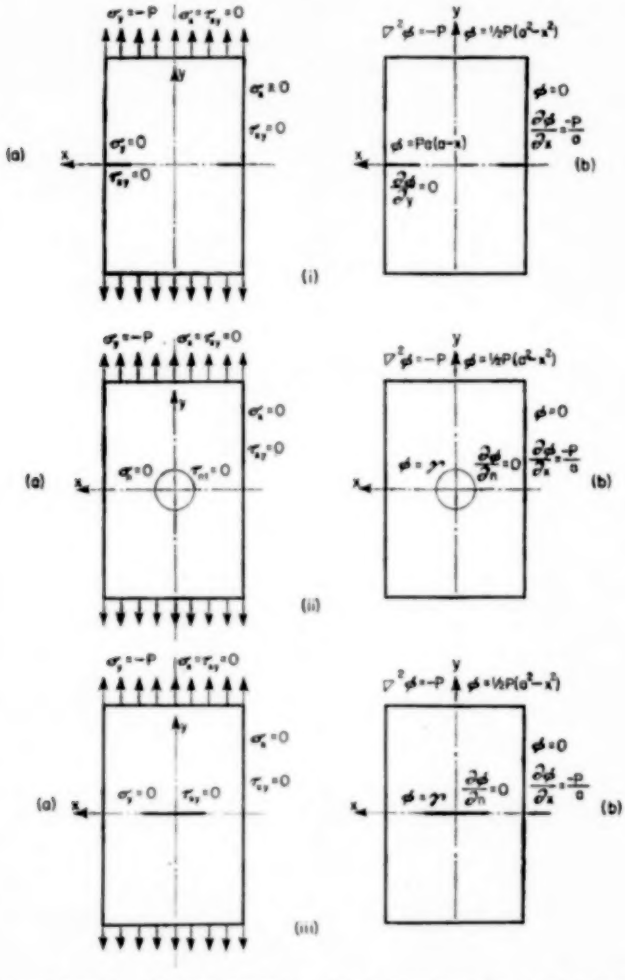

FIG. 1. (i) External cracks. (ii) Circular holes. (iii) Internal cracks. (a) Loading conditions. (b) Airy stress functions.

points. Subsequent double differentiation yields the stresses but, additionally, the sum of these stresses can be measured directly from the network.

For a simply connected region the boundary conditions may be expressed directly in terms of the Airy stress function, but for a multiply connected region an additional boundary condition is required.

(ii) *Determination of Airy stress function*

The stresses on any boundary, see Fig. 2, can be expressed in terms of X and Y the components of the surface stresses and the direction cosines l and m :

$$X = l\,\sigma_x + m\,\tau_{xy}, \quad Y = m\,\sigma_y + l\,\tau_{xy}. \tag{1}$$

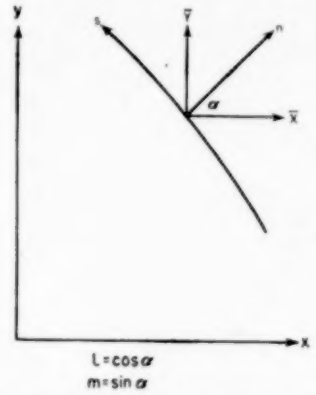

FIG. 2. The stresses on any boundary.

Since

$$\tau_x = \frac{\partial^2 \phi}{\partial y^2}, \quad \sigma_y = \frac{\partial^2 \phi}{\partial x^2}, \quad \tau_{xy} = -\frac{\partial^2 \phi}{\partial x\,\partial y}, \tag{2}$$

equations (1) can be written in terms of the Airy stress function ϕ and, on integration,

$$\frac{\partial \phi}{\partial n} = Al + Bm + \alpha l + \beta m. \tag{3}$$

Hence

$$\phi = \int_0^s (Bl + Am)\,ds + \alpha x + \beta y + \gamma \tag{4}$$

where

$$A = -\int_0^s Y\,ds, \quad B = \int_0^s X\,ds.$$

α, β and γ are constants of integration which for a simply connected region can be chosen arbitrarily. Therefore, when strains are specified on the boundary they can be represented by the Airy stress function and its normal gradient.

In the problems considered, not only were the normal and shearing stresses known on the loaded boundaries, $y = \pm b$ (Fig. 1), but the transverse stress was assumed to be zero. Hence, instead of having to specify ϕ and $\partial\phi/\partial n$ on these boundaries, $\nabla^2 \phi$ and ϕ can be used, which is more convenient for the electrical analogue.

If the body is multiply connected the constants are of importance and must be chosen to ensure that the rotations and displacements are continuous. On one boundary, usually the external boundary, the constants are chosen arbitrarily but their values on the internal boundaries are restricted by the continuity condition.

MICHELL (1899) first presented these conditions in terms of the Airy stress function; he deduced the equations for each internal boundary which must be satisfied to ensure single valuedness on the boundary. These are the rotation condition

$$\oint_I \frac{\partial}{\partial n}(\nabla^2 \phi)\, ds = 0 \tag{5}$$

and displacement conditions

$$\left.\begin{aligned} \oint_I \left\{ y \frac{\partial}{\partial n}(\nabla^2 \phi) - x \frac{\partial}{\partial s}(\nabla^2 \phi) \right\} ds = 0, \\ \oint_I \left\{ y \frac{\partial}{\partial s}(\nabla^2 \phi) + x \frac{\partial}{\partial n}(\nabla^2 \phi) \right\} ds = 0. \end{aligned}\right\} \tag{6}$$

For a multiply connected region the constants must be chosen so that these conditions are satisfied.

Twofold symmetry occurred in all the problems described in this paper and therefore α and β become zero, also the displacement conditions (6) are automatically satisfied.

There remains, however, the determination of γ and for this two alternative methods exist: either a superposition method, described by PRAGER (1946), or an iterative method due to SOUTHWELL (1948). During the experiments both methods were tried, SOUTHWELL's method being finally used as the superposition method entailed the summing of two solutions, with the attendant inaccuracies.

Using SOUTHWELL's method, various values of γ were tried until the one giving the correct solution of (5) was found; the nature of the electrical analogue is such that this presented no difficulty.

(iii) *Boundary conditions for cracks and holes*

The boundary conditions for cracks and holes require special mention. For a hole the normal stress and the shearing stress are both zero. When substituted in (3) and (4) this yields $\phi = \gamma$ and $\partial\phi/\partial n = 0$. A fine line internal crack may be considered as an ellipse whose minor axis is virtually zero, and again the normal and shearing stresses are zero, giving the same boundary conditions as for a hole. For the external crack a somewhat similar boundary condition applies (see Section 4)

3. ELECTRICAL ANALOGY

(i) *Description of electrical analogue*

The electrical analogue in effect provides a solution to the biharmonic equation when expressed in finite difference form. The principle of the analogy has been previously described (PALMER and REDSHAW 1955) and the electrical analogue used in the present instance is a very enlarged version of the prototype apparatus.

The electrical resistance network is described diagrammatically in Fig. 3. The lower network consists of a square grid built with resistors of uniform resistance value, a similar network forms the middle network and the upper network comprises a similar grid but without resistors. Corresponding nodes of the upper and lower nets are connected to the intermediate net through resistors whose

resistance value is large compared with that of the net resistors. The fineness of the net permits an optimum mesh separation of $\frac{1}{48} \times \frac{1}{32}$ and, by taking advantage of double symmetry, the whole net was used to represent one quarter of the plate.

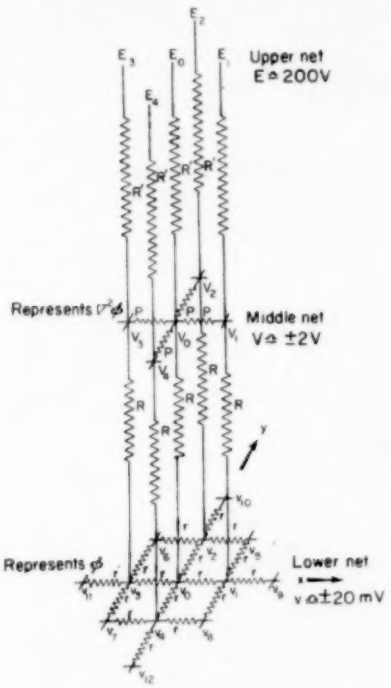

FIG. 3. Resistance network.

On the network an axis of symmetry is automatically ensured by doubling the resistance value of the boundary resistors. In the analogy a potential v on the lower net represents the Airy stress function and the potential V on the middle net represents the sum of the direct stresses $(\sigma_x + \sigma_y)$.

(ii) *Satisfaction of boundary conditions*

The satisfaction of a double boundary condition is required ; for the loaded edge a potential, representing a uniform stress, is applied to the middle net and the Airy stress function, as calculated by the method described in Section 2 (ii), is applied directly to the lower net, again in the form of a potential.

For the free edge $x = \pm a$ the Airy stress function ϕ and its normal gradient $\partial\phi/\partial n$ are specified, and this is analogous to setting the lower net boundary potential to v and its normal derivative to $\partial v/\partial n$. To achieve this, boundary potentials V are set on the middle net and adjusted until v and $\partial v/\partial n$ are brought to the assigned values on the lower net. This involves a type of electrical iteration process but with a little care and experience the desired conditions can rapidly be achieved.

For a hole or a crack the conditions are again that v and $\partial v/\partial n$ are specified. A description of the technique for setting up the boundary conditions on the electrical analogue is to form the subject of a separate paper.

4. Experimental Investigation

Three plane stress problems were investigated, with a rectangular plate of length breadth ratio 3/2. The problems selected were as follows:

(i) Two external cracks; i.e. a simply connected region.

(ii) A central circular hole; i.e. a multiply connected region to which an analytical solution exists for a finite width of plate.

(iii) An internal crack; i.e. a multiply connected region problem similar to that of the circular hole but presenting greater experimental difficulty. No known analytical solution exist, but an analytical solution for an internal crack in an *infinite* plate is available.

(i) *External crack*

The problem considered was that of a flat rectangular plate of length/breadth ratio 3/2 and having two symmetrically disposed cracks each $\frac{3}{16}$ of the plate width. The geometry, boundary and loading conditions of the problem are illustrated in Fig. 1. The half-length of the plate was represented by 48 mesh intervals, and therefore the half-width and each crack length by 32 and 12 units, respectively.

Using the concept of the slender ellipse, described in Section 2 (iii), the Airy stress function can be calculated to be $\phi = Pa\,(a - x)$, where P is the applied stress and $\partial\phi/\partial y = 0$.

The electrically analogous condition was applied to the electrical analogue, and the potentials at nodes on the middle and lower nets were measured as necessary. From the electrical measurements direct and shearing stresses were calculated in the manner described in the Appendix. The stress components σ_x, σ_y and τ_{xy} are shown in Fig. 4. No known theoretical or experimental results were available for comparison.

It should be noted that the stress at the end of the crack should be infinite, since an infinitely fine crack has been represented on the analogue, but, owing to the finite mesh used, the recorded stress at the end of the crack represents the average value of the stress over the area represented by the discrete interval.

As a check on the experiment the average longitudinal stress across a number of sections was calculated from the experimental results and expressed as a percentage of the applied stress. The agreement was good, an error of about 5 per cent in the section containing the crack being reduced in subsequent experiments to less than 2 per cent.

(ii) *Circular hole*

A rectangular plate of the same size as that used in the last experiment was selected, but in place of the external cracks the plate was perforated with a centrally placed circular hole whose diameter was $\frac{7}{3\frac{1}{2}}$ the breadth of the plate. As it was not possible to represent the curved boundary of the hole on the square network mesh, the boundary was considered to coincide with the nearest node. This technique has previously been found to be satisfactory and the result of the present experiment confirms this statement.

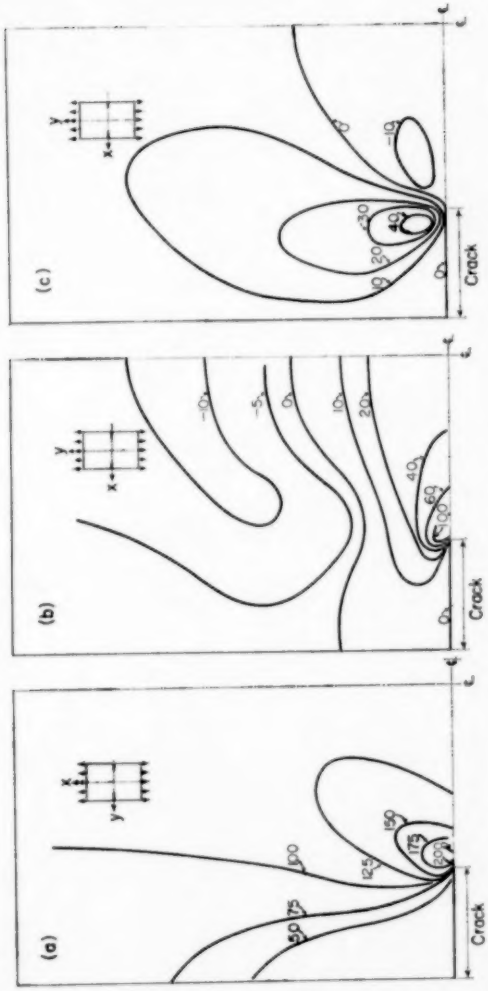

FIG. 4. External crack: stress fields. (a) Direct stress σ_y. (b) Transverse stress σ_x. (c) Shearing stress τ_{xy}. Applied stress = 100.

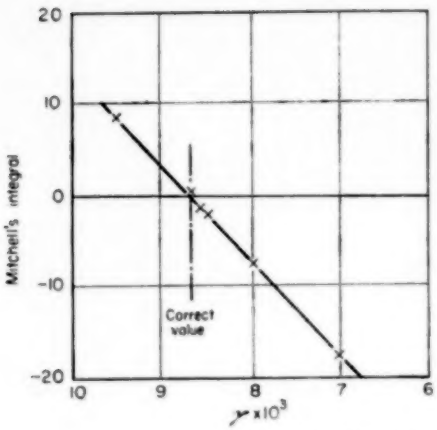

y	Michell's integral
7030	− 17·7
8057	− 7·7
8502	− 2·1
8582	− 1·6
8662	+ 0·03
9486	+ 8·5

Fig. 5. Michell's integral: circular hole.

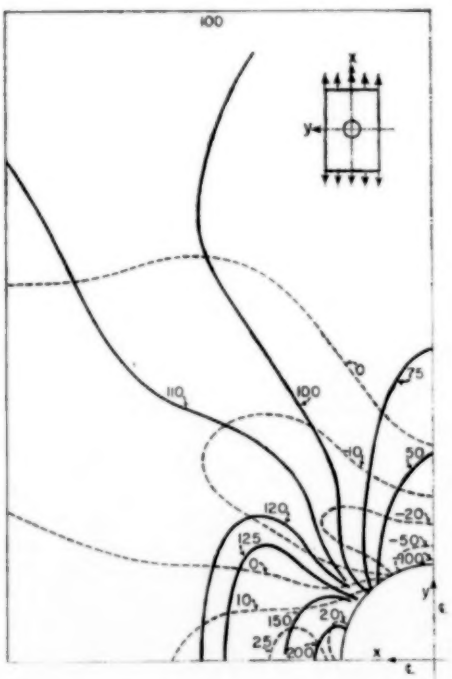

Fig. 6. Circular hole: direct stresses.
——— Direct stress; – – – – Transverse stress σ_θ. Applied stress = 100.

The loading conditions on the external boundary in terms of the Airy stress function are identical to those obtaining in the last problem. As shown in Section 2 (iii) the internal boundary conditions require γ to be constant and its normal derivative to be zero. The correct value of the function satisfies (5).

The iterative process necessary for setting up the internal boundary condition consists in choosing a probable value for the function, setting the condition in the electrical analogue, and measuring the potentials on the middle net in close proximity to the hole in order to evaluate the line integral in (5). Since $\nabla^2 \phi$ represents the middle net potential the line integral is simply the sum of the normal slope of the middle net potentials around the hole. It will thus be seen that only a few measurements need be taken, the rest of the board being left unscanned. The process has to be repeated for several values of the function until (5) it identically satisfied ; the iterative results are shown in Fig. 5. The experimental process was rapid and the correct value for γ was obtained after about five trials, each trial taking less than one hour. The correct value for γ was then set on the network and the field scanned completely. The direct stresses σ_y and σ_x were then calculated in the manner described in the Appendix, the results being shown in Fig. 6.

The tangential stress on the circumference of the hole, as determined by the experiment, has been compared in Fig. 7 with the analytical result obtained by

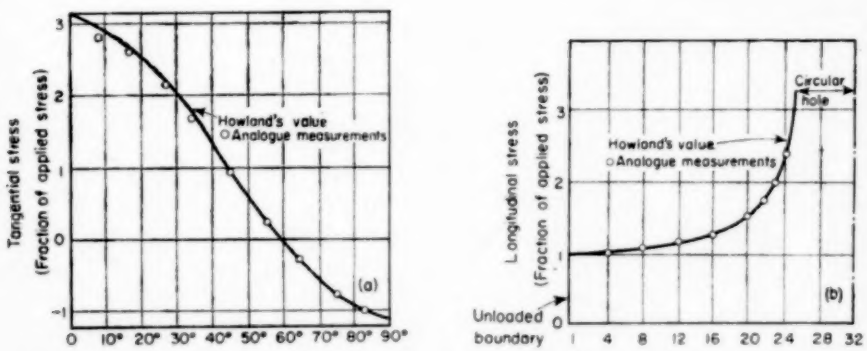

FIG. 7. (a) Tangential stress on circumference of circle. (b) Stress variation on cross section.

HOWLAND (1930) for a plate of finite width and infinite length, containing a circular hole. On the same Figure a comparison between the experimental and theoretical stress variation on the central cross section is given. It will be noted that the agreement in both cases is very good. It is interesting to observe that from a collection of photo-elastic results compiled by HEYWOOD (1952) the maximum tangential stress on the hole is given as 3·04, which lies between the present electrical analogue result of 3·00 and HOWLAND's value of 3·14.

(iii) *Internal crack*

With the same plate size as in the last two experiments an internal crack lying along the horizontal axis of symmetry was considered. Cracks varying in length from $\frac{1}{4}$ to $\frac{5}{8}$ × the width of the plate were considered.

The loading conditions on the external boundary were the same as for the previous experiments, but the method of interpreting the internal boundary loading condition varied from that for the circular hole. The difficulty lies in the fact that the integral condition (5), which has to be applied to the internal boundary, cannot be used satisfactorily because the infinite stress which should arise at the

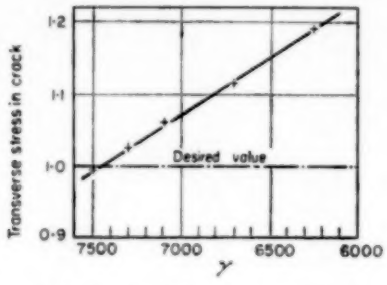

Fig. 8. Transverse stress for trial values of γ. All values are expressed as fractions of the applied stress.

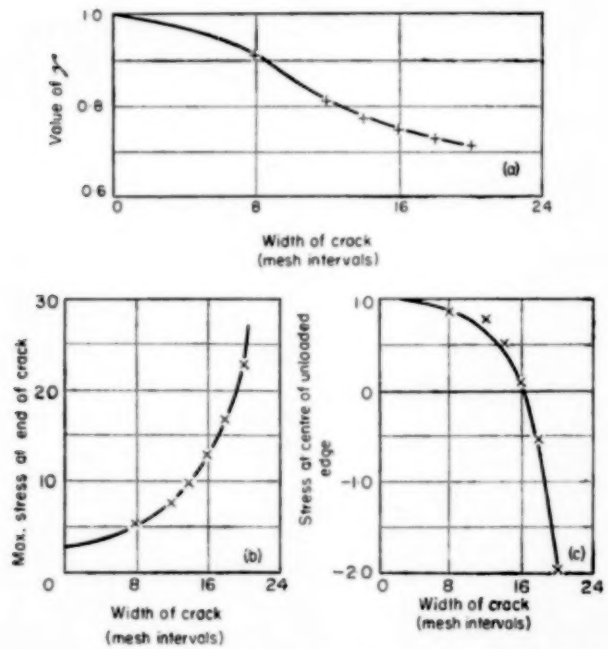

Fig. 9. (a) Variation of γ with width of crack. (b) Maximum stress. (c) Centre of unloaded edge.

end of the crack cannot be represented in the analogue because of the finite mesh of the network. An alternative condition was sought and it was decided to use the condition that the transverse stress at the centre of the crack is a compressive stress numerically equal to the applied tensile stress. This assumption would appear to be justified if the crack is considered to be an ellipse with an infinitely

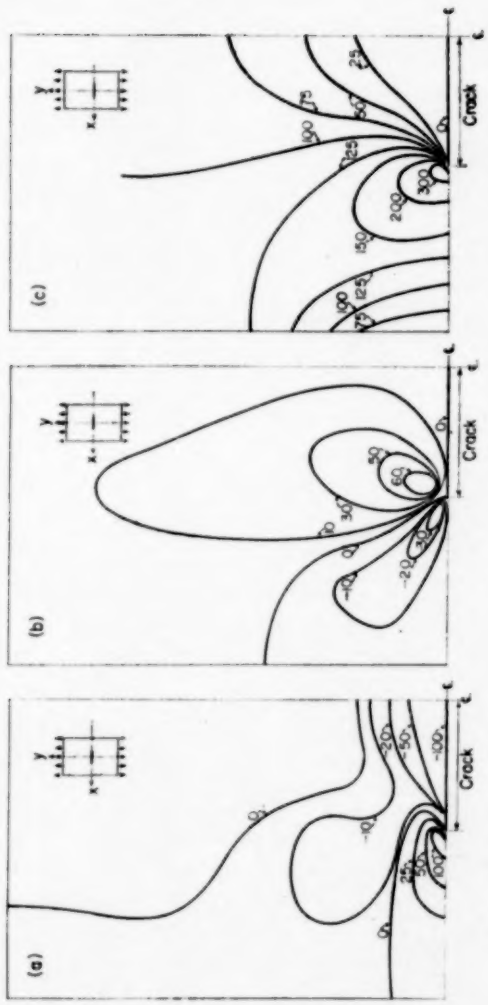

FIG. 10. Internal crack: stress fields. (a) Transverse stress σ_x. (b) Shearing stress τ_{xy}. (c) Direct stress σ_y. Applied stress $\sigma_y = 100$.

small minor axis, in which case it is well known theoretically that this stress condition is applicable. Apart from this, the iteration process for setting up the internal boundary condition was identical to that used for the circular hole. The manner in which the transverse stress varies with γ is shown in Fig. 8; it should be noted that the correct value of γ occurs when the transverse stress is unity.

Six crack widths were investigated by this method. For each experiment the value of γ, the maximum stress at the end of the crack, and the stress at the free unloaded edge on the centre of the plate normal to the direction of the applied stress, were determined and are plotted in Fig. 9.

During the experiments it was found that a crack exceeding $\frac{5}{6}$ of the plate width could not be set up on the electrical analogue because the stress at the end of the crack was very large, and could not be represented by an equivalent electrical potential.

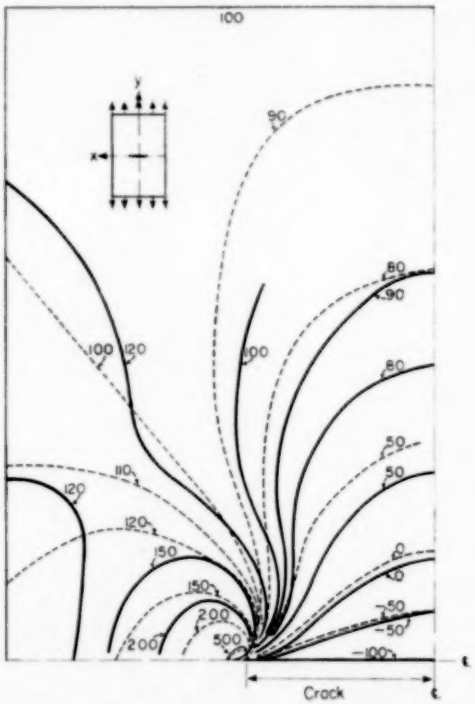

Fig. 11. Internal crack: principal stresses. —— Sum of principal stresses from analogue; - - - - Sum of principal stresses for infinite plate. Applied stress = 100.

It will be appreciated that the stress at the end of the crack should, for every crack length, be infinite but owing to the mesh size, as explained previously, finite stresses were obtained. Possibly the network may be considered to be acting analogously to a metallic plate which will experience plastic yielding at the edge of the crack.

A detailed analysis of the stresses for a crack width of $\frac{7}{16} \times$ the plate width are shown in Fig. 10. It is of interest to note that the average direct stress at the

section containing the crack, as found from the experiment, was 98·5 per cent of the applied stress. Fig. 11 gives a comparison between the analogue results for a finite plate and the theoretical results for an infinite plate (FROST and DUGDALE 1958)*. For the purpose of making a comparison the sum of the principal stresses have been presented in Fig. 11. It will be observed that a reasonable agreement is obtained in the region of the crack but, as would be anticipated, appreciable differences occur in the vicinity of the external boundary. The results of a photo-elastic experiment made at the University of Washington (CHENG *et. al.* 1959) on a rectangular plate with a central crack, but of different proportions to the plate considered here, showed the same trend in the distribution of the principal stresses at points remote from the crack. The agreement in the region of the crack was poor since the crack was formed by making a saw cut, the thickness of the cut being $\frac{1}{24}$ of the width of the crack as compared with the infinitely thin crack assumed for the electrical analogue. The mesh length used for the electrical analogue was $\frac{1}{16}$ that used in the photo-elastic experiment.

5. CONCLUSIONS

Within the limitations imposed by the size of the network the results obtained from the electrical analogue appear to be reasonable, and good agreement with the few analytical results available was obtained. In the case of a crack, the major limitations in the method lies in the inability to represent the infinite stress at the end of the crack, whereas for a circular hole this limitation does not apply and excellent results were obtained. It is probable that a closer approximation to the true results for a crack could be obtained if a graded mesh were constructed or if, in a future experiment, the results obtained for a portion of the field were reset to a finer mesh (PALMER and REDSHAW 1957). No attempt was made to introduce plastic yielding in the neighbourhood of the crack although, as mentioned in Section 4 (iii), this may be inherent in the electrical analogy.

It is considered that an investigation into the possibility of introducing plasticity into the analogy is very desirable in view of the importance of plastic yielding in problems of crack propagation.

REFERENCES

CHENG, Y. F., MILLS, D. B. and DAY, E. E.	1959	*Trend Engng Univ. Wash.* **11**, 15.
FROST, N. E. and DUGDALE, D. S.	1958	*J. Mech. Phys. Solids* **6**, 92.
HEYWOOD, R. B.	1952	*Designing by Photoelasticity*, p. 268, (Chapman & Hall).
HOWLAND, R. J. C.	1930	*Phil. Trans. Roy. Soc.* A **229**, 49.
MICHELL, J. H.	1899	*Proc. Lond. Math. Soc.* **31**, 100.
PALMER, P. J. and REDSHAW, S. C.	1955 1957	*Aero. Quart.* **6**, 13. *J. Sci. Inst.* **34**, 307.
PRAGER, W.	1946	*Quart. Appl. Math.* **111**, 377.
SOUTHWELL, R. V.	1948	*Proc. Roy. Soc.* A **193**, 147.

*Approximate formulae were derived by DUGDALE and quoted by FROST and DUGDALE. DUGDALE recorded that the formulae were previously given by T. POSCHL, *Math. Zeit.* 11, 89 (1912) and A. TIMPE, *Math. Zeit.* 17, 189 (1923).

Appendix

Calculation of Direct and Shearing Stresses from the Stress Function

Values of the stress function are obtained directly from the electrical analogue and these values have to be doubly differentiated to give the stresses. Numerous finite difference formulae exist for this purpose but it has been found that the following five point formula, written below, gives better results when applied to analogue readings than the more usual formulae, although the truncation error is actually greater. The purpose of the formula is to make the errors in the electrical readings of the same order as the truncation errors

$$h^2\left(\frac{\partial^2\phi}{\partial x^2}\right)_0 = \tfrac{1}{7}(2\phi_{11} - \phi_3 - 2\phi_0 - \phi_1 + 2\phi_9)$$

where the suffices denote the nodes of the networks as defined in Fig. A1.

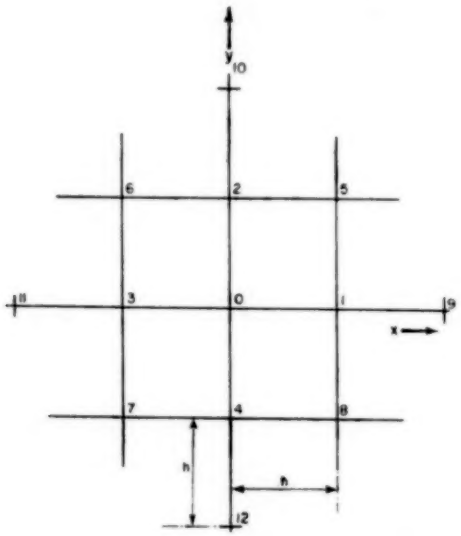

Fig. A1.

In the neighbourhood of boundaries the above formula cannot be used but since the middle net potentials equal $\partial^2\phi/\partial x^2 + \partial^2\phi/\partial y^2$ and since $\partial^2\phi/\partial y^2$ can still be calculated by the corresponding formula, $\partial^2\phi/\partial x^2$ may be obtained by subtraction. For the computation of the shearing stress the conventional formula

$$h^2\left(\frac{\partial\phi}{\partial x\,\partial y}\right)_0 = \tfrac{1}{4}(\phi_5 - \phi_6 + \phi_7 - \phi_8)$$

was used.

On occasions, recourse to graphically smoothing of the differentials was found to be necessary.

J. Mech. Phys. Solids, 1960, Vol. 8, pp. 187 to 193. Pergamon Press Ltd., London. Printed in Great Britain

TRAVELLING CRACKS IN ELASTIC MATERIALS UNDER LONGITUDINAL SHEAR*

By F. A. McClintock and S. P. Sukhatme
Department of Mechanical Engineering, Massachusetts Institute of Technology

(*Received* 3rd *May*, 1960)

Summary

The solution for the stress field around the tip of a crack subjected to longitudinal shear (anti-plane strain) and travelling with a constant velocity in an elastic medium, as given by Bilby and Bullough (1954), has been extended to a configuration analogous to the tensile case studied by Craggs (1960). As in the case of tensile cracks, the applied stress required for constant velocity is lower for higher crack velocity and there is a critical velocity approximately 0·6 times that of the shear wave velocity above which the crack will branch. Similar stress levels are found using two different fracture criteria: the Griffith energy criterion and the criterion of critical shear strain averaged over a critical area.

1. Introduction

Since the analysis of stress and strain around cracks subjected to longitudinal shear (anti-plane strain) is much easier than that around cracks subjected to tension, one may be tempted to extend the results of an analysis of the shear case to the tensile case by analogy. A comparison of the results when both modes of loading can be analysed, is helpful in determining the validity or the limitations of such an analogy. Two configurations of the travelling crack subjected to tension have been studied by Yoffé (1951) and Craggs (1960), and in this paper these results will be compared with those for the corresponding configurations subjected to shear. In addition, the analysis for longitudinal shear will be used to compare the energy criterion for fracture due to Griffith (1920) with the criterion of critical average strain in a local area, as used by Neuber (1937) and McClintock (1958). While the two criteria turn out to be similar in the elastic case, the criterion of a limiting value of the local average shear strain seems more appropriate for use when plastic deformation is present and the strain history becomes important.

Because of mathematical difficulties associated with the growing crack, it is convenient to study configurations in which the length of the crack or stressed region remains constant even though such configurations are physically rather implausible. The configuration of Fig. 1, in which the crack reseals itself spontaneously, is analogous to one considered by Yoffé (1951). In the configurations of Figs. 2 and 3 it is supposed that the crack length l is maintained constant by

*This research was supported by the United States Air Force, through the AF Office of Scientific Research and Development Command under Contract No. AF 18 (600)-957. Reproduction is permitted for any purpose of the United States government.

removing material at the face a distance l behind the tip of the crack at the rate at which the crack is progressing. The stress fields of Figs. 1 and 2 are identical since there can be no shear stress on the plane $X = -l$ in Fig. 1, while the only difference between the fields of Figs. 2 and 3 is a constant shear stress, τ_l. The

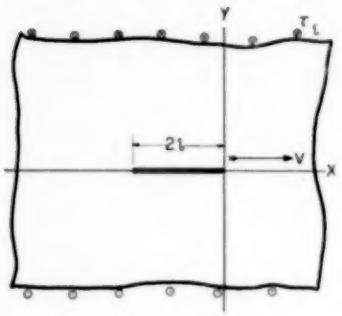

Fig. 1. Travelling crack under external stress.

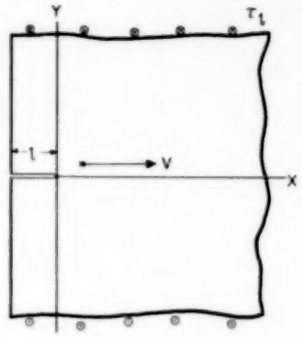

Fig. 2. Crack from eroding face under external stress.

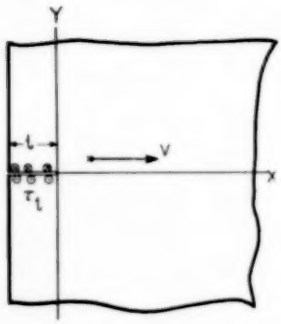

Fig. 3. Crack from eroding face under internal stress.

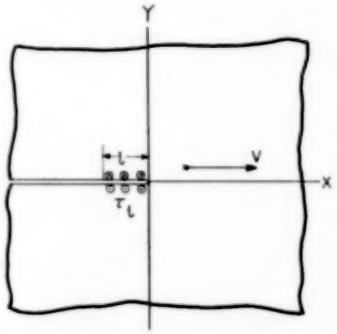

Fig. 4. Internal stress following tip of infinite crack.

stress distribution in these cases has been given by Bilby and Bullough (1954). The configuration of Fig. 4 is analogous to that studied by Craggs (1960). The crack is semi-infinite, the shear stress τ_l being applied over a length l behind the tip. In all cases the crack is supposed to be moving to the right with a constant velocity V in an elastic medium of density ρ and modulus of rigidity μ.

2. Stress Distributions

(a) *For the configurations of Figs.* 1, 2 *and* 3

The local distribution of stress around the tip of the crack can be found from Bilby and Bullough (1954) in terms of the applied shear stress τ_l, the crack dimension l, a constant factor m which in this case turns out to be $1/\sqrt{2}$ and a factor β defined by

$$\beta = \sqrt{1 - (V/c_2)^2}, \tag{1}$$

where c_2 is the shear wave velocity given by $c_2 = \sqrt{(\mu/\rho)}$. The resulting expression is

$$\left.\begin{aligned} \tau_Y &= \tau_l \cdot m \cdot \sqrt{\left(\frac{l}{2\beta}\right)} \cdot \left[\frac{\sqrt{(X^2/\beta^2) + Y^2} + (X/\beta)}{(X^2/\beta^2) + Y^2}\right]^{\frac{1}{2}}, \\ \tau_X &= -\frac{1}{\beta} \cdot \tau_l \cdot m \cdot \sqrt{\left(\frac{l}{2\beta}\right)} \cdot \left[\frac{\sqrt{(X^2/\beta^2) + Y^2} - (X/\beta)}{(X^2/\beta^2) + Y^2}\right]^{\frac{1}{2}}. \end{aligned}\right\} \tag{2}$$

(b) *For the configuration of Fig. 4*

The solution to this is found by transforming the dynamic problem into a static problem, which is solved with the aid of a conformal mapping.

In terms of coordinates moving with the crack at constant velocity, the equilibrium equation relates the shear stress gradients to the acceleration of the warping displacement, w:

$$\frac{\partial \tau_{XZ}}{\partial X} + \frac{\partial \tau_{YZ}}{\partial Y} = \rho \frac{\partial^2 w}{\partial t^2} = \rho V^2 \frac{\partial^2 w}{\partial X^2}. \tag{3}$$

Expressing the stresses in terms of strains, and the strains in terms of displacements and making the substitution

$$x = \frac{X}{\left[1 - (\rho V^2/\mu)\right]^{\frac{1}{2}}} = \frac{X}{\beta}, \qquad y = Y, \tag{4}$$

reduces (3) to Laplace's equation

$$\frac{\partial^2 w}{\partial x^2} + \frac{\partial^2 w}{\partial y^2} = 0, \tag{5}$$

subject to the boundary condition $\partial w/\partial y = \tau_l/\mu$ along $-l/\beta < x < 0$.

Thus the dynamic problem has been reduced to one of statics. It is most easily solved in terms of the stress function, ϕ, defined through

$$\tau_{xz} = \frac{\partial \phi}{\partial y}, \qquad \tau_{yz} = -\frac{\partial \phi}{\partial x}. \tag{6}$$

For equilibrium ϕ must satisfy Laplace's equation. The boundary conditions are

$$\left.\begin{aligned} &-l/\beta < x < 0, && \phi = -\tau_l (x + l/\beta), \\ &-\infty < x < -l/\beta, && \phi = 0, \\ &\text{at} \quad \infty, && \phi = 0. \end{aligned}\right\} \tag{7}$$

With the loaded length taken as unity for simplicity, the given region is mapped into a unit circle in the plane $w = u + iv$ by the transformation

$$z = \tfrac{1}{4}\left(\frac{w+1}{w-1}\right)^2. \tag{8}$$

In the notation of Fig. 5, the boundary conditions are

$$\phi(1, \psi) = 0 \quad \text{on the arc ADC,}$$

and

$$\phi(1, \psi) = -\tau_l \left[1 - \tfrac{1}{4}\cot^2(\psi/2)\right] \text{ on the arc ABC.}$$

The tip of the crack has been mapped into the point B. In the vicinity of B, which is non-singular, the first order approximation to the solution of Laplace's equation will be a plane whose equation can be found by letting $u = -1 + \epsilon$ and $v = 0$. Evaluation of the Poisson integral formula gives

$$\phi(\epsilon) = -\tau_l\left(1 - \frac{\epsilon}{\pi}\right), \tag{10}$$

and ϕ is locally independent of v.

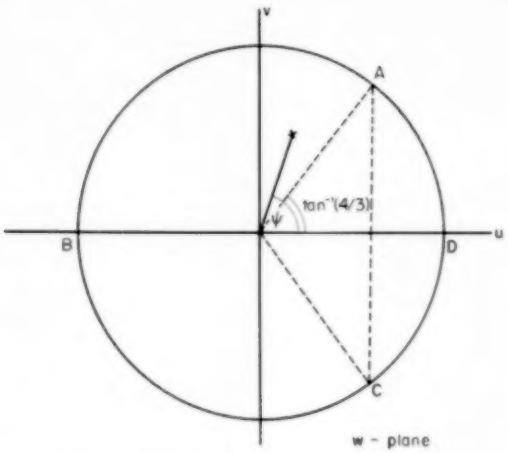

Fig. 5. Notation for transformed problem.

Transforming back to the x–y plane and using polar coordinates r and θ gives

$$\tau = \tau_l \cdot \frac{2}{\pi} \cdot \sqrt{\left(\frac{l/\beta}{r}\right)} \quad \text{and} \quad \delta = \theta/2, \tag{11}$$

where δ is the angle made by the total shear stress τ with the y-axis, the sense being positive in a counter-clockwise direction.

Since the stress distribution given by (11) is identical to that for the finite crack in the static case (Bilby and Bullough) with the exception that the value of the constant m is different, the dynamic state of stress around the tip of the infinite crack will also be given by (2) with a value of $m = 2/\pi$. Equation (2) indicates that the shear stress on the plane $Y = 0$, directly ahead of the moving crack, is unaffected by the crack velocity but that the shear stresses elsewhere are increased as a result of increasing crack velocities.

3. Branching Velocity

Following Yoffé (1951) it will be assumed that a crack will fork whenever the maximum shear stress is attained on two radial planes on either side of the plane of the crack rather than on the plane of the crack itself. When (2) is transformed to give the shear stress on a radial plane, $\tau_{\theta Z}$, (in terms of polar coordinates R, Θ) the relation plotted in Fig. 6 is obtained. For velocities greater than 0·57 c_2 where

c_2 denotes the shear wave velocity, the crack will tend to fork. This is similar to the value of 0·6 obtained by YOFFÉ (1951) and also to the values of 0·612 to 0·667 (as Poisson's ratio varies from $\frac{1}{4}$ to $\frac{1}{3}$) given by CRAGGS (1960) for the infinite crack with internal pressure following its tip.

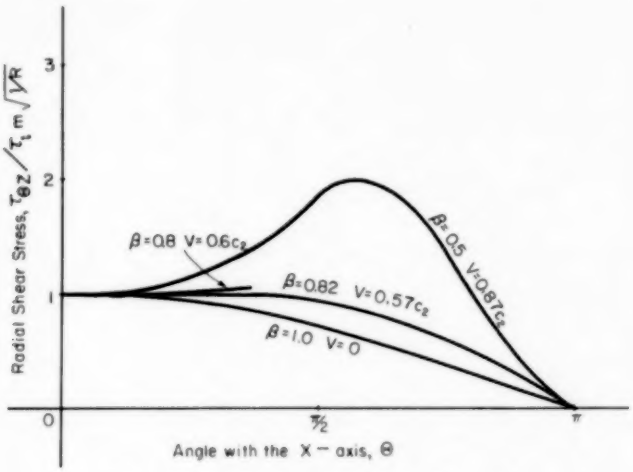

FIG. 6. Distribution of radial shear stress.

4. APPLIED STRESS FOR CRACK PROPAGATION

The applied stress required to maintain a constant velocity of the crack can be estimated from either the Griffith energy criterion or the criterion of a critical average strain over a certain region.

Griffith energy criterion

In order to apply the criterion the energy flowing into the region around the tip of the crack per unit increase in crack length per unit height in the Z-direction will be equated to twice the surface energy, α. We have

$$2\alpha = \int \tau \frac{\partial w}{\partial X} \cdot \mathbf{ds} \tag{12}$$

where the integral is taken around the boundary of an area enclosing the tip of the crack. Choosing, for the sake of convenience, the shape of the region around the crack tip to be a square with the tip of the crack as its centre and using (2), we get

$$l\tau_l^2 = \frac{\alpha\mu/m^2}{(1/\beta^3)\log\left\{\beta\left[1+\sqrt{1+(1/\beta^2)}\right]\right\} + (1/\beta)\tan^{-1}(1/\beta)}. \tag{13}$$

Criterion of local average shear strain

According to this criterion [NEUBER (1937) and MCCLINTOCK (1958)], fracture will occur when the average shear strain over a distance related to the structure of the material along the line directly ahead of the tip of the crack reaches some

critical value γ_f. In an elastic material this structural distance is taken to be an atomic or molecular spacing, a. Applying this criterion to (2) we get

$$l\tau_l^2 = \frac{a\mu^2\gamma_f^2}{4m^2} = \text{constant}. \tag{14}$$

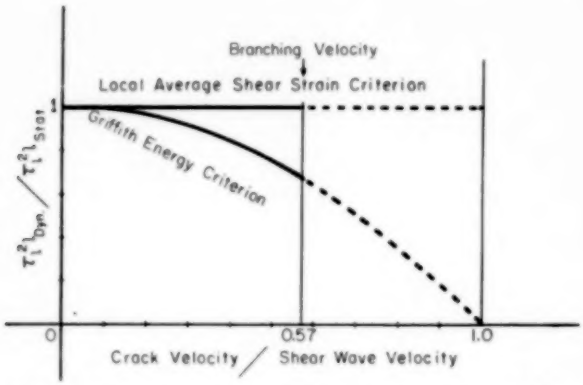

Fig. 7. Variation of applied shear stress with crack velocity.

Comparison between the two criteria

The two criteria can be compared if a relation between γ_f and α is obtained on physical grounds. Continuing with a linear stress–strain relation, the energy per unit area between two crystallographic planes a distance a apart is $a\mu\gamma_f^2/2$. Equating this to twice the surface energy since two surfaces are formed, solving for γ_f, and substituting in (14) yields

$$l\tau_l^2 = \frac{\mu\alpha}{m^2}. \tag{15}$$

In the static case the Griffith criterion (13) reduces to

$$l\tau_l^2 = 0{\cdot}60\,\frac{\mu\alpha}{m^2}. \tag{16}$$

Thus the two criteria give similar results. Some of the difference is no doubt due to the non-linear stress–strain relation at high strain.

In the dynamic case the energy criterion indicates a decrease in applied stress with increasing crack velocity, while the local average shear-strain criterion indicates no effect of velocity provided the average is taken along the line directly in front of the crack (Fig. 7). If, however, the average is taken over a region around the tip, the increase in stress at the sides of the crack will again result in a decrease in required applied stress with increasing crack velocity. The physical explanation for this decrease from the energy point of view seems to be that, if the applied stress were constant, the displacements would be greater at higher crack velocity so that energy would be fed in at a higher rate per unit crack growth. From the strain point of view the decrease in required applied stress is due to the higher local stresses and strains at either side of the tip of the crack.

5. Conclusion

For shear cracks the dependence of applied stress on crack velocity and the tendency of forking to occur above a given velocity are shown to be similar to what has previously been found for tensile cracks. Thus, in more difficult problems, such as the growing crack rather than the travelling crack, or the elastic–plastic case, there is reason to hope that a simpler shear analysis will provide some insight into the more difficult but more practical problem of tension. With the aid of the shear analysis two fracture criteria, the Griffith energy criterion and the local average shear strain criterion, are shown to yield similar results.

References

Bilby, B. A. and Bullough, R. 1954 *Phil. Mag.* **45**, 631.

Craggs, J. W. 1960 *J. Mech. Phys. Solids* **8**, 66.

Griffith, A. A. 1920 *Phil. Trans. Roy. Soc.* A **221**, 163.

McClintock, F. A. 1958 *J. Appl. Mech.* **25**, 582.

Neuber, H. 1937 *Kerbspannungslehre* (Springer, 2nd Ed. 1958).

Yoffé, E. H. 1951 *Phil. Mag.* **42**, 739.

J. Mech. Phys. Solids, 1960, Vol. 8, pp. 194 to 206. Pergamon Press Ltd., London. Printed in Great Britain

SOME KINETIC CONSIDERATIONS OF THE GRIFFITH CRITERION FOR FRACTURE—I

EQUATIONS OF MOTION AT CONSTANT FORCE

By J. P. Berry
General Electric Research Laboratory, New York

(*Received* 10*th May*, 1960)

Summary

The implications of the Griffith criterion for fracture in tension and cleavage have been investigated in the region where the crack is moving. An anomaly in behaviour is shown to arise if the Griffith criterion is assumed, *a priori*, to define the critical condition for the beginning of crack growth. The equations of motion have therefore been derived initially without reference to the criterion for fracture, and the effect of approaching the Griffith condition determined by adjustment of a dimensionless parameter. It is concluded that the details of the motion of a crack are determined by the stress condition existing at the point of fracture, and that the observed critical stress is (infinitesimally) greater than that given by the Griffith criterion and is probably determined by the size of the defect in the sample and the rate of straining.

1. Introduction

Since its formulation in 1921, the Griffith criterion for fracture (Griffith 1921, 1924) has found extensive use in the interpretation of the ultimate properties of materials. Though in its original form it referred specificially to fracture under a tensile stress, it has also been applied to other types of stress systems, notably cleavage (Benbow and Roesler 1957 ; Gilman 1959). In most studies, the criterion has usually been used to define the critical condition for fracture, and less attention seems to have been paid to the behaviour of the moving crack. Some of the treatments of this phase of the fracture process which have been published appear to be in error (Gilman 1959 ; Roberts and Wells 1954).

Under the usual conditions for the determination of the ultimate properties of a material, the sample, which is presumed to contain an adventitious crack, is subjected to forces of increasing magnitude until a critical point is reached, at which the crack spontaneously increases in size, and fracture ensues. In the present treatment, up to the critical point, the system is considered to possess only potential energy, and the increase in potential energy above the ground state will, of course, be equal to the work done on the system. Beyond the critical point, the system will possess both potential and kinetic energy. At any stage the potential energy and the work done on the system can be expressed in terms of the parameters of the system, and by a simple energy balance the kinetic energy can be taken as the difference between the work done on the system and the increase

in potential energy. From the expression for the kinetic energy, equations for the velocity (v_c) and acceleration (a_c) of the crack, as a function of its length, can be derived. Integration of the velocity equation gives the length–time relation for the crack. If the Griffith criterion is assumed, *a priori*, to define the critical condition for fracture, this last operation gives an integration constant which is infinite when the appropriate boundary conditions are inserted. To determine the reason for this result, the equations of motion have been derived initially without reference to the criterion for fracture, and the effect of approaching the critical condition corresponding to the Griffith criterion determined by adjustment of a dimensionless parameter. This general approach can be applied to both the tensile and cleavage types of experiment, as is demonstrated below.

2. Fracture in Tension

Following Griffith the sample is taken as a sheet of unit thickness containing a crack of length $2c_0$. Since only surface and strain energies are to be considered, the potential energy ground state is $H_0 = S_0 + 4\gamma c_0$, where S_0 represents the surface energy in the absence of the crack, and γ is the specific surface energy, i.e. the energy required to create unit area of surface as the crack increases in length. As shown by Griffith, when subjected to a stress σ, the strain energy of the sheet is increased because of the presence of the crack by an amount $\pi\sigma^2 c_0^2/E$, where E is the Young's modulus. Thus the total strain energy of the sheet is

$$\frac{A\sigma^2}{2E} + \frac{\pi\sigma^2 c_0^2}{E} = \frac{\sigma^2}{2E}(A + 2\pi c_0^2) \tag{1}$$

where A is the (infinite) area of the sheet. It is clear from the form of the strain energy expression that the effective elastic modulus of a sheet containing a crack of length $2c_0$ is $AE/(A + 2\pi c_0^2)$.

At the point of incipient fracture the potential energy is

$$H_1 = S_0 + 4\gamma c_0 + \frac{\sigma_c^2}{2E}(A + 2\pi c_0^2). \tag{2}$$

The work done on the sample at this stage is

$$W_1 = \frac{\sigma_c^2}{2E}(A + 2\pi c_0^2). \tag{3}$$

The crack can now increase in length while the applied stress remains constant. At any subsequent stage, therefore, the total energy is

$$H_2 = S_0 + 4\gamma c + \frac{\sigma_c^2}{2E}(A + 2\pi c^2) + K \tag{4}$$

where $2c$ is any arbitrary crack length (greater than $2c_0$), and K is the kinetic energy. Since the modulus of the sample has decreased, the constant stress has moved through a distance given by the change of strain. The total work done is therefore

$$W_2 = W_1 + A\sigma_c(\epsilon - \epsilon_c)$$

where ϵ is the strain corresponding to the crack length $2c$, and ϵ_c is the critical strain at the point of incipient fracture. Then

$$W_2 = \frac{A\sigma_c^2}{2E} + \frac{\pi\sigma_c^2}{E}(2c^2 - c_0^2). \tag{5}$$

Writing the energy balance as $H_2 = H_0 + W_2$, we obtain

$$K = \frac{\pi\sigma_c^2}{E}(c^2 - c_0^2) - 4\gamma(c - c_0). \tag{6}$$

The quantity $4E\gamma/\pi\sigma_c^2$ defines a length which may be taken as some multiple of the original crack length $2c_0$. Thus

$$nc_0 = \frac{4E\gamma}{\pi\sigma_c^2}$$

where n is a numerical factor. Then

$$K = \frac{\pi\sigma_c^2 c^2}{E}\left(1 - \frac{c_0}{c}\right)\left[1 - (n-1)\frac{c_0}{c}\right]. \tag{7}$$

MOTT (1948) has demonstrated that on dimensional grounds, the kinetic energy of the system must have the form

$$K = \frac{k\rho\sigma_c^2 c^2 v_c^2}{2E^2} \tag{8}$$

where k is a numerical constant, ρ is the density of the material, and v_c is the velocity of the crack. Inserting (8) in (7) and solving for v_c yields

$$v_c^2 = \frac{2\pi}{k}\frac{E}{\rho}\left(1 - \frac{c_0}{c}\right)\left[1 - (n-1)\frac{c_0}{c}\right]. \tag{9}$$

It is shown below that $n \leqslant 2$, and hence when c is large ($\ll c_0$) the velocity of the crack will tend to a limiting maximum value

$$v_m = \left(\frac{2\pi}{k}\right)^{\frac{1}{2}}\left(\frac{E}{\rho}\right)^{\frac{1}{2}}.$$

This expression is the same as that deduced by ROBERTS and WELLS (1954) from the Griffith criterion. Also, of course, $v_c = 0$ when $c = c_0$.

From (9) we obtain, by differentiation

$$a_c = \frac{\pi}{k}\frac{E}{\rho}\frac{c_0}{c^2}\left[n - 2(n-1)\frac{c_0}{c}\right] \tag{10}$$

where a_c is the acceleration of the crack, and when $v_c = 0$ $(c = c_0)$

$$a_c = \frac{\pi}{k}\frac{E}{\rho}\frac{(2-n)}{c_0}.$$

Hence $n \leqslant 2$.

From (6) the equation of motion of the crack is

$$a_c + \frac{v_c^2}{c} = \frac{\pi}{k}\frac{E}{\rho}\frac{1}{c}\left[2 - n\frac{c_0}{c}\right]. \tag{11}$$

Clearly (9) is a partial solution of the equation of motion, and (9) itself can be integrated to give the relation between the length of the crack and time in a general form:

$$\left.\begin{aligned} \frac{v_m}{c_0}t &= (\alpha-1)^{\frac{1}{2}}\left[\alpha-(n-1)\right]^{\frac{1}{2}} + n\ln\left\{(\alpha-1)^{\frac{1}{2}}+\left[\alpha-(n-1)\right]^{\frac{1}{2}}\right\} \\ &\qquad - \frac{n}{2}\ln(2-n); \\ v_m &= \left(\frac{2\pi}{k}\right)^{\frac{1}{2}}\left(\frac{E}{\rho}\right)^{\frac{1}{2}}, \qquad \alpha = \frac{c}{c_0}. \end{aligned}\right\} \tag{12}$$

The above equations have been derived without reference to a particular criterion for fracture, which merely serves to define the value of n.

3. Criterion for Tensile Fracture

In considering the fracture process from the standpoint of the kinetic energy, as given by (6), the half-length of the crack c_0 becomes critical for a particular value of stress σ_c in that the kinetic energy becomes positive, and increases for all values of c greater than c_0. The terms of the kinetic energy equation may be rearranged thus:

$$K = \frac{\pi\sigma_c^{\,2}c^2}{E} - 4\gamma c - \left(\frac{\pi\sigma_c^{\,2}c_0^{\,2}}{E} - 4\gamma c_0\right). \tag{6a}$$

Since $K = 0$ when $c = c_0$, and since $c \geqslant c_0$, the value of c_0 is given by the intersection of the abscissa and the ascending part of the plot of $(\pi\sigma_c^{\,2}c^2/E - 4\gamma c)$ versus c. According to the Griffith criterion, this point of intersection is the minimum in the curve, and corresponds to $n = 2$ (Fig. 1).

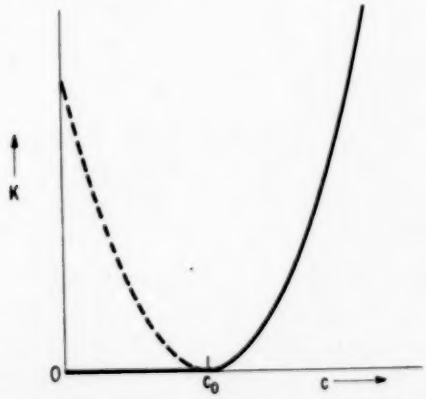

Fig. 1. Griffith condition for fracture in tension.

Assuming the Griffith criterion for fracture, the equations of motion can now be written explicitly:

$$v_c = v_m\left(1 - \frac{c_0}{c}\right), \tag{9a}$$

$$a_c = v_m^2 \cdot \frac{c_0}{c^2}\left(1 - \frac{c_0}{c}\right), \tag{10a}$$

and $a_c = 0$ when $v_c = 0$ $(c = c_0)$;

$$a_c + \frac{v_c^2}{c} = \frac{v_m^2}{c}\left(1 - \frac{c_0}{c}\right). \tag{11a}$$

A difficulty arises when the appropriate value of n is inserted into (12), since the integration constant then becomes infinite. The physical interpretation of this effect arises from the fact that the point defined by the Griffith criterion represents

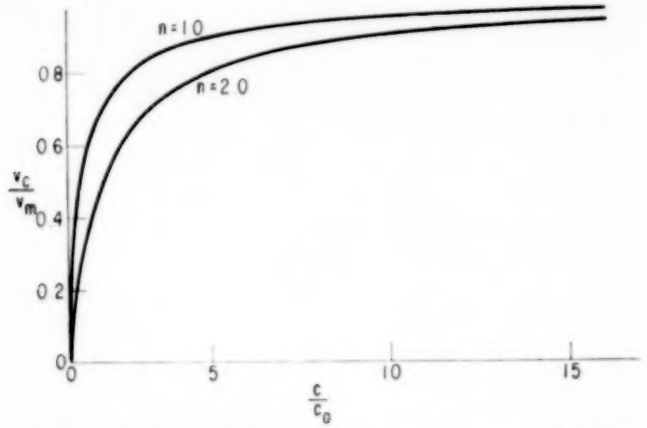

FIG. 2. Theoretical crack velocity–crack length relations at constant tensile stress

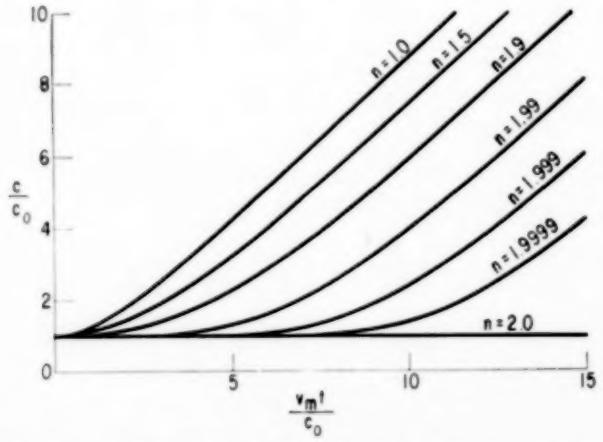

FIG. 3. Theoretical crack length–time relations at constant tensile stress.

an (unstable) equilibrium, and that the sample must be subjected to a stress infinitesimally greater than the critical Griffith value before the crack begins to increase in length. Thus for the Griffith criterion, since $n = 2$, both v_c and a_c are zero when $c = c_0$. Since, in practice, the stress on the sample is continuously

increased until the sample breaks, the observed ultimate stress σ_c will be greater than that defined by the Griffith criterion σ_g, and it is clear that the value of n must then be less than two. The actual value is determined by the magnitude of σ_c since

$$n\sigma_c^2 = \frac{4E\gamma}{\pi c_0} = 2\sigma_g^2.$$

Hence

$$n = \frac{2\sigma_g^2}{\sigma_c^2}.$$

As shown above, the detailed behaviour of the moving crack depends on n, and hence on the discrepancy between σ_c and σ_g. This is exemplified in Figs. 2 and 3.

It has been demonstrated that the effective modulus of a sheet containing a crack of length $2c_0$ is $AE/(A + 2\pi c_0^2)$, and since the Griffith criterion is defined by $\sigma_g^2 = 2E\gamma/\pi c_0$, the relation between stress and strain for this condition is

$$\epsilon_g = \frac{\sigma_g}{E} + \frac{8E\gamma^2}{A\pi\sigma_g^3}. \tag{13}$$

This equation gives the locus of the Griffith condition for fracture and the form of the relation is illustrated in Fig. 4. The significance of the locus is that the

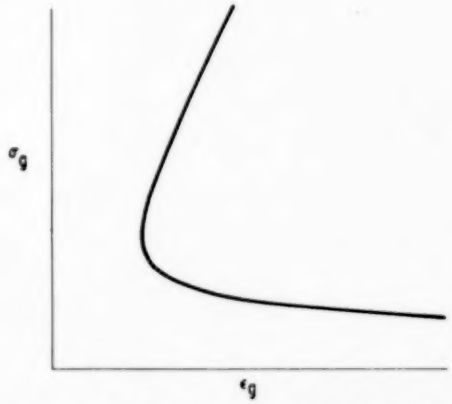

FIG. 4. Locus of the Griffith condition in tension.

Griffith criterion for fracture is satisfied at the point where the stress–strain curve for the sample intersects the locus, and for normal samples the point of intersection will be in the region where the slope of the locus is positive. It is plausible, therefore, that the discrepancy between σ_c and σ_g will be related to the angle θ between the two curves at this point. This angle is a monotonic function of the length $2c_0$ of the crack in the sample, and, on this basis, it would be predicted that the value of n will approach the ideal value of two as the length of the crack increases to the point where $\theta = \frac{1}{2}\pi$. As indicated in Fig. 3 and equation (10) this prediction implies that an initially small crack in a sample should have a high initial acceleration, and vice versa. Such a dependence of the mode of crack propagation on

initial size has been noted in Plexiglas. It would also be expected that the rate of stressing or straining would have an influence on n and hence on the behaviour of the moving crack.

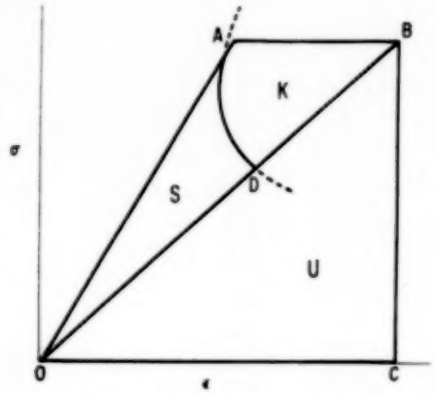

FIG. 5. Distribution of energy in a tensile fracture process.

A further interesting property of the locus of the Griffith condition is illustrated in Fig. 5. In the type of experiment already considered, a sample containing a crack of length $2c_0$ is extended to fracture, and the ultimate stress maintained constant as the crack increases in length. The stress–strain curve of the original sample is given in Fig. 5 by OA. At the point A the crack begins to increase in length, and at an arbitrary later stage the condition of the system is represented by the point B in the Figure. Clearly, the work performed on the system is given by the area OABC. The line OB is the stress–strain curve for the sample at the arbitrary later stage, when the crack length is $2c$, and hence the strain energy U of the system, is represented by the area OBC. It can be shown that the part of the work expended as surface energy is the area OAD bounded by the lines OA, OB, and the locus, and that the remaining area ADB is the kinetic energy of the system. Fig. 5 thus gives a graphical representation of equation (6).

4. FRACTURE IN CLEAVAGE

The analysis of the mechanical system by which a cleavage type of fracture is induced has been discussed by OBREIMOV (1930), by BENBOW and ROESLER (1957), and by GILMAN (1959). Only the last author considered the behaviour of the moving crack, though the treatment given is, in parts, incorrect. The system to be discussed is identical to that of GILMAN, with the exception that the origin of the coordinate system is taken as the point at which the forces are applied, rather than the tip of the crack in the sample (Fig. 6). The system is symmetrical about the midline, and each half may be treated by simple cantilever beam theory.

Adopting an approach analogous to that used above for tensile fracture, the potential energy ground state is

$$H_0 = S_0 + \gamma\pi c_0$$

where w is the width of the sample, and c_0 the original length of the crack.

As the applied force is increased to its critical value f_c the beam will be deflected and at the point of incipient failure the potential energy will be

$$H_1 = S_0 + \gamma w c_0 + \frac{f_c^2 c_0^3}{6EI} \tag{14}$$

where E is Young's modulus and I the moment of inertia of cross-section of the beam, i.e. one half of the sample. The last term in the expression is obtained from

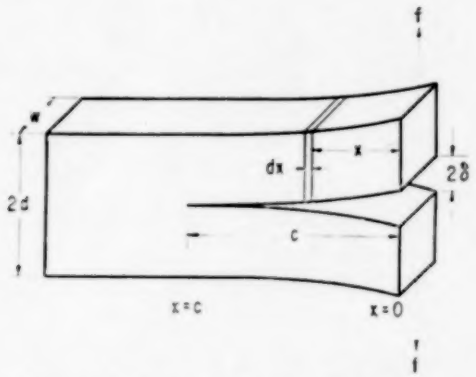

FIG. 6. Mechanical system for fracture in cleavage.

beam theory. (Provided that $c_0 > 3d$, the shear strain energy is less than 10 per cent of the bending strain energy and can be neglected.) The work done on the sample to this stage is

$$W_1 = \frac{f_c^2 c_0^3}{6EI}.$$

The conditions imposed by this type of cleavage process are that the applied forces are maintained at the constant value f_c as the crack increases in length. At any subsequent stage therefore the total energy of the system is

$$H_2 = S_0 + \gamma w c + \frac{f_c^2 c^3}{6EI} + K. \tag{15}$$

Since the point of application of the constant force f_c moves as the crack increases in length, work is performed continuously on the system. This work is $f_c(\delta - \delta_c)$, where δ_c and δ are the deflexions of the end of the sample at the point of incipient failure and at the arbitrary later stage when the crack length is c. Also from beam theory

$$\delta_c = \frac{f_c c_0^3}{3EI}, \qquad \delta = \frac{f_c c^3}{3EI}.$$

Thus the total work performed on the system is

$$W_2 = \frac{f_c^2 c_0^3}{6EI} + f_c(\delta - \delta_c) = \frac{f_c^2}{6EI}(2c^3 - c_0^3).$$

Since $H_2 = H_0 + W_2$,

$$K = \frac{f_c^2}{6EI}(c^3 - c_0^3) - \gamma w (c - c_0). \tag{16}$$

On dimensional grounds the quantity $6EI\gamma w/f_c^2$ defines a (length)^2. Let $6EI\gamma w\, f_c^2 = nc_0^2$, where n is a numerical factor. Then

$$K = \frac{f_c^2 c^3}{6EI}\left(1 - \frac{c_0}{c}\right)\left[1 + \frac{c_0}{c} - (n-1)\frac{c_0^2}{c^2}\right]. \tag{17}$$

The form of the kinetic energy term.

Consider an element of the beam of length dx lying between x and $(x + dx)$ from the extremity of the beam (Fig. 6). The vertical displacement at this point is

$$y = \frac{f}{6EI}(c - x)^2(2c + x).$$

When the crack is moving with a velocity $v_c = dc/dt$, the corresponding velocity in the y-direction is

$$\frac{dy}{dt} = \frac{f}{EI}c(c - x)v_c.$$

The mass of the moving element is $(\rho w d)\,dx$, where ρ, w, d are the density, width, and thickness, respectively, of the beam. Hence the kinetic energy of the element is

$$\frac{\rho w d}{2}\left(\frac{dy}{dt}\right)^2 dx.$$

Thus the kinetic energy of the beam is

$$K = \frac{\rho w d}{2}\left(\frac{f_c v_c}{EI}\right)^2 c^2 \int_0^c (c - x)^2\, dx$$

$$= \frac{\rho w d}{6}\left(\frac{f_c v_c}{EI}\right)^2 c^5.$$

Since $I = wd^3/12$, and the velocity of the longitudinal sound wave is $v_s = (E/\rho)^{\frac{1}{2}}$,

$$K = \frac{2f_c^2 c^5 v_c^2}{EIa^2 v_s^2}. \tag{18}$$

Introducing equation (18) in (17) and solving for v_c:

$$v_c^2 = \frac{d^2 v_s^2}{12c^2}\left(1 - \frac{c_0}{c}\right)\left[1 + \frac{c_0}{c} - (n-1)\frac{c_0^2}{c^2}\right]. \tag{19}$$

Since, as shown below, $n \leqslant 3$ this equation indicates that as c becomes large ($> c_0$) the velocity of the crack does not tend to a limiting maximum value, as in the case of tensile fracture, but tends to zero, since under the present conditions the relation between velocity and length of the crack becomes hyperbolic:

$$cv_c = \frac{dv_s}{2\sqrt{3}}.$$

Also, by differentiation of (19),

$$a_c = \frac{v_s^2 d^2}{24c^3}\left[4n\frac{c_0^2}{c^2} - 2 - 5(n-1)\frac{c_0^3}{c^3}\right] \tag{20}$$

and, when $c = c_0\,(v_c = 0)$,

$$a_c = \frac{v_s^2 d^2}{24c_0^3}(3-n)$$

and hence $n \leqslant 3$.

The equation of motion of the crack is

$$a_c + \frac{5v_c^2}{2c} = \frac{v_s^2 d^2}{24c^3}\left(3 - n\frac{c_0^2}{c^2}\right). \tag{21}$$

Equation (19) is again a partial solution of the equation of motion, but a general solution to the velocity equation has not been found.

As in the case of tensile fracture, the above equations are not related to a specific fracture criterion.

5. Criterion for Cleavage Fracture

The kinetic energy formula may be written in a form analogous to (6a):

$$K = \frac{f_c^2 c^3}{6EI} - \gamma\pi wc - \left(\frac{f_c^2 c_0^3}{6EI} - \gamma\pi wc_0\right). \tag{16a}$$

With regard to the value of the critical length c_0 corresponding to the constant force f_c, the considerations discussed above for tensile fracture can be applied to the present case. Thus c_0 is given by the intersection of the abscissa and the ascending part of the plot of $(f_c^2 c^3/6EI - \gamma\pi wc)$ versus c. The Griffith criterion defines this point as the minimum in the curve and here $n = 3$ (Fig. 7). However, the

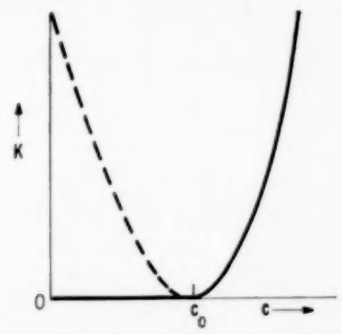

Fig. 7. Griffith condition for fracture in cleavage.

criterion adopted by Gilman is not, in fact, the Griffith criterion, but corresponds to the condition $n = 1$. Assuming the Griffith criterion, the equations describing the motion of the crack can be written explicitly:

$$v_c = \frac{v_s d}{2\sqrt{3c}}\left(1 - \frac{c_0}{c}\right)\left(1 + \frac{2c_0}{c}\right)^{\frac{1}{2}}, \tag{19a}$$

$$a_c = \frac{v_s^2 d^2}{12c^3}\left(1 - \frac{c_0}{c}\right)\left(\frac{5c_0^2}{c^2} - \frac{c_0}{c} - 1\right). \tag{20a}$$

Thus, when $c = c_0 (v_c = 0)$, $a_c = 0$.

The equation of motion is

$$a_c + \frac{5v_c^2}{2c} = \frac{v_s^2 d^2}{8c^3}\left(1 - \frac{c_0^2}{c^2}\right). \tag{21a}$$

Equation (19a) can be integrated for this special case. The result is

$$kt = \tfrac{1}{2}(\alpha - 1)[\alpha(\alpha + 2)]^{\frac{1}{2}} + 3\ln[\alpha^{\frac{1}{2}} + (\alpha + 2)^{\frac{1}{2}}] - \\ - \frac{2\sqrt{3}}{3}\ln\left[\frac{(3\alpha)^{\frac{1}{2}} + (\alpha + 2)^{\frac{1}{2}}}{(\alpha - 1)^{\frac{1}{2}}}\right] + \text{const.}, \tag{22a}$$

$$k = \frac{v_s d}{2\sqrt{3}c_0^2}, \qquad \alpha = \frac{c}{c_0}.$$

When the boundary conditions, $t = 0$ when $c = c_0$ $(v_c = 0)$, are introduced, the integration constant becomes infinite. This is analogous to the corresponding situation for tensile fracture, and the same conclusions may be drawn from the result. Thus, in order to make the crack increase in length, the applied force must be (infinitesimally) greater than that corresponding to the Griffith criterion (f_g). It would be possible, of course, to carry out a numerical integration of equation (19) for selected values of $n \sim 3$. This has not been done, but it is probable that the resulting curves would closely resemble these of Fig. 3. The obvious correspondence between Figs. 2 and 8 is a further indication of the similarity between the two cases when the Griffith criterion is applied to determine the condition for failure.

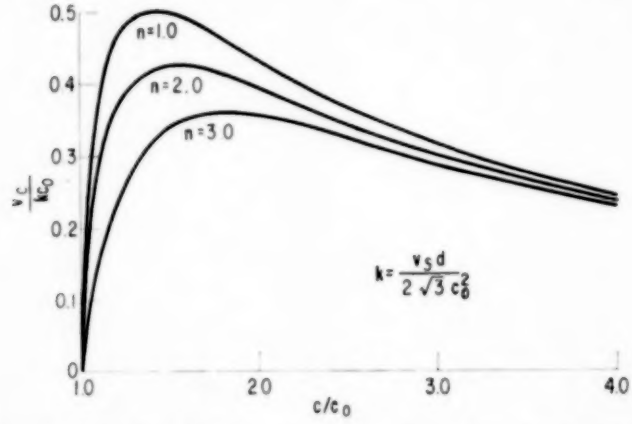

FIG. 8. Theoretical crack velocity–crack length relations at constant force in cleavage.

If the criterion used by Gilman is considered, the corresponding equations are

$$v_c = \frac{v_s d}{2\sqrt{3}c}\left(1 - \frac{c_0^2}{c^2}\right)^{\frac{1}{2}}, \tag{19b}$$

$$a_c = \frac{v_s^2 d^2}{12c^3}\left(\frac{2c_0^2}{c^2} - 1\right), \tag{20b}$$

$$a_c + \frac{5v_c^2}{2c} = \frac{v_s^2 d^2}{24c^3}\left(3 - \frac{c_0^2}{c^2}\right). \tag{21b}$$

Equation (20b) can also be integrated to give

$$kt = \frac{\alpha}{2}(\alpha^2 - 1)^{\frac{1}{2}} + \tfrac{1}{2}\ln\left[\alpha + (\alpha^2 - 1)^{\frac{1}{2}}\right], \tag{22b}$$

$$k = \frac{v_s d}{2\sqrt{3c_0^2}}, \qquad \alpha = \frac{c}{c_0}.$$

Apart from the difference in the numerical coefficients, which arise from the change in the kinetic energy term, these equations are identical to those derived by GILMAN (1959) or SUITS (1959).

The force-deflexion relation for a sample in cleavage is $f = 3EI\delta/c_0^3$, and the Griffith criterion for fracture gives $f_g = (2EI\gamma w)^{\frac{1}{2}}/c_0$. Hence the equation for the locus of the Griffith condition in this case is

$$\delta_g = \frac{(2\gamma w)^{\frac{5}{2}}(EI)^{\frac{1}{2}}}{3f_g^2} \tag{23}$$

The form of the curve is shown in Fig. 9, and, as discussed for the corresponding locus in tension, it provides a useful graphical interpretation of the kinetic energy

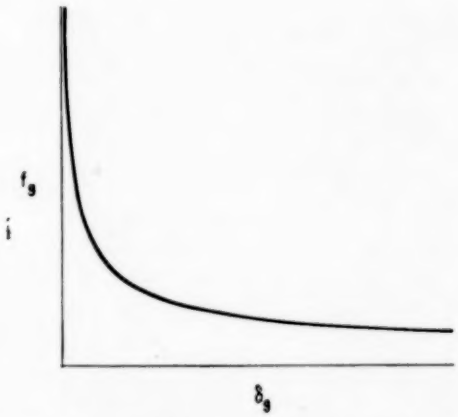

FIG. 9. Locus of the Griffith condition in cleavage.

equation (17). The angle between the force–deflexion line and the locus is again a monotonic function of c_0, but in cleavage this angle does not take on such small values as in tension experiments since the slope of the locus is always negative and since, in general, c_0 is large. Consequently the discrepancy between the observed critical force and that predicted by the Griffith criterion would not be expected to be as great in cleavage as in tension. Thus, in experiments in which the Griffith criterion is under investigation, cleavage experiments are preferable to those in tension in that a closer approach to ideal behaviour can probably be realized.

REFERENCES

BENBOW, J. J. and ROESLER, F. C. 1957 *Proc. Phys. Soc.* B **70**, 201.

GILMAN, J. J. 1959 *Fracture*, Proceedings of an International Conference on the Atomic Mechanisms of Fracture, Swampscott, Mass., p. 193. (Wiley, N.Y.).

GRIFFITH, A. A. 1921 *Phil. Trans. Roy. Soc.* A **221**, 163.

1924 *Proc. Int. Cong. Appl. Mech., Delft*, p. 55.

MOTT, N. F. 1948 *Engineering* **165**, 16.

OBREIMOV, J. W. 1930 *Proc. Roy. Soc.* A **127**, 290.

ROBERTS, D. K. and WELLS, A. A. 1954 *Engineering* **178**, 820.

SUITS, J. C. 1959 *Fracture*, Proceedings of an International Conference on the Atomic Mechanisms of Fracture, Swampscott, Mass., p. 223. (Wiley, N.Y.).

J. Mech. Phys. Solids, 1960, Vol. 8, pp. 207 to 216. Pergamon Press Ltd., London. Printed in Great Britain

SOME KINETIC CONSIDERATIONS OF THE GRIFFITH CRITERION FOR FRACTURE—II

EQUATIONS OF MOTION AT CONSTANT DEFORMATION

By J. P. Berry
General Electric Research Laboratory, New York

(*Received 8th June*, 1960)

Summary

The equations of motion of cracks in tensile and cleavage samples have been derived, assuming that the deformation of the sample is maintained constant after the critical condition for fracture has been attained. It is shown that the behaviour of cracks in tensile samples depends on their initial size and that large cracks are, in one sense, more stable than small cracks. The behaviour of cracks of all sizes in cleavage samples is shown to resemble that of large cracks in tensile samples.

1. Introduction

It has been shown (Berry 1960) that, if a sheet sample containing a crack is subjected to tensile forces, the theoretical value of the ultimate stress given by the Griffith criterion (σ_g) represents a lower, limiting value. Under such conditions the crack will not in fact increase in size, since both the initial velocity and the initial acceleration are zero. Consequently, in order to cause the crack to grow, the applied stress must be increased to a higher value (σ_c), so that the initial acceleration is finite. The discrepancy between σ_c and σ_g would be expected to depend on the size of the crack and the rate of stressing. From the equations already developed, it appears that if the stress is maintained constant at the maximum value σ_c, the behaviour of the moving crack depends critically on the discrepancy between σ_c and σ_g.

Using the same approach, it is of interest to consider the motion of the crack if, after achieving the critical stress σ_c, the sample is maintained at the corresponding critical strain ϵ_c while the crack grows. The analogous problem in cleavage will also be discussed. Consideration of these problems is facilitated by reference to the energy distribution diagrams, based on the locus of the Griffith condition, as previously described.

2. Fracture in Tension

The stress–strain relation for a sheet sample containing a central crack of length $2c_0$ is

$$\sigma = \frac{AE\epsilon}{(A + 2\pi c_0^2)} \tag{1}$$

where A is the area of the sheet (assumed large) and E is the Young's modulus of the material.

The equation for the locus of the Griffith condition is

$$\epsilon_g = \frac{\sigma_g}{E} + \frac{8E\gamma^2}{A\pi\sigma_g^3} \tag{2}$$

where ϵ_g is the strain corresponding to the Griffith critical stress σ_g and γ is the specific surface energy of the material. The form of the locus is illustrated in Fig. 1.

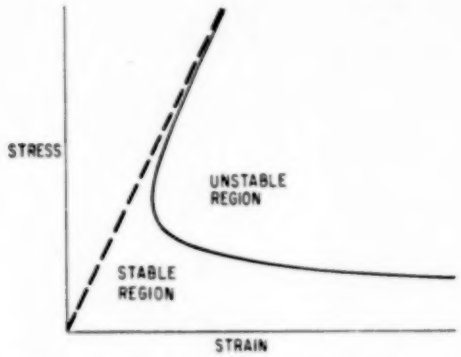

FIG. 1. Griffith locus for fracture in tension.

The attainment of the Griffith condition is given by the point of intersection of the stress–strain relation and the Griffith locus, which therefore defines regions of stability and instability of the crack in the sample. Both the predicted ultimate stress and the effective elastic modulus of the sample decrease continuously with increasing initial crack length, but the ultimate strain passes through a minimum for a particular value of the initial crack length, given by $c_0^2 = A/6\pi$. Thus, the minimum in the ultimate strain is determined by the size of the initial crack relative to the dimensions of the sample. As will be shown below, two different types of behaviour are to be expected under conditions of constant strain, depending on the relative size of the initial crack. For a sample containing a small crack, the point at which the Griffith criterion is satisfied lies on that part of the Griffith locus where the slope is positive. If the initial crack is large, the slope of the locus is negative when the Griffith criterion is satisfied. The change from positive to negative slope occurs at the condition for the minimum ultimate strain, i.e. when $c_0^2 = A/6\pi$. Consequently, in discussing the behaviour of the system at constant strain, it is convenient to characterize the relation between the initial crack size and sample dimension by a dimensionless parameter m where $m = A/\pi c_0^2$.

The effective elastic modulus of a sample containing a small crack ($m > 6$) is relatively high, as indicated by the line OA (Fig. 2). The critical condition is satisfied at the point A, and the crack can then increase in length. If the strain is maintained constant at the critical value, the modulus decreases and the stress therefore also decreases as the crack grows. Thus, at any arbitrary later stage, the condition of the system can be represented by the point B, and the line OB is the stress–strain relation for the sample containing the larger crack. It is clear

that, since the point *B* lies in the region of instability, the crack in the sample must continue to increase in length, the kinetic energy being represented by the area AEB. When the stress on the sample has decreased to the value indicated by point C, the relation between the crack length and the stress again satisfies the Griffith criterion. However, the system still possesses a large amout of kinetic

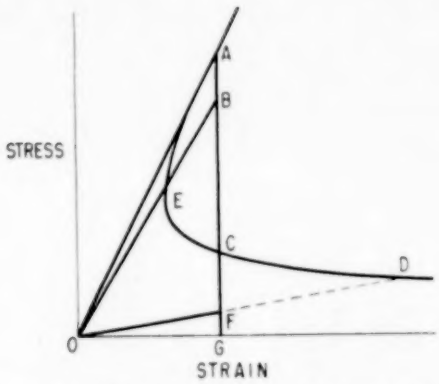

FIG. 2. Behaviour of a small crack in a tensile sample.

energy indicated by the area AEC, and consequently the crack continues to advance. As it does so, the surface energy increases at the expense of the strain energy and the kinetic energy. Eventually the kinetic energy will be reduced to zero and the crack will stop. If the point F represents this final condition the system now possesses only strain energy, given by the area OFG, and surface energy (OAECD). The total energy must be equal to the work performed on the system, i.e. the area OAG, and hence the area CFD is equal to the area AEC. Clearly the crack is now sub-critical in length with respect to the final value of the stress.

The Griffith condition relating the applied stress to the size of a crack in the sample is satisfied twice during the course of the experiment, first in the vicinity of the point A, and second at the point C. As already discussed (BERRY 1960) the attainment of the Griffith condition in a sample containing a crack, subjected to a tensile stress, is indicated by a minimum in the relation between the kinetic energy and crack length. From the above considerations, the kinetic energy is a maximum at the point C where the Griffith condition is again satisfied. Thus in both instances the same differential condition is fulfilled ($dK/dc = 0$), but in the first case this defines a minimum, and in the second it defines a maximum.

The effective elastic modulus of a sample containing a large crack ($m > 6$) is relatively low (Fig. 3), and the slope of the locus is negative at the point at which the Griffith criterion is satisfied. If the strain is held constant at the critical value (A), it is evident from Fig. 3 that the crack will increase in size. By the same line of argument as used above, when the Griffith criterion is again satisfied at the point B, the kinetic energy is a maximum, and is represented by the area ADB. The crack continues to grow until the system achieves the condition represented by the point C, i.e. until the area BCE is equal to the area ADB. In this case the amount by which the final crack size differs from that corresponding to the equili-

brium Griffith value will depend on the amount by which the Griffith stress (σ_g) is exceeded, i.e. on the distance DA. This fact marks the essential difference in behaviour between small and large initial cracks in samples subjected to this type of experiment. A small crack will increase in size by an amount which depends

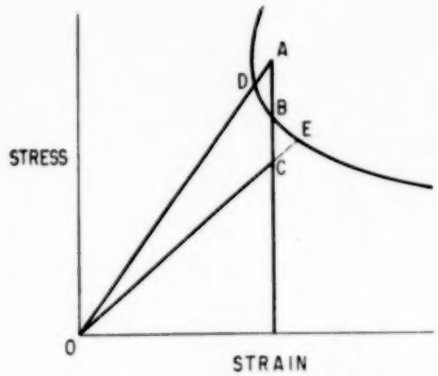

FIG. 3. Behaviour of a large crack in a tensile sample.

primarily on its initial size. A large crack will increase in size only by an amount depending on the discrepancy between σ_c and σ_g. Subject to the conditions of constant strain therefore, large cracks are, in this sense, more stable than small cracks.

3. EQUATIONS OF MOTION

The equations of motion which characterize the behaviour described above can be derived using the approach developed for the constant stress case. The kinetic energy of the system at constant strain in tension is

$$K = \frac{A^2 E\epsilon_c^2}{2}\left[\frac{1}{A + 2\pi c_0^2} + \frac{1}{A + 2\pi c^2}\right] - 4\gamma(c - c_0) \tag{3}$$

where $2c$ is any arbitrary crack length (greater than $2c_0$). Making the substitutions $A = m\pi c_0^2$ and $\alpha = c/c_0$, equation (3) reduces to

$$\frac{K}{4\gamma c_0} = \frac{(\alpha^2 - 1)(m + 2)}{n(m + 2\alpha^2)} - (\alpha - 1). \tag{4}$$

The parameter n in this equation corresponds to that defined for the constant stress case and the same conditions govern its value. Thus

$$nc_0 = \frac{4E\gamma}{\pi\sigma_c^2} = \frac{4\gamma}{\pi E}\left[\frac{A + 2\pi c_0^2}{A\epsilon_c}\right]^2,$$

and

$$n = \frac{2\sigma_g^2}{\sigma_c^2} = \frac{2\epsilon_g^2}{\epsilon_c^2}.$$

Equation (4) gives the dependence of the kinetic energy on the size of the initial crack (m), and the discrepancy between σ_c and σ_g or ϵ_c and ϵ_g (n), as discussed in

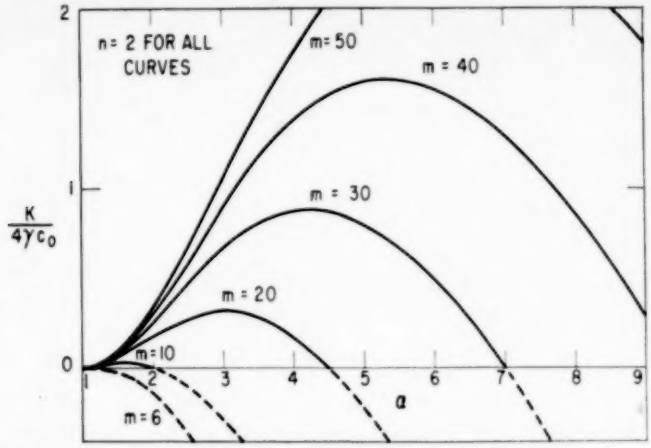

FIG. 4. Theoretical kinetic energy–crack length relations at constant tensile strain for different initial crack lengths.

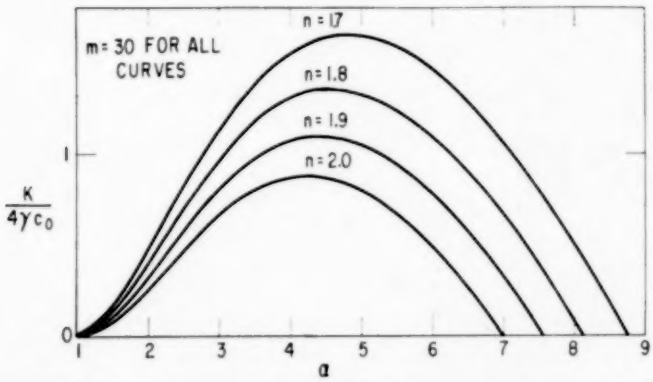

FIG. 5. Theoretical kinetic energy–crack length relations at constant tensile strain for a small crack.

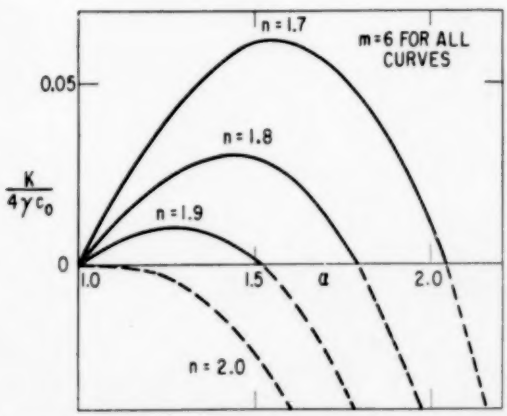

FIG. 6. Theoretical kinetic energy–crack length relations at constant tensile strain for a large crack.

qualitative terms above. This dependence is illustrated in Figs. 4, 5 and 6. Although, in drawing these Figures, the parameters n and m have been varied independently, some degree of interdependence would be expected, for the reasons already put forward. Thus, low values of n should be associated with large values of m, and vice versa.

Adopting analogous reasoning to that used by MOTT (1948) for the constant stress condition, the kinetic energy of the system at constant strain can be shown to be of the form

$$K = \frac{k' \rho c^2 v_c^2}{2} \cdot \frac{A^2 \epsilon_c^2}{(A + 2\pi c^2)^2} \tag{5}$$

where k' is a numerical constant, which would not be expected to be the same as that in the constant stress condition, ρ is the density of the material, and v_c is the velocity of the crack. Equating the two expressions for the kinetic energy [equations (3) and (5)] and making the appropriate substitutions for n, m and α gives

$$v_c^2 = \frac{2\pi}{k'} \cdot \frac{E}{\rho} \cdot \frac{(m + 2\alpha^2)^2}{\alpha^2 (m + 2)^2} \left[\frac{(m + 2)(\alpha^2 - 1)}{(m + 2\alpha^2)} - n(\alpha - 1) \right] \tag{6}$$

and when $\alpha = 1$, $v_c = 0$. The crack velocity–crack length relation again depends on both n and m, and the curves of Fig. 7 correspond to those of Fig. 4.

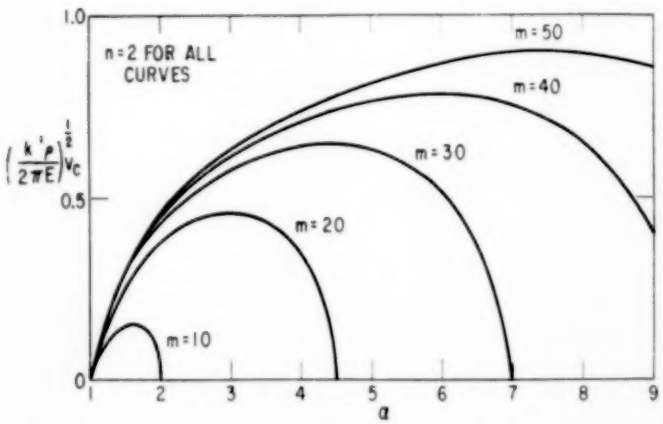

FIG. 7. Theoretical crack velocity–crack length relations at constant tensile strain for different initial crack lengths.

Differentiating equation (6) yields

$$a_c = \frac{\pi}{k'} \cdot \frac{E}{\rho c_0} \cdot \frac{1}{\alpha^3 (m + 2)^2} \left[2(m + 2)(m + 2\alpha^4) - n(m + 2\alpha^2) \{ m(2 - \alpha) + 2\alpha^2 (3\alpha - 2) \} \right] \tag{7}$$

where a_c is the acceleration of the crack, and when $\alpha = 1$ ($v_c = 0$)

$$a_c = \frac{\pi E}{k' \rho c_0} (2 - n).$$

As might be expected, the form of the equation for the initial acceleration is the same as in the constant stress case, and this imposes the same limits on the value of n, i.e. $n \leqslant 2$. The Griffith criterion is defined by the condition that $n = 2$, and thus, as before, under these conditions the initial acceleration is zero.

The generalized equation of motion is

$$a_c + \frac{v_c^2\,(m - 2\alpha^2)}{\alpha c_0\,(m + 2\alpha^2)} = \frac{2\pi E}{k'\,\rho} \cdot \frac{1}{\alpha c_0}\left[1 - \frac{n}{2\alpha}\left(\frac{m + 2\alpha^2}{m + 2}\right)^2\right]. \tag{8}$$

In considering the practical application of the above discussion it is clear that a restriction must be imposed on the value of m, the parameter that characterizes the relative size of the initial crack, if quantitative agreement with the theory is to be expected. This limitation is due to the method of calculating the elastic strain energy of the sheet sample containing a crack, in which it is assumed that the crack length is small compared to the dimensions of the sample. However, because of the stress concentration which occurs in the vicinity of the tip of the crack, most of the elastic energy is stored in a comparatively small volume, and serious deviation from theoretical behaviour may not obtrude until the ratio of the crack length to sample width is of considerable magnitude. For a square sample, when $m = 6$, this ratio is 0·46, and it is possible, therefore, that the quantitative description of the behaviour of ' large ' cracks according to the above theory is not to be expected. However, the qualitative behaviour of large cracks in samples of poly (methyl methacrylate) is in accord with the predictions of the theory.

4. Fracture in Cleavage

The type of sample which will be considered is that described previously (Berry 1960). The force–deflexion (f–δ) relation for such a sample containing a crack of length c_0 is

$$f = \frac{3EI\delta}{c_0^3} \tag{9}$$

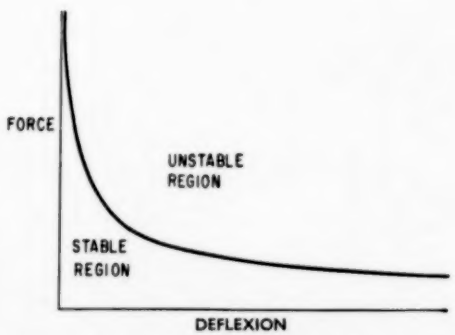

Fig. 8. Griffith locus for fracture in cleavage.

where E is Young's modulus and I is the moment of inertia of cross-section of one half of the sample.

The equation of the locus of the Griffith condition in cleavage is

$$\delta_g = \frac{(2\gamma w)^{\frac{1}{2}}(EI)^{\frac{1}{2}}}{3f_g^2}. \tag{10}$$

The form of the locus is illustrated in Fig. 8. It is clear that the Griffith locus in tension differs from that in cleavage in that in the latter case the slope of the locus is negative for all values of f_g. Thus, the considerations discussed for large cracks in tensile samples will apply to cracks of all sizes in cleavage. Hence, the increase in crack size at constant deflexion in cleavage will depend only on the amount by which the Griffith condition has been exceeded.

5. EQUATIONS OF MOTION

By the procedure already outlined, the kinetic energy of a cleavage sample at constant deflection is

$$K = \frac{3EI\delta_c^2}{2}\left[\frac{1}{c_0^3} - \frac{1}{c^3}\right] - \gamma w(c - c_0) \tag{11}$$

where c is any arbitrary crack length (greater than c_0).

In discussing the behaviour of the crack in a cleavage sample subjected to constant force, use was made of the parameter n, which was defined by the relation $nc_0^2 = 6EI\gamma w/f_c^2$. It can also be defined in terms of the constant deflection δ_c by $n = 2\gamma w c_0^4/3EI\delta_c^2$. As in the tensile case, n is a measure of the discrepancy

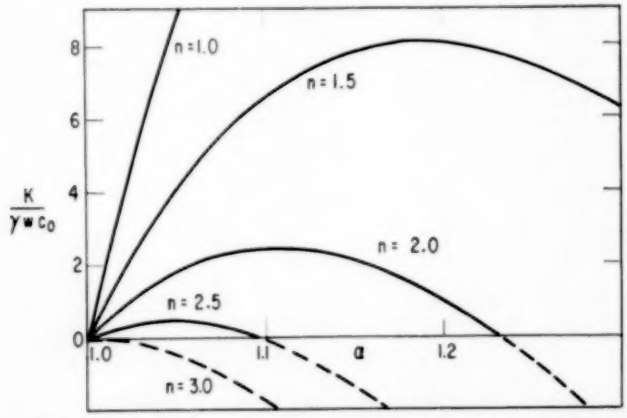

FIG. 9. Theoretical kinetic energy–crack length relations at constant deflexion in cleavage.

between the critical force according to the Griffith criterion (f_g), and that corresponding to the conditions under which the crack begins to increase in length (f_c). The relation between these quantities is $n = 3f_g^2/f_c^2 = 3\delta_g^2/\delta_c^2$. After making the appropriate substitutions for n and $\alpha\,(= c/c_0)$, equation (11) reduces to

$$\frac{K}{\gamma w c_0} = \frac{1}{n}\left[1 - \frac{1}{\alpha^3}\right] - (\alpha - 1). \tag{12}$$

The form of this relation is shown in Fig. 9.

It has been stated that the kinetic behaviour of cracks of all sizes in cleavage samples should resemble that of long cracks in tensile samples. This is indicated by the fact that the equation for the kinetic energy does not contain any term relating to the initial length of the crack, and by the close similarity between the curves of Fig. 9 and those of Fig. 6, which refer to the behaviour of initially large cracks in tensile samples.

Using methods analogous to those already described (Berry 1960), the kinetic energy of the system at constant deflexion in cleavage is

$$K = \tfrac{3}{35}\frac{wd}{c} \cdot E\delta_c^2 \cdot \frac{v_c^2}{v_s^2}, \tag{13}$$

and hence

$$v_c^2 = \tfrac{35}{24}\frac{d^2 v_s^2}{\alpha^2 c_0^2}\left[(\alpha^3 - 1) - n\alpha^3(\alpha - 1)\right]. \tag{14}$$

As before, when $\alpha = 1$, $v_c = 0$. The crack length–crack velocity relations are illustrated in Fig. 10.

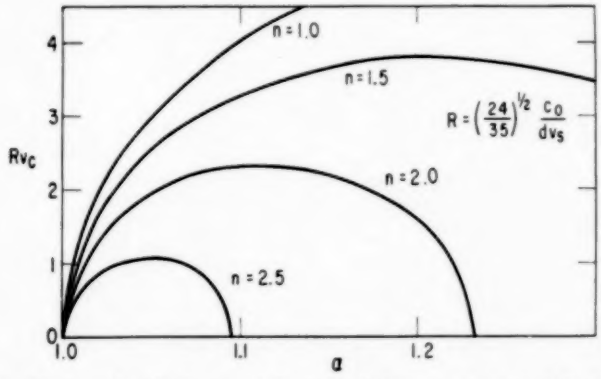

Fig. 10. Theoretical crack velocity–crack length relations at constant deflexion in cleavage.

By differentiation of (14), we obtain

$$a_c = \tfrac{35}{48}\frac{d^2 v_s^2}{\alpha^3 c_0^3}\left[(\alpha^2 + 2) - n\alpha^3(2\alpha - 1)\right] \tag{15}$$

where a_c is the acceleration of the crack, and when $\alpha = 1$ ($v_c = 0$)

$$a_c = \tfrac{35}{48}\frac{d^2 v_s^2}{c_0^3}(3 - n).$$

The equation for the initial acceleration has the same form as that for the corresponding case at constant force, and leads to the same limiting condition, that $n \leqslant 3$. Also, as before, the Griffith criterion is defined by the condition that $n = 3$, which implies that the initial acceleration is zero for this case.

The generalized equation of motion for a crack in a cleavage sample at constant deflexion is

$$a_c - \frac{v_c^2}{2\alpha c_0} = \tfrac{35}{48}\frac{d^2 v_s^2}{\alpha^3 c_0^3}(3 - n\alpha^4). \tag{16}$$

In contrast to the case for tensile samples, deviations from the theoretical form of the strain energy function in cleavage will arise when the initial crack is short. Thus a much wider range of experimental conditions, for which the theory would be expected to be valid, is available for testing the derived equations of motion.

In both types of experiment, tension and cleavage, the crack velocity–crack length relations are complex functions which have resisted integration. It is to be expected that the corresponding crack length–time relations would lead to the anomalies discussed earlier if the Griffith criterion is assumed to define the condition for the beginning of crack growth. This is indicated by the fact that for both types of experiment under these conditions, both the initial velocity and the initial acceleration of the crack are zero.

REFERENCES

BERRY, J. P. 1960 *J. Mech. Phys. Solids* **8**, 194.
MOTT, N. F. 1948 *Engineering* **165**, 16.

BOOK REVIEWS

S. H. Crandall and N. C. Dahl: **An Introduction to the Mechanics of Solids.** McGraw–Hill, New York, 1959, 444 pp., $8.50.

This book has been prepared for use as a text in the first course in applied mechanics in the Mechanical Engineering Department at the Massachusetts Institute of Technology. It assumes elementary Newtonian mechanics, and is intended to provide an introduction both to the rigorous theory of elasticity and plasticity, and to engineering design courses.

A feature of the book is the " more than usual care " taken to explain the precise process of solving equilibrium problems in applied mechanics. Starting from the practical engineering situation, this procedure begins by idealization, i.e. by ' distilling ' a representative and analysable model. The role of the free-body diagram is fully illustrated. The principles for analysing the model are then distinguished by three steps: (1) study of forces and equilibrium requirements; (2) study of deformations and geometric compatibility; (3) application of force-deformation relations. These points are persistently emphasized in the worked examples throughout the book. The diligent student can expect to acquire not only a sound technique, but also an explicit awareness of the role of the principles involved in applying mechanics. Many problems are provided at the end of each chapter.

Chapter I illustrates the above scheme in rigid-body statics, and Chapter II treats some simple cases of (mostly uniaxial) deformation. The next three chapters serve to amplify the above three steps in turn. Thus Chapter III, " Forces and moments transmitted by slender members," is chiefly concerned with the calculation of shear forces and bending moments in beams in statically determinate situations; Chapter IV gives a specification of stress and of strain, and Chapter V considers mechanical laws relating them. In Chapter V the generalized Hooke's law is derived from the elastic tensile test observations. Twenty-four pages are then devoted to a discussion of plastic yielding and hardening, and the Hencky and Lévy–Mises equations. This topic requires a level of sophistication rather above that of the rest of the book. Some complete engineering problems requiring a simultaneous consideration of all three steps are treated in the remaining four chapters, entitled " Torsion," " Stresses due to bending," " Deflections due to bending," and " Stability of equilibrium: buckling." In each of these the treatment is carried far enough for inelastic topics (e.g. the hinge mechanism of plastic collapse) to be briefly remarked on.

The many diagrams are a model of clarity.

M. J. Sewell

L. D. Landau and E. M. Lifshitz: **Theory of Elasticity.** Translated from Russian by J. B. Sykes and W. H. Reid. Pergamon Press, London, 1959, 134 pp., 40*s*.

This book, written primarily for physicists, gives a concise account of a number of important topics in classical elasticity. The theory of elasticity and thermoelasticity for isotropic bodies is developed in Chapter 1 and applied to a number of elementary problems including simple extension and simple deformations of cylinders and spheres, some of which are given as worked examples. The chapter also deals with the Boussinesq solution of the elastic problem for a half-space, and includes a treatment of the Hertz contact problem and a brief mention of plane strain. A discussion of the crystal classes, although more comprehensive than in many texts, is incomplete and omits several possible forms for the strain energy.

The largest section of the book (Chapter 2), deals with deformations of plates, shells and rods, the equations of equilibrium being derived from energy considerations. There is also a brief

treatment of plane stress and the flexure and torsion problems and an elementary account of the stability problem for struts.

Chapters 3 and 4 give an elementary treatment of elastic wave motion, including vibrations of rods and plates, and the effects of viscosity in solids. The latter effect is taken into account by assuming linear relations between stress and strain and their time rates of variation.

The book forms a useful introduction to the subject but no indication is given of the fundamental difficulties inherent in a number of problems e.g. the theory of thermoelasticity, the description of viscoelastic properties, and the approximations used in plate and shell theory.

J. E. ADKINS

Fracture: Edited by B. L. AVERBACH, D. K. FELBECK, G. T. HAHN and D. A. THOMAS. The Technology Press, Massachusetts Institute of Technology and John Wiley and Sons, New York; Chapman & Hall Ltd., London, 1959. pp. xvii + 646, £7.

THIS book records the proceedings of the International Conference on the Atomic Mechanisms of Fracture, held at Swampscott, Massachusetts in the spring of 1959. The twenty-seven papers presented at the Conference, which are printed in full with discussions, were concerned almost exclusively with the fine scale mechanisms of fracture in metals, ceramics and polymers. A valuable feature of the publication is the presentation of summarized reports of general discussions on the current status of knowledge in this field.

The classical work of Griffith on the fracture of glass fibres, published about forty years ago, provided the key to our understanding of the differences between the theoretical and real strengths of brittle solids. It remains the basis of many present-day ideas on fracture. Yet less then twenty years ago the fracture behaviour of metals was commonly discussed in terms of an unexplained and uncertain material constant, the critical stress for fracture. Elucidation of the role of plastic deformation in the fracture of engineering materials awaited developments in dislocation theory. Thus the work described in this book is largely the product of the last decade. It has been a period of remarkable progress.

In the first paper COTTRELL gives a lucid review of recent ideas on the brittle and ductile fracture behaviours of metals, and on the mechanisms of crack formation in creep and fatigue. Eight papers are devoted to cleavage fracture in body centred cubic metals, and a similar number to fracture in non-metals including ionic crystals, glasses and polymers. ANDERSON discusses modern views on the Griffith criterion for glass fracture and GILMAN gives a useful review on cleavage in a much wider context. Ten papers deal principally with fatigue, ductile fracture and intercrystalline failure at elevated temperatures. In fatigue much interest is focussed on the possible mechanisms whereby cracks are formed from the broad slip bands, often associated with "intrusions," which are observed to develop at the surface. Here, as elsewhere, it is clear that developments in experimental techniques, no less than advances in theory, are contributing to a refinement of ideas. Observations made at high magnifications, using fracture replicas and taper sections, are of particular interest. In both brittle fracture and fatigue details of the mechanisms of crack nucleation by dislocations remain uncertain. Observations on ionic crystals described by PARKER, MCEVILY and MACHLIN provide an insight into what may happen in metals.

The emphasis given to brittle fracture in steel reflects outstanding progress in this field. There is rather general agreement that cracks are nucleated by the conversion of glide dislocations into cavity dislocations. If these are to spread in the form of a growing crack, their concentration of elastic energy must not be dispersed by plastic flow. Theoretical ideas on the ductile–brittle transition advanced by PETCH and COTTRELL go far towards giving a unified picture, which takes account of the main effects of microstructure, temperature, strain rate and the degree of traxiality of the applied stress. Many problems remain unsolved, but such achievements are already sufficient to justify BARRETT'S comment that "The atomic mechanisms involved lie at the heart of the true understanding."

This book will be of unique value to research workers concerned with deformation and fracture. It is recommended to all who seek a scientific understanding of mechanical properties.

D. V. WILSON

J. Mech. Phys. Solids, 1960, Vol. 8, pp. 219 to 234. Pergamon Press Ltd., London. Printed in Great Britain

THE HERTZ PROBLEM FOR A RIGID SPHERICAL INDENTER AND A VISCOELASTIC HALF-SPACE

By S. C. Hunter
Brown University, Providence, R.I.

(*Received 22nd June, 1960*)

Summary

The penetration of a viscoelastic half-space by a rigid spherical indenter is investigated in a quasi static approximation. Solutions to the problem are obtained for monotonic contact radius and also when the radius possesses a single maximum. The analysis is used to estimate the duration of contact and coefficient of restitution for the Hertzian impact of a spherical indenter on a Maxwell solid.

1. Introduction

The present paper is concerned with the mechanical contact between a rigid spherical indenter and a viscoelastic half-space; the problem is of significance for the interpretation of Brinell hardness measurements and rebound (i.e. scleroscopic) tests on polymer materials.

The problem is one for which the boundary conditions are mixed since the surface displacement is prescribed within the contact region $r < r_1(t)$ while elsewhere on the surface the normal stress vanishes. In the absence of inertial forces many problems of this type are solvable by appeal to the similarity between the equations of elasticity and the transformed visco-elastic equations:

$$\partial \bar{\sigma}_{ij}/\partial x_j = 0, \qquad \bar{\sigma}_{ij} = \lambda(p)\,\bar{\epsilon}_{ii}\,\delta_{ij} + 2\mu(p)\,\bar{\epsilon}_{ij},$$

in which the bar denotes a Laplace transform with respect to time, p is the transform variable, while $\lambda(p)$ and $\mu(p)$ are the associated transform moduli (e.g. see Hunter 1960). As discussed by Lee (1955) and Lee and Radok (1960), provided the transformed boundary conditions are known *a priori*, the transformed viscoelastic equations lead to an elastic problem in the transformed variables; inversion of the (known) elastic solution then solves the original problem. However, once time dependent boundary regions are encountered, as in the present example, there exist boundary points subject to different boundary conditions at different instants of time. For this class of problem we only possess a partial history of the stress and displacement boundary conditions for some regions; thus it is no longer possible to construct the transformed boundary conditions, and the method fails.

For the contact problem considered here Lee and Radok found a solution of limited validity by the following device. The associated Hertz elastic problem leads to the equation

$$-\sigma_z = \frac{4\mu}{\pi R(1-\nu)}(r_1^2(t) - r^2)^{\frac{1}{2}}, \qquad r_1 > r, \tag{1.1}$$

for the distribution of normal stress σ_z over the contact region. A tentative solution of the viscoelastic problem is given by replacing the elastic constants in (1.1) by the corresponding integral or differential viscoelastic operators. The solution is tentative since, as the authors point out, prior valid manipulations of (1.1) (e.g. squaring each side) would lead to a different viscoelastic solution. The validity of the LEE and RADOK solution was established by showing that the associated displacement field conformed to the geometry of the indenter for the contact region.

The solution is valid provided $r_1(t)$ is a monotonic increasing function of time; once $r_1(t)$ passes through a maximum the solution fails by predicting the possibility of tensile stresses under the indenter. The mathematical reason for this failure will become evident from the present analysis which shows that extremum values of $r_1(t)$ are critical points for the solution. Physically the failure of the solution is attributable to the fact that the normal stress boundary condition implicit in the LEE and RADOK analysis is not $\sigma = 0$ for $r > r_1$, but rather

$$\int_0^t \frac{\partial \sigma}{\partial t'} \mu(t - t')\, dt' = 0, \qquad r > r_1, \tag{1.2}$$

where $\mu(t)$ is the stress relaxation function. For monotonic increasing $r_1(t)$ the hereditary integral condition (1.2) is satisfied and is equivalent to $\sigma = 0$ for $r > r_1$; however, once $r_1(t)$ passes through a maximum, there exist points where currently $\sigma = 0$ but for which equation (1.2) is violated.

The present method of solution (Section 2) devolves on expressing the transformed field quantities $\bar{u}$ and $\bar{\sigma}$ in terms of the eigenfunctions of the elastic Boussinesq problem,

$$\bar{u} = \sum_m \bar{a}(m, p)\, \psi_u(m, \mathbf{r}), \qquad \bar{\sigma} = \sum_m \bar{b}(m, p)\, \psi_\sigma(m, \mathbf{r}). \tag{1.3}$$

Here only the eigenfunctions ψ contain the space coordinate $\mathbf{r}$ while p only enters the coefficients $\bar{a}$ and $\bar{b}$. To apply the boundary conditions directly we remove the transforms in (1.3) obtaining (in an obvious notation)

$$u = \sum_m a(m, t)\, \psi_u(m, \mathbf{r}), \qquad \sigma = \sum_m b(m, t)\, \psi_\sigma(m, \mathbf{r}),$$

in which the time dependent coefficients a and b are related through an hereditary integral of the Volterra type.

The boundary conditions now lead to a pair of integral equations with kernels related by hereditary integrals. In the limiting case of an elastic solid the two kernels are identical functions and the solution of the equations has been effected by TITCHMARSH (1937). By following this method of analysis (Section 2) we transform the original dual equations into an equivalent pair in the complex plane. Solutions of these equations are obtained for monotonic $r_1(t)$ in Section 3, recovering the results given by LEE and RADOK. The more general case in which $r_1(t)$ increases monotonically from zero to a maximum and subsequently decreases monotonically to zero, is dealt with in Section 4.

Finally, we give a treatment of the scleroscope problem for the limiting case of a nearly elastic solid (Section 5). In this limit the impact duration T deviates only slightly from the Hertzian value while the coefficient of restitution is given by

$$e = 1 - \tfrac{4}{5}\eta T$$

where η is the mean inverse relaxation time of the solid.

2. Formulation of Basic Equations

The basis of the present analysis is founded in a paper by Lamb (1902) dealing with the axisymmetric Boussinesq problem. For a half-space $z > 0$ with the surface $z = 0$ subject to zero shear traction and an arbitrary radially symmetric distribution of normal pressure, Lamb gives the displacement field

$$u_r = \sum_m P(m)\left[1/2m(\lambda+\mu) - z/2\mu\right] J_1(mr)\, e^{-mz}, \tag{2.1}$$

$$u_z = -\sum_m P(m)\left[(\lambda+2\mu)/2m\mu(\lambda+\mu) + z/2\mu\right] J_0(mr)\, e^{-mz}. \tag{2.2}$$

Here r, z are cylindrical polar coordinates with z the axis of symmetry, u_r and u_z are radial and axial components of displacement, J_0 and J_1 are Bessel functions, λ, μ are the Lamé constants while m denotes a continuous spectrum of eigenvalues with $P(m)$ a distribution function to be determined.

The value of Lamb's results in the present context devolves on the fact that the basic eigenfunctions in which the displacement field is expanded are valid solutions of the transformed viscoelastic equations provided the elastic constants are replaced by their corresponding transform moduli. Thus, the Laplace transforms of the displacement field in a viscoelastic half space subject to similar surface conditions are given by

$$\bar{u}_r(\mathbf{r}, p) \equiv \int_0^\infty u_r(\mathbf{r}, t)\, e^{-pt}\, dt$$

$$= \sum_m P(m, p)\left[1/2m(\lambda(p)+\mu(p)) - z/2\mu(p)\right] J_1(mr)\, e^{-mz}, \tag{2.3}$$

$$\bar{u}_z(\mathbf{r}, p) = -\sum_m P(m, p)\left[(\lambda(p)+2\mu(p))/2\mu(p)\, m(\lambda(p)+\mu(p)) + z/2\mu(p)\right] J_0(mr)\, e^{-mz} \tag{2.4}$$

where P now depends on p and where $\lambda(p)$, $\mu(p)$ are defined by either the creep or relaxation functions in both shear and dilation. For example, if we define $\mu(t)$, $\mu^{-1}(t)$ as the normalized relaxation and creep functions in shear so that for*

$$\tau = \tau_0 H(t), \qquad \gamma = \tau_0 \mu^{-1}(t),$$

$$\gamma = \gamma_0 H(t), \qquad \tau = \gamma_0 \mu(t),$$

then the transform shear modulus is given by

$$\mu(p) = p\int_0^\infty e^{-pt}\mu(t)\, dt = \left\{p\int_0^\infty e^{-pt}\mu^{-1}(t)\, dt\right\}^{-1}. \tag{2.5}$$

While $\mu(t)$ and $\mu^{-1}(t)$ are not algebraically reciprocal functions, expansion in a power series about $t = 0$ yields

$$\mu(t) = \mu_D(1 - \eta t + \dots), \qquad \mu^{-1}(t) = \mu_D{}^{-1}(1 + \eta t - \dots), \tag{2.6}$$

where μ_D is the instantaneous shear modulus and η is a mean inverse relaxation time defined by

$$\eta = \int_0^\infty \tau^{-1} g(\tau)\, d\tau$$

*$H(t)$ is the Heaviside step function $H(t) = 0$, $t < 0$; $H(t) = 1$, $t > 0$.

in which $g(\tau)$ is the distribution function of relaxation times. We make use of the expansions (2.6) in Section 5.

To simplify the subsequent algebra we assume similar behaviour in both shear and dilation ; this assumption enables us to define an unequivocal value of Poisson's ratio independent of p:

$$\nu = \lambda(p)/2\left[\lambda(p) + \mu(p)\right].$$

There is no loss of generality in this assumption ; the appropriate modifications to the ensuing analysis merely entail replacing $\mu(t)$ and $\mu^{-1}(t)$ by somewhat different functions of time. With the assumption that ν is independent of p, equations (2.3) and (2.4) lead to the following expressions for the Laplace transforms of surface displacement and normal stress:

$$(\overline{u}_z)_{z=0} = \int_0^\infty \overline{\phi}_1(m, p)\, J_0(mr)\, dm, \tag{2.7}$$

$$-(\overline{\sigma}_z)_{z=0} = \{\mu(p)/(1-\nu)\} \int_0^\infty m\overline{\phi}_1(m, p)\, J_0(mr)\, dm, \tag{2.8}$$

in which

$$\overline{\phi}_1 = -(1-\nu)\, P/\mu(p)\, m.$$

The boundary conditions to be applied to (2.7) and (2.8) for the determination of $\overline{\phi}_1$ for the contact problem are of the form (a) u_z is prescribed by the geometry of the indenter for $r < r_1(t)$ where $r_1(t)$ is the radius of the contact circle, (b) $\sigma_z = 0$ for $r > r_1(t)$. As has already been discussed, the explicit appearance of boundary regions varying with time precludes an immediate solution for the transformed field quantities $\overline{u}_z$ and $\overline{\sigma}_z$; because of this we remove the transforms in (2.7) and (2.8) obtaining*

$$u_z = \int_0^\infty \phi_1(m, t)\, J_0(mr)\, dm, \tag{2.9}$$

$$-(1-\nu)\,\sigma_z = \int_0^\infty m\phi_2(m, t)\, J_0(mr)\, dm, \tag{2.10}$$

to which the boundary conditions may be applied directly. In (2.9) $\phi_1(m, t)$ is the inverse Laplace transform of $\overline{\phi}_1$ while ϕ_1 and ϕ_2 are related by the (equivalent) formulae

$$\phi_1(m, t) = \int_{-\infty}^t \mu^{-1}(t-t')\, \frac{\partial}{\partial t'}\, \phi_2(m, t')\, dt', \tag{2.11}$$

$$\phi_2(m, t) = \int_{-\infty}^t \mu(t-t')\, \frac{\partial}{\partial t'}\, \phi_1(m, t')\, dt', \tag{2.12}$$

which follows directly from (2.7), (2.8) and the convolution theorem for Laplace transforms. Without prejudice we assume the solid undisturbed prior to $t = 0$ so that the lower limits in equations (2.11), (2.12) may be taken as zero.

For a spherical indenter of radius R the boundary conditions are explicitly

$$\left.\begin{aligned} u_z &= \alpha(t) - r^2/2R, \qquad r \leqslant r_1(t), \\ \sigma_z &= 0, \qquad\qquad\quad r > r_1(t), \end{aligned}\right\} \tag{2.13}$$

*In the remainder of the paper we deal exclusively with surface displacements and stresses ; in equations (2.9) (2.10) and subsequently we omit the specification $z = 0$.

where *a priori* the indenter penetration $\alpha(t)$ is unknown for given r_1.

It is convenient to define

$$\Phi_i(mr_1(t), t) \equiv \phi_i(m, t) \qquad (i = 1, 2) \tag{2.14}$$

in terms of which equations (2.9) and (2.10) become

$$r_1(t)\, u_z = \int_0^\infty \Phi_1(y, t)\, J_0(xy)\, dy, \qquad x = r/r_1(t), \tag{2.15}$$

$$-(1-\nu)\, r_1^2(t)\, \sigma_z = \int_0^\infty y\, \Phi_2(y, t)\, J_0(xy)\, dy, \tag{2.16}$$

when the boundary conditions (2.13) become

$$\int_0^\infty \Phi_1(y, t)\, J_0(xy)\, dy = A(t) - B(t)\, x^2, \qquad x = r/r_1(t) < 1, \tag{2.17}$$

$$\int_0^\infty y\Phi_2(y, t)\, J_0(xy)\, dy = 0, \qquad x > 1, \tag{2.18}$$

with $A(t) = r_1(t)\, \alpha(t), \qquad B(t) = r_1^3(t)/2R.$ (2.19)

From equations (2.11), (2.12) and (2.14) the two kernels Φ_1, Φ_2 are related by

$$\Phi_2(mr_1(t), t) = \int_0^t \left\{\dot{\Phi}_1(mr_1(t'), t') + m\dot{r}_1(t')\, \Phi_1'(mr_1(t'), t')\right\} \mu(t - t')\, dt', \tag{2.20}$$

$$\Phi_1(mr_1(t), t) = \int_0^t \left\{\dot{\Phi}_2(mr_1(t'), t') + m\dot{r}_1(t')\, \Phi_2'(mr_1(t'), t')\right\} \mu^{-1}(t - t')\, dt', \tag{2.21}$$

where

$$\dot{\Phi}(x, t) = \partial\Phi/\partial t, \qquad \Phi'(x, t) = \partial\Phi/\partial x.$$

Equations (2.17), (2.18) comprise a pair of dual integral equations for the determination of the related functions Φ_1 and Φ_1. For an elastic solid for which $\mu(t) \equiv \mu_D$ and $\mu^{-1}(t) \equiv \mu_D{}^{-1}$, the two kernels Φ_1 and Φ_2 differ only by a multiplicative constant and the resulting integral equations are well known (Titchmarsh 1937, Busbridge 1938, Sneddon 1951). By following Titchmarsh's analysis for the present problem we arrive at the following pair of integral equations in the complex plane:

$$\frac{1}{2\pi i}\int_{k-i\infty}^{k+i\infty} \frac{\Gamma(\frac{1}{2}s)}{\Gamma(\frac{1}{2}+\frac{1}{2}s)}\, \frac{x_1(s, t)}{s-\omega}\, ds = \frac{A(t)}{1-\omega} - \frac{B(t)}{3-\omega}, \tag{2.22}$$

$$\frac{1}{2\pi i}\int_{k'-i\infty}^{k'+i\infty} \frac{\Gamma(1-\frac{1}{2}s)}{\Gamma(\frac{1}{2}-\frac{1}{2}s)}\, \frac{x_2(s, t)}{s-\omega}\, ds = 0, \tag{2.23}$$

which are entirely equivalent to (2.17), (2.18). In (2.22), (2.23) the integration contours lie on either side of the singularity $s = \omega$ and within the strip $0 < Re(s) < 1$,

$$\text{viz: } 0 < k' < Re(\omega) < k < 1$$

while the kernels x_i are defined by the Mellin transforms of Φ_i,

$$x_i(s, t) = \frac{\Gamma(\frac{1}{2}-\frac{1}{2}s)}{2^s\, \Gamma(\frac{1}{2}s)}\, F_i(s, t), \qquad (i = 1, 2) \tag{2.24}$$

$$F_i(s, t) = \int_0^\infty \Phi_i(y, t)\, y^{s-1}\, dy, \qquad 0 < Re(s) < 1. \tag{2.25}$$

From (2.20), (2.21), (2.24) and (2.25) we deduce the convolution integral relations connecting x_1 and x_2,

$$x_2(s,t) = \int_0^t \mu(t-t') \frac{\partial}{\partial t'} \left\{ x_1(s,t') \left[\frac{r_1(t)}{r_1(t')} \right]^s \right\} dt', \tag{2.26}$$

$$x_1(s,t) = \int_0^t \mu^{-1}(t-t') \frac{\partial}{\partial t'} \left\{ x_2(s,t') \left[\frac{r_1(t)}{r_1(t')} \right]^s \right\} dt', \tag{2.27}$$

which together with (2.22) and (2.23) define the spherical indenter problem for a viscoelastic solid.

The purpose in extracting $2^s \Gamma(\frac{1}{2}s)/\Gamma(\frac{1}{2} - \frac{1}{2}s)$ from the definition of the x_i functions in (2.24) is to ensure that the resulting ratios of Γ functions in (2.22) and (2.23) are functions of s which are regular and free from zeros, respectively in the domains $Re(s) > 0$, $Re(s) < 1$.

For an elastic solid (2.26) and (2.27) reduce to $x_2 = \mu_D x_1$ and the (unique) solution

$$x_1(s,t) = \pi^{-\frac{1}{2}} \left[\frac{A(t)}{1-s} - \frac{2B(t)}{3-s} \right] = \mu_D^{-1} x_2(s,t) \tag{2.28}$$

may be verified directly. For, if we complete the contour for the integral on the left side of (2.23) with a semi-circle in the left plane, the contour encloses no singularities of the integrand; further, on the semi-circle the integrand is of order $|s|^{-\frac{1}{2}}$ so that (2.23) is verified. Similarly, if we complete the contour for the integral in (2.22) with a semi-circle in the right plane, the only enclosed singularities are simple poles at $s = 1$, $s = 3$ respectively with residues

$$R(1) = \frac{\pi^{\frac{1}{2}} A(t)}{1-\omega}, \qquad R(3) = -\frac{\pi^{\frac{1}{2}} B(t)}{(3-\omega)}.$$

Here the integrand is of order $|s|^{-\frac{1}{2}}$ around the semi-circle so that (2.22) is verified.

The important results for the elastic contact problem are recovered as follows. From (2.24), (2.28) we have

$$F_1(s,t) = \pi^{-\frac{1}{2}} \left\{ \frac{2^{s-1}\Gamma(\frac{1}{2}s)}{\Gamma(3/2 - \frac{1}{2}s)} A(t) - \left[\frac{2^{s-1}\Gamma(\frac{1}{2}s)}{\Gamma(5/2 - \frac{1}{2}s)} - \frac{2^s \Gamma(1 + \frac{1}{2}s)}{\Gamma(5/2 - \frac{1}{2}s)} \right] B(t) \right\} \tag{2.29}$$

whose Mellin inversion is (TITCHMARSH 1937, p. 196)

$$\Phi_1(y,t) = \frac{2A(t)}{\pi} \frac{\sin y}{y} - \frac{2^{\frac{1}{2}} B(t)}{\pi^{\frac{1}{2}}} \{ y^{-\frac{1}{2}} J_{\frac{1}{2}}(y) - y^{-\frac{1}{2}} J_{\frac{3}{2}}(y) \}. \tag{2.30}$$

Substituting this expression into (2.15) and (2.16) and carrying out the resulting integrations (e.g. see ERDELYI *et al.* 1954) leads to

$$r_1(t)\, u_z = \begin{cases} A(t) - B(t)\, x^2, & x = r/r_1 < 1 \quad (2.31) \\ \dfrac{2A(t)}{\pi} \sin^{-1}(x^{-1}) - \dfrac{4B(t)}{3\pi x} F(3/2, \tfrac{1}{2}, 5/2, x^{-2}), & x > 1 \quad (2.32) \end{cases}$$

$$-(1-\nu) r_1^2(t)\, \sigma_z = \begin{cases} \mu_D \left[\dfrac{2A(t)}{\pi} (1-x^2)^{-\frac{1}{2}} + \dfrac{4B(t)}{\pi} (1-x^2)^{\frac{1}{2}} \right. \\ \qquad \left. - \dfrac{4B(t)}{\pi} x^2 (1-x^2)^{-\frac{1}{2}} \right], & x < 1 \quad (2.33) \\ 0, & x > 1. \end{cases}$$

To avoid singularities in σ_z at $x = 1$ we have to choose $A = 2B = r_1^3(t)/R$ [from (2.19)] so that we finally derive

$$-\sigma_z = \begin{cases} \dfrac{4\mu_D r_1}{\pi(1-\nu)R}(1 - r^2/r_1^2)^{\frac{1}{2}}, & r < r_1 \\ 0, & r > r_1 \end{cases} \tag{2.34}$$

$$u_z = \begin{cases} \dfrac{r_1^2}{R} - \dfrac{r^2}{2R}, & r < r_1 \\ \dfrac{2r_1^2}{\pi R}\left\{(1 - \tfrac{1}{2}x^2)\sin^{-1}(x^{-1}) + \tfrac{1}{2}(x^2-1)^{\frac{1}{2}}\right\}, & x = r/r_1 > 1 \end{cases} \tag{2.35}$$

in which we have expressed the hypergeometric function in (2.32) in terms of elementary functions.

It is convenient to denote the function on the right side of (2.30) by $f(y, t)$:

$$f(y,t) = \frac{r_1^3(t)}{R}\left\{\frac{2}{\pi}\frac{\sin y}{y} - \left(\frac{2}{\pi}\right)^{\frac{1}{2}}\left[y^{-\frac{1}{2}}J_{\frac{1}{2}}(y) - y^{-\frac{1}{2}}J_{\frac{1}{2}}(y)\right]\right\}. \tag{2.36}$$

This function is of importance in the solutions of (2.22), (2.23) for the viscoelastic case, which follows immediately.

3. Viscoelastic Solutions for Monotonic $r_1(t)$

We assume a solution for which

$$x_1 = x_1^{\circ}(s,t) \equiv \pi^{-\frac{1}{2}}\left[\frac{A(t)}{1-s} - \frac{2B(t)}{3-s}\right] \tag{3.1}$$

so that from the previous analysis (2.22) is satisfied. From (2.26)

$$x_2 = x_2^{\circ} \equiv \pi^{-\frac{1}{2}}\int_0^t \mu(t-t')\frac{\partial}{\partial t'}\left\{\left[\frac{A(t')}{1-s} - \frac{2B(t')}{3-s}\right]\left[\frac{r_1(t)}{r_1(t')}\right]^s\right\}dt' \tag{3.2}$$

which is a regular function of s in the half-plane $Re(s) < 1$ provided that $r_1(t) > r_1(t')$ for all $t > t'$. Thus, for monotonically increasing $r_1(t)$, (2.23) is satisfied and (3.1), (3.2) provide a solution to the problem. Further, the solution is unique, as may be seen from the following argument. We write

$$x_1 = x_1^{\circ} + x_1^{(1)} \qquad x_2 = x_2^{\circ} + x_2^{(1)}$$

so that (2.22), (2.23) become

$$\frac{1}{2\pi i}\int_{k-i\infty}^{k+i\infty}\frac{\Gamma(\frac{1}{2}s)}{\Gamma(\frac{1}{2}+\frac{1}{2}s)}\frac{x_1^{(1)}}{(s-\omega)}\,ds = 0, \tag{3.3}$$

$$\frac{1}{2\pi i}\int_{k'-i\infty}^{k'+i\infty}\frac{\Gamma(1-\frac{1}{2}s)}{\Gamma(\frac{1}{2}-\frac{1}{2}s)}\frac{x_2^{(1)}}{(s-\omega)} = 0, \tag{3.4}$$

where, because the problem is linear,

$$x_1^{(1)}(s,t) = \int_0^t \mu^{-1}(t-t')\frac{\partial}{\partial t'}\left\{x_2^{(1)}(s,t)\left[\frac{r_1(t)}{r_1(t')}\right]^s\right\}dt'. \tag{3.5}$$

Following Titchmarsh we have $\Gamma(1-\frac{1}{2}s)/\Gamma(\frac{1}{2}-\frac{1}{2}s)$ is a regular function of s without zeros for $Re(s) < Re(\omega)$ so that equation (3.4) shows $x_2^{(1)}$ to be regular in the same domain; thus, from (3.5), $x_1^{(1)}$ is regular in the same domain provided $r_1(t)$ is a monotonically increasing function. It follows that

$$\frac{1}{2\pi i}\int_{k'-i\infty}^{k'+i\infty}\frac{x_1^{(1)}}{s-\omega}\,ds = 0. \tag{3.6}$$

On the other hand $\Gamma(\frac{1}{2}s)/\Gamma(\frac{1}{2}+\frac{1}{2}s)$ is a regular function of s without zeros for $Re(s) > Re(\omega)$ so that

$$\frac{1}{2\pi i}\int_{k-i\infty}^{k+i\infty}\frac{x_1^{(1)}}{s-\omega} = 0. \tag{3.7}$$

Moving the line of integration from k' to k in (3.6) gives

$$x_1^{(1)}(\omega, t) = \frac{1}{2\pi i}\int_{k-i\infty}^{k+i\infty}\frac{x_1^{(1)}(s,t)}{s-\omega}\,ds$$

and by (3.7)

$$x_1^{(1)}(s,t) = 0, \qquad 0 < Re(s) < 1. \tag{3.8}$$

However, since we have proved incidentally that $x_1^{(1)}$ is regular in the entire complex plane, then by a well known theorem, $x_1^{(1)}$ is at most a constant and by analytic continuation of (3.8) $x_1^{(1)}$ vanishes identically for all s.

To obtain nonsingular stresses at the circle of contact we have to make the same choice for $A(t)$ as previously, namely

$$A(t) = 2B(t) = r_1^2(t)/R$$

so that the displacement determined by x_1° is identical with that for an elastic solid. The stress field is determined by

$$x_2^\circ = R^{-1}\left(\frac{1}{1-s}-\frac{1}{3-s}\right)\int_0^t \mu(t-t')\frac{\partial}{\partial t'}\left\{r_1^3(t')\left[\frac{r_1(t)}{r_1(t')}\right]^s\right\}dt'. \tag{3.9}$$

Comparing this expression with the elastic solution (2.28) and using the result that the Mellin transform of $f(ny)$ is n^{-s} times the transform of $f(y)$, we find the corresponding

$$\phi_2 = \int_0^t \mu(t-t')\frac{\partial}{\partial t'}f\left(yr_1(t)/r_1(t'), t'\right)dt'$$

where f is defined by (2.36).

The stress under the ball is given by

$$-(1-\nu)r_1^2(t)\sigma_z = \int_0^t dt'\,\mu(t-t')\int_0^\infty y\frac{\partial}{\partial t'}f\left(y\frac{r_1(t)}{r_1(t')}, t'\right)J_0\left(y\frac{r}{r_1(t)}\right)dy.$$

Carrying out the y integration using previously obtained results leads finally to

$$\sigma_z = \begin{cases} -\dfrac{4}{\pi R(1-\nu)}\displaystyle\int_0^t \mu(t-t')\frac{d}{dt'}\left(r_1^2(t')-r^2\right)^{\frac{1}{2}}dt', & r_1(t') > r \\ 0, & r > r_1(t) \end{cases} \tag{3.10}$$

in which the restriction on r implies that the effective lower limit in the integral is the solution of the equation $r_1(t) = r$.

Since $\mu(t-t') > 0$ while $\{r_1^2(t')-r^2\}^{\frac{1}{2}}$ is a monotonic increasing function of time, (3.10) yields compressive stresses for all points under the ball.

The solution (3.10) is that previously obtained by RADOK and LEE (1960) who note that, once $r_1(t)$ passes through a maximum (3.10) may predict tensile stresses within the circle of contact, and is thereby invalid. The reason for the failure is quite clear in the present analysis, since once there exist times $t' < t$ for which $r_1(t') > r_1(t)$, the value of x_2° given by (3.9) is no longer a regular function of s for $Re(s) < 0$ and (2.23) is violated. The correct solution for the case where $r_1(t)$ is a continuous function with a single maximum is given in Section 4.

Finally, in anticipation of the rebound problem for which the present analysis is valid prior to the point of maximum penetration, we derive the total resisting force for the indenter together with the equation of motion. The total resistive force given by (3.10) is

$$F = -\frac{8}{R(1-\nu)}\int_0^{r_1(t)} r\,dr\int_0^t \mu(t-t')\frac{d}{dt'}\left(r_1^2(t')-r^2\right)^{\frac{1}{2}}dt' \tag{3.11}$$

in which the effective lower limit of the time integral is the solution of $r_1(t) = r$. As written in (3.11), the evaluation of the double integral in the r, t' plane implies first an integration with r constant, followed by a summation over horizontal strips lying beneath the $r_1(t')$ curve (Fig. 1a), By inverting the order of integration so that the final summation is carried out over vertical strips (Fig. 1b), the integration with respect to r may be carried out explicitly to yield

$$\begin{aligned} F &= -\frac{8}{R(1-\nu)}\int_0^t \mu(t-t')\frac{d}{dt'}\int_0^{r_1(t')} r\left(r_1^2(t')-r^2\right)^{\frac{1}{2}}dr \\ &= -\frac{8}{3R(1-\nu)}\int_0^t \mu(t-t')\frac{d}{dt'}\left(r_1^3(t')\right)dt' \end{aligned} \tag{3.12}$$

in which the lower limit of the time integral is here truly zero. Equation (3.12) is also derived by RADOK and LEE by a somewhat different method.

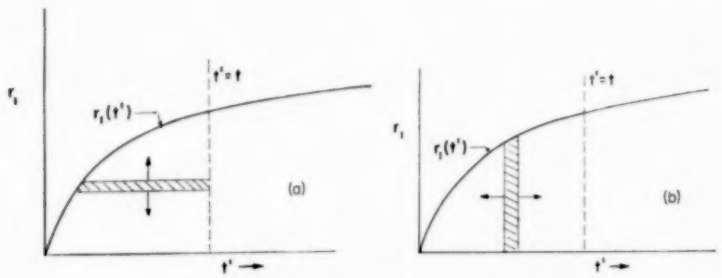

FIG. 1. Evaluation of resistive force on indenter.
(a) The integral (3.11). (b) The integral (3.12).

Since the surface displacement is identical with that for the corresponding elastic problem, the indenter penetration is given by (c.f. (2.35)).

$$\alpha = r_1^2(t)/R \tag{3.13}$$

so that by Newton's third law and (3.12) the equation of motion of the indenter prior to maximum penetration is

$$M\ddot{\alpha}(t) = -\frac{8R^{\frac{1}{2}}}{3(1-\nu)}\int_0^t \mu(t-t')\frac{d}{dt'}\left(\alpha^{\frac{3}{2}}(t')\right)dt' \tag{3.14}$$

or equivalently

$$-\alpha^{\frac{3}{2}}(t) = \frac{3M(1-\nu)}{8R^{\frac{1}{2}}}\int_0^t \mu^{-1}(t-t')\frac{d^3\alpha(t')}{dt'^3}dt' \tag{3.15}$$

in which M is the indenter mass. We return to equation (3.15) in Section 5.

4. VISCOELASTIC SOLUTION WHERE $r_1(t)$ POSSESSES A SINGLE MAXIMUM

In this section we derive a solution where $r_1(t)$ is of the form depicted in Fig. 2, i.e. a continuous function of time with a single maximum occurring at $t = t_m$. For $t \leqslant t_m$, $r_1(t) > r_1(t')$ for $t > t'$, while for $t > t_m$ there exist values of t' in the range $t_1(t) > t' > t$ for which $r_1(t) < r_1(t')$. Here $t_1(t)$ is the solution of the equation

$$r_1(t) = r_1(t_1), \qquad t > t_m, \qquad t_1 < t_m.$$

For $t < t_m$ we already have the solution given by (3.1) and (3.2). For $t > t_m$ we make the substitution

$$x_2 = x_2^{(2)} + \frac{\pi^{-\frac{1}{2}}}{R}\left(\frac{1}{1-s} - \frac{1}{3-s}\right)\int_0^{t_1} \mu(t-t')\frac{\partial}{\partial t'}\left\{r_1^3(t')\left[\frac{r_1(t)}{r_1(t')}\right]^s\right\} dt' \tag{4.1}$$

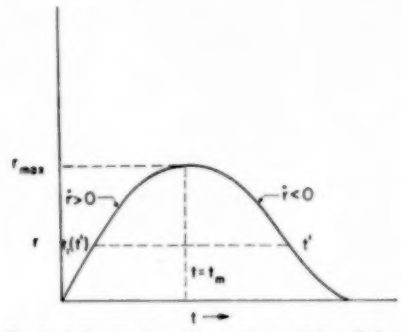

FIG. 2. Typical loading path $r_1(t)$ considered in Section 4.

in which the integral term is a regular function of s for $Re(s) < 0$. Since (2.23) shows that x_2 is regular in the same region, $x_2^{(2)}$ is likewise regular. The corresponding value of x_1 for $t > t_m$ is given by

$$x_1 = \int_0^t \mu^{-1}(t-t')\frac{\partial}{\partial t'}\left\{x_2(s,t')\left[\frac{r_1(t)}{r_1(t')}\right]^s\right\} dt'.$$

Substituting for x_2 from (3.2) for $t < t_m$ and from (4.1) for $t > t_m$ yields (after some algebra)

$$x_1 = \frac{\pi^{-\frac{1}{2}}}{R}\left(\frac{1}{1-s} - \frac{1}{3-s}\right)\left\{r_1^3(t) - \int_{t_m}^t \mu^{-1}(t-t')\frac{\partial}{\partial t'}\left[\int_{t_1(t')}^{t'} \mu(t'-t'')\times\right.\right.$$
$$\left.\left.\frac{\partial}{\partial t''}\left\{r_1^3(t'')\left(\frac{r_1(t)}{r_1(t'')}\right)^s\right\} dt''\right] dt'\right\} + \int_{t_m}^t \mu^{-1}(t-t')\frac{\partial}{\partial t'}\left[\left(\frac{r_1(t)}{r_1(t')}\right)^s x_2^{(2)}(s,t')\right] dt'. \tag{4.2}$$

For all relevant t'' in the double integral term in (4.2), $r_1(t) < r_1(t'')$. It follows that with the exception of simple poles at $s = 1$, $s = 3$ the terms in (4.2) not involving $x_2^{(2)}$ are regular functions of s for $Re(s) > 0$. Inserting (4.2) into (2.22) yields ultimately

$$\frac{1}{2\pi i}\int_{t_m}^t \int_{k-i\infty}^{k+i\infty} \mu^{-1}(t-t')\frac{\Gamma(\frac{1}{2}s)}{\Gamma(\frac{1}{2}+\frac{1}{2}s)}\frac{\partial}{\partial t'}\left[x_2^{(2)}\left(\frac{r_1(t)}{r_1(t')}\right)^s\right]\frac{dt'\,ds}{s-\omega} = \frac{Q(t)}{1-\omega} \tag{4.3}$$

where

$$Q(t) = A(t) - r_1^3(t)/R +$$
$$+ R^{-1}\int_{t_m}^t \mu^{-1}(t-t')\frac{d}{dt'}\left\{\int_{t_1(t')}^{t'} \mu(t'-t'')\frac{d}{dt''}\left(r_1^2(t'')\,r_1(t)\right) dt''\right\} dt'. \tag{4.4}$$

The unique solution of (4.3) regular in $Re(s) < 0$ may be shown to be

$$x_2^{(2)} = \frac{\pi^{-\frac{1}{2}}}{1-s}\int_{t_m}^t \mu(t-t')\frac{d}{dt'}\left[\frac{r_1(t)}{r_1(t')}Q(t')\right] dt'$$

and in contrast with the remaining terms in (4.1) leads to singular stresses at the contact circle. It follows that $x_2^{(2)}$ vanishes so that $Q(t)$ can only be a constant multiple of $r_1(t)$. However, in the limit $t \to t_m + 0$, (4.4) gives

$$Q(t_m) = A(t_m) - r_1^3(t_m)/R$$

and since $A(t)$ $(\equiv \alpha(t) r_1(t))$ is continuous while for $t < t_m$, $\alpha(t) \equiv r_1^2(t)/R$, we must have $Q(t_m) = 0$. It follows that $Q(t)$ is identically zero and the indenter penetration given by

$$R\alpha(t) = r_1^2 - \int_{t_m}^{t} \mu^{-1}(t-t') \frac{d}{dt'} \left[\int_{t_1(t')}^{t'} \mu(t'-t'') \frac{d}{dt''} (r_1^2(t'')) \, dt'' \right] dt', \qquad t > t_m. \tag{4.5}$$

From (4.2) with $x_2^{(2)} = 0$, we confirm the displacement under the ball as

$$u_z = \alpha(t) - r^2/2R, \qquad r < r_1(t),$$

with α given by (4.5) For $r > r_1(t)$ a much more complicated result follows which entails (among other terms) hereditary integrals of the functions appearing on the right hand side of (2.35). From this result, in the limit $r = r_1(1+\delta)$ where $\delta \ll 1$, it may be shown that the indenter and free surface are separated by the positive quantity

$$\frac{8\sqrt{2}}{3\pi} \cdot \frac{\mu(t - t_1(t))}{\mu_D R} r_1^2 \delta^{\frac{3}{2}} \tag{4.6}$$

in the derivation of which the logarithmic variation of $\mu(t-t_1)$ over the time taken for the contact circle to contract from $r_1(1+\delta)$ to r_1 has been assumed negligible. The separation (4.6) is to be compared with the value

$$\frac{8\sqrt{2}}{3\pi R} \cdot r_1^2 \delta^{\frac{3}{2}}$$

obtaining during the penetration process (and for the corresponding elastic problem).

From (4.1), with $x_2^{(2)} = 0$, we find for the stress under the ball

$$\sigma_z = \begin{cases} -\dfrac{4}{\pi(1-\nu)R} \displaystyle\int_0^{t_1(t)} \mu(t-t') \frac{d}{dt'} \{r_1^2(t') - r^2\}^{\frac{1}{2}} dt', & r_1(t') > r \\ 0, & r > r_1(t) \end{cases}$$

and since $\{r_1^2(t') - r^2\}^{\frac{1}{2}}$ is monotonically increasing in the integration range,* the stresses are everywhere compressive. Evaluating the total resistive force by the same procedure adopted for (3.11) leads to

$$F = -\frac{8}{3R(1-\nu)} \int_0^{t_1(t)} \mu(t-t') \frac{d}{dt'} (r_1^3(t')) \, dt' \tag{4.7}$$

which differs from (3.12) only in that $t_1(t)$ replaces t as the upper limit of the integral.

For prescribed $r_1(t)$ conforming to Fig. 2 we have obtained a complete solution of the indentation problem for a viscoelastic solid. However, the problem of dominant physical interest is that of dynamic impact, for which $r_1(t)$ is not prescribed ; rather the present results required to be supplemented by Newton's third law

$$F = M\ddot{\alpha}(t) \tag{4.8}$$

which then determines $r_1(t)$ concomitantly with $\alpha(t)$. For $t < t_m$ we have already carried out this procedure to the point where we obtained a single nonlinear integro-differential equation for $\alpha(t)$, namely (3.15). In general, for $t > t_m$, (4.5), (4.7) and (4.8) appear not to lead to a single equation for $\alpha(t)$ except under certain limiting circumstance discussed in the final Section below.

5. Dynamic Impact Problem

A solution of the impact problem for a solid of arbitrary mechanical properties appears to be feasible only on a numerical basis. However, for a solid which is nearly elastic in the sense that the creep and relaxation functions are adequately approximated by the expansions (2.6) over the impact period, we can obtain

*As in (3.10) the lower limit on the integral is effectively the point where $r_1(t) = r$ $(t < t_m)$.

an analytic solution to terms linear in the parameter η. The solution so obtained is valid provided

$$\eta T \ll 1$$

where T is the total impact duration.

To terms linear in η, we may replace equations (2.6) by

$$\mu(t) = \mu_D e^{-\eta t} \qquad \mu^{-1}(t) = \mu_D^{-1}(1 + \eta t) \tag{5.1}$$

which, in addition to simplifying the subsequent analysis, are the exact reciprocal functions for a Maxwell solid.

With $\mu^{-1}(t)$ given by (5.1), the equation of motion of the indenter for $t < t_m$ (3.15) reduces to the differential equation

$$\ddot{\alpha} + \eta(\dot{a} - V) = -\frac{8R^{\frac{1}{2}}\mu_D}{3M(1-\nu)}\alpha^{\frac{3}{2}}, \qquad t < t_m, \tag{5.2}$$

with boundary conditions

$$\dot{a} = V, \qquad \alpha = 0, \qquad t = 0,$$

where V is the initial impact velocity.

For $t > t_m$, substitution of (5.1) into (4.5) yields

$$R\alpha = r_1^2(t) - \int_{t_m}^{t} (1 + \eta(t - t')) \frac{d}{dt'} \left[\int_{t_1(t')}^{t'} e^{-\eta(t'-t'')} \frac{d}{dt''} r_1^2(t'')\, dt'' \right] dt'.$$

On differentiating this equation we obtain the surprisingly simple result

$$R\dot{a} = e^{-\eta(t-t_1)} \frac{d}{dt_1}\left(r_1^2(t_1)\right) \frac{dt_1}{dt} \tag{5.3}$$

or, since $r_1(t) = r_1(t_1)$,

$$R\dot{a} = e^{-\eta(t-t_1)} \frac{d}{dt}\left(r_1^2(t)\right), \qquad t > t_m, \tag{5.4}$$

which replaces the equation

$$R\alpha = r_1^2(t), \qquad t < t_m, \tag{5.5}$$

for $t < t_m$. We note that at $t = t_m$, r_1 is a maximum and therefore $\dot{r}_1(t_m) = 0$. It follows from (5.4) and (5.5) that α is likewise a maximum so that optimum penetration and contact radius occur concurrently ; this latter result may be proved more generally for a solid with arbitrary properties.

The total force resisting the indenter for $t > t_m$ is given by [equation (4.7)]

$$F = -\frac{8\mu_D}{3R(1-\nu)} \int_0^{t_1(t)} e^{-\eta(t-t')} \frac{d}{dt'}\left(r_1^3(t')\right) dt'$$

from which we deduce

$$\frac{dF}{dt} + \eta F = -\frac{8\mu_D}{3R(1-\nu)} \frac{dt_1}{dt} e^{-\eta(t-t_1)} \frac{d}{dt_1}\left(r_1^3(t_1)\right)$$

or, since $F = M\ddot{\alpha}$,

$$M(\dddot{\alpha} + \eta\ddot{\alpha}) = -\frac{8\mu_D}{3R(1-\nu)} \frac{dt_1}{dt} e^{-\eta(t-t_1)} \frac{d}{dt_1}\left(r_1^3(t_1)\right). \tag{5.6}$$

Alternatively,

$$M(\ddot{\bar{\alpha}} + \eta\ddot{\alpha}) = -\frac{8\mu_D}{3R(1-\nu)} e^{-\eta(t-t_1)} \frac{d}{dt}(r_1^3(t)). \tag{5.7}$$

Since (5.3) permits the determination of $\ddot{\alpha}(t)$, $\ddot{\bar{\alpha}}(t)$ entirely in terms of t, $t_1(t)$ and $r_1(t_1)$ (presumed known from the solution of (5.2) since $t_1 < t_m$), (5.6) constitutes a complicated differential equation for $t_1(t)$. Fortunately, to terms linear in η, a much simpler treatment is possible. We observe that, in the limit $\eta \to 0$, the problem reduces to that of elastic impact for which the function $r_1(t)$ is symmetrical about $t = t_m$ and for which

$$t_1 = 2t_m - t. \tag{5.8}$$

For the viscoelastic case therefore it is reasonable to expect that, for small η,

$$t_1 = 2t_m - t + \eta\theta(t) + 0(\eta^2)$$

and this may be verified by the procedure outlined above. However, if we confine attention to (5.4) and (5.7), it is seen that t_1 only enters by virtue of the exponential factor $\exp[-\eta(t-t_1)]$ and so to terms linear in η we can replace t_1 by the zeroth order approximation (5.8), obtaining for $t > t_m$

$$R\ddot{\alpha} = e^{-2\eta(t-t_m)} \frac{d}{dt}(r_1^2(t)),$$

$$\ddot{\bar{\alpha}} + \eta\ddot{\alpha} = -\frac{8\mu_D}{3MR(1-\nu)} e^{-2\eta(t-t_m)} \frac{d}{dt}(r_1^3(t)).$$

To terms linear in η the elimination of α between these two equations leads to

$$\ddot{Z} - 3\eta\dot{Z} = -\frac{8\mu_D R^{\frac{1}{2}}}{3M(1-\nu)} \frac{d}{dt}(Z^{\frac{3}{2}}) \tag{5.9}$$

where

$$Z = \frac{r_1^2(t)}{R}. \tag{5,10}$$

A first integration of (5.9) gives

$$\ddot{Z} - \ddot{Z}(t_m) - 3\eta(\dot{Z} - \dot{Z}(t_m)) = -\frac{8\mu_D R^{\frac{1}{2}}}{3M(1-\nu)} \{Z^{\frac{3}{2}} - Z^{\frac{3}{2}}(t_m)\}. \tag{5.11}$$

At $t = t_m$, $\dot{Z}(t_m) = 0$ so that from (5.4) and (5.10) for $t = t_m + 0$, $\ddot{Z} = \ddot{\alpha}$. For $t < t_m$, $Z(t) \equiv \alpha(t)$ and the continuity of $F(\equiv M\ddot{\alpha})$ implies, from (5.2),

$$\ddot{Z}(t_m) + \eta(\dot{Z}(t_m) - V) = -\frac{8\mu_D R^{\frac{1}{2}}}{3M(1-\nu)} Z^{\frac{3}{2}}(t_m).$$

With $\dot{Z}(t_m) = 0$, (5.11) becomes therefore

$$\ddot{Z} - \eta(3\dot{Z} + V) = -\frac{8\mu_D R^{\frac{1}{2}}}{3M(1-\nu)} Z^{\frac{3}{2}} \tag{5.12}$$

which provides an equation of motion for the ejection part of the cycle. The solution of (5.12) is subject to the boundary conditions at $t = t_m$, (a) $\dot{Z}(t_m) = 0$, (b) $Z(t_m)$ continuous from the solution of (5.2) for $t < t_m$.

The approximate solutions of (5.2) and (5.12) are effected in the Appendix. The principal results to emerge are the following estimates of the coefficient of

restitution e and impact duration T:

$$e = 1 - \tfrac{4}{5}\eta T_0, \qquad T = T_0(1 - 0{\cdot}037\,\eta T_0),$$

where T_0 is the elastic impact duration

$$T_0 = 2{\cdot}94\left(\frac{15M(1-\nu)}{32R^{\frac{1}{2}}\mu_D}\right)^{\frac{2}{5}} V^{-\frac{1}{5}}$$

and where η may be regarded as the mean inverse relaxation time of the solid.

The present approximation, valid for $\eta T_0 \ll 1$, is pertinent for solids whose properties are nearly 'glass-like' at the temperature of testing. Since the modification to the Hertzian impact duration is negligible, measurement of T determines the essentially dynamic quantity $\mu_D/(1-\nu)$ while measurement of e provides an estimate of η.

ACKNOWLEDGMENT

The author is indebted to the Commonwealth Fund of New York for the award of a Harkness Fellowship, during the tenure of which the present work was undertaken.

REFERENCES

BUSBRIDGE, I. W.	1938	*Proc. Lond. Math. Soc.* **44**, 115.
ERDELYI, A.	1954	*Tables of Integral Transforms*, Vol. 2 (McGraw-Hill, New York).
HUNTER, S. C.	1960	*Progress in Solid Mechanics*, Vol 1 (North-Holland Publishing Company, Amsterdam).
LAMB, H.	1902	*Proc. Lond. Math. Soc.* **34**, 276.
LEE, E. H.	1955	*Quart. Appl. Math.* **13**, 183.
LEE, E. H. and RADOK, J. R. M.	1960	*J. Appl. Mech.* (To be published).
SNEDDON, I. N.	1951	*Fourier Transforms* (McGraw-Hill, New York).
TITCHMARSH, E. C.	1937	*Theory of Fourier Integrals* (Clarendon Press, Oxford).

APPENDIX

Approximate solutions of equations of motion

With $\mathbf{Z} = r_1^2/R$, the equations of motion for the indenter are

$$\ddot{\mathbf{Z}} + \eta(\dot{\mathbf{Z}} - V) = -\frac{8\mu_D R^{\frac{1}{2}}}{3M(1-\nu)}\mathbf{Z}^{\frac{3}{2}}, \qquad t < t_m, \tag{A1}$$

$$\ddot{\mathbf{Z}} - \eta(3\dot{\mathbf{Z}} + V) = -\frac{8\mu_D R^{\frac{1}{2}}}{3M(1-\nu)}\mathbf{Z}^{\frac{3}{2}}, \qquad t > t_m. \tag{A2}$$

In terms of the dimensionless variables

$$\omega = \mathbf{Z}/\alpha_0, \qquad \xi = Vt/\alpha_0,$$

(A1) and (A2) become

$$\frac{d^2\omega}{d\xi^2} + K\left(\frac{d\omega}{d\xi} - 1\right) = -\tfrac{5}{4}\omega^{\frac{3}{2}}, \qquad \omega = 0, \quad \frac{d\omega}{d\xi} = 1, \quad \xi = 0, \tag{A3}$$

$$\frac{d^2\omega}{d\xi^2} - K\left(3\frac{d\omega}{d\xi} + 1\right) = -\tfrac{5}{4}\omega^{\frac{3}{2}}, \qquad \omega = \omega_m, \quad \dot{\omega}(\xi_m) = 0, \quad \xi = \xi_m. \tag{A4}$$

Here

$$K = \eta\alpha_0/V, \qquad \text{and} \qquad \alpha_0 = \left[\frac{15M(1-\nu)}{32R^{\frac{1}{2}}\mu_D}V^2\right]^{\frac{2}{5}}.$$

α_0 is the maximum penetration for an elastic solid while ξ_m is the point for which (A3) first yields $d\omega/d\xi = 0$; the corresponding value of $\omega = \omega(\xi_m)$ is denoted by ω_m.

Writing $v = d\omega/d\xi$, a formal integration of (A3) leads to

$$v^2 = c + 2K\omega - \omega^{\frac{5}{2}} + 2K\int_{\omega}^{\beta} v\,d\omega' \tag{A5}$$

where c and β are integration constants related by the boundary condition

$$1 = c + 2K\int_{0}^{\beta} v\,d\omega'. \tag{A6}$$

We proceed on the assumption that $K \ll 1$; this is equivalent to the assumption $\eta T \ll 1$ already adopted in the derivation of (A2). Equation (A5) is in a form suitable for iteration; a first iteration leads to

$$v^2 = c + 2K\omega - \omega^{\frac{5}{2}} + \int_{\omega}^{\beta} (c + 2K\omega' - \omega'^{\frac{5}{2}})^{\frac{1}{2}}\,d\omega'. \tag{A7}$$

Now $v = 0$, $\omega = \omega_m$ is a movable singularity of (A3) and in order that (A7) should provide a uniformly valid second approximation for all ω in the range $0 < \omega < \omega_m$ we have to choose $\beta = \omega_m$, $c = \omega_m^{\frac{5}{2}} - 2K\omega_m$. The actual value of ω_m is then given by (A6)

$$1 = \omega_m^{\frac{5}{2}} - 2K\omega_m + \int_{0}^{\omega_m} \{\omega_m^{\frac{5}{2}} - \omega^{\frac{5}{2}} - 2K(\omega - \omega_m)\}^{\frac{1}{2}}\,d\omega. \tag{A8}$$

In the limit $K \to 0$, $\omega_m = 1$. For $K \ll 1$ we anticipate $\omega_m = 1 + \Omega$ with $\Omega \ll 1$. With this assumption, we have on expanding (A8) to first order terms in K, Ω,

$$\Omega = \tfrac{4}{5}K(1 - I_1) \tag{A9}$$

where

$$I_1 = \int_0^1 (1 - y^{\frac{5}{2}})^{\frac{1}{2}}\,dy = \tfrac{2}{9}\frac{\Gamma(\frac{1}{2})\,\Gamma(\frac{2}{5})}{\Gamma(\frac{9}{10})} \simeq 0{\cdot}817.$$

To the same order the time to maximum penetration is given by

$$\xi_m = \int_0^{\omega_m} d\omega/v = I_2 + K[I_3 - I_4 - I_2(1 - I_1)/5]$$

where I_2 is the Hertz integral

$$I_2 = \int_0^1 \frac{dy}{(1 - y^{\frac{5}{2}})^{\frac{1}{2}}} = \tfrac{2}{5}\frac{\Gamma(\frac{1}{2})\,\Gamma(\frac{2}{5})}{\Gamma(\frac{9}{10})} \simeq 1{\cdot}47$$

and where

$$I_3 = \int_0^1 \frac{(1-y)}{(1 - y^{\frac{5}{2}})^{\frac{1}{2}}}\,dy \simeq 0{\cdot}842,$$

$$I_4 = \int_0^1 \frac{dy\displaystyle\int_y^1 (1 - x^{\frac{5}{2}})^{\frac{1}{2}}\,dx}{(1 - y^{\frac{5}{2}})^{\frac{1}{2}}} \simeq 0{\cdot}473.$$

I_3 and I_4 were evaluated by numerical integration.

The values

$$\omega_m = 1 + \tfrac{4}{5}K(1 - I_1), \qquad v = 0$$

provide the starting point for the integration of (A4), which may be treated in an identical manner. In this way we obtain for total impact time

$$\frac{VT}{x_0} = 2I_2 + K\left[2I_3 - 4I_4 - 2I_2(1 - I_1)/5\right]$$

or, on inserting numerical values and substituting for K in terms of η,

$$T = T_0(1 - 0{\cdot}037\eta T_0)$$

in which $T_0 = 2I_2x_0/V$ is the elastic impact time.

The value of v at $\omega = 0$ determines the ejection velocity V_e. To first order in K we find

$$v = 1 + 2KI_1$$

and from (5.4)

$$V_e/V \simeq ve^{-\eta T_0} \simeq (1 + \eta T_0 I_1/I_2)(1 - \eta T_0)$$

or, since $I_1/I_2 = 5/9$,

$$V_e/V = 1 - \tfrac{4}{9}\eta T_0.$$

J. Mech. Phys. Solids, 1960, Vol. 8, pp. 235 to 254. Pergamon Press Ltd., London. Printed in Great Britain

ASSESSMENT OF THE STRAIN-RATE SENSITIVITY OF METALS BY INDENTATION WITH CONICAL INDENTERS

By C. D. Davis and S. C. Hunter
Armament Research and Development Establishment, Fort Halstead

(*Received* 24*th June*, 1960)

Summary

An impact indentation test is described for investigating the behaviour of metals and alloys subjected to stress cycles of a few milliseconds duration. The test consists of the normal impact of a conically tipped tungsten carbide indenter on a plane surface of the specimen at impact velocities in the range 2–30 cm/sec. An analysis of impact indentation is made, using a quasi-stationary approach; relations between impression dimensions, contact duration and impact velocity are obtained and verified experimentally. Comparison of the impact test results with those derived from hardness measurements, using the same indenter, affords an assessment of the strain rate sensitivity of the material. Results are reported for a wide range of materials, including copper, aluminium, iron, various steels and non-ferrous alloys.

1. Introduction

The dependence of the deformation behaviour of metals and alloys upon the rate of loading has received much attention over the last two decades, the most fruitful experimental investigations being essentially dynamic versions of the standard tensile and compression testing techniques [e.g. Baron (1956), Crum and Mavis (1958), Gohlke (1957), Hawkyard and Freeman (1954), Johnson *et al.* (1953), Maiden and Campbell (1958), Strella *et al.* (1958)]. This type of experimental approach can, with careful design, give dynamic stress–strain curves with strains covering the region 0–50 per cent, but the strain-rates attainable (1–10^3 sec^{-1}) are usually confined to a limited range by the inertial properties of the apparatus. This limitation, however, applies to all known methods of dynamic testing, and hence a complete description of the strain-rate sensitive behaviour of a given material, necessitating the determination of the manifold of stress–strain curves with strain-rate as the variable parameter, would require a large number of different experimental arrangements.

However, the stress–strain relationship for metals is a relatively insensitive function of the strain-rate parameter and therefore stress–strain curves derived from arbitrary loading cycles, but over a limited range of test durations (e.g. 10^{-2}–10^{-3} sec), are closely similar. Under these circumstances it is legitimate to characterize the dynamic behaviour of a metal by the order of magnitude of the loading duration and we may then refer to dynamic testing in the second, millisecond and microsecond region. Internal ballistic problems (e.g. gun stresses during firing) are almost entirely concerned with millisecond behaviour, while terminal ballistics (e.g. target attack) are an admixture of millisecond and microsecond behaviour.

In the present work a description is given of an experiment requiring comparatively simple equipment, which assesses the average strain-rate sensitivity of a material (i.e. the ratio of the dynamic and static flow stresses) over a limited region of strain of order 10 per cent and for test durations in the millisecond region. This average strain-rate sensitivity, while of little or no use in fundamental investigations into strain-rate phenomena, would be useful as a 'design factor' or 'figure of merit' when the structural use of new materials is under consideration. This figure of merit is determined by the correlation of the indentations made statically and dynamically in the material using a conical indenter.

2. Apparatus and Experimental Procedure

The indenters consisted of conical tungsten carbide tips of 45° and 68° semi-angles, brazed onto mild steel adaptors which fitted both a pendulum block and a Vickers hardness machine.

The specimens were in the form of disks 0·975 in. diameter and 0·1in. thick. A few disks of 0·20 in. and 0·05 in. thick were also indented, and the results did not differ significantly from those on the 0·1in. specimens. It was concluded that a thickness of 0·1in. was sufficient to avoid any errors due to plastic deformation extending right through the specimen. For impact indentation the disks were securely clamped by a peripheral retaining ring to an anvil of similar material; in turn the latter was attached to an inertial block (mass $\sim$ 100 kg) by another retaining ring, lead foil being inserted between anvil and inertial block to ensure good mechanical contact. The object of the inertial block was to dissipate the elastic waves produced by the impact.

All the test surfaces were ground and polished, the final polishing being made using a diamond-paste impregnated wheel. The cold-worked surface layers were then removed, by vacuum annealing in the case of aluminium and copper, but otherwise by chemical etching.

The composition, hardness numbers and heat treatment of the materials examined are shown in Table 1.

For impact indentation the indenter was rigidly mounted on a steel pendulum block (mass $\sim$ 1 Kg) suspended by eight light strings. The suspension design prevented yawing in the pendulum motion; this, allied with careful positioning of the specimen, ensured that at the instant of impact the pendulum velocity was normal to the vertical testing surface of the specimen. The suspension length ($\sim$ 6 ft) was chosen to permit impact velocities of up to 30 cm/sec with release of the pendulum from small angular displacements about the equilibrium position. Under these circumstances the impact velocity V could be derived from the formula $V = 2\pi f\Delta$ where Δ is the horizontal displacement and f the frequency of free vibration of the pendulum. Experimentally Δ lay between 2 cm and 15 cm and was measured to the nearest 0·1 mm. Thus V was given to better than 1 per cent; corrections for pendulum damping were sufficiently small ($\sim \frac{1}{2}$ per cent) to be neglected.

The static indentations were made using a standard Vickers hardness machine, but with the conical indenter replacing the usual diamond pyramid indenter. The loading time was in the range 10–15 sec giving a ratio of strain-rates for dynamic and static indentation of about 10^4.

The diameters of the residual impressions were measured in two perpendicular directions with the microscope of a Vickers hardness machine, while the contact durations ($\sim 10^{-3}$ sec) were measured by the timing device described by Vincent *et al.* (1957) in which the making and breaking of electrical contact between the indenter and specimen was used to start and stop a microsecond counter. To ensure good electrical contact during impact the indenter was frequently cleaned with absolute alcohol.

3. Theoretical Mechanics of Indentation

(*i*) *Calculation of indentation parameters and duration of contact*

The quasi-static approach to impact problems, which avoids the difficulties due to stress-wave propagation, was used by Hertz [for a readily accessible account see Vincent *et al.* (1957)] in the analysis of the elastic impact of two spheres.

TABLE 1. *Composition, heat treatment and hardness of specimen materials*

Specimen	*Materials and Composition*	*Heat Treatment*	*V.P.N.*
Al	99·83% Aluminium. Si 0·096, Fe 0·07, Cu 0·003, Mn 0·002	Annealed 2 hr at 350°C	20
Cu	H.C. Copper. 0. 0·033%. Other impurities < 0·005	Annealed 2½ hr at 550°C *in vacuo*	41
Mo	Molybdenum. Nominal carbon content 0·01%	Stress relieved 1 hr at 1350°C	186
DSP	Aluminium Alloy. DTD 687 special purity base. Cu 1·27, Mg 2·13, Zn 5·45	Solution treated ½ hr/465°C quenched. Aged 12 hr/135°C	176
FSP	Aluminium Alloy. DTD 687 special purity base. Cu 1·29, Mg 2·57, Zn 5·48	Solution treated ½ hr/465°C quenched. Aged 12 hr/135°C	187
Mild Steel	B.S 970 En 3 Mild Steel, C 0·13, Si 0·25, Mn 0·84, S 0·046, P 0·03, Ni 0·09, Cr 0·04	Stress relieved 1 hr at 650°C	133
WDDJ	Armco iron	Heated in air 1 hr/930°C air cooled	112
WFSW	Normalized S.G. Iron. C 3·33, Si 2·15, Mn 0·24, Ni 0·52, S 0·011. Mg 0·033	Annealed 1 hr/860°C furnace cooled	166
WFST	Normalized S.G. Iron. Composition as for WFSW	—	267
WCQW	Grey cast iron. C 3·23 (total), 0·71 (combined), Si 1·44, Mn 0·79, S 0·091, P 0·44, Ni 0·50	As cast	233
WCQY	Steel. C 0·89, Si 0·32, Mn 0·28	Heated in air 1 hr/760°C air cooled	253
WFSM	19% Chromium Steel. C 0·09, Si 0·58, Mn 0·52, Ni 0·66, Cr 19·3, Mo 0·41, Ti 0·24	—	179
WFAK	Austenitic stainless steel. C 0·10, Si 0·77, Mn 0·75, Ni 9·20, Cr 18·67, Mo 0·03, Ti 0·72	—	157
WEGF	Steel. C 0·31, Si 0·19, Mn 0·72, Ni. 2·68, Cr 0·72, Mo 0·42	Hardened by oil quench from 820°C. Tempered 550°C	379
W Alloy	Sintered tungsten heavy alloy. 1% total Ni and Co	—	313
Nilo 36	Iron nickel alloy. (Invar). 36% Ni.	—	168

This analysis led to the prediction that the contact time T and the impact velocity V were related by an expression of the form

$$T = KV^{-\frac{1}{5}}$$

which was subsequently verified by the low velocity impact experiments of, amongst others, Andrews (1929, 1931). The Hertzian relation was also shown by Hunter (1957) to hold for the impact of a sphere on the plane surface of a massive body. This success suggests the validity of the quasi-static approximation for the problem of the impact of a conical indenter with the plane surface of a massive specimen; however, the fact that here the basic theoretical plasticity problem has not yet proved amenable to analysis means that we are unable to discuss the precise significance of the approximation as was the case for the Hertzian elastic problem. Nevertheless it is reasonable to argue that the physical grounds for the validity of the quasi-static approximation should be similar in the two cases.

The physical basis for the validity of the quasi-static approximation for the elastic impact of a small body and a massive one is twofold.

(i) The impact duration must be long enough for the passage of a large number of elastic waves back and forth along the relevant directions (i.e. those involving compression) of the small body.

(ii) The quasi-static state of the massive body can be realized from outgoing waves only.

In the present work, (i) is satisfied since the deformation of the indenter is wholly elastic and the time of travel of an elastic wave back and forth in the indenter mass is about 20 μsec which is a small fraction of the observed contact durations (ca. 2000 μsec).

The possibility of a quasi-static state arising from outgoing waves alone was discussed by Hunter (1954) for the associated problem of the propagation of spherically symmetric outgoing waves generated by a transient pressure pulse at an internal cavity face. It was shown that the time required for the medium to respond quasi-statically to a step function pressure pulse is of the order $2a/c_0$ where a is the cavity radius and c_0 is the propagation velocity of elastic waves in the medium.

Returning, then, to the conical indenter impact problem we might expect the corresponding time for quasi-static response to be of the order $t = d/c_0$ where d is the indentation diameter. Anticipating the relationships between d, V and T obtained subsequently, we may derive

$$\frac{t}{T} \simeq \frac{1{\cdot}4\,V}{c_0}.$$

It follows that the massive body responds quasi-statically provided that V obeys the inequality

$$\frac{1{\cdot}4\,V}{c_0} \ll 1$$

which for $c_0 \simeq 5 \times 10^5$ cm/sec is well satisfied for the present range of impact velocities.

The immediately preceding discussion implies that a knowledge of the stress system produced in static indentations with a conical indenter would be a sufficient basis for an adequate description of the corresponding impact process. This knowledge is much less complete than for (elastic) spherical indentation and we are compelled to rely on well-established semi-empirical relations derived from static loading experiments and supported to some extent by theoretical work on related problems.

In the various theoretical indentation problems studied by HILL (1950) and SHIELD (1955) it is a common result that the mean pressure P over the surface of the indenter is given by a relation of the form

$$P = cY \tag{1}$$

where Y is the flow-stress of the material (assumed constant) and c is a numerical constant of magnitude $c \simeq 3$. Equation (1) is valid for a non-hardening rigid/plastic material. In particular this result has been obtained for indenters in the shape of (a) a two-dimensional plane punch, (b) a two-dimensional wedge and (c) a flat circular punch. The mathematical difficulties associated with axisymmetric problems of plasticity have so far precluded exact solutions for the conical indenter but it is not unreasonable that an equation of the form (1) should be valid. Experimental support for this is given by DUGDALE (1954) for indentation with lubricated cones of cold-worked materials, which are a reasonably close approach to the ideal plastic–rigid material. It was found that for a given cone angle, the mean indentation pressure P bore a constant ratio to the shear yield stress k over a wide range of loads; this leads to a relation between P and Y of form (1) if it can be assumed that the von Mises yield criterion is applicable.

Other experimental information is complicated by the existence of work-hardening in all real materials. An extensive study by TABOR (1951) of the Vickers diamond indenter yields the empirical result that (1) is valid (again with $c \simeq 3$) provided that Y is interpreted as the flow stress on the compressive stress–strain curve for a particular finite strain value (8 per cent in the cases examined). To date this result has received no detailed theoretical backing but is well supported by experimental evidence for a wide variety of materials. There is, however, general theoretical support for the form of the result (i.e. the interpretation in terms of a strain value independent of indentation size) in that all pyramid diamond impressions entail an element of geometrical similarity. Geometric similarity is likewise a feature of conical indentations and a similar interpretation of equation (1) is permissible but with a different strain value. This representative strain value would be expected to be a function of the semi-angle of the cone.

In what follows we shall assume the validity of an equation of type (1) to evaluate the residual impression dimensions and duration of impact as functions of the initial impact velocity for a rigid conical indenter. The results obtained are compared with experimental evidence in Section 4.

By integrating the equation connecting the motion of the indenter with the resistance to penetration ($P = cY_i$)* we show in the Appendix that the maximum penetration x_0 is given by

$$x_0 = \left(\frac{3m}{2\pi c\, Y_i \tan^2\theta}\right)^{\frac{1}{4}} V^{\frac{1}{2}} \tag{2}$$

*The subscripts i and s refer to impact and static indentation respectively.

and the corresponding maximum diameter (d_i) of the indentation is

$$d_i = 2x_0 \tan\theta = 2\left(\frac{3m\tan\theta}{2\pi c\, Y_i}\right)^{\frac{1}{3}} V^{\frac{2}{3}}. \tag{3}$$

The loading duration T derived by further integration is

$$T = 1{\cdot}4\left(\frac{3m}{2\pi c\, Y_i \tan^2\theta}\right)^{\frac{1}{3}} V^{-\frac{1}{3}} \tag{4}$$

where V is the impact velocity, m the pendulum mass and θ the semi-angle of the cone. The $\frac{2}{3}$ power law relationship between d_i and V is originally due to Tabor (1951).

These relations are derived for idealized conical indenters but in practice the tip of the cone is rounded into an approximately spherical cap, on account of which the idealized height of the cone and hence the depth of impression is reduced by a distance h. Correcting for this we show

$$d_i \simeq 2\tan\theta\left(\frac{3m}{2\pi c\, Y_i \tan^2\theta}\right)^{\frac{1}{3}} V^{\frac{2}{3}}, \tag{5}$$

$$T \simeq \left(\frac{3m}{2\pi c\, Y_i \tan^2\theta}\right)^{\frac{1}{3}} V^{-\frac{1}{3}}\left(1 - 0{\cdot}7\,\frac{h}{x_0}\right). \tag{6}$$

Equations (5) and (6) have been obtained for the loading cycle; immediately following this, the mean pressure $P = cY$ between specimen and indenter unloads to zero, ejecting the indenter with a finite velocity V_e (say). It is probable that the unloading process is mostly elastic although the possibility of reversed plastic flow in the vicinity of the base of the impression cannot necessarily be discounted. At the termination of the unloading process the impression dimensions will have changed only by an elastic order of magnitude so that to an accuracy of order 10^{-3} the formula (5) for the impression diameter remains valid. However, the present work demonstrates that the duration of elastic unloading is not necessarily small compared with the loading time given by (6), and an estimate of the duration is necessary

With the present limited knowledge of the detailed mechanics and stress system associated with the indentation process it is hardly possible to formulate a precise account of the elastic unloading process. Instead we make use of a model somewhat akin to that suggested by Tabor (1951) in the parallel problem for a spherical indenter. It is assumed that during unloading geometrical similarity of the impression is maintained and at the termination of the process the impression depth has contracted from x_0 to x_1 where from general considerations one might expect

$$\left(\frac{x_0 - x_1}{x_0}\right) \sim \left(\frac{Y}{E}\right)^r < 1$$

where r is an exponent of order unity, and E is Young's modulus.

Further, during the unloading we assume the mean pressure between indenter and specimen is

$$P = P_0\left(\frac{x - x_1}{x_0 - x_1}\right)^n \tag{7}$$

where n is (as yet) a second free parameter and $P_0 (\equiv cY_i)$ is the initial value of P at $x = x_0$. With these asumptions, integration of the equation of motion of the indenter during the unloading phase,

$$m\ddot{x} = -P_0 \left(\frac{x - x_1}{x_0 - x_1}\right)^n A \tag{8}$$

is shown in the Appendix to give an unloading duration of

$$T' = \tfrac{2}{3} \left(\frac{V_e}{V}\right) \left(\frac{3m}{2\pi c\, Y_i \tan^2 \theta}\right)^{\frac{1}{2}} V^{-\frac{1}{2}} \int_0^{\frac{\pi}{2}} \sin^p \phi d\phi \tag{9}$$

where ϕ is a function of $(x - x_1)/(x_0 - x_1)$.

In this analysis we derive

$$\left(\frac{V_e}{V}\right)^2 \simeq \left(\frac{3}{n+1}\right) \left(\frac{x_0 - x_1}{x_0}\right) \tag{10}$$

where V_e is the rebound velocity of the indenter and V the impact velocity. The right hand side of (10) is a measure of the elastic strain recovery (Y_i/E) independent of impression size and impact velocity. Accordingly (10) predicts a constant value of the ratio (V_e/V) for all impact velocities. This result was subsequently verified experimentally, though the precise value depends on the specimen material and angle of the indenter. Using this constant ratio we derive from equations (6) and (9) the total contact time T_c as

$$T_c = T + T' = \left[1{\cdot}4 \left(1 - 0{\cdot}7 \frac{h}{x_0}\right) + k \frac{V_e}{V}\right] \left(\frac{3m}{2\pi c\, Y_i \tan^2 \theta}\right)^{\frac{1}{2}} V^{-\frac{1}{2}} \tag{11}$$

where $k = \frac{2}{3} \int_0^{\frac{\pi}{2}} \sin^p \phi d\phi$.

If h is ignored T_c is proportional to $V^{-\frac{1}{2}}$.

(*ii*) *Estimation of strain-rate sensitivity*

During static indentation the indenter is pressed slowly into the specimen under constant load until deformation ceases. At this point the load Mg is entirely supported by the pressure between the indenter and specimen and we can write

$$Mg = PA$$

where P and A are as defined in the Appendix. Hence, by using an equation of type (1), viz. $P = cY_s$, we obtain

$$Mg = \tfrac{1}{4} \cdot \pi d_s^2\, cY_s \tag{12}$$

which is also to be compared with experimental results.

The geometrical constant c occurs only in the product of cY and therefore cannot be found unless Y is known from other sources. Although it is known that $c \simeq 3$, ignorance of its exact value in the present work precludes the determination of Y_i and Y_s individually.

However, if the quasi-static approach leads to a valid description of the impact process, it is reasonable to assume that the same value of c is pertinent to both the impact and static indentations. On this assumption, c can be eliminated

between (5) and (12) giving the ratio Y_i/Y_s (defined here as the average strain-rate sensitivity λ) in the form

$$\lambda = \frac{Y_i}{Y_s} = \frac{3m \tan \theta}{Mg} \cdot \frac{d_s^2}{S_d^3} \tag{13}$$

where S_d is the slope of the indentation diameter vs. (impact velocity)$^{\frac{1}{3}}$ plot from equation (5).

(*iii*) *Frictional effects*

Modification of the indentation analysis to allow for frictional effects is made difficult by the lack of any precise model describing them. A proposed model due to Hankins (1925) postulates the existence of a coefficient of friction μ between the indenter and indentation, and incorporating this idea into (1) leads to re-writing it in the form

$$P = c_0 (1 + \mu \cot \theta) Y \tag{14}$$

where c_0 is a numerical function of θ alone. As was pointed out by Tabor it is doubtful if this model is satisfactory on general physical grounds for it suggests that for a flat cylindrical punch ($\theta = 90°$) the yield pressure is independent of the friction between the indenter and indentation, and this is known to be untrue. Fair agreement was obtained by Hankins between experimental and theoretical results on the basis of this model for indenter semi-angles up to 70°, although the quoted values of μ are probably spurious due to his neglect of the dependence of frictionless indentation pressure on cone angle (see Bishop *et al.* 1945). However, as no use is made here of absolute magnitudes of μ, this model, in the absence of a better one, will be adopted in the following.

If the coefficients of friction μ_i and μ_s (the subscripts i and s have their usual meanings) are both constant, the forms of (5), (6) and (12) will be unchanged by the substitution for c of a different constant $c_0 (1 + \mu \cot \theta)$ and therefore the constancy of μ can be adduced from the linearity of the experimental results plotted according to (5) and (12).

Substitution of $c = c_0 (1 + \mu \cot \theta)$ into equations (5) and (12) leads to (13) having the form

$$\lambda = \frac{Y_i}{Y_s} = \left(\frac{1 + \mu_s \cot \theta}{1 + \mu_i \cot \theta} \right) \cdot \frac{3m \tan \theta}{Mg} \cdot \frac{d_s^2}{S_d^3} \tag{15}$$

and here λ depends on the unknown values of μ_s and μ_i.

In what follows we shall assume $\mu_s \simeq \mu_i$ and

$$\frac{1 + \mu_s \cot \theta}{1 + \mu_i \cot \theta} \simeq 1$$

which reduces (15) to the form of (13). The assumption $\mu_s \simeq \mu_i$ is not easily justified experimentally except for a material whose strain-rate sensitivity is a relatively insensitive function of the work-hardening i.e. of the 'representative' strain associated with the semi-angle of the cone. Of the materials tested here it is believed that the high tensile steels conform closest to this specification; for these materials the experimental values of λ derived using semi-angles of $\theta = 45°$, $\theta = 68°$ are sufficiently close to prove the validity of the above assumption. For other materials (notably the annealed f.c.c. metals) the two values of λ differ

slightly ; while this may be partly attributable to a difference between μ_s and μ_i it is thought that the dominant contribution arises from a true variation of flow stress ratio (Y_i/Y_s) with strain.

A secondary reason supporting the assumption $\mu_s \simeq \mu_i$ arises from considering the more detailed mechanics of the indentation process. It is at once apparent that the frictional coefficient defined for the indentation experiment bears little or no relation to the corresponding quantity measured in sliding experiments. In the first instance the normal pressures involved here are several orders of magnitude greater ; secondly, in the indentation process there is hardly any question of sliding ; rather the indenter is continuously compressing the specimen material into intimate contact. Under these circumstances it seems likely that apart from strain-rate sensitive features the indentation mechanics are exactly similar for both the static and dynamic impressions.

4. Results and Discussions

(*i*) *Indentation diameter results*

A wide range of materials was tested ; for details of materials and heat treatment etc., see Table 1. Fig. 1 shows plots of indentation diameter vs. (impact velocity)$^{\frac{2}{3}}$ for annealed copper, and austenitic stainless steel. Results for both indenters are presented.

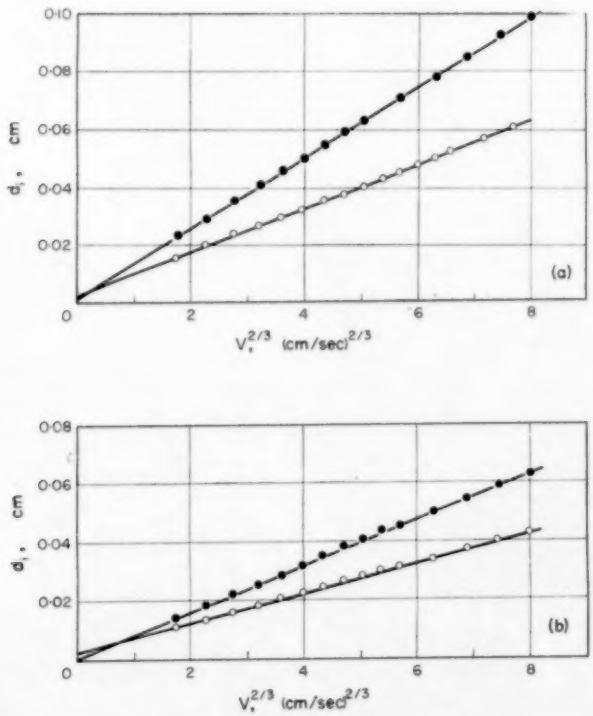

Fig. 1. Indentation diameter, d_i vs. (impact velocity, V)$^{\frac{2}{3}}$ for (a) annealed copper, (b) austenitic stainless steel. ○, 90° indenter ; ●, 136° indenter.

According to the proposed theoretical model, (5) predicts a linear relation between d_i and $V^{\frac{1}{3}}$; this is amply confirmed by the excellent straight lines obtained for which the statistically estimated slopes possess standard deviations varying from $\pm \frac{1}{2}$ to ± 3 per cent. In repeat experiments on different specimens of the same material, the statistically estimated slopes usually differ by less than the sum of their individual deviations.

While none of the plots precisely intersect the origin as required by (5), the intercepts are relatively small, varying from $-0{\cdot}0008$ to $0{\cdot}002$ cm; for a particular material the larger intercepts are usually associated with the 90° indenter.

The mean values and standard errors of the two groups of intercepts are $0{\cdot}00149 \pm 0{\cdot}000076$ cm and $0{\cdot}00041 \pm 0{\cdot}000156$ cm respectively for the 90° and 136° indenters; the value 6·4 for the ratio of the difference between the two means to its standard error implies a probability of the two sets of intercepts belonging to the same family of less than 0·2 per cent. This suggests that the intercepts are quantities related predominantly to the individual indenter rather than the specimen material; physically it seems likely that to some extent the intercept magnitudes devolve on deviations of the tip geometry from the ideal, i.e. on the parameter h; direct (somewhat inaccurate) estimation of h for the two indenters gave values of $0{\cdot}0018$ (90°) and $0{\cdot}0009$ cm (136°) which are of the same orders of magnitude as the mean intercept values quoted above. However, we are unable to reconcile an equation of the type

$$d = S V^{\frac{1}{3}} + K$$

as suggested by Fig. 1, with the model proposed in Section 3 for which the relation between d and V is considerably more involved.

The remarkably good linearity of the indentation diameter plots is adduced as evidence for both the validity of (1) and the constancy, within the limits of experimental accuracy, of the dynamic frictional coefficient μ_i; comparable evidence for the static coefficient μ_s was provided by load vs. (diameter)^2 plots for copper and aluminium.

The dynamic indentation diameter results may be summarized as providing excellent support for the theoretical model based on (1) and the assumption of a quasi-stationary state.

(*ii*) *Contact duration results*

Correlation of the contact duration results with the theoretical prediction of (11),

$$T_c = \left[1{\cdot}4\left(1 - 0{\cdot}7\,\frac{h}{x_0}\right) + k\left(\frac{V_e}{V}\right)\right]\left(\frac{3m}{2\pi c\, Y_i \tan^2\theta}\right)^{\frac{1}{5}} V^{-\frac{1}{5}}, \qquad (16)$$

is rather more difficult than for the indentation diameters. Complicating features are the unknown parameters h, k and V_e/V and the dependence of x_0 upon V which precludes a simple linear plot of T_c in terms of an elementary power of V. On the other hand, for the limit of an ideal tip ($h = 0$) or for a large impression ($h/x_0 \ll 1$, and with the additional experimentally justifiable assumption $(V_e/V) = \text{const.}$, (16) predicts a linear relation between T_c and $V^{-\frac{1}{5}}$. It is therefore convenient to plot T_c as a function of $V^{-\frac{1}{5}}$ since, for $(h/x_0) \ll 1$, we expect a linear relation while the presence of a non-vanishing h should be indicated by systematic deviations of the graph from linearity.

Fig. 2 shows plots of T_c vs. $V^{-\frac{1}{3}}$ corresponding to the indentation diameter plots of Fig. 1. The remaining experimental results are similar.

It is at once apparent that the scatter on the contact duration results is much greater than that for the indentation diameters; so much so that any existing deviations from linearity are completely masked. The scatter appears more pro-

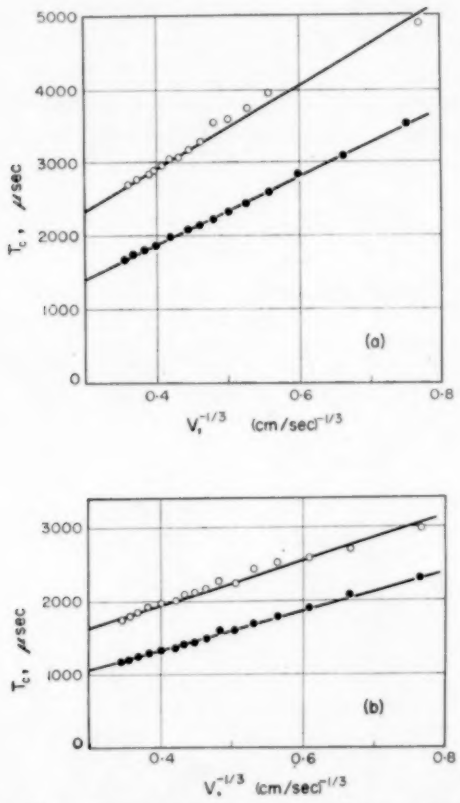

FIG. 2. Contact time, T_c vs. (impact velocity, V)$^{-\frac{1}{3}}$ for (a) annealed copper, (b) austenitic stainless steel. ○, 90° indenter; ●, 136° indenter.

nounced for the 90° indenter than for the 136° indenter. If the scatter is partly associated with the tip geometry, this result might seem reasonable since visual observation of the indenters indicates a value of $h = 0{\cdot}0018$ cm* for the 90° cone and of 0·0009 cm* for the 136° cone. On the other hand, part of the scatter is probably attributable to persistence of arcing between specimen and indenter after mechanical contact has ceased; another contributing factor may be continued contact of indenter and specimen during ejection of the indenter due to twisting of the pendulum induced by slight misalignment of pendulum and specimen. Evidence that such twisting did occur is provided by the appearance of score marks in some of the impressions. It is interesting to note that both these effects

*h was obtained experimentally by estimation of the diameter of the rounded tip with the measuring eyepiece of the microscope of the Vickers hardness tester.

lead qualitatively to longer contact durations than those suggested theoretically; to some extent this is borne out by a more detailed analaysis of the experimental results (below).

In the absence of any detailed treatment of these effects it was decided to analyse the results for the 136° indenter on the assumption $h = 0$; this is justified to some extent by the comparative linearity of the plots T_c vs. $V^{-\frac{1}{3}}$ for the 136° indenter. Further, for the 136° indenter and with the visually estimated value of h, the quantity $(0{\cdot}7\ h/x_0)$ is at most 0·07 and assumes this magnitude only for the smallest impressions.

More explicitly, since the extrapolated contact duration plots fail to intersect the origin by some hundreds of microseconds, we compare the experimental slopes with the theoretical value

$$S_t = \left[1{\cdot}4 + k\left(\frac{V_e}{V}\right)\right]\left(\frac{3m}{2\pi c\ Y_i \tan^2\theta}\right)^{\frac{1}{3}}$$

derived from (16) in the limit $h = 0$.

Table 2. *Comparison of theoretical and experimental slope ratios and of calculated and measured contact times*

Specimen material	V (cm/sec)	$\frac{V_e}{V}$	R^*	$\frac{S_d}{S_t}$	T_c *meas.* (μsec)	T_c *calc.* (μsec)
99·83 % Aluminium annealed	2·25	0·14	3·04	3·4	4120	4050
	15·76				2310	2120
Armco iron annealed	2·25	0·22	2·82	3·1	2231	2280
	15·76				1291	1190
0·89 % C. Steel	2·25	0·32	2·59	2·6	2080	2000
	15·76				1160	1050
Austenitic stainless steel	2·25	0·32	2·59	2·8	2381	2320
	15·76				1341	1210
Grey cast iron (as cast)	2·25	0·37	2·49	2·0	2641	2270
	15·76				1471	1190

$$^*R = \frac{2\tan\theta}{1{\cdot}4 + 1{\cdot}53\,(V_e/V)}$$

For practical purposes it is most convenient to compare the slope ratios

$$\frac{S_d}{S_t} = \frac{2\tan\theta}{1{\cdot}4 + k\,(V_e/V)} \tag{17}$$

where S_d is the previously defined slope of the d_i vs. $V^{\frac{1}{3}}$ plots. Equation (17) contains one free parameter k (since V_e/V is experimentally determinable),

$$k = \tfrac{8}{5}\int_0^{\frac{\pi}{2}} \sin^p\phi\, d\phi,$$

and we have attempted to compare the experimental slope ratio to the right hand side of (17) with a single choice of k.

As mentioned previously, measurement of ejection velocity V_e over a range of impact velocities V, showed that for each material the ratio V_e/V was constant. Some experimental values of V_e/V have been entered in Table 3. Using all values of V_e/V the best choice of k was found to be $k = 1{\cdot}53$. The experimental slope ratio S_d/S_t is compared with

$$R = \frac{2 \tan \theta}{1{\cdot}4 + 1{\cdot}53\ V_e/V}$$

in Table 2 for a few materials. The agreement is fair.

Table 2 also displays, for some materials tested, two experimental values of T_c obtained at impact velocities of 2·25 and 15·76 cm/sec. These may be compared with the theoretical values derived using $k = 1{\cdot}53$; as can be seen from the table the calculated times are usually less than the observed values by amounts up to 300 or 400 μsec, the discrepancy showing no significant difference for the two impact velocities. The agreement between the two sets of figures is very reasonable considering the necessarily approximate description of the unloading process while the existence of arcing and pendulum twisting affords an explanation of the positive difference between the theoretical and calculated values of T_c.

It is of some interest to note that with $k = 1{\cdot}53$, the exponent n appearing in (7) is approximately $n = 2$. Thus, the elastic unloading phase for the 136° indenter is governed by a mean pressure

$$P = P_0 \left(\frac{x - x_1}{x_0 - x_1} \right)^2$$

where $(x_0 - x_1)/x_0$ is measured experimentally by V_e/V [equation (10)].

In analysing the results for the 90° indenter we have again chosen $k = 1{\cdot}53$ although there is no *a priori* reason why the same value of n (and hence k) should hold for both indenters; however, no single value of k gives very good agreement between theoretical and experimental slope ratios and in the absence of any evidence to the contrary the choice $k = 1{\cdot}53$ has been adopted.

Accurate determination of the slopes of the contact time vs. (impact velocity)$^{-1}$ plots was precluded by the scatter of the measured contact times, which also concealed any deviations due to tip flattening. However, if tip flattening were significant, it would be expected that the values of

$$\frac{2 \tan \theta}{1{\cdot}4 + 1{\cdot}53\,(V_e/V)}$$

would in general be less than the measured, albeit inaccurate, slope ratios, while the difference between the two would be expected to be less for the pure, softer materials where larger impression diameters would lessen the significance of (h/x_0) in the factor $(1 - 0{\cdot}7\ h/x_0)$. Examination of the results shows that these expectations were qualitatively fulfilled but no consistent estimation of h was possible from the magnitudes of the discrepancies.

Somewhat better agreement between theory and experiment is obtained for the 90° indenter results if some account is taken of the tip flattening parameter h; while experimental scatter precludes comparison of the experimental plots of

T_c vs. $V^{-\frac{1}{2}}$ with the resultant non-linear theoretical curve, it is still possible to compare theoretical values of T_c derived from equation (11) (for assigned values of h and k) with the experimental figures. As before the value $k = 1{\cdot}53$ has been adopted, and, in the absence of a more accurate estimate, we choose $h = 0{\cdot}0018$ cm.

As previously, the experimental values of T_c exceed the theoretical estimates; however, the present discrepancies, while of the same order of magnitude as those for the 136° indenter, are distinctly larger. This result might reasonably be attributed to either or both the arcing and twisting phenomena proposed previously. For a given impact velocity the 90° indenter is ejected at a lower velocity than the 136° indenter. Under these circumstances the 90° indenter spends a longer time within the vicinity of the specimen and this in turn leads to (a) an increased arcing time* and (b) an increased probability of the indenter making continued contact with the walls of the impression during ejection.

In conclusion, it is felt that the contact duration results afford reasonable support for the theoretical model of the indentation process proposed in Section 3.

(*iii*) *Static indentation results*

From (12) the theoretically predicted relation between M and d_s^2 is linear with zero intercept. This result was confirmed experimentally for both indenters on copper and invar specimens. From these it follows that the conventionally defined hardness values are independent of the load and that a valid estimate of the static flow-stress is given from experiments with a single value of M by the formula

$$cY_s = \frac{4Mg}{\pi d_s^2}.$$

In practice a number of impressions were made, using one value of M in conjunction with the mean diameter d_s.

Repeated static experiments on different specimens of the same material were extremely reproducible, since, with the exception of annealed copper, the difference of the mean diameters for the two groups was less than the sum of the individual standard deviations. In the exceptional case of copper, the indentations were characterized by marked 'sinking in' of the material near the indentation peripheries.† This feature, which to a lesser extent occurred with the aluminium impressions, produces a lack of definition of the impressions and leads to some difficulties in assessing d_s.

It was noticeable that with the same load the 136° indenter always produced larger diameter impressions than the 90° indenter. This is in agreement with earlier work of Bishop *et al.* (1945) who found that, with unlubricated indenters on hardened copper, the mean indentation pressure P decreased with increasing indenter angle. The three parameters which could affect the impression diameter with change of indenter angle are the geometrical constant c_θ (a function of θ alone), the mean flow-stress Y_s (dependent on the strain-pattern produced) and the coefficient of friction μ_s (appearing in the term $\mu_s \cot \theta$). Dugdale (1954) in his work on cold-worked materials (which are close approximations to the ideal plastic–rigid solid and hence are described by a nearly constant value of Y_s) shows that

*An elementary model suggests an arcing time proportional to V_e^{-1}.

†Tabor (1951) states that 'sinking in' is a common feature of impressions made in annealed metals.

c_0 (the constant for frictionless indentation) is an increasing function of θ in the range $15° < \theta < 70°$. This would produce an increase of P with increasing indenter angle. The observed decrease in P thus devolves entirely on the decrease in the expression $\mu_s \cot \theta$ and a probable decrease in Y_s corresponding to the lower representative strain associated with the blunter cone.

(*iv*) *Strain-rate sensitivity*

The average strain-rate sensitivities, from (13) are tabulated in Table 3 for all the materials tested (see Table 1) and for both indenters. In the same table the present results are compared with those of other authors who used more conventional testing methods.

With the exceptions of molybdenum, copper, aluminium and grey cast iron, the results of repeat experiments are in close agreement. The somewhat low value $\lambda = 1{\cdot}58$ obtained with the 90° indenter on one molybdenum specimen is attributed to specimen variability, as are the scattered results for the other three materials concerned ; however, the discrepancy between λ values from any pair of nominally identical specimens tested with the same indenter, lies within, or almost within, the sum of the two individual standard deviations on λ.

For many of the materials tested (spheroidal graphite iron ; normalized 0·89% C steel ; 2·68% Ni, Cr, Mo steel ; 19% Cr steel ; austenitic stainless steel) the λ values derived using both indenters differ only by a few per cent. For the remainder of the materials the two λ values deviate ; the discrepancy for these solids is believed to reflect the variation of strain-rate sensitivity with strain. In particular for molybdenum, mild steel and Armco iron, which all exhibit upper yield point phenomena, the λ value is believed to represent a compromise between the initially large upper yield point ratios and the somewhat lesser flow stress ratios obtained at larger strains ; here for molybdenum and Armco iron, the sharper cone angle, associated with the larger representative strain, tends to yield smaller values for λ than the 136° indenter. On the other hand, annealed copper and aluminium exhibit larger λ values for the sharper indenter ; this result is in qualitative agreement with Baron's (1956) work on annealed tough pitch copper which shows that for strains up to about 20 per cent of the ratio of dynamic to static flow-stress is an increasing function of strain.

For the remaining materials tested (Al alloys, Tungsten Heavy alloy and Nilo 36) the mechanical properties are insufficiently detailed to effect a comparison with the present results ; for these three materials the 136° indenter gives larger λ values than the 90° indenter. This suggests that here the flow stress ratio is a decreasing function of strain, in contrast to the results for aluminium and copper. The present results for the aluminium alloys are everywhere higher than those reported by Baron (1956) for duralumin but agree more closely with his low temperature tests on that material.

As mentioned in Section 3 (*iii*) discrepancies in λ values from the two indenters may be partly attributable to a difference between μ_s and μ_i. In view of this, it is felt that perhaps slightly greater weight should be attached to the value of λ obtained with the 136° indenter for which the expression $(1 + \mu_s \cot \theta)/(1 + \mu_i \cot \theta)$ is nearer to unity for given values of μ_s and μ_i.

TABLE 3. *Tabulated values of the slopes (S_d) of d_i vs. $V^{\frac{1}{3}}$ plots, static indentation diameters (d_s) and average strain-rate sensitivities λ.*

Specimen	2θ	*M* (Kg)	S_d $\times 10^5$	d_s (cm) $\times 10^4$	λ *present experiments*	*Ratio* $\frac{\text{dynamic stress}}{\text{static stress}}$ *from other work*			
						5% *strain*	10% *strain*	15% *strain*	*U.T.S.*
Al	90°	10	1064 ± 7	675 ± 9	1·40 ± 0·043	1·45(1)		1·4(1)	1·33(2)
	136°	10	1615 ± 12	776 ± 11	1·31 ± 0·047				
Cu	90°	20	763 ± 4	592 ± 2	1·48 ± 0·046	1·2(1)		1·2(1)	1·37(2)
	136°	20	1204 ± 8	714 ± 5	1·34 ± 0·034	1·20(3)	1·21(3)	1·24(3)	1·22(2)
Mo	90°	20	496 ± 6	335 ± 6	1·71 ± 0·089				
	136°	20	716 ± 10	369 ± 10	1·70 ± 0·115	2·1 (U)*	2·02 (L)*		1·43*
DSP	90°	20	600 ± 6	353 ± 4	1·07 ± 0·041				
Al alloy	136°	20	808 ± 6	373 ± 7	1·21 ± 0·053	1·07(1)†		1·06(1)†	
FSP	90°	20	595 ± 4	338 ± 4	1·01 ± 0·032				
Al alloy	136°	20	804 ± 5	360 ± 9	1·14 ± 0·055	0·97(3)	0·99(3)	>1·00(3)	
Mild steel	90°	10	587 ± 2	271 ± 4	1·36 ± 0·043	1·27(3)	1·24(3)	1·21(3)	
	136°	10	—	299 ± 5	—	2·0 (U)(3)	1·5 (L)(3)		20% strain
WDDJ	90°	20	605 ± 3	417 ± 5	1·47 ± 0·038	1·54(3)	1·40(3)	1·33(3)	1·28(3)
Armco iron	136°	20	852 ± 7	461 ± 9	1·58 ± 0·072				
WFSW	90°	20	557 ± 4	339 ± 5	1·27 ± 0·042				
S.G. iron	136°	20	783 ± 5	372 ± 6	1·32 ± 0·079				
WFST	90°	20	472 ± 7	270 ± 5	1·29 ± 0·070				
S.G. iron	136°	20	671 ± 7	290 ± 6	1·29 ± 0·060				
WCQW	90°	20	545 ± 14	302 ± 11	1·06 ± 0·114				
Grey cast iron	136°	20	732 ± 10	320 ± 10	1·20 ± 0·090				
WCGY	90°	20	483 ± 2	270 ± 5	1·29 ± 0·037				
0·089C Steel	136°	20	680 ± 5	290 ± 6	1·29 ± 0·055				
WFSM	90°	20	546 ± 5	333 ± 5	1·27 ± 0·052				
Cr. steel	136°	20	783 ± 9	367 ± 11	1·26 ± 0·073				
WFAK	90°	20	527 ± 3	314 ± 2	1·26 ± 0·024	1·38(3)	1·27(3)	1·20(3)	1·15(3)
Stainless steel	136°	20	797 ± 6	367 ± 10	1·22 ± 0·072				
WEGF	90°	20	452 ± 2	236 ± 2	1·13 ± 0·021	1·09(3)	1·16(3)	1·09(3)	
Ni, Cr steel	136°	20	620 ± 3	246 ± 6	1·17 ± 0·054				
W alloy	90°	20	440 ± 3	253 ± 3	1·41 ± 0·036				
sintered	136°	20	610 ± 3	274 ± 7	1·51 ± 0·078				
Nilo 36	90°	20	583 ± 3	344 ± 3	1·12 ± 0·028				
invar	136°	20	815 ± 5	378 ± 6	1·21 ± 0·044				

(1) Hawkyard and Freeman (1954)
(2) Clark and Wood (1950)
(3) Baron (1956)

* Private communication from Ward, E. W.
† A.W.10 Aluminium alloy

5. Conclusions

The quasi-static approach utilizing the semi-empirical equation (1) led to a valid description of the impact indentation process for a conical indenter. The theoretical model implied relations between impact velocity, impression dimensions and contact duration, which were subsequently verified experimentally.

The values of λ derived here represent estimates of the average strain-rate sensitivity over the strain region 0–10 per cent, such estimates being useful as design factors in problems of limited plastic flow. The experimental simplicity of that part of the apparatus required to drive λ (i.e. without measurement of contact time) compares favourably with conventional methods of dynamic testing; in particular the method recommends itself as a rapid means of dynamic testing complementary to standard hardness testing procedures. The most time-consuming process is that of subjecting the experimental information to statistical analysis, but where access to an electronic computer is not available, the slope of the d vs. $V^{\frac{1}{2}}$ relations can be estimated by ordinary graphical means to within ± 2 per cent. The corresponding deviation on λ is then ± 6 per cent compared with that of ± 3 per cent given by statistical treatment.

It is recommended that conical indenters used in impact testing should not have included angles of less than 120°, a convenient angle to choose being that of the Vickers diamond pyramid which is 136°.

Finally it is wished to emphasize the versatility of the method in testing a wide range of materials many of which for reasons of brittleness, high density or poor machinability do not readily lend themselves to testing in the dynamic extensions of the conventional tensile and compressive procedures. In brief, the range of materials includes any which are susceptible to ordinary static hardness testing with a tungsten carbide indenter.

Acknowledgments

Acknowledgments are made to our colleagues Mr. B. D. Burns for helpful advice and criticism and Mr. H. G. Baron who supplied most of the materials tested.

References

Andrews, J. P. 1929 *Phil. Mag.* **8**, 781.
1931 *Ibid.* **9**, 593.
Baron, H. G. 1956 *J. Iron Steel Inst.* **182**, 354.
Bishop, R. F., Hill, R. and Mott, H. F. 1945 *Proc. Phys. Soc. Lond.* **57**, 147.
Clark, D. S. and Wood, D. S. 1950 *Trans. Amer. Soc. Metals* **42**, 45.
Crum, R. G. and Mavis, F. T. 1958 *Bull. Amer. Soc. Test. Mat.* **231**, 88.
Dugdale, D. S. 1954 *J. Mech. Phys. Solids* **2**, 265.
Gohlke, W. 1957 *Z. Ver. Dtsch. Ing.* **99**, 579.
Hawkyard, J. B. and Freeman, P. 1954 *Brit. Iron & Steel Res. Ass. Report* MW/E/58/54.
Hankins, G. A. 1925 *Proc. Inst. Mech. Engrs* **1**, 611.
Hill, R. 1950 *The Mathematical Theory of Plasticity* (Clarendon Press, Oxford).

HUNTER, S. C.	1954	Unpublished Ministry of Supply Report.
	1957	*J. Mech. Phys. Solids* **5**, 162.
JOHNSON, J. E., WOOD, D. S. and CLARK, D. S.	1953	*J. Appl. Mech.* **20**, 523.
MAIDEN, C. J. and CAMPBELL, J. D.	1958	*Phil. Mag.* **3**, 872.
SHIELD, R. T.	1955	*Proc. Roy. Soc.* A **233**, 267.
STRELLA, S., SIGLER, H., CHMURA, M. and HOLMAN, B.	1958	*Bull. Amer. Soc. Test. Mat.* **228**, 50.
TABOR, D.	1951	*The Hardness of Metals* (Clarendon Press, Oxford).
VINCENT, B. J., GEE, R. and HUNTER, S. C.	1957	*Conference on Properties of Materials at High Rates of Strain* (Session 2, Paper 5) Institution of Mechanical Engineers, London.

APPENDIX

The equation of motion of the pendulum during the loading cycle is

$$m\ddot{x} + PA = 0 \qquad \text{A(1)}$$

where m is the pendulum mass, x the penetration distance and A is the normally projected area of the indenter in contact with the specimen. From the geometry of the cone

$$A = \pi x^2 \tan^2 \theta \qquad \text{A(2)}$$

in which θ is the semi-angle of the cone. From (1) in the text, and A(1) and A(2) we obtain

$$\ddot{x} + \frac{\pi c\, Y_i \tan^2 \theta}{m} \cdot x^2 = 0, \qquad \text{A(3)}$$

a differential equation to be solved subject to the boundary conditions

$$x = 0, \qquad \dot{x} = V, \qquad t = 0$$

where V is the initial impact velocity. A first integration of A(3) gives

$$\tfrac{1}{2}(V^2 - \dot{x}^2) = \left(\frac{\pi c\, Y_i \tan^2 \theta}{3m}\right) x^3. \qquad \text{A(4)}$$

The maximum penetration x_0 occurs when $\dot{x} = 0$, for which A(4) gives

$$x_0 = \left(\frac{3m}{2\pi c\, Y_i \tan^2 \theta}\right)^{\frac{1}{3}} V^{\frac{2}{3}} \qquad \text{A(5)}$$

while the corresponding diameter d_i of the impression is

$$d_i = 2x_0 \tan \theta = 2 \tan \theta \left(\frac{3m}{2\pi c\, Y_i \tan^2 \theta}\right)^{\frac{1}{3}} V^{\frac{2}{3}}. \qquad \text{A(6)}$$

In terms of x_0 A(4) may be re-written

$$\dot{x} = V\left[1 - \left(\frac{x}{x_0}\right)^3\right]^{\frac{1}{2}} \quad \text{or} \quad t = V^{-1} \int_0^x \frac{dq}{[1 - (q/q_0)^3]^{\frac{1}{2}}}$$

from which the duration T of the loading cycle is

$$T = V^{-1} \int_0^{x_0} \frac{dq}{[1 - (q/q_0)^3]^{\frac{1}{2}}} = \frac{x_0}{V} \int_0^1 \frac{ds}{(1 - s^3)^{\frac{1}{2}}}.$$

Using the result

$$\int_0^1 \frac{ds}{(1-s^3)^{\frac{1}{3}}} = \frac{2}{3}\int_0^{\frac{\pi}{2}} (\sin\phi)^{\frac{1}{3}}\, d\phi = \frac{\Gamma(\frac{1}{3})\,\Gamma(\frac{1}{2})}{3\Gamma(\frac{5}{6})} = 1{\cdot}403$$

together with A(5) gives finally

$$T \simeq 1{\cdot}4\left(\frac{3m}{2\pi c\, Y_i \tan^2\theta}\right)^{\frac{1}{3}} V^{-\frac{1}{3}}. \qquad \text{A(7)}$$

The reduction (h) in the idealized height of the cone due to flattening of the tip leads to some modification in A(5), A(6) and A(7):

$$x_0 = \left(\frac{3mV^2}{2\pi c\, Y_i \tan^2\theta} + h^3\right)^{\frac{1}{3}} - h, \qquad \text{A(8)}$$

$$d_i = 2\tan\theta\left(\frac{3mV^2}{2\pi c\, Y_i \tan^2\theta} + h^3\right)^{\frac{1}{3}}, \qquad \text{A(9)}$$

$$T = \left(\frac{3m}{2\pi c\, Y_i \tan^2\theta}\right)^{\frac{1}{3}} V^{-\frac{1}{3}}\, F\left(1 - \frac{h}{x_0}\right), \qquad \text{A(10)}$$

where

$$F\left(1 - \frac{h}{x_0}\right) \simeq 1{\cdot}4\left(1 - 0{\cdot}7\,\frac{h}{x_0}\right)$$

to better than $\frac{1}{2}$ per cent for the values of (h/x_0) obtaining in the experiments reported here.

In the present experiments the initial impact velocity V is everywhere sufficiently large to make the h^3 term entering the parentheses of A(9) negligible and we are then left with the expressions for the loading cycle:

$$d_i = 2\tan\theta\left(\frac{3m}{2\pi c\, Y_i \tan^2\theta}\right)^{\frac{1}{3}} V^{\frac{1}{3}}, \qquad \text{A(11)}$$

$$T \simeq 1{\cdot}4\left(\frac{3m}{2\pi c\, Y_i \tan^2\theta}\right)^{\frac{1}{3}} V^{-\frac{1}{3}}\left(1 - 0{\cdot}7\,\frac{h}{x_0}\right). \qquad \text{A(12)}$$

During the unloading cycle it is assumed that geometrical similarity of the impression is maintained and that the impression depth contracts from x_0 to x_1. Further, choosing for the mean pressure between specimen and indenter

$$P = P_0\left(\frac{x - x_1}{x_0 - x_1}\right)^n \qquad \text{A(13)}$$

where n is a free parameter and $P_0\,(\equiv cY_i)$ is the initial value of P at $x = x_0$, we may write the equation of motion of the indenter as

$$m\ddot{x} = -P_0\left(\frac{x - x_1}{x_0 - x_1}\right)^n A \qquad \text{A(14)}$$

where $A = \pi(x + h)^2\tan^2\theta$ is the projected area of the impression. However, as the change in impression dimensions due to elastic recovery is small, A will be taken as constant and equal to $\pi(x_0 + h)^2\tan^2\theta$ in what follows.

The first integration of A(14) together with the boundary conditions $\dot{x} = 0$ at $x = x_0$ gives

$$\dot{x}^2 = \frac{2P_0 A(x_0 - x_1)}{m(n+1)}\left[1 - \left(\frac{x - x_1}{x_0 - x_1}\right)^{n+1}\right]. \qquad \text{A(15)}$$

At $x = x_1$, $\dot{x} = V_e$, and so

$$V_e^2 = \frac{2P_0 A(x_0 - x_1)}{m(n+1)}. \qquad \text{A(16)}$$

The unloading time T' is obtained from A(15) in the form

$$T' = \sqrt{\left\{\frac{m(n+1)}{2P_0 A(x_0 - x_1)}\right\}} \int_{x_1}^{x_0} \frac{dx}{\sqrt{\left\{1 - \left(\frac{x - x_1}{x_0 - x_1}\right)^{n+1}\right\}}} \qquad \text{A(17)}$$

which can be reduced to

$$T' = \sqrt{\left\{\frac{m(n+1)(x_0 - x_1)}{2P_0 A}\right\}} \int_0^1 \frac{du}{\sqrt{(1 - u^{n+1})}}. \qquad \text{A(18)}$$

The equations

$$P_0 = cY_i$$

$$x_0 + h = \left(\frac{3m}{2\pi c\, Y_i \tan^2\theta}\right)^{\frac{1}{3}} V^{\frac{1}{3}}$$

enable A(16) and A(18) to be written in the form

$$\left(\frac{V_e}{V}\right)^2 = \frac{3}{(n+1)}\left(1 - \frac{x_1 + h}{x_0 + h}\right) = \frac{3}{(n+1)}\left(\frac{x_0 - x_1}{x_0 + h}\right) \simeq \frac{3}{(n+1)}\left(\frac{x_0 - x_1}{x_0}\right) \qquad \text{A(19)}$$

$$T' = \frac{2}{3}\left(\frac{V_e}{V}\right)\left(\frac{3m}{2\pi c\, Y_i \tan^2\theta}\right)^{\frac{1}{3}} V^{-\frac{1}{3}} \int_0^{\frac{\pi}{2}} \sin^p \phi\, d\phi \qquad \text{A(20)}$$

where $p = (1 - n)/(1 + n)$ and the integral has been simplified by the substitution $\sin^2\phi = u^{n+1}$. Also, in A(19) the assumption $x_0 \gg h$, valid for most of the present experimental results, has been introduced.

Crown Copyright reserved. Reproduced by permission of the Controller of H.M. Stationery Office.

J. Mech. Phys. Solids, 1960, Vol. 8, pp. 255 to 261. Pergamon Press Ltd., London. Printed in Great Britain

PLASTIC YIELDING IN ANELASTICITY

By M. Reiner
Technion, Israel Institute of Technology, Haifa

(*Received* 11*th July*, 1960)

Summary

By means of the application of a yield criterion, according to which yielding takes place when that part of the stress-work which is conserved reaches a definite maximum value, it is shown that from the constitutive equation of anelasticity two phenomena follow. On one hand, when the load is constant, yielding can take place after some time in creep. On the other hand, when a constant rate of strain is applied, the yield stress increases with the rate of strain.

1. The generally accepted yield criterion for the 'ideal plastic body' is one due to von Mises (1913) in accordance with which plastic yielding takes place when the second invariant of the stress-deviator $\Pi_{s\,(0)}$ reaches a certain limit. Let ϑ be the yield stress and $\vartheta_{(0)}$ its deviator, then

$$\Pi_{s\,(0)} = -\tfrac{1}{2}\left[\vartheta^2_{xx\,(0)} + \vartheta^2_{yy\,(0)} + \vartheta^2_{zz\,(0)} + 2\vartheta^2_{yz} + 2\vartheta^2_{zx} + 2\vartheta^2_{xy}\right]. \tag{1.1}$$

Let ϑ_t be the maximum (tangential) shear stress in yielding in a state of simple shear; then from (1.1)

$$-\Pi_{s\,(0)} = \vartheta_t^2. \tag{1.2}$$

The ideal plastic body is assumed to be isotropic, to be perfectly elastic below the yield point, and not to yield under an isotropic stress. To a first approximation metals behave in this manner, and the theory of plasticity as treated, for instance, by Hill (1950) "is related specifically to the properties of metals" insofar as coming under the picture of a 'Hooke-body' (H)*. In the Hooke-body, stress s and strain ϵ are single-valued functions of one another. Let μ be the modulus of rigidity; then Hooke's law is postulated as

$$s_{(0)} = 2\mu\,\epsilon_{(0)} \tag{1.3}$$

where the index (0) indicates the deviator, and s and ϵ stand for the tensors s_{ij} and ϵ_{ij}. It has, however, more recently been realized that *internal friction* in metals cannot be disregarded in many phenomena, and largely as a result of Zener's work (1948) a new approach to the theory of elasticity of metals has been developed under the term 'anelasticity.' Anelasticity is not 'inelasticity' because it is assumed that, when the strained body is unloaded, all strain ultimately disappears, and the original shape (and volume) is completely recovered, even if this takes time. However, in anelasticity stress and strain are not single-valued functions

*See Reiner (1958), p. 448.

of one another. The 'rheological equation' in this case, which has to replace (1.3) is written by ZENER as

$$s + T_{\text{rel}}\,\dot{s} = M\,(\epsilon + T_{\text{ret}}\,\dot{\epsilon}) \tag{1.4}$$

where T_{rel} is a 'relaxation time,' T_{ret} a 'retardation time' and M a 'modulus of elasticity.' These terms will be defined more specifically later.

In the same manner as 'elastic' metals, anelastic metals are liable to plastic yielding. It is obvious that the von Mises criterion (1.1) is here not applicable. The question therefore arises as to an appropriate yield criterion for anelasticity. It is the purpose of the present paper to deal with this problem.

2. While the von Mises yield criterion is always written in terms of stress as in (1.1), it is obvious that for a Hooke-body it can as well be written in terms of strain. Let θ be the yield strain, then from (1.3)

$$\theta_{(0)} = \vartheta_{(0)}/2\mu, \tag{2.1}$$

and (1.1) becomes

$$\Pi_{\epsilon\,(0)} = -\tfrac{1}{2}\left[\theta^2_{xx\,(0)} + \theta^2_{yy\,(0)} + \theta^2_{zz\,(0)} + 2\theta^2_{yz} + 2\theta^2_{zx} + 2\theta^2_{xy}\right] \tag{2.2}$$

with

$$-\Pi_{\epsilon\,(0)} = \theta_t^{\,2} = \vartheta_t^{\,2}/4\mu^2 \tag{2.3}$$

The fact that this relation does not hold in anelasticity makes the von Mises criterion inapplicable. We shall, however, do well in following Occam's principle*, that is we shall apply von Mises' criterion *as far as possible*. This can be done by giving (1.1) a physical interpretation. Such interpretation is due to HENCKY (1924). In accordance with HENCKY, yielding begins *when the elastic energy of distortion reaches a critical value*. A characteristic term exists for this energy since 1835. It is *resilience*, 'the work (per unit volume) required to deform an elastic body to the elastic limit.' Denoting the specific deviatoric stress-power by $\dot{w}_{(0)}$, we have

$$\dot{w}_{(0)} = s_{\alpha\beta\,(0)}\,\dot{\epsilon}_{\beta\alpha\,(0)} = 2\mu\epsilon_{\alpha\beta\,(0)}\,\dot{\epsilon}_{\beta\alpha\,(0)} \tag{2.4}$$

and by integration

$$w_{(0)} = \mu\epsilon_{\alpha\beta\,(0)}\,\epsilon_{\beta\alpha\,(0)} = s_{\alpha\beta(0)}\,s_{\beta\alpha\,(0)}/4\mu. \tag{2.5}$$

Let $R_{(0)}$ be the deviatoric resilience; then from (2.5)

$$\left.\begin{aligned}\vartheta^2 &= \vartheta_{\alpha\beta\,(0)}\,\vartheta_{\beta\alpha\,(0)} = 4\mu\,R_{(0)},\\ \theta^2 &= \theta_{\alpha\beta\,(0)}\,\theta_{\beta\alpha\,(0)} = R_{(0)}/\mu.\end{aligned}\right\} \tag{2}$$

These two equations are identical with (1.1) and (2.2), if we make

$$-\Pi_{s\,(0)} = 2\mu\,R_{(0)}, \qquad -\Pi_{\epsilon\,(0)} = R_{(0)}/2\mu. \tag{2.7}$$

So far we are still giving only a different interpretation to the usual yield criterion of the Hooke-body, but a slight modification of the procedure implied in it will serve our purpose.

3. The rheological equation which defines anelasticity was first derived by POYNTING and THOMSON (1902). They were also the first to introduce a mechanical model for the representation of rheological behaviour. The model is shown in

* 'Theories are not to be multiplied without necessity.'

Fig. 1. It consists of a spring (H_1) and dashpot (N) in series, coupled with another spring (H_2) in parallel. We may assume that anelasticity effects do not occur under isotropic pressure (or tension)*. We therefore apply the model upon the deviators of stress and strain, but shall drop the index (0) for simpler writing. ZENER has named a body which behaves in accordance with this model a ' standard linear solid,' while REINER (1958, p. 147) uses the designation ' Poynting–Thomson-body ' (*PTh*), and defines it as a combination ' in parallel ' of a Maxwell-body (M) and a Hooke-body (H), and accordingly denotes the two shear-moduli by μ_M and μ_H, with η the coefficient of viscosity. Examination of the model will show that the stress s is the sum of the stresses taken by the two components, or

$$s = s_H + s_M \tag{3.1}$$

while the strain ϵ, which the *PTh*-body suffers, is the same as the strains of each one of its components, or

$$\epsilon_H = \epsilon_M = \epsilon. \tag{3.2}$$

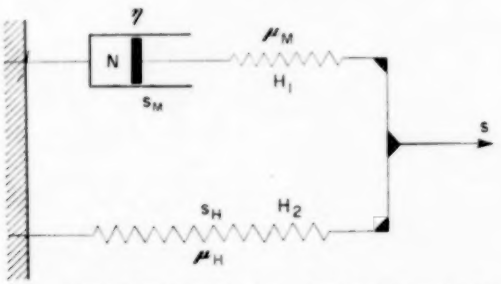

FIG. 1. Mechanical model of a ' standard linear solid.'

We can therefore write the rheological equation of the *PTh*-body in two equivalent forms. On the basis of (3.1) we find the stress s as a function of ϵ and $\dot{\epsilon}$ as follows:

$$s - s_0 \exp(-t/T_{\text{rel}}) = 2\mu_H \epsilon + 2\mu_M \exp(-t/T_{\text{rel}}) \cdot \int_0^t \dot{\epsilon} \exp(t/T_{\text{rel}})\, dt \tag{3.3}\dagger$$

On the basis of (3.2) we find

$$s + \dot{s}\frac{\eta}{\mu_M} = 2\mu_H \left(\epsilon + \dot{\epsilon}\eta \frac{\mu_H + \mu_M}{\mu_H \mu_M}\right) \tag{3.4}\ddagger$$

Equation (3.4) yields the following interpretation of Zener's parameters in (1.4):

$$T_{\text{rel}} = \frac{\eta}{\mu_M}, \qquad T_{\text{ret}} = \eta \frac{\mu_H + \mu_M}{\mu_H \mu_M}, \qquad M = 2\mu_H. \tag{3.5}$$

From (3.4) we find by integration the strain ϵ as a function of s as follows:—

$$\epsilon - \epsilon_0 \exp(-t/T_{\text{ret}}) = \frac{1}{2(\mu_H + \mu_M)} \left[s - s_0 \exp(-t/T_{\text{ret}})\right] + \\ + \frac{\mu^2_M}{2\eta(\mu_H + \mu_M)^2} \exp(-t/T_{\text{ret}}) \int_0^t s \exp(t/T_{\text{ret}})\, dt. \tag{3.6}$$

*Because, as expressed by ZENER (op. cit., p. 56), 'Generally no relaxation occurs under a pure hydrostatic pressure.'
†REINER (op. cit., p. 471).
‡Equation (3.4) can also be derived from (3.3) by differentiation with respect to time and elimination of the integral.

4. In order to apply as far as possible the Mises–Hencky yield criterion to our case we note that the resilience should not include stress-work which is dissipated through internal friction. REINER and WEISSENBERG (1939) have therefore generalized the Mises–Hencky yield criterion to include materials with internal friction, viscous or solid, by postulating that yielding takes place when that part of the distortional stress-work which is *conserved* as elastic energy in a unit volume of the body reaches a certain maximum value – the resilience. Applying this to our case, the stress-work expended upon the PTh-body is the sum of the stress-works expended upon its two components, or

$$w_{PTh} = w_H + w_M. \tag{4.1}$$

We find w_H from (2.5):

$$w_H = \mu_H \epsilon^2 = s_H^2/4\mu_H. \tag{4.2}$$

This is entirely conserved. In contradistinction the stress power of the M-component

$$\dot{w}_M = s_M \dot{\epsilon} = \frac{s_M \dot{s}_M}{2\mu_M} + \frac{s^2_M}{2\eta} \tag{4.3}^*$$

is partly conserved and partly dissipated through viscous resistance. In accordance with REINER and WEISSENBERG's theory only the first part on the right side of (4.3) has to be taken into account.

The total conserved stress-work is therefore

$$w_c = s_H^2/4\mu_H + s_M^2/4\mu_M. \tag{4.4}$$

This is also

$$w_c = \mu_H \epsilon^2 + (s - 2\mu_H \epsilon)^2/4\mu_M \tag{4.5}$$

and plastic yielding will take place when this expression reaches the value R.

5. We assume that through appropriate experiments† the parameters u_H, μ_M and η of the material or, what comes to the same, T_{ret}, T_{ret} and μ_H have been determined. We now put a specimen of the material in a testing machine to determine at what stage it will yield plastically. We have to distinguish two kinds of machines. In the first kind the cylindrical specimen is loaded in tension by gradually increasing loads and the (normal) tensile stress ϑ_n‡ is determined at which yielding takes place. In every single case s = constant = s_c. We can then integrate (3.6) and find, assuming that we start in every case with an unstrained and unstressed specimen ($\epsilon_0 = 0$, $s_0 = 0$),

$$\epsilon = \frac{s_c}{2\mu_H}\left[1 - \frac{\mu_M}{\mu_H + \mu_M} \exp\left(-t/T_{ret}\right)\right]. \tag{5.1}$$

In this case our yield criterion gives, from (4.5) with $s_c = \vartheta_n$,

$$\vartheta_n^2 = 4\mu_H R\left[1 - \frac{2\mu_M}{\mu_H + \mu_M} \exp\left(-t/T_{ret}\right) + \frac{\mu_M}{\mu_H + \mu_M} \exp\left(-2t/T_{ret}\right)\right]^{-1}. \tag{5.2}$$

*REINER (op. cit., p. 522).

†For instance instantaneous reaction, creep, damping, etc.

‡We mean, of course, $\vartheta_{n(0)}$, i.e. the *deviator* of the tensile stress.

When the stress ϑ_n is applied, plastic yielding will accordingly take place after the lapse of time

$$t = T_{\text{rel}} \ln \left\{ \frac{1}{1 - \sqrt{\left[1 - \frac{\mu_H + \mu_M}{\mu_M}\left(1 - \frac{4\mu_H R}{\vartheta_n^2}\right)\right]}} \right\}. \tag{5.3}$$

We see that, if the stress applied is

$$\bar{\vartheta}_n = 2\sqrt{[(\mu_H + \mu_M) R]}, \tag{5.4}$$

$t = 0$ and plastic yielding will set in *at once*. On the other hand, when a smaller stress of magnitude

$$\bar{\bar{\vartheta}}_n = 2\sqrt{(\mu_H R)} \tag{5.5}$$

is applied, it will take infinite time ($t = \infty$) for yielding to be reached. If $s_c < \bar{\bar{\vartheta}}_n$, there will be no yielding, however long we may wait. If $\bar{\bar{\vartheta}}_n < s_c < \bar{\vartheta}_n$, there will be yielding after the lapse of time $0 < t < \infty$ to be found from (5.3).

This is qualitatively in accordance with experience. If plastic yielding takes time to arrive, it will lead to what is known as 'creep fracture.' Anelasticity is accordingly of necessity connected with what may be named 'static fatigue.'

The strain corresponding to the yield stress is, from (5.1),

$$\theta_n = \frac{\vartheta_n}{2\mu_H}\left\{1 - \frac{\mu_H}{\mu_H + \mu_M}\left[1 - \sqrt{\left(1 - \frac{\mu_H + \mu_M}{\mu_M}\left(1 - \frac{4\mu_H R}{\vartheta_n^2}\right)\right)}\right]\right\} \tag{5.6}$$

and is in the two extreme cases

$$\bar{\theta} = \frac{\bar{\vartheta}_n}{2(\mu_H + \mu_M)} = \sqrt{\left(\frac{R}{\mu_H + \mu_M}\right)}, \qquad \bar{\bar{\theta}} = \frac{\bar{\bar{\vartheta}}_n}{2\mu_H} = \sqrt{\frac{R}{\mu_H}}, \tag{5.7}$$

with, in general, $\bar{\theta}_n < \theta_n < \bar{\bar{\theta}}_n$.

6. The other, and usual, kind of testing machine is one in which $\dot{\epsilon}$ is roughly constant, say $= \dot{\epsilon}_c$. For this we have from (3.3), assuming that we start with an unstressed specimen ($s_0 = 0$),

$$s = 2\mu_H \epsilon + 2\mu_M T_{\text{rel}} \left[1 - \exp\left(-t/T_{\text{rel}}\right)\right] \dot{\epsilon}_c. \tag{6.1}$$

Introducing ϵ/t for $\dot{\epsilon}_c$, the yield criterion gives from (4.5)

$$\theta_n = \sqrt{\left(\frac{R}{\mu_H + \alpha^2 \mu_M}\right)} \tag{6.2}$$

where

$$\alpha = \frac{T_{\text{rel}}}{t}\left[1 - \exp\left(-t/T_{\text{rel}}\right)\right] \tag{6.3}$$

when $t/T_{\text{rel}} = 0$, $\alpha = 1$, and when $t/T_{\text{rel}} = \infty$, $\alpha = 0$. For any $0 < t/T_{\text{rel}} < \infty$, α varies monotonically from 1 to 0, being always positive, and smaller than 1. In accordance with (6.2) θ_n varies between $\sqrt{(R/\mu_H + \mu_M)}$ and $\sqrt{R/\mu_H}$ as in the previous case [compare (5.7)]. From (6.2) and (6.3) we have

$$t = \frac{1}{\dot{\epsilon}_c}\sqrt{\frac{(R/\mu_M)}{(\mu_H/\mu_M) + \alpha^2}} \tag{6.4}$$

from which we can calculate the time τ, when yielding will take place with a given constant rate of extension $\dot{\epsilon}_c$.

If we thus know τ, we introduce this value for t in (6.3) and find the limiting α, and thus in turn from (6.2) the yield strain θ_n.

We now write from (6.1), (6.2) and (3.5, 1)

$$\vartheta_n = 2\mu_H \theta_n + 2\eta \beta \dot{\epsilon}_c \tag{65.}$$

where

$$\beta = 1 - \exp(1 - t/T_{rel}). \tag{6.6}$$

This coefficient varies between 0 and 1. We see that when the specimen is extended with a constant rate ($\dot{\epsilon}_c$) yielding will take place when a definite strain (θ_n) is reached. The stress at the yield point (ϑ_n), however, increases with the rate of strain. This also is qualitatively in accordance with experience. There exists a large body of experimental results showing the increase of the yield stress with the rate of strain in metals and other materials.

7. CONCLUSIONS

Two phenomena observed in metals and other materials have until now not been traced to a common source. They are ' static fatigue leading to creep fracture ' and ' increase of yield stress with rate of strain.' We have shown that both are inherent in anelasticity as defined by a linear relation between stress, strain and their time derivatives, and/or as represented by a mechanical model which consists of a Maxwell-body and a Hooke-body coupled in parallel. The causal connection was effected by means of REINER and WEISSENBERG's yield criterion, in accordance with which yielding takes place when that part of the stress-work which is conserved as elastic energy reaches a certain maximum value R. Two methods of testing, namely (i) by constant load (s_c), and (ii) by constant rate of strain ($\dot{\epsilon}_c$) were considered in detail. In the first case it was found that there is *instantaneous* yielding when the load produces a certain yield stress $s_c = \bar{\vartheta}$. If the stress is less than $\bar{\vartheta}$, but larger than $\underline{\vartheta}$, with $\underline{\vartheta} < \bar{\vartheta}$, yielding takes place in creep after the lapse of some time which, in the limiting case $s_c = \underline{\vartheta}$, is infinite. If $s_c < \underline{\vartheta}$, there is no yielding. To the yield stresses $\bar{\vartheta}$ and $\underline{\vartheta}$ correspond single valued yield strains $\bar{\theta}$ and $\underline{\theta}$.

In the second case yielding takes place when the yield *strains* $\bar{\theta}$ and $\underline{\theta}$ are reached, the first when the rate of strain is very large approaching infinite, the second when it is very small approaching zero, with other yield strains $\underline{\theta} < \theta < \bar{\theta}$ corresponding to rates of strain $\infty > \dot{\epsilon} > 0$. The yield stress ϑ, however, is not a single valued function of θ, but increases with the rate of strain.

ACKNOWLEDGMENT

This research has been sponsored in part by the Air Research and Development Command of the United States Air Force through the European Office, A.R.D.C.

REFERENCES

HENCKY, H. 1924 *Z. Angew. Math. Mech.* **4**, 223.

HILL, R. 1950 *Mathematical Theory of Plasticity* (Clarendon Press, Oxford).

Mises, R. von	1913	*Göttinger Nachr. Math.-Phys. Klasse* 582.
Poynting, J. H. and Thomson, J. J.	1902	*Properties of Matter* (Griffin, London).
Reiner, M.	1958	*Encyclopaedia of Physics* (Ed. Fluegge, S.), Vol. 6, p. 434 (Springer, Berlin).
Reiner, M. and Weissenberg, K.	1939	*Rheol. Leafl.* **10**, 12.
Zener, C.	1948	*Elasticity and Anelasticity of Metals* (University of Chicago Press).

J. Mech. Phys. Solids, 1960, Vol. 8, pp. 262 to 279. Pergamon Press Ltd., London. Printed in Great Britain

THE DYNAMIC PLANE DEFORMATION OF AN IDEAL PLASTIC–RIGID SOLID

By A. J. M. Spencer*
Atomic Weapons Research Establishment, Aldermaston

(*Received 4th August*, 1960)

Summary

This paper is concerned with the motion under plane strain conditions of an ideal plastic–rigid solid, when the inertial forces are not negligible. It is shown that the equations for such a motion can be expressed in a particularly simple form when referred to a system of moving curvilinear coordinates which is a generalization of the system defined by the slip-line field in quasi-static plane plasticity. A perturbation method of solving the equations is described; in this, approximate solutions to dynamic problems are obtained as perturbations of a known (usually quasi-static) solution. The method is illustrated by application to problems of indentation of a plastic–rigid half-space by stationary and moving loads.

1. Introduction

The theory of the deformation of plastic solids under dynamic conditions has been studied by various authors. For example, Taylor (1958), Karman and Duwez (1950) and others have considered the propagation of longitudinal plastic waves; Symonds and others and Hopkins and others have treated the dynamic deformation of beams and plates respectively (references to this work are given by Goodier and Hodge, 1958); and Hopkins (1960) has reviewed work on spherically symmetric deformations.

In all the examples quoted the treatment has been facilitated by the fact that it is possible to analyse the problem in terms of two independent variables, namely time and one space coordinate. In this paper the plane deformation of an ideal plastic–rigid solid under dynamic conditions is considered; the analysis therefore involved two space variables as well as time. The theory is based on the well-developed theory of quasi-static plane plastic strain which is here extended to the case in which inertial terms are included. The general problem is formulated in a fundamental system of coordinates and an approximate method of solution is described, with examples.

As with any theory which treats an idealized material, the ideal plastic–rigid theory has limitations in its application to real materials. Those which apply in quasi-static as well as in dynamic motion have been discussed frequently in the past and need not be stated here; it may be noted, however, that the assumption of plastic–rigid behaviour also precludes any consideration of elastic waves, and so may lead to erroneous results if material velocities are comparable with the

*Now in Department of Theoretical Mechanics, University of Nottingham.

velocities of elastic waves in real materials. A further assumption, which is of no consequence in the quasi-static theory, but which further limits the dynamic theory, is that the yield stress is independent of strain-rate. Although these assumptions restrict the value of the plastic–rigid theory, this theory seems to be a necessary first step towards the construction of more elaborate and realistic theories, and may itself be adequate to describe some physical situations.

The arrangement of the work is as follows. In Section 2 the governing equations are stated and their characteristic surfaces and bicharacteristic curves in (x, y, t) space are determined. It is shown that the equations have formal simplicity when referred to a system of coordinates which is a generalization of the system defined by the slip-line field in quasi-static plasticity.

In Section 3 a perturbation method of solution of the equations of Section 2 is described. In this a known solution (usually a quasi-static solution) is taken, and dynamic solutions are regarded as perturbations of this original solution. The method can be applied if the stresses due to the inertia of the material are small compared to the yield stress.

In Sections 4–7 the theory is illustrated by application to the problem of surface indentation of a semi-infinite body by the application of surface pressure or displacement to a segment $|x| \leqslant a$ of the surface $y = 0$. In Sections 4 and 5 a is taken to be constant; in Section 6 a is considered to be a function of time. In Section 7 the work done in surface indentation is evaluated approximately.

2. Equations of Plane Plastic Strain

We denote by σ_x, σ_y, τ_{xy} the components of stress referred to a fixed system of rectangular coordinates (x, y); v_x, v_y the components of particle velocity; f_x, f_y the components of particle acceleration; and by ρ the constant density of the material. Then the equations which govern the motion of an ideal plastic–rigid solid which satisfies either a von Mises or a Tresca yield criterion, and is undergoing deformation under conditions of plane strain, are as follows:

(i) The equations of motion

$$\frac{\partial \sigma_x}{\partial x} + \frac{\partial \tau_{xy}}{\partial y} = \rho f_x, \qquad \frac{\partial \tau_{xy}}{\partial x} + \frac{\partial \sigma_y}{\partial y} = \rho f_y. \tag{1}$$

(ii) The yield criterion

$$(\sigma_x - \sigma_y)^2 + 4\,\tau_{xy}^2 = 4k^2, \tag{2}$$

where k is a constant.

(iii) The incompressibility condition

$$\frac{\partial v_x}{\partial x} + \frac{\partial v_y}{\partial y} = 0. \tag{3}$$

(iv) The condition that the principal axes of the stress and strain-rate tensors are coincident

$$(\sigma_x - \sigma_y)/2\tau_{xy} = \left(\frac{\partial v_x}{\partial x} - \frac{\partial v_y}{\partial y}\right) \Big/ \left(\frac{\partial v_x}{\partial y} + \frac{\partial v_y}{\partial x}\right). \tag{4}$$

The acceleration components f_x, f_y are given in terms of v_x, v_y by the relations

$$\left.\begin{aligned} f_x &= \frac{\partial v_x}{\partial t} + v_x \frac{\partial v_x}{\partial x} + v_y \frac{\partial v_x}{\partial y}, \\ f_y &= \frac{\partial v_y}{\partial t} + v_x \frac{\partial v_x}{\partial x} + v_y \frac{\partial v_y}{\partial y}. \end{aligned}\right\} \quad \text{(v)} \tag{5}$$

Equations (1)–(5) are in principle sufficient to determine σ_x, σ_y, τ_{xy}, v_x and v_y as functions of x, y and t, if suitable boundary and initial conditions are specified.

We begin by investigating the characteristic surfaces in (x, y, t) space of the system of equations (1)–(5). The notation to be used follows, in the main, that of HILL (1950). Proceeding by analogy with the theory of quasi-static plane plastic deformation, we define the α- and β-lines at a time t to be the curves in the (x, y) plane whose tangents at any point at time t are directed in the principal directions of the shearing stress at that point. The α- and β-lines at a given instant are two families of plane curves, and are distinguished by the convention that if the α- and β-lines through a point are regarded as a pair of right-handed curvilinear coordinate axes, the line of action of the algebraically greatest principal stress lies in the first and third quadrants. The α- and β-lines collectively are called slip-lines. The use of this term will be justified later.

If ϕ denotes the angular rotation, measured anti-clockwise, of an α-line from the x-axis, we may write

$$\left.\begin{aligned} \sigma_x &= -p - k \sin 2\phi, \\ \sigma_y &= -p + k \sin 2\phi, \\ \tau_{xy} &= k \cos 2\phi, \end{aligned}\right\} \tag{6}$$

where p and ϕ are scalar functions of position and time. The yield condition (2) is now identically satisfied. Substituting for the stress components, equation (1) becomes

$$\left.\begin{aligned} \frac{\partial p}{\partial x} + 2k \cos 2\phi \frac{\partial \phi}{\partial x} + 2k \sin 2\phi \frac{\partial \phi}{\partial y} + \rho f_x &= 0, \\ \frac{\partial p}{\partial y} + 2k \sin 2\phi \frac{\partial \phi}{\partial x} - 2k \cos 2\phi \frac{\partial \phi}{\partial y} + \rho f_y &= 0, \end{aligned}\right\} \tag{7}$$

and (4) may be written

$$\cos 2\phi \left(\frac{\partial v_x}{\partial x} - \frac{\partial v_y}{\partial y}\right) + \sin 2\phi \left(\frac{\partial v_x}{\partial y} + \frac{\partial v_y}{\partial x}\right) = 0. \tag{8}$$

When the expressions (5) for f_x, f_y are substituted into (7), equations (3), (7) and (8) form a system of four first-order quasi-linear differential equations, with p, ϕ, v_x and v_y as dependent variables, and x, y, t as independent variables. It is this system of equations which will be studied.

The condition that a surface $\theta(x, y, t) = 0$ shall be a characteristic surface of the equations, that is a surface on which the normal derivatives of p, ϕ, v_x and v_y are not uniquely determined by the equations if p, ϕ, v_x and v_y are known on the surface, is

$$\begin{vmatrix} \partial\theta/\partial x & 2kA & \rho C & 0 \\ \partial\theta/\partial y & 2kB & 0 & \rho C \\ 0 & 0 & \partial\theta/\partial x & \partial\theta/\partial y \\ 0 & 0 & A & B \end{vmatrix} = 0, \tag{9}$$

where

$$\left.\begin{aligned} A &= \cos 2\phi\,(\partial\theta/\partial x) + \sin 2\phi\,(\partial\theta/\partial y), \\ B &= \sin 2\phi\,(\partial\theta/\partial x) - \cos 2\phi\,(\partial\theta/\partial y), \\ C &= (\partial\theta/\partial t) + v_x\,(\partial\theta/\partial x) + v_y\,(\partial\theta/\partial y). \end{aligned}\right\} \tag{10}$$

Expanding the determinant and inserting the expressions for A and B, we obtain from (9), after simplification

$$[\cos\phi\,(\partial\theta/\partial x) + \sin\phi\,(\partial\theta/\partial y)]^2\,[\sin\phi\,(\partial\theta/\partial x) - \cos\phi\,(\partial\theta/\partial y)]^2 = 0. \tag{11}$$

The determinant expressing the characteristic condition therefore resolves into two distinct factors, each repeated, neither of which contains terms in $\partial\theta/\partial t$. Thus there are four families of characteristic surfaces which are coincident in pairs. This coincidence is a generalization of the familiar result in quasi-static plane plasticity that the characteristics of the stress and velocity equations coincide, and are the slip-lines. From (11) and the definition of the slip-lines, it follows that each characteristic surface $\theta(x, y, t) = 0$ is either a plane $t =$ constant or a surface which intersects the planes $t =$ constant in α- or β-lines. The bicharacteristic curves through a given point degenerate to become the envelope of the characteristic surfaces through the point, and are in fact the pair of slip-lines through the point. Since the slip-lines, regarded as curves in (x, y, t) space, are plane curves in the planes $t =$ constant, relations along the bicharacteristics through a point $P_0(x_0, y_0, t_0)$ can give no information about the dependent variables at times subsequent to t_0, and in this sense the system of equations is parabolic.

Since it has been shown that derivatives of v_x and v_y may be discontinuous across a characteristic surface, and hence across a bicharacteristic curve, the use of the term slip-line for the bicharacteristics is justified.

In view of these properties of the equations, it is appropriate to refer them to t, and to a system of moving curvilinear coordinates in the (x, y) plane which at any instant are defined by the two families of slip-lines at that time, which in turn are completely defined by the current value of the angle ϕ. We denote by ds_α, ds_β, elements of length along the α- and β-lines respectively at a time t, so that

$$\left.\begin{aligned} (\partial/\partial x) &= \cos\phi\,(\partial/\partial s_\alpha) - \sin\phi\,(\partial/\partial s_\beta), \\ (\partial/\partial y) &= \sin\phi\,(\partial/\partial s_\alpha) + \cos\phi\,(\partial/\partial s_\beta). \end{aligned}\right\} \tag{12}$$

We also denote by v_α, v_β, the components of particle velocity in the directions of the α- and β-lines respectively at time t, and by f_α, f_β, the components of particle acceleration in the directions of the α- and β-lines at time t. Thus

$$v_\alpha = v_x\cos\phi + v_y\sin\phi, \qquad v_\beta = -v_x\sin\phi + v_y\cos\phi\,; \tag{13}$$

$$f_\alpha = f_x\cos\phi + f_y\sin\phi, \qquad f_\beta = -f_x\sin\phi + f_y\cos\phi. \tag{14}$$

From (12), (13) and (14), equations (3), (7) and (8) are readily seen to be equivalent to

$$\partial (p + 2k\phi)/\partial s_\alpha + \rho f_\alpha = 0, \tag{15}$$

$$\partial (p - 2k\phi)/\partial s_\beta + \rho f_\beta = 0, \tag{16}$$

$$\partial v_\alpha/\partial s_\alpha - v_\beta (\partial \phi/\partial s_\alpha) = 0, \tag{17}$$

$$\partial v_\beta/\partial s_\beta + v_\alpha (\partial \phi/\partial s_\beta) = 0. \tag{18}$$

When the acceleration components f_α, f_β are zero, (15) and (16) reduce to HENCKY's equations for the stress field in quasi-static plane plastic flow; equations (17) and (18) are an expression of GEIRINGER's equations for the velocity field in plane plastic flow.

It remains to express f_α and f_β in terms of v_α, v_β and ϕ. From (5), (12), (13) and (14) we find, after some manipulation and use of (17) and (18),

$$\left.\begin{aligned} f_\alpha &= \frac{\partial v_\alpha}{\partial t} + v_\beta \left(\frac{\partial v_\alpha}{\partial s_\beta} - v_\beta \frac{\partial \phi}{\partial s_\beta} - \frac{\partial \phi}{\partial t} \right), \\ f_\beta &= \frac{\partial v_\beta}{\partial t} + v_\alpha \left(\frac{\partial v_\beta}{\partial s_\alpha} + v_\alpha \frac{\partial \phi}{\partial s_\alpha} + \frac{\partial \phi}{\partial t} \right). \end{aligned}\right\} \tag{19}$$

In (19) the expressions $\partial v_\alpha/\partial t$, $\partial v_\beta/\partial t$ and $\partial \phi/\partial t$ denote the time rates of change of v_α, v_β and ϕ respectively, referred to fixed curvilinear coordinates which coincide instantaneously with the α- and β-lines.

As in the quasi-static theory, a velocity field which satisfies (17) and (18) and the boundary conditions does not generally define a unique solution of a given problem. Moreover, a stress field in a plastic region can be accepted only if a stress field can be constructed in the rigid regions, which is in equilibrium, or permits only rigid body motion, does not violate the yield criterion, and will support the tractions on the boundary of the rigid region.

It may be remarked that THOMAS (1952) has discussed characteristic surfaces in three-dimensional time-dependent plasticity from a completely different viewpoint.

3. Perturbation Method of Solution

Despite their formal simplicity the numerical solution of equations (15)–(19) in cases of interest will at best be an extremely lengthy procedure, and we are led to consider approximate methods. In this Section a perturbation method of solution will be formulated.

It is first noted that in many cases the terms involving the squares and products of v_α, v_β $\partial v_\alpha/\partial s_\beta$ and $\partial v_\beta/\partial s_\alpha$ in the expressions (19) for f_α and f_β will, when these expressions are inserted in (15) and (16), be small in comparison to other terms appearing in (15) and (16). More specifically, we may have

$$\rho c^2 \ll 2k \tag{20}$$

where c is a typical particle velocity occurring in a problem. It will be assumed that this condition is satisfied.

We seek solutions of (15)–(18) of the form

$$\left.\begin{aligned} p &= p^\circ + \epsilon p' + \epsilon^2 p'' + \ldots\ldots\ldots, \\ \phi &= \phi^\circ + \epsilon \phi' + \epsilon^2 \phi'' + \ldots\ldots\ldots, \\ f_\alpha &= f_\alpha^\circ + \epsilon f_\alpha' + \epsilon^2 f_\alpha'' + \ldots\ldots\ldots, \\ f_\beta &= f_\beta^\circ + \epsilon f_\beta' + \epsilon^2 f_\beta'' + \ldots\ldots\ldots, \end{aligned}\right\} \tag{21}$$

where ϵ is a small dimensionless constant. We require that the terms involving squares and products of v_α, v_β and their space derivatives shall appear as terms of order ϵ in the expressions for f_α and f_β, that is, we require that v_α and v_β may be expressed in the forms

$$\left.\begin{aligned} v_\alpha &= \epsilon^{\frac{1}{2}}(V_\alpha^\circ + \epsilon V_\alpha' + \epsilon^2 V_\alpha'' + \ldots\ldots), \\ v_\beta &= \epsilon^{\frac{1}{2}}(V_\beta^\circ + \epsilon V_\beta' + + \epsilon^2 V_\beta'' + \ldots\ldots). \end{aligned}\right\} \tag{22}$$

In order that the derivatives of v_α, v_β and ϕ with respect to time shall appear as terms of the correct order, the substitution

$$t = \epsilon^{\frac{1}{2}}\tau \tag{23}$$

is also made.

The solution will be referred to the system of orthogonal curvilinear coordinates which is defined by the angle ϕ°, and the coordinate curves of this system will be called an ' initial slip-line field,' in contrast to the field defined by ϕ, called the ' perturbed slip-line field.' The angle ϕ° is in general a function of time, as well as of position. In order to transform equations (15)–(19) to equations referred to the initial slip-line field, we use the relations

$$\left.\begin{aligned} (\partial/\partial s_\alpha) &= \cos(\phi - \phi^\circ)(\partial/\partial s_\alpha^\circ) + \sin(\phi - \phi^\circ)(\partial/\partial s_\beta^\circ), \\ (\partial/\partial s_\beta) &= -\sin(\phi - \phi^\circ)(\partial/\partial s_\alpha^\circ) + \cos(\phi - \phi^\circ)(\partial/\partial s_\beta^\circ), \end{aligned}\right\} \tag{24}$$

where $\partial/\partial s_\alpha^\circ$ and $\partial/\partial s_\beta^\circ$ denote differentiation along the slip-lines of the initial field.

We now insert (21), (22), (23) and (24) in equations (15)–(19), express all the resulting terms in the equations as series of powers of ϵ, and equate coefficients of successive powers of ϵ in the equations to zero. This procedure yields a sequence of sets of linearized equations, which determine, in turn, p°, ϕ°, V_α°, V_β°; p', ϕ', V_α', V_β'; p'', ϕ'', V_α'', V_β''; and so on, as functions of time and of position with respect to the initial slip-line field. We will formulate explicity the equations obtained by equating to zero coefficients of the three lowest powers of ϵ which occur in equations (15)–(19).

The terms of lowest order in (15)–(19) give

$$\left.\begin{aligned} &\partial(p^\circ + 2k\phi^\circ)/\partial s_\alpha^\circ + \rho f_\alpha^\circ = 0, \\ &\partial(p^\circ - 2k\phi^\circ)/\partial s_\beta^\circ + \rho f_\beta^\circ = 0, \\ &\partial V_\alpha^\circ/\partial s_\alpha^\circ - V_\beta^\circ(\partial\phi^\circ/\partial s_\alpha^\circ) = 0, \\ &\partial V_\beta^\circ/\partial s_\beta^\circ + V_\alpha^\circ(\partial\phi^\circ/\partial s_\beta^\circ) = 0, \\ &f_\alpha^\circ = \partial V_\alpha^\circ/\partial\tau - V_\beta^\circ(\partial\phi^\circ/\partial\tau), \\ &f_\beta^\circ = \partial V_\beta^\circ/\partial\tau + V_\alpha^\circ(\partial\phi^\circ/\partial\tau). \end{aligned}\right\} \tag{25}$$

A solution p°, ϕ°, V_α°, V_β° of (25) will be called an ' initial solution,' and solutions which include terms of higher order in ϵ will be regarded as perturbations of the initial solution. The boundary conditions satisfied by the initial solution may differ at most by quantities of order ϵ from the boundary conditions of the problem which is to be solved by the perturbation method. In applications, the initial solution will usually be the solution of a quasi-static problem, and the initial slip-line field will be the slip-line field of this quasi-static problem. The equations (25) for the initial solution reduce to the quasi-static equations of plastic plane strain when $f_\alpha^\circ = f_\beta^\circ = 0$. This condition is satisfied in two important cases, namely (i) problems of steady motion, in which $\partial V_\alpha^\circ/\partial\tau = \partial V_\beta^\circ/\partial\tau = \partial\phi^\circ/\partial\tau = 0$, and (ii) problems in which $V_\alpha^\circ = V_\beta^\circ = 0$, that is, non-steady motion problems in which $\rho\partial v_\alpha/\partial t$ and $\rho\partial v_\beta/\partial t$ are everywhere of order $\epsilon k/a$, where a is a typical length, and the non-linear terms in the expressions (19) for the acceleration components are of order $\epsilon^2 k/a$. Note that in problems of type (ii) it is not necessary that $\partial\phi^\circ/\partial\tau = 0$, so that perturbation solutions may be developed for problems in which ϕ° varies with time, if a suitable initial solution can be found.

The equations for the first-order perturbations p', ϕ', V_α' and V_β' are obtained by equating to zero coefficients of the next higher power of ϵ in (15)–(19), after making the substitutions (21)–(24). These equations are

$$
\left.\begin{aligned}
&\partial(p' + 2k\phi')/\partial s_\alpha^\circ + \phi' \partial(p^\circ + 2k\phi^\circ)/\partial s_\beta^\circ + \rho f_\alpha' = 0,\\
&\partial(p' - 2k\phi')/\partial s_\beta^\circ - \phi' \partial(p^\circ - 2k\phi^\circ)/\partial s_\alpha^\circ + \rho f_\beta' = 0,\\
&\partial V_\alpha'/\partial s_\alpha^\circ - V_\beta' \partial\phi^\circ/\partial s_\alpha^\circ - V_\beta^\circ \partial\phi'/\partial s_\alpha^\circ + \phi'(\partial V_\alpha^\circ/\partial s_\beta^\circ - V_\beta^\circ \partial\phi^\circ/\partial s_\beta^\circ) = 0,\\
&\partial V_\beta'/\partial s_\beta^\circ + V_\alpha' \partial\phi^\circ/\partial s_\beta^\circ + V_\alpha^\circ \partial\phi'/\partial s_\beta^\circ - \phi'(\partial V_\beta^\circ/\partial s_\alpha^\circ + V_\alpha^\circ \partial\phi^\circ/\partial s_\alpha^\circ) = 0,\\
&f_\alpha' = \partial V_\alpha'/\partial\tau - V_\beta' \partial\phi^\circ/\partial\tau + V_\beta^\circ(\partial V_\alpha^\circ/\partial s_\beta^\circ - V_\beta^\circ \partial\phi^\circ/\partial s_\beta^\circ - \partial\phi'/\partial\tau),\\
&f_\beta' = \partial V_\beta'/\partial\tau + V_\alpha' \partial\phi^\circ/\partial\tau + V_\alpha^\circ(\partial V_\beta^\circ/\partial s_\alpha^\circ + V_\alpha^\circ \partial\phi^\circ/\partial s_\alpha^\circ + \partial\phi'/\partial\tau).
\end{aligned}\right\} \quad (26)
$$

The equations for the second-order perturbations p'', ϕ'', V_α'' and V_β'' are derived in a similar manner, and are

$$
\left.\begin{aligned}
&\partial(p'' + 2k\phi'')/\partial s_\alpha^\circ + \phi' \partial(p' + 2k\phi')/\partial s_\beta^\circ + \\
&\qquad + \phi'' \partial(p^\circ + 2k\phi^\circ)/\partial s_\beta^\circ + \rho f_\alpha'' + \tfrac{1}{2}\rho\phi'^2 f_\alpha^\circ = 0,\\
&\partial(p'' - 2k\phi'')/\partial s_\beta^\circ - \phi' \partial(p' - 2k\phi')/\partial s_\alpha^\circ - \\
&\qquad - \phi'' \partial(p^\circ - 2k\phi^\circ)/\partial s_\alpha^\circ + \rho f_\beta'' + \tfrac{1}{2}\rho\phi'^2 f_\beta^\circ = 0,\\
&\partial V_\alpha''/\partial s_\alpha^\circ - V_\beta'' \partial\phi^\circ/\partial s_\alpha^\circ - V_\beta' \partial\phi'/\partial s_\alpha^\circ - V_\beta^\circ \partial\phi''/\partial s_\alpha^\circ + \\
&\qquad + \phi'(\partial V_\alpha'/\partial s_\beta^\circ - V_\beta' \partial\phi^\circ/\partial s_\beta^\circ - V_\beta^\circ \partial\phi'/\partial s_\beta^\circ) + \\
&\qquad + \phi''(\partial V_\alpha^\circ/\partial s_\beta^\circ - V_\beta^\circ \partial\phi^\circ/\partial s_\beta^\circ) = 0,\\
&\partial V_\beta''/\partial s_\beta^\circ + V_\alpha'' \partial\phi^\circ/\partial s_\beta^\circ + V_\alpha' \partial\phi'/\partial s_\beta^\circ + V_\alpha^\circ \partial\phi''/\partial s_\beta^\circ - \\
&\qquad - \phi'(\partial V_\beta'/\partial s_\alpha^\circ + V_\alpha' \partial\phi^\circ/\partial s_\alpha^\circ + V_\alpha^\circ \partial\phi'/\partial s_\alpha^\circ) - \\
&\qquad - \phi''(\partial V_\beta^\circ/\partial s_\alpha^\circ + V_\alpha^\circ \partial\phi^\circ/\partial s_\alpha^\circ) = 0,\\
&f_\alpha'' = \partial V_\alpha''/\partial\tau - V_\beta'' \partial\phi^\circ/\partial\tau + V_\beta'(\partial V_\alpha^\circ/\partial s_\beta^\circ - V_\beta^\circ \partial\phi^\circ/\partial s_\beta^\circ - \partial\phi'/\partial\tau) + \\
&\qquad + V_\beta^\circ(\partial V_\alpha'/\partial s_\beta^\circ - V_\beta^\circ \partial\phi'/\partial s_\beta^\circ - V_\beta' \partial\phi^\circ/\partial s_\beta^\circ - \partial\phi''/\partial\tau),\\
&f_\beta'' = \partial V_\beta''/\partial\tau + V_\alpha'' \partial\phi^\circ/\partial\tau + V_\alpha'(\partial V_\beta^\circ/\partial s_\alpha^\circ + V_\alpha^\circ \partial\phi^\circ/\partial s_\alpha^\circ + \partial\phi'/\partial\tau) + \\
&\qquad + V_\alpha^\circ(\partial V_\beta'/\partial s_\alpha^\circ + V_\alpha^\circ \partial\phi'/\partial s_\alpha^\circ + V_\alpha' \partial\phi^\circ/\partial s_\alpha^\circ + \partial\phi''/\partial\tau).
\end{aligned}\right\} \quad (27)
$$

In deriving (27), use has been made of (25).

It will be observed that across lines of discontinuity in the velocity field, $f_\alpha', f_\alpha'', \ldots$; $f_\beta', f_\beta'', \ldots$ will in general take infinite values unless the normal component of velocity across the line of discontinuity is zero, and that infinities may also arise in the velocity equations if velocity discontinuities occur. The perturbation method cannot be applied without modification in such cases. As in the quasi-static theory, the correct approach in such cases seems to be to regard the lines of discontinuity as the limits of narrow regions through which the tangential component of velocity changes rapidly, and to adopt a limiting process.

In applying equations (25), (26) and (27) to the solution of particular problems, boundary conditions and conditions of continuity at interfaces between different regions must be applied in the perturbed slip-line field and not in the initial field.

4. Surface Indentation of a Semi-infinite Solid. Relation between Pressure and Surface Velocity

In this and the following Sections we consider the problem of the indentation of a plastic–rigid solid occupying the half-space $y < 0$ by the application of prescribed surface pressures or displacements to the surface $y = 0$, $|x| < a$. In this Section and the next a will be taken to be constant ; in Section 6 a is a function of time. It is assumed that the deformation is sufficiently small for changes in surface geometry to be neglected, so that boundary conditions may be regarded as being

applied on the undeformed surface $y = 0$. The solution therefore applies strictly to the initial motion of the plastic–rigid material, but should give a useful approximation as long as the depth of indentation remains small compared with its width.

The perturbation method of solution will be used to solve this problem approximately. As an initial slip-line field we use one which gives a solution of the quasi-static punch indentation problem. It is well known that there is no unique velocity field which solves this problem; however, if for simplicity we consider only configurations which are symmetrical about $x = 0$, every possible field can be regarded as a special case of that illustrated in Fig. 1. For instance if in Fig. 1 A and B

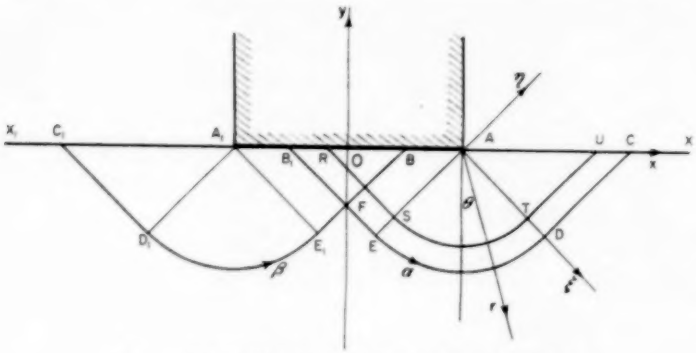

Fig. 1. Initial slip-line field for surface indentation.

coincide, the field resembles that originally proposed by Prandtl (1920), whereas when B coincides with the origin O, the field reduces to that due to Hill (1949). It will be shown that the solution of the dynamic problem throws some light on this problem of uniqueness of the velocity field.

In Fig. 1, the surface of the punch is represented by $A_1 A$, and the deforming region is $OCDFD_1 C_1$, the region exterior to this being rigid. The lengths OA, OB are denoted a, b respectively. The initial slip-lines are straight lines in ACD, $A_1 C_1 D_1$ and $A_1 AEE_1$, and are straight lines and circular arcs in ADE and $A_1 D_1 E_1$. Since the configuration is symmetrical, we refer to the region $B_1 ACDE$ only. As illustrated in Fig. 1, (r, θ) are polar coordinates centred on A, the line $\theta = 0$ coinciding with the downward vertical through A.

The initial solution for the stress field is

(i) Region $B_1 AE$: $p^\circ = k(1 + \pi)$, $\phi^\circ = -\frac{1}{4}\pi$. (28)

(ii) Region ADE: $p^\circ = k(1 + \frac{1}{2}\pi - 2\theta)$, $\phi^\circ = \theta$. (29)

(iii) Region ACD: $p^\circ = k$, $\phi^\circ = \frac{1}{4}\pi$. (30)

For the initial velocity solution the material is assumed to be at rest, that is

$$V_\alpha^\circ = V_\beta^\circ = 0, \tag{31}$$

and all motion is regarded as a perturbation of this stationary state. It is readily verified that (28)–(31) satisfy equations (25). The normal surface pressure on the surface $A_1 A$ is Q_0, where

$$Q_0 = k(2 + \pi). \tag{32}$$

There is no applied tangential stress on $A_1 A$, and the surface AX is stress-free.

For the dynamic problem, let $Q(x, t)$ denote the pressure applied to the surface $A_1 A$, and $W(x, t)$ the downward vertical component of velocity of points which initially lie on this surface. For simplicity, it is assumed that $Q(x, t)$ and $W(x, t)$ are even functions of x in $-a < x < a$. The surface AX remains stress-free, and there is no applied tangential stress on $A_1 A$. Hence $\phi = -\frac{1}{4}\pi$ on $A_1 A$, so that if W_α and $-W_\beta$ denote components of velocity on $A_1 A$ directed along the α- and β-lines respectively, then

$$W = (W_\alpha + W_\beta)/\sqrt{2}. \tag{33}$$

In the dynamic problem, the α-line through B_1 is denoted $B_1 F' E' D' C'$, where F' lies on $x = 0$, C' lies on $y = 0$, and the centred fan of β-lines through A is bounded by AE' and AD'. The configuration is illustrated in Fig. 3 for a special case, to be described later, in which B_1 coincides with A_1.

When σ_y and τ_{xy} are expressed in terms of p and ϕ by means of (6), it is seen that the boundary conditions to be satisfied in the dynamic problem are

$$p = Q(x, t) - k, \quad \phi = -\tfrac{1}{4}\pi, \quad \text{on } A_1 A. \tag{34}$$

$$v_\alpha = W_\alpha, \quad v_\beta = -W_\beta, \quad \text{on } A_1 A. \tag{35}$$

$$p = k, \quad \phi = \tfrac{1}{4}\pi, \quad \text{on } AC'. \tag{36}$$

Also, since the α-line segment $F' E' D' C'$ is the boundary of a rigid region, we have

$$v_\beta = 0, \quad \text{on } F' E' D' C'. \tag{37}$$

Either $Q(x, t)$ or $W(x, t)$ is regarded as given on $A_1 A$, and W_α and W_β are related to W by (33).

From (34)–(37), and the surface values of p°, ϕ°, $V_\alpha{}^\circ$ and $V_\beta{}^\circ$ given by (28)–(31), it follows that the conditions to be satisfied by the first-order perturbation terms p', ϕ', $V_\alpha{}'$, $V_\beta{}'$ are

$$\epsilon p' = Q(x, t) - Q_0, \quad \phi' = 0, \quad \text{on } A_1 A. \tag{38}$$

$$\epsilon^{\frac{1}{2}} V_\alpha{}' = W_\alpha, \quad \epsilon^{\frac{1}{2}} V_\beta{}' = -W_\beta, \quad \text{on } A_1 A. \tag{39}$$

$$p' = 0, \quad \phi' = 0, \quad \text{on } AC'. \tag{40}$$

$$V_\beta{}' = 0, \quad \text{on } F' E' D' C'. \tag{41}$$

It is, of course, implicit in this formulation that $Q(x, t) - Q_0$ shall be of order ϵk and that $W(x, t)$ shall be of order $\epsilon^{\frac{1}{2}}(k/\rho)^{\frac{1}{2}}$.

Noting that the β-lines of the initial solution are everywhere straight lines in $B_1 ACDE$, it is clear from (28)–(30) that $\partial p^\circ/\partial s_\beta{}^\circ = \partial\phi^\circ/\partial s_\beta{}^\circ = 0$ throughout $B_1 ACDE$. Inserting these values, with the values $V_\alpha{}^\circ = V_\beta{}^\circ = 0$, $\partial\phi^\circ/\partial\tau = 0$, in (26), we obtain for $B_1 ACDE$

$$\left.\begin{aligned}
&\partial(p' + 2k\phi')/\partial s_\alpha{}^\circ + \rho f_\alpha{}' = 0,\\
&\partial(p' - 2k\phi')/\partial s_\beta{}^\circ - \phi'\,\partial(p^\circ - 2k\phi^\circ)/\partial s_\alpha{}^\circ + \rho f_\beta{}' = 0,\\
&\partial V_\alpha{}'/\partial s_\alpha{}^\circ - V_\beta{}'\,\partial\phi^\circ/\partial s_\alpha{}^\circ = 0, \quad \partial V_\beta{}'/\partial s_\beta{}^\circ = 0,\\
&f_\alpha{}' = \partial V_\alpha{}'/\partial\tau, \quad f_\beta{}' = \partial V_\beta{}'/\partial\tau.
\end{aligned}\right\} \tag{43}$$

From the fourth of these equations, V_β' is constant on each initial β-line in $B_1\,ACDE$. Since $V_\beta^\circ = 0$, the condition (41) for V_β' on $F'\,E'\,D'\,C'$ may, to the required order in ϵ, be applied on the initial α-line $FEDC$, so it follows that $V_\beta' = 0$ in $BCDF$. In $B_1\,BF$, from (28), $\partial\phi^\circ/\partial s_\alpha^\circ = 0$. Thus at all points of $B_1\,ACDE$ the third of (43) reduces to $\partial V_\alpha'/\partial s_\alpha^\circ = 0$, and it follows that V_α', and consequently f_α', is constant at any given time along any initial α-line in $B_1\,ACDE$. The first of equations (43) may therefore be integrated immediately along each of the initial α-lines. Taking for definiteness the typical α-line $RSTU$ illustrated in Fig. 1, we obtain

$$p_R' - p_U' + 2k(\phi_R' - \phi_U') = \rho l\,\partial V_\alpha'/\partial\tau, \tag{44}$$

where p_R', p_U' are the values of p' at R, U respectively, ϕ_R', ϕ_U' are the values of ϕ' at R, U respectively, V_α' is evaluated on $RSTU$, and l is the length $RSTU$, and is equal to $(2 + \frac{1}{2}\pi)(a - x_R)/\sqrt{2}$, x_R being the value of x at R. Inserting this value of l and the boundary conditions (38), (39) and (40) in (44), making the substitution $t = \epsilon^{\frac{1}{2}}\tau$, and omitting the suffix from x_R, we have

$$Q(x,t) = Q_0 + \rho(2 + \tfrac{1}{2}\pi)\,2^{-\frac{1}{2}}(a - x)\,\partial W_\alpha(x,t)/\partial t. \tag{45}$$

Two cases now arise, according to whether $|x|$ is greater or less than b. If $b < x < a$, then R lies on the surface BA, which is part of the boundary of the region $BCDF$, and we have shown that $V_\beta' = 0$ in this region. Hence $W_\beta = 0$ and, from (33), $W_\alpha = \sqrt{2}\,W$, on BA. We therefore have, from (45)

$$Q(x,t) = Q_0 + \rho(2 + \tfrac{1}{2}\pi)(a - x)\,\partial W(x,t)/\partial t, \tag{46}$$

for $b < x < a$. Similarly

$$Q(x,t) = Q_0 + \rho(2 + \tfrac{1}{2}\pi)(a + x)\,\partial W(x,t)/\partial t, \tag{47}$$

for $-b > x > a$. If $-b < x < b$, integration along the β-line through R in the region $BA_1 - C_1\,D_1\,E_1$ leads to the relation, analogous to (45)

$$Q(x,t) = Q_0 + \rho(2 + \tfrac{1}{2}\pi)\,2^{-\frac{1}{2}}(a + x)\,\partial W_\beta(x,t)/\partial t. \tag{48}$$

Equations (45) and (48) are compatible with each other and with (33) only if

$$\frac{\partial W_\alpha(x,t)}{\partial t} = \frac{(a+x)}{a\sqrt{2}}\frac{\partial W(x,t)}{\partial t}, \quad \frac{\partial W_\beta(x,t)}{\partial t} = \frac{(a-x)}{a\sqrt{2}}\frac{\partial W(x,t)}{\partial t}, \tag{49}$$

and then

$$Q(x,t) = Q_0 + \rho(2 + \tfrac{1}{2}\pi)(a^2 - x^2)(2a)^{-1}\,\partial W(x,t)/\partial t \tag{50}$$

in $-b < x < b$.

It is remarkable that equations (46), (47) and (50), giving the required relations between $Q(x,t)$ and $W(x,t)$, have been derived without it being necessary to determine p' and ϕ' in the deforming region; in fact no use has been made of the second of equations (43). The relations (46), (47) and (50) are valid only as long as $W(x,t)$ is positive; if $W(x,t)$ becomes negative, the sign of Q_0 must be reversed, in order that the rate of plastic working shall be positive. It is noted that $Q(x,t) = Q_0$ at $x = \pm a$, if $\partial W/\partial t$ is to be finite at $x = \pm a$.

The total vertical force applied to the surface, per unit length in the z direction, is

$$R(t) = 2\int_0^a Q(x,t)\,dx$$
$$= 2aQ_0 + 2\rho(2 + \tfrac{1}{2}\pi)\left[\int_0^b (a^2 - x^2)(2a)^{-1}(\partial W(x,t)/\partial t)\,dx + \right.$$
$$\left. + \int_b^a (a - x)(\partial W(x,t)/\partial t)\,dx\right]. \qquad (51)$$

In the case of indentation of a medium initially at rest, $\partial W(x,t)/\partial t$ is initially positive. It may be shown from (51) that, for $\partial W(x,t)/\partial t > 0$, $R(t)$ has its minimum value when $b = a$. In this case the initial field is that illustrated in Fig. 2.

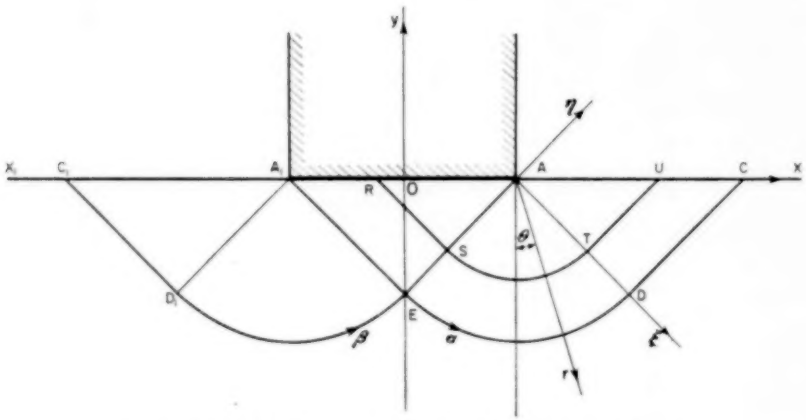

FIG. 2. Initial slip-line field for surface identation when $b = a$.

$Q(x,t)$, W_α and W_β are then given by (49) and (50) on the entire surface $-a < x < a$, and the velocity field is determined by these values of W_α and W_β and the result that V_α' is constant along each initial α-line, and V_β' is constant along each initial β-line. Of the infinity of mathematically possible velocity fields, it is expected that the actual one is that which minimizes $R(t)$.

If a quasi-statically deforming plastic–rigid solid is regarded as the limit, as v_α, $v_\beta \to 0$, of a dynamically deforming plastic–rigid solid, and if minimizing $R(t)$ is accepted as a criterion for uniqueness, then we obtain the velocity field described above as the solution which must be chosen from all possible solutions which are symmetrical about $x = 0$, for the initial motion in the problem of quasi-static surface indentation. For indentation by a flat rigid punch, this velocity field differs both from that proposed by PRANDTL and from that proposed by HILL, and is characterized by the fact that v_α decreases linearly along any β-line, from a maximum value at A to zero on the α-line through A_1, and by a similar relation for v_β along the α-lines. This field, of course, is not necessarily obtained if other properties of real materials, such as workhardening, are taken into consideration.

The possibility that b may be a function of time has not been taken into account. For non-zero W, it seems unlikely that b should vary with time, since in such a case $\partial\phi^\circ/\partial\tau$ would be non-zero in parts of the field, and this would introduce infinite accelerations, and consequently infinite stress gradients, into the field.

5. Surface Indentation. Perturbed Slip-line Field

For many purposes equations (46), (47) and (50), which relate the surface pressure to the surface velocity, give all the information that is required. It is, however, of interest to determine the form of the perturbed slip-line field and, furthermore, a complete solution of the first-order perturbation equations is essential if it is intended to proceed to higher order perturbations.

It was shown in Section 4 that the case $b = a$ is of particular interest, and for brevity we will consider this case only. The initial slip-line field is then that illustrated in Fig. 2, and W_α and W_β are related to W by (49) in $-a < x < a$. In other respects the formulation is the same as in the preceding section.

It is convenient to introduce, in addition to the polar coordinates (r, θ) previously defined, a system (ξ, η) of rectangular Cartesian coordinates, illustrated in Fig. 2, and defined by

$$\xi = (x - a - y)/\sqrt{2}, \quad \eta = (x - a + y)/\sqrt{2}. \tag{52}$$

Then derivatives with respect to the initial system of α- and β-lines can be expressed as follows:

$$\partial/\partial s_\alpha{}^\circ = \partial/\partial\xi, \quad \partial/\partial s_\beta{}^\circ = \partial/\partial\eta \qquad \text{in } A_1AE', \tag{53}$$

$$\partial/\partial s_\alpha{}^\circ = \partial/r\partial\theta, \quad \partial/\partial s_\beta{}^\circ = -\partial/\partial r \qquad \text{in } AD'E', \tag{54}$$

$$\partial/\partial s_\alpha{}^\circ = \partial/\partial\eta, \quad \partial/\partial s_\beta{}^\circ = -\partial/\partial\xi \qquad \text{in } AC'D'. \tag{55}$$

Since V_α' is constant on each α-line, $V_\alpha' = V_\alpha'(-\eta)$ in A_1AE', $V_\alpha' = V_\alpha'(r)$ in $AD'E'$, and $V_\alpha' = V_\alpha'(\xi)$ in $AC'D'$, where V_α' is the same function of its argument in each region. Also $V_\beta' = V_\beta'(-\xi)$ in A_1AE', and $V_\beta' = 0$ in $AC'D'E'$. The boundary conditions on A_1A give

$$\left.\begin{aligned} \epsilon^3\, V_\alpha'(\zeta) &= W_\alpha(a - \sqrt{2}\,\zeta, t) = \frac{a\sqrt{2} - \zeta}{a}\, W(a - \sqrt{2}\,\zeta, t), \\ \epsilon^3\, V_\beta'(\zeta) &= -W_\beta(a - \sqrt{2}\,\zeta, t) = -\frac{\zeta}{a}\, W(a - \sqrt{2}\,\zeta, t), \end{aligned}\right\} \tag{56}$$

where, as before, the first argument of W denotes distance measured along OX. The relations between W_α, W_β and W are derived from (49), it being assumed that $W_\alpha = W_\beta = W = 0$ at $t = 0$.

In the first two of equations (43) we now substitute for f_α' and f_β' from the last two of (43), and insert the values (28)–(30) of p° and ϕ°, and the relations (53)–(55) for $\partial/\partial s_\alpha{}^\circ$ and $\partial/\partial s_\beta{}^\circ$. There results

$$\left.\begin{aligned} &\partial(p' + 2k\phi')/\partial\xi + \rho\,\partial V_\alpha'(-\eta)/\partial\tau = 0 \\ &\partial(p' - 2k\phi')/\partial\eta + \rho\,\partial V_\beta'(-\xi)/\partial\tau = 0 \end{aligned}\right\} \quad \text{in } A_1AE', \tag{57}$$

$$\left.\begin{aligned} &\partial(p' + 2k\phi')/\partial\theta - \rho r\,\partial V_\alpha'(r)/\partial\tau = 0 \\ &\partial(p' - 2k\phi')/\partial r - 4k\phi'/r = 0 \end{aligned}\right\} \quad \text{in } AD'E', \tag{58}$$

$$\left.\begin{aligned} &\partial(p' + 2k\phi')/\partial\eta + \rho\,\partial V_\alpha'(\xi)/\partial\tau = 0 \\ &\partial(p' - 2k\phi')/\partial\xi = 0 \end{aligned}\right\} \quad \text{in } AC'D'. \tag{59}$$

The solution is commenced in the region $AC'D'$. Integrating (59) and applying the conditions (40), we find

$$p' = 2k\phi' = \tfrac{1}{2}\rho(\xi - \eta)\,\partial V_\alpha'(\xi)/\partial\tau, \tag{60}$$

in $AC'D'$.

In the region $AD'E'$, (58) give on integration,

$$\left.\begin{aligned} p' &= -\tfrac{1}{2}\rho\theta\left[r\frac{\partial V_\alpha'(r)}{\partial\tau} + \frac{1}{r}\int_0^r r\frac{\partial V_\alpha'(r)}{\partial\tau}\,dr\right] + \rho G(r), \\ 2k\phi' &= -\tfrac{1}{2}\rho\theta\left[r\frac{\partial V_\alpha'(r)}{\partial\tau} - \frac{1}{r}\int_0^r r\frac{\partial V_\alpha'(r)}{\partial\tau}\,dr\right] + \rho H(r), \end{aligned}\right\} \tag{61}$$

where $G(r)$ and $H(r)$ are functions which satisfy

$$dG/dr - dH/dr - 2H/r = 0. \tag{62}$$

An arbitrary function of θ which arises in the integration of (58) has been set equal to zero in order to satisfy the requirement that ϕ' is finite as $r \to 0$.

The functions $G(r)$, $H(r)$ (of which only one is independent) are determined by the conditions that $p^\circ + \epsilon p'$, $\phi^\circ + \epsilon\phi'$ are continuous across AD'. To the present order of approximation the equation of AD' is $d\eta/d\xi = \epsilon\phi'$, where ϕ' is given by (60), with $\eta = 0$. Hence, on AD', to first order in ϵ,

$$\eta = \frac{\epsilon\rho}{4k}\int_0^\xi \xi \frac{\partial V_\alpha'(\xi)}{\partial\tau}\, d\xi.$$

On AD', therefore, from (30) and (60), and to order ϵ

$$\left.\begin{aligned} p^\circ + \epsilon p' &= k + \tfrac{1}{2}\epsilon\rho\xi\, \partial V_\alpha'(\xi)/\partial\tau, \\ 2k(\phi^\circ + \epsilon\phi') &= \tfrac{1}{2}\pi k + \tfrac{1}{2}\epsilon\rho\xi\, \partial V_\alpha'(\xi)/\partial\tau. \end{aligned}\right\} \tag{62}$$

Since, on AD', to first order in ϵ, $\xi = r$ and $\eta = r(\theta - \tfrac{1}{4}\pi)$, the equation of AD' may also be written

$$\theta = \tfrac{1}{4}\pi + \frac{\epsilon\rho}{4k}\frac{1}{r}\int_0^r r \frac{\partial V_\alpha'(r)}{\partial\tau}\, dr.$$

Substituting this value of θ into (29) and (61), we find that on AD', to order ϵ

$$\left.\begin{aligned} p^\circ + \epsilon p' &= k - \tfrac{1}{8}\epsilon\rho\left\{\tfrac{1}{4}\pi r \frac{\partial V_\alpha'(r)}{\partial\tau} + (1 + \tfrac{1}{4}\pi)\frac{1}{r}\int_0^r r\frac{\partial V_\alpha'(r)}{\partial\tau}\, dr - 2G(r)\right\}, \\ 2k(\phi^\circ + \epsilon\phi') &= \tfrac{1}{2}\pi k - \tfrac{1}{2}\epsilon\rho\left\{\tfrac{1}{4}\pi r \frac{\partial V_\alpha'(r)}{\partial\tau} - (1 + \tfrac{1}{4}\pi)\frac{1}{r}\int_0^r r\frac{\partial V_\alpha'(r)}{\partial\tau}\, dr - 2H(r)\right\}. \end{aligned}\right\} \tag{64}$$

Continuity requires that (63) and (64) shall determine the same values of $p^\circ + \epsilon p'$ and $\phi^\circ + \epsilon\phi'$. This determines the functions $G(r)$ and $H(r)$ as

$$G(r) = \tfrac{1}{8}(1 + \tfrac{1}{4}\pi)\left[r\frac{\partial V_\alpha'(r)}{\partial\tau} + \frac{1}{r}\int_0^r r\frac{\partial V_\alpha'(r)}{\partial\tau}\, dr\right],$$

$$H(r) = \tfrac{1}{8}(1 + \tfrac{1}{4}\pi)\left[r\frac{\partial V_\alpha'(r)}{\partial\tau} - \frac{1}{r}\int_0^r r\frac{\partial V_\alpha'(r)}{\partial\tau}\, dr\right].$$

It is readily verified that $G(r)$ and $H(r)$ satisfy the necessary condition (62). When these values of $G(r)$ and $H(r)$ are inserted in (61), we obtain

$$\left.\begin{aligned} p' &= \tfrac{1}{8}\rho(1 + \tfrac{1}{4}\pi - \theta)\left[r\frac{\partial V_\alpha'(r)}{\partial\tau} + \frac{1}{r}\int_0^r r\frac{\partial V_\alpha'(r)}{\partial\tau}\, dr\right], \\ 2k\phi' &= \tfrac{1}{8}\rho(1 + \tfrac{1}{4}\pi - \theta)\left[r\frac{\partial V_\alpha'(r)}{\partial\tau} - \frac{1}{r}\int_0^r r\frac{\partial V_\alpha'(r)}{\partial\tau}\, dr\right], \end{aligned}\right\} \tag{65}$$

in $AD'E'$.

In the region A_1AE', equations (37) integrate to give

$$\left.\begin{aligned} p' &= \tfrac{1}{8}\rho\{-\xi[\partial V_\alpha'(-\xi)/\partial\tau + \partial V_\alpha'(-\eta)/\partial\tau] + (\xi - \eta)\,\partial V_\beta'(-\xi)/\partial\tau + \\ &\qquad + F(\xi) + F(\eta)\}, \\ 2k\phi' &= \tfrac{1}{8}\rho\{\xi[\partial V_\alpha'(-\xi)/\partial\tau - \partial V_\alpha'(-\eta)/\partial\tau] - (\xi - \eta)\,\partial V_\beta'(-\xi)/\partial\tau - \\ &\qquad - F(\xi) + F(\eta)\}, \end{aligned}\right\} \tag{66}$$

where the condition $\phi' = 0$ on A_1A has been imposed, and F is as yet an arbitrary function of its argument. The treatment of the conditions of continuity of $p^\circ + \epsilon p'$ and $\phi^\circ + \epsilon\phi'$ across

AE' is somewhat similar to the treatment of the continuity conditions across AD' except that it is necessary to use in addition the result, from (56), that $V_\beta'(0) = 0$. It is found that all the continuity conditions are satisfied if

$$F(\zeta) = -\tfrac{1}{2}\rho(1+\tfrac{1}{2}\pi)\,\zeta\,\partial V_\alpha'(-\zeta)/\partial\tau,$$

and thus

$$\left.\begin{aligned} p' &= -\tfrac{1}{2}\rho\{(2+\tfrac{1}{2}\pi)\,\xi\,\partial V_\alpha'(-\xi)/\partial\tau + [\xi + (1+\tfrac{1}{2}\pi)\,\eta]\,\partial V_\alpha'(-\eta)/\partial\tau - \\ &\qquad - (\xi-\eta)\,\partial V_\beta'(-\xi)/\partial\tau\}, \\ 2k\phi' &= \tfrac{1}{2}p\{(2+\tfrac{1}{2}\pi)\,\xi\,\partial V_\alpha'(-\xi)/\partial\tau - [\xi + (1+\tfrac{1}{2}\pi)\,\eta]\,\partial V_\alpha'(-\eta)/\partial\tau - \\ &\qquad - (\xi-\eta)\,\partial V_\beta'(-\xi)/\partial\tau\}, \end{aligned}\right\} \tag{67}$$

in A_1AE'.

On the surface A_1A, $\xi = \eta = -(a-x)/\sqrt{2}$. If these values of ξ and η, with the boundary value (38) of p' and the expressions (56) for V_α' and V_β', are inserted in (67), the relation (50) between $Q(x,t)$ and $W(x,t)$ is again obtained.

As a specific example, let us consider the indentation of a plane surface by a flat rigid punch of width $2a$. $W(x,t)$ is then independent of x in $-a < x < a$, so that the expressions (56) for V_α' and V_β' become

$$\left.\begin{aligned} \epsilon^{\frac{1}{2}}\,V_\alpha'(\zeta) &= \frac{a\sqrt{2}-\zeta}{a}\,W(t), \\ \epsilon^{\frac{1}{2}}\,V_\beta'(\zeta) &= -\frac{\zeta}{a}\,W(t). \end{aligned}\right\} \tag{68}$$

From (50), the resultant downward force exerted by the punch is, to order ϵ

$$\begin{aligned} R(t) = 2\int_0^a Q(x,t)\,dx &= 2\int_0^a \{Q_0 + \rho(2+\tfrac{1}{2}\pi)(a^2-x^2)(2a)^{-1}\,dW(t)/dt\}\,dx \\ &= 2aQ_0 + \tfrac{2}{3}\rho a^2(2+\tfrac{1}{2}\pi)\,dW(t)/dt. \end{aligned} \tag{69}$$

Equations (60), (65) and (67) become respectively

$$p' = 2k\phi' = \tfrac{1}{2}\rho\epsilon^{-1}(\xi-\eta)(a\sqrt{2}-\xi)\,a^{-1}\,dW(t)/dt, \tag{70}$$

in $AC'D'$;

$$\left.\begin{aligned} p' &= \tfrac{1}{2}\rho\epsilon^{-1}(1+\tfrac{1}{4}\pi-\theta)\,r(\tfrac{2}{3}a\sqrt{2}-\tfrac{4}{3}r)\,a^{-1}\,dW(t)/dt, \\ 2k\phi' &= \tfrac{1}{2}\rho\epsilon^{-1}(1+\tfrac{1}{4}\pi-\theta)\,r(\tfrac{1}{2}a\sqrt{2}-\tfrac{2}{3}r)\,a^{-1}\,dW(t)/dt, \end{aligned}\right\} \tag{71}$$

in $AD'E'$;

$$\left.\begin{aligned} p' &= -\tfrac{1}{2}\rho\epsilon^{-1}\{(3+\tfrac{1}{2}\pi)\,\xi\,a\sqrt{2} + (1+\tfrac{1}{2}\pi)(\xi^2+\eta^2+\eta\,a\sqrt{2}) + 2\xi\eta\}\,a^{-1}\,dW(t)/dt, \\ 2k\phi' &= \tfrac{1}{2}\rho\epsilon^{-1}(1+\tfrac{1}{2}\pi)(\xi-\eta)(\xi+\eta+a\sqrt{2})\,a^{-1}\,dW(t)/dt, \end{aligned}\right\} \tag{72}$$

in A_1AE'.

Using the above expressions for ϕ', the equations of the perturbed slip-lines are readily found to first order in ϵ. They are:

$$\alpha\text{-lines}: \quad \xi = \xi_0 - \frac{\rho}{4ka}\,\eta(\xi_0 - \tfrac{1}{2}\eta)(a\sqrt{2}-\xi_0)\,dW/dt,$$

$$\beta\text{-lines}: \quad \eta = \eta_0 - \frac{\rho}{4ka}\,\xi[\tfrac{1}{3}\xi^2 - \tfrac{1}{2}(a\sqrt{2}+\eta_0)\,\xi + \eta_0\,a\sqrt{2}]\,dW/dt,$$

in $AC'D'$;

$$\alpha\text{-lines}: \quad r = r_0 + \frac{\rho}{8ka}(1+\tfrac{1}{4}\pi-\theta)^2 r_0^2(\tfrac{1}{2}a\sqrt{2}-\tfrac{2}{3}r_0)\,dW/dt,$$

$$\beta\text{-lines}: \quad \theta = \theta_0 + \frac{\rho}{4ka}(1+\tfrac{1}{4}\pi-\theta_0)\,r(\tfrac{1}{2}a\sqrt{2}-\tfrac{1}{3}r)\,dW/dt,$$

in $AD'E'$;

$$\alpha\text{-lines}: \quad \eta = \eta_0 + \frac{\rho}{4ka}(1 + \tfrac{1}{2}\pi)\,\xi\,(\tfrac{1}{3}\xi^2 + \tfrac{1}{2}\xi\,a\sqrt{2} - \eta_0^2 - \eta_0\,a\sqrt{2})\,dW/dt,$$

$$\beta\text{-lines}: \quad \xi = \xi_0 + \frac{\rho}{4ka}(1 + \tfrac{1}{2}\pi)\,\eta\,(\tfrac{1}{3}\eta^2 + \tfrac{1}{2}\eta\,a\sqrt{2} - \xi_0^2 - \xi_0\,a\sqrt{2})\,dW/dt,$$

in A_1AE'. In these equations, ξ_0, η_0, r_0 and θ_0 are parameters which characterize the various families of slip-lines.

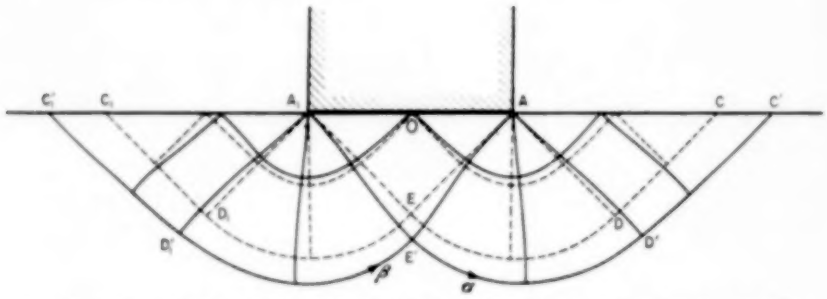

FIG. 3. Perturbed slip-line field for identation by a flat rigid punch when $b = a$ and $(\rho a/2k)\,dW/dt = \frac{1}{4}$. – – – Initial slip-lines; ——— Perturbed slip-lines.

The field of perturbed α- and β-lines is illustrated in Fig. 3 for the case

$$\frac{\rho a}{2k}\frac{dW}{dt} = \tfrac{1}{4}.$$

With this comparatively large value of dW/dt the second-order terms would probably have a significant effect on the field; the form of the perturbed field is, however, shown more clearly with a large value of dW/dt.

6. Surface Indentation by a Moving Load

It is now considered that pressure or surface displacement is applied to the surface of a semi-infinite solid over the surface $y = 0$, $|x| < a$, where now $a = a(\tau)$. In all other respects the conditions of the problem are the same as in Section 5.

The initial solution is again given by (28)–(31), but now, through the relations

$$r^2 = [x - a(\tau)]^2 + y^2, \quad \tan\theta = [x - a(\tau)]/(-y), \tag{73}$$

p° and ϕ° depend implicitly on τ. Since $\partial p^\circ/\partial\tau$ does not appear in equations (25), and $\partial\phi^\circ/\partial\tau$ appears in (25) only when multiplied by ${V_\alpha}^\circ$ or ${V_\beta}^\circ$, and ${V_\alpha}^\circ = {V_\beta}^\circ = 0$ in the present problem, the validity of (28)–(31) as an initial solution is not affected by the dependence of p° and ϕ° on τ.

The boundary conditions are again given by equations (38)–(41) where now A_1, A and C' are moving points. The (ξ, η) coordinate system is again defined by (52), with the constant a replaced by a function $a(\tau)$. The (ξ, η) and (r, θ) systems of coordinates are now in motion relative to the fixed (x, y) system of coordinates. Referred to fixed coordinates which coincide with the instantaneous positions of the (ξ, η) and (r, θ) systems, the formulae for differentiation along the α- and β-lines are still given by (53)–(55). As in Section 5, the initial slip-line field is chosen to be that illustrated in Fig. 2.

When the relations $\partial p^\circ/\partial {s_\beta}^\circ = \partial\phi^\circ/\partial {s_\beta}^\circ = {V_\alpha}^\circ = {V_\beta}^\circ = 0$ are inserted in (26), equations (43) are obtained as before, except that now ${f_\alpha}'$ and ${f_\beta}'$ are given by

$${f_\alpha}' = \partial {V_\alpha}'/\partial\tau - {V_\beta}'\,\partial\phi^\circ/\partial\tau, \quad {f_\beta}' = \partial {V_\beta}'/\partial\tau + {V_\alpha}'\,\partial\phi^\circ/\partial\tau. \tag{74}$$

As in Sections 4 and 5, the solution of the third and fourth of equations (43) is

$$\left.\begin{aligned} V_\alpha' &= V_\alpha'(-\eta), \quad V_\beta' = V_\beta'(-\xi), && \text{in } A_1AE',\\ V_\alpha' &= V_\alpha'(r), \quad V_\beta' = 0, && \text{in } ADE',\\ V_\alpha' &= V_\alpha'(\xi), \quad V_\beta' = 0, && \text{in } ACD', \end{aligned}\right\} \tag{75}$$

where

$$\epsilon^{\frac{1}{2}} V_\alpha'(\zeta) = W_\alpha(a - \zeta\sqrt{2}, t), \quad \epsilon^{\frac{1}{2}} V_\beta'(\zeta) = -W_\beta(a - \zeta\sqrt{2}, t). \tag{76}$$

Since $\partial\phi^\circ/\partial\tau = 0$ in A_1AE', and $V_\beta' = 0$ in $ACD'E'$, from (74)

$$f_\alpha' = \partial V_\alpha'/\partial\tau = \epsilon^{\frac{1}{2}}\,\partial V_\alpha'/\partial t \tag{77}$$

throughout the region under consideration. $\partial V_\alpha'/\partial t$ is to be interpreted as the derivative of V_α' with respect to t, evaluated at a fixed point (x, y).

The expressions for f_α' are obtained from (76) and (77) by inserting the appropriate argument in (76), differentiating to obtain the total derivative of V_α' with respect to t, regarding η, ξ and r functions of t, and in the resulting expressions evaluating $\partial\eta/\partial t$, $\partial\xi/\partial t$ and $\partial r/\partial t$ at a fixed point (τ, y), by differentiation of (52) and (73). This procedure gives

$$\left.\begin{aligned} \epsilon f_\alpha' &= \frac{\partial W_\alpha(a + \eta\sqrt{2}, t)}{\partial t} + \left(\frac{da}{dt} + \sqrt{2}\,\frac{\partial\eta}{\partial t}\right)\frac{\partial W_\alpha(a + \eta\sqrt{2}, t)}{\partial x}\\ &= \frac{\partial W_\alpha(a + \eta\sqrt{2}, t)}{\partial t}, \end{aligned}\right\} \tag{78}$$

in A_1AE';

$$\left.\begin{aligned} \epsilon f_\alpha' &= \frac{\partial W_\alpha(a - r\sqrt{2}, t)}{\partial t} + \left(\frac{da}{dt} - \sqrt{2}\,\frac{\partial r}{\partial t}\right)\frac{\partial W_\alpha(a - r\sqrt{2}, t)}{\partial x}\\ &= \frac{\partial W_\alpha(a - r\sqrt{2}, t)}{\partial t} + (1 + \sqrt{2}\sin\theta)\,\frac{da}{dt}\,\frac{\partial W_\alpha(a - r\sqrt{2}, t)}{\partial x}, \end{aligned}\right\} \tag{79}$$

in ADE';

$$\left.\begin{aligned} \epsilon f_\alpha' &= \frac{\partial W_\alpha(a - \xi\sqrt{2}, t)}{\partial t} + \left(\frac{da}{dt} - \sqrt{2}\,\frac{\partial\xi}{\partial t}\right)\frac{\partial W_\alpha(a - \xi\sqrt{2}, t)}{\partial x}\\ &= \frac{\partial W_\alpha(a - \xi\sqrt{2}, t)}{\partial t} + 2\,\frac{da}{dt}\,\frac{\partial W_\alpha(a - \xi\sqrt{2}, t)}{\partial x}, \end{aligned}\right\} \tag{80}$$

in ACD'.

The solution will be confined to finding the relation between $Q(x, t)$ and $W(x, t)$ on A_1A, to the accuracy of the first order perturbation. This relation follows from the first of equations (43) which, on integrating along a typical initial α-line $RSTU$, gives

$$p_R' - p_U' + 2k(\phi_R' - \phi_U') = \rho\int f_\alpha'\,ds_\alpha^\circ, \tag{81}$$

where the integral is along $RSTU$, and the notation is the same as in (44). Now, on RS, $-\eta\sqrt{2} = a - x_R$; on ST, $r\sqrt{2} = a - x_R$; and on TU, $\xi\sqrt{2} = a - x_R$. Inserting these values in the expressions (78)–(80) for f_α', evaluating the integral along $RSTU$, and substituting the appropriate boundary values of p' and ϕ' at R and U, we obtain

$$Q(x, t) = Q_0 + \rho(2 + \tfrac{1}{2}\pi)\,2^{-\frac{1}{2}}(a - x)\left\{\frac{\partial W_\alpha(x, t)}{\partial t} + \frac{da}{dt}\,\frac{\partial W_\alpha(x, t)}{\partial x}\right\}. \tag{82}$$

This reduces to (45) when $a(t)$ is a constant.

Similarly,

$$Q(x, t) = Q_0 + \rho(2 + \tfrac{1}{2}\pi)\,2^{-\frac{1}{2}}(a + x)\left\{\frac{\partial W_\beta(x, t)}{\partial t} - \frac{da}{dt}\,\frac{\partial W_\beta(x, t)}{\partial x}\right\}, \tag{83}$$

so that

$$(a - x)\left\{\frac{\partial W_\alpha(x,t)}{\partial t} + \frac{da}{dt}\frac{\partial W_\alpha(x,t)}{\partial x}\right\} = (a + x)\left\{\frac{\partial W_\beta(x,t)}{\partial t} - \frac{da}{dt}\frac{\partial W_\beta(x,t)}{\partial x}\right\}. \tag{84}$$

This relation, with (33), determines W_α and W_β in terms of W. $Q(x,t)$ is then given by either (82) or (83).

Equation (84) shows that W_α is constant at $x = -a(t)$, and W_β is constant at $x = a(t)$. If the material starts from rest, these constants must be zero, since neither W_α nor W_β may be negative if the rate of plastic working is to be non-negative everywhere in the field. It follows that in this example there is no velocity discontinuity across the bounding slip-lines $A_1 E' D' C'$ and $AE' D_1' C_1'$. If there were velocity discontinuities across these curves, a point initially outside the deforming regions would instantaneously acquire a finite velocity if the slip-line field moved in such a way that the point entered the deforming region. Such a motion would imply the existence of infinite accelerations and stress gradients, and the perturbation method could not be applied without modification in such a case.

The solutions obtained in this and the preceding sections are incomplete in the sense that it has not been proved that it is possible for the rigid region to support the tractions across $C_1' D_1' E' D' C'$. In principle this problem may be investigated by seeking to extend the perturbed slip-line field in $C_1' D_1' E' D' C'$ into the rigid region in the manner described by BISHOP (1953). Since the rigid region is at rest, quasi-static stress fields are appropriate for the extended field. For a complete solution, the extension must be shown to be possible for each instantaneous position of the dynamic field in $C'_1 D'_1 E' D' C'$. BISHOP has demonstrated how the extension can be made for quasi-static punch indentation. From the manner in which his solution was derived it seems probable that the perturbed slip-line fields can be extended in a similar way, provided that the variation from the quasi-static configuration is not too great, but this conjecture has not been verified.

7. Work Done in Surface Indentation

It is of interest to compare the work done in forming a surface cavity under dynamic loading with the work done in forming a similar cavity under quasi-static conditions. The work done in a deformation of the type described in Sections 4–6 between the times $t = 0$ and $t = T$ is

$$E = \int_0^T dt \int_{-a(t)}^{a(t)} Q(x,t)\, W(x,t)\, dx, \tag{85}$$

where, correct to the first order perturbation terms, $Q(x,t)$ and $W(x,t)$ are related by (33), (82), (83) and (84). The problem of Sections 4 and 5, in which $a(t)$ is a constant, is included as a special case. From (85) and (33)

$$E = 2^{-\frac{1}{2}} \int_0^T dt \int_{-a(t)}^{a(t)} Q(x,t)\left[W_\alpha(x,t) + W_\beta(x,t)\right] dt. \tag{86}$$

The expressions (82) and (83) for $Q(x,t)$ are now substituted in (86), giving

$$E = E_S + E_K^{(\alpha)} + E_K^{(\beta)}, \tag{87}$$

where

$$E_S = \int_0^T dt \int_{-a(t)}^{a(t)} Q_0\, W(x,t)\, dx, \tag{88}$$

$$E_K^{(\alpha)} = \tfrac{1}{2}\rho\,(2 + \tfrac{1}{2}\pi) \int_0^T dt \int_{-a(t)}^{a(t)} (a - x)\left\{\frac{\partial W_\alpha(x,t)}{\partial t} + \frac{da}{dt}\frac{\partial W_\alpha(x,t)}{\partial x}\right\} W_\alpha(x,t)\, dx, \tag{89}$$

$$E_K^{(\beta)} = \tfrac{1}{2}\rho\,(2 + \tfrac{1}{2}\pi) \int_0^T dt \int_{-a(t)}^{a(t)} (a + x)\left\{\frac{\partial W_\beta(x,t)}{\partial t} - \frac{da}{dt}\frac{\partial W_\beta(x,t)}{\partial x}\right\} W_\beta(x,t)\, dx. \tag{90}$$

The term E_S simply represents the work that would be done in forming a surface cavity which at all corresponding times is similar to the cavity under consideration, but which is formed in a quasi-static deformation.

The terms $E_K^{(\alpha)}$ and $E_K^{(\beta)}$ also have simple physical interpretations. The expression (89) may be written

$$E_K^{(\alpha)} = \tfrac{1}{4}\rho\,(2 + \tfrac{1}{2}\pi)\int_0^T dt \int_{-a(t)}^{a(t)} (a - x)\left\{\frac{\partial}{\partial t}\left[W_\alpha{}^2(x, t)\right] + \frac{da}{dt}\frac{\partial}{\partial x}\left[W_\alpha{}^2(x, t)\right]\right\} dx.$$

After integrating the last term by parts with respect to x, and using the fact that $W_\alpha(x, t)$ vanishes at $x = -a$, this becomes

$$E_K^{(\alpha)} = \tfrac{1}{4}\rho\,(2 + \tfrac{1}{2}\pi)\int_0^T dt \int_{-a(t)}^{a(t)} \frac{\partial}{dt}\left\{(a - x)\,W_\alpha{}^2(x, t)\right\} dx,$$

which, changing the order of integration, gives finally

$$E_K^{(\alpha)} = \tfrac{1}{4}\rho\,(2 + \tfrac{1}{2}\pi)\left\{\int_{-a(T)}^{a(T)} \left[a(T) - x\right] W_\alpha{}^2(x, T)\,dx - \int_{-a(0)}^{a(0)} \left[a(0) - x\right] W_\alpha{}^2(x, 0)\,dx\right\}. \quad (91)$$

It may be verified that the first and second integrals in (91) represent respectively the final and initial kinetic energies of the system due to the components of velocity directed along the α-lines to the accuracy of the first-order perturbation theory. This follows from integrating the expression $\frac{1}{4}\rho V_\alpha{}'^2$ over the region $A_1\,AC'\,D'\,E'$. Similarly

$$E_K^{(\beta)} = \tfrac{1}{4}\rho\,(2 + \tfrac{1}{2}\pi)\left\{\int_{-a(T)}^{a(T)} \left[a(T) + x\right] W_\beta{}^2(x, t)\,dx - \int_{-a(0)}^{a(0)} \left[a(0) + x\right] W_\beta{}^2(x, 0)\,dx\right\}, \quad (92)$$

and $E_K^{(\beta)}$ represents the change of kinetic energy due to motion directed along the β-lines. Hence $E_K^{(\alpha)} + E_K^{(\beta)}$ represents the total increase of kinetic energy of the system between $t = 0$ and $t = T$.

If the system is initially and finally at rest, then $E_K^{(\alpha)} = E_K^{(\beta)} = 0$. We therefore find that, to the accuracy of the first-order perturbation theory, the work done in forming a given surface cavity in a rigid–plastic medium which is initially and finally at rest is the same when the deformation occurs under dynamic loading conditions as when it occurs under quasi-static loading. The difference between the amounts of work done in otherwise similar dynamic and quasi-static surface indentations is therefore a quantity of order ϵ^2 or less.

Acknowledgments

I should like to thank Dr. H. G. Hopkins for helpful discussions of the work described in this paper.

This paper is published by permission of the Director of the Atomic Weapons Research Establishment, Aldermaston.

References

Bishop, J. F. W. 1953 *J. Mech. Phys. Solids* **2**, 43.

Goodier, J. N. and Hodge, P. G. 1958 *Elasticity and Plasticity. Surveys in Applied Mathematics*, Vol. 1 (John Wiley, New York).

Hill, R. 1949 *Quart. J. Mech.* **2**, 40.

1950 *The Mathematical Theory of Plasticity* (Clarendon Press, Oxford).

Hopkins, H. G. 1960 *Dynamical Expansion of Spherical Cavities in Metals. Progress in Solid Mechanics*, Vol. 1 (North Holland Publishing Company, Amsterdam).

Karman, T. von and Duwez, P. 1950 *J. Appl. Phys.* **21**, 987.

Prandtl, L. 1920 *Nachr. Ges. Wiss. Göttingen* (1920), 74.

Taylor, G. I. 1958 *Scientific Papers*, Vol. 1, pp. 456, 467. (Cambridge University Press).

Thomas, T. Y. 1952 *J. Rat. Mech. Anal.* **1**, 343.

J. Mech. Phys. Solids, 1960, Vol. 8, pp. 280 to 292. Pergamon Press Ltd., London. Printed in Great Britain

AN ELASTIC TREATMENT OF GROUND MOVEMENT DUE TO MINING—I. ISOTROPIC GROUND

By D. S. Berry
Department of Mining Engineering, University of Nottingham

(*Received* 19*th August*, 1960)

Summary

So long as the excavation is comparatively deep the seam thickness may be considered infinitesimal and the convergence of opposing points in roof and floor may be treated as a discontinuity in displacement at a single point. A result in plane elasticity can then be used to find the solution for a partially closed excavation of infinite length in an infinite medium, and from this solution are derived those for an unclosed and a completely closed panel. The corresponding results for a semi-infinite medium are found only approximately for the unclosed and partially closed panels, but exactly for complete closure. In the last case the expression for the displacement at the plane boundary is independent of the elastic constants and forms an unequivocal limit with which actual subsidence profiles may be compared. In British coalfields the magnitude of maximum subsidence is almost always greater than that given by the bounding expression, and the discrepancy cannot be explained on grounds of minor departures from the basic assumptions. It follows that these assumptions must be drastically modified before agreement may be expected.

1. Introduction

There is considerable disagreement among mining engineers concerning the mechanism of subsidence following the extraction of minerals. Some of this disagreement undoubtedly reflects major differences in behaviour in radically different circumstances: experiences gained in British coal mining may be very dissimilar from those obtained in other coalfields or in the extraction of other minerals. It is not intended to give here a complete survey of past and current theories of subsidence, but merely a brief sketch of the main ideas, which will serve as a background to the present work. Comprehensive surveys of the subject have been given by Briggs (1929) and Grond (1950), while a wide variety of opinion is represented in papers read at conferences in Liège (1951) and Leeds (1957).

Far from thinking of subsidence as an elastic deformation, most early writers appear to have favoured the idea of a practically clean break of the ground, upwards from the edges of the excavation, along a surface with generators either normal to the excavation or at an angle to the normal; it was thought that no movement at all occurred outside the region enclosed by this surface, unless it was due to flow of unconsolidated surface deposits. This conception was later modified by supposing that fragmentation of the roof in the centre of the excavation left the unbroken parts of the roof strata free to bend like cantilever beams until they fractured approximately above the edges of the excavation and subsided into the

cavity: the process was repeated by successive strata until the subsidence reached the surface. Some authors believe that a region of fragmented rock spreads out from the centre of the roof until it reaches the surface, while the ground outside the region of broken rock remains undisturbed. However, increasing support is now being given to the idea that fragmentation of the overlying rock is often arrested long before it reaches the surface, and that thereafter the deformation is chiefly elastic: the greater the depth of the working the more important, one supposes, is the elastic effect.

Most elastic treatments of ground movement to be found in the literature fall in two main categories. The first contains theoretical accounts of the simpler problems, chiefly the effects of openings of circular and elliptical cross-section representing shafts, roadways etc.: references to much of this work are to be found in a book by ISAACSON (1958). The second comprises investigations of more complicated problems undertaken by means of experimental models, either for the estimation of stress distributions photoelastically, or for the direct measurement of displacements. Of the last kind are the gelatine models of WHETTON, KING and co-workers (notably, WHETTON and KING 1957), which are of considerable interest but suffer from some defects to be discussed shortly. The theoretical work of HACKETT (1957, 1959) on an unclosed excavation, falls into neither of these categories, but forms the first stage in the present project.

Not very much is known about the elastic properties of coal measure rocks, but they are clearly inhomogeneous in the mass and almost certainly anisotropic even in small samples. Nevertheless the departures from homogeneity and isotropy have been almost totally disregarded in previous work and it seemed better, in a first attempt at a more sophisticated theoretical investigation, to retain these simple assumptions until they were shown to be inconsistent with practical measurements. The present treatment ignores, too, the fact that there is certainly some region, smaller or larger, of broken rock in the vicinity of the excavation; but if this region is small compared with the entire deformed region, its effect may be taken into account in applying the results of this work. However, they cannot be expected to predict stress and displacement fields in the immediate neighbourhood of an excavation. The treatment is based on the fact that if the mine is sufficiently deep, the thickness of the excavated panel is comparatively small, and the strains will be classically small: in the past it has been insufficiently recognized that displacements of the magnitude occurring in mining, although large compared with those of laboratory elasticity measurements, may still be infinitesimal in their own context. In addition to being comparatively thin the panel must be, for our purpose, comparatively long, so that there is substantially plane strain over cross-sections remote from the ends: then the problem is two-dimensional and the ground is represented by a homogeneous isotropic elastic half-plane.

Comparison of the results of the present work with measurements of subsidence show, without a doubt, that the basic assumptions are not wholly correct for British coal-mining conditions. It is not possible, on this theory, to accommodate surface subsidence of the magnitude encountered in practice. Moreover, the results predict measurable displacements over a much greater area than that actually affected. These discrepancies have led us to extend the work to the study of transversely isotropic materials with otherwise similar assumptions,

and an account will be published shortly, followed by a treatment of the three dimensional problem.

These conclusions mean that any theoretical or experimental elastic model of large-scale ground movements is quite inadequate in simulating coal-mining subsidence in this country if both homogeneity and isotropy are assumed. It appears that the gelatine models of WHETTON and KING (1957) were constructed to such a scale as to register subsidence extending not much farther than that found in field measurements: as we have seen, a homogeneous isotropic model will exhibit appreciable effects over a much wider area if it is made on an adequate scale. Again, the depth of their elastic medium seems insufficient, certainly in the experiments where it goes no deeper than the 'seam': there is then no allowance for uplift of the floor of the excavation, which, by the present results, would reduce the lowering of the roof by nearly a half, and so nearly halve the surface subsidence.

The results of the present work have been examined in more detail by SALES (1959), and a thorough discussion, from the mining engineer's viewpoint, is to be submitted to a mining journal.

2. FORMULATION OF THE PROBLEM

Although it is, in a sense, the weight of the ground which causes it to deform, the elastic problem is not a body-force problem, since the gravitational force is the same before and after mining. It is convenient to use the term 'primitive stress' (which has some currency) for the stress distribution existing in the undisturbed ground, and 'induced stress' for the increase in stress associated with mining. Then, on the assumptions stated in the Introduction, the consequent displacement is related to the induced stress by the equations of classical isotropic elasticity. Little is known about the primitive stress distribution, but it enters into the calculation of the induced stress and displacement only in so far as the traction it exerts across the surfaces exposed by the excavation must be cancelled by the induced stress field. The latter must be zero at infinity and exert no traction across the ground surface. The displacement is also zero at infinity.

It is supposed that the seam of coal which is extracted is so thin in comparison with its depth and the width of the excavation that the thickness can be treated as an infinitesimal and that a point on the lower boundary of the seam can be given the same coordinate as the nearest point on the upper boundary. The site of the excavation then becomes, in two dimensions, a single straight line, and convergence of opposing points in roof and floor of the excavation can be treated as a discontinuity in displacement at a *single* point. Clearly, a solution based on this assumption will not be valid at the edges of the excavated panel, but this is hardly important since in any case the deformation is known to depart from elastic conditions in the vicinity of an actual excavation: it is quite possible, however, that a solution of this kind may be valid outside a reasonably small region including the excavation.

It is convenient to distinguish three conceivable states of the excavation: (i) non-closure, in which roof and floor do not meet at any point, (ii) partial closure, in which they meet over part of the excavation, and, (iii) complete closure, in which roof and floor meet throughout the excavation. The first and second states

have a common limit, namely the condition of point contact, while the third state is a limiting form of the second. These three states have as their counterparts in the idealized model three forms of displacement discontinuity. Case (i) is really the crack problem in reverse, with the edges of the crack overlapping instead of drawing apart. Case (ii) may be considered as a double reversed crack problem with the extra condition that the interval between the two cracks is subjected to a constant displacement discontinuity, $-t$, where t is the seam thickness. In case (iii) the constant discontinuity covers the whole interval representing the excavation. Whether case (i) or case (ii) occurs depends upon the magnitude of the traction at the excavation and the other parameters involved. Case (iii) is the limit of (ii) as the ratio of the traction to the shear modulus tends to infinity: although this case is not physically realizable it yields some useful results.

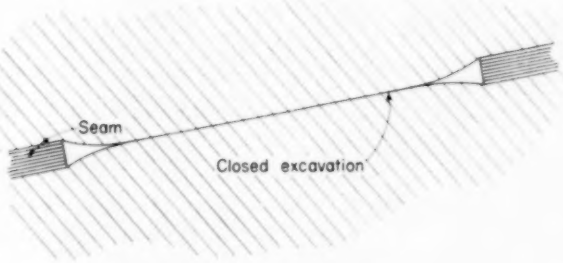

FIG. 1. Partial closure.

The problem is simplified considerably if it is supposed that the induced stress exerts a normal and constant traction, p, on the unclosed parts of the excavation. This condition would probably be fulfilled to sufficient accuracy either if the excavation were approximately horizontal, or, with a tilted panel, the primitive stress were hydrostatic and the difference in depth between the sides of the panel were comparatively small.

In this paper the infinite medium is treated first. Complex potential solutions are given for case (ii), partial closure, from which the other two solutions are derived quite simply as limits. The partial closure problem (though not in the mining context) has previously been considered by MOSSAKOVSKII and ZAGUBIZHENKO (1954) to the extent of finding the relation between the length of closure and the other parameters, but the complete solution was not calculated. The solution for a crack in an infinite plane is well known (WESTERGAARD 1939) and has been studied in the present context by HACKETT (1957, 1959), while a constant discontinuity over a finite line may be readily obtained as the sum of two edge dislocations, equal in magnitude but opposite in sign, originating one at each end of the line of excavation (SALES 1959).

The paper continues with a general method for the deduction of the complex potentials for a given discontinuity in the half-plane from those for the same discontinuity in the whole plane. For case (iii) this method gives an exact solution to the given problem, but for cases (i) and (ii) the traction condition at the excavation is no longer satisfied. The discrepancy is reduced by increasing the depth, so that the results are still useful for sufficient depth.

The most remarkable result emerging from this work is the expression for the displacement at the boundary of the half-plane in case (iii), complete closure. The displacement is independent of the elastic constants and so forms an unambiguous limit for the homogeneous isotropic medium.

3. Infinite Medium

It is assumed for the present that the ground surface is at an infinite distance from the excavation, which occupies the interval $|x| < a$ of the line $y = 0$. Roof and floor are supposed to meet in the interval $|x| \leqslant b$, while in the intervals $b \leqslant |x| < a$ the induced stress exerts a normal traction, p. The displacement and the induced stress must be zero at infinity. Writing Δv for the discontinuity in displacement, we have, on $y = 0$,

$$\Delta v = -t, \quad |x| \leqslant b; \quad \Delta v = 0, \quad |x| > a;$$

$$\sigma_y = p, \quad b \leqslant |x| < a; \quad \tau_{xy} = 0, \quad b \leqslant |x| < a.$$

In addition, if the contact at $|x| = b$ is to be *non-adhesive*, σ_y must be bounded there.

The solution of this problem follows from some general results on cracks by Muskhelishvili (1953). The displacement and stress fields are given by

$$\left.\begin{aligned} 2\mu\,(u + iv) &= (3 - 4\nu)\,\phi(z) - z\,\overline{\Phi}(\bar{z}) - \overline{\psi}(\bar{z}), \\ \sigma_x + \sigma_y &= 2\left[\Phi(z) + \overline{\Phi}(\bar{z})\right], \\ \sigma_x - \sigma_y + 2i\,\tau_{xy} &= -2\left[z\,\overline{\Phi}'(\bar{z}) + \overline{\Psi}(\bar{z})\right], \end{aligned}\right\} \tag{1}$$

where

$$\Phi(z) = \tfrac{1}{2}\,p\left[1 - (z^2 - b^2)^{\frac{1}{2}}\,(z^2 - a^2)^{-\frac{1}{2}}\right], \tag{2}$$

$$\Psi(z) = -z\,\Phi'(z), \tag{3}$$

$$\phi(z) = \int_{\infty}^{z} \Phi(z)\,dz, \tag{4}$$

$$\psi(z) = \int_{\infty}^{z} \Psi(z)\,dz = \phi(z) - z\,\Phi(z), \tag{5}$$

and $z = x + iy$. If the z-plane is cut along the intervals $b < |x| < a$ of $y = 0$ the function (2) is single-valued and the stress field is given unambiguously. However, the functions (4) and (5) remain multivalued unless a further cut is made, $|x| \leqslant b$ being the obvious choice.

The complex conjugate functions are defined so that $\overline{\Phi}(x) = \Phi(x)$ and $\overline{\phi}(x) = \phi(x)$ on the uncut intervals of $y = 0$. On $|x| < b$, $\sigma_y < p$ and $\tau_{xy} = 0$, so that contact is non-adhesive on the whole of that interval.

The relation between b and the other parameters is found by considering the increase in complex displacement around an anti-clockwise contour, C, enclosing the interval $b < x < a$ of the real axis. In an obvious notation

$$
\begin{aligned}
-it &= [u + iv]_C \\
&= \frac{2(1-\nu)}{\mu} \int_C \Phi(z)\, dz \\
&= -\frac{p(1-\nu)}{\mu} \int_C \left(\frac{z^2 - b^2}{z^2 - a^2}\right)^{\frac{1}{2}} dz,
\end{aligned}
$$

using equations (1) to (5). Further calculation shows that

$$
\begin{aligned}
\frac{\mu t}{2pa(1-\nu)} &= \frac{1}{a} \int_b^a \left(\frac{x^2 - b^2}{a^2 - x^2}\right)^{\frac{1}{2}} dx \\
&= E(k) - \frac{b^2}{a^2} K(k) \qquad (6)
\end{aligned}
$$

where $k = (1 - b^2/a^2)^{\frac{1}{2}}$ and $K(k)$, $E(k)$ are the complete elliptic integrals of the first and second kinds respectively. The right-hand side of (6) is a monotonic decreasing function of b/a, unity at $b/a = 0$, zero at $b/a = 1$. Equations (1) to (6) represent the required solution of case (ii).

In case (i) the interval of prescribed displacement discontinuity vanishes and the solution is obtained by putting $b = 0$ in (2), so that

$$
\Phi(z) = \tfrac{1}{2} p \left[1 - z(z^2 - a^2)^{-\frac{1}{2}}\right] \qquad (7)
$$

and

$$
\phi(z) = \tfrac{1}{2} p \left[z - (z^2 - a^2)^{\frac{1}{2}}\right], \qquad (8)
$$

both regular in the plane cut along the interval $|x| < a$ of $y = 0$. It is easy to show that, on $|x| \leqslant a$, $y = 0$,

$$
-\Delta v = \frac{2p}{\mu}(1-\nu)(a^2 - x^2)^{\frac{1}{2}}.
$$

This quantity remains less than t for all $|x| \leqslant a$ so long as

$$
\frac{\mu t}{2pa(1-\nu)} > 1, \qquad (9)
$$

so that (9) is the condition for no contact between roof and floor. The equality

$$
\frac{\mu t}{2pa(1-\nu)} = 1 \qquad (10)
$$

is the condition for point contact at $x = 0$, which is a limiting state of both cases (i) and (ii). When

$$
\frac{\mu t}{2pa(1-\nu)} < 1 \qquad (11)
$$

there is contact over a finite interval $2b$, given by (6).

The solution for case (iii) may be obtained as the limit of that for case (ii) by letting $b \to a$. In (6) we let $k \to 0$ and hence $\mu t/pa \to 0$. By expanding the right-hand side of (6) in powers of k^2 and inverting, we find that

$$
k^2 = 1 - b^2/a^2 = \frac{2\mu t}{\pi pa(1-\nu)} \left\{1 - \frac{\mu t}{4\pi pa(1-\nu)} + O\left[\left(\frac{\mu t}{pa}\right)^2\right]\right\}. \qquad (12)
$$

Substitution for b^2 from (12) into (2) leads to the expression

$$\Phi(z) = \frac{\mu a t}{2\pi(1-\nu)} \cdot \frac{1}{(a^2 - z^2)} \left\{1 + O\left(\frac{\mu t}{pa}\right) + O\left[\frac{\mu a t}{p(a^2 - z^2)}\right]\right\}.$$

In the limit we have the complex potential

$$\Phi(z) = \frac{\mu a t}{2\pi(1-\nu)} \cdot \frac{1}{(a^2 - z^2)} \tag{13}$$

for complete closure, valid except at $z = \pm a$. Corresponding to the potential (4) we have

$$\phi(z) = \frac{\mu t}{4\pi(1-\nu)} \log\left(\frac{z+a}{z-a}\right). \tag{14}$$

The constant displacement discontinuity described by these potentials is equivalent to a Weingarten dislocation formed by the superposition of two edge dislocations at $z = -a$ and $z = a$, with Burgers vectors $-t$ and t, respectively, in the y direction. The Airy stress function for an edge dislocation is well known (KOEHLER 1941) and the superposition of the two leads to the stress function

$$\chi(x, y) = \frac{\mu t}{4\pi(1-\nu)} \left[(x+a) \log\left\{\frac{(x+a)^2 + y^2}{t^2}\right\} - \right.$$
$$\left. - (x-a) \log\left\{\frac{(x-a)^2 + y^2}{t^2}\right\}\right], \tag{15}$$

which is easily shown to be equivalent to the complex variable solution above.

4. HALF-PLANE

The first part of this Section is concerned with a general result on displacement discontinuities or dislocations inside a half-plane with a traction-free boundary. Suppose that the equations (1) together with the functions

$$\phi(z) = f(z), \quad \psi(z) = g(z), \tag{16}$$

represent a stress distribution which is bounded in the whole plane with the exception of a finite number of singularities in $y < 0$ associated with discontinuities in that part of the plane. We wish to find functions $f_1(z)$, $g_1(z)$, regular in $y < 0$, such that the complex potentials

$$\phi(z) = f(z) + f_1(z), \quad \psi(z) = g(z) + g_1(z), \tag{17}$$

yield a stress distribution exerting no traction on $y = 0$. From equations (1) the condition for this to be so is

$$\phi'(x) + \bar{\phi}'(x) + x\phi''(x) + \psi'(x) = 0$$

or

$$f_1'(x) + \bar{f}_1'(x) + x f_1''(x) + g_1'(x) = -f'(x) - \bar{f}'(x) - x f''(x) - g'(x).$$

This equation is clearly satisfied if both

$$f_1'(z) + z f_1''(z) + g_1(z) = -\bar{f}'(z) \tag{18}$$

and

$$\bar{f}_1'(z) = -f'(z) - z f''(z) - g'(z). \tag{19}$$

These equations may be integrated to give

$$z f_1'(z) + g_1(z) = -\bar{f}(z), \tag{20}$$

$$\bar{f}_1(z) = -z f'(z) - g(z). \tag{21}$$

From (21)

$$f_1(z) = -z\bar{f}'(z) - \bar{g}(z), \tag{22}$$

and from (19) and (20)

$$g_1(z) = -\bar{f}(z) + z\left[\bar{f}'(z) + z\bar{f}''(z) + \bar{g}'(z)\right]. \tag{23}$$

The functions (22) and (23) satisfy the requirement of regularity in $y < 0$ since their singularities are all in $y > 0$, and are of the right order at infinity: hence the problem is solved.

In order to find functions $f(z)$ and $g(z)$ representing an arbitrarily oriented discontinuity of the type discussed in the previous section we must first transform the defining equations. Let (x', y') now denote the initial coordinate system, so that the discontinuity lies on the interval $|x'| < a$ of $y' = 0$, and let $\phi_0(z')$, $\psi_0(z')$ now denote the complex potentials (4) and (5). The transformation

$$z' = (z + ih)\,e^{-i\alpha} \tag{24}$$

translates the discontinuity so that it lies between the points $z = -ih \pm ae^{i\alpha}$.

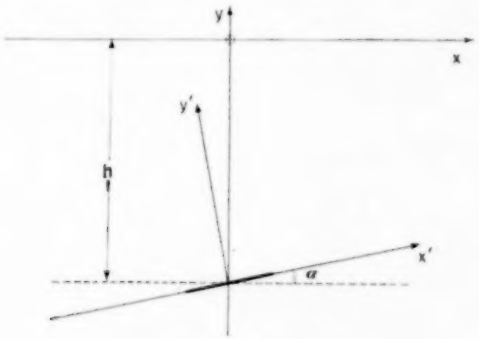

FIG. 2.

The equations relating the displacement and stress fields in the (x, y) coordinate system to those in the (x', y') system are

$$\left.\begin{aligned} u + iv &= e^{i\alpha}(u' + iv'),\\ \sigma_x + \sigma_y &= \sigma_{x'} + \sigma_{y'},\\ \sigma_x - \sigma_y + 2i\tau_{xy} &= e^{2i\alpha}(\sigma_{x'} - \sigma_{y'} + 2i\tau_{x'y'}), \end{aligned}\right\} \tag{25}$$

and substitution from (1) into these equations together with the substitution (24) leads to

$$\left.\begin{aligned} 2\mu(u + iv) &= e^{i\alpha}\{(3 - 4\nu)\phi_0[(z + ih)e^{-i\alpha}] - \\ &\quad - (z + ih)e^{-i\alpha}\bar{\phi}_0'[(\bar{z} - ih)e^{i\alpha}] - \bar{\psi}_0[(\bar{z} - ih)e^{i\alpha}]\},\\ \sigma_x + \sigma_y &= 2\{\phi_0'[(z + ih)e^{-i\alpha}] + \bar{\phi}_0'[(\bar{z} - ih)e^{i\alpha}]\},\\ \sigma_x - \sigma_y + 2i\tau_{xy} &= -2e^{2i\alpha}\{(z + ih)e^{-i\alpha}\bar{\phi}_0''[(\bar{z} - ih)e^{i\alpha}] + \\ &\quad + \bar{\phi}_0'[(\bar{z} - ih)e^{i\alpha}]\}. \end{aligned}\right\} \tag{26}$$

Now the functions (16) must satisfy the relations (1), and hence

$$\left.\begin{aligned} 2\mu(u + iv) &= (3 - 4\nu)f(z) - z\bar{f}'(\bar{z}) - \bar{g}(\bar{z}),\\ \sigma_x + \sigma_y &= 2\left[f'(z) + \bar{f}'(\bar{z})\right],\\ \sigma_x - \sigma_y + 2i\tau_{xy} &= -2\left[z\bar{f}''(\bar{z}) + \bar{g}'(\bar{z})\right]. \end{aligned}\right\} \tag{27}$$

Comparison of (26) and (27) shows that the required functions are

$$f(z) = e^{i\alpha} \phi_0 [(z + ih) e^{-i\alpha}], \tag{28}$$

$$g(z) = e^{-i\alpha} \psi_0 [(z + ih) e^{-i\alpha}] - ih \phi_0' [(z + ih) e^{-i\alpha}]. \tag{29}$$

By means of (5) $g(z)$ may be expressed in terms of $\phi_0(z)$ and its derivative with the result

$$g(z) = e^{-i\alpha} \phi_0 [(z + ih) e^{-i\alpha}] - [(z + ih) e^{-2i\alpha} + ih] \phi_0' [(z + ih) e^{-i\alpha}]. \tag{30}$$

Then, from (17), (22), (23), (28) and (30), the solution for the given discontinuities in a half-plane is given by the potentials

$$\phi(z) = e^{i\alpha} \{\phi_0 [(z + ih) e^{-i\alpha}] - \bar{\phi}_0 [(z - ih) e^{i\alpha}] - [(z + ih) e^{-i\alpha} - (z - ih) e^{i\alpha}] \bar{\phi}_0' [(z - ih) e^{i\alpha}]\}, \tag{31}$$

$$\psi(z) = e^{-i\alpha} \{\phi_0 [(z + ih) e^{-i\alpha}] - \bar{\phi}_0 [(z - ih) e^{i\alpha}] - [(z + ih) e^{-i\alpha} + ih e^{i\alpha}] \phi_0' [(z + ih) e^{-i\alpha}]\} + z\bar{\phi}_0' [(z - ih) e^{i\alpha}] + z e^{2i\alpha} [(z + ih) e^{-i\alpha} - (z - ih) e^{i\alpha}] \bar{\phi}_0'' [(z - ih) e^{i\alpha}] \tag{32}$$

with, from (2) and (4),

$$\phi_0(z) = \bar{\phi}_0(z) = \tfrac{1}{4} p \int_{\infty}^{z} [1 - (z^2 - b^2)^{\frac{1}{2}} (z^2 - a^2)^{-\frac{1}{2}}] \, dz. \tag{33}$$

The solution given by equations (31) to (33) is for a prescribed displacement discontinuity on the line $\mathrm{Im}[(z + ih) e^{-i\alpha}] = 0$ identical to that obtained in an *infinite* medium under the action of a constant normal traction p on the unclosed intervals $b < |\mathrm{Re}[(z + ih) e^{-i\alpha}]| < a$, where p satisfies the condition (ii). If b is made zero in (33) the solution is for the elliptical discontinuity obtained in the *infinite* medium when p satifies condition (9) or (10). The introduction of the traction-free boundary at $y = 0$ alters the tractions exerted at the discontinuity so that equations (31) to (33) do not represent the solution to the problem of prescribed normal traction at the excavation. We shall investigate later to what extent they may be used as an approximation to the required solution. However, if we let $b \to a$, the interval on which traction was originally specified now vanishes and the potentials (31) and (32) together with

$$\phi_0(z) = \bar{\phi}_0(z) = \frac{\mu l}{4\pi(1 - \nu)} \log\left(\frac{z + a}{z - a}\right) \tag{34}$$

give the exact solution for a constant displacement discontinuity

$$\Delta(u + iv) = -ile^{i\alpha}$$

on the interval $-a < \mathrm{Re}[(z + ih) e^{-i\alpha}] < a$ of $\mathrm{Im}[(z + ih) e^{-i\alpha}] = 0$. This is the complete closure solution, case (iii), for the half-plane.

From (25) and (1) the traction exerted on the line of the discontinuity is given by

$$\sigma_{y'} + i\tau_{x'y'} = \phi'(z) + \bar{\phi}'(\bar{z}) + e^{2i\alpha} [\bar{z}\phi''(z) + \psi'(z)] \tag{35}$$

with

$$\mathrm{Im}[(z + ih) e^{-i\alpha}] = 0$$

and $\phi(z)$ and $\psi(z)$ given by (31) and (32). Equation (35) can be put in the form

$$\sigma_{y'} + i\tau_{x'y'} = \phi_0'(z') + \bar{\phi}_0'(\bar{z}') - (z' - \bar{z}') \phi_0''(z') + F(\zeta, \bar{\zeta}) \tag{36}$$

where $z' = (z + ih) e^{-i\alpha}$ and $\zeta = (z - ih) e^{i\alpha}$. Here, the functions of z' and $\bar{z}'$ represent the solution of the original problem of the infinite medium and have the sum p on $b < |x'| < a$, $y' = 0$; while $F(\zeta, \bar{\zeta})$ is the additional traction introduced by imposing the traction-free boundary at $y = 0$. It can be shown that

$$F(\zeta, \bar{\zeta}) = p \cdot \frac{a^2 - b^2}{\zeta^2} [G(\zeta, \bar{\zeta}) + O(a^2/|\zeta^2|)] \tag{37}$$

where $G(\zeta, \bar{\zeta})$ is a function certainly satisfying the inequality $|G| < 43/4 + 15\,|h/\zeta| + 6\,|h^2/\zeta^2|$ and the notation $O(a^2/|\zeta^2|)$ is used to indicate terms which are of the order of magnitude of $a^2/|\zeta^2|$ as that quantity tends to zero.

Equations (36) and (37) imply that equations (31) to (33) constitute an approximation to the half-plane solution having a comparative discrepancy of $O(a^2/h^2)$. We suppose that in (37) terms of smaller order of magnitude than $G(\zeta, \bar{\zeta})$ may be neglected, and use the fact that $|\zeta| > 2h - a$ for points on the discontinuity. Then the modulus of the contribution of $F(\zeta, \bar{\zeta})$ to the complex traction is less than $p/10$ if

$$\frac{a^2}{(2h-a)^2}\left[\frac{43}{4} + \frac{15h}{2h-a} + \frac{6h^2}{(2h-a)^2}\right] < \frac{1}{10}.$$

It is not difficult to show that this inequality certainly holds if $h/2a > 4$. When $\alpha = 0$, $|\zeta| > 2h$ and it is easier to make an estimate of the magnitude of $F(\zeta, \bar{\zeta})$. In fact, we then have the inequality

$$|F(\zeta, \bar{\zeta})| < \frac{5\,p\,(a^2 - b^2)}{8h^2}\left[1 + \frac{15}{32}\frac{a^2}{h^2} + O\left(\frac{a^4}{h^4}\right)\right]. \tag{38}$$

In this case, neglecting the term $O(a^4/h^4)$, it is found that the contribution to the traction does not exceed $p/10$ if $h/2a > 1{\cdot}3$. These results indicate that, at least when the discontinuity is nearly parallel to the free surface, equations (31) to (33) may give a fair approximation to the exact solution even when the ratio of depth to width, $h/2a$, is not very large. In the half-plane, the criteria (9), (10) and (11) will no longer hold, and the critical ratio will become a function of a/h and α. Nevertheless, the original ratio will remain a good approximation for a/h sufficiently small.

5. Displacement at the Surface

The most easily and accurately measured of the effects of mining is the displacement at the surface. From (1), (31) and (32), the displacement on $y = 0$ is given by

$$(u + iv)_0 = 2e^{i\alpha}\frac{1-\nu}{\mu}\{\phi_0[(x + ih)\,e^{-i\alpha}] - \phi_0[(x - ih)\,e^{i\alpha}] + \\ + 2i\,(x\sin\alpha - h\cos\alpha)\,\phi_0'[(x - ih)\,e^{i\alpha}]\} \tag{39}$$

where ϕ_0 is given by (33) for partial closure, or by (34) for complete closure. For partial closure and non-closure ($b = 0$) the result holds only approximately, being subject to the limitations discussed in the previous section. For complete closure we find that

$$(u + iv)_0 = \frac{te^{i\alpha}}{2\pi}\left\{\log\frac{[(x + ih)\,e^{-i\alpha} + a]\,[(x - ih)\,e^{i\alpha} - a]}{[(x + ih)\,e^{-i\alpha} - a]\,[(x - ih)\,e^{i\alpha} + a]} + \right. \\ \left. + \frac{4ia\,(h\cos\alpha - x\sin\alpha)}{(x - ih)^2\,e^{2i\alpha} - a^2}\right\}. \tag{40}$$

This is the exact result, and it is clearly independent of the elastic constants.

In the case of non-closure, when $b = 0$ in (33), the elastic constants do not enter into the function $\phi_0(z)$, so that they occur in (39) in the factor $(1 - \nu)/\mu$ only. On the other hand, in the partial closure case the expression depends on the elastic constants by means of b also.

When $\phi_0(z)$ is given by (33) and h is sufficiently large, (39) has the following expansion :

$$(u + iv)_0 = -2p(a^2 - b^2)\frac{1-\nu}{\mu}\left(\frac{h\cos\alpha - x\sin\alpha}{x^2+h^2}\right)^2(x+ih)\times$$
$$\times\left[1 + \frac{3a^2+b^2}{12(x^2+h^2)}q(x) + O\left(\frac{a^4}{h^4}\right)\right] \quad (41)$$

where

$$q(x) = \frac{x-ih}{x+ih}e^{2i\alpha} + 2 + 3\frac{x+ih}{x-ih}e^{-2i\alpha}, \quad (42)$$

so that the inequality

$$\frac{3a^2+b^2}{12(x^2+h^2)}q(x) \leqslant 2\frac{a^2}{h^2}$$

is certainly satisfied. Equation (41) thus affords a convenient approximation even when $h/2a$ is not very large. Certainly, for values $h/2a \geqslant 4$, when the approximation to the partial closure solution for general α may be reckoned to be reasonably close, the first term of the expansion (41) will be all that is required for comparison with actual surface displacement measurements. In the range $h/2a \geqslant 5/2$, the partial closure approximation of the previous section is good for a nearly horizontal excavation and the ratio of the second term to the first in the expansion (41) is not more than 2/25.

Except for complete closure ($b \to a$), (41) has a comparative discrepancy of $O(a^2/h^2)$, so long as it is regarded as the result for constant and normal traction at the free surface of the excavation, and it follows that the exact form of the second term in the expansion is unknown. For complete closure, however, this term stands, and the limiting expansion can be found by means of (12). Bearing these points in mind, we write for the three cases:

(i) *Non-closure*

$$(u + iv)_0 = -2pa^2\frac{1-\nu}{\mu}\left(\frac{h\cos\alpha - x\sin\alpha}{x^2+h^2}\right)^2(x+ih)\left[1 + O\left(\frac{a^2}{h^2}\right)\right], \quad (43)$$

(ii) *Partial closure*

$$(u + iv)_0 = -2p(a^2 - b^2)\frac{1-\nu}{\mu}\left(\frac{h\cos\alpha - x\sin\alpha}{x^2+h^2}\right)^2(x+ih)\left[1 + O\left(\frac{a^2}{h^2}\right)\right], \quad (44)$$

(iii) *Complete closure*

$$(u + iv)_0 = -\frac{4at}{\pi}\left(\frac{h\cos\alpha - x\sin\alpha}{x^2+h^2}\right)^2(x+ih)\left[1 + \frac{a^2q(x)}{3(x^2+h^2)} + O\left(\frac{a^4}{h^4}\right)\right] \quad (45)$$

where $q(x)$ is given by (42). It may be shown that in these expressions the factor independent of x is equal in each case to $2/\pi$ times the area of the appropriate displacement discontinuity in the infinite medium. Since, to the order of approximation considered, the discontinuity is the same in the half-plane as in the whole plane, each case may be represented by the single expression

$$(u + iv)_0 = -\frac{2}{\pi}A\left(\frac{h\cos\alpha - x\sin\alpha}{x^2+h^2}\right)^2(x+ih)\left[1 + O\left(\frac{a^2}{h^2}\right)\right] \quad (46)$$

where A is the area of the discontinuity, or, in practical terms, the volume closure

per unit length of the infinite rectangular panel. The vertical displacement given by this approximation is indicated in Fig. 3.

For a given size of excavation, A increases steadily with $p(1-\nu)/\mu$. The rate of increase is approximately linear until, according to condition (10), point contact is made in the neighbourhood of $p(1-\nu)/\mu = \frac{1}{2}t/a$, when $A \simeq \frac{1}{2}\pi at$. Thereafter the rate of increase becomes less, and as $p(1-\nu)/\mu \to \infty$, $b \to a$ by equation (12) and $A \to 2at$ exactly. Thus, to the degree of accuracy indicated, the complete closure solution provides for the surface displacement a bound which is independent of the elastic constants. Moreover, the magnitude of the displacement in the bounding case is greater than that at incipient closure by a factor of approximately $4/\pi$ only.

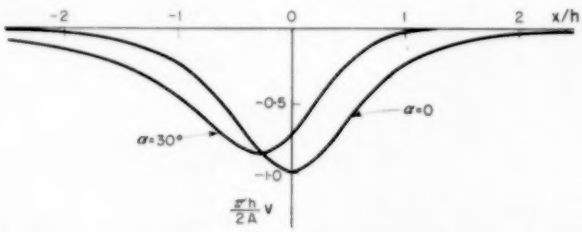

Fig. 3. Approximate vertical displacement at surface, h large.

In comparing these results with actual measurements one should bear in mind the effects of likely deviations from the postulated model. There are two respects in which the actual situation will probably differ from the ideal without destroying its validity; and the effect of both departures seems to be to reduce the expected subsidence. In the first place, the panel may well be insufficiently long to be considered infinite, and the effect of having the ends at a finite distance is almost certainly to reduce the displacement. (It is certainly so in the complete closure case, as will be shown in the paper on the three-dimensional problem). Secondly, when the ground around the excavation is broken to some extent, more space is occupied by the broken material than if it remains continuous, and the convergence of points just outside the fractured zone is less than predicted: this again has the effect of decreasing the displacement.

However, when the subsidence measurements recorded in the literature are examined, it is found that almost without exception the magnitude of maximum subsidence is in excess of that given by the bounding expression, equation (45). Moreover, the shape of the subsidence profile indicated by the present results is much flatter than that observed in practice, so that displacements of measurable magnitude extend much farther from the centre of the trough than those actually found.

A more detailed comparison of these results with field measurements will be made elsewhere, but the present remarks are intended to show that it is of little use to consider subsidence in British coal-measure rocks as the deformation of a homogeneous, isotropic, elastic medium: at least one of the major assumptions must be modified.

ACKNOWLEDGMENTS

The author is grateful for much helpful discussion on various aspects of the problem to his colleagues, Mr. T. W. SALES, Dr. P. HACKETT, Professor F. B. HINSLEY and particularly to Professor R. HILL who was responsible for the fundamental idea of the excavation as a dislocation. The author is indebted to the National Coal Board for financial support during the period of this work, which is part of an extended investigation of strata control carried out by a theoretical group in the University of Nottingham.

REFERENCES

BRIGGS, H. 1929 *Mining Subsidence* (Arnold, London).

GROND, G. J. A. 1950 *Iron Coal Tr. Rev.* **160**, 1323, 1377, 1445; **161**, 37, 85, 135, 197, 249, 295, 353, 394.

HACKETT, P. 1957 Ph.D. Thesis, University of Nottingham.

1959 *Trans. Instn. Min Engrs, Lond.* **118**, 421.

ISAACSON, E. DE. ST. Q. 1958 *Rock Pressure in Mines* (Mining Publications, London).

KOEHLER, J. S. 1941 *Phys. Rev.* **60**, 397.

LEEDS 1957 *Proceedings of the European Congress on Ground Movement.*

LIÈGE 1951 *Proceedings of the International Conference about Rock Pressure and Support in the Workings* (Annales des Mines de Belgique, Brussels).

MOSSAKOVSKII, V. I. and ZAGUSIZHENKO, P. A. 1954 *Dokl. Akad. Nauk SSSR* (N.S.) **94**, 409.

MUSKHELISHVILI, N. I. 1953 *Some Basic Problems of the Mathematical Theory of Elasticity*, Trans. by J. R. M. RADOK (Noordhoff, Groningen).

SALES, T. W. 1959 M.Sc. Thesis, University of Nottingham.

WESTERGAARD, H. M. 1939 *J. Appl. Mech.* **6**, 249.

WHETTON, J. T. and KING, H. J. 1957 *Proceedings of the European Congress on Ground Movement, Leeds*, p. 27.

NOTICE

PIB SYMPOSIUM

ON

ELECTROMAGNETICS AND FLUID DYNAMICS OF GASEOUS PLASMA

THE eleventh annual international Polytechnic Institute of Brooklyn Symposium, scheduled for 4–6 April 1961 in New York City, will be devoted to "Electromagnetics and Fluid Dynamics of Gaseous Plasma." The area of interest covers collective electromagnetic and fluid dynamic phenomena and their self-consistent analytical description in the temperature range characteristic of the transition between partially and fully ionized gaseous plasmas.

Typical of the subjects planned for discussion at the Symposium are:

1. Microscopic and Macroscopic Theories of Non-equilibrium Magneto-Fluidynamics.
   (a) Distribution function versus moment approaches (cut-off procedures)
   (b) Elastic and inelastic collision contributions
   (c) Effects of heat conductivity, viscosity, etc.
   (d) Effects of particle trapping, instabilities

2. Linear Wave Propagation in Uniform and Non-Uniform Plasmas
   (a) Classification of wave types (harmonic and other small disturbances)
   (b) Surface waves
   (c) Effects of plasma discontinuities
   (d) Plasma radiation (random and ordered)
   (e) Experimental wave techniques

3. Nonlinear Wave Propagation in Uniform and Non-Uniform Plasmas
   (a) Shocks
   (b) Dissipation and excitation phenomena
   (c) Harmonic generation and parametric effects
   (d) Boundary layer effects
   (e) Experimental techniques

4. Possible Applications of Magneto-Fluidynamics
   (a) Electromechanical forces in moving plasmas
   (b) Plasma generators
   (c) Plasma jets
   (d) Confinement and stability

This year the symposium is being organized by the Department of Aerospace Engineering and the Microwave Research Institute of the Polytechnic Institute of Brooklyn in cooperation with the Institute of Radio Engineers and the Institute of the Aeronautical Sciences and with the co-sponsorship of the Air Force Office of Scientific Research, the Office of Naval Research, and the U.S. Army Signal Corps.

In keeping with tradition, the symposium will endeavour to serve the twofold purpose of providing both a review of the present state of research in the above plasma fields and a forum for discussion of recent outstanding advances of interest to engineers, mathematicians and phys-

icists involved in plasma research. The programme will comprise both invited and a limited number of contributed papers and will conclude with a round-table discussion of some future trends in plasma research. Further information may be obtained from Professors MARTIN BLOOM and ENRICO LEVI, Co-Chairmen of the Symposium Committee.

The closing date for submission of papers or 200 word abstracts is 20 December 1960. Correspondence should be addressed to:

Symposium Committee,
Polytechnic Institute of Brooklyn,
55 Johnson Street,
Brooklyn 1, New York, U.S.A.

END OF VOL.